Journal of Sensors

Sensors and Applications in Agricultural and Environmental Monitoring 2021

Lead Guest Editor: Yuan Li
Guest Editors: Zhenxing Zhang, Jingwei Wang, Ajit Ghosh, Liu Hongxiao, and Ya-Dan Du

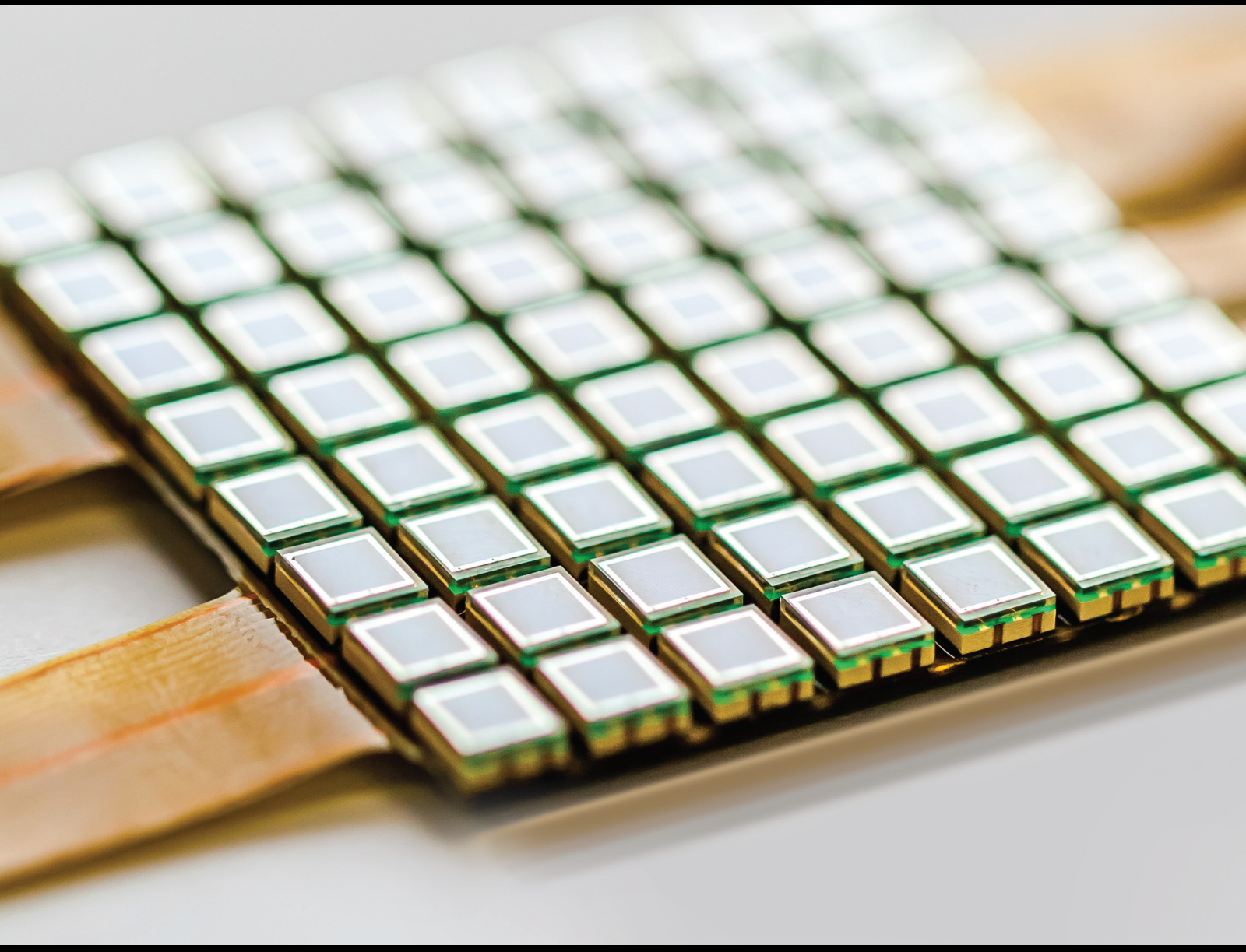

Sensors and Applications in Agricultural and Environmental Monitoring 2021

Journal of Sensors

Sensors and Applications in Agricultural and Environmental Monitoring 2021

Lead Guest Editor: Yuan Li
Guest Editors: Zhenxing Zhang, Jingwei Wang, Ajit Ghosh, Liu Hongxiao, and Ya-Dan Du

Contents

Contents

Hindawi
Journal of Sensors
Volume 2023, Article ID 7020104, 17 pages
https://doi.org/10.1155/2023/7020104

Research Article

Energy-Efficient Resource Scheduling and Computation Offloading Strategy for Solar-Powered Agriculture WSN

Juan Gao,[1] Runze Wu,[1] Jianhong Hao,[1] Chen Xu,[2] Haobo Guo,[1] and Haonan Wang[1]

[1]*Electrical and Electronic Engineering Department, North China Electric Power University, Beijing 102206, China*
[2]*School of Artificial Intelligence, Beijing University of Posts and Telecommunications, Beijing 100876, China*

Correspondence should be addressed to Runze Wu; wurz@ncepu.edu.cn

Received 25 March 2022; Revised 23 September 2022; Accepted 26 September 2022; Published 11 April 2023

Academic Editor: Zhenxing Zhang

IoT-based smart agriculture plays a significant role in building a high-yield, sustainable, and intelligent modern agriculture. However, limited battery capacity and low-power processors of sensors cannot accommodate the exponential expansion of data from smart agriculture sensing terminals. To overcome the challenges, we introduced solar harvesting and multiaccess edge computing (MEC) to investigate sustainable monitoring of smart agriculture in solar-powered MEC-enabled WSNs. Considering the cyclical and day-night fluctuations of solar energy, we formulate a joint optimization problem for resource scheduling and computation offloading strategy to maximize the minimum weighted computation capacity across the time slots under solar energy constraints. To solve the mixed-integer nonlinear program (MINLP), we propose a multiply-iterated decoupling optimization algorithm by jointly optimizing a computation offloading strategy, energy provision of the solar-powered hybrid access point (HAP), and local CPU frequency as well as time scheduling. Simulation results show that the proposed algorithm can efficiently use solar energy to balance network calculations, improve network energy efficiency, and realize unmanned and sustainable agricultural WSN.

1. Introduction

1.1. Background. The flourishing development of IoT has brought new opportunities and challenges to modern agriculture, especially in precision agriculture and smart irrigation applications [1]. Wireless sensor networks (WSNs), as the sensing layer of IoT, can achieve comprehensive sensing and timely response to environmental status with their highly scalable and ubiquitous architecture, which can effectively assist the smart agriculture systems in maximizing yields and minimizing wastage [2]. However, the characteristics of sensors, including the low-power processor and energy-constrained battery, make it difficult to process complex tasks sustainably. It seriously affects the upgrade application of agriculture WSNs, especially in precision agriculture, where WSN not only needs to consume more energy to continuously monitor feature parameters, such as soil moisture, soil nutrients, crop growth, and pests, but also requires to pay more computation to process data and transmit commands with low latency [3]. Therefore, how to tackle the energy constraints and computation limitations of sensors simultaneously is a critical problem in the development of sustainable agriculture WSN.

Conventional sensors are powered by limited capacity batteries. Networks that prolong the network lifetime by regularly replacing batteries can result in significant maintenance costs and serious environmental pollution. To satisfy the energy requirements for comprehensive monitoring, existing research focuses on either open-source or cost-saving approaches [4]. Specific energy-efficient approaches for battery-constrained WSNs cover clustering-based schemes [5], node deployment strategies [6], node scheduling algorithms [7], energy-efficient routing schemes [8], and energy-efficient joint designs [9], all of which prolong the network lifetime at the expense of network performance and fail to inherently provide a sustainable energy supply to the network. Moreover, the deployment of batteries in soil and water quality monitoring applications is not allowed since it is necessary to prevent environmental damage caused by battery leakage or damage. Based on RF, wireless

power transfer (WPT) technology can provide a continuous and controlled energy supply for sensors and effectively solve the energy constraint problem [10]. However, the existing wireless energy mainly derives from high-capacity batteries or the nearby power grid, which is problematic in agricultural applications due to the difficulty of introduction and high maintenance costs. Renewable environmental energy sources, such as solar energy, wind energy, thermal energy, and vibration, can provide a continuous, convenient, and clean energy supply for remote agriculture by virtue of their wide distribution and accessibility [11]. Solar energy, as the most popular ambient microenergy source, enjoys a higher power density (15 mW/cm^2), greater geographic flexibility, easier installation, and periodicity available, making it particularly appropriate for the perpetual energy supply of nodes in agricultural WSNs [12].

To make up for the limited computing capacity of sensors, the majority of agricultural systems use cloud computing to process, analyse, and store large amounts of heterogeneous data through multiple network layers, which imposes a significant burden on the information and communication infrastructure, causing enormous energy costs and more significant information return latency [13]. It obviously fails to match the low latency requirements of precision agriculture with exponentially increasing monitoring tasks. The multiaccess edge computing (MEC) allows the sensors to offload intensive computations to nearby servers located at the edge of the radio access network, thus facilitating better performance than the cloud computing paradigm in terms of latency, effective bandwidth, energy consumption, and load balancing, which is considered to be a promising solution to enhance the computing capability of WSN [14]. Existing MEC research has mainly focused on networks that rely on limited batteries [15] or stable and controllable RF signals [16] for energy supply, achieving maximum computation rate [17], minimum energy consumption [18], and maximum energy efficiency [19] by jointly optimizing offloading decisions and resource allocation, which makes it difficult to apply in remote agricultural IoT with the requirement of unmanned, low-latency, comprehensive state monitoring. It is significant to build a solar-powered MEC green agricultural IoT to satisfy the requirements of smart agriculture for comprehensive sensing and real-time processing. However, due to the randomness and volatility of solar energy, research on energy-efficient offloading decisions and resource scheduling of MEC based on solar energy supply faces significant challenges.

1.2. Related Works. In MEC systems, it is essential to design efficient offloading decision and resource scheduling for improving network performance in terms of energy efficiency, spectral efficiency, latency, and lifetime [14]. Compared to single-user offloading [20], the multiuser offloading decision is more suitable for the smart agricultural IoT as it requires a combination of communication resources and collaboration between multiple users [18].

From the perspective of task features, there are two basic computation offloading decisions for MEC, such as binary and partial offloading [14]. Partial offloading allows a task to be partitioned into two parts, with one executed locally and the other offloaded for edge computing, which is mostly used for high-volume and complex tasks such as environmental monitoring and healthcare applications. Binary offloading requires a task to be executed as a whole packet either locally or offloaded to a remote MEC server, which is more suitable for applications with high relevance, such as anomaly detection. Research on binary and partial offloading is also abundant [16, 21, 22]. In [21], Zhou et al. investigated the optimal resource allocation for maximizing the network computation efficiency under the partial and binary offloading mode. Mao et al. [22] designed the online partial offloading and resource allocation algorithm to tradeoff between energy efficiency and delay. In [16], Bi et al. proposed two efficient solution algorithms (such as the coordinate descent method and the ADMM-based method) to tackle the binary combinatorial computing mode selection. Partial offloading is a relaxed form of binary offloading from a mathematical point of view, which is simpler to compute since it eliminates the discrete random variables. However, in many practical scenarios, especially those suffering from timing characteristics, computing tasks may not be arbitrarily divisible; thus, the binary offloading will be considered in this work.

From the energy supply perspective, traditional MEC are powered by limited capacity batteries. Researchers have focused on proposing excellent offload decisions and resource allocation strategies that can reduce node energy consumption and prolong network lifetime, but this is limited. In [15], Xu et al. investigated the energy minimization task offloading and resource allocation for MEC in NOMA-HetNets under the constraints of QoS requirements. Literature [23] proposes a cooperative offloading technique based on the Lagrangian Suboptimal Convergent Computation Offloading Algorithm (LSCCOA) to minimize weighted sum of transmit power consumption. Considering the limitations and complexity of the integrated batteries in nodes, more and more scholars are focusing on introducing WPT to provide continuous and controlled energy supply for sensors sensing, forwarding, etc., thus improving network energy efficiency and prolonging network lifetime [24]. In a wireless powered multiuser MEC system, Literature [16] jointly optimized the binary offloading mode and the transmission time allocation to maximize the sum computation rate of all the devices. Literature [18] proposed a power minimized resource scheduling strategy by jointly optimizing downlink energy beamforming, uplink computation offloading, and local task execution at users. To enhance computation efficiency and prolong the network lifetime, Literature [17] jointly optimizes the allocation of the communication, computing, and energy resources with the aid of WPT in Full-Duplex (FD) mode. In [25], Li et al. proposed a joint user association and dynamic offloading scheme to enhance the computing capability and achieve sustainable device operation. Different from the works in [18] where channel state information (CSI) is assumed to be fixed, the authors in [26] consider a practical scenario with casual task state

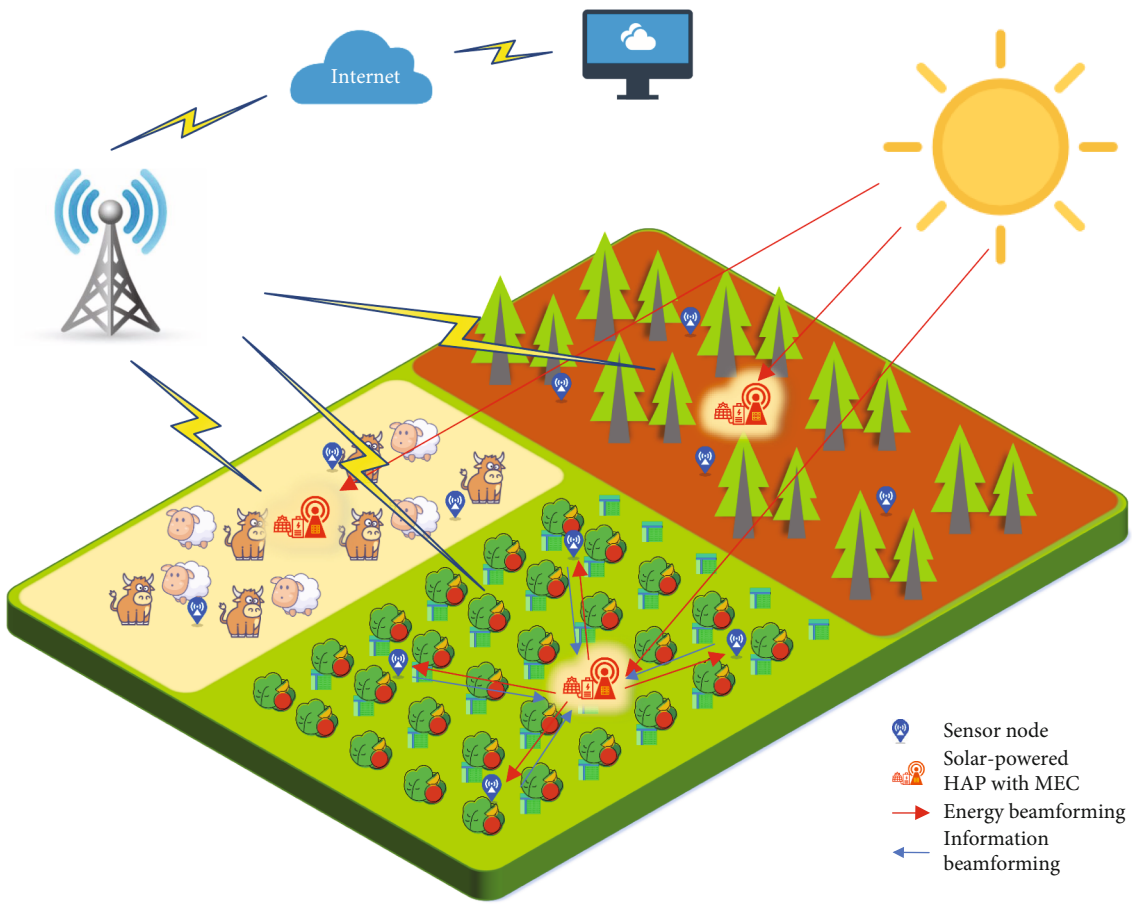

Figure 1: The overview of solar-powered MEC-enabled agriculture WSN. The HAP (embedded MEC) consistently harvests and stores solar energy for charging a set of battery-free sensor nodes and processing tasks offloaded by sensor nodes that makes offloading decisions.

information (TSI) and CSI and propose a real-time resource allocation strategy to minimize the total system energy consumption. However, these studies are based on the continuous and stable energy transmitting power provided by high-capacity batteries or the nearby power grid, which is not suitable for the agricultural environment far from cities and complex terrain, so we need to find a more suitable energy source for agricultural WSNs. Given the stochastic and volatile nature of environmental energy, few existing studies on renewable energy-powered MEC are available. In [27], the multiuser energy consumption and computing resource minimization problem for hybrid renewable energy and grid supply is studied under energy harvesting and QoS constraints. Literature [28] investigated the decentralized partially observable offloading problem in the multiuser EH-enabled system, in which multiple IoT devices cooperate to maximize the network performance while meeting QoE requirements. Although MEC-based optimal offloading decisions and resource scheduling problems have been studied under conventional battery supply, WPT supply, and renewable energy access supply, all of these have failed to fully exploit both the periodic cleanliness of solar energy and the continuous controllability advantages of WPT through technological complementarity in MEC networks to meet the operational requirements of precision agricultural IoT.

1.3. Contributions. In this paper, we consider a solar-powered multinode MEC-enabled WSN system, as shown in Figure 1, where a solar-powered hybrid access point (HAP) integrated with a MEC server jointly recharges all sensors and computes the offloading task. Each sensor uses up the charged energy to make the optimal offloading decision given the system objective. In particular, we are interested in maximizing the minimum weighted system computation capacity as indicated by throughput across the time slots subject to the periodicity and day-night variability of solar energy. To our knowledge, this is the first paper that studies the optimal design in a multinode solar-WPT-powered MEC network using binary offloading strategy for agricultural WSN. Our contributions are detailed below.

(1) We constructed a solar-powered multinode MEC-enabled agricultural WSN framework to achieve balanced system computation capacity, which is necessary for building efficient, clean, unmanned sustainable smart agriculture

(2) We formulate a maximize the minimum weighted system throughput problem for Solar-Powered MEC-enabled WSN to determine the computation offloading strategy of each node in each time slot

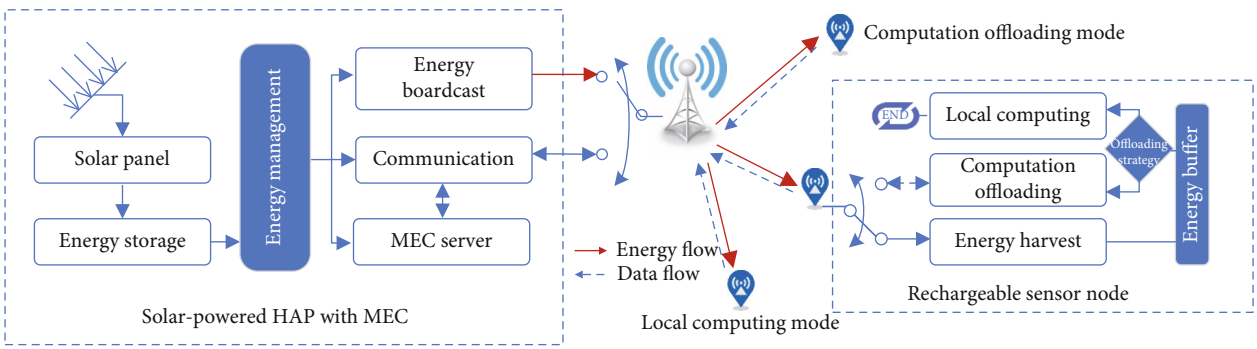

Figure 2: A block diagram of the energy broadcasting and task computing. The HAP harvest-store-broadcast energy for member nodes to perform local computing or computation offloading.

and the time trade-off between energy broadcast and transmission, which jointly optimize the energy provision of solar-powered HAP, multinode computation offloading strategy, and local CPU frequency as well as computing offloading time schedule

(3) To solve the mixed-integer nonlinear program (MINLP), we propose a multiply-iterated decoupling optimization method. First, we initialize a computation offloading strategy to obtain a semiclosed-form solution for the optimal local CPU frequency and the optimal edge computation communication time allocation subject to a specific HAP energy provision. We then propose a low-complexity algorithm to compute the optimal solution for HAP energy provision and time allocation by using the dual and successive convex approximation (SCA) methods. Subsequently, we propose a coordinate descent (CD) method to update the previous computation offloading strategy and finally get the optimal solution of the model by several iterations of the loop

The rest of the paper is organized as follows. Section 2 introduces the system model and assumption. Section 3 formulates the maximize the minimum weighted system throughput problem for solar-powered MEC-enabled battery-free WSN. Section 4 presents the details of the multiply-iterated decoupling optimization method for the nonconvex problem mentioned above. Section 5 evaluates the simulation results, and Section 6 concludes the paper.

2. System Model and Assumption

We consider a solar-powered multinode MEC-enabled WSN system with perfect CSI as shown in Figure 2, where a solar-powered HAP integrated with a MEC server consistently harvests and stores solar energy with battery capacity $B_j^{\max}$, then employs WPT to charge a set $N \triangleq \{1, 2, \cdots, n\}$ of battery-free sensor nodes and compute offloading tasks. It is assumed that all channels are reciprocity and follow a quasistatic block fading model [29], in which the channel gain of a channel remains constant over a slot but varies between slots. Each node makes full use of recharged energy to perform environmental monitoring and task computing, which follows a binary offloading strategy, i.e., operating in either local computing or computation offloading at each slot. Local computing is where the sensor node performs the generated computing tasks by the on-chip microprocessor, which has low computing capability due to energy and size constraints. Computation offloading means that the sensor node offloads the entire task to the MEC server embedded in HAP with much more processing power, which provides cloud-like computation capability for WSN to realize the requirements of computationally intensive applications in precision agriculture. To achieve real-time state monitoring for smart agriculture, we need to guarantee that the network sensor nodes are in a full-time sensing state, which imposes greater requirements for better management of the HAP's energy provision and offloading decisions of the network. This is illustrated in Figure 2.

2.1. Time Scheduling Model. Considering the periodicity and day-night variability of solar harvesting, we propose a time division computing offloading scheduling (TDCOS) to improve the system computation capacity and solar energy utilisation of each time slot. To avoid interference, we assume that HAP and its member nodes run on different frequencies. Each node adopts a half-duplex time mode to communication with a HAP and uses time division multiple access (TDMA) to achieve computation offloading to avoid cochannel interference. Consider a finite time horizon T with a whole day as shown in Figure 3, which is divided into K slots with duration $\tau = T/K$. Let $T \triangleq \{1, \cdots, k, \cdots, K\}$ denote the set of the time slots k. Each time slot $k$is divided into the following two intervals: (1) energy broadcast time, where HAP charges all devices for a time τ_{bro} simultaneously; (2) computing offloading time, where each node chooses to operate at either local computing or computing offloading based on the system throughput within a time slot; then, each offload node takes turns uploading tasks in their allocated time slots τ_i. In this case, task offloading can occupy the rest of the time slot after energy broadcasting of HAP, as shown in the following equation.

$$\sum_{i=1}^{N} \tau_i + \tau_{bro} \leq \tau. \tag{1}$$

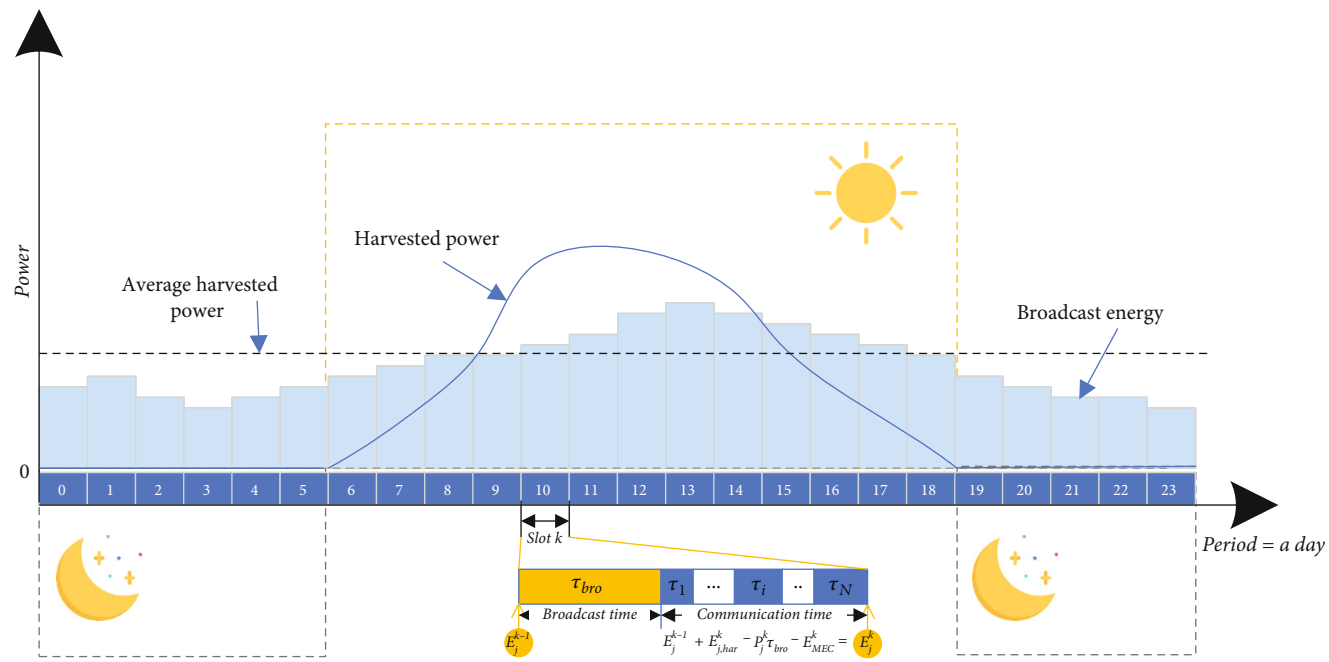

Figure 3: Time slot allocation during a solar-harvesting period. A period (a day) is divided equally with time interval 1 h, and each slot is composed of the broadcast time and task offloading time. The harvested energy of HAP is scheduled to reduce the impact from day-night variability of solar energy.

2.2. Energy Harvest Model. We consider a solar-powered HAP equipped with a solar panel of size W_p and has a rechargeable battery with capacity $B_j^{\max}$, as shown in Figure 2. We assume that solar energy arriving at HAP follows the m-state Markov chain model [30],where each state $m \in \{1, \cdots, M\}$ represents an EH profile expressed as a probability distribution with a given mean μ_m and variance ρ_m. Specifically, letting ψ_j^k represent the solar intensity on the HAP at time slot k, the solar-harvested energy of HAP at slot k can be expression by the following equation.

$$E_{j,har}^k = \eta_j \psi_j^k W_p \tau, \quad \forall k \in T, \tag{2}$$

where $\eta_j \in (0, 1)$ denotes the solar energy conversion rate of HAP. Within each time slot k of period T, the HAP converts the available energy E_j^{k-1} at the start of time slot k to charge all member nodes with wireless power transfer (WPT) and process tasks offloaded by some nodes on the MEC server, followed by storing the residual solar energy in the battery for the next slot. Let P_j^k denote the transmitting power of HAP, which characterizes the antenna performance of HAP and is satisfied with $0 \le P_j^k \le P_j^{\max}$. Here, E_{MEC}^k denotes the energy consumption of HAP processing the tasks offloaded by nodes. Consequently, the available energy of HAP at the end of slot k can be defined as the following equation.

$$E_j^k = E_j^{k-1} + E_{j,har}^k - P_j^k \tau_{bro} - E_{MEC}^k, \quad \forall k \in T, \tag{3}$$

where the broadcast energy $P_j^k \tau_{bro}$ of HAP is constrained by $P_j^k \tau_{bro} \le E_j^{k-1}$ as a result of the causal energy limitations. Also, to ensure proper monitoring at night within the constraints of day-night variability of solar-harvesting, we need to further constrain the lower limit of available energy for the HAP at any time slot as shown in the following equation.

$$P_j^k \tau_{bro} + E_{MEC}^k \le E_j^{k-1}, \quad \forall k \in T. \tag{4}$$

For avoiding energy overflow, E_j^k is limited by the capacity of the HAP battery $B_j^{\max}$, as shown in the following equation.

$$0 \le E_j^k \le B_j^{\max}, \quad \forall k \in T. \tag{5}$$

During the energy broadcasting phase, each member node harvests the wireless energy for task monitoring and offloading during the time slot. Let h_{ij}^k denote the channel gain from the HAP to node i based on the Rayleigh fading model [31]. Ignoring interference from noise, we can get the charged energy of each node at slot k, which can be expressed as the following equation.

$$E_i^k = P_j^k h_{ij}^k \eta_i \tau_{bro}, \quad \forall k \in T, i \in N, \tag{6}$$

where $\eta_i \in (0, 1)$ denotes the energy-harvesting efficiency, which can be considered as a fixed value since the transmitting power is usually small in WSNs. In order to establish a sustainable agricultural WSN, we need the network to

achieve energy neutral operation (ENO), which means the energy harvesting and consumption of HAP is balanced in one period. The mathematical expression is as in the following equation.

$$\left|E_j^N - E_j^0\right| \le \varepsilon, \tag{7}$$

where ε denotes the acceptable error range.

2.3. Computing Model. For each node, task computing can be performed locally or alternatively by offloading to the MEC server embedded in HAP. Here, we introduce the set of binary offloading variable $S^k \triangleq \{s_1^k, \cdots, s_i^k, \cdots, s_N^k\}$, where $s_i = 0$ denotes that the node i decides to offload its computation task to the MEC server. Otherwise, $s_i = 1$. Based on the given computing offloading strategy, the detailed operation of each node is illustrated as follows.

2.3.1. Local Computing. When node i makes the decision of local computing, it would perform the task computation independently of the others with the charged energy. Let δ_i indicate the number of CPU cycles required to complete a task with unit data size and f_i^{loc} denote the CPU frequency, which characterizes the computational power of the node and satisfies with $0 \le f_{i,loc}^k \le f_{\max}^{loc}$. It is assumed that $\Phi_{i,loc}^k$ is the total throughout on local computing at the slot k; the corresponding energy consumption and computation latency can be calculated as shown in the Equations (8) and (9), respectively.

$$E_{i,loc}^k = \kappa_{mob,i}\left(f_{i,loc}^k\right)^3 \delta_i \Phi_{i,loc}^k, \quad \forall k \in T, i \in N, \tag{8}$$

$$t_{i,loc}^k = \frac{\Phi_{i,loc}^k \delta_i}{f_{i,loc}^k}, \quad \forall k \in T, i \in N, \tag{9}$$

where $\kappa_{mob,i}$ denotes energy consumption parameters, which depend on the chip architecture [32]. Notice that local computing can last for the entire time slot τ, since the energy charging and local computing can be done simultaneously based on the circuit as shown in Figure 2. Accordingly, the total local computing throughput $\Phi_{i,loc}^k$ are constrained by computation latency and energy consumption in the Equations (10) and (11), respectively.

$$0 \le t_{i,loc}^k \le \tau, \quad \forall k \in T, i \in N, \tag{10}$$

$$0 \le E_{i,loc}^k \le E_i^k, \quad \forall k \in T, i \in N. \tag{11}$$

2.3.2. Computing Offloading. Apart from local computing, each node needs to take turns using up the charged energy for offloading the entire task to the MEC server embedded in HAP, and downloading the computation results after MEC server has completed the task calculation when offloading decision $s_i = 0$. According to the Shannon theory [33], the available offload computing rate of node i, denoted by $r_{i,off}^k$, can be calculated by the following equation.

$$r_{i,off}^k = W \log_2\left(1 + \frac{p_{i,off}^k h_{ij}^k}{N_0}\right), \quad \forall k \in T, i \in N, \tag{12}$$

where W denotes the communication bandwidth and N_0 denotes the receiver noise power. Let $p_{i,off}^k = E_i^k/\tau_i^k$ denote the offloading transmitting power of node i at time slot k. The total throughput $\Phi_{i,off}^k$ of each offload node in its allocated time τ_i can be calculated by the following equation.

$$\Phi_{i,off}^k = \tau_i^k r_{i,off}^k = W\tau_i^k \log_2\left(1 + \frac{p_{i,off}^k h_{ij}^k}{N_0}\right), \quad \forall k \in T, i \in N. \tag{13}$$

After receiving the raw data of all the member nodes, the HAP computes and sends back the output result back to the corresponding node. Given that the calculation results at MEC are smaller and the downlink transmission rate is higher, the downlink energy consumption and latency can be ignored [34]. Thus, the energy consumption of computation offloading at the MEC server, denoted byE_{MEC}^k, can be expressed as the following equation.

$$E_{MEC}^k = \kappa_{mob,j}\left(f_{MEC}\right)^3 \delta_j \Phi_{ij,off}^k, \quad \forall k \in T, i \in N, \tag{14}$$

where $\kappa_{mob,j}$ is the capacitance coefficient specified by the MEC server's CPU architecture and f_{MEC} is the CPU frequency of the HAP during each slot, which is fixed during the calculation cycle of the task by the DVFS technique [35].

3. Problem Formulation

In this subsection, we formulate a maximize the minimum weighted system computation problem for the solar-powered MEC-enabled battery-free WSN to determine the computation offloading strategy of each node in each time slot and the time trade-off between energy broadcast and transmission, which jointly optimize the multinode computation offloading strategy $\{S^k\}$, the amount of energy provision by solar-powered HAP $\{P_j^k, \tau_{bro}\}$, and local CPU frequency $\{f_i^{loc}\}$, as well as computing offloading time scheduling $\{\tau\}$. Here, we qualify the volume of network computation in terms of throughput. Accordingly, the weighted total throughput maximization problem is formulated as the following equation.

$$\mathbf{P0} \max_{\{P,\tau,s,f\}} \min_k \sum_{i=1}^N w_i\left[s_i \Phi_{i,loc}^k + (1 - s_i)\Phi_{i,off}^k\right], \tag{15}$$

Subject to

$$C1: 0 \le P_j^k \le P_j^{\max}, \quad \forall k \in T, \tag{16}$$

$$C2: 0 \le E_j^k \le B_j^{\max}, \quad \forall k \in T, \tag{17}$$

$$C3: P_j^k \tau_{bro}^k + E_{MEC}^k \le E_j^{k-1}, \quad \forall k \in T, \tag{18}$$

$$C4: \left|E_j^N - E_j^0\right| \le \varepsilon, \tag{19}$$

$$C5: \sum_{i=1}^{N} \tau_i^k + \tau_{bro}^k \le \tau, \quad \forall i \in N, k \in T, \tag{20}$$

$$C6: s_i^k \in \{0, 1\}, \quad \forall i \in N, k \in T, \tag{21}$$

$$C7: f_{\min} \le f_{i,loc}^k \le f_{\max}, \quad \forall i \in N, k \in T, \tag{22}$$

$$C8: 0 \le t_{i,loc}^k \le \tau, \quad \forall i \in N, \tag{23}$$

where $w_i \in [0, 1]$ is a weight factor that accounts for the priorities of different nodes and is specified by the application layer. $C1$ is the transmission power constraint which ensures that the transmission power of the HAP is nonnegative and bounded by the maximum transmission power $P_j^{\max}$ depending on the system architecture. Battery capacity constraint $C2$ ensures that the battery energy level of HAP is upper bounded by the battery capacity $B_j^{\max}$. Energy consumption constraint $C3$ specifies that the energy consumption for broadcasting and computation offloading does not exceed the available energy of HAP at the start of the time slot, which can effectively guarantee the energy requirements for night-time network monitoring. $C4$ is an energy neutral operation (ENO) constraint wherein the energy harvesting and consumption of HAP is balanced in one period. Time slot constraint $C5$ specifies that all nodes need to accomplish energy charging and computational offloading within one time slot. $C6$ indicates that the variables of offloading decision variables are 0-1 binary decision variables. The frequency constraint $C7$ denotes that the local CPU frequency should be limited within a range of $[f_{\min}, f_{\max}]$. $C8$ indicates that the local computing time of the node cannot exceed the duration of a time slot. Due to the combinatorial nature of the multinode computing offloading strategy and its strong coupling with resource scheduling, problem (**P0**) is hard to tackle.

4. Joint Optimization Method

In this section, we introduce a joint optimization between resource scheduling and computation offloading strategy to maximize the minimum weighted system throughput for solar-powered MEC-enabled battery-free WSN. In response to this mixed-integer nonlinear program (MINLP), we propose a multiply-iterated decoupling optimization method, where we first initialize a computation offloading strategy $S^k(0)$ to obtain a semiclosed-form solution for the optimal local CPU frequency $f_{i,loc}^{k*}$ and the optimal edge computation communication time allocation subject to a certain HAP energy provision. We then propose a low-complexity algorithm to compute the optimal solution Γ^{k*} for HAP energy provision and time allocation. Subsequently, we propose a coordinate descent (CD) method to update the previous computation offloading strategy and finally get the optimal solution of the model. Next, we propose a corresponding solution for each iteration.

4.1. Optimal Local Computing. In this subsection, we investigate the optimization of the local CPU computation frequency given the computation offload strategy. From problem (**P0**), it can be seen that independently optimizing the local CPU frequency f_i^{loc} does not affect the performance of other nodes when the $\Gamma^k = P_j^k \tau_{bro}^k$ is fixed. Combining Equations (8)–(11) and constraint $C7$, we can conclude $f_{i,loc}^k$ by the following equation.

$$f_{i,loc}^k \in \left[\left(\frac{E_i^k}{\kappa_{mob,i}\tau}\right)^{1/4}, f_{\max}\right], \quad \forall i \in N, k \in T. \tag{24}$$

Note that the function $\Phi_i^{loc}(f_i^{loc})$ is monotonically decreasing on the domain. Hence, we can obtain the optimal semiclosed solution for the local CPU frequency for each node, which is shown in the following equation.

$$f_{i,loc}^{k*} = \min\left[\left(\frac{E_i^k}{\kappa_{mob,i}\tau}\right)^{1/4}, f_{\min}\right], \quad \forall i \in N, k \in T. \tag{25}$$

To ensure that the network works properly, $E_{i,loc}^k \ge \kappa_{mob,i} f_{\min}^4 \tau$ needs to be satisfied. By substituting f_i^{loc*} into Equation (8), we can obtain the maximum local computing data volume by the following equation.

$$\Phi_{i,loc}^{k*} = \frac{E_i^k}{\kappa_{mob,i}\left(f_{i,loc}^k\right)^3 \delta_i} = \eta_1 \left(\Gamma^k h_{ij}^k\right)^{1/4}, \quad \forall i \in N, k \in T, \tag{26}$$

where $\eta_1 \triangleq (\eta\tau^3/\kappa_{mob,i}\delta_i^4)^{1/4}$ is a fixed parameter.

4.2. Joint Iterative Optimization of Broadcast Power and Transmission Time. In this subsection, we continue to study the optimal computation offloading resource scheduling with the assumption that S^k is known and Γ^k is fixed. Here, we first transform problem (**P0**) into problem (**P1**) by removing the variables $f_{i,loc}^{k*}$ and making formal transformations to the objective function, which can be formulated as the following equation.

$$\mathbf{P1} \max_{\{P,\tau,s\}} \min_k \sum_{i=1}^{N} w_i s_i \eta_1 \left(\Gamma^k h_{ij}^k\right)^{1/4} + \sum_{i=1}^{N} w_i \left(1 - s_i^k\right) W_p \tau_i^k \log_2\left(1 + \frac{\Gamma^k \left(h_{ij}^k\right)^2}{\tau_i^k N_0}\right),$$
$$\text{s.t.} \quad C1 \sim C6. \tag{27}$$

To solve the problem (**P1**) for nodes with offloading decision, we need to adopt the iteration optimization algorithm for offloading time allocation and energy broadcast scheduling. Let $\tau^k(l)$ and $\Gamma^k(l)$ denote the set of variables related to offloading time and energy charging allocation for nodes in the l-th iteration, respectively. Specifically, each iteration can be divided into two steps. Firstly, the optimal

Input: given a computation offloading strategy$S^k = \{s_1^k, s_2^k, \cdots, s_n^k\}$.
Output: the optimal $\{P_j^{k*}, \tau_{bro}^{k*}, \tau^{k*}\}$ to Problem (P2) given S^{k*}.
1Initialize $\Gamma^k(0)$ and $l = 1, \alpha(0), \beta(0)$
2Repeat
3Calculate local CPU frequency according to Equation (25);
4Repeat
5Calculate edge offloading time allocation according to Equation (32);
6Update $\lambda_1, \lambda_3, \lambda_4$ according to Equations (33)–(35);
7Until $\lambda_1, \lambda_3, \lambda_4$ converges;
8Let $\tau^{k*}(l) \longleftarrow \max_{i=1,\cdots,n} \Phi_i^k(l)$;
9Repeat
10Repeat
11Calculate energy provision according to Equation (43);
12Update μ_3, μ_4, μ_5, according to Equations (44)–(46);
13Until μ_3, μ_4, μ_5, converges;
14Repeat
15Calculate $\alpha_i^k(l_p)$, $\beta_i^k(l_p)$ according to Equations (39) and (40);
16Update number of iterations $l = l + 1$;
17Until Γ^k converges;
18Update outer loop iterations $l = l + 1$ and toleranceξ^l
19Until $\xi^l \le \sigma$
20Let $\Gamma^{k*}(l) \longleftarrow \max_{i=1,\cdots,n} \Phi_i^k(l)$
21Calculate the optimal energy broadcast power P_j^{k*} and corresponding time τ_{bro}^* according to Equations (48) and (49)
22Return the optimal solution by $f^*, \mathbf{P}, \tau$

Algorithm 1: Iterative algorithm with combination of SCA and Lagrangian dual theory for optimal resource scheduling.

offloading time allocation of iteration l is derived from the given value of $\Gamma^k(l-1)$. Then, with the fixed value of $\tau^k(l)$, the optimal energy broadcast scheduling $\Gamma^k(l)$ is obtained. The iterative algorithm is repeated until it converges to stopping criterion $\xi^l \le \sigma$; then, we can obtain a closed-form solution for optimal offloading time allocation and energy broadcast scheduling for problem (**P1**). The criterion is specified by the total throughput variation value ξ^l, which can be expressed by the following equation.

$$\xi^l = \left\| \begin{matrix} \sum_{i=1}^{N} w_i \left[s_i^k \Phi_{i,loc}^k(l) + \left(1 - s_i^k\right) \Phi_{i,off}^k(l) \right] \\ - \sum_{i=1}^{N} w_i \left[s_i^k \Phi_{i,loc}^k(l-1) + \left(1 - s_i^k\right) \Phi_{i,off}^k(l-1) \right] \end{matrix} \right\|, \quad \forall i \in N, k \in T. \tag{28}$$

As shown in Algorithm 1, we need to solve problem (P2) and problem (P3) to obtain an optimal solution for offloading time allocation and energy broadcast scheduling, respectively. The problem P2 is shown as the following equation.

$$\text{P2} \max_{\tau^k} \sum_{i \in \{s_i^k = 1\}} w_i W_p \tau_i^k \log_2 \left(1 + \frac{\Gamma^k(l-1)\left(h_{ij}^k\right)^2}{\tau_i^k N_0} \right), \text{s.t.} \quad C2 \sim C6. \tag{29}$$

Obviously, problem (P2) is a convex problem, so we can introduce Lagrangian multipliers $\boldsymbol{\lambda} = \{\lambda_i | \lambda_i \ge 0\}$ with constraints $C1 \sim C5$ to form a partial Lagrangian and achieve the optimal objective value $\{\tau^*\}$ by the strong duality, as is shown in the following equation.

$$\begin{aligned} L(\tau, \lambda) = & \sum_{i \in \{s_{i=1}\}} w_i W_p \tau_i^k \log_2 \left(1 + \frac{\Gamma^k(l-1)\left(h_{ij}^k\right)^2}{\tau_i^k N_0} \right) \\ & - \lambda_1 \left(E_j^k - B_j^{\max} \right) - \lambda_2 \left(\Gamma^k - E_j^{k-1} \right) \\ & - \lambda_3 \left(\sqrt{\left(E_j^N - E_j^0 \right)^2} - \varepsilon \right) \\ & - \lambda_4 \left(\sum_{i=1}^{N} \tau_i^k + \tau_{bro}^k - \tau \right). \end{aligned} \tag{30}$$

The corresponding dual function can be calculated by the following equation.

$$d(\lambda) = \underset{\tau}{\text{maximize}} \{ L(\tau, \lambda), \tau_i \ge 0 \}. \tag{31}$$

According to KKT condition $\partial L / \partial \tau_i^k(l) = 0$,we can obtain the optimal $\{\tau^*\}$ which satisfies the following equation.

$$\frac{\tau_i^{k*}(l)}{\Gamma^k(l-1)} = \frac{\eta_2\left(h_{ij}^k\right)^2}{(-W(x))^{-1}-1}, \quad \forall k \in T, i \in \{i|s_i = 0\}, \quad (32)$$

where $W(x)$ denotes the Lambert-W function and is satisfied with$x = -(1/\exp\,(1+\lambda_4/(w_i W_p + (\lambda_1+\lambda_3)\eta_3)))$.

Then, the solution of the dual problem $\min_{\boldsymbol{\lambda}} d(\lambda)$ can be determined by a subgradient method as shown in Equations (33) and (34).

$$\lambda_1^{l+1} = \left[\lambda_1^l + \sigma_{\lambda_1}\left(E_j^k - B_j^{\max}\right)\right]^+, \quad (33)$$

$$\lambda_3^{l+1} = \left[\lambda_3^l + \sigma_{\lambda_3}\left(\sqrt{\left(E_j^N - E_j^0\right)^2} - \varepsilon\right)\right]^+, \quad (34)$$

$$\lambda_4^{l+1} = \left[\lambda_4^l + \sigma_{\lambda_4}\left(\sum_{i=1}^N \tau_i + \tau_{bro} - \tau\right)\right]^+. \quad (35)$$

Here, $[x]^+ = \max\,(x, 0)$. With the fixed value τ_i^{k*} found above, Problem (P1) can be transformed into Problem (P3), which can be shown as Equation (35).

$$\textbf{P3} \max_{\{P\tau_0\}} \sum_{i=1}^N w_i s_i \eta_1 \left(\Gamma^k(l) h_{ij}^k\right)^{1/4} + \sum_{i=1}^N w_i(1-s_i) W \tau_i^{k*}(l) \log_2\left(1 + \frac{\Gamma^k(l)\left(h_{ij}^k\right)^2}{\tau_i^{k*}(l) N_0}\right),$$
$$\text{s.t.} \quad C2 \sim C6. \quad (36)$$

Obviously, Problem (P3) is a nonconvex problem because the second term of the objective function is a convex function. In order to solve this problem, we use the SCA approach [36] to propose the energy broadcast scheduling algorithm with logarithmic approximation. Instead of directly dealing with the highly nonconcave rate function, we apply the logarithmic approximation method to convert the throughput function into $\widehat{\Phi}_i^{off}(P_j^k \tau_{bro}(l_p))$, which is shown in Equation (36).

$$\widehat{\Phi}_{i,off}^k\left(\Gamma^k(l_p)\right) = W_p \tau_i^{k*} \alpha_i^k(l_p) + W_p \tau_i^{k*} \beta_i^k(l_p) \log_2\left(\frac{\Gamma^k(l_p)\left(h_{ij}^k\right)^2}{\tau_i^{k*} N_0}\right), \quad (37)$$

where $\alpha(l_p)$ and $\beta(l_p)$ are the parameter variable in the SCA process, which can be calculated as seen in Equations (37) and (38), respectively. l_p is the iteration number in the SCA process. $\widehat{\Phi}_{i,off}^k(\Gamma^k(l_p))$ denotes the low bound of the original throughput function $\widehat{\Phi}_{i,off}^k(\Gamma^k(l))$, which is satisfied with $\Phi_{i,off}^k(\Gamma^k(l)) \geq \widehat{\Phi}_{i,off}^k(\Gamma^k(l_p))$.

$$\alpha_i^k(l_p) = W_p \tau_i^{k*}(l) \log_2\left(1 + \frac{\Gamma^k(l_p-1)\left(h_{ij}^k\right)^2}{\tau_i^{k*}(l) N_0}\right) - W_p \tau_i^{k*} \beta(l_p) \log_2\left(\frac{\Gamma^k(l_p-1)\left(h_{ij}^k\right)^2}{\tau_i^{k*}(l) N_0}\right), \quad (38)$$

$$\beta_i^k(l_p) = \frac{\Gamma^k(l_p-1)\left(h_{ij}^k\right)^2 / \tau_i^{k*}(l) N_0}{1 + \Gamma^k(l_p-1)\left(h_{ij}^k\right)^2 / \tau_i^{k*}(l) N_0}. \quad (39)$$

Unfortunately, $\widehat{\Phi}_{i,off}^k(\Gamma^k(l_p))$ is still a nonconcave function owing to the existence of logarithmic function $\log_2(\Gamma^k(l_p)(h_{ij}^k)^2/\tau_i^{k*} N_0)$. Let $\widehat{\Gamma}^k = \log_2(\Gamma^k)$; then, the logarithmic function can be converted into a log-sum-exp function and the problem (P3) can be reformulated into a convex problem (P4), which is shown as Equation (39).

$$\textbf{P4} \max_{\{P\tau_0\}} \sum_{i=1}^N w_i s_i^k \eta_1 \left(e^{\Gamma^k(l_p)} h_{ij}^k\right)^{1/4} + \sum_{i=1}^N w_i\left(1 - s_i^k\right) W_p \tau_i^k(l) \times \left[\alpha(l_p) + \beta(l_p) \log_2\left(\frac{e^{\Gamma^k(l_p)}\left(h_{ij}^k\right)^2}{\tau_i^{k*}(l) N_0}\right)\right],$$
$$\text{s.t.} \quad C1, C4, C5, C6,$$
$$C2: 0 \leq E_j^k(l_p) \leq B_j^{\max},$$
$$C3: e^{\Gamma^k(l_p)} \leq E_j^{k-1}, \quad \forall k \in T, \quad (40)$$

where $\alpha(l_p) = \{\alpha_i^k(l_p)|i \in N\}$ and $\beta(l_p) = \{\beta_i^k(l_p)|i \in N\}$. Utilizing Lagrangian duality, we propose the SCA-based power allocation algorithm based on the logarithmic approximation method. The Lagrangian duality of the problem is defined as Equation (40).

$$\begin{aligned} L\left(\widehat{\Gamma}^k(l_p), \mu\right) = & \sum_{i=1}^N w_i s_i \eta_1 \left(e^{\widehat{\Gamma}^k(l_p)} h_{ij}^k\right)^{1/4} \\ & - \sum_{i=1}^N w_i(1-s_i) W \tau_i^k(l) \left[\alpha(l_p) + \beta(l_p) \log_2\left(\frac{e^{\widehat{\Gamma}^k(l_p)}\left(h_{ij}^k\right)^2}{\tau_i^{k*}(l) N_0}\right)\right] \\ & - \mu_1\left(P_j^k - P_j^{\max}\right) - \mu_2\left(E_j^k - B_j^{\max}\right) - \mu_3\left(e^{\widehat{\Gamma}^k(l_p)} - E_j^{k-1}\right) \\ & - \mu_4\left(\sqrt{\left(E_j^N - E_j^0\right)^2} - \varepsilon\right) - \mu_5\left(\sum_{i=1}^N \tau_i + \tau_{bro} - \tau\right). \end{aligned} \quad (41)$$

Input: initial computation offloading strategy $S^k(0)$.
Output: an approximate solution $\{P_j^{k*}, \tau_{bro}^*, f_{\text{local}}^*, \tau^*, S^*\}$.
Initialization: $l \longleftarrow 0$
Repeat
$l \longleftarrow l+1$
For each node i do
Calculate $R_i^k(l)$ in Equation (20) using Algorithm 1
End
Let $V^{k*}(l) \longleftarrow \max_{i=1,\cdots,n} R_i^k(l)$ and $i^{k*}(l) \longleftarrow \arg\max_{i=1,\cdots,n} R_i^k(l)$;
Update $S^k(l) \longleftarrow S_{i_l^*}^k(l-1)$ using Equation (51);
Until $V_l^* \le 0$:
Let $S^* = S^k(l)$ and calculate the optimal resource scheduling $\{P_j^{k*}, \tau_{bro}^*, f_{\text{local}}^*, \tau^*\}$
Return the optimal computation offloading strategy $\{P_j^{k*}, \tau_{bro}^*, f_{\text{local}}^*, \tau^*, S^*\}$ to P1

Algorithm 2: Coordinate descent algorithm for computation offloading strategy optimization.

The corresponding dual function can be shown as Equation (41).

$$D(\mu) = \underset{\left\{\widehat{\Gamma}^k(l_p)\right\}}{\text{maximize}} \left\{ L\left(\widehat{\Gamma}^k(l_p), \mu\right) \right\}. \tag{42}$$

According to KKT condition $\partial L / \partial \Gamma^k(l_p) = 0$, we can obtain the optimal $\{\Gamma^k(l_p)^*\}$ which satisfies Equation (42).

$$\Gamma^k(l_p)^* = \sqrt{\frac{(\mu_4 - \mu_3 - \mu_5)\left(h_{ij}^k\right)^4 w_i s_i^k \eta}{\left[w_i(1-s_i)W_p + (\mu_3 + \mu_5)\eta_3\right]\tau_i^{k*}(l)\beta(l_p)}}, \quad \forall i \in N, k \in T. \tag{43}$$

The solution of the dual problem $\min_{\mu} D(\mu)$ can be determined by a subgradient method as shown in Equations (42) and (43).

$$\mu_3^{l_p+1} = \left[\mu_3^{l_p} + \varepsilon_{\mu_3}\left(E_j^k - B_j^{\max}\right)\right]^+, \tag{44}$$

$$\mu_4^{l_p+1} = \left[\mu_4^{l_p} + \varepsilon_{\mu_4}\left(e^{\widehat{\Gamma}^k(l_p)} - E_j^{k-1}\right)\right]^+, \tag{45}$$

$$\mu_5^{l_p+1} = \left[\mu_5^{l_p} + \varepsilon_{\mu_5}\left(\sqrt{\left(E_j^N - E_j^0\right)^2} - \varepsilon\right)\right]^+. \tag{46}$$

By substituting energy broadcast scheduling $\Gamma^k(l)^* = \Gamma^k(l_p)^*$ and computation offloading time scheduling $\{\tau^{k*}\}$ into $C5$, we can get the optimal solution of broadcast power P_j^{k*} and time τ_{bro}^* by Equations (44) and (45), respectively.

$$\tau_{bro}^{k*} = \tau - \sum_{i=1}^{N} \tau_i^{k*}, \quad \forall i \in N, k \in T, \tag{47}$$

$$P_j^{k*} = \frac{\Gamma^{k*}}{\tau_{bro}^{k*}}, \quad \forall k \in T. \tag{48}$$

Algorithm 1 shows the pseudocode of iterative optimisation with combination of SCA and Lagrangian dual theory for optimal resource scheduling.

4.3. Coordinate Descent for Computing Mode Optimization. In this subsection, we introduce the coordinate descent (CD) method [37] to jointly optimize the N binary decision variable $\mathbf{S}^k = \{s_1^k, s_2^k, \cdots, s_n^k\}$, which can significantly lower the computational complexity and faster convergence by along the direction of only one variable s_i at a time; see the pseudocode of Algorithm 2 for details. First, we initialize a binary decision variable $\mathbf{S}^k(0)$ in slot k and denote $\mathbf{S}^k(l-1)$ as the computation offloading strategy at $(l-1)$th iteration, where the optimal system throughput $V^{S^k(l-1)}$ can be solved by Algorithm 1. In order to find the optimal decision in each iteration, we switch the decision variables for each node i in turn and calculate its system throughput gain $R_i^k(l)$ in the (l)th iteration, which can be calculated by Equation (50).

$$\mathrm{R}_i^k(l) = V^k\left(\mathbf{S}_i^k(l-1)\right) - V^k\left(\mathbf{S}^k(l-1)\right), \tag{49}$$

where $\mathbf{S}_i^k(l-1)$ denotes the switched computation offloading strategy with node i and can be calculated by Equation (51).

$$\mathbf{S}_i^k(l-1) = \left[S_1^k(l-1), S_2^k(l-1), \cdots, S_i^k(l-1) \oplus 1, \cdots, S_n^k(l-1)\right], \tag{50}$$

where $\oplus$ denotes the modulo-2 summation operator. Obviously, $R_i^k(l) > 0$ denotes a better decision for node i in $(l-1)$th iterations, and we need $\mathbf{S}^k(l) = \mathbf{S}_i^k(l-1)$ and vice versa. Therefore, the optimal decision under this iteration is obtained by comparing the selection of the best

$i_l^* = \arg \max_{i=1,\cdots,n} R_i^k(l)$. Meanwhile, R^k increases monotonically with the number of iterations and the optimal value is bounded, so the method can converge to the optimal value.

Next, we consider the complexity of the proposed algorithm. Here, the complexity of the proposed algorithm is calculated based on the two stages. During the computation offloading strategy definition phase, the number of iterative updates for each strategy increases linearly with n, and the complexity is $O(n)$, where n is the number of nodes. In iteration optimization phases of $\Gamma^k(l)$ and τ^k, the number of messages exchanged in each iteration which is equal to the total number of nodes with computational complexity is $O(n^2)$. Therefore, the overall complexity of the proposed algorithm is $O(n^3)$.

5. Results and Discussion

In this section, we evaluate the proposed algorithm for solar-powered agriculture WSN in terms of the system average throughput, energy efficiency, and relevant parameters against the existing *All Local Computing*, *All Offloading*, *Algorithm* [16], and *Optimal*. *All Local Computing* means the sensor uses the charged energy to process their tasks locally. *All Offloading* denotes that the sensor offloads all computing tasks to the MEC for processing. *Algorithm* [16] is presented to address maximizing the computation rate of all users for WPT-powered WSN by jointly optimizing the individual computing mode selection and the system transmission time allocation where it is assumed that HAP is well powered and the transmitting power is fixed. *Optimal* refers to finding the optimal mode and allocating energy employing exhaustive enumeration. All except *Algorithm* [16] use the same energy provision constraint as the *proposed*. The following firstly illustrates the simulation environment and then presents the simulation results.

5.1. Simulation Setup. We consider a coverage area of 100 m × 100 m with total node number [5, 10, 15, 21, 25] for solar-powered multinode MEC-enabled agriculture WSN, which includes a HAP-integrated MEC and several sensor nodes randomly distributed. HAP are equipped with a 1 m × 1 m solar panel, which has an energy-harvesting efficiency of 20%. Solar energy arrivals are calculated in a similar way to [30], which follows the hidden Markov model with four states, including *excellent*, *good*, *fair*, and *poor*. The distribution of each state has a mean of 94.6, 76.0, 45.6, and 17.9, and variance of 0.31, 1.55, 1.48, and 0.71, respectively. The HAP has a battery with a capacity of 10 kJ, and the maximum transmitting power is set to 5 W. All nodes recharge themselves with energy efficiency 0.51, and the parameter of computing efficiency is set 109. The local CPU frequency of each node is set ranging from 0.2 GHz to 2 GHz, and the CPU frequency of each MEC server is set as 4 GHz. The channel gain from the sensor node to HAP follows the Rayleigh fading channel model, where the path loss factor is set varying from 2.0 Hz to 3.5 Hz. The system bandwidth is set to 200 kHz, and the noise spectral density is set to -95 dB/Hz. The numerical experiments are performed by the Monte Carlo method as follows. All nodes are randomly distributed in the sensing area for 100 times, and the corresponding maximum throughput is calculated, which are probabilistically distributed by interval, and the number with the highest throughput value from the highest probability interval is selected as the optimal throughput of this network, and the corresponding offloading calculation decision and resource scheduling scheme is the best. All the simulations are performed on a desktop computer with an Intel Core i7-8700U 3.2 GHz CPU and 24 GB memory.

5.2. Performance for Network. To achieve sustainable monitoring for solar-powered agriculture WSNs, we propose a joint optimization method for resource scheduling and computation offloading strategy to maximize the minimum system throughput of each time slot during one period under the solar energy periodicity and volatility constraints. Figure 4 shows in detail the variation of system throughput over time and the system period energy efficiency under two different algorithms. Here, the period energy efficiency is defined as the ratio of network throughput to network energy consumption during one period, where the energy consumption mainly comes from the energy broadcast and the energy consumption of the MEC in HAP and can be measured as the solar-harvested of HAP, which can be expressed as Equation (50).

$$EE = \frac{\sum_{k=1}^{T}\sum_{i=1}^{N} w_i \left[s_i^k \Phi_{i,loc}^k + \left(1 - s_i^k\right) \Phi_{i,off}^k \right]}{\sum_{k=1}^{T} E_{j,har}^k}, \quad \forall i \in N, k \in T. \tag{51}$$

Figure 4 illustrates the variation of the system throughput over time under different weather conditions. It is obvious to observe that the system throughput of *Algorithm* [16] fluctuates significantly at different time slots within one period compared to the proposed, which can reach the maximum during the day but zero at night. This is because *Algorithm* [16] is designed to maximize the system computation rate with the assumption that the HAP is always energetic and that the transmit power is constant. This is clearly not applicable to highly volatile solar energy. Conversely, the proposed has a balanced throughput across time slots by maximizing the minimum one slot throughput to balance the energy broadcast by the HAP across time slots, which can achieve a rational energy allocation and storage during the day to ensure normal monitoring at night. Also, it is evident from Figure 4 that the proposed can achieve a higher system period energy efficiency than the *Algorithm* [16] by managing the broadcast power of harvested solar energy. Compared to rainy days, the system has higher throughput and energy efficiency on sunny days because it has more solar energy and its value varies less over time. More notably, the algorithm proposed in this paper has better stability in terms of throughput either over diurnal or climate change processes, which shows that it is more adaptable to real-time energy changes in the network.

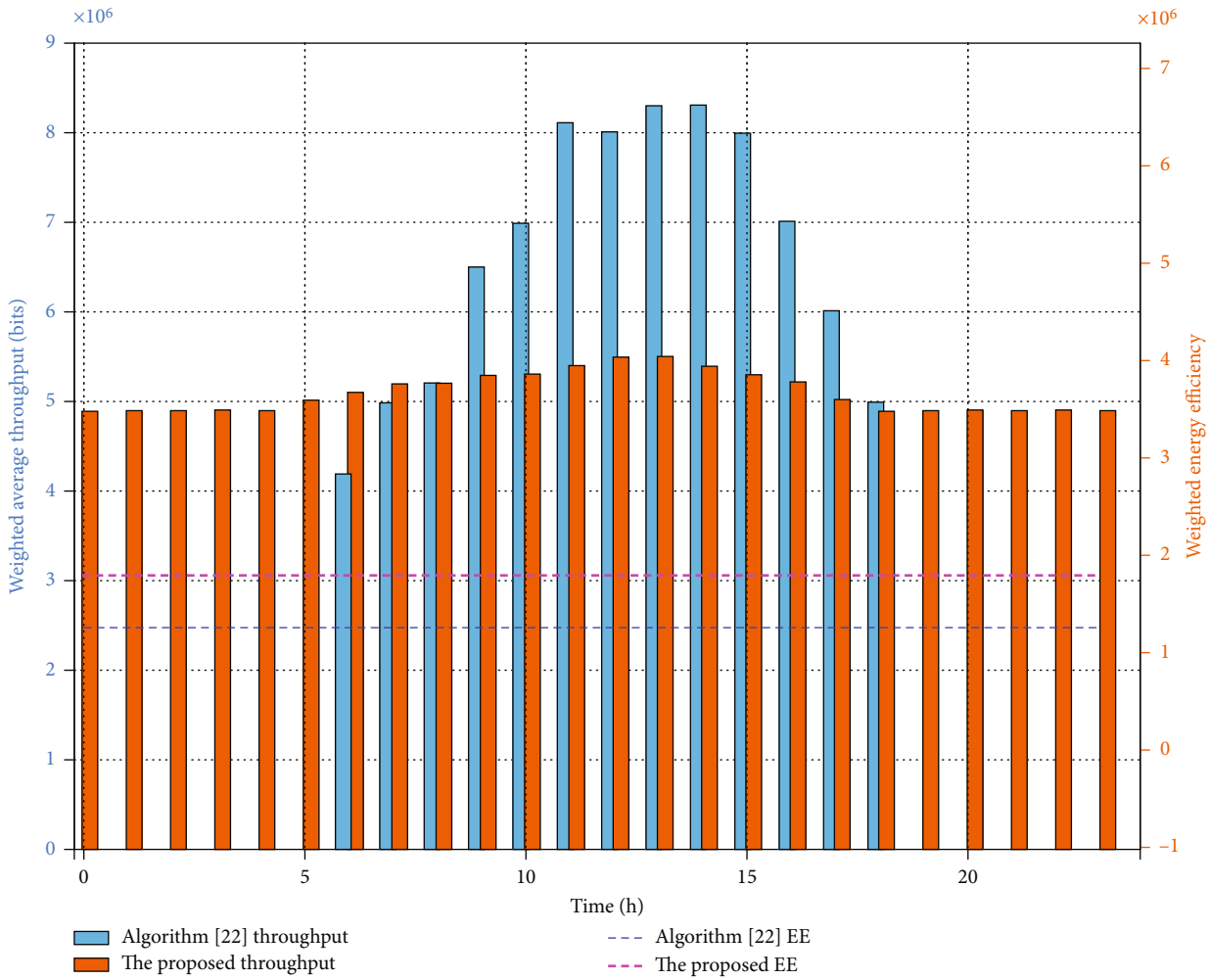

(a)

Figure 4: Continued.

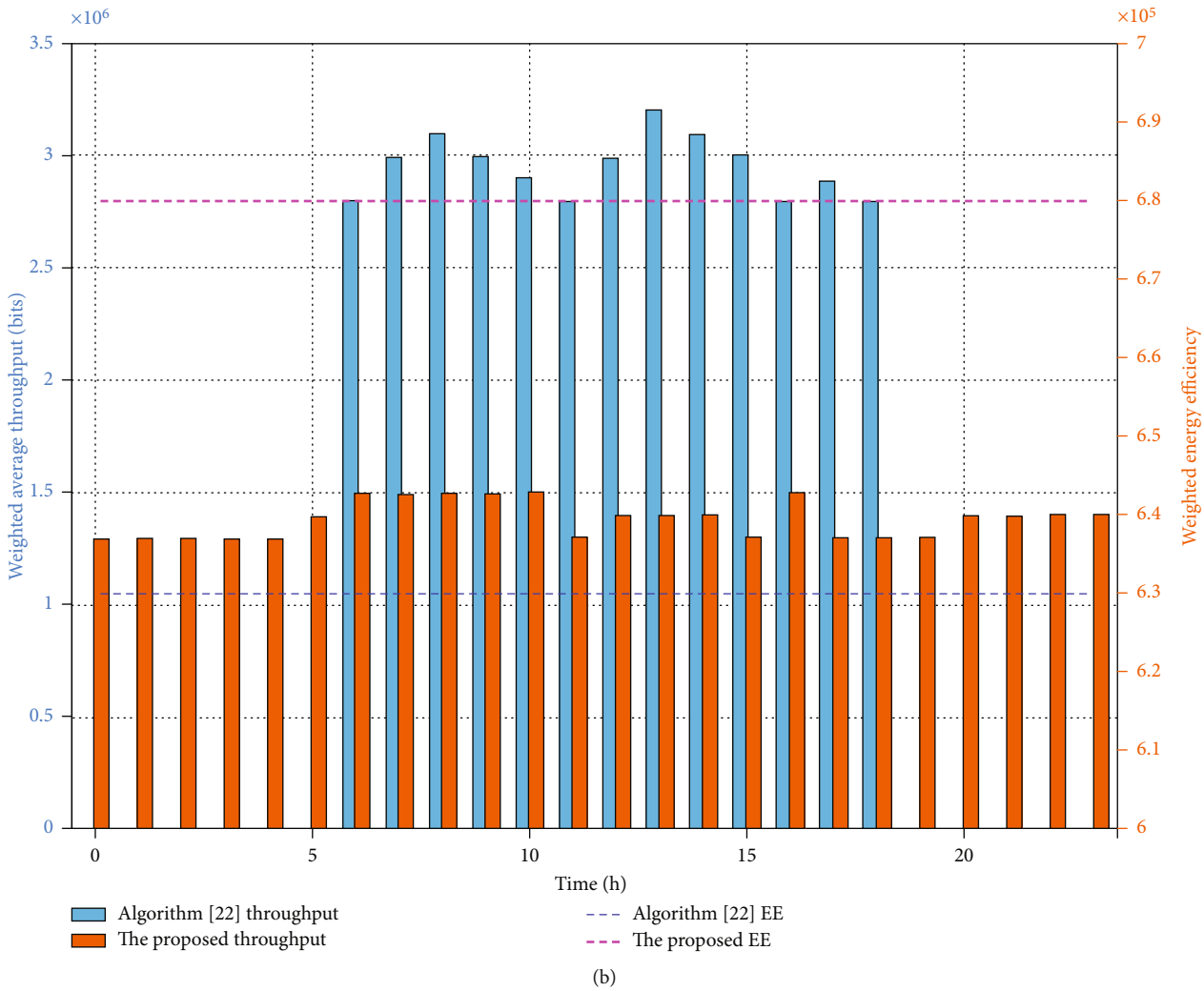

Figure 4: Plot of the weighted sum throughput of each slot and weighted energy efficiency versus the time with respect to (a) sunny and (b) rainy.

Figure 5 shows the effect of different algorithms on the system average throughput during one period versus total node number for path loss factor $\alpha = 2.4$. It is obvious that the *proposed* can achieve near-optimal performance and is superior to the other algorithms as the number of nodes increases. As more nodes are added gradually, the system average throughput of all the above algorithms increases, especially in the offload mode. But when the number of nodes is particularly large, the throughput in the offload mode drops abruptly. The reason for this is that when the number of nodes exceeds a threshold, wireless channel interference will increase, and this will lead to a reduction in offload link capacity. However, the local computing mode grows smoothly with the number of nodes due to the high independence of each node.

Figures 6(a) and 6(b) compare the effects of the path loss factor α and the average distance $\bar{d}$ between HAP and nodes on the system average throughput under different algorithms, respectively, where both α and $\bar{d}$ are important factors that affect the channel state. It can be seen from Figure 6(a) that, for a given $\bar{d}$, the average throughput of the above algorithms all suffer varying degrees of decline as the channel state deteriorates with α increasing from 2 to 3.5. *All Offloading* is close to optimal performance when α is small and drops significantly as α increases, which is because task offloading suffers from both the energy broadcast downlink state and the data transmission uplink state. In contrast, local computation has a more moderate degradation due to its dependence on the downlink state only. Note that the *Proposed* is perfectly aligned with the optimal algorithm because it jointly optimizes energy scheduling and offloading strategy, which drives the network to choose more local computing to reduce losses as the channel state progressively deteriorates. In Figure 6(b), we compare the average throughput variation of systems with different algorithms when the average distance $\bar{d}$ of HAP-to-nodes varies from 10 m to 50 m when $\alpha = 2.4$. We observe that the throughput of the above methods decreases as the average distance increases, because the distance between HAP and nodes affects the channel gain h_{ij}, which affects the

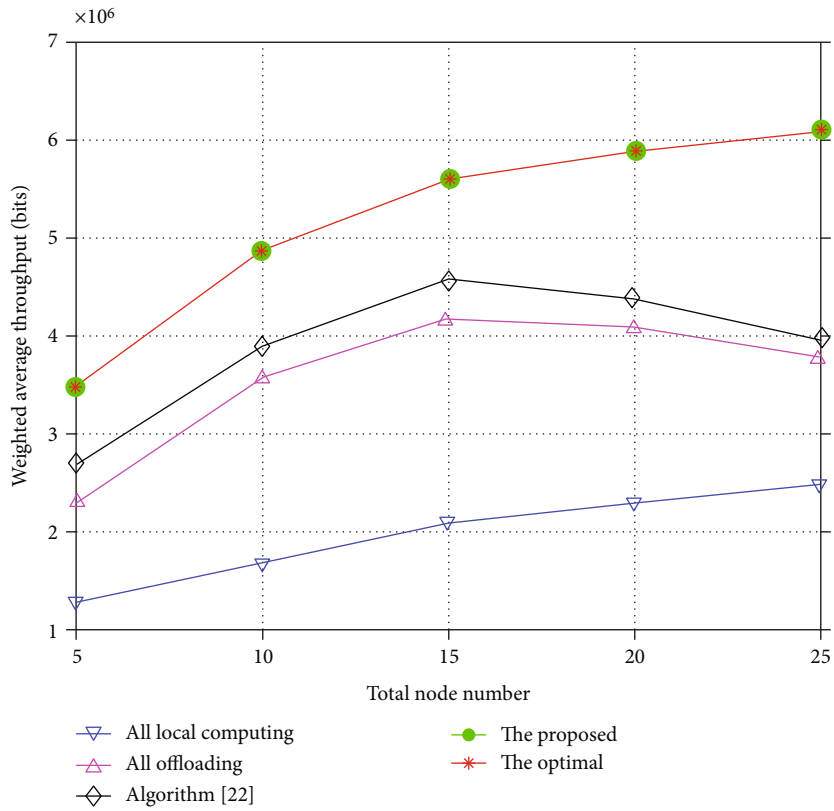

Figure 5: Plot of weighted average throughput versus total node number.

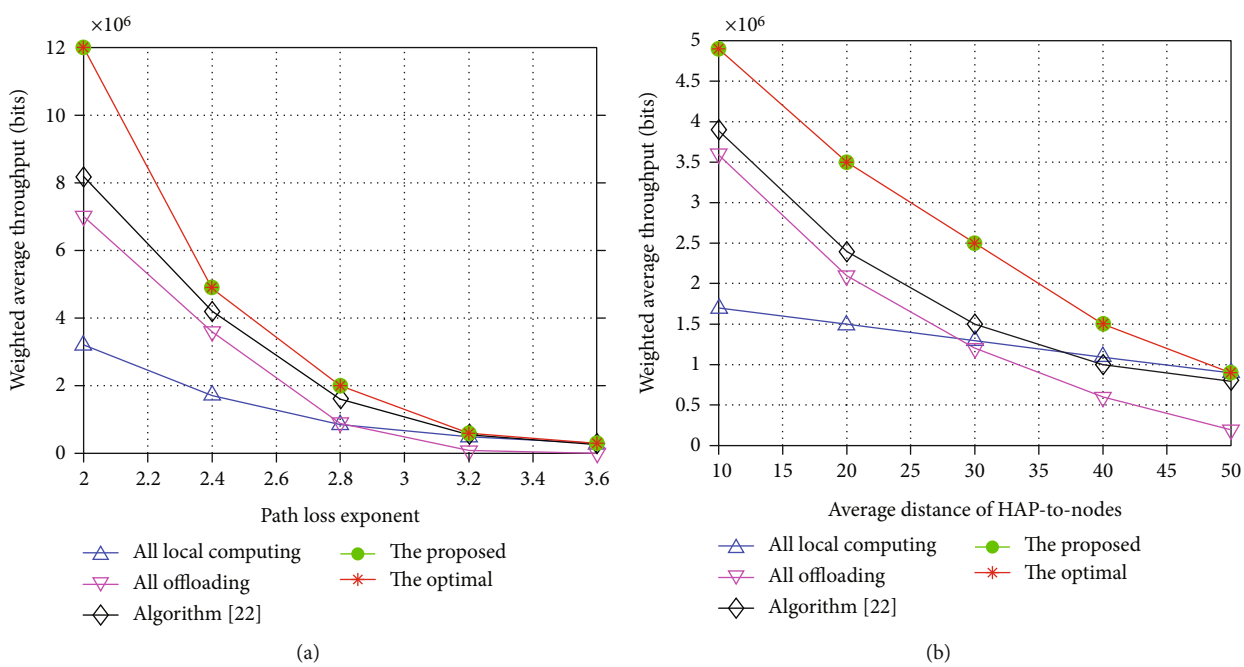

Figure 6: Plot of weighted average throughput with respect to (a) path loss exponent α when $\bar{d} = 20$ and (b) average distance $\bar{d}$ of HAP-to-nodes when $\alpha = 2.4$.

harvested energy E_i of node i and subsequently affects local throughput $\Phi_{i,loc}$ and computation offloading throughput $\Phi_{i,off}$, as in α. Comparing Figures 6(a) and 6(b), we can observe that α and $\bar{d}$ have a similar effect on system throughput, as both α and $\bar{d}$ influence network throughput by regulating the channel state.

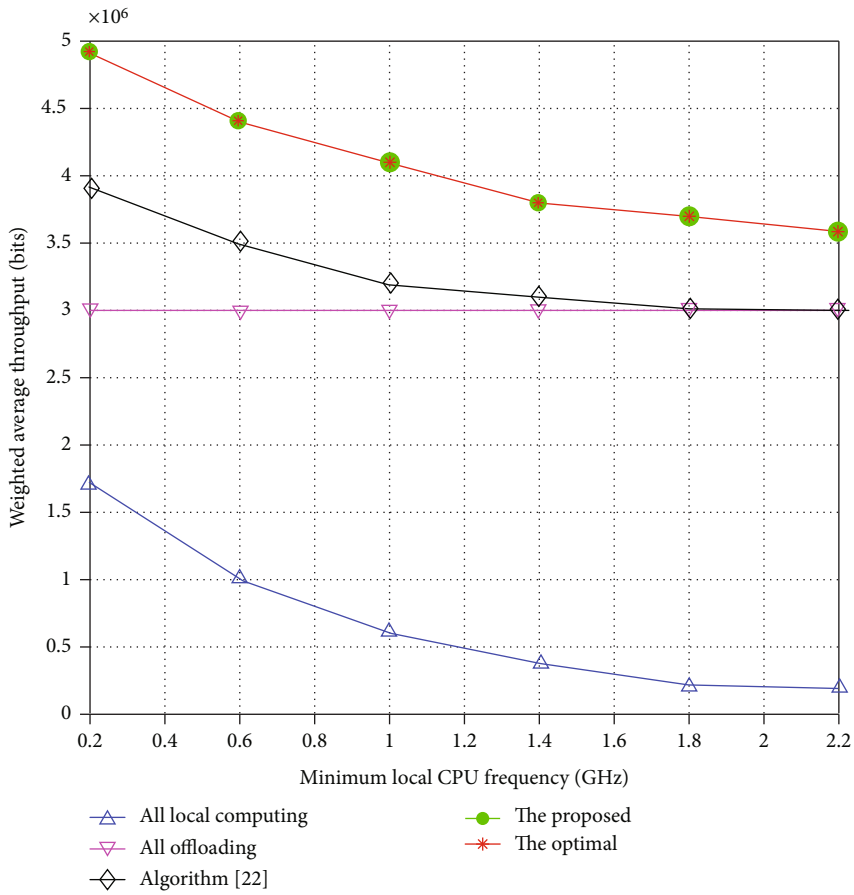

Figure 7: Plot of weighted average throughput versus minimum local CPU frequency.

Finally, we investigated the effect of the local minimum local CPU frequency on the network average throughput under different algorithms in Figure 7, from which we can observe that as the minimum local CPU frequency gradually increases, the average throughput under *all local computing* is affected the most with a significant downward trend, with some impact under the *proposed*, but almost no impact under *all offloading*. This is because the increase of the minimum local CPU frequency can drive more nodes to choose offloading. It is interesting to note that when the minimum local CPU frequency gradually increases to a certain value, the throughput under proposed tends to under offloading. This is because all nodes of the network would choose the computation offloading when the minimum local CPU frequency is greater than a certain threshold.

6. Conclusions

This paper studied a real-time environmental monitoring system for solar-powered MEC-enabled smart agriculture. To alleviate the cyclical and day-night fluctuation influence of solar energy on network performance, we formulated a joint resource scheduling and computation offloading strategy optimization problem, which maximizes the minimum weighted computation capacity across the time slots by jointly optimizing the computation offloading strategy, energy provision of the solar-powered hybrid access point (HAP), local CPU frequency as well as time scheduling. Based on the coordinate descent method and successive convex approximation theory, we developed a multiply-iterated decoupling optimization algorithm to solve the strong coupling between binary offloading strategy, broadcast power, and time allocation. The simulation results demonstrate that the proposed algorithm outperforms in terms of energy efficiency and computational volume time slot balance and can better adapt to solar energy variations to meet the real-time status monitoring requirements of the smart agriculture IoT.

In order to further improve green energy utilization, future research can be extended as follows. First, the assumption of the solar harvesting rate in this paper is linear. In practice, it varies nonlinearly with the transmitting power, so it will be more relevant to examine the optimal offloading decision under the nonlinear harvesting conditions. Next, HAP broadcast power can be extended by using MIMO technology to reduce interference and improve energy utilization. In addition, NOMA-based protocols can be used instead of TDMA-based multinode task offloading to improve the network's spectral efficiency. Finally, the long-term optimization model of network energy can be constructed by considering the time-varying nature of

network energy state information, channel state information, and task state information.

Data Availability

The data are available from the corresponding author upon request.

Conflicts of Interest

The authors declare that they have no conflicts of interest.

Acknowledgments

This work was partially supported by the National Natural Science Foundation of China (NSFC) under Grant 62071179.

References

[1] O. Friha, M. A. Ferrag, L. Shu, L. Maglaras, and X. Wang, "Internet of things for the future of smart agriculture: a comprehensive survey of emerging technologies," *IEEE/CAA Journal of Automatica Sinica*, vol. 8, no. 4, pp. 718–752, 2021.

[2] D. Popescu, F. Stoican, G. Stamatescu, L. Ichim, and C. Dragana, "Advanced UAV-WSN system for intelligent monitoring in precision agriculture," *Sensors*, vol. 20, no. 3, p. 817, 2020.

[3] M. Ayaz, M. Ammad-Uddin, Z. Sharif, A. Mansour, and E. H. M. Aggoune, "Internet-of-Things (IoT)-based smart agriculture: toward making the fields talk," *IEEE Access*, vol. 7, pp. 129551–129583, 2019.

[4] A. Boukerche, Q. Wu, and P. Sun, "Efficient green protocols for sustainable wireless sensor networks," *IEEE Transactions on Sustainable Computing*, vol. 5, no. 1, pp. 61–80, 2020.

[5] C. Iwendi, P. K. R. Maddikunta, T. R. Gadekallu, K. Lakshmanna, A. K. Bashir, and M. J. Piran, "A metaheuristic optimization approach for energy efficiency in the IoT networks," *Software: Practice and Experience*, vol. 51, no. 12, pp. 2558–2571, 2021.

[6] E. A. Khalil and S. Ozdemir, "Reliable and energy efficient topology control in probabilistic wireless sensor networks via multi-objective optimization," *The Journal of Supercomputing*, vol. 73, no. 6, pp. 2632–2656, 2017.

[7] R. Wan, N. Xiong, and N. T. Loc, "An energy-efficient sleep scheduling mechanism with similarity measure for wireless sensor networks," *Human-centric Computing and Information Sciences*, vol. 8, no. 1, pp. 1–22, 2018.

[8] T. D. Nguyen, J. Y. Khan, and D. T. Ngo, "A distributed energy-harvesting-aware routing algorithm for heterogeneous IoT networks," *IEEE Transactions on Green Communications and Networking*, vol. 2, no. 4, pp. 1115–1127, 2018.

[9] C. Buratti and R. Verdone, "Joint scheduling and routing with power control for centralized wireless sensor networks," *Wireless Networks*, vol. 24, no. 5, pp. 1699–1714, 2018.

[10] X. Gu, L. Grauwin, D. Dousset, S. Hemour, and K. Wu, "Dynamic ambient RF energy density measurements of Montreal for battery-free IoT sensor network planning," *IEEE Internet of Things Journal*, vol. 8, no. 17, pp. 13209–13221, 2021.

[11] A. Riaz, M. R. Sarker, M. H. M. Saad, and R. Mohamed, "Review on comparison of different energy storage technologies used in micro-energy harvesting, WSNs, low-cost microelectronic devices: challenges and recommendations," *Sensors*, vol. 21, no. 15, p. 5041, 2021.

[12] H. Sharma, A. Haque, and Z. A. Jaffery, "Solar energy harvesting wireless sensor network nodes: a survey," *Journal of Renewable and Sustainable Energy*, vol. 10, no. 2, article 023704, 2018.

[13] P. Corcoran and S. K. Datta, "Mobile-edge computing and the internet of things for consumers: extending cloud computing and services to the edge of the network," *IEEE Consumer Electronics Magazine*, vol. 5, no. 4, pp. 73-74, 2016.

[14] B. Ali, M. A. Gregory, and S. Li, "Multi-access edge computing architecture, data security and privacy: a review," *IEEE Access*, vol. 9, pp. 18706–18721, 2021.

[15] C. Xu, G. Zheng, and X. Zhao, "Energy-minimization task offloading and resource allocation for mobile edge computing in NOMA heterogeneous networks," *IEEE Transactions on Vehicular Technology*, vol. 69, no. 12, pp. 16001–16016, 2020.

[16] S. Bi and Y. J. Zhang, "Computation rate maximization for wireless powered mobile-edge computing with binary computation offloading," *IEEE Transactions on Wireless Communications*, vol. 17, no. 6, pp. 4177–4190, 2018.

[17] S. Mao, S. Leng, K. Yang, X. Huang, and Q. Zhao, "Fair energy-efficient scheduling in wireless powered full-duplex mobile-edge computing systems," in *GLOBECOM 2017-2017 IEEE Global Communications Conference*, Singapore, 2017.

[18] F. Wang, J. Xu, X. Wang, and S. Cui, "Joint offloading and computing optimization in wireless powered mobile-edge computing systems," *IEEE Transactions on Wireless Communications*, vol. 17, no. 3, pp. 1784–1797, 2018.

[19] L. Shi, Y. Ye, X. Chu, and G. Lu, "Computation energy efficiency maximization for a NOMA-based WPT-MEC network," *IEEE Internet of Things Journal*, vol. 8, no. 13, pp. 10731–10744, 2021.

[20] F. Wang, X. Jie, and S. Cui, "Optimal energy allocation and task offloading policy for wireless powered mobile edge computing systems," *IEEE Transactions on Wireless Communications*, vol. 19, no. 4, pp. 2443–2459, 2020.

[21] F. Zhou and H. Rose Qingyang, "Computation efficiency maximization in wireless-powered mobile edge computing networks," *IEEE Transactions on Wireless Communications*, vol. 19, no. 5, pp. 3170–3184, 2020.

[22] S. Mao, S. Leng, S. Maharjan, and Y. Zhang, "Energy efficiency and delay tradeoff for wireless powered mobile-edge computing systems with multi-access schemes," *IEEE Transactions on Wireless Communications*, vol. 19, no. 3, pp. 1855–1867, 2019.

[23] J. H. Anajemba, T. Yue, C. Iwendi, M. Alenezi, and M. Mittal, "Optimal cooperative offloading scheme for energy efficient multi-access edge computation," *Access*, vol. 8, pp. 53931–53941, 2020.

[24] Y. Mao, C. You, J. Zhang, K. Huang, and K. B. Letaief, "Mobile edge computing: Survey and research outlook," 2017, https://arxiv.org/abs/1701.01090v3.

[25] B. Li, Z. Fei, J. Shen, X. Jiang, and X. Zhong, "Dynamic offloading for energy harvesting mobile edge computing: architecture, case studies, and future directions," *Access*, vol. 7, pp. 79877–79886, 2019.

[26] F. Wang, H. Xing, and X. Jie, "Real-time resource allocation for wireless powered multiuser mobile edge computing with

energy and task causality," *IEEE Transactions on Communications*, vol. 68, no. 11, pp. 7140–7155, 2020.

[27] F. Zhao, Y. Chen, Y. Zhang, Z. Liu, and X. Chen, "Dynamic offloading and resource scheduling for mobile-edge computing with energy harvesting devices," *IEEE Transactions on Network and Service Management*, vol. 18, no. 2, pp. 2154–2165, 2021.

[28] Q. Tang, R. Xie, F. R. Yu, T. Huang, and Y. Liu, "Decentralized computation offloading in IoT fog computing system with energy harvesting: a dec-POMDP approach," *IEEE Internet of Things Journal*, vol. 7, no. 6, pp. 4898–4911, 2020.

[29] W. Yang, G. Durisi, T. Koch, and Y. Polyanskiy, "Quasi-static multiple-antenna fading channels at finite blocklength," *IEEE Transactions on Information Theory*, vol. 60, no. 7, pp. 4232–4265, 2014.

[30] M.-L. Ku, Y. Chen, and K. J. R. Liu, "Data-driven stochastic models and policies for energy harvesting sensor communications," *IEEE Journal on Selected Areas in Communications*, vol. 33, no. 8, pp. 1505–1520, 2015.

[31] B. Sklar, "Rayleigh fading channels in mobile digital communication systems.I. Characterization," *IEEE Communications magazine*, vol. 35, no. 7, pp. 90–100, 1997.

[32] W. Zhang, Y. Wen, K. Guan, D. Kilper, H. Luo, and D. O. Wu, "Energy-optimal mobile cloud computing under stochastic wireless channel," *IEEE Transactions on Wireless Communications*, vol. 12, no. 9, pp. 4569–4581, 2013.

[33] C. E. Shannon, "A mathematical theory of communication," *ACM SIGMOBILE mobile computing and communications review*, vol. 5, no. 1, pp. 3–55, 2001.

[34] X. Chen, L. Jiao, W. Li, and X. Fu, "Efficient multi-user computation offloading for mobile-edge cloud computing," *IEEE/ACM transactions on networking*, vol. 24, no. 5, pp. 2795–2808, 2016.

[35] C. Jiang, T. Fan, H. Gao et al., "Energy aware edge computing: a survey," *Computer Communications*, vol. 151, pp. 556–580, 2020.

[36] B. R. Marks and G. P. Wright, "Technical note—a general inner approximation algorithm for nonconvex mathematical programs," *Operations Research*, vol. 26, no. 4, pp. 681–683, 1978.

[37] P. Breheny and J. Huang, "Coordinate descent algorithms for nonconvex penalized regression, with applications to biological feature selection," *The annals of applied statistics*, vol. 5, no. 1, pp. 232–253, 2011.

Hindawi
Journal of Sensors
Volume 2022, Article ID 1628537, 21 pages
https://doi.org/10.1155/2022/1628537

Review Article

WSN Protocols and Security Challenges for Environmental Monitoring Applications: A Survey

Kofi Sarpong Adu-Manu,[1] Felicia Engmann,[2] Godwin Sarfo-Kantanka,[1] Godwill Enchill Baiden,[1] and Bernice Akusika Dulemordzi[1]

[1]*Department of Computer Science, University of Ghana, Legon, Accra, Ghana*
[2]*School of Technology, Ghana Institute of Management and Public Administration, Accra, Ghana*

Correspondence should be addressed to Kofi Sarpong Adu-Manu; ksadu-manu@ug.edu.gh

Received 25 March 2022; Revised 26 June 2022; Accepted 20 July 2022; Published 21 August 2022

Academic Editor: Zhenxing Zhang

In recent years, communication technology has improved exponentially, partly owing to the locations and nature of the deployment of sensor nodes. Wireless sensor networks (WSNs) comprise these sensor nodes and can provide real-time physical and environmental measurements. The sensor nodes have limited power, which reduces their lifespan, especially when placed in human-inaccessible locations. This paper reviews energy-efficient protocols for environmental monitoring applications and energy harvesting-wireless sensor networks. The dynamic deployment and communication challenges associated with environmental monitoring applications (EMAs) make this paper take into account the WSN protocol stack, focusing on the physical layer, network layer (routing), and medium access control (MAC). The paper will delve deeper into the security challenges of deploying sensor nodes for environmental monitoring applications (EMAs). The paper further describes scientific approaches that churn out innovative and engineering applications that must be followed to improve environmental monitoring applications.

1. Introduction

Environmental monitoring is aimed at identifying the status of a changing environment using data collection tools. Data collection tools employed for determining the status of the changing environment rely on data acquisition systems (DAS). DAS uses measurement devices that are designed to allow for gathering representative samples. The samples depend on the device's intrusiveness, sampling accuracy, and sample storage [1–3]. These measurement devices have varying degrees of impact depending on the application and the data gathering method. For example, the sensitivity of the measured physical value to external influences may vary depending on the type of application. The traditional way of collecting the status of the changing environment has proven ineffective, having data reliability, delays, and security challenges [4]. Hence, in recent times, the introduction of technological devices such as sensor nodes capable of forming a wireless sensor network (WSN) is used to sense the changes in the environment and wirelessly communicate the sensed data to a base station for processing.

WSNs are distributed systems comprised of several nodes and base stations (BS) to monitor physical environmental conditions [5]. Each sensor node contains a wireless radio transceiver to communicate with other nodes and the BS. Sensor nodes communicate via insecure radio channels prone to interference and fading [6].

WSNs are used in several applications and deployed on land (terrestrial), underground, and underwater. Recently, they have been used in multimedia applications and mobile applications such as animal tracking, air quality monitoring, forest fire warning, and flood detection, among the terrestrial applications of WSNs. WSNs monitor soil conditions underground, particularly for agricultural and mining purposes. Underwater applications include freshwater quality, climate change, ocean monitoring for aquatic life, and

assessing coral reef alterations underwater—WSNs track events such as video, audio, and imaging in multimedia applications. They are utilised in real-time monitoring of hazardous compounds, target tracking, and rescue and search applications in mobile applications [7, 8]. Despite the capabilities presented by WSNs, they are also associated with challenges in various application domains. Table 1 summarises some of these challenges and their associated recommended solutions when WSNs are utilised in the different application domains.

Researchers have studied the design of protocols that can address these challenges in a variety of application domains, taking into account the challenges of the application [9–13]. The protocols are intended to operate at the sensor network protocol stack (physical, link, network, and transport layers). Protocol design is aimed at helping with data collection, aggregation, processing, and communication to maximize network lifetime and uptime [14]. Protocols govern the operation of sensor nodes in a sensor network, specify the requirements and guidelines for operation, and ensure that the sensor network fulfils its intended use [8]. A wide range of protocols is designed in communication networks to overcome the challenges discussed in Table 1 and improve network performance. These protocols extend the operationality of the network to perform some intended function.

In WSNs, data packets are transmitted to the BS in two ways: single-hop or multihop. The node sends the generated packet directly to the base station in a single hop. In contrast, in multihop, source nodes send packets to the BS via a multipath, with each node in the path forwarding the received (or, in the case of the source node, generated) packet to another node until the packet reaches the BS [6]. WSNs face some challenges, which include energy consumption, sensor node deployment, routing algorithms, energy efficiency, cluster-head (CH) selection, resilience, etc. Researchers have developed several routing and medium access control (MAC) protocols to address these issues. Optimisation algorithms have also been designed to determine the best path between the transmitter and receiver nodes to save energy and extend the network lifetime.

Designing efficient communications and network protocols for WSNs for EMAs manages sensor node operation in their deployable environment and achieves successful sensor node objectives [15]. The variability of EMAs and their peculiar characteristics should be considered when designing efficient protocols suitable for gathering accurate and timely data from sensors in the field. A unique channel is frequently used to communicate between wireless sensor nodes. The channel has the property that only one node can send a message at any time. As a result, shared channel access necessitates the implementation of a MAC protocol among the sensor nodes [16]. The MAC protocol is aimed at managing access to the shared wireless medium to meet the underlying application's performance requirements.

On the other hand, routing protocols are essential during data transmission to create optimum paths from sensed data to be transmitted from source to destination [17]. Maintaining optimum paths in WSNs for EMAs is critical to maximizing the nodes' lifespan and data throughput. Another essential feature of the WSN is the maintenance of a secured network [18]. The different applications in EMAs require that their security solutions are provided with the objectives and application needs in mind.

The paper explores how WSNs for EMAs are affected by new security vulnerabilities at the physical, network, and data link layers. To appreciate the security challenges in EMAs, the paper discusses the WSN protocol stack, energy-efficient protocols, and energy harvesting protocols suitable for environmental monitoring applications. There are further discussions on the design requirements, simulation environments for EMA protocol designs, quality-of-service requirements, and network topology requirements. Finally, the paper presents the security issues in WSN for EMAs, detailing the threats at the nodal and network levels and their prevention and countermeasures.

2. WSN Protocol Stack

WSNs are distinguished by their adaptable network topology, which various networking protocols enable at multiple layers. Designing efficient and reliable communication protocols for WSNs for EMAs is difficult due to different constraints on the sensor platform and the different environments' lack of certainty and dynamics [19]. An analysis of the design requirements of protocols for WSNs for EMAs is provided in this section. Physical, data link, network, transport, and application are the five core layers of the WSN protocol stack, of which three (physical, data link, and network) will be explored in this section.

The physical, data link, network, transport, and application layers of the wireless sensor network protocol stack are similar to the classic open system interconnection (OSI) paradigm. In each of these layers, several activities are undertaken. The physical layer handles frequency selection, carrier frequency production, signal detection, modulation, and data encryption. The data link layer handles the multiplexing of data streams, data frame detection, medium access, and error correction. In a communication network, it enables reliable point-to-point and point-to-multipoint connections. The data given by the transport layer is routed by the network layer [8]. In WSNs, the network layer design must consider energy consumption, communication, aggregation, and other factors. The transport layer aids in data-flow maintenance and may be necessary if WSNs are accessed over the Internet or other external networks. Depending on the sensing duties, different forms of application software can be set up and employed at the application layer. The following section discusses the routing protocols for managing the increasing energy requirement of sensor nodes to monitor environmental applications such as photosynthesis, soil carbon flux, and soil salinity.

2.1. Routing Protocols. Routing protocols in EMAs determine optimum dynamic routes for exchanging information between sensor nodes depending on the application-specific requirements. These application-specific requirements of the routing protocols include throughput, capacity, coverage, network performance, end-to-end delay, real-time delay, and

Table 1: Challenges in WSN application domains.

Application domain	Challenges	Recommended solutions
Terrestrial	Limited power supply Data redundancy Data latency	Energy minimisation techniques Design of efficient routing protocols Use of energy harvesting Implement an effective node deployment strategy (e.g., multihop) Short transmission range
Underground	Difficulty in deployment High signal losses High levels of attenuation Higher energy cost Difficulty in battery replacement	Design of efficient data communication protocols
Underwater	Limited bandwidth of the acoustic channels Low link quality of acoustic channels Significant propagation delays due to the speed of sound Energy limitation with sensor nodes Creation of the Doppler effect due to the relative motion of the transmitter and the receiver Nodes are susceptible to corrosion	Design of efficient underwater data communication precools
Multimedia	High bandwidth demand High energy consumption Provisioning of quality of service due to variable delays and channel capacity High demand for data processing Challenges with cross-layer design Data compression	In-network processing Filtering Design of efficient compression techniques Design of cross-layer protocols
Mobile	Unreliable data transfer Uncontrolled mobility results in poor network performance Localization and coverage Unstable contact detection due to shorter contact durations	Design of efficient mobility-aware protocols for message exchanges Design of efficient mobility-aware power management protocols

collision. They are helpful, especially in mobile applications such as battlefields, disaster zones, animal tracking, water monitoring (freshwater/ocean), and air quality. Some EMAs are time-sensitive, while others have bandwidth constraints. The sensor nodes are either powered by fixed-energy batteries or rechargeable batteries. Battery-powered WSNs for EMAs are expected to operate for at least two (2) years without failure [20]. However, most applications of EMAs are deployed in areas where changing or recharging batteries is a difficult task. Generally, routing protocols are classified into route discovery protocols, network organization protocols, and protocol operations, as shown in Figure 1.

There are three route discovery protocols: reactive, proactive, and hybrid. There are four network organization protocols: flat-based, hierarchical-based, location-based, and data-centric. Based on their operation and how the protocols work in a deployable environment, routing protocols are classified as negotiation-based, multipath-based, query-based, quality-of-service-based, and coherent-based protocols [21, 22]. The following sections cover each category in detail, providing examples for each.

2.1.1. Discovery Protocols. Discovery routing protocols are discussed in this section. Developments of discovery routing protocols are presented in Figure 2.

(1) Proactive Protocols. Proactive protocols are table-driven protocols. Proactive routing techniques store the routes without any route matching. These protocols keep track of every sensor node's connectivity to other nodes in the sensor network at any given time. Proactive routing protocols enable every sensor node to send periodic updates and have a clear and consistent network topology view. Proactive routing keeps a fresh list of destinations and associated paths by frequently disseminating routing tables over the sensor network. Examples of proactive routing protocols include destination sequence vector (DSDV), optimised link state routing (OLSR), and wireless routing protocol (WRP). Other proactive protocols proposed in the literature include source tree adaptive routing (STAR); global state routing (GSR); cluster head gateway, switch routing (CGSR); and fisheye state routing (FSR) [23–25]. The popular examples discussed in this paper are DSDV and OLSR.

DSDV is a proactive table-driven protocol that uses the Bellman-Ford routing technique. Through sequence numbers, DSDV ensures loop-free operation. Every mobile node in the network keeps a routing table that lists all of the network's possible destinations and the number of hops required to reach each one. A sequence number is assigned to each entry by the destination node. The sequence

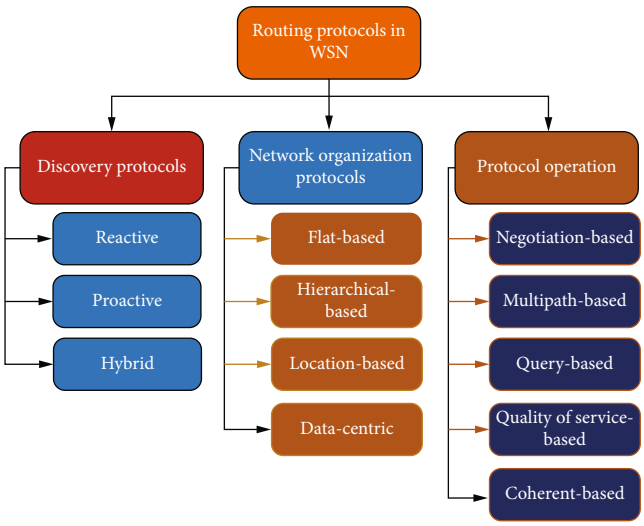

Figure 1: Classification of routing protocols.

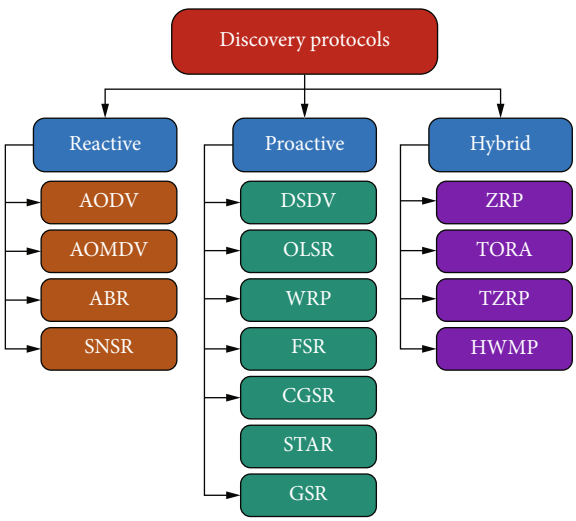

Figure 2: Discovery routing protocols.

numbers let the mobile nodes distinguish between old and new routes, preventing routing loops [26].

OLSR is a proactive protocol where frequent topology changes cause flooding of the network with erratic updates. The OLSR reduces the maximum time interval for updating control overhead messages to optimise the link-state information. The critical concept of OLSR is the multipoint relays (MPRs), which are selected nodes that forward broadcast packets during the flooding of the network. The MPR reduces the control overhead of flooding since only MPRs generate link-state information. Therefore, the flooding of the network with control overhead messages reduces when OLSR is employed [27]. OLSR only transmits partial link-state information between MPRs and their MPR selectors for route calculations. This approach reduces the computational cost of route calculations and hence minimal delay in establishing routes. This protocol is best for networks where larger subsets of the network communicate with other larger subsets of the same network. It is suitable for networks where the source/destination pair with time. It is also suitable for applications that do not allow for long delays and operate in dense networks. However, it is disadvantageous in mobile networks where the frequent change in topology increases the exchange of control overhead messages, increasing the cost of energy and memory use [27].

(2) Reactive Protocols. Reactive protocols are designed, so sensor nodes within the network initiate a route discovery process only when a route to a destination node is required. The routes are subjected to computation because the sensor node computes its route based on demand [20]. The routes that have been established are created and maintained in two stages: route discovery and route maintenance. The route discovery occurs on-demand by flooding the network with route request (RRQ) packets. When a route is discovered, the destination responds with a route reply (RREP) containing the route information traversed by the RREQ. Ad hoc on-demand distance vector (AODV), ad hoc on-demand multipath distance vector (AOMDV), associativity-based routing (ABR), sequence number-based secure routing (SNSR), signal stability routing (SSR), and dynamic source routing (DSR) are popular examples of reactive protocols [25, 26, 28]. More popular reactive protocols are discussed here. They are best suitable for applications where the sensors are mobile and have their routes changing frequently.

AODV reduces control traffic by generating path requests on-demand and constructs its routes without prior knowledge using an RREQ and RREP request loop between the source and destination nodes. RREQ packets are broadcast as part of the route-building process. When a node receives an RREQ packet, it checks its record to see if it has previously received an RREQ packet. If a packet is not logged when received, the node resends it [28]. Ad hoc on-demand multipath distance vector (AOMDV) is a modified version of the AODV routing protocol. AOMDV is a protocol with multiple routes, disjoint paths, and no loops from source to destination. AOMDV uses hop count during the advertisement. AOMDV is designed to keep multiple disjoint loop-free paths in route discovery. The AOMDV protocol reduces energy consumption and packet loss in WSNs. Compared to AODV, it performs better in applications with high traffic loads. The essence of the AOMDV protocol is guaranteeing that multiple pathways discovered are loop-free and discontinuous and identifying such paths fast utilising a flood-based route discovery method. AOMDV route update rules are critical for maintaining loop-freeness and applying disjointness properties locally at each node [29].

When a source node has packets to send to a destination node, dynamic source routing (DSR) checks its cache first to see if it has a route to that destination. A new packet header is constructed to include the destination's path if a route is available. Suppose no route is found in the cache. In that case, the node initiates the discovery process by sending an RREQ broadcast packet with the source and destination node identifiers of the route to be discovered and a unique identifier for the RREQ. Associativity-based routing (ABR)

is an on-demand routing protocol initiated by the source node. ABR employs both point-to-point and broadcast routing techniques. In ABR, the destination node decides on a route based on the property of "associativity." The chosen route is used, and all other routes are discarded because the decision is based on the property of "associativity," resulting in long-lived routes. ABR is divided into three stages (route discovery, route reconstruction, and route deletion).

(3) Hybrid Protocols. Hybrid routing methods combine the benefits of proactive and reactive routing strategies and their drawbacks. In some scenarios, hybrid routing is preferable. These hybrid protocols can achieve consistency across proactive and reactive protocols. Because nodes must keep high-level topological information, these protocols have a drawback in that they require more memory and power. Examples of hybrid routing protocols include zone routing protocol (ZRP), two-zone routing protocol (TZRP), temporarily ordered routing algorithm (TORA), and hybrid wireless mesh protocol (HWMP). A description of the most popular hybrid routing protocol is provided [25, 26]. ZRP was created to work in a zoned network. The node in ZRP maintains routes to all the routing zone's destinations. Intrazone routing protocol (IARP), interzone routing protocol (IERP), and bordercast resolution protocol are the three subprotocols of ZRP (BRP). When the route is within the zone, intrazone routing protocol (IZRP) is used, and when it is outside the zone, interzone routing protocol (IERP) is used [26].

2.1.2. Network Organization Protocols. Sensor nodes collaborate to complete the tasks of the app for which they were deployed. Sensor nodes with extreme energy constraints have limited computation, storage, and communication capabilities. Some network-level protocols are designed to address the limited computing, storage, and communication capabilities of WSNs. These include flat-based routing protocols, hierarchical protocols, data-centric protocols, and location-based protocols. In flat-based protocols, all nodes are treated as peers. Hierarchical protocols are a type of protocol that is based on clusters. Data-centric protocols are intended to disseminate information throughout the network, whereas location-based protocols are aimed at addressing sensor network concerns by utilising node position information. In each of these categories, several routing algorithms have been proposed. The following sections provide brief descriptions of the various network organization protocols, as illustrated in Figure 3.

(1) Hierarchical Protocols. Hierarchical routing protocols enable large-scale network deployment through self-organization capabilities. The primary goal of the hierarchical routing protocol is to keep sensor nodes' energy consumption as low as possible by performing data aggregation and fusion to reduce the amount of data transmitted to the base station [30]. In Figure 3, a list of hierarchical routing protocols is designed for use in WSNs. Details of these protocols are low energy adaptive clustering hierarchy (LEACH), power-efficient gathering in sensor information systems (PEGASIS), and hybrid energy-efficient distributed (HEED) clustering. Also, we have protocols such as the threshold-sensitive energy-efficient sensor network (TEEN), base station-controlled dynamic clustering protocol (BCDCP), concentric clustering scheme (CCS), and adaptive threshold sensitive energy-efficient protocol (APTEEN). Finally, hierarchical routing protocols also designed for large-scale networks include energy-efficient clustering scheme (EECS), self-organizing protocol (SOP), energy-balanced chain-cluster routing protocol (EBCRP), chain-based hierarchical routing protocol (CHIRON), energy-aware data aggregation tree (EADAT), balanced aggregation tree routing (BATR), power-efficient data gathering and aggregation protocol (PEDAP), and enhanced tree routing (ETR).

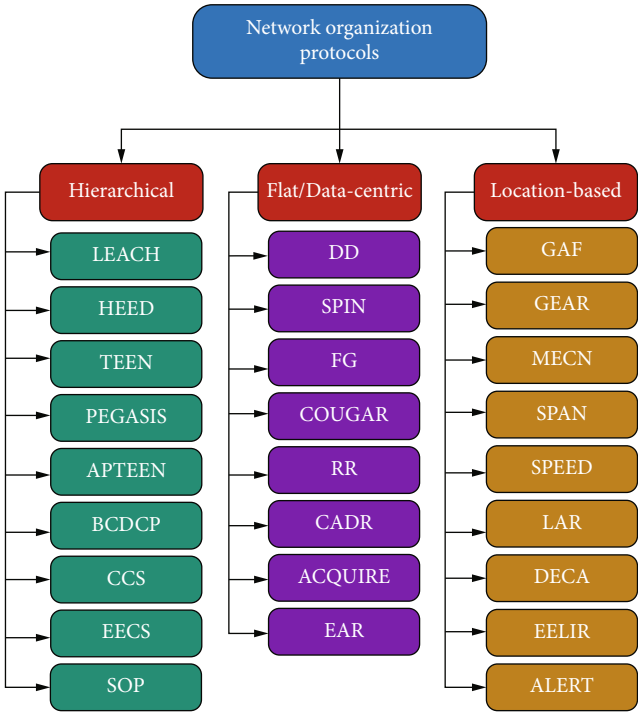

Figure 3: Network organization protocols.

Hierarchical routing protocols are divided into four types: cluster-based (LEACH, TEEN, HEED, APTEEN), chain-based (PEGASIS, CHIRON, EBCRP, CCS), tree-based (EADAT, BATR, ETR, PEDAP), and grid-based (SOP, BCDCP). Figures 4–7 illustrate the four hierarchical routing protocols employed for environmental monitoring applications depending on the requirements.

We describe two popular hierarchical protocols (LEACH and PEGASIS) suitable for environmental monitoring applications due to their flexibility in handling the routing information. LEACH (low-energy adaptive clustering hierarchy) is a routing algorithm that collects and delivers data to a sink node or base station. LEACH is the most widely used energy-efficient cluster-based hierarchical routing protocol for EMAs in WSNs. It employs localized coordination to enable scalability and robustness in dynamic networks.

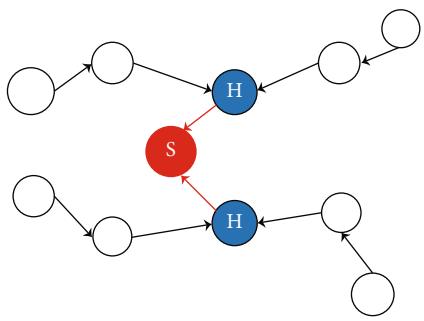

Figure 4: Chain-based.

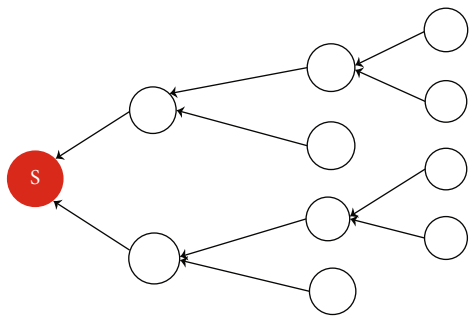

Figure 5: Tree-based.

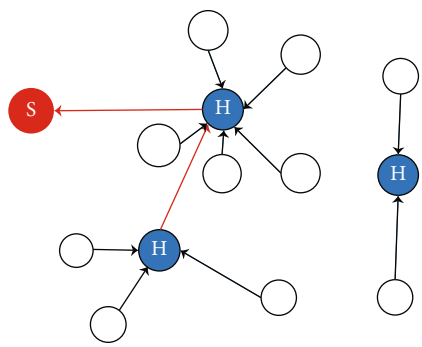

Figure 6: Grid-based.

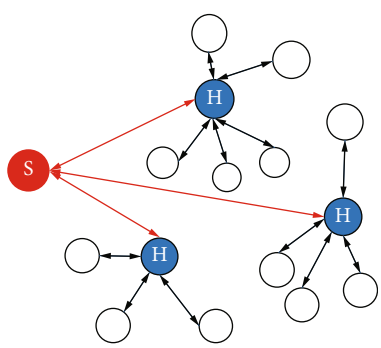

Figure 7: Cluster-based.

LEACH incorporates data fusion into the routing protocol to reduce the information transmitted to the base station and organizes the network into clusters using a hierarchical approach. A cluster head is responsible for each cluster. The cluster head carries out multifaceted tasks [10, 30, 31].

In PEGASIS, nodes are connected in a chain, with one node connected to the opposite and the last node connected to the base station. The advantage of PEGASIS is that it reduces the amount of data transferred between contiguous nodes by moving information obtained by detector nodes from one node to the next until the last node transmits the data to the final terminal and restricts the number of transmissions and receptions between nodes. Two main impediments challenge the use of PEGASIS in environmental monitoring applications. First, the base station acts as a single leader, which can cause bottlenecks. Secondly, PEGASIS generates excessive disruption for remote nodes in the chain. These two challenges can be solved by enabling concurrent transmission between neighbouring nodes, which reduces the latency incurred during connection with the base station. Other ideas include using signal coding or only permitting data to be transmitted simultaneously between far apart nodes [31].

(2) Flat/Data-Centric Protocols. It is not practical to issue global identifiers to each node in many sensor network applications. The lack of global identifiers and the random deployment of sensor nodes make selecting a set of sensor nodes to interrogate problematic. As a result, data is often transported to a deployment location with a high level of redundancy. The solution to these challenges led to developing a data-centric routing protocol [21]. Examples of flat/data-centric routing protocols include gradient-based routing (GBR), COUGAR, and constrained anisotropic diffusion routing (CADR). The others are directed diffusion (DD), flooding and gossiping (FG), energy-aware routing (EAR), active query forwarding in sensor networks (ACQUIRE), and rumor routing (RR). Two popular examples (SPIN and directed diffusion) of data-centric protocols discussed are provided in this paper.

SPIN stands for "sensor protocols for information via negotiation," a data-centric, negotiation-based family of WSN information dissemination protocols. The fundamental goal of these protocols is to efficiently distribute data collected by source nodes to the rest of the network's sensor nodes. Simple protocols such as flooding and gossiping are frequently recommended to achieve information distribution in WSNs. Each node in the network must send a copy of the data packet to its neighbours until the information reaches all nodes in the network [6, 9, 22]. Directed diffusion is a data-centric routing approach. There must be a list of attribute-value pairs (interval, name of objects, duration, and area). If a node is interested in specific data, the sink broadcasts the inquiry to its neighbours. The interest is cached by the nodes that get it to use later. The data is compared to the values in the cached interests. Within the interest, there are additional gradient fields. The gradient is a reply link to the neighbour who sent the interest [22, 32]. This data-centric strategy is used to acquire and deliver information because it is energy efficient, saving energy, and extending the network's lifespan. The directed diffusion routing protocol does not require addressing because all communication is node-to-node [22].

(3) Location-Based Protocols. A source node sends a packet to a destination node in a location-based routing (LBR) protocol, and the destination node appends to each packet by the source node. Packets received by intermediate nodes along the path to the destination node use the location information in the packet and deliver it to the next one-hop neighbours. They are geographically closest to the destination. The operation is repeated until the data packets arrive at the destination node. Because of the locality, location-based routing necessitates the minor state in each node. Because advertisements of routing tables, as in traditional routing protocols, are not required, it has a low communication overhead. As a result, route creation and maintenance are no longer needed with location-based routing. Location-based routing is used in more extensive networks where node positions change and the destination node's location is known to the source [33]. LBR makes use of node location information to improve efficiency and scalability. In LBR, each node in the network must be aware of its location information, obtained via GPS or other techniques. Also, each node must be informed of the position of its one-hop neighbour node, and the source must know where the destination node is located.

LBR generally requires accurate location information, which can be acquired through some sort of localization technique. Because location information is critical for many EMA WSNs, such as animal tracking and forest fire monitoring, it is expected that each wireless sensor node in the network will be equipped with some form of localization device. Location-based routing is categorised into GPS-based and non-GPS-based protocols. The sensor nodes may be deployed as mobile or static in each category. LBR employs greedy algorithms to forward packets from the source node to the destination node. It is critical in preserving the energy of the sensor nodes. Examples of location-based routing protocols are illustrated in Figure 3. Details of these protocols are geographic adaptive fidelity (GAF), geographical and energy-aware routing (GAER), minimum energy communication network (MECN), sensor protocols for information via negotiation (SPAN), SPEED (a real-time routing protocol for sensor networks), location-based energy-efficient intersection routing (EELIR), anonymous location-based efficient routing protocol (ALERT), energy-efficient geographic forwarding algorithm for wireless ad hoc and sensor network (DECA), improved hybrid location-based ad hoc routing protocol (IHLAR), location-based routing protocol (LBRP), selective bordercast in ZRP (SBZRP), and location-based selective bordercast in ZRP (LBZRP). In this paper, GAF and GEAR are described.

The geographic and energy-aware routing (GEAR) algorithm employs geographic information to route queries to the most relevant places. In many location-aware systems, notably sensor networks, disseminating information to a geographic region is valuable. GEAR uses an energy-aware and geographically informed neighbour selection algorithm to route a packet to the target region instead of flooding the query or packet across the whole network. On the contrary, interest is inundated throughout the entire network in directed diffusion. As a result, GEAR saves more energy than directed diffusion.

Geographical adaptive fidelity (GAF) is a location-based routing technology considering energy consumption. Sensor networks will find it informative and applicable. Algorithms control the network's nodes, turning them on and off to save energy while maintaining high fidelity. For the covered space, GAF develops a virtual grid. Each node receives its current location through GPS, associated with a virtual grid point. Regarding packet routing costs, nodes belonging to the same grid are regarded as the same.

2.1.3. Protocol Operation Routing. Protocol operation is another way to categorise routing protocols in WSNs. This category can be divided into five major sections based on protocol processes. Some subcategories include multipath, query, negotiation, quality-of-service, and coherent-based routing protocols. Examples of these protocols are presented in Figure 8.

In WSNs, data processing is critical, and several strategies are applied to lower processing costs to save energy. In this case, the obtained data can be handled logically. In coherent data processing-based protocols, the sensor nodes perform the bare minimum of processing locally [34]. Data is sent to sink nodes after minimal data processing in coherent routing. Tasks like time-stamping and duplicate elimination are often included in the minimum processing. Coherent processing is frequently used to produce energy-efficient routing [35]. Examples of protocols include the multiple winner algorithm (MWA) and single winner algorithm (SWA).

The protocol may use various methods to transmit data from source to destination in multipath routing. Multiple routes improve network fault tolerance while significantly increasing energy consumption and protocol overhead. An extension of the method evaluates only the path with the highest energy nodes. When a better path is found, the protocol changes to it. The network's reliability can be strengthened using the multipath routing protocol in severely unstable conditions. A large packet can be broken down into smaller chunks and sent via numerous channels. A message can still be produced even if one of the subpackets is lost owing to connection issues [16]. Some multipath routing protocols include energy-constrained multipath routing (ECMP) and multiconstrained quality-of-service multipath routing (MCMP).

A node initiates a query and propagates it across the network in query-based routing. The query is sent to each node; only the node with matching data receives responses. Rather than disseminating the queries throughout the network, the node could send them down a random path and wait for a response. If none of the other nodes responds, the node can broadcast it to the entire network [36]. Quality-of-service (QoS-based) routing ensures that a wireless network will deliver the expected results. Latency (delay), throughput, error rate, and energy consumption are a few quality-of-service parameters in WSNs, which differentiates traffic flows by treating packets differently based on their nature. The quality-of-service routing protocol is also in charge of

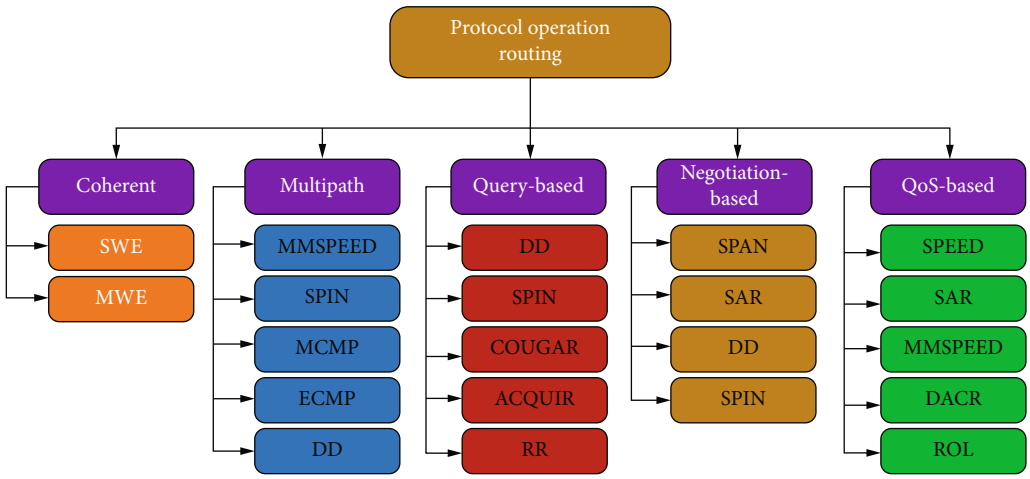

Figure 8: Protocol operation routing protocols.

prioritising data flows to maintain a predefined performance level. When delivering data in applications where parameters such as delay, resources, and bandwidth are critical, the routing protocol must maintain the quality and specifications of the required parameter. The quality-of-service routing protocol balances energy consumption and other metrics [37]. Sequential assignment routing (SAR) is a typical QoS-based routing protocol. Flooding and gossiping in WSNs can cause the network to implode; thus, a single node may get several copies of data. Negotiation-based protocols are intended to prevent duplicate packets from propagating. In wireless sensor networks (WSNs), sensor nodes exchange negotiation messages to send redundant data to the next node. It reduces network congestion and conserves energy.

Routing protocol categories (route discovery protocols, network organization protocols, and protocol operation) are beneficial in specific application areas. These protocols provide myriad challenges and energy requirements when used for specialised purposes. Table 2 highlights most of the application areas, challenges, and energy requirements for the various forms of routing protocols.

3. Energy-Efficient Protocols

Data communication is a critical challenge in many WSN applications. As a result, it is advantageous to construct and develop easily accessed resources to give data in WSNs. The number and position of nodes in WSNs make recharging or replacing batteries impossible. As a result, energy consumption is a universal design concern for WSNs. Researchers have concentrated on reducing energy dissipation at all stages of system design, from hardware to protocols to algorithms. As a result, it is critical for the network to carefully define the parameters of the protocols in the network stack to achieve the required energy efficiency and meet the quality-of-service requirements. The following is a discussion of some energy-efficient protocols used in the WSN architecture at the physical, link, and network layers.

3.1. Energy-Efficient Physical Layer Protocols. The Zigbee protocol suite is the preferred physical layer protocol for environmental monitoring. It is widely considered due to its low duty cycle for energy-efficient implementations. The communication range of Zigbee is within 100 m, with a reduced communication range of 30 m for indoor applications [38]. Using precision agriculture and farming applications, Zigbee enabled supervised irrigation, water quality management, pesticide and fertiliser control, and total field surveillance [39]. Other implementations of Zigbee include investigating signal propagation and strength distribution characteristics of wireless sensor networks in date palm orchards with application-efficient specific parameters such as signal strength on the spacing between nodes, the leaf density, and antenna height of the base station. Cattle grazing-field implementation [40, 41], greenhouse [42, 43], livestock monitoring [44], and smart beehives [45] are some current implementations using Zigbee.

3.1.1. LoRa (Long Range Radio). LoRa is a digital wireless data communication technology spread-spectrum radio modulation (EP2763321 from 2013 and US7791415 from 2008) derived from chirp spread spectrum (CSS) technology. It uses the unlicensed free radio frequency bands 169 MHz, 433 MHz, and 868 MHz in Europe and 915 MHz in the US.

LoRa is presented in two ways: the physical layer shown as LoRa on devices and the upper layers presented as the long range wide area network (LoRaWAN) [46]. LoRa provides a low-cost, secure bidirectional mobile communication for IoTs and other machine-to-machine (M2M) for high throughput systems. These systems typically run on 3G or Ethernet networks, WiFi, or cellular technologies. The LoRa has been implemented in smart bee monitoring farms to ensure communication of the colony activities [47]. Greenhouses measure air temperature, humidity, light intensity, and soil moisture [48]. LoRa's advantage is its scalability to several nodes and adaptability to interference and noise. Another implementation involves real-time monitoring using a multisensor combination module (MSCM) and LoRa. In the implementation, wetland parameters include

Table 2: Application areas, challenges, and energy requirements of routing protocols.

Categories of routing protocols		Application areas	Challenges	Energy requirements
Route discovery	Reactive	Animal tracking, habitat monitoring	Continuous energy source, size of sensor nodes, frequent change in node position, latency, security	Energy harvesting sources, rechargeable batteries
	Proactive	Infrastructure systems, hospice care, weather forecasting, military surveillance	Significant overhead for storing routing tables in sensor nodes, not suitable for mobile applications	Fixed energy batteries, capacitors, rechargeable batteries. Mobile energy transmitters
	Hybrid	Sewage and gully pot monitoring	Require more memory and power, mobility	Mobile energy transmitters, energy harvesting nodes
Network organization		Animal tracking, military surveillance, crop farming, forest fires, disasters. Habitat monitoring, disaster monitoring	Size of sensor nodes, energy source, number of nodes, modulation schemes	Fixed energy batteries, rechargeable batteries
Protocol operations		Smart farming, structural monitoring, earthquake monitoring, water quality monitoring, air quality monitoring, climate change monitoring	Energy consuming, topology control, maintaining energy-neutral operation (ENO), mobility of nodes, antenna sensitivity	Supercapacitors, rechargeable batteries, energy harvesting sources (primarily solar)

water temperature, pH, conductivity, turbidity, dissolved oxygen, and water level [11]. A recent work by authors considers the inability of the elderly and disabled farmers to monitor and oversee agricultural tasks on farms. In their implementation, LoRa radios were used to run several software applications from speech processing software, voice recognition, and other assistive artificial intelligence (AI) features. However, LoRA may only transmit data not exceeding a few kbps (not suitable for video capturing) over longer distances (not exceeding 3 km). The work by the authors included smartphones and tablets intercepting voice commands generated to be transmitted to a remote agent's device, usually at the farm's end. Applications on the agent's device are designed using raspberry pi and other programming facilities like the Arduino Uno unit with a WiFi radio module. Countries with existing implementations include smart gardens, vineyard crops in Spain, irrigation on kiwi and corn farms in Italy, and banana farming in Columbia.

3.1.2. Bluetooth. Bluetooth is another short-range communication protocol in environmental monitoring applications. It is usually implemented between movable portable devices such as laptops over 10 m distances. Due to its availability on most handheld devices, it can be used for multilevel agricultural applications. Agricultural implementations include weather information, soil moisture, temperature, and irrigation. Bluetooth is beneficial due to its low energy consumption, wide availability of devices, and ease of use. It has also been used in other monitoring environments, such as disaster prediction and monitoring [49], food storage systems [50], and environmental monitoring in small spaces [51].

3.1.3. Sigfox. Sigfox is the name of the company and the low power wireless area network (LPWAN) operator. It is one protocol gaining popularity in IoT and environmental monitoring applications in several countries, cooperating with various mobile network operators. Sigfox provides a software-based communication platform that allows the complexities of network computing to be carried out on the cloud instead of the devices. Their unique setup with mobile cellular networks provides an extensive network of global devices transmitting data without setting up or maintaining a connection [52]. Therefore, the Sigfox setup removes network bottlenecks such as signalling overheads, providing a robust and optimised network protocol. It uses the radio frequency channel on the 100 Hz band, with a data rate of 100 bps. It is based on the ultra narrow band (UNB). It uses a differential binary phase shift keying (DBPSK) modulation scheme, with scattered nodes accessing the network using random frequency time division multiple access (RFTDMA) [53].

Narrowband Internet of Things (NB-IoT) is developed by the 3rd Generation Partnership Project (3GPP) to scale up WSN applications and make them more dependable. NB-IoT uses an unlicensed frequency band in long-term evolution (LTE) and consumes more power than LoRaWAN due to its constant need for synchronisation. It implements orthogonal frequency-division multiplexing (OFDM) and frequency division multiple access (FDMA), increasing its power consumption. However, its applications require low latency and high data rates.

Other less implemented physical layer protocols in environmental monitoring include Bluetooth LE and mobile cellular technologies such as GPRS, 3G, and 4G. Due to their high energy consumption, mobile technologies are limited in IoTs and environmental monitoring applications. In contrast, the high data rate they provide may not be helpful in many applications [54–61]. Table 3 summarises the characteristics of energy-efficient physical layer protocols for environmental monitoring applications.

3.2. Energy-Efficient Routing Protocols. Energy-efficient routing is aimed at increasing the network lifetime by

Table 3: Characteristics of energy-efficient physical layer protocols.

Protocol	Standard	Power consumption	Security capability	Applications	Limitations	Range	Topology
Bluetooth	IEEE 802.15.1 (no more). The current standard is Bluetooth 5.3	Low (100 mW)	128-bit AES	Fire and disaster monitoring, food storage, greenhouse monitoring	Line of sight between communicating devices	1-10 m	Point-to-point
Zigbee	IEEE 802.15.4	Low (36.9 mW)	128-bit AES	Temperature and fire monitoring in underground mines, agriculture, cattle grazing, bee hives, and greenhouse monitoring	Line of sight between communicating devices	1-75 m and more	Mesh
LoRa	IEEE 802.15.4g	Low (100 mW)	AES CCm 128B	Greenhouse monitoring, voice detection techniques in farming, irrigation monitoring	Scalability, the maximum data rate of 250 kbps	2-5 km (urban) and 15 km (rural)	Star of stars
WiFi	IEEE 802.11a,b,g,n	High (835 MW)	128-bit AES	Air pollution, earthquake detection, temperature and humidity sensing, humiture and optical sensing	High power consumption, security, long access time (13.74 s)	100 m	Star
Sigfox	Sigfox	Low	Key generation, message encryption sequence	Water quality prediction, air quality monitoring, and optimum farming parameters	Mobility of nodes can only be deployed in a few countries, and communication is limited from the base station to the nodes	100 km	Star
NB-IoT	3GPP	Medium	NSA/AES 256	Water quality monitoring, air pollution, industrial environment	High power, high data rate		Star

considering the energy cost of the communication path. The routing protocols generally are categorised based on clustering, the mode of the protocol's functionality, the node's participation, and the network structure [20]. The general challenges for environmental monitoring include security, scalability, node deployment strategies, connectivity, and coverage. In mitigating these challenges, energy consumption is integral in implementing these solutions.

The challenges of WSN applications are diversified based on the application areas, which influences the routing protocols and quality-of-service parameters. For example, underwater communications in underwater wireless sensor networks (UWSN) use acoustic signals for propagation, unlike radio frequency (RF) signals that are used in terrestrial wireless sensor networks (TWSN). These acoustic signals are at lower magnitudes of 1500 m/s, five times lower than in TWSNs. Quality parameters such as delay are critical in acoustic mediums, which may be negligible for terrestrial environments. A centralised routing protocol, proposed by authors in [62], is based on a full-duplex communication that implements network management (gateway managers) and routing agents. These agents periodically probe the network for the statuses of the nodes to allow the gateways to determine a priori the optimum path between neighbouring nodes to avoid congestion for high traffic applications. Other protocols implemented in [63, 64] were based on water depth and temperature. Fire hazard monitoring applications require adaptive routing to ensure efficient real-time data delivery. The routing protocols for such emergency services include the real-time routing protocol with proposed load distribution [65] and improvement [66].

3.3. Energy-Efficient MAC Protocols. Using energy-efficient MAC protocols in WSN is aimed at meeting the challenges of general WSNs such as latency, throughput and fairness, channel utilisation, and scalability. Latency refers to the time it takes from a source node to reach the destination node. Its requirements in WSN are application dependent. The throughput is also a measure of successful data received by the destination node. Fairness here refers to the ability of the destination node to receive a fair amount of data from each sensor node in the network. Therefore, the MAC protocols ensure optimal results, with energy efficiency integral to its operations. To ensure energy efficiency, MAC protocols must overcome the challenges of multiple transmissions in the networks, such as energy losses due to control overheads, idle listening, collisions, and overhearing.

Environmental monitoring applications require MAC protocols that adapt to mission-critical applications. These applications require a quick response time. The applications may be deployed in inaccessible human environments. Hence, efficient energy management systems are needed to prolong the network lifetime. Examples include volcanic eruption-prone areas, surveillance applications,

environmental monitoring and control systems, and health care systems. The quality-of-service (QoS) parameters identified for MAC protocol implementation in any set of mission-critical system is similar and may be applied to other systems. ADMC-MAC is a mission-critical MAC protocol using regression techniques to decide the duty cycle of sensor nodes [67].

4. Energy Harvesting-Based Protocols

The slow development in battery technologies makes energy harvesting (EH) a viable solution to the energy challenge in environmental monitoring protocols. Using energy harvesting in environmental monitoring hampers the destruction of environmental pollution from the disposal of batteries. Energy harvesting is increasingly becoming important in IoT implementations due to the massive number of sensor nodes deployed for some applications, primarily working for long periods without human interferences.

Energy challenges like traditional WSN applications may not constrain energy harvesting due to energy availability. Some identified EH sources in environmental monitoring include sunlight, vibration, sound, wind, thermal, electromagnetic waves, and body heat and movement. Hence, some applications apply architectures such as mobile, stationary, or hybrid. They may also be classified as single-tier, multi-tier, or homogeneous [68]. Sources like solar energy, commonly used in many applications, use the photovoltaic energy harvesting approach. In photovoltaic energy harvesting, solar light energy is converted into electrical energy to recharge the batteries of WSN nodes. The highest energy conversion for outdoor solar energy harvesting was 15 mW/cm^2 and an efficiency of about 30%. It is the preferred renewable energy source. It is primarily available in the environment where sensor nodes are deployed and have the highest energy conversion efficiency. Solar energy harvesting does not pollute the environment but requires little preservation and may be stored for several years. Solar harvesters may be deployed in applications that include agriculture (farms), forest monitoring, greenhouse monitoring, and animal monitoring. Recently, commercial applications have been deployed by Crossbow Inc. USA, using Mote View 2.0 for measuring parameters such as temperature, humidity, pressure, acceleration, and light. The application uses the Zigbee protocol for communication with an expandable distance of 100 m to 1.5 km. An example of implementation was discussed in the survey by authors in [69] which reviewed the literature on solar energy harvesting WSN (SHE-WSN).

A smart agricultural application simulated by the authors in [70] is intended to extend the network lifetime using solar energy harvesting. Using similar tools described by Sharma et al., the lifetime of nodes deployed on a farm was extended from 5.75 days when energy harvesting was not implemented to 115.75 days. With an increase in throughput of 160 kbits/s from 100 kbits/s, the duty cycle of these sensor nodes could be adjusted upwards to more than 25% (which is a message transmitted every 4 s) since energy is no longer the main challenge of these networks. The network setup consists of MICAz WSN nodes deployed at fixed locations in a mapped-out area on a smart farm. Sensor nodes are connected to a gateway/base station powered by the main supply. Sensor nodes transmit their data to relays through multihop transmits for forwarding to the gateway. The network supports bidirectional communication from the gateway directly with the deployed sensor nodes.

For a comprehensive review of up-to-date energy harvesting WSNs (EH-WSN), the reader may refer to [14] for references. An energy harvesting–based clustering protocol is proposed by authors in [71] to improve network stability and efficiency. Their approach includes the selection of the cluster head for each cluster based on the node's energy level, the amount of energy harvested, and the number of its neighbours. The leach-based clustering protocol uses a lower threshold of 0.1 J and a higher threshold of 1 J to compete in the cluster head selection. Other protocols implementing prediction models that may be difficult in WSN are made possible due to energy harvesting. Weather forecasting-based applications include implementations in IproEnergy [72], autoregressive (AR) models [73], ARIMA models [74], and reinforcement learning applications using Q-learning [75].

Mechanical kinetic energy harvesting converts mechanical motions and vibration harnessed from the environment into electrical energy. This energy source is self-power sensing, convenient, energy-saving, sustainable, and eco-friendly. It is applied in aerospace, biomedical engineering, and military and environmental monitoring applications [76]. However, mechanical energy has few implementations in WSN due to low conversion efficiency, low power output, and conversion being time-dependent and may even cause damage to the device. It requires unique modulation of the energy source to harness the energy from the ambient environment. Applications depending on mechanical include structural condition monitoring, smart devices and cities, biomedical and wearable devices, and machine monitoring. Biomass, which converts organic materials from plants and animals, has seen applications in WSNs where devices deployed in unreachable locations harvest energy from organic ambient sources. Examples of sources include corn, soyabeans, woody plants, paper, cotton, food, wood wastes, and animal and human sewage. Authors in [77] harvested energy from switchgrass, while authors in [78] mentioned the extraction of Xenopus oocytes from female frogs to power capacitors in their application.

5. Environmental Monitoring Application Design Requirements

Environmental monitoring applications are different in many ways. Some of the applications are dynamically deployed, and others are statically deployed. In dynamic deployments, the nodes are primarily mobile, and in static deployments, the nodes are positioned at various points in the environment. In each of these deployments, the design requirements may differ. Also, environmental monitoring applications are characterised by energy efficiency, network

complexity, scalability, data transmission, bandwidth, and processing storage. These characteristics are critical design criteria considered in EMAs. Different topologies associated with the various applications determine the routing and MAC protocols employed for the energy-constrained sensor node. Efficient routing protocols schedule routes efficiently to minimise the amount of energy consumed by the nodes to prolong the lifetime of the sensor network. With efficient routing, gains are made in data communication. MAC layer protocol requirements such as duty cycling, slot scheduling, time synchronisation, node prioritisation, and efficient channel utilisation improve performance and increase network lifespan. MAC protocol implementation in WMAs achieves high reliability, effective scheduling, and efficient time synchronisation in EMAs [79].

5.1. Quality-of-Service Requirements. Quality of service (QoS) guarantees that the network provides the expected results. In WSNs for EMAs, there are essential parameters that the application may be designed to achieve. These QoS parameters include throughput, delay, packet delivery ratio, and energy consumption. For example, in forest fire monitoring, the nodes are deployed to access real-time data and remotely acquire data from forest zones for decision-makers to make decisions based on the data received from the sensor nodes. The sensor nodes report any unusual temperature, smoke, oxygen levels, and humidity that may be collected to mitigate forest fires. Collecting and studying event data from the forest employ sensors that may trigger alarms, calculate and track humidity levels and temperature variations, and detect smoke patterns. From such sensor networks, throughput and data reliability are essential. Also, measuring delay is crucial because the different sensors may collect the data in specified periods. This means that delays in sensor data reporting may cause forest fires. The sensor nodes' energy efficiency will optimise network performance and uptime. For example, in forest fires, sensor nodes must operate in the forest for a long time. Therefore, efficient energy consumption or low energy consumption of the sensor nodes' energy will make the node live longer. Energy-aware sensor network architecture (SNA) techniques are paramount in such networks [80]. Therefore, protocols designed at the various layers must be energy-aware to enhance the overall network lifetime.

5.2. Topology Requirements. WSN network topology is the physical or logical placement or arrangement of sensor nodes in an observed area of interest. It also includes how sensor nodes communicate within the network to collect data from the environment and transmit it to a base station via a sink node [81]. Topology requirements in WSN for EMAs vary depending on the environment and application. Network topologies are typically application-specific, and the structure serves as an essential foundation in EMAs [82]. Network topologies must be designed to balance the energy consumed by sensor nodes while the network lifetime is maximized. The topology of a network can directly impact its performance [83].

WSN topologies such as basic peer-to-peer, linear, star, tree, a cluster tree, or mesh are used in EMAs to monitor and set up the sensor network. Sensor nodes may be deployed remotely at an area of interest to acquire data wirelessly using one WSN topology to monitor agriculture, the environment, or water resources. Topologies can be built either statically or dynamically. Several sensor nodes can freely move in dynamic topologies in some application domains (for example, water quality monitoring and oceanography). The topology can self-organize when individual sensor nodes fail or deplete their energy. In dynamic topologies, when new nodes are added to the network after some nodes fail, the identity of the new node enters the network without changing the topology [81].

In WSNs for EMAs, the transmission power of the nodes determines the network topology, which directly impacts network performance [82]. The network topology in EMAs can be designed to accommodate mobile or static sensor nodes and a sink. Mobile nodes in a sensor network are typically designed to deal with the dynamic network topology required for node mobility. Because node mobility in WSNs makes the topology dynamic, the communication protocol becomes more complicated, necessitating more processing resources and energy. The network topology may generate minimal heavy traffic load depending on the network size and application domain (animal tracking, water quality, oceanography, fire monitoring). The sensor node in an EMA must be able to reconfigure itself for different network topologies (such as star and tree topology). All sensor nodes directly communicate with the sink node in the star topology. Most sensor nodes in a tree or mesh communicate with neighbours to maintain connectivity with the sink node [84].

EMAs' network topology requirements should consider the number of nodes and the distance between neighbour nodes to determine node placement density, network diameter, and coverage. The minimum number of data relays between sensor nodes is used when packets are transmitted between nodes in the network [85]. Researchers developing applications to monitor the environment must consider network topology requirements because network functionality and stability are critical to meeting application objectives. To determine the type of topology, it is also necessary to consider the traffic load density. Network topologies should be well-designed to be fault-tolerant, reconfigurable, energy-efficient, and scalable [86].

6. WSN Security Approaches for EMAs

WSN application security is a complex problem to solve. It requires finding the best method to maximize network performance while dealing with complex restrictions. The goal is to find a reasonable balance between efficiency, energy efficiency, and routing protocol design. Wireless sensor networks (WSNs) are being utilised for various applications, including environmental monitoring applications (EMAs), like a new computer and network infrastructure platform, and operational security is a significant problem. Security issues in WSN for EMAs are more concerned with the reliability of the network, positioning of the nodes

Table 4: Security attacks at the layer(s) on the OSI model.

Network layers	Security attacks	Effects of network/node	Defense mechanism
Application	Message corruption, DoS, disrupt or intercept confidential data	Increases packet reception time Reduces data reliability	Firewalls and the use of antiviruses
Transport	Session hijacking, DoS	Degradation of energy Fake packets are injected Data integrity, availability, and authenticity are affected	Provision of authentication Reducing packet response rate
Network	Wormhole, blackhole, sinkhole, Sybil, selective forwarding, spoofing, altered or replayed routing information, internet smurf	Continuous request to send packets floods the network Generation of false messages Creation of routing loops Causes selective forwarding	Encryption Authorisation Probing Monitoring firewalls
Data link	Traffic analysis, HELLO flood, monitoring, channel exhaustion, 802.11 disruptions (MAC)	Retransmission of data The decreased energy level of the sensor node Nodes may miss the transmission Degradation in network performance	Error correction Use of virtual private networks Reprogramming senor devices
Physical	Jamming, node malfunctioning, node destruction, tampering (direct node attack), DoS, radio interference, interception	Corrupts or sends a large number of packets Sensor node physically tampered Addition of other sensor nodes Network services get stopped (data collection) Network energy is exploited	Hiding Region mapping Spread-spectrum techniques such as DSSS and FHSS

(localization), and the topological characteristics that may affect data collection, data processing, and increased delay in the network [18, 87].

In WSNs, a security attack is defined as any attempt to expose, steal, manipulate, modify, or obtain unauthorised access to information in the sensor network [87]. A wireless sensor network is highly vulnerable to attacks because the sensor nodes are physically unprotected. In WSN, there are two types of attacks: active and passive. The attackers just monitor the communication channel in a passive attack, but they modify the data stream in an active attack. Passive attacks include eavesdropping, node dysfunction, node destruction, and traffic analysis. Active attacks occur when an adversary attempts to disrupt the operation of the network under attack. Active attacks include denial-of-service (DoS), sinkhole attacks, flooding, and Sybil. At various tiers of the network, many attacks exist. The attackers aim to exploit the nodes directly at the physical layer. Jamming is a denial-of-service attack in which the victim's computer's functions are disrupted. There are various attacks at various layers of the network. Table 4 presents security attacks at the layers on the OSI model. At the physical layer, attackers attempt to exploit the nodes physically. Physical layer threats put data availability, integrity, and confidentiality at risk. The data link layer is responsible for framing, addressing, error correction, and flow control. At this layer, a variety of attacks may occur. When two separate nodes send data on the same frequency, the packet's data varies by a small amount. As a result, the packet becomes unusable, and the data is deleted. An attacker may cause these collisions [5, 87].

For communication, many networks employ a two-way handshake. An attacker can make a constant request to send the packet. The network link may be flooded as a result. Interrogation is the term used to describe this type of attack. The network layer handles packet routing from one node to another. Several attacks at this layer in wireless sensor networks take advantage of the routing mechanism. In WSNs, the transport layer ensures that the entire message is delivered in the exact sequence. At this level, some attacks can be made. New connection requests are produced repeatedly in floating till the resources reach their maximum capacity.

To develop secure WSNs, application designers must consider security objectives (integrity, availability, authorisation, authentication, and confidentiality). Data integrity ensures that data is not tampered with by unauthorised parties. Data availability ensures that authorised system stakeholders have immediate and unrestricted access to the system's and network's resources. The most critical aspect of security is availability. The authority to access the data is primarily concerned with maintaining the confidentiality of the information. Authentication requires genuine access to sensor nodes and the network by application designers throughout implementation. The sensor nodes must provide authorised data to stakeholders while operating the network [5]. Encryption techniques are used to protect the privacy of system resources and operations. As a result, data confidentiality is conditional on a certain level of information [88].

6.1. Types of Security Threats in EMAs. Security targets in WSNs for EMAs apply to the wireless medium between sensor nodes, and the sensor devices are susceptible to attacks and vulnerabilities. The environmental monitoring applications are designed to achieve specific objectives. Some applications such as water quality, air quality, animal tracking, and forest fire are life-threatening, endangering the lives of humans and animals. They require essential security measures to ensure that the nodes remain operational 100% of the time. Security attacks of the sensor nodes may cause the nodes to malfunction, disrupt the network, and

Table 5: Description of various security threats.

Attack	Description
Denial of service (DoS)	This attack overflows the network with traffic, utilises more bandwidth, and causes services or resources to become unavailable to the user. This type of attack is most common in all WSN applications. It is aimed at interrupting the system, making it unavailable or unusable, which attacks its availability and efficiency.
Selective forwarding	In this situation, the attacker installs a malicious node which masquerades as a genuine node, which may refuse to forward or simply discard specific messages. This jeopardises the availability and integrity of system data.
Sinkhole	This exploits the network by adding a node that collects all data as though it were the base station. This threatens the confidentiality of the system where applicable.
Sybil attack	In this case, the compromised node assumes several identities (creating the illusion of being present in multiple locations) to connect with a large number of nodes. This poses a risk to the network's confidentiality.
Wormhole	The attack records the information to a different location before transmitting it or a portion of it. This is a threat to data integrity.
HELLO flood	The HELLO packet is transmitted to the nodes, and the attacked device may be misidentified as a neighbour seeking to communicate with it. Its objective is to use network resources. The availability of network resources is jeopardised as a result.
Spoofed, altered, or replayed routing information	This is a more direct attack whereby the attacker can wreak havoc on the network by sending falsified error messages or establishing routing loops. This compromises the network's integrity and availability.
Blackhole	With this attack, the targeted node is forced to transmit the reply to the malicious node by providing fake route information. This disrupts availability.
Node destruction	This attack seeks to either disable the node so that a compromised node with the same identifier may take its place or prohibit it from gathering data.
Monitor and eavesdropping	The goal of this exploit is to obtain network information. This jeopardises confidentiality.
Traffic analysis	The goal is to capture and analyse messages to derive information from communication patterns. Its threat stems from its capacity to function even when data are encrypted and compromised confidentiality.
Node replication	This attack duplicates nodes and uses them to set up multiple attacks.
Message corruption	This attack takes three significant steps: it accepts a message, alters it to make it incomprehensible, and finally sends it to its intended recipient—the integrity and availability of data are being compromised.
Jamming	Jamming disrupts the sensor nodes' RF signals, rendering them inoperable and compromising availability.
Node malfunctioning	Node malfunctioning creates erroneous data that might jeopardise the integrity of the cluster heads' data-aggregation process.

introduce delays in data communication, halting the monitoring process and degrading the overall quality of service. Table 5 illustrates the attacks and descriptions of the various security threats.

Also, when the sensor nodes and network are attacked, the attackers may reprogram the nodes to transmit false data readings, which may endanger the lives of humans and animals.

Attackers may also cause the sensor nodes to continuously send packets until they are exhausted, drain their energy, and die. Table 6 depicts some common types of attacks and the environmental monitoring application they affect, which an attacker may exploit to render the sensor network inefficient affecting its intended use.

6.2. Node and Network Security Approaches in Environmental Monitoring Applications. This paper has established that wireless sensor networks (WSNs) have minimal operational energy, limited memory capacity, and constrained computing abilities. These nodes can sense, record, and monitor environmental conditions. The sensor node and the sensor network have a lot of practical uses, but they are also challenged with several deployment problems of which security is paramount. The node is deployed in hostile environments, making them physically vulnerable to attacks (adversaries and natural disasters). When sensor nodes are deployed in hostile environments, the kind of topology formed because of the node depleting its energy or being damaged by animals is unclear. The section examines different security approaches suitable for specific operations in WSNs for EMAs. Some data gathered from sensor nodes in EMAs may be sensitive. Hence, there is a need to safeguard the node, network and sensed data to prevent any attack or tampering. The data obtained from the sensor nodes and transferred to a base station require levels of authorisation and authentication to access it. These security

Table 6: Threats in environmental applications.

Threat	Animal tracking	River/ocean monitoring	Forest fire detection	Air quality	Precision agriculture	Earth/ landslide	Active	Passive
Denial of service	×	×	×	×	×	×	×	
Selective forwarding		×	×	×	×	×		×
Sinkhole	×		×	×	×	×	×	
Sybil			×	×		×	×	
Wormhole		×	×	×	×	×	×	
HELLO flood	×	×	×	×	×	×		×
Spoofed, altered, or replayed routing information	×			×	×		×	
Blackhole	×		×		×	×	×	
Node destruction	×	×	×	×	×	×	×	
Monitor and eavesdropping	×	×		×	×			×
Traffic analysis	×				×		×	
Node replication	×		×	×	×	×	×	
Message corruption	×	×	×	×	×	×	×	
Jamming	×	×	×	×	×	×	×	
Node malfunction	×	×	×	×	×	×	×	

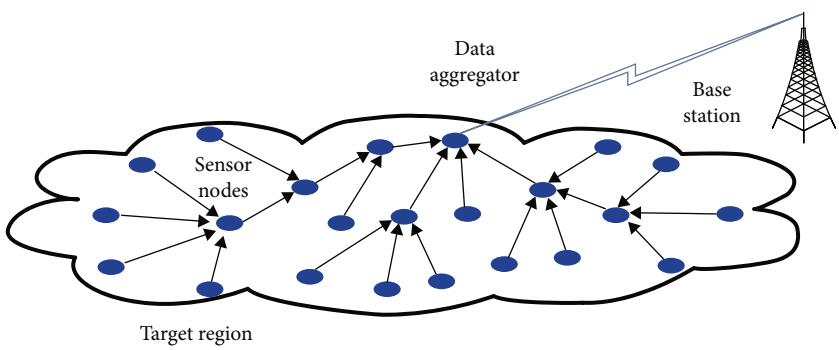

Figure 9: Data aggregation in a wireless sensor network (adapted from [92]).

levels will prevent unauthorised data from getting into the hands of the wrong users [89].

6.2.1. Secure Data Aggregation. The sensor nodes in EMAs collect enormous amounts of data. The sensed data must be aggregated to avoid overload at the base station. As illustrated in Figure 9, data aggregation is how sensed data is processed and combined en route by intermediary sensor nodes. In a typical WSN, many sensor nodes gather application-specific data from the environment and transfer it to a centralized base station for processing, analysing, and use by the application [90]. The basic strategy is to analyse data from multiple sensor nodes as transmitted collectively. The plain text sensed by the deployable environment's nodes may be encrypted before being transferred to the base station. For example, water quality data such as pH or dissolved oxygen sensed by nodes deployed in a river is encrypted after sensing and transmitted to the base station. Before data aggregation operations can be performed on the data, the encrypted water quality data is decrypted at the base station [91, 92]. In real-time applications, data aggregation occurs to prevent false alarms. Data can be aggregated within a node, across a network, at the sink, or the base station. All of these data collection points require some level of security. Where sensitive data is being collected, as in military deployments, encryption may be needed to prevent data from being read and compromised by adversaries [93].

6.2.2. Access Control. Access control is a security strategy that governs who has access to and uses resources in a computing environment. It is a fundamental security concept used to mitigate risk. The two types of access control are physical and logical access control. Physical access control is used to restrict access to physical IT assets. Logical access control governs all communication systems, files, and data connections. Nodes are fixed or mounted on endangered species (for example, turtles) in animal tracking applications to track their movements. Physical access to the nodes is impossible while the animals are in motion. Still, logically, the algorithms or protocols are accessible to researchers who track the position of the animals and all data residing on the node. This could be applied to the battlefield, forest

fire, and water resource monitoring. Farmers can have physical and logical control over agricultural monitoring and use the necessary security at each level to provide the restrictions required for the device and the data [94].

6.2.3. Secure Routing. Nodes in WSNs for environmental monitoring communicate to transfer data from one node to another. Data exchange between nodes necessitates a secure pathway to avoid data compromise. Because nodes in a WSN route packets over multiple paths, secure routing techniques must be used to secure the route. Secure routing is a set of transport and network security controls that apply to routing protocols and individual nodes. However, to establish the network architecture (reactive, proactive, or hybrid), nodes must communicate with their peers to use one of the routing protocols. Safe routing and secure data forwarding are two approaches to routing security used in EMAs. Secure routing necessitates node collaboration to share accurate routing information and keep the network connected. Secure data forwarding requires the protection of data packets from corruption, dropping, and manipulation by an untrusted source.

6.2.4. Secure Localization. The positional information of nodes mounted on animals and floating in water sources is critical in mobile-based sensor deployments such as animal tracking and water quality monitoring. For example, in the case of animal tracking, the location of endangered species such as turtles, elephants, and others will provide information. Localization computes the location or position of sensor nodes in WSNs. Because of the dynamic nature of the applications, WSN deployment has shifted from static to dynamic (mobile). Because such networks are dynamic, node localization is also variable, making the process critical in WSNs. Knowledge of a network entity's physical location is useful in various applications. The primary factor in location determination is a group of particular nodes known as anchor/beacon nodes, which are resource privileged and have more excellent storage and computing capacity. Other unknown nodes calculate their position in various ways based on the location of anchor/beacon nodes. As a result, malicious anchor/beacon nodes must be prevented from providing false location information, as unknown nodes rely entirely on them to compute their position [95].

6.2.5. Cryptographic Algorithms. The communication infrastructure (radios in the network) in WSNs for EMAs may also be compromised. If the radio is compromised, it will no longer be able to securely communicate the data obtained from the sensor nodes. Furthermore, the data obtained from the sensor nodes may necessitate additional security at the base station and backup systems if the base station is attacked. As a result, using cryptographic algorithms to provide the desired security is critical. Cryptographic algorithms are methods and procedures for securing a system linked with keys. The crypto security of an environmental monitoring application against attacks and malicious infiltration can be defined by two factors: (1) the strength of the keys and the efficiency of procedures and protocols associated with the keys and (2) the protection of the keys through key management (secure key generation, storage, distribution, use, and destruction). Poor algorithms embedded in a robust key management framework are just as likely as good algorithms embedded in a weak key management framework to fail. Data encryption, authentication, and digital signatures are tasks that require using cryptographic algorithms [96].

6.3. Challenges of WSNs for EMAs. Wireless sensor networks' intense constraints and demanding application environments make computer security for such systems more complicated than traditional networks. Some challenges, like most systems, have a negative impact on the system's operations and resources. WSNs are not immune to challenges, particularly in terms of security. Wireless communication is less secure due to its distributed nature, allowing easy interception. An adversary can easily intercept, change, or rerun any message. An attacker can easily intercept legal packets and inject malicious ones [97].

6.3.1. Constrained Resources. A constrained resource is one in which you have a finite supply. Sensor nodes in WSNs are subject to resource constraints such as limited power, restricted communication bandwidth, limited processing capability, and limited storage capacity due to their varying sizes and cost. Wireless channels in the network are typically unstable when sensor data is shared among nodes or transferred for data processing, resulting in unpredictable transmission delays and packet losses. Energy constraints, for example, require strategies to save energy to enable nodes to operate for a longer time since sensor nodes mainly rely on batteries. The deployment type also affects the communication and connectivity between nodes in the network. This challenge also requires optimal node deployment schemes to ensure effective communication among the nodes in the network in EMAs.

6.3.2. Node Failure. Sensor nodes are the main components of the wireless sensor network for environmental monitoring applications. They operate unattended and are capable of adapting to their deployable environment. Due to its size, it comes with stringent energy requirements because, on most occasions, the nodes are not inaccessible to humans. Hence, its battery and other hardware cannot fail to operate since monitoring will not be possible. Sensor nodes comprise sensing, energy, transceiver, and processing units. The node fails to operate if any of these components fail, affecting the overall network's operation. In EMAs, node failure means no sensing can occur, and there will be an optimal communication medium [93].

6.3.3. Network Converge and Fault Tolerance. Typically, sensor nodes fail because of a lack of power, physical harm, or environmental interferences, and such failures should not impact the WSN's intended mission. Fault tolerance refers to a WSN's capacity to maintain sensor functionality in the face of node failures. Fault-tolerance protocols and algorithms must be designed to handle their specified performance levels. For example, tolerance can be minimal in a

house, but tolerance levels must be quite high for environmental monitoring to maintain operation [98].

6.3.4. Data Privacy. Data privacy is the ability to control when, how, and to what extent data or information is shared or divulged to others. WSNs in EMAs, like most data systems, collect sensitive information, necessitating the need to protect its privacy, which in turn protects its confidentiality. However, the data collected by the sensors can be obtained by an attacker using a powerful receiver, resulting in a privacy breach [99]. Furthermore, a hacker can quickly introduce harmful messages into the network by using wireless communication, allowing easy eavesdropping and potentially breaching data privacy.

6.3.5. Location and Positioning of Nodes. Localization techniques are critical in applications such as animal tracking, where the location of the animals at a given time is required, particularly in the case of endangered species. Localization is a technique used in WSNs for EMAs to determine the location of sensor nodes. WSNs are thousands of tiny nodes, making GPS installation on each sensor node impractical. Furthermore, even when GPS is installed on sensor nodes, it does not provide ideal localization results. Establishing location references on each sensor node in a dense network is practically impossible [100]. It thus creates a problematic situation in which the sensor nodes must define their current position without the support of any special equipment such as a global positioning system.

6.3.6. Propagation Delay. The nodes in EMAs are strategically placed throughout the deployment area to achieve detection and identification probabilities close to 100% for specified parameters [101]. However, even when the nodes detect the required parameters, propagation delays affect their transmission during in-node or in-network communication and a node sink communication. The propagation delay is the time it takes packets to travel through the transmission medium and is limited by the speed of light. For example, if the source and destination are both in the same deployment area or region but are 100 meters apart, the propagation delay can be estimated to be 1 microsecond. If they are separated by 500 meters in a different deployment environment, the delay can be estimated to be 0.1 seconds [102]. Factors influencing node propagation with underwater nodes differ from those influencing node propagation with tracking animals on land in environmental monitoring applications. As a result, the number of packets transmitted between the source and destination nodes may vary depending on the environment and channel conditions. Delays in packet transmission have serious consequences for WSNs used in environmental monitoring applications that require a response time of fewer than 200 milliseconds. When the propagation delay exceeds the threshold in such applications as forest fire monitoring, battlefield, and freshwater quality, it may affect stakeholders' decisions to avoid the effects if no such delays occur.

7. Conclusion

The applications of WSN technology for environmental monitoring have been discussed in this paper. The paper reviewed vital protocols used in WSNs for EMAs, focusing on some protocols in the WSN protocol stack. Given the importance of security in environmental monitoring applications, this review discussed wireless sensor network routing protocols, security implementations, the types of security threats in environmental monitoring applications, node and network security practices, and some suggested WSN challenges for EMAs. Researchers interested in designing protocols at the physical, data link, and network layers should consider the type of applications and the associated peculiarities. The paper also examines some essential protocols researchers use to track animals, water quality, and forest health.

Data Availability

No data is available.

Conflicts of Interest

The authors declare that there is no conflict of interest regarding the publication of this paper.

Acknowledgments

This work was funded in part by the BANGA-AFRICA, University of Ghana, under the Seed Research Grant UG-BA/SRG-001/2022.

References

[1] K. S. Adu-Manu, C. Tapparello, W. Heinzelman, F. A. Katsriku, and J.-D. Abdulai, "Water quality monitoring using wireless sensor networks," *ACM Transactions on Sensor Networks*, vol. 13, no. 1, pp. 1–41, 2017.

[2] W. Honghui, T. Xianguo, L. Yan et al., "Research of the hardware architecture of the geohazards monitoring and early warning system based on the IoT," *Procedia Computer Science*, vol. 107, pp. 111–116, 2017.

[3] B. Jiang, G. Huang, T. Wang, J. Gui, and X. Zhu, "Trust based energy efficient data collection with unmanned aerial vehicle in edge network," *Transactions on Emerging Telecommunications Technologies*, vol. 33, no. 6, article 3942, 2020.

[4] S. Bader, *Enabling autonomous environmental measurement systems with low-power wireless sensor networks terms with low-power wireless sensor networks, [Ph.D. thesis]*, Mid Sweden University, Faculty of Science, Technology and Media, Department of Information Technology and Media, Sweden, 2011.

[5] M. Keerthika and D. Shanmugapriya, "Wireless sensor networks: active and passive attacks - vulnerabilities and countermeasures," *Global Transitions Proceedings*, vol. 2, no. 2, pp. 362–367, 2021.

[6] M. Almazaideh and J. Levendovszky, "Novel reliable and energy-efficient routing protocols for wireless sensor networks," *Journal of Sensor and Actuator Networks*, vol. 9, no. 1, 2020.

[7] F. Engmann, K. S. Adu-Manu, J.-D. Abdulai, and F. A. Katsriku, *Applications of prediction approaches in wireless sensor networks*, IntechOpen, London, 2021.

[8] H. M. A. Fahmy, "Energy harvesting projects for WSNs," in *Wireless Sensor Network*, Springer, Cham, 2020.

[9] M. Y. Arafat, M. A. Habib, and S. Moh, "Routing protocols for UAV-aided wireless sensor networks," *Applied Sciences*, vol. 10, no. 12, p. 4077, 2020.

[10] I. Daanoune, B. Abdennaceur, and A. Ballouk, "A comprehensive survey on LEACH-based clustering routing protocols in wireless sensor networks," *Ad Hoc Networks*, vol. 114, article 102409, 2021.

[11] Y. Jia, "LoRa-based WSNs construction and low-power data collection strategy for wetland environmental monitoring," *Wireless Personal Communications*, vol. 114, no. 2, pp. 1533–1555, 2020.

[12] O. I. Khalaf and G. M. Abdulsahib, "Energy efficient routing and reliable data transmission protocol in WSN," *International Journal of Advances in Soft Computing and Its Applications*, vol. 12, no. 3, pp. 45–53, 2020.

[13] V. Pandiyaraju, R. Logambigai, S. Ganapathy, and A. Kannan, "An energy efficient routing algorithm for WSNs using intelligent fuzzy rules in precision agriculture," *Wireless Personal Communications*, vol. 112, no. 1, pp. 243–259, 2020.

[14] K. S. Adu-Manu, N. Adam, C. Tapparello, H. Ayatollahi, and W. Heinzelman, "Energy-harvesting wireless sensor networks (EH-WSNs)," *ACM Transactions on Sensor Networks (TOSN)*, vol. 14, no. 2, pp. 1–50, 2018.

[15] F. Engmann, F. A. Katsriku, J.-D. Abdulai, and K. S. Adu-Manu, "Reducing the energy budget in WSN using time series models," *Wireless Communications and Mobile Computing*, vol. 2020, Article ID 8893064, 15 pages, 2020.

[16] A. Kochhar, P. Kaur, P. Singh, and S. Sharma, "Protocols for wireless sensor networks: a survey," *Journal of Telecommunications and Information Technology*, vol. 1, no. 2018, pp. 77–87, 2018.

[17] K. Sohraby, D. Minoli, and T. Znati, *Wireless sensor networks: technology, protocols, and applications*, John wiley & Sons, United States, 2007.

[18] M. Elhoseny, A. E. Hassanien, M. Elhoseny, and A. E. Hassanien, "Secure data transmission in WSN: an overview," *Studies in Systems, Decision and Control*, vol. 165, pp. 115–143, 2019.

[19] J. Yang, *Design and implementation of large-scale wireless sensor networks for environmental monitoring applications*, University of North Texas, United States, 2010.

[20] A. Sarkar and T. Senthil Murugan, "Routing protocols for wireless sensor networks: what the literature says?," *Alexandria Engineering Journal*, vol. 55, no. 4, pp. 3173–3183, 2016.

[21] B. Abidi, A. Jilbab, and M. E. Haziti, "Routing protocols for wireless sensor networks: a survey," in *Advances in Ubiquitous Computing*, pp. 3–15, Academic Press, United States, 2020.

[22] N. Shabbir and S. R. Hassan, "Routing protocols for wireless sensor networks (WSNs)," in *Wireless Sensor Networks - Insights and Innovations*, Intecopen Science, 2017.

[23] S. Arjunan and P. Sujatha, "Lifetime maximization of wireless sensor network using fuzzy based unequal clustering and ACO based routing hybrid protocol," *Applied Intelligence*, vol. 48, no. 8, pp. 2229–2246, 2018.

[24] U. Draz, A. Ali, M. Bilal et al., "Energy efficient proactive routing scheme for enabling reliable communication in underwater Internet of Things," *IEEE Transactions on Network Science and Engineering*, vol. 8, no. 4, pp. 2934–2945, 2021.

[25] D. Kothandaraman, S. Naik Korra, A. Balasundaram, and S. Magesh Kumar, "Sequence number based secure routing algorithm for IoT networks," *Materials Today: Proceedings*, 2021.

[26] F. Tabbana, "Performance analysis of AODVDSDV and ZRP routing protocols," *Wireless Sensor Networks using NS2 Tool*, vol. 10, pp. 279–297, 2020.

[27] K. S. Adu-Manu, F. Katsriku, J.-D. Abdulai, J. M. Gómez, and W. Heinzelmann, "Network lifetime maximization with adjustable node transmission range," in *Smart Cities/Smart Regions–Technische, wirtschaftliche und gesellschaftliche Innovationen*, pp. 693–707, Springer Vieweg, Wiesbaden, 2019.

[28] O. A. Osanaiye, O. O. Ogundile, and F. Aina, "Evaluating DoS jamming attack on reactive routing protocol in wireless sensor networks," *African Journal of Science, Technology, Innovation and Development*, pp. 1–8, 2021.

[29] P. Sarao, "Ad hoc on-demand multipath distance vector based routing in ad-hoc networks," *The Journal of Communication*, vol. 14, no. 4, pp. 2953–2953, 2019.

[30] L. Chan, K. Gomez Chavez, H. Rudolph, and A. Hourani, "Hierarchical routing protocols for wireless sensor network: a compressive survey," *Wireless Networks*, vol. 26, no. 5, pp. 3291–3314, 2020.

[31] A. K. Singh, A. Bhalla, P. Kumar, and M. Kaushik, "Hierarchical routing protocols in WSN: a brief survey," in *2017 3rd International Conference on Advances in Computing, Communication & Automation (ICACCA)(Fall)*, pp. 1–6, Dehradun, India, September 2017.

[32] K. Haseeb, N. Islam, A. Almogren, I. U. Din, H. N. Almajed, and N. Guizani, "Secret sharing-based energy-aware and multi-hop routing protocol for IoT based WSNs," *IEEE Access*, vol. 7, pp. 79980–79988, 2019.

[33] A. Ghaffari and H. R. Bannaeian, "QoS-based routing protocols for wireless sensor networks: a survey," *World Applied Sciences Journal*, vol. 14, no. 6, pp. 866–875, 2011.

[34] R. Zagrouba and A. Kardi, "Comparative study of energy efficient routing techniques in wireless sensor networks," *Information*, vol. 12, no. 1, p. 42, 2021.

[35] J. N. Al-Karaki and A. E. Kamal, "A taxonomy of routing techniques in wireless sensor networks," in *Handbook of Sensor Networks: Compact Wireless and Wired Sensing Systems*, pp. 116–139, CRC Press, 2004.

[36] F. Lakrami, N. Elkamoun, and M. E. Kamili, "Advances in ubiquitous networking," *Lecture Notes in Electrical Engineering*, vol. 366, pp. 287–300, 2016.

[37] B. Bhushan and G. Sahoo, "Routing protocols in wireless sensor networks," *Studies in Computational Intelligence*, vol. 776, 2019.

[38] J. J. Cancela, M. Fandiño, B. J. Rey, and E. M. Martínez, "Automatic irrigation system based on dual crop coefficient, soil and plant water status for *Vitis vinifera* (cv Godello and cv Mencía)," *Agricultural Water Management*, vol. 151, pp. 52–63, 2015.

[39] M. Usha Rani and S. Kamalesh, "Energy efficient fault tolerant topology scheme for precision agriculture using wireless

sensor network," in *2014 IEEE International Conference on Advanced Communications, Control and Computing Technologies*, pp. 1208–1211, Ramanathapuram, India, May 2014.

[40] M. Gameil and T. Gaber, "Wireless sensor networks-based solutions for cattle health monitoring: a survey," in *International Conference on Advanced Intelligent Systems and Informatics*, pp. 779–788, Springer, Cham, 2020.

[41] B. Sharma and D. Koundal, "Cattle health monitoring system using wireless sensor network: a survey from innovation perspective," *IET Wireless Sensor Systems*, vol. 8, no. 4, pp. 143–151, 2018.

[42] Y. Liu and C. Bi, "The design of greenhouse monitoring system based on ZigBee WSNs," in *2017 IEEE international conference on computational science and engineering (CSE) and IEEE international conference on embedded and ubiquitous computing (EUC)*, pp. 430–433, Guangzhou, China, 2017.

[43] Z. Yiming, Y. Xianglong, G. Xishan, Z. Mingang, and W. Liren, "A design of greenhouse monitoring & control system based on ZigBee wireless sensor network," in *2007 International Conference on wireless communications, networking and Mobile computing*, pp. 2563–2567, Shanghai, China, September 2007.

[44] T. Hidayat, R. Mahardiko, and S. T. D. Franky, "Method of systematic literature review for Internet of Things in ZigBee smart agriculture," *2020 8th International Conference on Information and Communication Technology, ICoICT*, 2020, pp. 20–23, Yogyakarta, Indonesia, 2020.

[45] S. Cecchi, S. Spinsante, A. Terenzi, and S. Orcioni, "A smart sensor-based measurement system for advanced bee hive monitoring," *Sensors*, vol. 20, no. 9, p. 2726, 2020.

[46] L. Joris, F. Dupont, P. Laurent, P. Bellier, S. Stoukatch, and J. M. Redoute, "An autonomous Sigfox wireless sensor node for environmental monitoring," *IEEE Sensors Letters*, vol. 3, no. 7, pp. 01–04, 2019.

[47] S. Gil-Lebrero, F. J. Quiles-Latorre, M. Ortiz-López, V. Sánchez-Ruiz, V. Gámiz-López, and J. J. Luna-Rodríguez, "Honey bee colonies remote monitoring system," *Sensors*, vol. 17, no. 1, 2016.

[48] S. S. Reka, B. K. Chezian, and S. S. Chandra, "A novel approach of IoT-based smart greenhouse farming system," in *Green Buildings and Sustainable Engineering*, Springer, 2019.

[49] M. Y. Cheng, K. C. Chiu, Y. M. Hsieh, I. T. Yang, J. S. Chou, and Y. W. Wu, "BIM integrated smart monitoring technique for building fire prevention and disaster relief," *Automation in Construction*, vol. 84, pp. 14–30, 2017.

[50] S. Kaushik and C. Singh, "Monitoring and controlling in food storage system using wireless sensor networks based on Zigbee & Bluetooth modules," *International Journal of Multidisciplinary in Cryptology and Information Security*, vol. 2, no. 3, pp. 7–10, 2013, http://warse.org/pdfs/ijmcis01232013.pdf.

[51] S. Aram, A. Troiano, F. Rugiano, and E. Pasero, "Low power and Bluetooth-based wireless sensor network for environmental sensing using smartphones," in *Artificial Intelligence Applications and Innovations*, pp. 332–340, Springer, 2012.

[52] P. Di Gennaro, D. Lofú, D. Vitanio, P. Tedeschi, and P. Boccadoro, "WaterS: a Sigfox-compliant prototype for water monitoring," *Internet Technology Letters*, vol. 2, no. 1, article e74, 2019.

[53] F. Pitu and N. C. Gaitan, "Surveillance of SigFox technology integrated with environmental monitoring," in *2020 15th International Conference on Development and Application Systems, DAS 2020 - Proceedings*, pp. 69–72, Suceava, Romania, 2020.

[54] A. Chehri and R. Saadane, "Zigbee-based remote environmental monitoring for smart industrial mining," in *SCA2019: The Fourth International Conference on Smart City Applications*, pp. 2–7, Casablanca Morocco, 2019.

[55] M. Dangana, S. Ansari, Q. H. Abbasi, S. Hussain, and M. A. Imran, "Suitability of NB-IoT for indoor industrial environment: a survey and insights," *Sensors*, vol. 21, no. 16, p. 5284, 2021.

[56] S. Duangsuwan, A. Takarn, R. Nujankaew, and P. Jamjareegulgarn, "A study of air pollution smart sensors LPWAN via NB-IoT for Thailand smart cities 4.0," *2018 10th International Conference on Knowledge and Smart Technology: Cybernetics in the Next Decades, KST*, 2018, pp. 206–209, Chiang Mai, Thailand, 2018.

[57] M. Ibrahim, A. Elgamri, S. Babiker, and A. Mohamed, "Internet of Things based smart environmental monitoring using the Raspberry-Pi computer," *2015 5th International Conference on Digital Information Processing and Communications, ICDIPC*, 2015, pp. 159–164, Sierre, Switzerland, 2015.

[58] Y. Liu, A. Liu, N. Zhang, X. Liu, M. Ma, and Y. Hu, "DDC: dynamic duty cycle for improving delay and energy efficiency in wireless sensor networks," *Journal of Network and Computer Applications*, vol. 131, pp. 16–27, 2019.

[59] K. Lokesh Krishna, J. Madhuri, and K. Anuradha, "A ZigBee based energy efficient environmental monitoring alerting and controlling system," *2016 international conference on information communication and embedded systems, ICICES*, 2016, Chennai, India, 2016, 2016.

[60] J. A. Lossio-Ventura and H. Alatrista-Salas, "Information management and big data: SIMBig overview," in *6th International Conference, SIMBig 2019*, Lima, Peru, 2016.

[61] S. Zafar, G. Miraj, R. Baloch, D. Murtaza, and K. Arshad, "An IoT based real-time environmental monitoring system using Arduino and cloud service," *Engineering, Technology & Applied Science Research*, vol. 8, no. 4, pp. 3238–3242, 2018.

[62] G. G. Xie and J. H. Gibson, "A network layer protocol for UANs to address propagation delay induced performance limitations," *Oceans Conference Record (IEEE)*, vol. 4, no. - November, pp. 2087–2094, 2001.

[63] H. Yan, Z. J. Shi, and J. H. Cui, "DBR: depth-based routing for underwater sensor networks," *Networking 2008 Ad Hoc and Sensor Networks, Wireless Networks, Next Generation Internet*, vol. 4982, pp. 72–86, 2008.

[64] M. Zorzi, P. Casari, N. Baldo, and A. F. Harris, "Energy-efficient routing schemes for underwater acoustic networks," *IEEE Journal on Selected Areas in Communications*, vol. 26, no. 9, pp. 1754–1766, 2008.

[65] A. A. Ahmed and N. Fisal, "A real-time routing protocol with load distribution in wireless sensor networks," *Computer Communications*, vol. 31, no. 14, pp. 3190–3203, 2008.

[66] A. Ali Ahmed, "An enhanced real-time routing protocol with load distribution for mobile wireless sensor networks," *Computer Networks*, vol. 57, no. 6, pp. 1459–1473, 2013.

[67] G. Sakya and V. Sharma, "ADMC-MAC: energy efficient adaptive MAC protocol for mission critical applications in WSN," *Sustainable Computing: Informatics and Systems*, vol. 23, pp. 21–28, 2019.

[68] D. K. Sah and T. Amgoth, "Renewable energy harvesting schemes in wireless sensor networks: a survey," *Information Fusion*, vol. 63, pp. 223–247, 2020.

[69] H. Sharma, A. Haque, and Z. A. Jaffery, "Solar energy harvesting wireless sensor network nodes: a survey," *Journal of Renewable and Sustainable Energy*, vol. 10, no. 2, 2018.

[70] H. Sharma, A. Haque, and Z. A. Jaffery, "Maximization of wireless sensor network lifetime using solar energy harvesting for smart agriculture monitoring," *Ad Hoc Networks*, vol. 94, article 101966, 2019.

[71] S. M. Bozorgi, A. Shokouhi Rostami, A. A. R. Hosseinabadi, and V. E. Balas, "A new clustering protocol for energy harvesting-wireless sensor networks," *Computers and Electrical Engineering*, vol. 64, pp. 233–247, 2017.

[72] H. K. Qureshi, U. Saleem, M. Saleem, A. Pitsillides, and M. Lestas, "Harvested energy prediction schemes for wireless sensor networks: performance evaluation and enhancements," *Wireless Communications and Mobile Computing*, vol. 2017, 14 pages, 2017.

[73] T. Xie, G. Zhang, H. Liu, F. Liu, and P. Du, "A hybrid forecasting method for solar output power based on variational mode decomposition, deep belief networks and autoregressive moving average," *Applied Sciences*, vol. 8, no. 10, p. 1901, 2018.

[74] A. G. Salman and B. Kanigoro, "Visibility forecasting using autoregressive integrated moving average (ARIMA) models," *Procedia Computer Science*, vol. 179, no. 2019, pp. 252–259, 2021.

[75] M. Prauzek, N. R. A. Mourcet, J. Hlavica, and P. Musilek, "Q-learning algorithm for energy management in solar powered embedded monitoring systems," in *2018 IEEE Congress on Evolutionary Computation, CEC 2018 - Proceedings*, Rio de Janeiro, Brazil, 2018.

[76] H. X. Zou, L. C. Zhao, Q. H. Gao et al., "Mechanical modulations for enhancing energy harvesting: principles, methods and applications," *Applied Energy*, vol. 255, article 113871, 2019.

[77] V. Larnaudie, M. D. Ferrari, and C. Lareo, "Switchgrass as an alternative biomass for ethanol production in a biorefinery: perspectives on technology, economics and environmental sustainability," *Renewable and Sustainable Energy Reviews*, vol. 158, article 112115, 2022.

[78] J. Singh, R. Kaur, and D. Singh, "Energy harvesting in wireless sensor networks: a taxonomic survey," *International Journal of Energy Research*, vol. 45, no. 1, pp. 118–140, 2021.

[79] B. Paharia and K. Bhushan, "A comprehensive review of distributed denial of service (DDoS) attacks in fog computing environment," in *Handbook of Computer Networks and Cyber Security: Principles and Paradigms*, Springer, 2019.

[80] K. S. Adu-manu, *A study into lifetime maximization of wireless sensor networks for water quality monitoring, [Ph.D. thesis]*, University of Ghana, 2020.

[81] W. Tiberti, F. Caruso, L. Pomante, M. Pugliese, M. Santic, and F. Santucci, "Development of an extended topology-based lightweight cryptographic scheme for IEEE 802.15.4 wireless sensor networks," *International Journal of Distributed Sensor Networks*, vol. 16, no. 10, Article ID 155014772095167, 2020.

[82] C. Mallick and S. Satpathy, "Challenges and design goals of wireless sensor networks: a sate-of-the-art challenges and design goals of wireless sensor networks: a sate-of-the-art review," *International Journal of Computer Applications*, vol. 179, no. 28, pp. 42–47, 1970.

[83] J. Hou and Y. Zhang, "Mobile-service based approach for topology control of wireless sensor networks," *Wireless Personal Communications*, vol. 102, no. 2, pp. 1839–1851, 2018.

[84] G. M. E. Rahman and A. W. Khan, "LDAP: lightweight dynamic auto-reconfigurable protocol in an IoT-enabled WSN for wide-area remote monitoring," *Remote Sensing*, vol. 12, no. 19, p. 3131, 2020.

[85] A. Sobchuk, Y. Kravchenko, M. Tyshchenko, P. Gawliczek, and O. Afanasyeva, "Analytical aspects of providing a feature of the functional stability according to the choice of technology for construction of wireless sensor networks," in *2019 IEEE International Conference on Advanced Trends in Information Theory (ATIT)*, pp. 102–106, Kyiv, Ukraine, 2019.

[86] M. Dong, H. Li, Y. Li, Y. Deng, and R. Yin, "Fault-tolerant topology with lifetime optimization for underwater wireless sensor networks," *Sādhanā*, vol. 45, no. 1, 2020.

[87] R. Jadhav and V. Vatsala, "Security issues and solutions in wireless sensor networks," *International Journal of Computer Applications*, vol. 162, no. 2, pp. 14–19, 2017.

[88] V. Ekong and U. Ekong, "A survey of security vulnerabilities in wireless sensor networks," *Nigerian Journal of Technology*, vol. 35, no. 2, p. 392, 2016.

[89] J. Bhola, S. Soni, and G. K. Cheema, "Recent trends for security applications in wireless sensor networks - a technical review," in *Proceedings of the 2019 6th International Conference on Computing for Sustainable Global Development, INDIACom 2019*, pp. 707–712, New Delhi, India, 2019.

[90] S. Roy, M. Conti, S. Setia, and S. Jajodia, "Secure data aggregation in wireless sensor networks," *Networks*, vol. 7, no. 3, pp. 1040–1052, 2012.

[91] A. Aseeri and R. Zhang, "Secure data aggregation in wireless sensor networks: enumeration attack and countermeasure," in *ICC 2019 - 2019 IEEE International Conference on Communications (ICC)*, Shanghai, China, 2019.

[92] S. Ozdemir and Y. Xiao, "Secure data aggregation in wireless sensor networks: a comprehensive overview," *Computer Networks*, vol. 53, no. 12, pp. 2022–2037, 2009.

[93] A. J. Watt, M. R. Phillips, C. E. Campbell, I. Wells, and S. Hole, "Wireless sensor networks for monitoring underwater sediment transport," *Science of the Total Environment*, vol. 667, pp. 160–165, 2019.

[94] A. Razaque and S. S. Rizvi, "Secure data aggregation using access control and authentication for wireless sensor networks," *Computers & Security*, vol. 70, pp. 532–545, 2017.

[95] M. B. Shanthi and D. K. Anvekar, "Secure localization for underwater wireless sensor networks based on probabilistic approach," in *Proceedings of 2018 2nd International Conference on Advances in Electronics, Computers and Communications, ICAECC 2018*, pp. 1–6, Bangalore, India, 2018.

[96] E. Barker and Q. Dang, *Recommendation for key management – part 3: application-specific key management guidance*, vol. 800-57, NIST Special Publication, 2007.

[97] V. Kumar, A. Jain, and P. N. Barwal, "Wireless sensor networks: security issues, challenges and solutions," *International Journal of Information & Computation Technology*, vol. 4, no. 8, pp. 859–868, 2014, http://www.irphouse.com.

[98] C. S. Kingsly and J. G. C. Chandran, "Critical study on constraints in wireless sensor network applications,"

International Journal of Engineering Research & Technology, vol. 2, no. 7, pp. 1311–1316, 2013.

[99] N. Sharma and R. Bhatt, "Privacy preservation in WSN for healthcare application," *Procedia Computer Science*, vol. 132, pp. 1243–1252, 2018.

[100] J. Kuriakose, S. Joshi, R. Vikram Raju, and A. Kilaru, "A review on localization in wireless sensor networks," *Adv. Intell. Syst. Comput.*, vol. 264, pp. 599–610, 2014.

[101] A. J. Garcia-Sanchez, F. Garcia-Sanchez, F. Losilla et al., "Wireless sensor network deployment for monitoring wildlife passages," *Sensors*, vol. 10, no. 8, pp. 7236–7262, 2010.

[102] S. Khanvilkar, F. Bashir, D. Schonfeld, and A. Khokhar, "Multimedia networks and communication," in *The Electrical Engineering Handbook*, pp. 401–425, University of Illinois, Chicago, 2005.

Hindawi
Journal of Sensors
Volume 2022, Article ID 3314881, 16 pages
https://doi.org/10.1155/2022/3314881

Research Article

Tenant-Centric Attribute Semantic Access Control Policy Model for the Cloud Service Platform

Yang Yu,[1,2] **Linfu Sun**,[1,2] **and Shuhai Wang**[1,2]

[1]*School of Computing and Artificial Intelligence, Southwest Jiaotong University, Chengdu 611756, China*
[2]*Manufacturing Industry Chain Collaboration and Information Support Technology Key Laboratory of Sichuan Province, Southwest Jiaotong University, Chengdu 610031, China*

Correspondence should be addressed to Linfu Sun; slxbr615765@163.com

Received 16 March 2022; Accepted 21 April 2022; Published 4 July 2022

Academic Editor: Yuan Li

In the open Internet environment, there is a cross-platform access control problem that when a tenant needs to access the business resources of other collaborative platforms through the cloud service platform, the cloud service platform only supports the tenant to access the business resources within the platform. When tenants need to access business resources through the cloud service platform, the authorization method of the cloud service platform is static and the authorization granularity is coarse-grained, so dynamic fine-grained authorization is not supported. To solve the above problems, based on ABAC, this paper proposes a tenant-centric attribute semantic access control policy model for cloud service platforms. The model and its application framework can automatically evaluate whether it has cloud service platform or cross-platform access control rights according to the change of the tenant's attributes so as to determine whether it can obtain the corresponding business resources. Through a practical case analysis, we prove that the application of ASACPM and its application framework to the cloud service platform have good flexibility, scalability, and practicability. In addition, we design some experimental scenarios to verify that the performance of ASACPM and its application framework meet our expectations and have good reliability, validity, and rationality.

1. Introduction

The cloud computing is an emerging business computing model that uses the Internet to access shared basic resources anytime, anywhere, on-demand, and conveniently, which is regarded as a major innovation in the information industry and has received widespread attention from the academia, industry, and business community [1, 2]. At the same time, it is also a challenging field that covers all aspects of the information industry and is driving the transformation of information technology to socialization, intensification, and specialization. The governments, hospitals, research institutions, and industry giants use cloud computing to solve their growing computing and storage problems [3, 4].

The cloud service platform (CSP) is a third-party public service platform that draws on the idea of cloud computing and uses software as a service (SaaS) as its core application mode, which adopts information technology and Internet of Things technology to share the business resources (i.e., business data, business processes, and business services) of different enterprises to different tenants, thus breaking the "information island" [5, 6]. The CSP hosts data, services, and applications for tenants in the pay-as-you-go feature, breaking the traditional service mode and automatically allocating business resources according to tenant needs, thereby saving enterprise costs, lowering information thresholds, and enjoying professional information services [7, 8]. The CSP builds an application environment based on a flexible and scalable multitenant architecture feature to meet the diverse application needs and personalized form requirements of tenants [9, 10].

In the open Internet environment, the application mode and characteristics of CSP bring the following problems: first, when tenants access business resources of other collaborative platforms, CSP only supports tenants to access business resources within the platform, so there is a problem of

cross-platform access control. For example, CSP and other collaborative platforms all adopt the traditional access control model, and it is impossible for CSP tenants to access the business resources of other collaborative platforms and vice versa. Second, when tenants access business resources, the CSP authorization method is static and the authorization granularity is coarse-grained, so dynamic fine-grained authorization is not supported. For example, the type of enterprise, role category, and collaboration relationship all change dynamically with the increase or decrease of enterprises in the enterprise alliance, and the permissions of enterprises to access CSP (that is, grant or cancel permissions) should have changed dynamically, but in fact, the existing CSP is to preset the permissions of tenants. The platform cannot automatically adjust the corresponding access permissions according to the changes of the properties of the tenants, and the granularity of authorization is coarse-grained.

Third, CSP has many characteristics, such as many types of enterprises, large number of tenants, wide range of roles, and complex and dynamic collaboration relationship, which pose new challenges for CSP to build an access control model.

In order to solve the above problems, based on attribute-based access control (ABAC) [5, 10], this paper proposes a tenant-centric attribute semantic access control policy model (ASACPM) for the CSP. In ASACPM, access requests, access decisions, and evaluation results are formally described through attribute semantics, where access request is used to describe the requester, requested business resources, current environment, credentials and access methods, etc., and access decision is used to evaluate the adaptation result of the access request and the policy set, and the evaluation result is used to determine whether the tenant can access the service resource. In the application framework of ASACPM, the access decision mechanism is used to evaluate whether the tenant has CSP or cross-platform access control rights, the attribute synchronization mechanism is used to ensure the consistency of the AA of CSP and the AA of collaborative platform (CP), and the dynamic fine-grained authorization mechanism ensures that the CSP has better flexibility and scalability.

2. Related Work

This section focuses on reviewing and analyzing the recent academic results of traditional access control models and attribute-based access control models. The traditional access control model is divided into the following three categories according to the authorization method: the discretionary access control (DAC) model, the mandatory access control (MAC) model, and the role-based access control (RBAC) model [11, 12] The traditional access control model is based on the identities or fixed identifiers and is suitable for the centralized and closed network environments. According to the application mode and characteristics of the CSP, the traditional access control model is difficult to adapt to the open and shared Internet environment.

In recent years, domestic and foreign scholars have carried out a lot of research on the traditional access control model, and based on this, combined with the characteristics of cloud computing or cloud services, some improved access control models are put forward. Reference [13] proposed an emergency-RBAC (E-RBAC) model, which controlled the system in emergency situations according to the model constraints. Taking medical and dispensing scenarios as examples, the effectiveness of the model was verified. Reference [14] proposed a cloud computing access control model based on RBAC, which introduced the dynamic variable mechanism and security level into the access control strategy, improving the security and flexibility of access control to a certain extent. Reference [15] introduced the concept of trust degree into the RBAC model and proposed a dynamic RBAC model based on trust in cloud computing environment, which first gave the calculation method of trust degree and then assigned permissions to users according to their role information and trust degree, improving the security of cloud resource or service access process. However, the above references [13–15] did not give a cross-domain or cross-platform access control method. Reference [16] proposed an adaptive model based on cloud computing environment on the basis of RBAC model, which solved the problem of dynamic change of roles, but the access request of the model was relatively high in the process of dynamic role transformation. Reference [17] proposed a fine-grained access control mechanism in the cloud computing environment, which was used to deal with the dynamic changes of user permissions, but it was difficult to manage and control permissions in the face of dynamic changes of multiple types of roles and reduce the flexibility and scalability of the cloud computing platform. Reference [18] proposed a role-based access control model using smart contracts, which utilized the smart contract technology of Ethereum to realize the cross-organizational utilization of roles and ensured the security and adaptability of the platform. However, the corresponding permissions cannot be automatically adapted according to the needs of tenants. Although the above references improve the traditional access control model, it is still not fully suitable for building a dynamic and fine-grained access control model.

In the aspect of the attribute-based access control model, reference [19] proposed a fine-grained access control scheme based on ciphertext policy attribute encryption (CPABE) and trusted execution environment (TEE), which could be used to mitigate sensitive information attacks and improve confidentiality, but this scheme did not consider cross-domain or cross-platform access control methods. Reference [20] proposed an attribute-based access control policy model and gave definition, decision-making process, and access control policy of the model, but how to implement the model was not described in detail. Reference [21] proposed a new decentralized access control scheme for secure data storage in clouds that supported anonymous authentication, which could effectively protect the privacy of the data, but it did not involve cross-domain or cross-platform data storage. Reference [22] proposed a new distributed access control scheme, which supported the storage security of anonymous

users to verify data, prevented replay attacks, and supported the creation, modification, and reading of data stored in the cloud; however, the scheme did not involve cross-domain or cross-platform data storage. Reference [23] proposed an access control architecture model for restricted medical resources in IoT, which provided authorized users with fine-grained access to services based on policies while protecting valuable resources from unauthorized access. Although the above references improve the attribute-based access control model, it is also not fully applicable to constructing a dynamic and fine-grained access control model.

In summary, in the Internet environment, it is a series of challenging problems to research and meet the access control requirements of different tenants, explore the access decision mechanism and dynamic fine-grained authorization mechanism, and realize the cross-platform access control of tenants. Therefore, this paper solves the above problems by building ASACM.

3. The Modeling Process of the ASACPM

3.1. Formal Definition of the ASACPM. In this section, the concepts of the ASACPM are defined and used throughout this paper. The ABAC does not directly define the authorization between the subjects and the objects but uses a multirelationship among the subject attributes, the object attributes, and the environment attributes to define the authorization. So far, there is no unified formal definition of the ABAC. This paper draws on the formal definition of the existing ABAC [5, 10] and then optimizes it based on this and finally gives the formal definition of the ASACPM.

Definition 1. The basic elements of ASACPM are composed of subject, object, environment, certificate, and action, among which subject refers to the tenant (i.e., the requester), object refers to the business resources of CSP or CP, environment refers to the context in which transactions are processed, certificate refers to the SSL certificate issued by certificate authority (CA), and action refers to the access mode of the tenant which is usually related to the object. Subject, object, and environment are represented by attributes (i.e., entities).

Definition 2. In the ASACPM, all entities are described by attributes. The attribute is a variable consisting of the specified data type and value field, which can be represented by $\mathrm{Att} = (\mathrm{attn}, \mathrm{type}, \mathrm{Val}, \mathrm{R}(\mathrm{Val}))$. Among them, attn indicates the attribute name, type indicates the data type, Val indicates the value range, and R(Val) indicates the relationship between different values as shown in Table 1. In Table 1, $\succ$ means precedence, $\succcurlyeq$ means inheritance, the meaning of $\prec$ and $\preccurlyeq$ is the opposite of $\succ$ and $\succcurlyeq$, Val means the value of the attribute, and $\mathrm{val}_1, \mathrm{val}_2 \in \mathrm{Val}$.

Definition 3. The attribute value pair (avp) represents the specific value of the attribute, which can be represented by $\mathrm{avp} = (\mathrm{attn}, =, \mathrm{val})$, and its mathematical expression is $\mathrm{attn} = \mathrm{val}$. In this paper, Savp, Oavp, and Eavp are used to represent the attribute value pairs of the subject, the object, and the environment, respectively.

Table 1: The relationship between different values.

Relationship	Mathematical expression
Comparative relationship	$\mathrm{R}(\mathrm{Val}) = \{(\mathrm{val}_1 \bowtie_c \mathrm{val}_2) \mid \bowtie_c \in \{\leq, <, \geq, >, \neq, =\}\}$
Partial ordering relation	$\mathrm{R}(\mathrm{Val}) = \{(\mathrm{val}_1 \bowtie_p \mathrm{val}_2) \mid \bowtie_p \in \{\preccurlyeq, \prec, \succcurlyeq, \succ, \neq, =\}\}$

Definition 4. The attribute predicate value pair (apvp) can be represented by $\mathrm{apvp} = (\mathrm{attn}, \bowtie_r, \mathrm{val})$. Among them, $\bowtie_r \in \{\leq, <, \geq, >, \neq, =, \preccurlyeq, \prec, \succcurlyeq, \succ\}$ is a relational expression operator to limit the range of values of the attribute. Its mathematical expression is $\mathrm{attn} \bowtie_r \mathrm{val}$. In this paper, the Sapvp, Oapvp, and Eapvp are used to represent the attribute predicate value pairs of the subject, the object, and the environment, respectively.

Definition 5. The evaluation results of evaluating the apvp based on the avp are divided into three cases as shown in Table 2.

Definition 6. The tenant's standard access request (SAR) is defined as $\mathrm{SAR} = (\mathrm{s}, \mathrm{o}, \mathrm{e}, \mathrm{c}, \mathrm{a})$, where $\mathrm{s} = \{\mathrm{Savp}_1, \mathrm{Savp}_2, \cdots, \mathrm{Savp}_l\}$ represents the set of the Savp, $\mathrm{o} = \{\mathrm{Oavp}_1, \mathrm{Oavp}_2, \cdots, \mathrm{Oavp}_m\}$ represents the set of the Oavp, $\mathrm{e} = \{\mathrm{Eavp}_1, \mathrm{Eavp}_2, \cdots, \mathrm{Eavp}_n\}$ represents the set of the Eavp, *c* represents the tenant certificate, and *a* indicates the tenant's access method to the requested business resource, which includes browsing, adding, editing, deleting, and approving.

Definition 7. The ASACPM's policy is defined as $\mathrm{Pol} = (\mathrm{S}, \mathrm{O}, \mathrm{E}, \mathrm{C}, \mathrm{A}) \longrightarrow \mathrm{P}$, and the set of the policy is defined as $\mathrm{POL} = \{\mathrm{Pol}_1, \mathrm{Pol}_2, \cdots, \mathrm{Pol}_n\}$, where $\mathrm{S} = \{\mathrm{Sapvp}_1, \mathrm{Sapvp}_2, \cdots, \mathrm{Sapvp}_n\}$ represents the set of the Sapvp, $\mathrm{O} = \{\mathrm{Oapvp}_1, \mathrm{Oapvp}_2, \cdots, \mathrm{Oapvp}_n\}$ represents the set of the Oapvp, $\mathrm{E} = \{\mathrm{Eapvp}_1, \mathrm{Eapvp}_2, \cdots, \mathrm{Eapvp}_n\}$ represents the set of the Eapvp, $\mathrm{C} = \{\mathrm{C}_1, \mathrm{C}_2, \cdots, \mathrm{C}_n\}$ represents the set of the tenant certificate, $\mathrm{A} = \{\mathrm{A}_1, \mathrm{A}_2, \cdots, \mathrm{A}_n\}$ indicates the set of the access method (i.e., browsing, adding, editing, deleting, and approving), and $\mathrm{P} \in \{\mathrm{permit}, \mathrm{deny}\}$ represents the permission flag.

Definition 8. The evaluation results of evaluating the policy based on the SAR are divided into two cases as shown in Table 3.

When the Pol is applicable to the SAR (i.e., $[\mathrm{Pol}]_{\mathrm{SAR}} = \mathrm{True}$), since Pol's permission flag is $\mathrm{P} \in \{\mathrm{permit}, \mathrm{deny}\}$ (i.e., $[\mathrm{Pol}]_{\mathrm{SAR}} = \mathrm{True}$ has two states, the permissible state and the denial state), this paper defines the permissible state as $[\mathrm{Pol}]_{\mathrm{SAR}} = \mathrm{True}^+ = \mathrm{permit}$ and the denial state as $[\mathrm{Pol}]_{\mathrm{SAR}} = \mathrm{True}^- = \mathrm{deny}$. In Table 3, if the $[\mathrm{Pol}]_{\mathrm{SAR}}$ is true (i.e., $[\mathrm{Pol}]_{\mathrm{SAR}} = \mathrm{True}$), then the final evaluation results (FERs) of the $[\mathrm{Pol}]_{\mathrm{SAR}}$ refer to the cases 1 and 2 in Table 4, and if the $[\mathrm{Pol}]_{\mathrm{SAR}}$ is false (i.e., $[\mathrm{Pol}]_{\mathrm{SAR}} = \mathrm{False}$),

Table 2: The evaluation results of evaluating the apvp based on the avp.

Cases	Evaluation results
Case 1	Description: given avp and apvp, if their attribute names are the same and the value of the avp is within the range defined by the apvp, then the evaluation result of the avp on the apvp is true; otherwise, the evaluation result is false, and the mathematical expression is as follows: $[\text{apvp}]_{\text{avp}} = \begin{cases} \text{True}, (\text{avp.attn} = \text{apvp.attn}) \wedge (\text{avp.val} \in \text{apvp.val}) \\ \text{False, otherwise} \end{cases}$
Case 2	Description: given the set of the attribute value pairs $\text{AVP} = \{\text{avp}_1, \text{avp}_2, \cdots, \text{avp}_n\}$ and apvp, if $\exists \text{avp}_i \in \text{AVP}$ makes $[\text{apvp}]_{\text{avp}_i}$ true, then the evaluation result (i.e., $[\text{apvp}]_{\text{AVP}}$) of the AVP on the apvp is true; otherwise, the evaluation result is false, among which $i \in N^*$, and the mathematical expression is as follows: $[\text{apvp}]_{\text{avp}} = \begin{cases} \text{True}, \bigvee_{i=1}^{n} [\text{apvp}]_{\text{avp}_i \in \text{AVP}} = \text{True} \\ \text{False, otherwise} \end{cases}$
Case 3	Description: given AVP and the set of the attribute predicate value pairs $\text{APVP} = \{\text{apvp}_1, \text{apvp}_2, \cdots, \text{apvp}_n\}$, if $\forall \text{apvp}_i \in \text{APVP}$ makes $[\text{apvp}_i]_{\text{AVP}}$ true, then the evaluation result (i.e., $[\text{APVP}]_{\text{AVP}}$) of the AVP on the APVP is true; otherwise, the evaluation result is false, among which $i \in N^*$, and the mathematical expression is as follows: $[\text{APVP}]_{\text{AVP}} = \begin{cases} \text{True}, \bigwedge_{i=1}^{n} [\text{apvp}_i \in \text{APVP}]_{\text{AVP}} = \text{True} \\ \text{False, otherwise} \end{cases}$

Table 3: The evaluation results of evaluating the policy based on the SAR.

Cases	Evaluation results
Case 1: single policy	Description: given $\text{SAR} = (s, o, e, c, a)$ and $\text{Pol} = (S, O, E, C, A) \longrightarrow P$, if $[S]_s \wedge [O]_o \wedge [E]_e \wedge (c \in C) \wedge (a \in A)$ is true, then the evaluation result (i.e., $[\text{Pol}]_{\text{SAR}}$) of the SAR on Pol is true, namely, Pol applies to SAR. Otherwise, the evaluation result is false, namely, Pol does not applies to SAR; the mathematical expression is as follows: $[\text{Pol}]_{\text{SAR}} = \begin{cases} \text{True}, [S]_s \wedge [O]_o \wedge [E]_e \wedge (c \in C) \wedge (a \in A) = \text{True} \\ \text{False, otherwise} \end{cases}$
Case 2: policy set	Description: given $\text{SAR} = (s, o, e, c, a)$ and $\text{POL} = \{\text{Pol}_1, \text{Pol}_2, \cdots, \text{Pol}_n\}$, if $\exists \text{Pol}_i \in \text{POL}$ makes $[\text{Pol}_i]_{\text{SAR}}$ is true, then the evaluation result (i.e., $[\text{POL}]_{\text{SAR}}$) of SAR on POL is true, namely Pol_i in POL applies to SAR. Otherwise, the evaluation result is false, namely, $\forall \text{Pol}_i$ in POL does not applies to SAR; the mathematical expression is as follows: $[\text{POL}]_{\text{SAR}} = \begin{cases} \text{True}, \bigvee_{i=1}^{n} [\text{Pol}_i \in \text{POL}]_{\text{SAR}} = \text{True} \\ \text{False, otherwise} \end{cases}$

Table 4: The final evaluation results.

Cases	Evaluation results	FERs
Case 1	$[\text{Pol}]_{\text{SAR}} = \text{True}^+$ $[\text{POL}]_{\text{SAR}} = [\text{Pol}_1]_{\text{SAR}} \vee [\text{Pol}_2]_{\text{SAR}} \vee \cdots = \text{True}^+ \vee \text{True}^+ \vee \cdots = \text{True}^+$	{permit}
Case 2	$[\text{Pol}]_{\text{SAR}} = \text{True}^-$ $[\text{POL}]_{\text{SAR}} = [\text{Pol}_1]_{\text{SAR}} \vee [\text{Pol}_2]_{\text{SAR}} \vee \cdots = \text{True}^- \vee \text{True}^- \vee \cdots = \text{True}^-$	{deny}
Case 3	$[\text{POL}]_{\text{SAR}} = [\text{Pol}_1]_{\text{SAR}} \vee [\text{Pol}_2]_{\text{SAR}} \vee \cdots = \text{True}^+ \vee \text{True}^- \vee \cdots = \text{True}^+ \vee \text{True}^-$	{permit, deny}
Case 4	$[\text{Pol}]_{\text{SAR}} = \text{False}$ $[\text{POL}]_{\text{SAR}} = [\text{Pol}_1]_{\text{SAR}} \vee [\text{Pol}_2]_{\text{SAR}} \vee \cdots = \text{False} \vee \text{False} \vee \cdots = \text{False}$	{False}

then the FER of the $[\text{Pol}]_{\text{SAR}}$ refers to the case 4 in Table 4.

In Table 3, if the $[\text{POL}]_{\text{SAR}}$ is true (i.e., $[\text{POL}]_{\text{SAR}} = \text{True}$), then obviously, the $\bigvee_{i=1}^{n} [\text{Pol}_i]_{\text{SAR}} = [\text{Pol}_1]_{\text{SAR}} \vee [\text{Pol}_2]_{\text{SAR}} \vee \cdots \vee [\text{Pol}_n]_{\text{SAR}}$ is true; namely, there is one or more $[\text{Pol}]_{\text{SAR}}$ such that the $[\text{POL}]_{\text{SAR}}$ is true. If one $[\text{Pol}]_{\text{SAR}}$ is true, then the FERs are the same as the result of Table 3, and if at least two $[\text{Pol}]_{\text{SAR}}$ are true, then after performing the disjunction operation, the FERs of the $[\text{POL}]_{\text{SAR}}$ refer to the cases 1-3 in Table 4. If the $[\text{POL}]_{\text{SAR}}$ is false (i.e., $[\text{POL}]_{\text{SAR}} = \text{False}$; specifically, all $[\text{Pol}]_{\text{SAR}}$ is false), then after performing the disjunction operation, the FER of $[\text{POL}]_{\text{SAR}}$ refers to the case

4 in Table 4. When the FER is {permit, deny}, this type of result can be handled by the rejection priority principle, the license priority principle, the first application principle, and the unique application principle [24].

In summary, given the set of logical variable as $U = \{[\mathrm{Pol}_1]_{\mathrm{SAR}}, [\mathrm{Pol}_2]_{\mathrm{SAR}}, \cdots, [\mathrm{Pol}_n]_{\mathrm{SAR}}\}$ and the function of U as $[\mathrm{POL}]_{\mathrm{SAR}} = \bigvee_{i=1}^{n} [\mathrm{Pol}_i]_{\mathrm{SAR}}$, ask if there is a logical variable $[\mathrm{Pol}]_{\mathrm{SAR}}$ in U that satisfies $[\mathrm{POL}]_{\mathrm{SAR}}$. Obviously, this is a typical SATISFIABILITY problem (SAT for short), according to the Cook's theorem; the SAT problem is the NP-complete problem. It can be deduced that the access control problem in this paper is also the NP-complete problem.

Based on the above definition, this paper gives the mathematical expressions of the conditions, constraints, and objective functions necessary for the ASACPM (access control problem). Among them, the mathematical expressions of the conditions and constraints of the ASACPM are as follows.

$$\begin{cases} \mathrm{SAR} = (s, o, e, c, a), \forall \mathrm{SAR} \in \mathrm{CSP}, \\ \mathrm{POL} = \{\mathrm{Pol}_1, \mathrm{Pol}_2, \cdots, \mathrm{Pol}_n\}, \mathrm{Pol} = (S, O, E, C, A) \longrightarrow P. \end{cases} \tag{1}$$

In this paper, the conditions and their constraints (i.e., Equation (1)) are divided into multivariate relationship and affiliation relationship. Among them, the multivariate relationship refers to the relationship between the entity attributes of the SAR (i.e., s, o, e) and attribute conditions of the Pol (i.e., S, O, E). The affiliation relationship refers to whether the certificate and action (i.e., c, a) of the *SAR* belong to Pol's certificate set and action set (i.e., C, A), where the entity attribute refers to the subject attribute, the object attribute, and the environment attribute (i.e., Definition 1).

The mathematical expression of the ASACPM objective function is as follows.

$$[\mathrm{Pol}]_{\mathrm{SAR}} = \begin{cases} \mathrm{True}, \left([S]_s \wedge [O]_o \wedge [E]_e \wedge (c \in C) \wedge (a \in A) = \mathrm{True}\right), \\ \mathrm{False}, \text{otherwise}, \end{cases} \tag{2}$$

$$[POL]_{SAR} = \begin{cases} \mathrm{True}, \bigvee_{i=1}^{n} [Pol_i \in POL]_{SAR} = \mathrm{True}, \\ \mathrm{False}, \text{otherwise}. \end{cases} \tag{3}$$

Given the conditions and constraints (Equation (1)), the ASACPM first obtains the evaluation result by calculating the objective function (Equations (2) and (3)) and then obtains the FER based on the evaluation result and Table 4 and finally according to the FER which determines whether the tenant has access to the platform's business resources. In the policy evaluation, $[\mathrm{Pol}]_{\mathrm{SAR}}$ in Equations (2) and (3) is true if and only if all the multivariate relationships and affiliation relationships are true; that is, Pol applies to SAR.

3.2. Implementation of the ASACPM. Policy evaluation algorithm (PEA) is the core algorithm for implementing ASACPM. It is mainly used to evaluate whether a tenant's access request meets the requirements of the policy set. The detailed process and pseudocode are as follows:

Step 1. Given the necessary conditions as $\mathrm{SAR} = (s, o, e, c, a)$ and $\mathrm{POL} = \{\mathrm{Pol}_1, \mathrm{Pol}_2, \cdots, \mathrm{Pol}_n\}$, the constraints are $\forall SAR \in CSP$ and $Pol = (S, O, E, C, A) \longrightarrow P$, that is, Equation (1).

Step 2. The conditional SAR and POL (i.e., Equation (1)) are taken as parameters to the objective function (i.e., Equations (2) and (3)) for the calculation to obtain the evaluation result.

Step 3. According to the evaluation result and Table 4, the FER is obtained.

4. Application Framework of the ASACPM

4.1. Framework of the ASACPM. The overall framework of the tenant-centric attribute semantic access control policy model for cloud service platform is shown in Figure 1. It consists of four modules, namely, tenant and platform module, CA module, web module, and decision module. These modules can not only complete the corresponding tasks independently. They can also communicate with each other and work together. The tenant first initiates an access request and then establishes an SSL secure channel to evaluate the access request and next return the result to form a complete closed loop. The detailed description of the meaning and function of each module is as follows.

4.1.1. Tenant and Platform Module. Tenants (i.e., requesters) refer to enterprise users in the enterprise alliance consisting of suppliers, manufacturers, distributors, service providers, and agents. The CSP is a third-party public service platform that provides business resources (such as business data, business services, and business processes) to different tenants through the Internet, while the CP can also provide different business resources for the tenants (complementing the resources of the CSP). This paper builds the ASACPM so that the tenant can not only access the business resources of the CSP but also access the business resources of the CP through the CSP, thereby breaking the "information island."

4.1.2. CA Module. The CA is responsible for the issuance and management of SSL certificate, including tenant certificates and server certificates. The main role of the SSL certificate is to implement data encryption transmission and communication entity identity authentication [7], so it can solve many security problems of business resources in the open Internet environment. In ASACPM, SSL certificate can be used not only to build authorization relationships between tenant and business resource but also to establish trust relationships between tenant and server or between cloud platform and collaborative platform. Therefore, when the tenant first uses the platform, the unique tenant certificate is issued by the CA, and this certificate is also saved to the policy administration point of the decision-making body to form the tenant certificate set of the policy which is one of

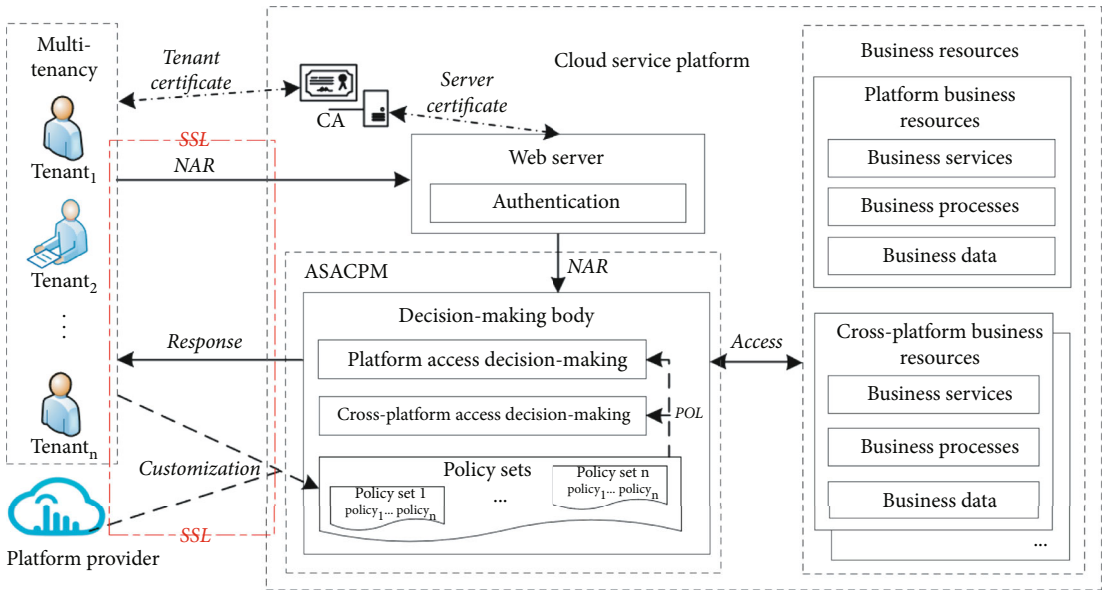

Figure 1: The framework of the tenant-centric attribute semantic access control policy model for cloud service platform.

the basic elements of the calculation of the objective function (Equations (2) and (3)). The version adopted by SSL is V3.0, and the specification adopted by CA is X.509 V3.

4.1.3. Web Module (Web Server). When the tenant accesses the business resources of the CSP, a secure SSL channel (that is, data encryption transmission) is established between the tenant and the web server. When an SSL session is generated, firstly, the web server sends the server certificate to the tenant, and the tenant automatically analyzes the server certificate and verifies the identity of the web server. Secondly, the tenant sends the tenant certificate to the web server, and the web server verifies the identity of the tenant. The verification content includes the certificate authority, the validity period of the certificate, and whether the certificate has been tampered with or revoked. Finally, after the two parties authenticate successfully and establish an SSL secure channel, the web server sends the received tenant's native access request (NAR) to the decision-making body. In addition, this paper mainly focuses on the access control and dynamic fine-grained authorization of business resources. Therefore, the specific processes of constructing SSL secure channel and identifying communication entity authentication can be referred to reference [7], which will not be researched in detail in this paper.

4.1.4. Decision Module (Decision-Making Body). According to the conditions and constraints (Equation (1)) and the objective function (Equations (2) and (3)), the decision-making body is divided into conditional part and decision part, which are described in detail below.

(i) Conditional part: the policy/policy set is formulated by the tenant and the platform provider according to the sharing requirements of the business resources and the management requirements of the CSP, respectively, which is a necessary condition for the access decision. The policy consists of explicit element and implicit element; among them, the explicit element refers to the subject, the object, the environment, and the action; the entity attribute set of the first three elements and action set need to be customized by the tenant (platform provider) and stored in the policy administration point of the decision-making body; and the implicit element refers to the certificate, which is composed of the tenant certificate set and stored in the policy administration point of the decision-making body, so it does not require tenant (platform provider) customization. The access request has five elements: the subject, the object, the environment, the certificate, and the action, respectively, for describing the entity attribute set of the requester, the entity attribute set of the requested business resource, the entity attribute set of the current environment, the tenant certificate, and the access method. It is another necessary condition for the access decision. Since the business resources accessed by tenants may belong to different platforms, this article divides access request into platform access request and cross-platform access request

(ii) Decision part: the ASACPM's access decision mechanism is based on conditions and constraints (Equation (1)) through the calculation of the objective function (Equations (2) and (3)) to obtain the evaluation results, and then based on the evaluation results and Table 4 to obtain the FERs, and finally based on the FERs whether the tenant has access to the platform's business resources. Since access requests are divided into the platform access request and cross-platform access request, the access decision mechanism is divided into the platform access decision and cross-platform access decision, and the

detailed description refers to Section 4.2. The ASACPM's attribute synchronization ensures attribute authority consistency across platforms and provides support for access decision mechanisms, and the detailed description refers to Section 4.3. The ASACPM's dynamic fine-grained authorization mechanism restricts dynamic tenant access requests by increasing the policy's attribute conditions, and the detailed description refers to Section 4.4

4.2. Access Decision Mechanism. The eXtensible Access Control Markup Language (XACML) [25] is an open standard language based on the eXtensible Markup Language (XML) that can be used to determine the general access control policy language for request/response and the framework for executing authorization policies. This language is well interoperable, versatile, and extensible while also supporting dynamic fine-grained access control. This paper adopts XACML to provide a unified writing specification for tenant's access request, platform's policy, and decision-making, which makes the access control system of different platforms universal and then gives the detailed process of access decision implementation.

According to the process of executing the authorization policy, the decision-making body is divided into the policy enforcement point (PEP), the policy decision point (PDP), the attribute authority (AA), and the policy administration point (PAP), in which PEP and PAP belong to the conditional part, PDP belongs to the decision part, and AA can belong to both the conditional part and the decision part. The platform access decision and cross-platform access decision include the PEP, PDP, AA, and PAP, and their functions are described in detail as follows:

(i) The function of the PEP is to translate the NAR into the SAR based on the attribute table provided by the AA and then obtain the decision result from the PDP. If the FER is permit, the tenant is permitted access to the business resource; otherwise, the tenant is denied access to the business resource

(ii) The function of the PDP is to calculate the objective function (Equations (2) and (3)) according to the conditions and constraints (Equation (1)) to obtain the evaluation result and obtain the FER based on the evaluation result and Table 4

(iii) The function of the AA is to store and manage the attribute table (which includes the subject, the object, and the environment) and the relationship between attributes and their values and provide attribute support for the PEP and PDP

(iv) The function of the PAP is to store and manage the policy sets formulated by the tenant and provide the necessary condition (i.e., policy sets) for PDP.

4.2.1. Platform Access Decision Mechanism

(1) Process of Platform Access Decision. The process of platform access decision is shown in Figure 2. When a tenant accesses the business resources of the CSP, first the CSP establishes an SSL channel between the tenants and the web server according to the tenant certificate and server certificate, and then, the web server sends the received NAR to the decision-making body, and finally, the decision-making body executes the platform access decision mechanism to obtain the final evaluation result.

Step 1. When the tenant initiates the NAR, the identity of tenant and web server is authenticated according to the tenant certificate and the server certificate, then the SSL channel between them is established, and next, the NAR is sent to the web server.

Step 2. The web server receives the NAR and sends the NAR to the decision-making body of the CSP.

Step 3. After the PEP of the decision-making body receives the NAR, the process of the platform access decision handling NAR is as follows.

(a) The AA provides attribute support for PEP and PDP, including the attribute tables and relationship between attributes and their values

(b) The PEP transforms the NAR into SAR = (s, o, e, c, a) based on the attribute table provided by the AA. Since all the object (i.e., business resource) stored in the object attribute table of the AA has a corresponding subordinate label (i.e., the platform to which the resource belongs), the PEP can identify the SAR as the platform access request and send the SAR to the PDP

(c) The PDP receives the SAR, which obtains the policy set POL = $\{\mathrm{Pol}_1, \mathrm{Pol}_2, \cdots, \mathrm{Pol}_n\}$ from the PAP. In the case where the given conditions are SAR and POL, the evaluation result is calculated by Algorithm 1, and the calculation process needs to map the entity attribute of the policy to a specific value or a range of values according to the relationship between the attribute and its value provided by the AA

(d) The PDP obtains the FER (i.e., mapping the evaluation result to the FER) based on the evaluation result and Table 4 and then sends the FER to the PEP

Step 4. The PEP performs the FER, which permits or denies the tenant access to the CSP's business resources.

(2) Platform Access Decision Algorithm. Platform access decision algorithm (PADA) is one of the core algorithms for implementing access decision mechanism, which is mainly used to process platform access requests initiated by tenants.

4.2.2. Cross-Platform Access Decision Mechanism

(1) Process of Cross-Platform Access Decision. The process of cross-platform access decision is shown in Figure 3. When a

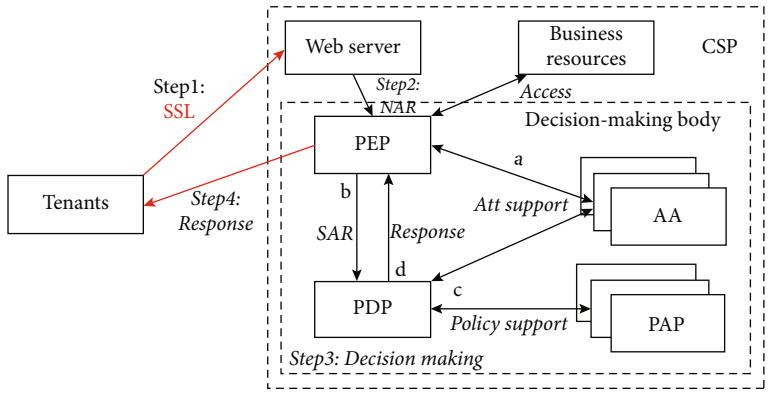

Figure 2: The process of platform access decision.

Input: Given $SAR = (s, o, e, c, a)$ and $POL = \{Pol_1, Pol_2, \cdots, Pol_n\}$, among them, $Pol = (S, O, E, C, A)$
Output: FER
Policy_Evaluation $(SAR = (s, o, e, c, a)$, $POL = \{Pol_1, Pol_2, \cdots, Pol_n\})$ /∗ (Equation (1)) ∗/
FOR each k in n do
IF $[S(k)]_s \wedge [O(k)]_o \wedge [E(k)]_e \wedge (c \in C(k)) \wedge (a \in A(k)) = True$ /∗ Performing the conjunction operation (namely Equations (2) and (3)) ∗/
    $[Pol_k]_{SAR} = True$
    $[POL]_{SAR} + = \vee [Pol_k]_{SAR}$
  ELSE
    $[Pol_k]_{SAR} = False$
    $[POL]_{SAR} + = \vee [Pol_k]_{SAR}$
END IF
END FOR
$[POL]_{SAR} = [Pol_1]_{SAR} \vee [Pol_2]_{SAR} \vee \cdots \vee [Pol_k]_{SAR}$ /∗ Performing the disjunction operation (namely Eq. (2)) ∗/
$[POL]_{SAR} \longrightarrow FER$ /∗$[POL]_{SAR}$ maps to FER∗/
Return FER
End Policy_Evaluation

Algorithm 1: Policy evaluation algorithm (PEA).

Input: Tenant's NAR
Output: *Permit* or *deny* to access business resources for the CSP
$\forall NAR$
PEP_Fuction (NAR)
    Getting attribute tables from the AA
    Translating NAR to SAR
    Executing PDP_Fuction (SAR)
    Executing FER
    Permit or *deny* to access business resources
END PEP_Fuction
PDP_Fuction (SAR)
    Getting SAR from the PEP
    Getting $POL = \{Pol_1, Pol_2, \cdots, Pol_n\}$ from the PAP
    Getting the relationship between attributes and their values from the AA
    Policy_Evaluation (SAR, POL) /∗ Executing **Policy Evaluation Algorithm (PEA)**∗/
    Return FER
END PDP_Fuction

Algorithm 2: Platform access decision algorithm (PADA).

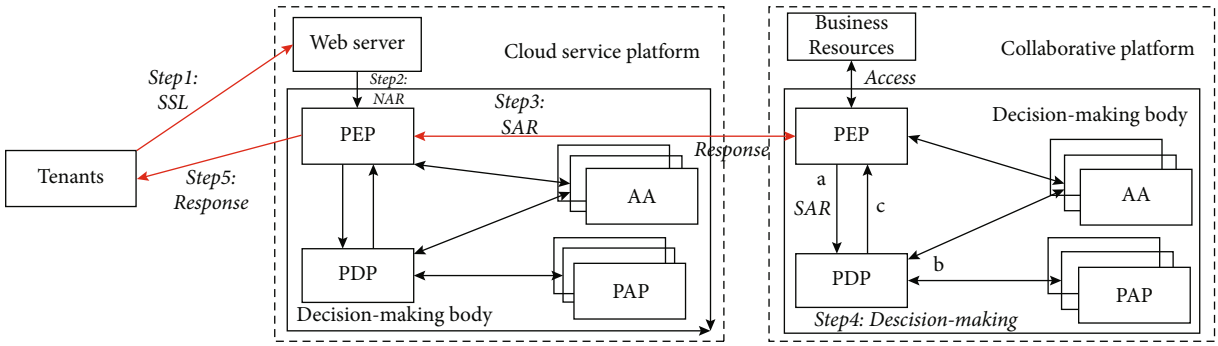

Figure 3: The process of cross-platform access decision.

Input: Tenant's *NAR*
Output: *Permit* or *deny* to access business resources of the CP
1: $\forall NAR$
2: CSP.PEP_Fuction (*NAR*)
3: Getting attribute tables from the AA
4: Translating *NAR* to *SAR*
5: IF *SAR* is the cross-platform access request
6: Sending *SAR* to CP.PEP
7: ENDIF
8: END CSP.PEP_Fuction
9: CP.PEP receives *SAR* and verifies the integrity of *SAR*
10: CP.PEP_Fuction (*SAR*)
11: Executing CP.PDP_Fuction (*SAR*)
12: Executing *FER*
13: *Permit* or *deny* to access business resources of the CP
14: END CP.PEP_Fuction
15: CP.PDP_Fuction (*SAR*)
16: Getting *SAR* from the CP.PEP
17: Getting $POL = \{Pol_1, Pol_2, \cdots, Pol_n\}$ from the CP.PAP
18: Getting the relationship between attributes and their values from the *CP.AA*
19: Policy_Evaluation (*SAR*, *POL*)/∗ Execute **Policy Evaluation Algorithm (PEA)**∗/
20: Return *FER*
21: END CP.PDP_Fuction

Algorithm 3: Cross-platform access decision algorithm (CADA).

tenant accesses the business resources of the CP through the CSP, first the CSP establishes an SSL channel between the tenants and the web server according to the tenant certificate and server certificate, and then, the web server sends the received NAR to the decision-making body, and finally, the decision-making body executes the cross-platform access decision mechanism to obtain the final evaluation result.

Step 1. When the tenant initiates the NAR, the identity of tenant and web server are authenticated according to the tenant certificate and the server certificate, then the SSL channel between them is established, and next, the NAR is sent to the web server.

Step 2. The web server receives the NAR and sends the NAR to the decision-making body of the CSP.

Step 3. After the CSP.PEP (i.e., the PEP of the decision-making body of the CSP) receives the NAR, it is transformed into SAR = (s, o, e, c, a) based on the attribute table provided by the AA. Since all the object (i.e., business resource) stored in the object attribute table of the AA has a corresponding subordinate label (i.e., the platform to which the resource belongs), the CSP.PEP can identify the SAR as the cross-platform access request and send the SAR to the decision-making body of the CP.

Step 4. After the CP. PEP (it has a similar meaning to the CSP.PEP) receives SAR, the process of the cross-platform access decision handling SAR is as follows.

(a) The CP.PEP verifies the integrity of the SAR and sends it to the CP.PDP

(b) The CP.PDP receives the SAR, which obtains the policy set $POL = \{Pol_1, Pol_2, \cdots, Pol_n\}$ from the CP.PAP. In the case where the given conditions are SAR and POL, the evaluation result is calculated by Algorithm 1, and the calculation process needs to map the entity attribute of the policy to a specific value or a range of values according to the relationship between the attribute and its value provided by the CP.AA

(c) The CP.PDP obtains the FER (i.e., mapping the evaluation result to the FER) based on the evaluation result and Table 4 and then sends the FER to the CP.PEP

Step 5. The CP.PEP performs the FER, which permits or denies the tenant access to the CP's business resources based on the CSP.

(2) Cross-Platform Access Decision Algorithm. Cross-platform access decision algorithm (CADA) is one of the core algorithms for implementing access decision mechanism, which is mainly used to process cross-platform access requests initiated by tenants.

4.3. Attribute Synchronization Mechanism

4.3.1. Methods of Attribute Synchronization. The dynamic characteristics of CSP lie in the fact that new enterprises join and old enterprises exit from the enterprise alliance at any time [7, 10]. Therefore, the CSP grants or cancels the access permissions of the enterprise users with the dynamic characteristics, which makes the information of the subject attribute (SA) often change. If the SA changes, the CSP needs to update the subject attribute table in the AA and then informs the CP to update the subject attribute table in the AA; that is, the CSP needs to ensure the consistency of the AA of different platforms. If the attribute table of the CSP or CP is not updated, it will affect the policy evaluation (i.e., the calculation of Equations (2) and (3) will be affected).

When the CSP or CP updates the SA in the subject attribute table, if the SA is being used by other operations, a conflict will occur. Therefore, this paper introduces the PV operation [26] to solve the mutual exclusion problem of attribute update and invoke of the CSP or CP (i.e., attribute synchronization problem), the PV operation is related to the processing of semaphore, and the P operation and V operation must appear in pairs. The P and V are from the initials of Dutch words, P is usually explained as proberen (i.e., "to test" or " to try"), and V is usually explained as verhogen (i.e., "increase") [27]. We set a semaphore $\mathcal{S}$ for the SA. If the SA is not invoked by other operations, the initial value $\mathcal{S} = 1$ is given. If the SA is invoked by another operations, the initial value $\mathcal{S} = 0$ is given.

The detailed definition of the PV operation: executing a P operation means that the platform performs the attribute update operation, so the value of $\mathcal{S}$ is decremented by 1. When $\mathcal{S} \geq 0$, which means that the platform can update the SA in the subject attribute table, and when $\mathcal{S} < 0$, which means that the SA is invoked by other operations and the platform cannot perform the update operation, the update operation is in the wait state. Executing a V operation means releasing the update operation of the platform or the SA invoked by other operations, so the value of $\mathcal{S}$ is incremented by one. When $\mathcal{S} \leq 0$, it means that the update operation in the wait state is awakened to make it run (i.e., executing the update operation).

```
Input:  S = 0 or S = 1
Output: Performing the update operation
IF the attribute or its value is changed
    IF the attribute or its value is invoked
        S = 0
        Executing P_Operation (S)
        Executing V_Operation (S)
    ELSE
        S = 1
        Executing P_Operation (S)
        Executing V_Operation (S)
    END IF
END IF
P_Operation (S: Semaphore)
    S = S − 1
    IF S < 0
        Wait (S)
    ELSE
        Performing the update operation
    END IF
END P_Operation
V_Operation (S: Semaphore)
    S = S + 1
    IF S = <0
        Resume (S)
        Performing the update operation
    ELSE
        Releasing the update operation
    END IF
END V_Operation
```

Algorithm 4: Attribute synchronization algorithm (ASA).

The PV operation can not only update the subject attribute table but also update other attribute tables and relationships between attributes and their values. Attribute synchronization (i.e., the PV operation) not only ensures the consistency the AA of the CSP and the AA of the CP but also solves the mutual exclusion problem of attribute update and invoke, and it is also the basis of access control mechanism and dynamic fine-grained authorization mechanism.

4.3.2. Attribute Synchronization Algorithm. Attribute synchronization algorithm (ASA) adopts PV operation to solve the mutual exclusion problem of attribute updating and invoking (i.e., attribute synchronization problem).

4.4. Dynamic Fine-Grained Authorization Mechanism. The ASACPM defines a dynamic fine-grained authorization mechanism that determines the tenant's permissions based on the SAR evaluation of the Pol and applies to an open,

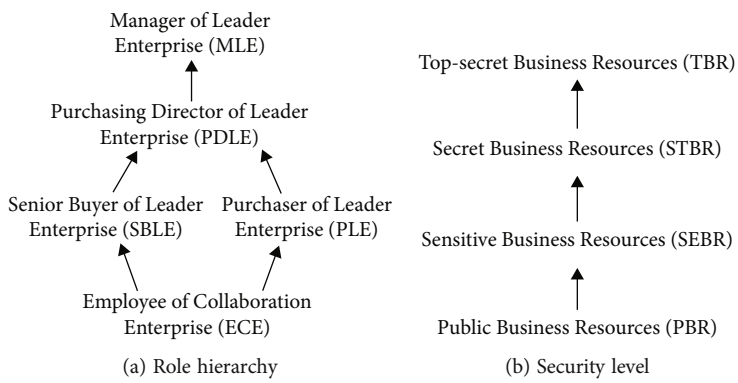

Figure 4: The relationship between different attribute values.

shared, and complex Internet environment. In the case that the SAR is unchanged, the owner of the business resource restricts the tenant's access to the business resources by increasing the attribute condition of the policy, thereby forming the finer-grained attribute condition constraint, and the formation process can refer to Section 5.1.

It can be seen from the above that the dynamic and fine-grained authorization mechanism of the model defines the multivariate relationship between the entity attributes of SAR and the attribute conditions of Pol. If and only if all multivariate relationships (i.e., $[S]_s$, $[O]_o$, and $[E]_e$) and affiliation relationships (i.e., $c \in C$ and $a \in A$) are true, $[\mathrm{Pol}]_{\mathrm{SAR}}$ or $[\mathrm{POL}]_{\mathrm{SAR}}$ (i.e., Equations (2) and (3)) can be true, thereby resulting in that Pol applies to SAR (i.e., the authorization is valid). When the entity attributes of SAR remain unchanged, we can conclude that the more attribute conditions of Pol, the finer the granularity of access control, which fully shows that the mechanism has good scalability.

In addition, when the AA of different platforms is the same and the policy set remains unchanged, no matter how the SA of the tenants in the enterprise alliance changes, the $[\mathrm{Pol}]_{\mathrm{SAR}}$ or $[\mathrm{POL}]_{\mathrm{SAR}}$ can only be true if all the multivariate relationships and affiliation relationships are true; that is, the tenant can access the business resources. Therefore, this mechanism can effectively solve the problem of dynamic characteristics of access permissions, which fully shows that it has good flexibility.

In summary, this paper makes the CSP not only have good scalability and flexibility through the dynamic fine-grained authorization mechanism but also can adapt to future development and application.

5. Analysis and Evaluation of the ASACPM

5.1. Case Analysis. The ASACPM and its application framework are applied to the ASP-/SaaS-based manufacturing industry value chain collaboration platform [24], and the specific process of the ASACPM and its application framework performing access decisions are described through corresponding business scenarios. We use the SA to represent the subject attribute, the OA to represent the object attribute, and the EA represent the environment attribute. According to the actual business requirements, the relationship between the attributes of some SAs and OAs is given, as shown in Figures 4(a) and 4(b), respectively, where the srole represents the role hierarchy of the SA and the obsl represents the security level of the OA. Each level of business resources includes business data, business services, and business processes.

Table 5 gives the SAR of the tenant, Table 6 shows the simple policy set (i.e., POL), and the definitions of the srole and obsl are shown in Figure 4.

Given the tenant's SAR (Table 5) and POL (Table 6) (i.e., given the input of Algorithm 1), the evaluation results (ERs) are calculated by Algorithm 1, and the ERs are mapped to the FERs, which are shown in Table 7. This paper assumes that "T^+" means True$^+$, "T^-" means True$^-$, and "F" means False; the default authorization is deny (i.e., "F" is deny).

It can be seen from Table 7 that for the SAR_2 and SAR_6, since there is no suitable policy in the POL, the FER is the default authorization (deny); that is, the tenant cannot add or browse the business resources of the CSP or CP. For the SAR_5, there are two suitable policies in the POL, the ER includes deny and permit. According to the license priority principle [5, 9], the FER is permit; that is, the tenant can delete the business resources of the CSP or CP, among which the license priority principle means that the ER of at least one policy is T^+, and the FER is {permit}.

Based on the above example, we describe in detail the implementation process of the dynamic fine-grained authorization mechanism of ASACPM and its application framework. It is known from Section 4.4 that this mechanism defines the multivariate relationship between the entity attributes of the SAR and the attribute conditions of the Pol, which limits the SAR by increasing the attribute condition of the Pol.

For example, we add an attribute condition to the S of the Pol_1 in Table 6 as shown in Table 8, give the tenant's SAR (Table 5), and then calculate the ERs based on the Pol_1 and SAR through Algorithm 1, and finally, the ERs are mapped to the FERs as shown in Table 9. It can be seen from Table 9 that the Pol_1 is not applicable to all SARs in Table 5, where st = CU represents the attribute condition added in the S, st represents the requester (i.e., tenant), and CU represents the automobile enterprise alliance, which

Table 5: The SAR of the tenant.

SAR	s	o	e	c	a
SAR_1	srole = ECE	obsl = PBR	etime = 11 : 30	C_1	Browsing
SAR_2	srole = SBLE	obsl = SEBR	etime = 13 : 30	C_2	Adding
SAR_3	srole = PLE	obsl = STBR	etime = 10 : 30	C_3	Editing
SAR_4	srole = PDLE	obsl = TBR	etime = 15 : 30	C_4	Approving
SAR_5	srole = MLE	obsl = STBR	etime = 10 : 30	C_5	Deleting
SAR_6	srole = ECE	obsl = PBR	etime = 11 : 30	None	Browsing

Table 6: The simple policy set.

POL	S	O	E	C	A	P
Pol_1	srole $\succcurlyeq$ ECE	obsl $\succcurlyeq$ PBR	8 : 30 < etime < 17 : 00	$\{C_1, \cdots, C_m\}$	Browsing	Permit
Pol_2	srole $\succcurlyeq$ SBLE	obsl = PBR	8 : 30 < etime < 17 : 00	$\{C_1, \cdots, C_m\}$	Browsing, adding	Permit
Pol_3	srole $\succcurlyeq$ PLE	obsl $\succcurlyeq$ STBR	9 : 30 < etime < 17 : 30	$\{C_1, \cdots, C_m\}$	Editing, deleting	Deny
Pol_4	srole $\succcurlyeq$ SBLE	obsl = SEBR	9 : 00 < etime < 18 : 00	$\{C_1, \cdots, C_m\}$	Editing	Permit
Pol_5	srole $\succcurlyeq$ PDLE	obsl = TBR	9 : 30 < etime < 17 : 30	$\{C_1, \cdots, C_m\}$	Approving	Deny
Pol_6	srole $\succcurlyeq$ PDLE	obsl$\preccurlyeq$STBR	7 : 00 < etime < 19 : 30	$\{C_1, \cdots, C_m\}$	Deleting	Permit

Table 7: The final evaluation results.

SAR	Pol_1	Pol_2	Pol_3	Pol_4	Pol_5	Pol_6	ERs	FERs
SAR_1	T^+	F	F	F	F	F	$\{T^+\}$	{permit}
SAR_2	F	F	F	F	F	F	$\{F\}$	{deny}
SAR_3	F	F	T^-	F	F	F	$\{T^-\}$	{deny}
SAR_4	F	F	F	F	T^-	F	$\{T^-\}$	{deny}
SAR_5	F	F	T^-	F	F	T^+	$\{T^-, T^+\}$	{deny, permit}
SAR_6	F	F	F	F	F	F	$\{F\}$	{deny}

Table 8: The Pol_1.

POL	S	O	E	C	A	P
Pol_1	srole $\succcurlyeq$ ECE, st = CQ	obsl $\succcurlyeq$ PBR	8 : 30 < etime < 17 : 00	$\{C_1, \cdots, C_m\}$	Browsing	Permit

means that the requester is affiliated with the automobile enterprise alliance.

The above cases fully demonstrate that ASACPM and its application framework can solve the access control problem of CSP through the access decision mechanism and dynamic fine-grained authorization mechanism. The application of these two mechanisms enables CSP not only to have good flexibility, scalability, and practicability but also to adapt to future development and applications.

5.2. Correctness Analysis. The ASACPM and its application framework proposed in this paper are through CA and SSL certificates to restrict attackers from invading CSP or CP to steal or tamper with tenant's business resources. So the

Table 9: The final evaluation results of the Pol_1.

SAR	Pol_1	ERs	FERs
SAR_1	F	$\{F\}$	{deny}
SAR_2	F	$\{F\}$	{deny}
SAR_3	F	$\{F\}$	{deny}
SAR_4	F	$\{F\}$	{deny}
SAR_5	F	$\{F\}$	{deny}
SAR_6	F	$\{F\}$	{deny}

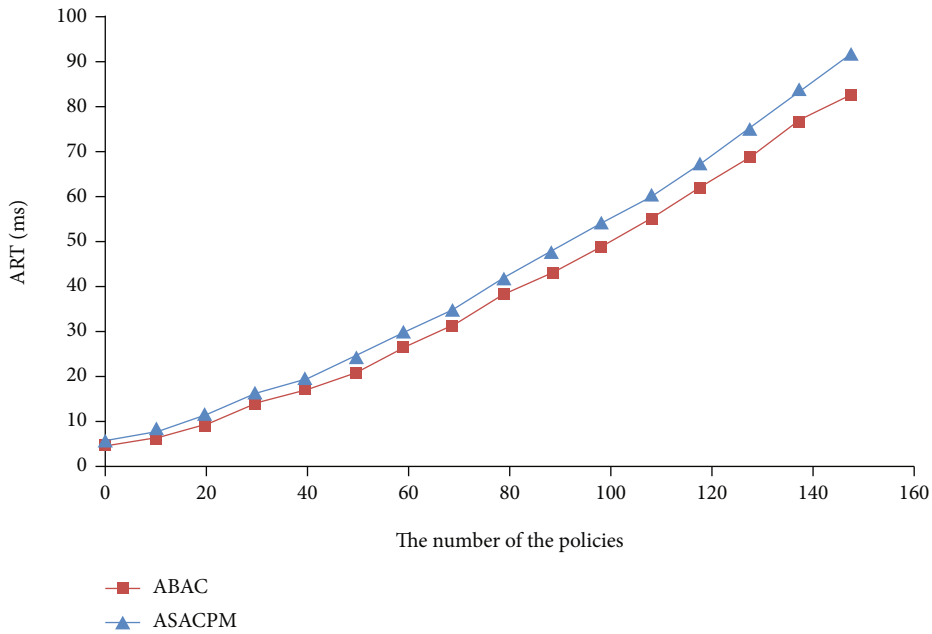

Figure 5: Comparison of the execution overhead of ABAC and ASACPM.

ASACPM and its application framework ensure that the confidentiality and integrity of business resources will not be destroyed by attackers. In order to prove this conclusion is correct, we use the reductio ad absurdum (RAA) to prove the safety performance of the model.

We assume that the attacker obtains the correct tenant certificate and obtains access permission of the CSP by repeatedly sending the virtual attribute set in a polynomial time. Attacking this target requires the following three parameters $<x, y, z_i>$, where x represents the number of attributes required to access the business resources of the CSP or CP, y represents the number of attribute conditions of all policy sets, $y \gg x$, and z_i represents the number of values for each attribute. The attempted time required for the attacker to find the correct combination is $C_y^x = A_y^x/x! = y!/(x!(y-x)!)$. Therefore, the computational complexity of finding out the correct access permissions is $T(x, y, z_i) = C_y^x \times \prod_{i=1}^{i} z_i = y!/(x!(y-x)!) \times \prod_{i=1}^{i} z_i$. This attempt cannot be accomplished within a polynomial time, which has conflict with the assumed condition, so the correctness of the above conclusion is proved.

5.3. Model Evaluation. The ASACPM and its application framework are applied to the ASP-/SaaS-based manufacturing industry value chain collaboration platform, and a thousand policies are written for evaluating the performance of ASACPM and its application framework. Development tools include XACML, JDK1.7, Eclipse4.5, and Mysql5.6. LAN is taken as the test environment, the computer configuration at client side is Intel Core i7-4790 3.6 G, 8 G memory, and Windows 10 enterprise operating system, and the computer configuration at server side is Intel Core i7-4790 3.6 G, 16 G memory, and Windows server 2012 operating system.

In the execution overhead experiment of the ABAC and ASACPM, the NAR of 16 different tenants is arbitrarily selected, the NAR is sent to the decision-making body first, and then, the different policy sets (the number of policies in each policy set is different and is within 0-160) are evaluated based on the NAR, and next, the result is returned to the tenant, and the time spent in the entire process is called the response time. The same NAR was repeatedly performed 20 times, and the corresponding response time was recorded and then averaged to form an average response time (ART). Under different access control schemes (ABAC and ASACPM), the relationship between the number of the policies in the policy set and the ART is shown in Figure 5.

It can be seen from Figure 5 that the difference in execution overhead between ABAC and ASACPM is relatively small, and as the number of policies increases, their ART is also growing. In the case of the same number of policies, the ABAC's ART is slightly slower than the ASACPM's ART, but their gap is within 10 ms. The ASACPM proposed in this paper needs to establish an SSL secure channel, so its implementation overhead is relatively long, but its security is better than the ABAC (i.e., the data plaintext transmission). In combination with actual needs, the number of policies and the amount of data transmission are usually small, and their ART is relatively short, so the execution overhead of the ASACPM has little effect on the overall performance of the CSP.

In the experiment on the access decision, we divide the experimental scenario according to the type of the access decision and then evaluate different policy set (the number of policies in each policy set is different and is within 0-1000) based on different NAR. Repeat the execution of the same NAR 20 times, record the corresponding decision-making time, and then take the average to form

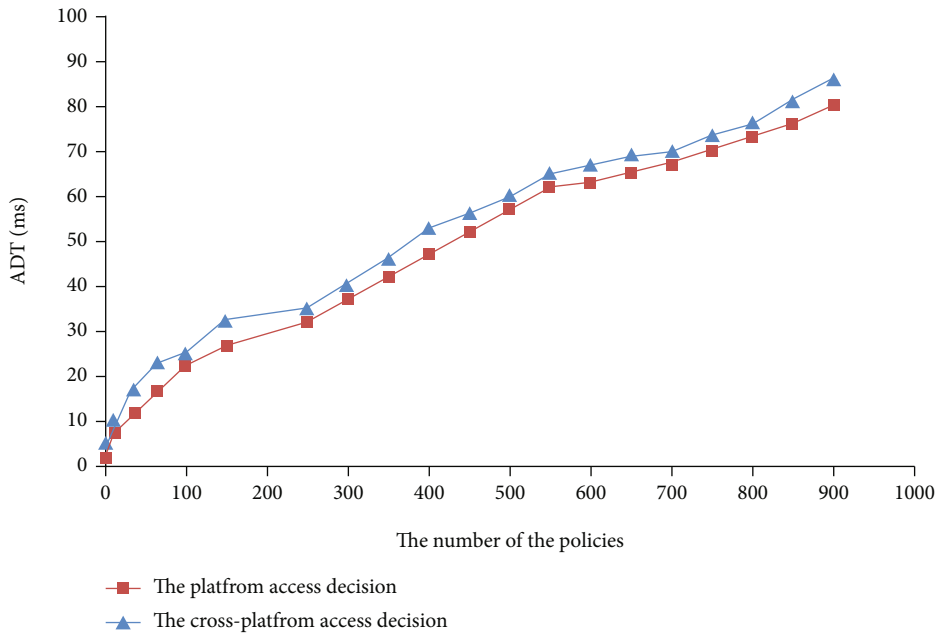

Figure 6: Comparisons of relationship between the number of the policies and ADT.

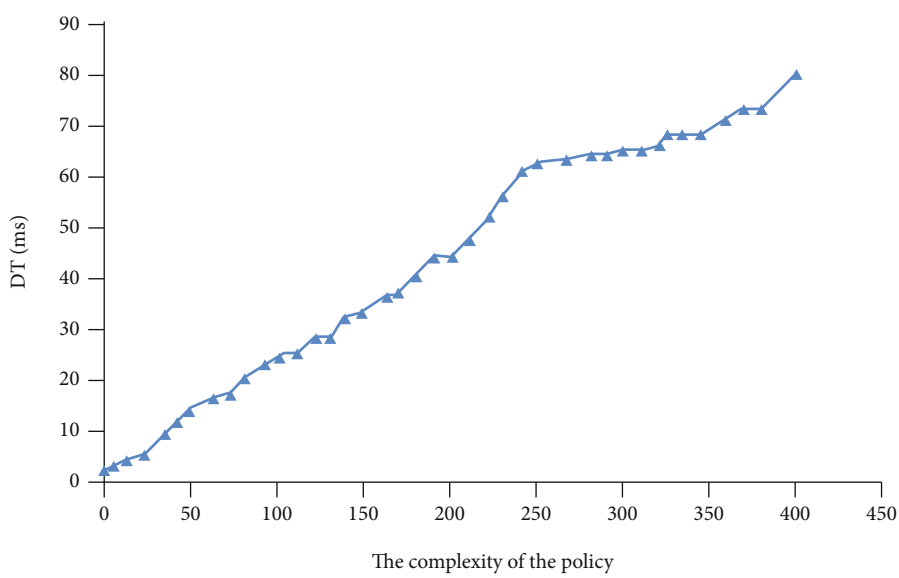

Figure 7: The relationship between the complexity of the policy and the DT.

the average decision-making time (ADT). In the scenario where the access decision is different types, the relationship between the number of the policies in the policy set and the ADT is as shown in Figure 6.

It can be seen from Figure 6 that the ADT of the platform access decision and cross-platform access decision is slowly increasing with the increase of the number of policies. The ADT of the cross-platform access decision is relatively long. In the case where the number of policies is the same, the ADT gap between it and the platform access decision is within 7 ms. In combination with actual needs, when evaluating policies based on the SAR, since the number of policies is usually less than 200 and the ADT is relatively short, the impact of the access decision on the overall performance of the CSP is relatively small.

In the experiment on the dynamic fine-grained authorization, the complexity of a policy is related to the number of the attribute conditions it owns. The more the attribute conditions of the policy, the higher its complexity and the finer the granularity of access control. In this experiment, we first give the SAR of the tenant, then arbitrarily select 40 policies, next evaluate the policies based on the SAR, and finally record their decision time (DT). The relationship between the complexity of the policy and the DT is shown in Figure 7.

It can be seen from Figure 7 that as the complexity of the policy increases (i.e., the granularity of the access control is also finer), the corresponding DT is also gradually increasing, and we can conclude that the relationship between them is proportional. In combination with actual requirements, the complexity of the policy is usually within 200 attribute conditions, and the corresponding DT has a small gap. Therefore, the dynamic fine-grained authorization has less impact on the overall performance of the CSP.

In summary, in the Internet environment, the above experimental results show that the performance of the ASACPM and its application framework proposed in this paper meets our expectations and is generally satisfactory.

6. Conclusions

In the Internet environment, traditional cloud service platforms have cross-platform access control problems and do not support dynamic fine-grained authorization methods. This paper proposes a tenant-centric attribute semantic access control policy model for cloud service platforms. First, this paper formally describes ASACPM through attribute semantics and evaluates whether the tenant's access request conforms to the requirements of the policy set through ASACPM. Secondly, this paper presents the application framework of ASACPM, in which the access decision mechanism is used to evaluate whether the tenant has CSP or CP access control permissions, the attribute synchronization mechanism is used to ensure the consistency of the AA of the CSP and the AA of the CP, and the dynamic fine-grained authorization mechanism ensures better flexibility and scalability of CSP. Finally, through a practical case analysis, this paper proves that the application of ASACPM and its application framework to CSP has good flexibility, scalability, and practicability. In addition, we design some experimental scenarios to verify that the performance of ASACPM and its application framework meets our expectations and has good reliability, validity, and rationality.

Since the application framework of ASACPM adopts CA and SSL certificate to ensure the security, integrity, and confidentiality of data, its execution overhead is relatively high in the application process. Therefore, the main work in the future is to further optimize the web server and shorten the construction time of the SSL secure channel. In addition, the visual interface and policy customization format are optimized to improve the experience of tenants.

Data Availability

The data used to support the findings of this study are included within the article.

Conflicts of Interest

The authors declare that they have no conflicts of interest.

Acknowledgments

This work was supported by the National Key R&D Plan of China (Nos. 2018YFB1701500 and 2018YFB1701502).

References

[1] Z. C. Zhou and L. Zhao, "Cloud computing model for big data processing and performance optimization of multimedia communication," *Computer Communications*, vol. 160, pp. 326–332, 2020.

[2] S. N. Mthunzi, E. Benkhelifa, T. Bosakowski, C. G. Guegan, and M. Barhamgi, "Cloud computing security taxonomy: from an atomistic to a holistic view," *Future Generation Computer Systems*, vol. 107, pp. 620–644, 2020.

[3] L. Wang, D. Chen, Y. Hu, Y. Ma, and J. Wang, "Towards enabling cyberinfrastructure as a service in clouds," *Computers & Electrical Engineering*, vol. 39, no. 1, pp. 3–14, 2013.

[4] M. Z. Wang and Q. L. Zhang, "Optimized data storage algorithm of IoT based on cloud computing in distributed system," *Computer Communications*, vol. 157, pp. 124–131, 2020.

[5] Y. Yu, L. Sun, and Y. Ma, "Access control model for attribute-based cloud manufacturing collaboration platform," *Computer Integrated Manufacturing Systems*, vol. 23, no. 1, pp. 196–202, 2017.

[6] Y. Yu, L. F. Sun, C. H. Ren, and M. Han, "Bilateral matching model of business resources for multi-service value chain," *Computer Integrated Manufacturing Systems*, vol. 27, no. 5, pp. 1397–1409, 2021.

[7] Y. Yu, L. Sun, Y. Ma, and S. Wang, "Data security model for industrial chain collaborative SaaS platform," *Computer Integrated Manufacturing Systems*, vol. 22, no. 12, pp. 2911–2919, 2016.

[8] M. Hasan and B. Starly, "Decentralized cloud manufacturing-as-a-service (CMaaS) platform architecture with configurable digital assets," *Journal of Manufacturing Systems*, vol. 56, pp. 157–174, 2020.

[9] X. Li, G. Feng, and C. Chen, "The access control model based on attribute," *Journal of Communications*, vol. 29, no. 4, pp. 90–98, 2008.

[10] Y. Yu, L. Sun, and Y. Ma, "Multi-tenant form customization technology for collaborative cloud service platform in industrial chain," *Computer Integrated Manufacturing Systems*, vol. 22, no. 9, pp. 2235–2244, 2016.

[11] K. Ma, G. Yang, and Y. Xiang, "RCBAC: a risk-aware content-based access control model for large-scale text data," *Journal of Network and Computer Applications*, vol. 167, article 102733, 2020.

[12] Y. D. Wang, J. H. Yang, C. Xu, X. Ling, and Y. Yang, "Survey on access control technologies for cloud computing," *Journal of Software*, vol. 26, no. 5, pp. 1129–1150, 2015.

[13] F. Nazerian, H. Motameni, and H. Nematzadeh, "Emergency role-based access control (E-RBAC) and analysis of model specifications with alloy," *Journal of Information Security and Applications*, vol. 45, pp. 131–142, 2019.

[14] Z. Tan, Z. Tang, and R. Li, "Research on trust-based access control model in cloud computing," in *IEEE Joint International Information Technology and Artificial Intelligence Conference*, pp. 339–344, Washington, DC, USA, 2011.

[15] M. Zhao and Z. Yao, "Cloud computing access control model based on RBAC," *Journal of Computer Applications*, vol. 32, no. S2, pp. 267–270, 2012.

[16] Y. Jung and M. Chung, "Adaptive security management model in the cloud computing environment," in *International Conference on Advanced Communication Technology*, pp. 1664–1669, Washington, DC, USA, 2010.

[17] G. Lin, S. He, and H. Huang, "The cloud computing access control model based on behavior security model," *Journal of Communication*, vol. 33, no. 3, pp. 59–66, 2012.

[18] J. P. Cruz, Y. Kaji, and N. Yanai, "RBAC-SC: role-based access control using smart contract," *IEEE Access*, vol. 6, pp. 12240–12251, 2018.

[19] Y. K. Fan, S. L. Liu, G. Tan, and F. Qiao, "Fine-grained access control based on trusted execution environment," *Future Generation Computer Systems*, vol. 109, pp. 551–561, 2020.

[20] X. Cheng, X. Chen, B. Zhang, and Y. Yang, "Attribute-based access control policy model," *Computer Engineering*, vol. 36, no. 15, pp. 130–133, 2010.

[21] S. Ruj, M. Stojmenovic, and A. Nayak, "Decentralized access control with anonymous authentication of data stored in clouds," *IEEE Transactions on Parallel and Distributed Systems*, vol. 25, no. 2, pp. 384–394, 2014.

[22] K. Fan, H. Y. Xu, L. X. Gao, H. Li, and Y. Yang, "Efficient and privacy preserving access control scheme for fog-enabled IoT," *Future Generation Computer Systems*, vol. 99, pp. 134–142, 2019.

[23] S. Pal, M. Hitchens, V. Varadharajan, and T. Rabehaja, "Policy-based access control for constrained healthcare resources in the context of the Internet of Things," *Journal of Network and Computer Applications*, vol. 139, pp. 57–74, 2019.

[24] Southwest Jiaotong University, "ASP/SaaS-based manufacturing industry value chain collaboration platform," 2022, http://www.autosaas.cn/.

[25] A. Liu, C. Fei, J. Hwang, and X. Tao, "Designing fast and scalable XACML policy evaluation engines," *IEEE Transactions on Computers*, vol. 60, no. 12, pp. 1802–1817, 2011.

[26] A. Ren, X. Wang, X. Luo, and L. Ruan, *Operating System Practical Tutorial*, Tsinghua University Press, 3th edition, 2012.

[27] A. Silberschatz, G. Gagne, and P. Galvin, *Operating System Concepts*, John Wiley & Sons, Inc., 8th edition, 2008.

Hindawi
Journal of Sensors
Volume 2022, Article ID 5001953, 10 pages
https://doi.org/10.1155/2022/5001953

Research Article

Research on Data Fusion Method Based on Multisource Data Awareness of Internet of Things

Fanglei Sun[1] and Zhifeng Diao[2]

[1]*School of Creativity and Art, Shanghai Tech University, Shanghai 201210, China*
[2]*College of Design and Innovation, Tongji University, Shanghai 200082, China*

Correspondence should be addressed to Zhifeng Diao; zfdiao@alumni.tongji.edu.cn

Received 21 March 2022; Revised 14 May 2022; Accepted 24 May 2022; Published 2 July 2022

Academic Editor: Yuan Li

The diversity of big data in Internet of Things is one of the important characteristics that distinguish it from traditional big data. Big data of Internet of Things is often composed of a variety of data with different structural forms. The description of the same thing by these different modal data has certain independence and strong relevance. Accurately and efficiently extracting and processing the hidden fusion information in the big data of the Internet of Things is helpful to solve various multimodal data analysis tasks at present. In this paper, a multimodal interactive function fusion model based on attention mechanism is proposed, which provides more efficient and accurate information for emotion classification tasks. Firstly, a sparse noise reduction self-encoder is used to extract text features, Secondly, features are extracted by encoder. Finally, an interactive fusion module is constructed, which makes text features and image features learn their internal information then the combination function is applied to the emotion classification task.

1. Introduction

A protocol for sharing system information in wireless sensor networks, an energy-aware multipoint relay protocol based on hybrid MAC, is proposed. Simulation results show that compared with on-demand DMDS, it can reduce the corresponding power consumption. Compared with the traditional system data sharing protocol, this protocol has short transmission delay [1]. Surveillance and spatial perception systems that need to capture panoramic images new challenges are posed in data fusion. Image fusion of multisensor array can be realized by data acquisition and computer operation. This paper discusses the design considerations, delay, control loop for source data aggregation, health monitoring, and data rate processing of such systems [2]. The mission of advanced volume sensor is to develop a low-cost detection system that identifies ship damage management status and provides real-time threat level information for damage management events. NRL built two prototype systems with multicockpit sensors. The test results show that the prototype of volume sensor is equivalent to or better than commercial video detection system and point detection system in key quality indicators of fire detection. [3]. We investigate and demonstrate dedicated surveillance services based on UAV fleet. Its purpose is to provide support for threat detection through data fusion, enhance the situational awareness of operators, and reduce the workload of operators. Therefore, a distributed monitoring system is proposed to enhance the detection capability, high-level data fusion capability, and autonomous capability of UAV [4]. In this paper, a new distraction detection method is proposed. Naturalistic driving data and video surveillance records from the Shanghai Naturalistic Driving Study were used for analysis. The application program deals with complex interference by weighing focus characteristics, which provides method basis and technical support for driver behavior early warning system [5]. Domain adaptive learning is a special transfer learning method. The source domain and the target domain usually have different data distributions, but they must perform the same tasks. We have verified the proposed method for domain adaptive classification tasks on PointDA-10 dataset. Empirically, it shows strong performance comparable to the

standard, even better than the most advanced performance [6]. Network security situational awareness is an effective way to analyze complex network security situation. This paper puts forward the concept and model of network security situational awareness and puts forward a new network security situational awareness model. We focus on the attributes of multisource data in network security research and introduce situational awareness algorithm based on data fusion. The results may reflect the overall security status of the network [7]. For companies that build situational awareness based on multisource data, image development is becoming more and more important. This paper introduces an image development application that uses only image content to detect objects of interest, and automatically creates and saves spatial and temporal relationships among images, cameras, and objects. [8]. Data fusion technology is widely used in automatic object recognition system. The problems of data aggregation systems are intrinsically complex, not only accidental but also vague. A method to determine the basic probability reported by each sensor is proposed. Fusion of sensor reports using classic Dempster combination rules [9]. A new method of mobile station position tracking under LOS/NLOS mixed conditions is proposed. The algorithm has good flexibility. It can support various measurement methods and asynchronous or synchronous observation data, which is especially suitable for future interoperable positioning systems [10]. A new method for early detection of breast cancer using ultrawideband microwave imaging technology is proposed. Then, based on the fusion concept of TOA data, the position and scattering intensity of main scatterers are estimated. Compared with existing methods, this method has higher computational efficiency because the scanning process is localized in several candidate positions [11]. In order to determine the reliability of each sensor and how to fuse the measured data of sensors, a data fusion method based on fuzzy theory is proposed, and its measurement application is studied. The measurement example shows that this method is feasible, can give priority to stable and reliable sensors, has good measurement effect, is simple and effective, and is convenient for real-time measurement [12]. We make use of comparative advantages to overcome the limitations of different technologies and data sources, it is necessary to develop basic methods, which promotes the development of data fusion methods to improve material position estimation in this paper. The results show that method has the ability to improve position estimation and can resist measurement noise and future technical development [13]. This paper introduces a method of synthesizing high-resolution and low-resolution data for the scanning system. According to the complexity of parts, the modeling process can be partially or fully automated. This method of combining data improves the flexibility of scanning and maintains the accuracy of results [14]. In data fusion, linear combination method is a very flexible method, because it can give different weights to different systems. We find that some medium power functions are more effective in combining data than in simple weighting mode, and data combination can be realized as efficiently as in simple weighting mode [15].

2. Data Perception Method

2.1. Artificial Data Perception Method. The programmer uses a common programming language or a specially designed scripting language to write a personalized data-aware wrapper according to the specific structure of each web page. Because the wrapper's data awareness rules are identical to the page structure, the quality and efficiency of data awareness are usually higher. The shortcoming of this method is that once the page changes, the wrapper loses its data perception ability and needs manual modification, and the maintenance cost is relatively high, which is not suitable for large-scale commercial use.

2.2. Semiautomatic Data Perception Method. Because of the high learning cost and maintenance cost of manually constructed data-aware wrapper, semiautomatic data-aware wrapper came into being. This method requires certain manual operation and assists the generation of wrapper through data annotation. Usually, these annotation operations are relatively simple, and annotators can complete them without mastering programming knowledge. The commonly used semiautomatic data-aware wrappers are divided into two categories: one is the wrapper constructed by inductive derivation, including pattern rule method and template tree matching method. The other is a wrapper constructed by machine learning method, which trains statistical models from the feature data of web pages to realize data perception and analysis.

2.3. Automatic Data Perception Method. The methods that can generate data perception rules without user participation and manual labeling of training samples are collectively called automatic data perception methods. Commonly used automatic data-aware wrappers are divided into three categories: (1) ontology-based data-aware wrappers, (2) visual-based data-aware wrappers, and (3) repetitive similar subtree-based data-aware wrappers, all of which can adaptively adjust data-aware rules to adapt to the changes of web page structure.

3. Feature Fusion Model

3.1. Summary of AE-IFF Model. The purpose of this model is to correctly predict the emotional polarization of texts. The bottom layer of the model is a text attribute separation module and image attribute separation module. The main work is to transform the text from $X = \{x_1, x_2, \cdots, x_M\}$ to $Y = \{y_1, y_2, \cdots, y_M\} \in \mathbb{R}^{d_w \times M}$, where d_w represents the word vector dimension, and converts the image into a fixed-size vector. The next layer of the model is a feature synthesis module, which includes a fine-grained attention mechanism, which learns to share hidden representations of text and images interactively and allows modal synthesis. Above the model is a fully integrated layer, which combines two different primary and secondary functions of the module as the input of the classifier to perform the emotion classification task.

3.2. Text Function Decoding Module. The function of the text element extraction layer is to map each word to a small dimensional vector called an embedded word. There is a lot of noise in the text data of social media, which affects the accuracy of feature extraction. In order to eliminate interference and obtain more efficient functions, this chapter uses sparse noise reduction automata to extract text functions.

3.2.1. Construction of a Rare Automatic Encoder. In the previous article, the concept, basic principle, and formal representation of automatic encoder have been briefly described. When the hidden layer unit is smaller than the input unit, the automatic encoder will have a better effect in feature extraction. In contrast, if the number of units is just the opposite of the above, an additional sparsity constraint needs to be added to the loss function of an automatic encoder, which is called a sparse automatic encoder.

In this section, some improvements are made to the common automatic encoder by adding sparsity constraints. Inspired by the fact that the number of activated neurons in the brain is very small, we make the activation in neural network in sparse form.

Assuming that the input is X and the activation of the J th hidden unit is $\widehat{\rho}$, the average activation function is shown in

$$\widehat{\rho} = \frac{1}{m\sum_{i=1}^{m} h_j(x^i)}. \tag{1}$$

After the average activation is defined, the sparsity constraint ρ can be given as shown in

$$\widehat{\rho}_j = \rho. \tag{2}$$

In the above formula, ρ is usually called sparse parameter. In order to achieve the above biological characteristics, ρ is usually equal to a very small value. This paper makes an empirical study on the selection of sparse parameters. According to the survey, in many published literatures, researchers mostly choose the number far less than 1 as the sparse parameter. In order to control the weight of the function, a superparameter a is introduced, and the final function is shown in

$$\begin{aligned} &L_{\text{sparse}}\left(W, W', b_1, b_2; X\right) \\ &\quad = L\left(W, W', b_1, b_2; X\right) + \beta \sum_{j=1}^{s_2} KL\left(\rho \middle\| \widehat{\rho}_j\right), \end{aligned} \tag{3}$$

$$\mathrm{KL}\left(\rho \middle\| \widehat{\rho}_j\right) = \rho \log \frac{\rho}{\widehat{\rho}_j} + (1-\rho) \log \frac{1-\rho}{1-\widehat{\rho}_j}. \tag{4}$$

In addition, $\mathrm{KL}(\rho \| \widehat{\rho}_j)$ is called KL divergence, which is used to measure the different degrees between p and $\widehat{\rho}_j$. $L_{\text{sparse}}(W, W', b_1, b_2; X)$ is used to indicate the loss function of sparse automatic encoder. Similar to the selection method of sparse constraints, β can be set to 3 or 5. In fact, the setting method of these parameters has a good effect in practical application. Obviously, β cannot be 0, because this will eliminate the effect.

3.2.2. Construction of Noise Reduction Self-Encoder. Noise reduction self-encoders are usually used to learn more robust features. In addition to the normal encoding and decoding stages, it also includes the destruction operation before encoding. The destruction operation is mainly to destroy the input matrix of eigenvectors in the original data, which is similar to adding some artificial noise. The destruction of the original data by the noise reduction self-encoder can be expressed by

$$X_c = \text{rand}\,(C_l) \times X. \tag{5}$$

In the above formula, rand $(\cdot)$ generates a matrix with the same dimension as X. After obtaining the data, encoding and decoding can be performed using corrupted data, as shown in

$$h = f(W \times X_c + b_1). \tag{6}$$

In contrast, the decoding process remains unchanged. It should be noted that when calculating the actual loss value $L(\cdot)$, the difference between the initial data and the original data is still compared. There are three common damage operations for noise reduction automatic encoders:

(1) Gaussian noise: $\tilde{X} = X \sim x(X, \sigma^2 I)$

(2) Masking noise: randomly selecting some pixels in sample X and setting the value to 0

(3) Salt and pepper noise: a single pixel is randomly selected based on a binomial distribution and the value is set to a predefined maximum or minimum value

It should be noted that the automatic encoder for noise reduction is not used for noise reduction in practical application, but for learning more effective and robust features. As for the specific meaning of effectiveness, in this section, it refers to using the features learned by the automatic noise reduction encoder to obtain higher classification accuracy. The weight matrix can be initialized with $[-1/\sqrt{\text{fan}_{\text{in}} + \text{fan}_{\text{out}}}, -1/\sqrt{\text{fan}_{\text{in}} + \text{fan}_{\text{out}}}]$ or $[-4/\sqrt{\text{fan}_{\text{in}} + \text{fan}_{\text{out}}}, -4/\sqrt{\text{fan}_{\text{in}} + \text{fan}_{\text{out}}}]$, which can avoid the nondifferentiable weights.

3.2.3. Training Sparse Noise Reduction Self-Encoder. Generally speaking, the difference between noise attenuation self-encoder and sparse noise attenuation self-encoder is that the latter introduces scarcity constraint to the loss function. The training method of sparse noise reduction self-encoder mainly includes the following five steps:

(1) The original dataset X is damaged, and the result X_c is obtained

(2) Forward propagation with X_c as input, and then, output Y is obtained

(3) Calculate the loss value

(4) Optimize bias using back propagation

(5) Repeat 2-5 until the function converges

In general, histograms allow us to measure the similarity between original text data and reconstructed text data from a statistical point of view. However, due to the low dimension and strict preprocessing of commonly used social media texts, the evaluation results obtained by histogram are not clear. Therefore, this paper uses correlation coefficient to evaluate the compatibility of text data before and after reconstruction, and the calculation method of correlation coefficient is shown in

$$\mathrm{Corr} = \frac{\sum_{i=1}^{n}(x_i - \bar{x}) \times (y_i - \bar{y})}{\sqrt{\sum_{i=1}^{n}(x_i - \bar{x})\sum_{i=1}^{n}(y_i - \bar{y})}}. \tag{7}$$

In the above formula, x_i represents the original data, y_i represents the reconstructed data, and X and Y are the mean values of x_i and y_i, respectively.

By using sparse noise reduction self-encoder, the model can extract the most representative key features from the text dataset, reduce the interference of noise, improve the robustness of text features, and effectively overcome the overfitting problem.

3.3. On Feature Extraction of Image. We have already introduced the basic principle and structural characteristics of variational self-encoder. The purpose of this section is to extract image features containing emotional information from image data.

Variational self-encoder is a variational extended model of automatic encoder, which is similar to classical automatic encoder. After the decoder reconstructs the encoded result, the reconstructed model is obtained. The model remaps its own hidden features to the probability distribution of the decoded result. The smaller the error between the new probability distribution and the old original distribution, the better the effect of the model.

The network of variable self-encoders has two components, and its loss function can be expressed by

$$L(\phi, \mu, a) = E_{q\phi(d|a)}\left[\log p_\mu(a|d)\right] - D_{KL}\left(q_\phi(d|a)\middle\|p_\mu(d)\right). \tag{8}$$

Loss functions usually consist of two subterms.

Data itself has certain independence, and some vectors in the original features can well represent their independent characteristics. In this section, the variant $\beta-$VAE of variational self-encoder is used for experiments. $\beta-$VAE introduces unwrapping prior into variational self-encoder; it can prove the independence of data by using different variables. This expansion prior enables the encoder to learn a concise representation of data, which is beneficial to the subsequent emotion analysis tasks in this section and improves the overall performance of the model. The loss function of $\beta-$VAE can be expressed by

$$L(\phi, \mu, a) = E_{q\phi(d|a)}\left[\log p_\mu(a|d)\right] - \beta D_{KL}\left(q_\phi(d|a)\middle\|p_\mu(d)\right). \tag{9}$$

As can be seen from the above equation, $\beta-$VAE introduces an adjustable hyperparameter β, which can keep a balance between potential variable dimensional changes and the accuracy of reconstructed data. Gauss's transcendental homogeneity also sets invisible constraints behind the learning process. The teacher of the model is associated with the value of β, so the value of β must be constantly adjusted in the experiment, so that the model can use extended representation to learn different levels of functions.

The function of attention mechanism in neural network mentioned in this paper is very similar to the relationship between human visual attention mechanism and brain. The function of attention mechanism is to screen some key information from complex information, and then downstream tasks use these key information to achieve the expected goals. By analyzing the global features of input data, the attention module learns the intrinsic meaning of feature expression and selectively extracts features containing key information.

In this paper, we construct new input data according to the feature γ generated by the pretrained encoder and input it into the attention module, $\gamma \in R^{b\times h\times w\times c}$. As shown in equations (10)–(13), the original feature C fuses the

Table 1: Basic information of dataset.

Dataset	Number of samples	Characteristic dimension	Category
Chess	3196	36	2
Chair	1000	64	2

Table 2: Classifier integration scheme.

Number of base classifiers	Base classifier combination	Difference
2	(SVM, ANN)	0.68
	(SVM, Bayes)	0.78
3	(SVM, ANN, Bayes)	0.81
	(SVM, SoftMax, random forest)	0.84
4	(SVM, ANN, KNN, Bayes)	0.85
	(random forest, SVM, ANN, Bayes)	0.84
5	(random forest, SVM, ANN, KNN, Bayes)	0.86

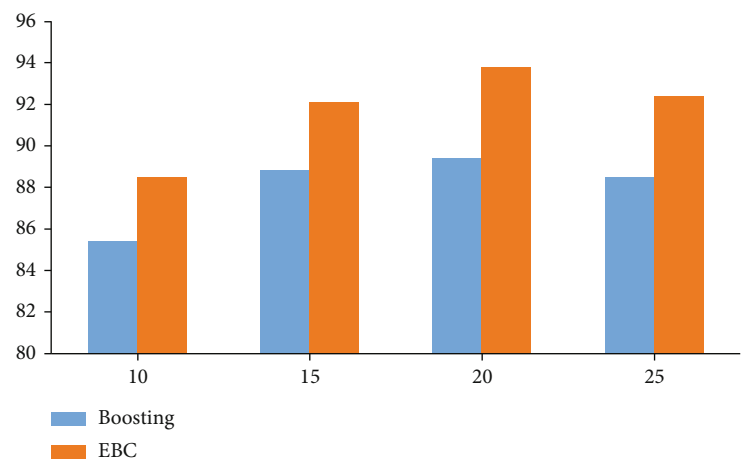

Figure 1: Voting method.

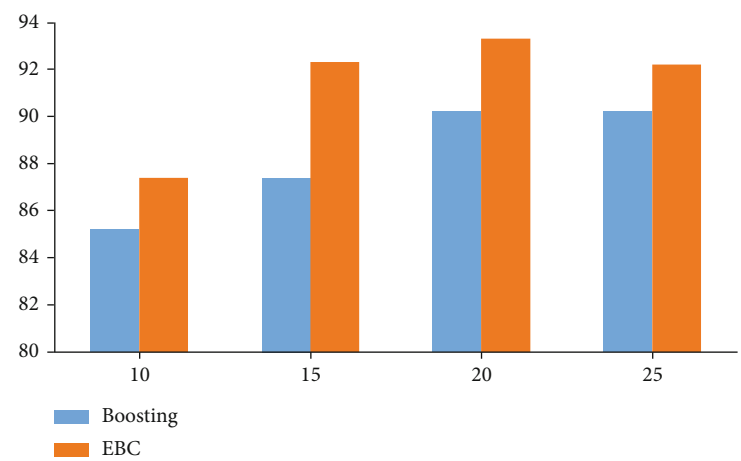

Figure 2: Linear combination method.

multisource information in the convolution kernel through convolution calculation and calculates new feature sequences Q and K, the size of the convolution kernel is 1, the dimension of the new feature sequence is $R^{a\times c}$, and $a = h \times w$. Then, we multiply the transpose matrix of Q and the transpose matrix of K to obtain the product of them. Finally, we standardize the results to obtain the final attention probability distribution a_{ij}, and the dimension of a_{ij} is $c \times c$. By comparing the attention weights of γ in each channel, this module enhances the effect of key attribute set and reduces the influence of redundant attributes on final attribute extraction, as shown in

$$Q = \text{reshape}(F_{\text{CNN}}(\gamma\,;\mu_1)), \tag{10}$$

$$K = \text{reshape}(F_{\text{CNN}}(\gamma\,;\mu_2)), \tag{11}$$

$$V = \text{reshape}(\gamma), \tag{12}$$

$$a_{ij} = \frac{\exp\left(Q_i \cdot K_j\right)}{\sum_{i=1}^{C}\exp\left(Q_i \cdot K_j\right)}. \tag{13}$$

Finally, the weighted sum of the weighted coefficient a_{ij} and the input feature vector of the original feature is carried out, and the summed result is fine-tuned with the scale coefficient β, so that the feature expression O_j containing key information can be obtained as shown in

$$O_j = \beta \sum_{i=1}^{c}\left(a_{ij} \cdot V_i\right) + \gamma_j. \tag{14}$$

In the above formula, β is initialized to 0, which will gain more and more weights in the process of learning features of the model.

3.4. Interactive Fusion Module. For feature extraction, this paper designs an interactive feature fusion module to fuse the two. The attributes of the first two modules are used as the input of the attribute fusion module, and the two input modes are combined to output from the target mode. Given a primary input $E = \{E_1, E_2, \cdots, E_n\} \in \mathbb{R}^{d_c \times n}$ and an auxiliary input $G = \{G_1, G_2, \cdots, G_l\} \in \mathbb{R}^{d_i \times l}$, the primary

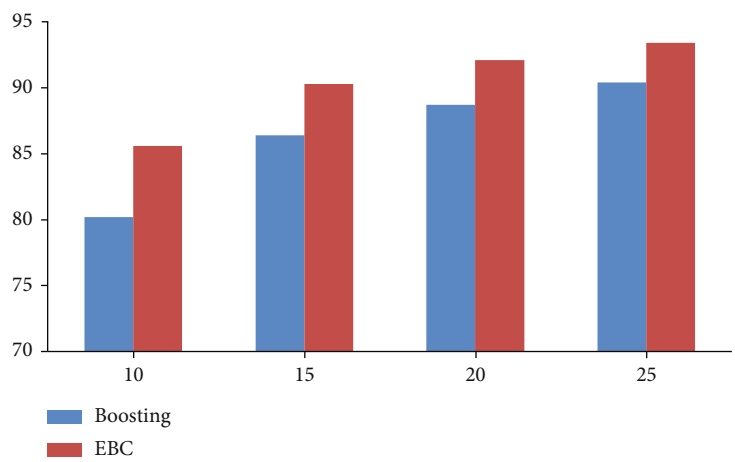

Figure 3: Voting method.

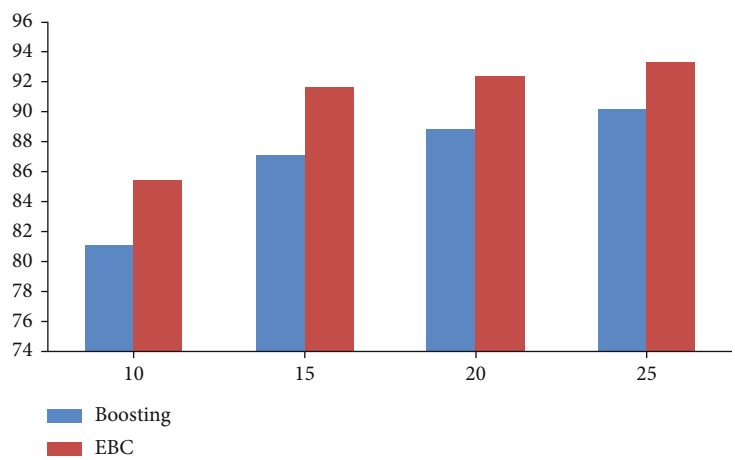

Figure 4: Linear combination method.

and secondary inputs are projected into the space vector at the same time, as shown in

$$E_{\text{emb}_i} = \tanh\left(P_{E_{\text{emb}}} E_i + C_{E_{\text{emb}}}\right), \tag{15}$$

$$G_{\text{emb}_i} = \tanh\left(P_{G_{\text{emb}}} G_i + C_{G_{\text{emb}}}\right). \tag{16}$$

In the above formula, d_v represents the dimension of space vector. In this section, the function of E_{emb} and G_{emb} is to calculate matrix $M \in \mathbb{R}^{n \times l}$, and matrix M can be expressed by

$$M_{ij} = {E_{\text{emb}_i}}^T G_{\text{emb}_i} \tag{17}$$

To measure the importance of secondary inputs, M is quantified using the softmax function as shown in

$$M_{ij} = \frac{\exp\left(M_{ij}\right)}{\sum_{j=1}^{l} \exp\left(M_{ij}\right)}. \tag{18}$$

Then, you get an attention-based auxiliary input J, as shown in

$$J = G \cdot M^T. \tag{19}$$

Finally, E and J are inputted to the full connection layer and then the fusion feature is obtained$U = \{U_1, U_2, \cdots, U_n\}$, as shown in

$$U = \tanh\left(P_u[E_i : J_i] + C_u\right), \tag{20}$$

where E_i and J_i are inputted to the full connection layer.

Through the modules mentioned before, the fused features are obtained. Some of which are text-based and image-supplemented features, and the other is image-based and text-supplemented features. We connect them, input the last full connection layer, use softmax function to process, and complete the task of emotion classification.

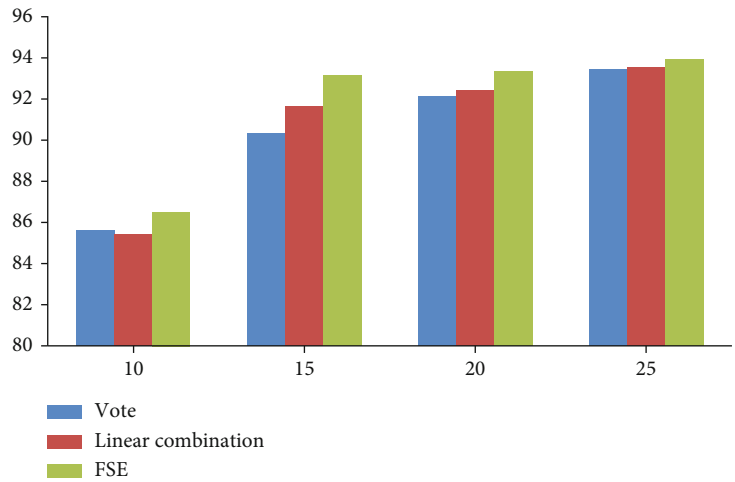

Figure 5: Recognition rate of classifier combinations of different sizes constructed by boosting method.

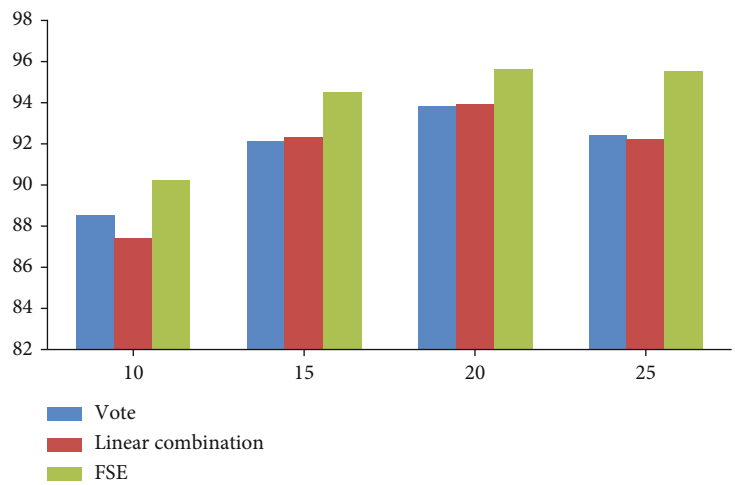

Figure 6: Recognition rate of classifier combinations of different sizes constructed by boosting method.

Table 3: Experimental results (MAE).

	MovieLens-100K	MovieLens-1M	MovieLens-10M
NMF	0.7677	0.7203	0.6788
SVD++	0.7422	0.6881	0.6146
PMF	0.7532	0.6685	0.635
ASDAE	0.7487	0.6911	0.62
Ours	0.7398	0.6681	0.6127

Table 4: Experimental results (RMSE).

	MovieLens-100K	MovieLens-1M	MovieLens-10M
NMF	0.9327	0.9254	0.9036
SVD++	0.911	0.8681	0.8165
PMF	0.9433	0.8821	0.8422
ASDAE	0.8801	0.8368	0.7865
Ours	0.867	0.8133	0.7516

4. Analyze the Experimental Results

4.1. Environment for the Experiment. The algorithm in this chapter is experimented with MatlabR2010b on a computer with 2.53 GHz CPU and 4 GB memory capacity. In the experiment, the chess dataset in UCI database is used as the experimental sample to simulate the image information obtained by sensors in real scene. The basic information is shown in Table 1. The data is classified into two categories: winning and nonwinning. Features have been extracted from the dataset, and each group is a 36-dimensional feature array. In the data sampling stage, 2000 samples are extracted as classifier training sets; we extract 400 samples as integrated training set; 500 samples are selected as the test set.

Taking 300 samples as training set; 500 samples are selected as the test set. Because the proposed model deals with the original data, the experimental dataset also uses the real dataset chain. The data are divided into two categories: chairs and nonchairs, and the picture resolution is 800∗800. In the feature extraction stage, ANN is used to extract features independently, and each sample forms a group of 64-dimensional feature arrays. In the data sampling stage,

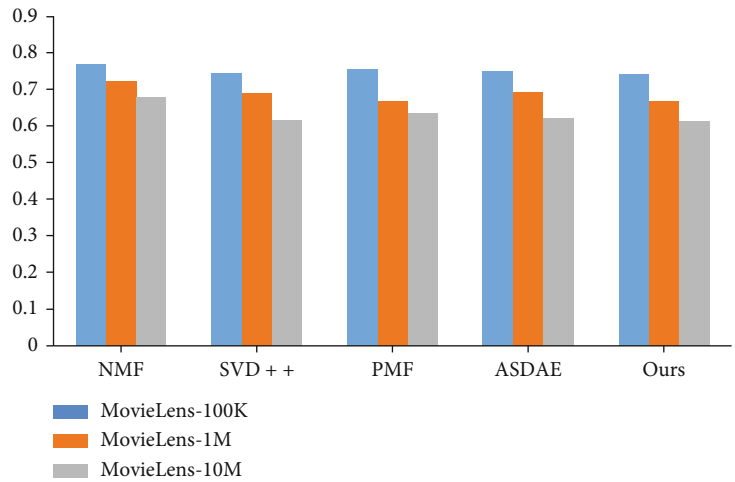

Figure 7: Experimental results (MAE).

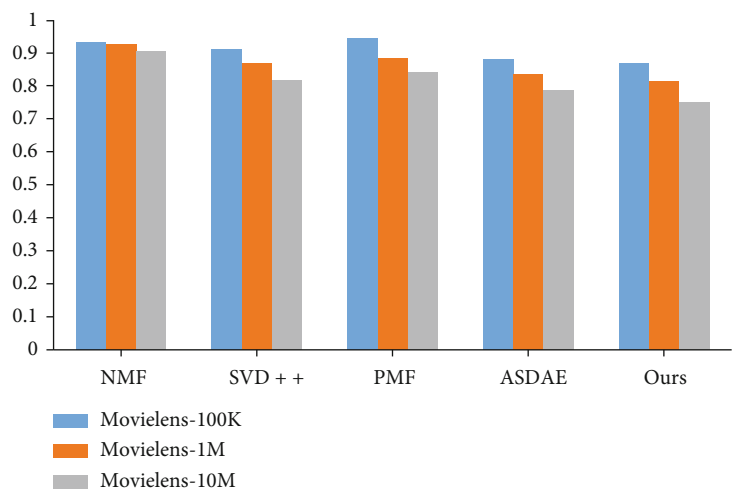

Figure 8: Experimental results (RMSE).

600 samples are extracted as classifier training sets; we extract 300 samples as integrated training set; 100 samples are selected as the integration test set.

4.2. Experimental Design

(i) Experiment 1: comparison of accuracy between selected base classifier and unselected ensemble classifier

Because there are many machine learning algorithms and the corresponding generalizations are countless, it is obviously unrealistic to enumerate all strong classifiers and select the best classifier. Therefore, only for the commonly used machine learning classifiers and chess datasets, the classification combination scheme is obtained by using the base classifier evaluation method proposed in this paper, as shown in Table 2.

Because the effect of boosting ensemble classifier is obviously better than bagging, in the comparative experiment, boosting algorithm is used to train and generate a new base classifier, that is, randomly select a subset of samples as the training set repeatedly. The base classifier is CART tree. Using boosting algorithm, some samples are randomly selected from the training samples to form 10, 15, 20, and 25 sample subsets, and the 10, 15, 20, and 25 base classifiers generated by them are combined to calculate their recognition rates and use them to identify the integrated training samples. According to the recognition rates, the group with the highest recognition rate is selected. The base classifier evaluation algorithm is used to select the corresponding number of base classifier combinations with the largest difference from common classifiers and finally calculate their respective recognition rates. Both of them use voting method and linear combination method to complete classifier integration. Figures 1 and 2 show the recognition rates of classifier combinations of different sizes directly constructed by boosting method, and Figures 3 and 4 show the recognition rates of base classifier evaluation method.

As can be seen from Figures 1–4, under the chess dataset, the accuracy of the integrated classifier without the base classifier evaluation method reaches the highest 90.2% when the

number of classifiers is 20 and 25. Under the condition of the same number of base classifiers, the recognition rate of the ensemble classifier using the base classifier evaluation method is up to 93.9% and 92.2%. Under the chair dataset, when the number of classifiers is 15, the recognition rate increases by 4.5% at the highest. Therefore, the evaluation method of base classifier can effectively improve the recognition rate of ensemble classifier. At the same time, it can be found that when constructing a multiclassifier ensemble system, the more classifiers, the better.

(i) Experiment 2: comparison between FSE integration method and common integration methods

In order to compare the difference between using FSE integration method and common integration methods, FSE integration method is added on the basis of Experiment 1. The specific results are shown in Figures 5 and 6.

As can be seen from Figures 5 and 6, under the chess dataset, the recognition rate of FSE integration method is nearly 2% higher than that of voting method and linear combination. The recognition rate is also about 1% higher under the chair dataset. Therefore, using FSE ensemble method can further improve the recognition accuracy of the final ensemble classifier.

4.3. Analysis of Experimental Results. The experimental results between the model proposed in this chapter and other comparison algorithms are shown in Tables 3 and 4. The trend chart is shown in Figures 7 and 8.

It can be seen from Table 4 that PMF is the worst performance among the comparison methods, and the method proposed in the article is the best performance. With the increase of data volume, the performance of different models is getting better and better. The method used in this paper shows the best performance.

The experimental results show that the MAE of the model in this chapter is 0.7398, 0.6681, and 0.6127 and RMSE is 0.8670, 0.8133, and 0.7516, respectively, on MovieLens-100K, MovieLens-1M, and MovieLens-10M datasets. Compared with other comparison methods, for example, the model of aSDAE, which performs well in the experiment, has MAE of 0.7487, 0.6911, and 0.6200 and RMSE of 0.8801, 0.8368, and 0.7865, respectively, on the three datasets. Moreover, the experimental results in Figures 7 and 8 can also intuitively show the improvement of the experimental performance of the design model in this section. This shows that this section can mine the feature combination relationship between multisource data well by introducing multisource data features and designing feature crossover mechanism, Therefore, it can be inferred that the model in this section can not only make full use of the interactive data between users and projects but also mine more meaningful information through automatic feature cross-mining, so as to achieve better recommendation.

This section introduces the model structure and composition of the recommended multisource neural cooperative filtering algorithm, which ensures the efficiency of the recommended model for MovieLens-100K, MovieLens-1M, and Movielens-public datasets. Compared with NMF, SVD++, PMF, and ASDAE, the proposed recommendation algorithm has higher accuracy.

5. Concluding

Now, although the algorithm of using multisource data for recommendation has made some progress, there are still many shortcomings that need to be solved and optimized. At the same time, there is a lot of room for improvement of the model, so we can design fusion strategies and recommendation strategies that meet different scenarios from different angles. Through the analysis and experimental verification of this paper, it can be concluded that the multisource data related to the recommendation task can be effectively fused, modeling user interest preferences more accurately, more fine-grained modeling of users' interest preference, and in-depth understanding of users can provide users with more targeted and valuable suggestions and can provide better recommendation results for different users. Better user interest modeling and more effective features can improve the ability of recommendation system more effectively.

Data Availability

The experimental data used to support the findings of this study are available from the corresponding author upon request.

Conflicts of Interest

The authors declare that they have no conflicts of interest.

References

[1] J. Zhang, K. T. Chen, M. Jia, and T. Baba, "Hybrid MAC-based multipoint relay with energy awareness for system data sharing in wireless sensor network," *Journal of Signal Processing*, vol. 16, no. 6, pp. 527–535, 2012.

[2] R. C. Downs, "Live panoramic surveillance and spatial awareness achieved through optimized array sensor at source data fusion," *Proceedings of SPIE-The International Society for Optical Engineering*, vol. 4363, pp. 198–206, 2001.

[3] C. P. Minor, D. A. Steinhurst, and K. J. Johnson, "A full-scale prototype multisensor system for damage control and situational awareness," *Fire Technology*, vol. 46, no. 2, pp. 437–469, 2010.

[4] P. Bouvry, S. Chaumette, G. Danoy et al., "Using heterogeneous multilevel swarms of UAVs and high-level data fusion to support situation management in surveillance scenarios," in *IEEE International Conference on Multisensor Fusion & Integration for Intelligent Systems*, Baden-Baden, Germany, 2017.

[5] Y. Zhang, J. Sun, and J. Wang, "Detecting driver distractions using a deep learning approach and multi-source naturalistic driving data Transportation Research Board (TRB)," *99th Annual Meeting*, vol. 25, 2020.

[6] R. Guo, Y. Zhou, J. Zhao, R. Yao, B. Liu, and X. Zhang, "Unsupervised spatial-awareness attention-based and multi-scale domain adaption network for point cloud classification,"

International Journal of Wavelets Multiresolution and Information Processing, vol. 19, no. 4, p. 2150007, 2021.

[7] G. Chen, J. P. Cai, and J. Yang, "Network security situation awareness based on multi-source data fusion," *Advanced Materials Research*, vol. 989-994, pp. 4885–4888, 2014.

[8] J. T. Thomas, D. Gains, and A. Malloy, "Content-based image exploitation for situational awareness," *Proceedings of SPIE - The International Society for Optical Engineering*, vol. 6956, article 695604, 2008.

[9] D. Yong, X. Su, and W. Dong, "Target recognition based on fuzzy Dempster data fusion method," *Defence Science Journal*, vol. 60, no. 5, pp. 525–530, 2010.

[10] L. Chen and W. U. Lenan, "Mobile positioning in mixed LOS/NLOS conditions using modified EKF banks and data fusion method," *IEICE Transactions on Communications*, vol. 92, no. 4, pp. 1318–1325, 2009.

[11] Y. Chen, E. Gunawan, and Y. Kim, "UWB microwave imaging for breast cancer detection: tumor/clutter identification using a time of arrival data fusion method," in *IEEE Antennas and Propagation Society International Symposium*, Albuquerque, NM, USA, 2006.

[12] F. Han, L. Zhu, and X. Zhi, "Measurement of multi-sensor data fusion method based on fuzzy theory," *Journal of Applied Optics*, vol. 30, no. 6, pp. 988–991, 2009.

[13] S. N. Razavi and C. T. Haas, "Reliability-based hybrid data fusion method for adaptive location estimation in construction," *Journal of Computing in Civil Engineering*, vol. 26, no. 1, pp. 1–10, 2012.

[14] J. Jamshidi, G. W. Owen, and A. R. Mileham, "A new data fusion method for scanned models," *Journal of Computing & Information Science in Engineering*, vol. 6, no. 4, pp. 340–348, 2006.

[15] S. Wu, Y. Bi, X. Zeng, and L. Han, "The experiments with the linear combination data fusion method in information retrieval," in *Asia-Pacific Web Conference on Progress in www Research & Development*, vol. 4976, Shenyang, China, 2008.

Hindawi
Journal of Sensors
Volume 2022, Article ID 8318921, 10 pages
https://doi.org/10.1155/2022/8318921

Research Article

Intelligent English Translation and Optimization Based on Big Data Model

Xiao Yan Wang

Jiang Xi Institute of Economic Administrators, Nanchang, Jiangxi 330088, China

Correspondence should be addressed to Xiao Yan Wang; 000418@jiea.edu.cn

Received 17 March 2022; Revised 19 April 2022; Accepted 21 April 2022; Published 20 June 2022

Academic Editor: Yuan Li

With the development and popularization of communication technology, intelligent analysis using big data front-end in various fields is also skillful. In the study of English literature and short sentence translation, we should realize a fast and intelligent translation approach. Based on the analysis and research of big data, a set of online learning algorithms for English translation learning algorithms is compiled, which will greatly improve the efficiency and accuracy of translation. On the premise of online processing of big data English information, this paper shortens the processing time without affecting the translation accuracy. The radial function algorithm for big data reduces the complexity of big data, improves the computational efficiency of dealing with problems, and realizes the generalization of translation performance. The effective application of big data in the optimization practice of English translation will provide an effective theoretical way for accurate translation and realize intelligent model algorithm. The experimental results are summarized as follows: (1) with the increase of the number of translated texts, the translation time will also increase and the difficulty will increase. (2) The approximation value in radial basis function is used to evaluate the translation effect, and its error in 100 texts will decrease with the increase of literature, and its approximation state is consistent with the real state. (3) Among various translation techniques, conventional literal translation is still the usual method, and its feedback effect is also the best, which is the basic method of thinking according to data. (4) The evaluation of accuracy in intelligent calculation methods is different, from 100% accuracy under heterogeneous functions to 50% accuracy under unified algorithms, which shows that optimization methods need to be updated and improved in time.

1. Introduction

In the realization of text translation, this difficult work is based on the efficient analysis of the network and the Internet. In the face of the analysis of some advanced English literature, powerful data are often needed to support the experimental conditions, so the modeling of data sets should be carried out in time. Under the experimental exploration of big data model, the analysis speed is greatly improved, and the task can be completed efficiently and accurately. In this paper, incremental learning and scientific intelligent algorithm of function expression are adopted to realize high-performance intelligent translation. This paper probes into the present situation and existing problems of the training of sci-tech translators in colleges and universities and analyzes the objectives of the current training mode of sci-tech translators in colleges and universities [1]. It reveals the potential relationship between the linguistic features of passive structures in English original language and the translators' choices in translating passive structures and further confirms and expands the research conclusions [2]. Taking "A Brief History of Time", a scientific and technological reading, and the translation of some lines in "The Theory of Everything" as examples, this paper analyzes and discusses that scientific and technological translation also needs artistic theory [3]. On the basis of investigating the demands of non-English major college students' English listening and speaking learning based on WeChat, this paper designs a college students' English listening and speaking learning model based on WeChat [4]. The analysis of college English extracurricular learning activities under the background of "Internet plus Homework" can give some enlightenment to the reform and exploration of college English listening and speaking curriculum [5]. This paper

analyzes the informationization ability of college students' English mobile learning and further studies the strategies to improve the ability of mobile learning [6]. Based on the information flow combing of thematic progression mode, the translation forms are the stability of subject and the order of subject replacement [7]. This paper puts forward that the translation strategy is to make the recipient close to the source language and demonstrates that "alienation" strategy is used in translating culture-loaded words in Zhuang language [8]. Starting from the stages of Western translation competence research, this paper explores the origin of its theoretical research and its symbolic academic achievements [9]. Starting with the analysis of competence concept, we reexamine the composition of translation competence model and use appropriate tools and methods to solve the problems encountered in translation [10]. The practical teaching mode of translation for English majors in physical education colleges is constructed, and the teaching method of "process-oriented" is adopted [11]. This paper discusses how to use linguistic translation theory to guide sports English translation practice, defines the types and functions of sports texts by studying text types, and analyzes cases through literature review [12]. Constructing a perfect translation evaluation system makes it clear that scientific translation concepts should be established in college English translation teaching [13]. This paper discusses the teaching of college English translation and its innovation, to improve students' English translation ability and provide better services for social and economic development [14]. It shows that the first principle of translation is the purpose of translation, and the goal achieved has a great influence on the whole translation behavior [15].

2. Online Learning Method for Big Data

2.1. Online Learning Algorithm for Radial Basis Function Construction. The farther away from the center and the distance point, it is a monotone decreasing function, which is defined by Gaussian function theory. Assuming that a function can be approximated by a radial basis function, substituting it into a differential equation and forcing the error of the differential equation to take the minimum under a certain measure on a certain set of data points; thus, determining the coefficient a_j and even the point x_j, this method has also obtained very satisfactory results in some practical applications.

Gaussian function [16]. Formula expression:

$$h(x) = \exp\left(-\frac{(x-c)^2}{r^2}\right). \tag{1}$$

Its C and R represent the radial center and radius, and the distance decreases monotonously as the distance from the center is farther away.

Multiple quadratic radial basis functions [17]:

$$h(x) = \frac{\sqrt{r^2 + (x-c)^2}}{r}. \tag{2}$$

Multiquadratic radial basis function is a special function, which only increases monotonously with the distance from the center. The more obvious the meridian center is, the more obvious it is.

Radial basis function is a distance independent variable function between the measured point and the range point, which is formed by superposition linearity.

Radial basis function model [18]. The expression is as follows:

$$f(x) = \sum_{i=1}^{m} \beta\varphi(\|x - x_i\|). \tag{3}$$

The interpolation conditions that need to be satisfied are:

$$f(x_i) = F(x_i)(i = 1,\cdots,m). \tag{4}$$

Equations (3) and (4) are combined:

$$A \times \beta = F. \tag{5}$$

Among them,

$$A = \left[\begin{pmatrix} \phi(\|x_1 - x_1\|) & \cdots & \phi(\|x_1 - x_m\|) \\ \vdots & \ddots & \vdots \\ \phi(\|x_m - x_1\|) & \cdots & \phi(\|x_m - x_1\|) \end{pmatrix}\right], \quad F = \begin{bmatrix} F(x_1) \\ F(x_m) \end{bmatrix}. \tag{6}$$

Positive definite function, namely,

$$\widehat{\beta} = A^{-1} \times F. \tag{7}$$

Commonly used kernel functions are as follows.
Multiquadratic function [19] is:

$$\varphi(r) = \left(r^2 + c^2\right)^{1/2}. \tag{8}$$

Inverse multiquadratic function [20], namely,

$$\varphi(r) = \left(r^2 + c^2\right)^{-1/2}. \tag{9}$$

Thin plate spline function [21] is expressed as:

$$\varphi(r) = \left(\frac{r}{c}\right)^2 \log\left(\frac{r}{c}\right). \tag{10}$$

The calculation formula of logarithmic path function [22] is:

$$\varphi(r) = \frac{1}{1 + e^{r/c}}. \tag{11}$$

In the above expression, $c > 0$.

2.2. Data-Based Unified System Representation Algorithm. Realize structured and semistructured feature quantization, and form a tensor model, which also represents a big data

fusion model of data eigenvalues. When constructing features based on structured, semistructured, and unstructured data models, the basic fusion of models is obtained according to the corresponding data subtensor models. Under the fusion of the acquisition system of big data analysis platform, the data is converted to ensure the integrity of the structure. Implement data formulas for unstructured data, semistructured data, and structured data. Semistructured data is the data set of nodes, which has a hierarchical structure on each node, and the data model is obtained according to the tag type and object value. The flow chart is as follows in Figure 1.

The unified tensor model is obtained by coding high-dimensional data. Defined as:

$$T \in R^{I_1 \times I_2 \times \cdots \times I_P} T \in R^{I_1 \times I_2 \times \cdots \times I_P} T \in R^{I_1 \times I_2 \times \cdots \times I_P}. \tag{12}$$

Among them, R defines the different attributes of data in each stage, the extension of tensor, and the definition of operator.

Semitensor product [23]. Defined as:

$$X \infty Y := \sum_{i=1}^{m} X^i Y_i \in R^n. \tag{13}$$

X belongs to a row of vectors of R, and Y belongs to a row of vectors of R.

The half vectors of X and Y, namely,

$$X \infty Y := \left(Y^T \infty X^T\right) \in R^n. \tag{14}$$

Tensor expansion multiplication follows the function [24]. Expression:

$$f : A \infty B \longrightarrow C, C \in R^{I_1 \infty I_2 \infty I_n}. \tag{15}$$

AB associative law. Among them,

$$(A \infty B) \infty C = A \infty (B \infty C). \tag{16}$$

Two time operators of tensor extensibility constitute heterogeneous data sets, with time orders T1 and T2, and their dimensions are:

$$\begin{aligned} I_{i-1} &\in \{i_1, i_2\}, \\ I_{i-2} &\in \{i_2, i_3\}. \end{aligned} \tag{17}$$

This can be expressed as a merging time order.

2.3. Quantitative Model of Multisource Heterogeneous Data. In order to ensure the quantitative model of each kind of data, explain its data under different characteristics and stage characteristics.

Quantization of unstructured data. The formula is as follows:

$$T_{\text{video}} = R^{I_f \times I_w \times I_h \times I_c}, \tag{18}$$

where I is the stage data, R is the quantitative expression, and the data eigenvalue is obtained according to the fourth-order tensor model.

The semistructured data formula is as follows:

$$X \in R^{I_{er} \times I_{ec} \times I_{en}}, \tag{19}$$

where er is the row that identifies the matrix, ec is the column of the matrix, and en is the encoding of the elements.

In the managed database, the main data is stored and exiled, which is often represented by numbers or symbols, and then has matrix expressions.

2.4. Simulation Experiment for Big Data. Discretization algorithm in incremental efficient equation.

$$\begin{aligned} x_1 &= x_2, \\ x_2 &= -p_1 x_1 - p_2 x_2 - {x_1}^3 + q \cos(\omega t_1). \end{aligned} \tag{20}$$

Discretize it to get:

$$\begin{aligned} x_1(t+1) &= x_1(t) + x_2(t)\Delta t, \\ x_2(t+1) &= x_2(t) + \left(-p_1 x_1(t) - p_2 x_2(t) - {x_1}^3(t) + q \cos(\omega.t).\Delta t\right), \end{aligned} \tag{21}$$

When $t = 0.01$, $p = 1.1$, and q is the sample size, the incremental algorithm will be used to calculate the standard error to achieve the algorithm accuracy in order to avoid accidental errors. Standard error rate [25], that is,

$$\Delta = \sqrt{\frac{1}{n} \sum_{j=1}^{n} \frac{[y(j) - y(j)]^2}{y(j)^2}}. \tag{22}$$

Through the results of simulation experiments, the average sample error rate of training set and test set can be obtained, and the error can be improved again to a reliable range. With the increase of sample size, the accuracy is improved. After many experiments, the learning standardization is obtained, which is suitable for big data.

3. Analysis Based on Data Structure Model

3.1. Formal Theory for Big Data Model. Big data mainly takes two forms: static big data and dynamic streaming data. Dynamic big data will be used when dealing with limited data, while static data is mainly taught by learning methods. The main form of them is to reduce the training time of the process, but there are disadvantages of single collection and reverse data collection. Therefore, it is necessary to improve the characteristics of the model, so that the data flow has the characteristics of infinity, disorder, real-time, and suddenness. The number of texts translated each time is not fixed, but changes in different phrases and long sentences based on the special meaning of the article. By adding and deleting the training set of the text, no matter the text changes dynamically based on the number of words, the time of each practice training set will not change, which improves the translation efficiency and can also translate strong and difficult sentences by 90.

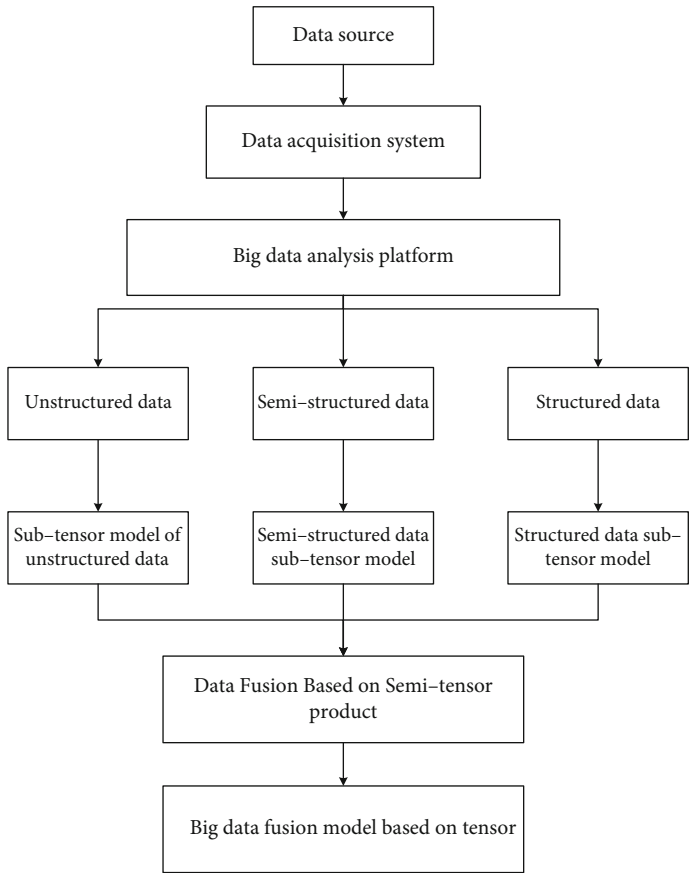

Figure 1: Flow chart of big data fusion model.

First, the essence of data analysis is to verify rather than explore to get a conclusion.

Second, the verification in data analysis can only be falsification rather than confirmation in essence. Strictly speaking, all data-based verifications of the reliability of models and assumptions need to pay attention to the p value.

Third, a model, the biggest assumption is the model itself.

Fourth, a model has not been falsified by data, which does not mean that the model is right, and other models are wrong. It is more likely that a model has not been falsified by data, indicating that the model is OK, but it does not rule out that there are other models that are more suitable.

Fifth, the model is not as complex as possible, but as simple as possible on the premise that it can explain the problem.

Sixth, finding valuable variables depends on domain knowledge and mastery of DGP (data generation process).

3.2. The Central Idea of Big Data Model in Computing Convergence. In some specific translation fields, the model cannot make use of all big data. Compared with the traditional model structure, it cannot represent high-dimensional data variables. Therefore, according to the connection of data eigenvalues, the extended format of high dimension and dimension between data is constructed. There are two basic steps in the formation of big data model:

(1) Data collection

Structured data under different circumstances, such as data in database, text data, audio data, and other data with complete structure, need to be collected. Classify the collected data and send them to the big data platform for the next detailed calculation. When collecting, it is necessary to ensure the authenticity of the data without changing the original format of the data.

(2) Quantitative phase of data

According to the structural data submitted in the early stage, the main data feature is to deal with the quantitative situation. Its main situation is to transform the data uniformly, ensure the structure and feature value unchanged in the process, and encode and merge the missing data in time if there are features missing, so as to reduce the small-scale quality weakening of the data.

When considering the internal relations in phased data fusion, first, it is necessary to ensure the new features of data, and second, it is necessary to ensure the stability of the internal structure of data. Tensioned data structures have the same attributes, and multisource heterogeneous represents unified variables with lower order.

3.3. Analyze Big Data Management Technology. Object-relational database management and system domain model are

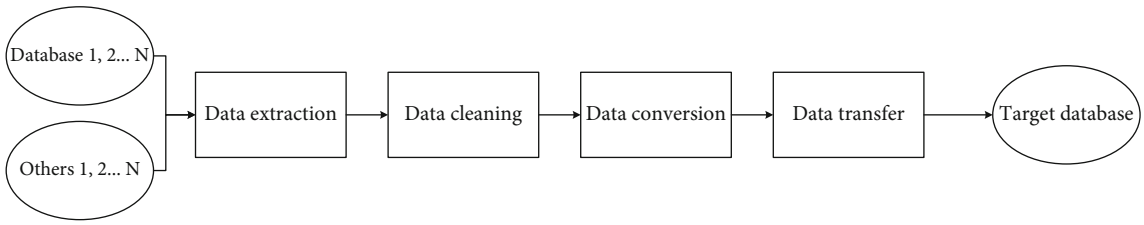

Figure 2: ETL process architecture.

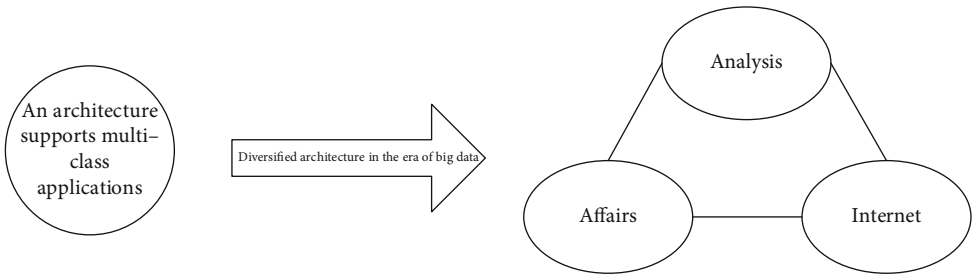

Figure 3: NoSQL schema diagram.

all technical means accompanied by Internet of Things, cloud computing, and spatial data collection. Small data has evolved into the characteristics of big data, and the technical means also present the digital era, dealing with the concept of big data strategically and professionally. Structured data is simply a database, which realizes logical expression and real data by the structure of two-dimensional table. The off-line errors of sample data sets are compared and judged, and the average sample error rate is obtained by dividing the standard error by the total sample data one by one. Institutional data integration must gain insight into and make decisions on huge information assets, so as to realize a new data processing mode. The data set of big data cannot complete all the collection, storage, and management in a certain period of time. The concept of big data management is defined as:

(1) At present, the popularity of software technology and the efficient operation of software tools, in the realization of management, deal with the later improvement of the scale of the operating conditions

(2) After the decision information is quantified, it is modeled, and a data set expressed by grammar is formed for the next summary

(3) It is impossible to implement collection, storage, and management in an all-round way at the same time, so internal management is extremely important and the most solid foundation, to realize comprehensive control for summary work

(i) Understand and support the information needs of enterprises

(ii) Capture, store, protect, and ensure the integrity of data assets

(iii) Ensure data quality

(iv) Ensure data security

(v) Ensure efficient use of data

Turn big data into a basic resource, which is simple and practical, get data management mode from storage, management, and analysis stage, and transform it into reprint of target data planning. The ETL data transformation process is shown in the following Figure 2.

Split the process of data flow into E, T, and L. The ETL framework mainly uses the intermediate processes of data extraction, data cleaning, data conversion, and data transfer to complete the data set of goal planning. In the ETL architecture, the data flow is from the source data flow to the ETL tool, which is a separate data processing engine. Generally, all the data transformation work is realized on a separate hardware server, and then, the data is loaded into the target data warehouse. The performance in the framework is easy for people to understand and make the copywriting ideas clearer. Data extraction needs to select useful data. Nowadays, the main means are automatic extraction and full data extraction, which shorten the time and improve the extraction efficiency compared with traditional manual extraction. The data cleaning needs to filter the wrong data, missing data, and repeated data to avoid affecting the quality of the data and ensure the quality of the data in the application process. The filter data for manual screening and machine quality inspection to achieve the secondary use of the standard greatly increase the data versatility. The task of the transformation process is to synchronize some data with inconsistent progress through transformation, and some particles and regular dynamics will be the transformation of coordinate system. Loading is to load the processed data into the target database and provide the data to the system for use.

3.4. Technical Analysis Based on Big Data Application. In strict compliance with the correct execution of the database, the complete data storage needs to meet the most basic criteria: consistency, isolation, atomicity, and persistence, that is, a

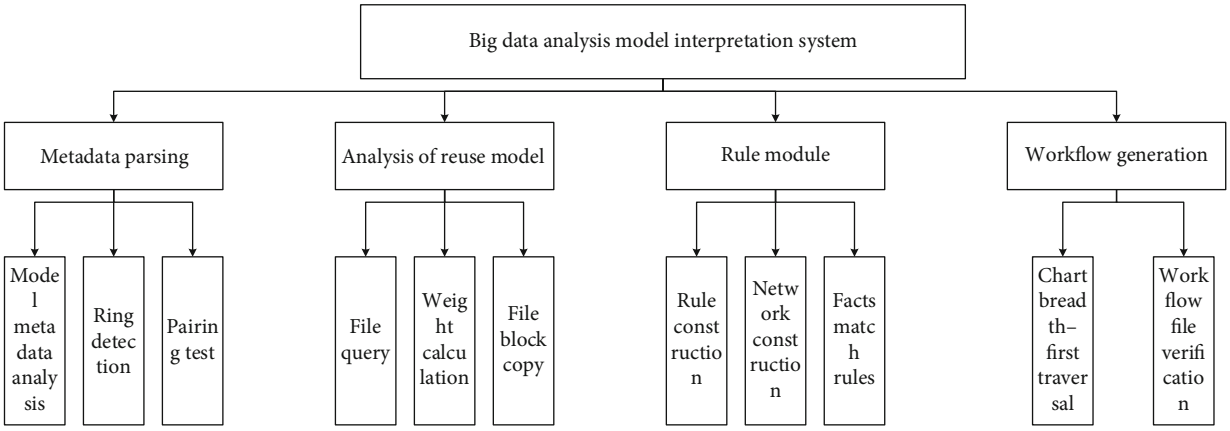

Figure 4: Module explanation frame diagram.

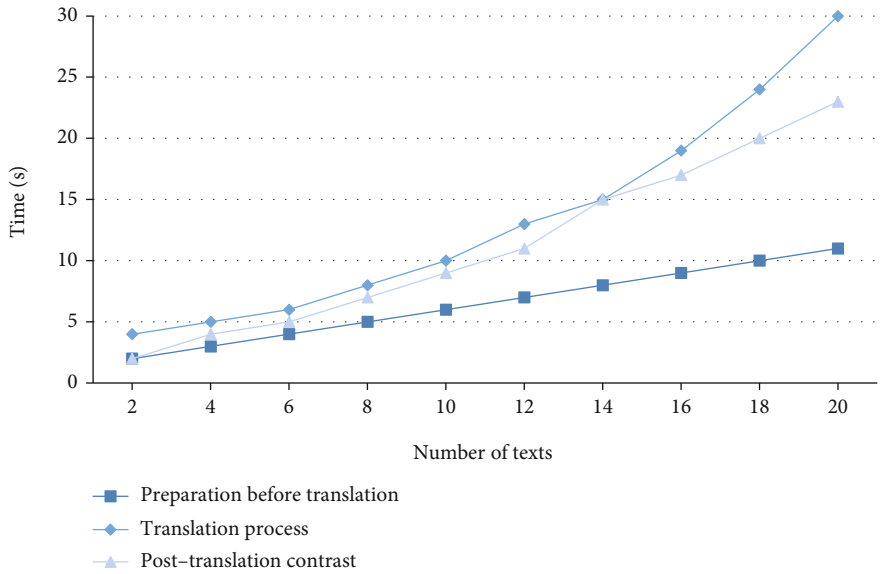

Figure 5: Statistical chart of text quantity translation time under intelligence.

new structure data storage system with high scalability using NoSQL, which will divide and index data. The structure diagram of its old and new transformation is as follows in Figure 3.

Using NoSQL technology to store data will effectively improve query efficiency, reduce the proportion of memory, and clearly identify the location data that is not good at it. This can not only meet the demand of large amount of data but also ensure the comprehensive and persistent functions of the whole system. Under the advantages of high performance and concurrent function of cluster technology, data can be shared to achieve comprehensive utilization of data, and the overload of the system can also be reduced, and the fault and fault-tolerant points of the database will be upgraded and updated.

3.5. Research on the Operation of Data Model. The model data needs to be analyzed and read metadata, and the corresponding directed graph is constructed and aggregated on the reused model through ring measurement and node matching. The big data analysis work based on the rule engine will be divided into componentization and module reuse requirements. The module diagram divided by function is shown in Figure 4.

In the face of data module interpretation frame diagram, the main metadata analysis, and restoration into a framework analysis diagram, for hierarchical division of the model framework file, the parsing, detection, and pairing under metadata parsing need to be restored to acyclic graphs. The analysis of the model is mainly the directory operation of file copying, weight calculation, and file query. The planning module needs to build rules and build network security to finally realize the matching of facts; workflow generation module is responsible for checking the flow direction of nodes and description files.

4. Strategies of English Intelligent Translation and Optimization

4.1. Intelligent English Translation Method. In today's education stage, English teaching tasks have become the key training direction, and the basic preparation stage of Chinese-English

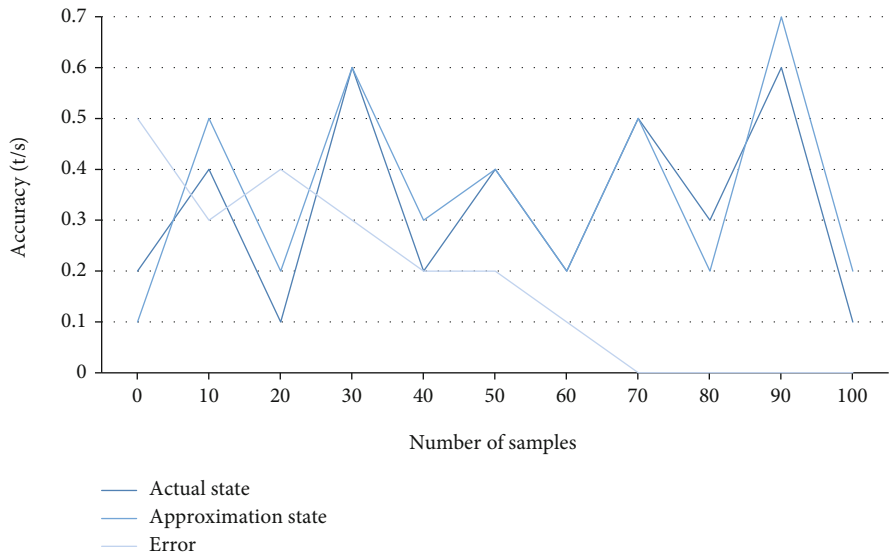

Figure 6: Approximation performance based on radial basis function online translation.

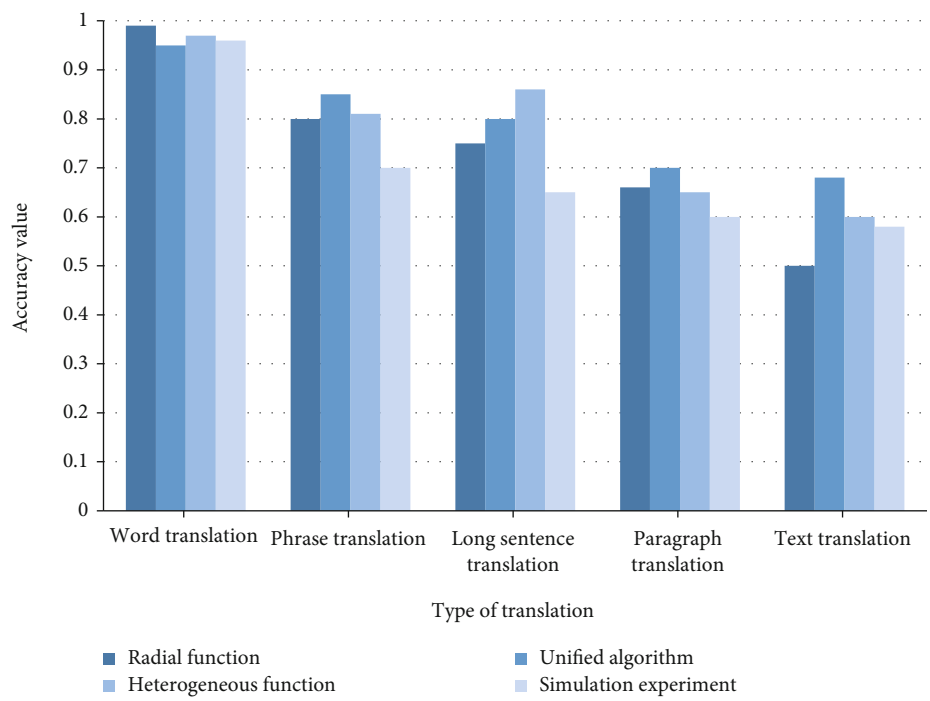

Figure 7: Comparison of translation accuracy.

translation is supported by big data network platform. Under the condition of intelligent and efficient completion progress in the translation process, it will be a brand-new breakthrough stage for English in actual translation. Compared with the translated texts of data sets, the accuracy of translation is particularly important, especially for some overseas documents. That is to say, intelligent optimization is adopted to improve the rapidity and accuracy of English translation. Compared with English translation in different stages under intelligent method, the usage time is shown in Figure 5.

Before translation, it is necessary to have an early understanding of the types, features, concepts, and translation requirements of all texts. In view of the increase of the number of translated texts, this paper makes a detailed time analysis of the whole translation work. As can be seen from the figure, with the increase of the number of translated texts, the working hours will also increase obviously. It takes the most time in the translation process, which is also the most difficult work, and the later processing and comparison work will be relatively simple.

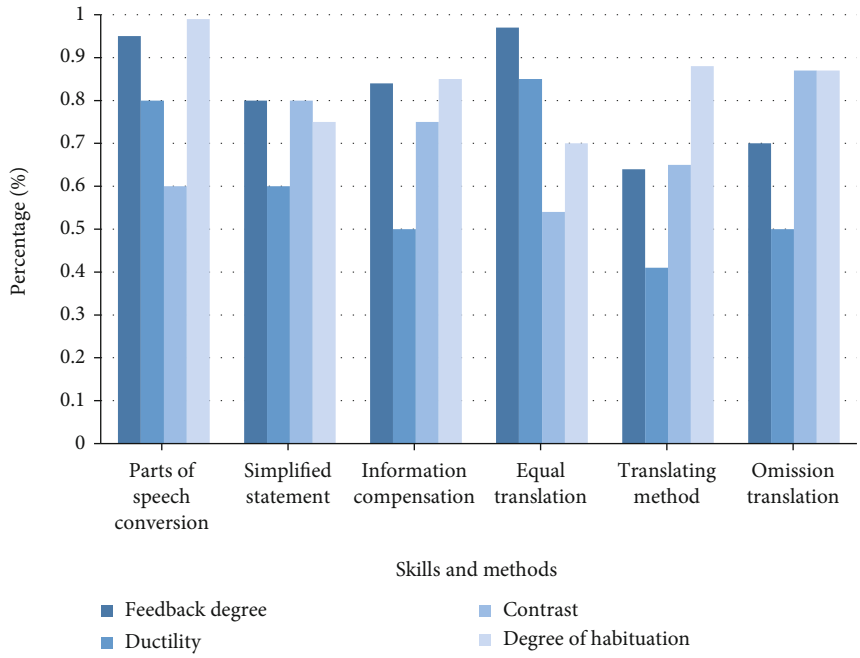

Figure 8: Statistical chart of practical skills.

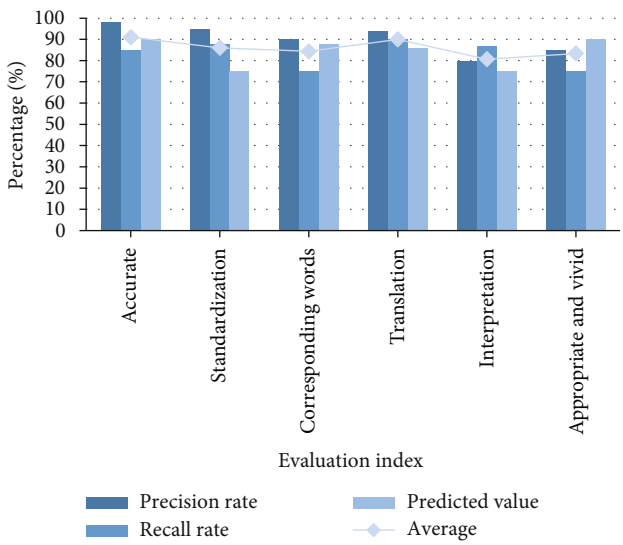

Figure 9: Statistical chart of evaluation index of original model.

4.2. Online Translation Effect Based on Radial Basis Function. The effectiveness of the model is verified by online learning method under simulation experiment, and the next algorithm is optimized according to the simulation experimental results. 100 samples of text are selected to realize the translation simulation experiment, which analyzes the accuracy of the algorithm according to the real and predicted results. The experimental results are shown in Figure 6.

The accuracy of radial function is calculated in the form of approximation value, which is displayed in the form of actual state, approximation state, and error. The experimental results show that the calculated values of the approximate state and the actual state are close to coincide in the online translation of 100 samples, which also shows that the online intelligent translation has high calculation accuracy and can accurately translate the text. When the text translation approaches 70, the calculation error will also drop to 0, which is the effect of improving approximation ability and prediction accuracy.

4.3. Analysis of Data Unified Algorithm in English Translation. In order to achieve a comprehensive and detailed translation of English practice results, the data set will be unified and standardized before the work is carried out. On the basis of unified data algorithm, we can realize accurate translation of English contents, which mainly focuses on the investigation and practice of tasks in evaluation. Its various translation accuracy pairs under big data are shown in Figure 7.

As shown in the experimental results in Figure 7, each intelligent computing method can achieve 100% accuracy in word analysis, but with the increase of difficulty, the translation accuracy of text type is only 50%. When words are expressed in multiple meanings, there will be relatively large differences, which will lead to different semantics of text meanings. Text translation based on radial function cannot meet the experimental requirements, which leads to an increase in translation error rate.

4.4. Translation Skills at the Lexical Level. The actual meaning of Chinese in English is much more profound. English sentences often present spherical structure, while Chinese sentences have strong branch relevance, and mainly analyze the feedback effect of text translation in these methods, and the test results are as follows in Figure 8.

Therefore, in the process of translation, many techniques are used to achieve practical results, such as part-of-speech conversion, simplification, information compensation, equivalent translation, order-changing translation, and ellipsis translation.

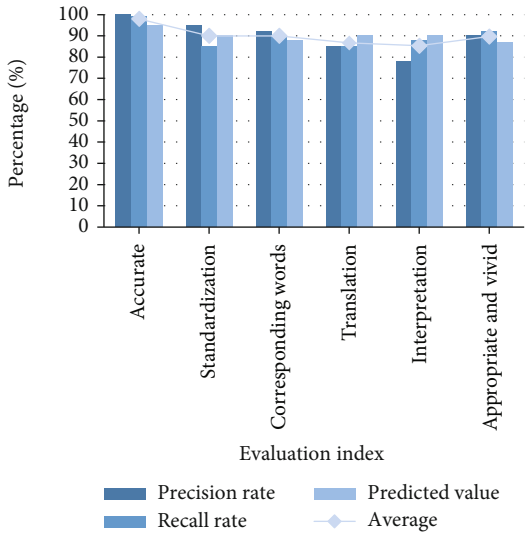

Figure 10: Statistical chart of evaluation index of new model.

He is good at finding out the subject structure in complex sentence structure, especially the subject and predicate of the main sentence, and taking it as the starting point of sentence understanding and translation. The ingenious use of skills depends on people's personal thinking habits. When using a variety of methods to analyze and explain, it can be seen according to the use of different groups of people and feedback. Conventional techniques are realized through literal translation, but in the face of some special methods, it is obviously rarely used by many people. For example, only 50% of people have used it in order-changing translation, while the number of people who use literal translation is very small.

4.5. Summary and Analysis of English Translation Optimization. Starting from the context and getting rid of the surface meaning, we will deal with the translation accurately and flexibly to achieve smooth sentences and clearer regulations. In order to correctly understand the intention of the original text, we should straighten out the internal logical relationship and find reasonable sentence patterns to express it. Compared with the traditional big data processing technology, it can no longer be used in large-scale and highly concurrent network storage structure, and it is in the bottleneck of inability to upgrade and innovate in flexibility and convenience. Therefore, in order to deeply study the development and accuracy of English translation methods, it is the road of change that should be reformed now. With the introduction of the new model, people's interest in reading is greatly enhanced, and the difficulty of translation is reduced. With the continuous evolution of the index model, the analysis dimension of the business field corresponding to the model is gradually clear, and with the accumulation of historical data, it is natural for machine learning to do big data analysis based on these indicators. Its expanded model analysis checks the consistency of statements as shown in Figures 9 and 10.

In the statistical chart of the comparative experiment between the old and new models, based on the analysis of evaluation indicators, after updating the new big data model, the translation accuracy of English has been greatly improved. As far as the accuracy rate is concerned, it has increased from 98% to 100%, and the proportion of each average index has also increased relatively, giving full play to the advantages of the new model. The recall rate of text has a downward trend, that is, it proves that users can play their good effects and make good feedback after using it.

5. Conclusion

With the development of big data, more and more people will apply it to practice, so according to the significance and value of education and assessment industry, it is extremely valued. Therefore, in the assessment and analysis of English talents training, English translation is an important transitional process. In the face of a large number of text translation work, intelligent calculation is needed to realize the efficient and accurate implementation of data processing. In this paper, based on the intelligent optimization of English translation, the experimental analysis will be carried out, and the incremental learning method and the radial function big data model will be used to deeply study the optimization means. The development of big data has promoted the all-round development of education, economy, and system and has also achieved new value significance in English education and training in the education industry. In the era of data development, most educators have shown great interest in English learning. Based on the deepening of foreign exchanges, foreign education is extremely important, which will effectively cultivate talents and move towards deeper learning. In the training of professionals to get comprehensive development, to accept the comprehensive and coordinated development of foreign economy, education, and culture, the results of a large number of text experiments are aimed at improving the translation accuracy, that is, confirming the proposed optimization methods for each working stage. The research results of this paper are as follows: (1) the optimization of English translation methods is the main form in the era of big data, and simple analysis and processing of this set of data will be useful numerical variables for variable realization. (2) By improving the basis function and adopting incremental learning algorithm, the overall performance of designing the big data model will verify the effectiveness of its translation. (3) The simulation experiment is to verify the accuracy of the model, realize the processing of flow-like big data, and build an online English translation model in time. (4) It solves the problem of large amount of text, strengthens the applicability of the model to many kinds of word meanings, achieves effective translation of all contents, and studies in batches in time, which is the main method to effectively reduce time.

Prospects and challenges of experimental content: (1) the complexity and fast updating speed of English literature lead to the reduction of the practicability of relevant data, which is also an important challenge. (2) The extensiveness and spatio-temporal characteristics of big data model may lead to the lack of guarantee of data quality and the increase of translation errors. (3) There will be dynamic system fission in modular analysis, so the process data of sustainable development should be used when creating value. (4) There

is a difference in difficulty between simple vocabulary and high-level vocabulary translation, and it is still necessary to solve the difficult problems in mode up to now.

Data Availability

The experimental data used to support the findings of this study are available from the corresponding author upon request.

Conflicts of Interest

The author declared that there are no conflicts of interest regarding this work.

References

[1] L. Beibei, L. Na, and Z. Jun, "Discussion on the training mode of sci-tech translation talents in colleges and universities under the background of "the belt and road initiative"," *Shanghai Translation*, vol. 6, no. 3, pp. 74–79, 2019.

[2] L. Dingjia and W. Kefei, "Research on Chinese translation of English passive structure-multivariate analysis based on big data," *Audio-visual Teaching of Foreign Languages*, vol. 2, no. 1, pp. 45–52, 2020.

[3] L. Xianyu, "Sci-tech translation from the perspective of translation theory–taking a brief history of time and the theory of everything as examples," *China Sci-tech Translation*, vol. 2, no. 29, pp. 40–59, 2016.

[4] C. Yangli, "An empirical study on English listening and speaking learning demands of non-English majors based on WeChat," *Audio-Visual Education Research*, vol. 35, no. 10, pp. 66–72, 2014.

[5] L. Li and L. Yuanxia, "Innovative research on the design of college English listening and speaking extracurricular learning activities under the background of "internet plus homework"," *Journal of Weinan Normal University*, vol. 34, no. 8, pp. 75–81, 2019.

[6] Z. Qian and H. Songshan, "Investigation and analysis of college students' English mobile learning ability," *Journal of Ningbo institute of Education*, vol. 21, no. 4, pp. 84–88, 2019.

[7] P. Fasheng, "Research on English translation strategies of Chinese prose under subject-driven principle," *Foreign Language Teaching and Research*, vol. 48, no. 1, pp. 128–161, 2016.

[8] C. Guangxiao, "The application of foreignization translation strategy in Zhuang culture-loaded words," *Journal of Heilongjiang Teacher Development College*, vol. 40, no. 2, pp. 116–118, 2021.

[9] W. Chuanying, "From "natural translator" to PACTE model: a restricted view of Western translation competence research," *China Science and Technology Translation*, vol. 25, no. 4, pp. 32–35, 2012.

[10] C. Weijuan and S. Xiaolan, "Reflection on PACTE's translation competence model," *Journal of Sichuan Institute of Education*, vol. 28, no. 7, pp. 79–92, 2012.

[11] Z. Yinghong, "Research on translation practice teaching mode for English majors in physical education colleges," *Journal of Nanjing Institute of Physical Education*, vol. 13, no. 13, p. 125, 2014.

[12] B. Yuan, "Sports English translation research from the perspective of linguistic translation theory," *Journal of Chengdu Institute of Physical Education*, vol. 45, p. 73, 2019.

[13] Y. Rongjing, "Research on problems and countermeasures of English translation teaching in colleges and universities," *Educational Theory and Practice*, vol. 18, no. 38, pp. 55-56, 2018.

[14] K. Lifang, "College English translation teaching and its innovation research," *Industry and Technology Forum*, vol. 5, no. 18, pp. 160-161, 2019.

[15] X. Li, "Skills and strategies of English translation teaching from the perspective of Skopostheorie," *Journal of Zhejiang Institute of Water Resources and Hydropower*, vol. 1, no. 31, pp. 84-85, 2019.

[16] C. Hui, "Key consciousness in English teaching," *English Teachers*, vol. 20, no. 24, pp. 174–179, 2020.

[17] L. Zhiyong, "English teaching research based on behaviorist learning theory," *Educational Modernization*, vol. 4, no. 30, pp. 145–162, 2017.

[18] K. Wang, "Analysis of six major changes in English curriculum standards for ordinary senior high schools (2017 edition)," *China Foreign Language Education*, vol. 11, no. 2, pp. 11–19, 2018.

[19] H. Xiaoli, "Discussion on diversified development model of higher vocational education–comment on research on development model of higher vocational education," *Chemistry Education*, vol. 41, no. 18, p. 113, 2020.

[20] S. Haiyan, D. Hongwei, and J. Nan, "Research on the application of Internet technology in English listening and speaking teaching–review of college English listening and speaking teaching research under network environment: theory, model and evaluation," *Educational Theory and Practice*, vol. 37, no. 8, p. 65, 2017.

[21] Z. Yanling, "Investigation and research on English teachers' beliefs in middle schools under the new curriculum concept–one of the comparative studies on English teachers' beliefs in pre-service and vocational schools," *Journal of Xuchang University*, vol. 32, no. 3, pp. 149–152, 2013.

[22] L. Meiyan, "A preliminary study on the design of open English homework in junior high school," *Asia-Pacific Education*, vol. 5, no. 15, pp. 32-33, 2016.

[23] D. Z. Cheng, H. S. Qi, and Y. Zhao, "Analysis and Control of Boolean Networks:A Semi-tensor Product Approach," *Journal of Xuchang University*, vol. 37, no. 5, 2011.

[24] D. Liu, "Research on the training of sports English translation talents under the background of internationalization of sports culture industry," *Science and Technology Innovation Herald*, vol. 22, no. 6, pp. 205-206, 2017.

[25] T. Zuo, "Research on college English translation teaching reform under the background of cultural differences," *Journal of Suzhou Institute of Education*, vol. 15, no. 22, pp. 95-96, 2019.

Hindawi
Journal of Sensors
Volume 2022, Article ID 1510868, 12 pages
https://doi.org/10.1155/2022/1510868

Research Article

Application of the Neural Network Based on the Multilayer Perceptron Genetic Algorithm in Chinese-English Two-Way Translation

Yuxiu Yu

School of Foreign Languages, University of Sanya, China

Correspondence should be addressed to Yuxiu Yu; yuxiuyu@sanyau.edu.cn

Received 11 March 2022; Revised 15 April 2022; Accepted 18 April 2022; Published 16 June 2022

Academic Editor: Yuan Li

With the increasing application of the perceptron genetic algorithm neural network in Chinese-English two-way translation, there are many translation problems to be solved. In order to solve the translation problem of Chinese-English parallel corpus, the multilayer perceptron method, genetic word alignment model (GA), language model, and neural network method (including the translation model and bilingual pretraining model) are designed, which are combined into the ga-mlp-nn combination model to measure the parallelism of Chinese and English sentences from different emphases. The results show that the ga-mlp-nn model has good performance in filtering high-quality parallel corpus. The final experimental results show that compared with a single system, the improved multisystem fusion method based on weight multiplication has achieved better results in the test set. In the last five groups of evaluation results, the system submitted in this paper ranks second and first in multiple datasets, which has a certain reference value for the research of corpus filtering.

1. Introduction

With the development and in-depth application of information technologies such as mobile Internet and mobile communication, the number of online users in major social media platforms and e-commerce platforms has increased sharply. As one of the important ways of information interaction between enterprises, platforms, and consumers, online comments came into being with a huge number. An online comment is the user's comment on a specific topic through the network platform. It is the user's feeling and evaluation based on their own use or experience of products/services [1]. Because the online comments are rich in consumers' feelings and expectations after the product/service experience, involving preferences, needs, and evaluation in terms of quality, design, price, and service, the commercial value is becoming increasingly prominent, which has attracted great attention from enterprises, platforms, and consumers. However, due to the cross-platform interaction and information diffusion effect, the comment information of some topics, especially hot issues, is growing explosively. In the face of a large amount of comment information, it is often difficult to effectively distinguish the valuable comment information and correctly judge the true situation of products/services. In addition, due to the anonymity of users, the difference of motivation to evaluate products/services, and noncontact in the network platform, the quality of comment information is uneven and the authenticity of comments is uneven. In view of the overload and uneven authenticity of online comments, the cost of information screening is greatly increased and the efficiency is greatly reduced. It is not operable to manually screen the useful information of online comments [2]. Therefore, how to scientifically and effectively mine the useful information of online comments has become an important research topic, which is very important for the decision-making efficiency and effect of enterprises, platforms, and consumers.

Most of the existing studies on comment usefulness use the number of comments, text depth, and text emotion as the main factors affecting comment usefulness and rarely consider the impact of the professionalism of the comment content on comment usefulness. The innovative

contributions of this paper include the following: (1) The multilayer perceptron method and statistical method are used to screen and filter the expected value. (2) The GA MLP neural network is used as classifier for comment usefulness recognition. This paper creatively analyzes the influence of the proposed features on the usefulness of comments and obtains the best feature combination. And (3) compared with a single system, the improved multisystem fusion method based on weight multiplication has achieved better results in the test set. It provides a reference value for the translation of Chinese-English parallel corpora.

Based on this, this paper uses the knowledge adoption model and multilayer perceptron neural network to identify the information usefulness of online comments. This paper is divided into five parts. The first part is the research background, and the second part is the literature review to analyze the research results of the problem. The third part is the introduction of the multilayer backbone straight up genetic algorithm neural network and related systems. The fourth part is the specific experimental analysis. It shows how the multilayer perceptron genetic algorithm neural network deals with the translation of Chinese and English parallel corpora and compares it with the traditional methods. The fifth part is the round of the article.

2. Related Work

Theoretically, the usefulness of comment information depends on whether one thinks the that comment information is valuable and helpful to varying degrees [3]. In the existing studies, Yuanyuan et al. [4], Mudambi and Schuff [5], and Baek et al. [6] studied the factors affecting the usefulness of online comments from the text characteristics and found that the factors such as comment emotion, comment depth, comment grade, and reviewer reputation have a significant impact on the usefulness of comments. Chen and Xie constructed a normative model to judge the usefulness of comments and help consumers determine the best matching products [7]. Liu Wei and Pengtao and Zhang et al. constructed a theoretical model of two-way analysis based on the IAM (information acceptance model) to effectively identify the key factors affecting the usefulness of online comments on e-commerce platforms [8, 9]. Rui and Jian studied the impact of the inconsistency between the star rating of online comments and the average star rating of products on the usefulness of comments based on the attribution theory [10]. Liu et al. analyzed the impact of the number of comments, reviewer professionalism, reviewer reputation, and other factors on the usefulness of community online comments. In terms of the selection of influencing factors of comment usefulness, most of the existing studies consider the internal factors such as the star rating, number of comments, depth of comments, comment emotion, and external factors such as the identity, professionalism, and reputation of the comment publisher but few studies analyze the influencing factors from the professionalism of the comment content [11–18]. Because the comment information of each field contains its specific domain words, there are serious domain barriers. At present, there is no general method to effectively extract the factors related to the comment quality from the comment text. Existing studies show that compared with the feature extraction method without considering domain words, the feature extraction method based on the domain dictionary can enhance the expression ability of text features and improve the classification performance [19]. Therefore, this paper proposes a feature extraction method based on the domain dictionary to construct a measurement index of the comment text quality, so as to improve the recognition effect of comment usefulness.

In the existing research, there are a large number of theories that can be used to explain the usefulness of online comments, one of which is the knowledge adoption model (GA) [20]. The model holds that the information receiver's perception of information usefulness is the direct decision of knowledge adoption, and for a given information, the determinants of perceived information usefulness include the quality of the information itself and the credibility of the information source. Many scholars have studied the usefulness of online comments based on the GA model, For example, Cheung et al. and Huang et al. used the GA theory to study the usefulness of online comments [21, 22]. Erkan and Evans analyzed the usefulness of online comments and its effect on purchase intention on the basis of the GA theory [23]. It is not difficult to see that the GA theory has achieved good results in explaining the usefulness of online comments. In order to more comprehensively analyze the usefulness of comment information, this paper uses the GA model to construct the characteristics of the comment usefulness classification model from two aspects: the quality of the comment text and the credibility of the comment source.

At present, many researchers construct the judgment comment usefulness as a text binary classification problem. The solution to this kind of problem can adopt the text classification method based on machine learning, mainly including the support vector machine (SVM), decision tree, neural network, and Bayesian [24, 25].

3. Construction of the Multilayer Perceptron Genetic Algorithm Neural Network System (GA-MLP-NN)

Although a single perceptron cannot solve the XOR problem, it can realize the segmentation of complex space by combining multiple perceptrons. The two layers of perceptron are combined according to a certain structure and coefficients. The first layer of perceptron realizes two linear classifiers to divide the feature space, and an XOR operation can be realized by adding a layer of perceptron on the output of the two perceptrons. That is, it is composed of multiple perceptrons. Multilayer neural networks are also trained by the gradient descent algorithm, which is an algorithm dedicated to finding the extreme point of loss function to minimize the value of loss function. The so-called "learning" is to improve the model parameters

in order to minimize the loss through a large number of training steps.

The methods used in the system submitted in this paper can be divided into three categories: multilayer perceptron method, statistical method, and neural network method. The overall architecture of the system is shown in Figure 1. The multilayer perceptron method mainly designs a series of rules to filter corpus whose quality obviously does not meet the requirements. The statistical methods include the Zipporah system, genetic word alignment model, and language model. The purpose of filtering is achieved by statistical feature information on a large number of clean corpus. The neural network method includes a translation model and bilingual pretraining model. The model with strong generalization ability is trained on the clean corpus, and then, the translation corpus is filtered. Finally, according to the results of different methods, the excellent methods are weighted and fused to obtain the final clean corpus.

3.1. Multilayer Perceptron. The equivalent filtering methods of the sentence length ratio, maximum sentence length, and unique sentence are used to filter the corpus. According to his work, this paper formulates four rules:

(1) According to the length filtering rule, the sentence pairs with the length of more than 80 words at the source or the target end will be scored 0 points; otherwise, they will be scored 1 point

(2) According to the length ratio restriction rule, if the length ratio between the source and target sentences exceeds 1.7, 0 point will be recorded; otherwise, 1 point will be recorded

(3) Language identification rules: langid (https://github.com/saffsd/langid.py) is used to identify the source and target languages. If the language is incorrect, 0 point will be recorded; otherwise, 1 point will be recorded

(4) For the deduplication rule, record 1 point for the first occurrence of repeated sentences; otherwise, record 0 point

With the help of the abovementioned four rules, a four-dimensional feature can be obtained for a given sentence pair and the value of each dimension is 0 or 1.

3.2. Statistical Method

3.2.1. Zipporah System. As a part of the fusion system and achieved good results, the Zipporah system is a fast and scalable system, which can select "good data" of any size from a large number of translation data pools. For the training of neural machine translation model, the principle is as follows: firstly, the sentence is mapped to the feature space, which contains two features: adequacy score and fluency score. Then, logistic regression is used for binary classification and the categories are "good data" and "bad data," respectively. Finally, equation (1) is used for normalization to obtain the score of parallelism

$$S_Z(x) = \frac{x - x_{\min}}{x_{\max} - x_{\min}}, \tag{1}$$

where x is the score of the Zipporah system.

3.2.2. Genetic Word Alignment Model (GA). There are few word alignments for nonparallel sentence pairs, so this paper considers using word alignment for corpus filtering. First, use the fast align (https://github.com/clab/fast_align) word alignment tool to train on the translationless Chinese-English parallel corpus provided by the 16th National Machine Translation Conference (CCMT 2020), and then, predict the translation corpus. The word alignment score of sentence pairs can be obtained directly. In the fast align tool, the word alignment score is calculated by logarithmic summation of word alignment probability, so the longer the sentence, the smaller the word alignment score, which means that the system prefers short sentences. In order to reduce the impact of sentence length on the word alignment score, equation (2) is used to calculate the parallelism score in this paper:

$$S_{\text{avg}} = \frac{2S_{\text{align}}}{l_{\text{source}} + l_{\text{target}}}, \tag{2}$$

where S_{align} is the word alignment score of sentence pairs and l_{source} and l_{target} are the length of the source and target sentences, respectively.

After the word alignment scores of sentence pairs are processed according to equation (2), they are sorted according to the scores from high to low. After statistics, it is found that the number of sentence pairs with word alignment scores greater than or equal to −4.5 is about 4 million, about 100 million words. In this paper, it is determined that the quality of these sentence pairs is good and their scores after normalization should be high, so equation (3) is designed to normalize the scores:

$$S'_{\text{avg}} = \frac{-4.5}{S_{\text{avg}} - 4.5}. \tag{3}$$

3.2.3. Language Model. Because the language model can filter out nongrammatical data, this paper considers using the language model to filter the corpus. This paper selects the corpus without translation to generate the language model and uses the language model to calculate the perplexity (p) score of the dataset to be filtered.

Specifically, the srilm (https://github.com/BitSpeech/SRILM) tool is used to train a 5-gram language model for Chinese and English materials on the bilingual corpus without translation and this language model is used to calculate the confusion score of Chinese and English sentences in the bilingual corpus to be filtered. This paper uses two scoring strategies: the sentence level confusion score and word level confusion score.

In order to standardize the two piecewise functions to distinguish the differences between them, this paper standardizes the confusion score. In the standardized operation,

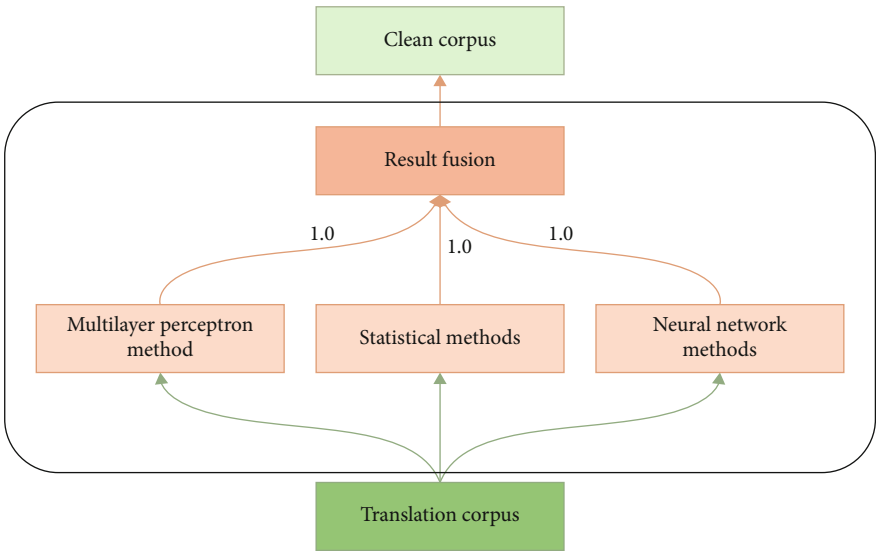

Figure 1: Construction diagram of the neural network system of the multilayer perceptron genetic algorithm.

a series of piecewise functions are designed according to experience. For the sentence level confusion score of Chinese corpus to be filtered, the normalized piecewise function designed in this paper is shown in formula (4) as follows:

$$S_1^L(x) = \begin{cases} 1 - 0.001p, & p \le 100, \\ 1 - \left((p-100)\dfrac{0.4}{900} + 0.1\right), & 100 < p \le 1000, \\ 1 - \left((p-1000)\dfrac{0.3}{9000} + 0.5\right), & 1000 < p \le 10000, \\ 0.1, & p > 10000. \end{cases} \tag{4}$$

For the sentence level confusion score of the English corpus to be filtered, the designed normalized piecewise function is shown in equation (5) as follows:

$$S_2^L(x) = \begin{cases} 1 - 0.003p, & p \le 100, \\ 1 - \left((p-100)\dfrac{0.4}{900} + 0.3\right), & 100 < p \le 1000, \\ 1 - \left((p-1000)\dfrac{0.15}{9000} + 0.7\right), & 1000 < p \le 10000, \\ 0.1, & p > 10000. \end{cases} \tag{5}$$

In addition, this paper considers the word level confusion score, calculates the word average confusion score of each sentence on the Chinese-English dataset and the word average confusion score on the overall dataset, and designs two piecewise functions to normalize the difference between them. Therefore, when calculating the average word confusion score of the overall dataset, this paper ignores sentences with a confusion degree of more than 10000.

For the word level confusion score of Chinese corpus to be filtered, the designed normalized piecewise function is shown in equation (6) as follows:

$$S_3^L(x) = \begin{cases} 1, p \le 0, \\ 1 - 0.003p, & 0 < p \le 100, \\ 1 - \left((p-100)\dfrac{0.6}{900} + 0.3\right), & 100 < p \le 1000, \\ 0.01, & p > 10000. \end{cases} \tag{6}$$

Finally, each parallel sentence pair will get 4 feature scores.

3.3. GA-MLP-NN Neural Network. The neural network is a highly parallel information processing system, which has very strong adaptive learning ability, does not depend on the mathematical model of the research object, and has good robustness to the changes of system parameters and external disturbances of the controlled object. GA-MLP-NN is a deep neural network, which overcomes the weakness that the perceptron cannot recognize linear inseparable data and can get better expression effect. The model is shown in Figure 2.

3.3.1. Translation Model. Based on the following assumption, if sentences a and B are parallel sentence pairs, then, the semantics of a and B are similar; when a is translated into a', the semantics of a' and B are still similar. In order to realize the abovementioned assumption, we should first train an English-Chinese translation model, then use the translation model to translate English sentences into corresponding translations, and finally calculate the similarity between the translation and the reference translation. For

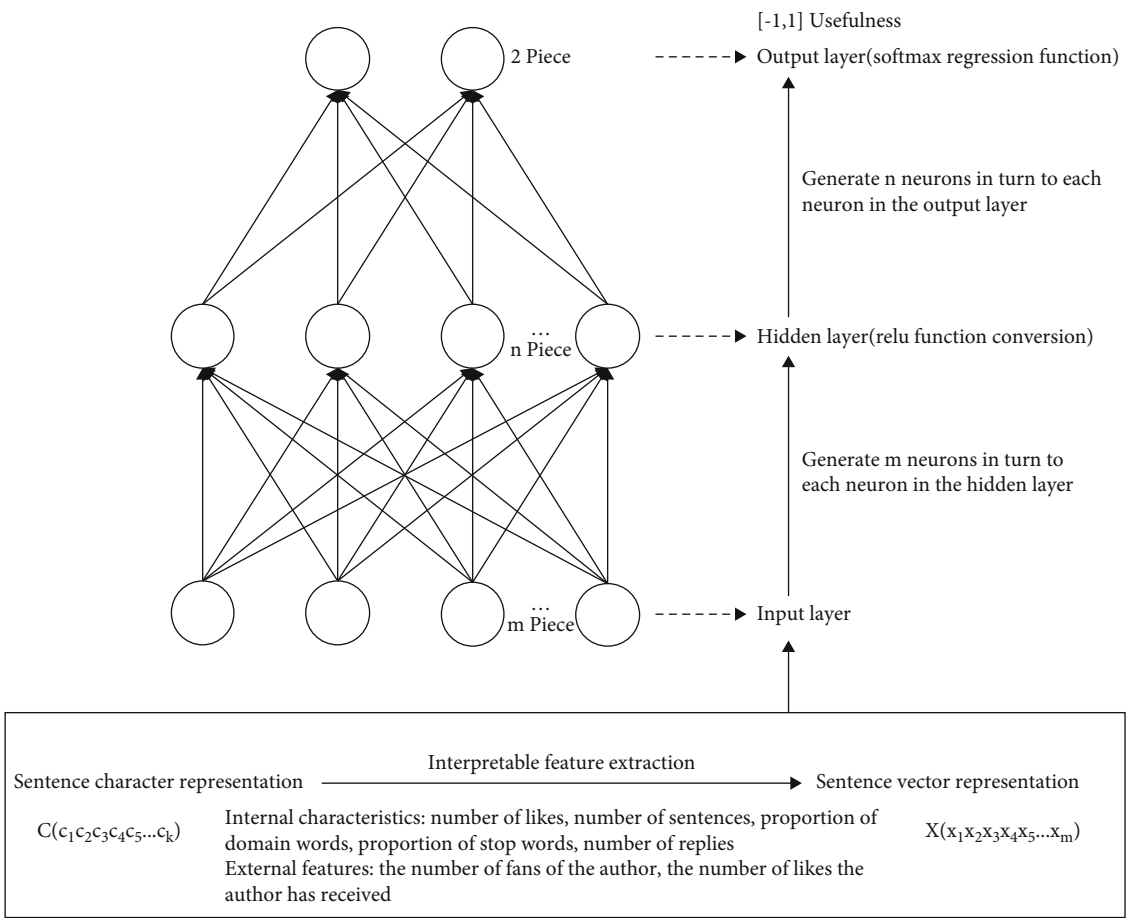

Figure 2: Schematic diagram of the GA-MLP-NN composite model.

similarity calculation, this paper uses two indicators: word-based editing distance and cosine similarity based on a pre-trained word vector, and finally forms a two-dimensional similarity feature.

3.3.2. Model Design. According to the abovementioned introduction, if you want to calculate the similarity between the translated translation and the reference translation, you should first get the translated translation, so you need a translation model. This paper adopts THUMT (https://github.com/THUNLP-MT/THUMT.git), an open-source neural machine translation tool of Tsinghua University. The system has less dependence and simple training and is suitable for rapid training of the neural machine translation system.

The training set data comes from the parallel corpus provided by the CCMT 2020 Chinese-English translation task, which is segmented and lowercased, and the sentence pairs with a length of more than 150 words are filtered to form about 10 million pairs of training data. The development set is the development set specified by the CCMT 2020 Chinese-English parallel corpus filtering task.

The main training parameters are selected by default and run for about 20 rounds. The five models with the highest bilingual translation evaluation results (BLEU) in the development set are saved; then, the models are averaged and fused into a final model, with the direction of English → Chinese, which is recorded as M_0. Then, M_0 is used to decode the Chinese and English sentences of parallel sentences with translation to obtain the corresponding Chinese translation.

3.3.3. Word-Based Editing Distance. This index is essentially the editing distance, but the granularity for calculating the matching degree of two sentences is words, not a single character. Let a' and b be Chinese sentences after two word segmentation, where a' is the translation of the English source sentence a; then, the editing distance $L_{a',b}(|a'|, |b|)$ can be calculated iteratively by equation (7) as follows:

$$L_{a',b}(i,j) = \begin{cases} \max(i,j), \min(i,j) = 0, \\ \min\left(L_{a',b}(i-1,j)+1, \right. \\ L_{a',b}(i,j-1)+1, \\ \left. L_{a',b}(i-1,j-1)+1_{(a'_i \neq b_j)}\right), \\ \text{others}, \end{cases} \tag{7}$$

where $|a'|$ and $|b|$ are the number of words in a' and b sentences, respectively, $L_{a',b}(i,j)$ is the distance between i words

before a' sentence and j words before b sentence, and a_i' and b_j are the i word of a' and the j word of b, respectively.

In the calculation process, a' is regarded as the translation and b as the reference. In translation data, b as the target does not necessarily correspond to the source. When a does not correspond to b, the distance between a' and b is large. It is considered that this sentence pair is less parallel to a and b, so the sentence pair can be filtered. On the contrary, a small distance means that the similarity between the translation model and the actual reference is high and the parallelism between the source sentence and the target sentence is high. According to the editing distance, the parallelism score of the final sentence pair is shown in equation (8) as follows:

$$s_{a,b} = 1 - \frac{L_{a',b}\left(\left|a'\right|, |b|\right)}{\max\left(\left|a'\right|, |b|\right)}. \tag{8}$$

3.3.4. Cosine Similarity. Since the translation model M_0 can translate the English source sentence a into the corresponding Chinese translation a', the semantic similarity between a' and b can be calculated only with the help of Chinese word vectors. The reason why two separate sets of Chinese and English word vectors are not used in this paper is that the language differences will cause the deviation of semantic space. This leads to inaccurate semantic similarity calculation. The data used for training the Chinese word vector is the same as the Chinese data in the machine translation training set. The training tool adopts the gensim (https://radimrehurek.com/gensim/models/word2vec.html) toolkit. The training window takes 5, and the words with word frequency lower than 5 are removed. Considering the high pressure of similarity calculation, the dimension is taken as 128 dimensions and trained for 10 rounds and the model is finally saved as M_1.

For a and b sentence pairs, a' is the Chinese translation of a; then, the parallelism score of the sentence pair can be obtained by using M_1 and cosine function, as shown in equation (9) as follows:

$$s_{a,b} = \cos\left(a', b|M_1\right). \tag{9}$$

3.3.5. Bilingual Pretraining Model. Considering that the pretraining model contains a lot of semantic knowledge, this paper uses the sentence-BERT (sense bidirectional encoder representations from transformation) model to fine tune the Chinese-English monolingual corpus given by CCMT2020; Chinese and English sentence vectors are obtained. However, the sentence vectors obtained in this way may have the problem of misalignment in the vector space between different languages, that is, sentences with the same meaning in different languages are mapped to different positions in the vector space. Therefore, when evaluating the parallelism between sentences in two different languages, this paper uses the ratio of the square of the Mahalanobis distance as the measurement index.

The Mahalanobis distance represents the covariance distance of data, which is an effective method to calculate the similarity of two unknown sample sets. Using the Mahalanobis distance is equivalent to the method of data conversion to eliminate the correlation and dimensional difference between different feature dimensions in the sample, so that the Euclidean distance can effectively measure the distance from the sample points to the distribution in the new distribution. Suppose that vector x represents μ. If the covariance matrix is a multivariable random vector of $\sum$, the Mahalanobis distance to the center is calculated as shown in (10) as follows:

$$d^2(x) = (x-\mu)^T \sum^{-1}(x-\mu) = \left\| \sum^{-(1/2)}(x-\mu) \right\|_2^2. \tag{10}$$

Here, $\sum^{-(1/2)}$ means finding the $-(1/2)$ power of each element in $\sum$.

In this system, firstly, each sentence vector is standardized so that it follows a random distribution with a mean value of 0. For each recentered Chinese-English sentence vector pair (l_1, l_2), three cases in the change space are considered, such as formula (11) as follows:

$$\begin{aligned} e_1 &= \sum^{-(1/2)} [l_1, 0], \\ e_2 &= \sum^{-(1/2)} [0, l_2], \\ e &= \sum^{-(1/2)} [l_1, l_2], \end{aligned} \tag{11}$$

where e_1, e_2, and e represent the vectors of splicing vectors $[l_1, 0]$, $[0, l_2]$, and $[l_1, l_2]$, respectively, in the Markov space. Through the abovementioned three cases, the following ratio of the squares of Markov distances can be used to measure the parallelism between two language sentences, as shown in formula (12) as follows:

$$m = \frac{\|e\|_2^2}{\|e_1\|_2^2 + \|e_2\|_2^2}. \tag{12}$$

If two sentences have the same meaning, the possibility of the sentence to vector e in the Markov space should not be less than the probability of the vector of isolated single sentences e_1 and e_2 in the Markov space. The greater the value of m, the higher the parallelism between the two sentences.

Finally, normalize the m value and use equation (13) to measure the parallelism between two sentences:

$$m' = 1 - m. \tag{13}$$

That is, the smaller the m', the higher the parallelism between the two sentences.

Table 1: BLEU value corresponding to each unit system.

System	BLEU
Stochastic system 0	16.59
Stochastic system 1	16.93
Rule	16.75
Zipporah	15.45
Word alignment model	17.04
Language model	16.92/16.38
Translation model	17.26/17.19
Bilingual pre-training model	17.18
Domain classifier	14.82

Table 2: CNN-based domain two classifier performance.

Category	p	R	F_1
News	82.8	99.0	90.2
Non-news	98.8	79.5	88.1

4. Results and Discussion

4.1. Data Processing. The development set, training set, and test set of the corpus filtering system in this paper are the Chinese-English news test set from WMT 2018 and WMT 2019 (including 3981 sentences and 2000 original texts and corresponding reference translations, respectively), the Chinese-English parallel corpus without translation in CCMT 2020 (9.02 million Chinese-English sentence pairs), and the parallel corpus with translation in CCMT 2020 (34.32 million Chinese-English sentence pairs).

Among them, the Jieba (https://github.com/fxsjy/jieba) word segmentation tool is used for Chinese corpus and Moses (https://statmt.org/moses/) script word segmentation and lowercase processing are used for English corpus. Because the amount of data is too large to prevent video memory overflow during decoding, the translation data after lowercase is truncated. At the same time, in order to alleviate the problem of out of vocabulary (OOV) and improve the processing ability of the model for rare words and OOV, this paper uses the method based on subword segmentation to segment Chinese corpus and English corpus with byte pair coding (BPE, http://github.com/resennrich/subword-nmt). In addition, in order to prevent the memory shortage and long decoding time caused by loading and decoding 34 million sentences at one time, this paper divides the translation data, each containing 2 million pieces of data. Finally, remove the sentences with a length of more than 150 words, and then, remove the sentences with language errors.

4.2. Evaluation Method. After the translation corpus is scored, it is sorted according to the score from high to low, so as to realize corpus filtering. This paper selects parallel sentence pairs containing about 100 million words, uses Marian, a neural machine translation tool designated by CCMT 2020 organizers, takes the previously selected parallel sentence pairs as a training set, trains them on Marian, and then tests them on the test set designated by CCMT 2020 organizers. The Bleu index commonly used in the field of machine translation is used as the evaluation index to evaluate the quality of the filtered corpus.

The final contestant shall provide the CCMT 2020 organizer with two filtered corpora of 100 million words and 500 million words. The CCMT 2020 organizer will take the corpora submitted by the contestants as the training set, use the Marian tool for training, ensure that all parameters are consistent during the training process, and conduct the test on the specified test set as the final result of the contestant.

4.3. GA-MLP-NN Single-System Experiment. Because of the specific relationship between each language system and Zipporah system, the translation system can be selected as the basis of each language system. The scores of translation data are sorted from high to low according to each system. It should be noted that if some systems have multiple scores, each score is added or multiplied to obtain the comprehensive score and the weight is 1.0. Then, use Marian, the machine translation tool provided by CCMT 2020 to train the neural machine translation system. Calculate the BLEU value between the translation results on the development set and the reference translation. Select the dominant features according to the corresponding Bleu value of each system, and try to combine the dominant features to get a better ranking.

Due to the limitation of computing resources, this paper only trains 10 rounds for each system and takes the highest Bleu value in the development set as the final score of the system. Refer to Table 1 for the score of each system. Among them, the random system randomly disrupts the data and similarly samples the parallel corpus of 100 million words, the random system 0 randomly disrupts the data only once, and the random system 1 randomly disrupts the data five times. In addition, in order to explore the influence of the domain on performance, this paper collects 1409 Chinese news samples and 1434 Chinese non-news samples from nontranslation parallel corpus, divides 200 news and 200 non-news samples into development sets, and trains a domain two classifier based on the convolutional neural network (CNN). As can be seen in Table 1, the results of random system 1 even exceed most systems. The best one is the similarity index between translation and reference based on the translation model. The domain classifier is the worst because the domain classifier is mainly used to select news corpus, and the results show that the proportion of news corpus in the test set may not be high, resulting in poor performance. It is noted that the top sentences in the corpus filtered by the translation model are not very sensitive to the sentence length, so a large number of sentences with moderate length are expected to rank first. Although the rule system can treat long sentences and short sentences indiscriminately, it cannot measure the degree of parallelism, so the effect is not prominent when it plays a role alone.

The domain classifier is used for the test of translation data, and the prediction probability of news data is taken as the score. For the performance of the domain 2 classifier, refer to Table 2. It can be seen that the performance of this

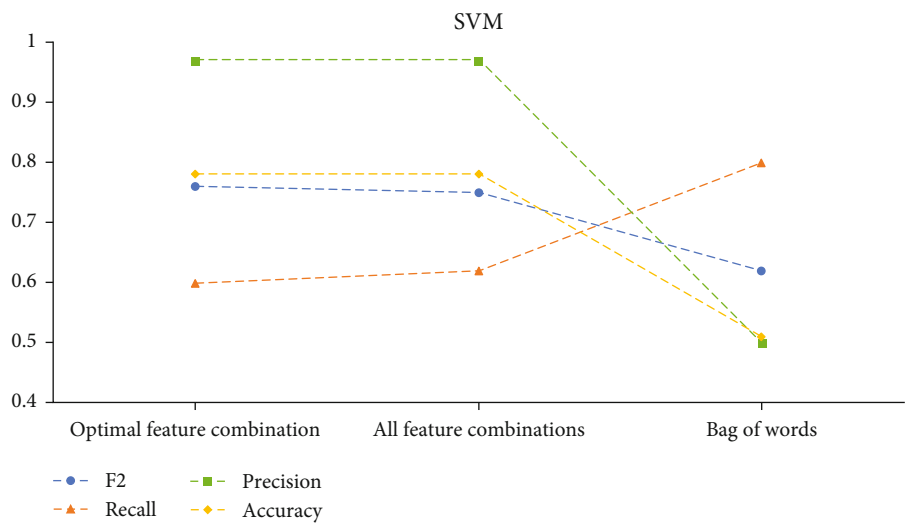

Figure 3: SVM result graph.

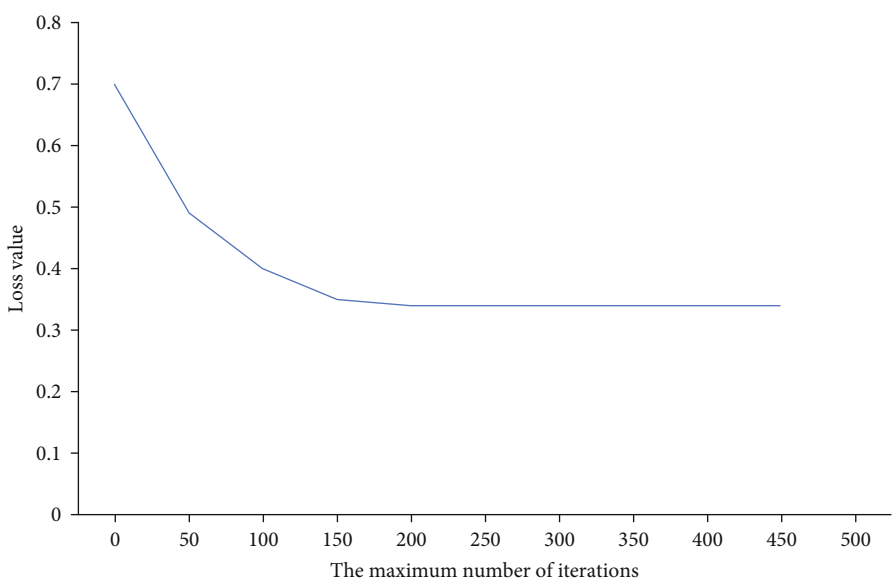

Figure 4: Schematic diagram of the number of iterations of GA-MLP-NN.

Table 3: Results of partial system integration.

System combination	BLEU	
	Addition	Multiplication
1,3	17.53	17.60
1,2,3	17.37	17.56
1,3,4	17.66	17.92
1,2,3,4	17.18	17.65
1,2,3,4,5	17.38	17.13
1,2,3,4,6	17.30	17.40

classifier is high, but in Table 1, the translation performance based on this classifier is very low, so it can be considered that in this task, the domain has little influence on the translation model. Therefore, the classifier is only used for verification, and it is not included in the final system in this paper.

4.4. Parameter Setting of the GA-MLP-NN Model. In the parameter setting of the GA MLP NN model, the process of superparameter optimization is as follows.

(1) Select a set of superparameters (automatic selection)

(2) Build the corresponding model

(3) Fit the model on the training data and measure its final performance on the validation data

(4) Select the next set of superparameters to try (auto select)

(5) Repeat the abovementioned process

(6) Finally, the performance of the model on the test data is measured

Table 4: Final evaluation results.

System	All test sets	WMT2020 news	BLEU WMT2020 biomedical	IWSI.T2020	CCMT2020	CCMT2019
1	16.8	15.3	9.1	17.7	13.6	18.4
2	16.0	15.8	9.3	16.1	13.9	19.0
3	14.2	14.3	6.8	14.3	12.9	17.5
4	14.2	14.2	6.8	14.3	13.1	17.1
5	13.6	15.7	8.3	12.0	12.8	18.8

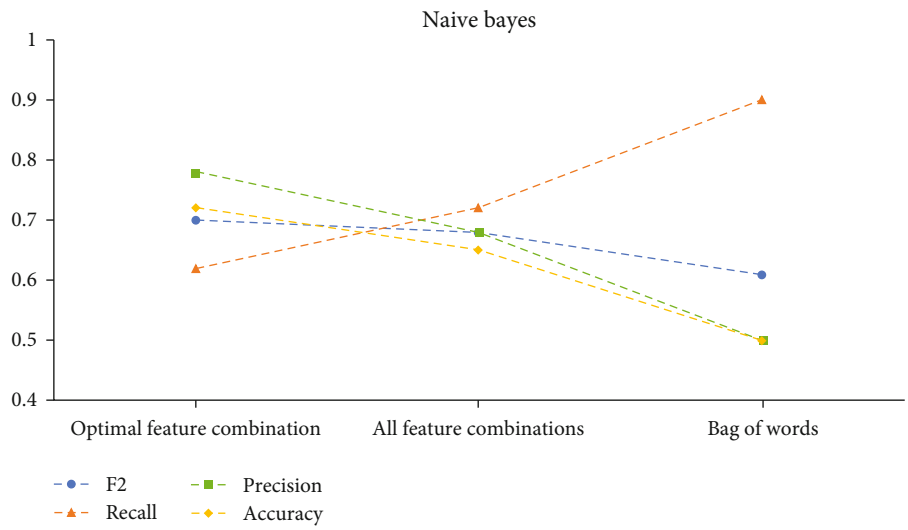

Figure 5: Naive Bayes result graph.

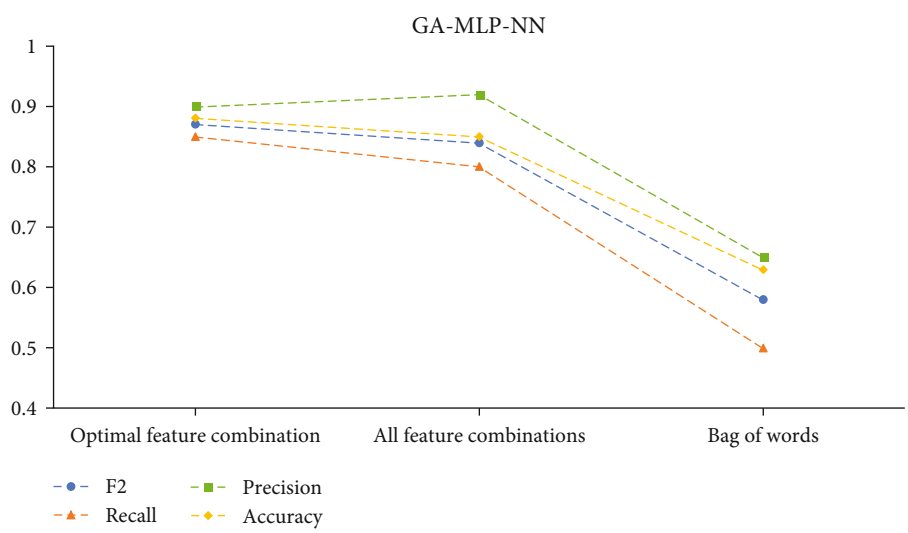

Figure 6: The result graph of the GA-MLP-NN combined model.

The key of this process is that given many sets of superparameters, the history of verification performance is used to select the next set of superparameters to be evaluated. It is necessary to systematically and automatically explore the possible decision space. According to experience, the recognition effect of the GA MLP NN classifier with the best performance is found.

The superparameter setting has an important impact on the recognition effect of the GA-MLP-NN classifier. Therefore, this paper has carried out many experiments on the super parameter setting of each group. Taking the number of iterations as an example, considering that the smaller the loss value of the model, the better the robustness of the model, the number of iterations of the model can be set through the loss value of the model. Specifically, the

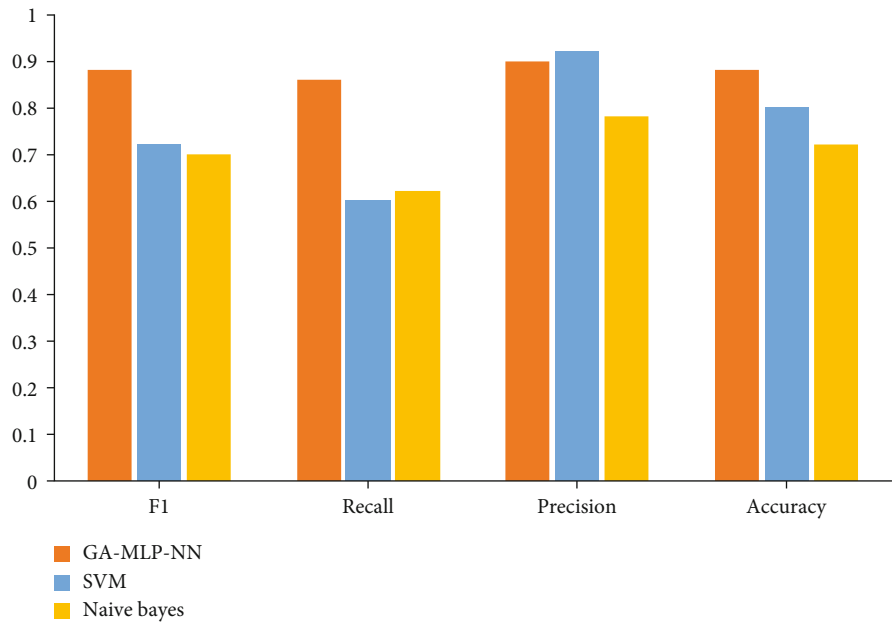

Figure 7: Comparison of the feature results of GA-MLP-NN and other models.

maximum number of iterations is set to 1, 50100, …, 500 and the maximum number of iterations for loss value convergence is selected according to its corresponding loss value. As shown in Figure 3, the loss value does not decrease after the maximum number of iterations is greater than or equal to 300 and is stable at about 0.3. Therefore, the maximum number of iterations of the GA-MLP-NN model is finally set to 300, as shown in Figure 4.

4.5. GA-MLP-NN System Experiment after Fusion. In this paper, it is considered that the translation model system, genetic word alignment model system, language model system, and bilingual pre training model system are relatively potential systems. Therefore, the combination of these systems is given priority to the fusion test, that is, to form the GA-MLP-NN combination model. The method of multisystem fusion is relatively simple, that is, the scoring of each system is fused. Then, reorder. There are two fusion methods: multiply by weight and add by weight. In most cases, only the fusion with the weight of 1.0 is tried. Table 3 shows some experimental results. It can be seen that the overall performance of the fusion system exceeds that of the single system. The main reason for the better performance of the fusion system is that different systems measure the parallelism of sentence pairs from different starting points, so the sentence pairs can be evaluated more comprehensively after multisystem fusion, which also shows the effectiveness of method fusion.

4.6. Submission System. It is not found that the more integrated the systems, the better performance. After a large number of tests, it is found that the robustness and BLEU value of "1,3,4" combination are high. Considering the complexity of the system, this paper selects "1,3,4" combination as the main system, because the multilayer perceptron method has been proved to be an effective means to improve the translation performance in WMT 2018 and WMT 2019 corpus filtering tasks. In addition, the pre training model has advantages in semantic extraction, so the combination of "1,2,3,4,6" is selected as the subsystem. The final evaluation results are shown in Table 4. It can be seen that the main system system2 submitted in this paper ranks second and first except the iwslt2020 dataset. Because the IWSLT2020 dataset is spoken language corpus, there are some differences between news corpus and spoken language corpus. This leads to the poor performance of the system on IWSLT2020 dataset, which also indicates that the training field will affect the filtering results.

4.7. Comparison between GA-MLP-NN and Classical Methods. In this paper, the recognition results of the GA MLP NN model are compared with those of classical methods such as naive Bayes, SVM, and support vector machine. The $f1f1$ value, recall, precision, and accuracy of the experimental results are analyzed and compared. The better the parameter value is, the higher the translation effect is. The results show that GA MLP NN model has good filtering performance for high-quality parallel corpus.

In order to further verify the recognition effect of the proposed method, the recognition results of the proposed method are compared with those of classical methods such as naive Bayes, SVM, and support vector machine. That is, the optimal feature combination (N_C, R_{RW}, N_F, and R_{SW}) and all features (N_C, R_{RW}, N_F, R_{SW}, N_G, and N_S) obtained based on the GA theory are used as feature representation, and the feature representation obtained by the word bag method is used to train the SVM classifier, naive Bayesian classic classifier model, and GA-MLP-NN neural network classifier. The $F1F1$ value, recall, precision, and accuracy of the experimental results are shown in Figures 5–6.

As can be seen in Figure 6, the $F1F1$ value, precision, and accuracy of the three classifiers trained by the feature representation based on the word bag method are lower than the recognition results of the classifiers trained by the other two feature representation methods based on the GA theory. The values of the three classifiers based on the optimal feature combination are better than those based on all feature combination and word bag method. Among them, the $F1F1$ value of the GA-MLP-NN classifier based on optimal feature combination is 3% higher than that based on all feature combinations and 33% higher than that based on the word bag method. The $F1F1$ value of the SVM classifier based on optimal feature combination is 2% higher than that based on all feature combinations and 11% higher than that based on the word bag method. The $F1F1$ value of naive Bayes based on the optimal feature combination is 1% higher than that based on all feature combinations, and 7% higher than that based on the word bag method. It can be seen that the selection of the optimal feature combination significantly improves the classification effect of the classifier and further verifies the feasibility and superiority of the method proposed in this paper.

As can be seen in Figure 7, GA-MLP-NN is much better than other classifiers in $f1f1$ value, recall, and accuracy. For the optimal feature combination of N_C, R_{RW}, N_F, and R_{SW}, the $F1F1$ value of the SVM classifier is 73.3% and the $F1F1$ value of the GA-MLP-NN classifier is 13.5% higher than that of the SVM classifier, reaching 86.8%. For the optimal feature combination of N_C, R_{RW}, N_F, and R_{SW}, the $f1f1$ value of the naive Bayesian classifier is 70% and the $f1f1$ value of the GA-MLP-NN classifier is 16.8% higher than that of the naive Bayesian classifier, which fully reflects the superiority of the GA-MLP-NN classifier trained by feature combination proposed in this paper.

5. Conclusion

In this paper, the ga-mlp neural network is used as a classifier for comment usefulness recognition. This paper creatively analyzes the impact of the proposed features on the usefulness of comments, measures the parallelism of Chinese and English sentences from different emphases, and obtains the best feature combination. Finally, the experimental results show that the $f1f1$ value of naive Bayes based on the optimal feature combination is 1% higher than that based on all feature combinations and 7% higher than that based on the word bag method. It can be seen that the selection of the optimal feature combination significantly improves the classification effect of the classifier and further verifies the feasibility and superiority of the method proposed in this paper. Compared with a single system, the improved multisystem fusion method based on weight multiplication has achieved better results in the test set. The application of the perceptron genetic algorithm neural network in Chinese-English two-way translation is solved. The system presented in this paper ranks second and first in multiple datasets, which has a certain reference value for corpus filtering research. However, this paper does not carry out the actual simulation verification of the adopted model and there are still some limitations. Further research is needed in the future.

Data Availability

The data used to support the findings of this study are included within the article.

Conflicts of Interest

The authors declare no conflicts of interest.

Acknowledgments

This study is supported by the Hainan Provincial Social Science Project of Foreign Language Base: a study on the construction of Hainan's local translation talent team under the background of new liberal arts (HNSK(JD)21-41).

References

[1] J. Wei, Z. Li, D. Yi, J. Jing, and W. Gang, "Analysis of the usefulness of online comments for user demand acquisition," *Chinese Journal of Computers*, vol. 36, no. 1, pp. 119–131, 2013.

[2] S. Shin, N. Chung, Z. Xiang, and C. Koo, "Assessing the impact of textual content concreteness on helpfulness in online travel reviews," *Journal of Travel Research*, vol. 58, no. 4, pp. 579–593, 2019.

[3] X. Liu, G. A. Wang, W. Fan, and Z. Zhang, "Finding useful solutions in online knowledge communities: a theory-driven design and multilevel analysis," *Information Systems Research*, vol. 31, no. 3, pp. 731–752, 2020.

[4] H. Yuanyuan, Y. Qiang, and L. Yijun, "Research on the influencing factors of the usefulness of online reviews based on film review data," *Journal of Management Science*, vol. 13, no. 8, pp. 78–88, 2010.

[5] S. M. Mudambi and D. Schuff, "Research note: what makes a helpful online review? A study of customer reviews on Amazon. com," *MIS Quarterly*, vol. 34, no. 1, pp. 185–200, 2010.

[6] H. Baek, J. Ahn, and Y. Choi, "Helpfulness of online consumer reviews: readers' objectives and review cues," *International Journal of Electronic Commerce*, vol. 17, no. 2, pp. 99–126, 2012.

[7] Y. Chen and J. Xie, "Online consumer review: word-of-mouth as a new element of marketing communication mix," *Management Science*, vol. 54, no. 3, pp. 477–491, 2008.

[8] L. Wei and X. Pengtao, "Research on the identification of factors affecting the usefulness of online reviews of O2O e-commerce platforms: taking the O2O model of the catering industry as an example," *China Management Science*, vol. 24, no. 5, pp. 168–176, 2016.

[9] Z. Yanhui, L. Zongwei, and Z. Yicheng, "The impact of information quality based on Taobao comment data on the usefulness of online comments," *Chinese Journal of Management*, vol. 14, no. 1, pp. 77–85, 2017.

[10] M. Rui and X. Jian, "The impact of scoring inconsistency on the usefulness of online reviews—from the perspective of attribution theory," *China Management Science*, vol. 26, no. 5, pp. 178–186, 2018.

[11] Z. W. Liu and S. Park, "What makes a useful online review? Implication for travel product websites," *Tourism Management*, vol. 47, pp. 140–151, 2015.

[12] A. H. Huang, K. Chen, D. C. Yen, and T. P. Tran, "A study of factors that contribute to online review helpfulness," *Computers in Human Behavior*, vol. 48, pp. 17–27, 2015.

[13] Y. Guopeng, "What kind of online reviews do consumers think is more useful?—the influence of social factors," *Management World*, vol. 12, pp. 115–124, 2012.

[14] Z. Liye, Y. Denghua, and Z. Jingyi, "The influence of online user review quality and reviewer rating on consumer purchase intention: the moderating effect of product involvement," *Management Review*, vol. 29, no. 2, pp. 87–96, 2017.

[15] A. Ghose and P. G. Ipeirotis, "Estimating the helpfulness and economic impact of product reviews: mining text and reviewer characteristics," *IEEE Transactions on Knowledge and Data Engineering*, vol. 23, no. 10, pp. 1498–1512, 2011.

[16] C. Shuqin, Q. Zhiyong, L. Cuiping, Y. Qian, and Z. Bipan, "Research on the influence of emotional intensity of negative online reviews on usefulness," *Management Review*, vol. 29, no. 2, pp. 79–86, 2017.

[17] B. Fang, Q. Ye, D. Kucukusta, and R. Law, "Analysis of the perceived value of online tourism reviews: Influence of readability and reviewer characteristics," *Tourism Management*, vol. 52, pp. 498–506, 2016.

[18] Y. Jianyuan, L. Yang, F. Miao, and L. Kai, "The interactive influence of user Q & A and online comments on consumer product attitudes," *Management Science*, vol. 33, no. 2, pp. 102–113, 2020.

[19] W. Chen, J. Zhu, M. Zhu, and T. Yao, "Text representation using domain dictionary," *Computer Research and Development*, vol. 42, no. 12, pp. 2155–2160, 2005.

[20] S. W. Sussman and W. S. Siegal, "Informational influence in organizations: an integrated approach to knowledge adoption," *Information Systems Research*, vol. 14, no. 1, pp. 47–65, 2003.

[21] C. Cheung, M. Lee, and N. Rabjohn, "The impact of electronic word-of-mouth," *Internet Research*, vol. 18, no. 3, pp. 229–247, 2008.

[22] Z. S. Chen, X. L. Liu, K. S. Chin, W. Pedrycz, K. L. Tsui, and M. J. Skibniewski, "Online-review analysis based large-scale group decision-making for determining passenger demands and evaluating passenger satisfaction: Case study of high-speed rail system in China," *Information Fusion*, vol. 69, pp. 22–39, 2021.

[23] I. Erkan and C. Evans, "The influence of eWOM in social media on consumers' purchase intentions: an extended approach to information adoption," *Computers in Human Behavior*, vol. 61, no. AUG., pp. 47–55, 2016.

[24] J. Chunhua and G. Feipeng, "Distributed data mining model DSVM based on support vector machine," *Systems Engineering - Theory & Practice*, vol. 30, no. 10, pp. 1855–1863, 2010.

[25] X. Binqing, Y. Yang, L. Xindan, and L. Haohua, "Research on the credit rating of small and micro enterprises based on fuzzy neural network," *Journal of Management Science*, vol. 19, no. 11, pp. 114–126, 2016.

Hindawi
Journal of Sensors
Volume 2022, Article ID 6710530, 12 pages
https://doi.org/10.1155/2022/6710530

Research Article

Analysis of Tourist Satisfaction Index Based on Structural Equation Model

Yan Peng[1,2] and Xiaolin Jiang[3]

[1]*School of International Education, Hunan Institute of Technology, Hengyang, Hunan 421008, China*
[2]*Lyceum of the Philippines University Batangas, P. Herrera cor. Dona Aurelia St., Kumintang Ibaba, Batangas City, 4200, Philippines*
[3]*School of Business, Hunan Institute of Technology, Hengyang Hunan 421002, China*

Correspondence should be addressed to Xiaolin Jiang; xiaolin_jiang@hnit.edu.cn

Received 17 March 2022; Accepted 4 May 2022; Published 11 June 2022

Academic Editor: Yuan Li

In the modern economy and society, traveling abroad has gradually become one of the ways for people to enjoy life. With the continuous development of tourism and the change of tourists' consumption concepts, tourists' satisfaction has been received by more and more tourism managers and operators. It pays attention to providing tourism products and services from the perspective of tourists and meets the personalized and diversified needs of tourists. Tourist satisfaction has become an important indicator to measure the level of tourism in a tourist destination. According to the structural equation model, this paper constructs the tourist satisfaction index analysis index, which can truly and efficiently detect the tourist satisfaction index, which is convenient for the scenic spot to find out the areas that need to be improved, and enhance the new attraction and service level of the scenic spot. The research results of the article show that (1) there is no significant difference in the satisfaction of tourists of different genders. In terms of influencing factor indicators, individual factors have not passed the T test. The difference in satisfaction of tourists of different ages is not obvious, but there are also individual factors that do not pass the significance test in terms of influencing factors. For the actual perceived quality, the observation index with a larger contribution rate to principal component 2 is mainly the tourists' evaluation of the satisfaction of the tourist attractions. (2) The test result of the structural equation-based satisfaction analysis model proposed in the article is the highest among the four models. According to the error curve, it can be concluded that with the increasing complexity of the data, for the other three models, the evaluation error of the tourist satisfaction evaluation model is getting larger and larger, and the errors of the models proposed in the article are basically controlled within 0.4. Therefore, it can be concluded that the satisfaction evaluation model based on structural equations can reduce the error of tourist satisfaction.

1. Introduction

With the increasing economic development, people's various needs have been paid more and more attention, and various leisure and tourism experiences have become increasingly diversified. Satisfaction has also become an important reference indicator to measure the competitiveness and development of a tourist attraction. This paper studies the tourist satisfaction of Daegu city tourism and proposes a structural equation model [1]. This article attempts to analyze the relationship between tourist satisfaction and loyalty in tourist destinations [2]. The purpose of the article is to provide two examples of advanced analysis, including a new nonlinear latent variable method to measure hygiene and pleasure factors in visitor satisfaction monitoring and the application of inferred causal theory to explore the antecedents of satisfaction [3]. Based on the American Customer Satisfaction Index model, this paper constructs a structural equation model of tourist satisfaction from four aspects: tourist experience, tourist perceived value, tourist satisfaction, and tourist loyalty [4]. Based on the American Customer Satisfaction Index, this paper takes AMOS (Analysis of Moment

Structure) and SPSS statistical software as examples to test the validity and practicability of the TSRTD (Tourist Satisfaction of Rural Tourism Destination) model [5]. The article proposes a framework of "experience value (functional value, situational value, emotional value, cognitive value, economic value), satisfaction and post-travel revisit and recommendation willingness" to investigate Kangyang Mountain tourism [6]. This paper proposes a tourist satisfaction model of a destination and takes Guilin as a case to study the causes and consequences of tourist satisfaction [7]. The research hypothesis of the article includes five main factors that lead to tourist loyalty, as well as some potential variables: corporate social responsibility, destination image, perceived value, tourist satisfaction, and tourist complaints [8]. This paper analyzes a specific wine tourism segment in the global context of tourism consumer behavior by examining the perceptions of winery tourists [9]. The article analyzes the data using structural equation modeling, draws theoretical and managerial implications based on the findings, and makes recommendations for future researchers [10]. This study is aimed at exploring the predictors of place attachment and measuring the impact of place attachment and its predictors on tourist satisfaction and how this satisfaction affects tourists' future revisiting [11]. In this paper, the method of exploratory factor analysis and structural equation model is used to propose a satisfaction model of urban forest tourists [12]. Based on structural equation modeling, this paper explores the relationship between travel satisfaction and destination loyalty intentions [13]. This paper uses AMOS software combined with structural equation model to explore the causal relationship of tourist satisfaction and obtains the relationship between various influencing factors and the direct and indirect effects between influencing factors and tourist satisfaction [14]. This paper builds a hypothesis model on the basis of previous research literature, collects data through on-site questionnaires, and establishes a structural equation model for hypothesis testing [15]. In the tourism market, there are obvious differences between different genders in tourism satisfaction. There are great differences in the evaluation of satisfaction of different customer groups by analyzing the different characteristics of tourists from different dimensions of data. The structural equation evaluation method proposed in this paper has objective fairness and has better performance in satisfaction evaluation compared with other methods.

2. Construction of Indicators and Model Structure

2.1. Satisfaction Index Model. The American Customer Satisfaction Index model is based on summarizing the Swedish Customer Satisfaction Index model and uses three observation variables: customerization quality, reliability quality, and overall quality to measure the latent variable perceived quality, and a new latent variable is added: perception value, as shown in Figure 1:

2.2. Construction of the Indicator System. At present, most of the construction of the tourist satisfaction evaluation system is based on the theory of customer satisfaction. In order to meet the needs of national mass tourism and improve the quality of tourism services, the China Tourism Academy has constructed a tourist satisfaction survey and evaluation covering all elements of tourism [16]. The construction of tourist satisfaction index system is shown in Tables 1 and 2:

3. Structural Equation Model Analysis of Tourist Satisfaction Indicators

3.1. Structural Model. The structural model describes the causal relationship between latent variables, and the equation is expressed as [20]

$$\eta = B\eta + \Gamma\xi + \tau. \tag{1}$$

Among them, $\eta = (\mathrm{n}_1, \mathrm{n}_2, \cdots, \mathrm{n}_n)$ is the vector composed of intrinsic latent variables, $\xi = (\xi_1, \xi_2, \cdots, \xi_n)$ is the vector composed of extrinsic latent variables, $B(m \times m)$ is the path coefficient matrix of intrinsic latent variables, $\Gamma(m \times n)$ is the path coefficient matrix of exogenous latent variables, and τ $(m \times 1)$ is the vector composed of residual terms, reflecting the unexplained part of η in the equation.

The measurement model is the measurement part of the structural equation model. It is composed of latent variables and their corresponding observed variables. The relationship between the observed variables and the latent variables is expressed as follows:

$$\begin{aligned} y &= \wedge_y + \varepsilon_y, \\ x &= \wedge_x \xi + \varepsilon_x. \end{aligned} \tag{2}$$

The equations that affect the measurement model are as follows [21]:

$$\begin{aligned} \eta &= \pi_\eta y + \delta_\eta, \\ \xi &= \pi_\xi + \delta_\xi. \end{aligned} \tag{3}$$

The measurement equations of exogenous latent variables and explicit variables are expressed as

$$x = \wedge_x \xi + \varepsilon_x, \tag{4}$$

represented by a matrix as [22]

$$\begin{bmatrix} x_1 \\ x_2 \end{bmatrix} = \begin{bmatrix} \lambda_{11} \\ \lambda_{21} \end{bmatrix} \xi + \begin{bmatrix} \delta_1 \\ \delta_2 \end{bmatrix}. \tag{5}$$

The measurement equations of endogenous latent variables and explicit variables are expressed as

$$y = \wedge_y \eta + \varepsilon_y. \tag{6}$$

The tourist satisfaction index habits are as follows:

$$\widehat{\eta} = \frac{1/n \sum_i^n \widehat{\eta}_{4i} - \min\left(\widehat{\eta}_{4i}\right)}{\max\left(\widehat{\eta}_{4i}\right) - \min\left(\widehat{\eta}_{4i}\right)}. \tag{7}$$

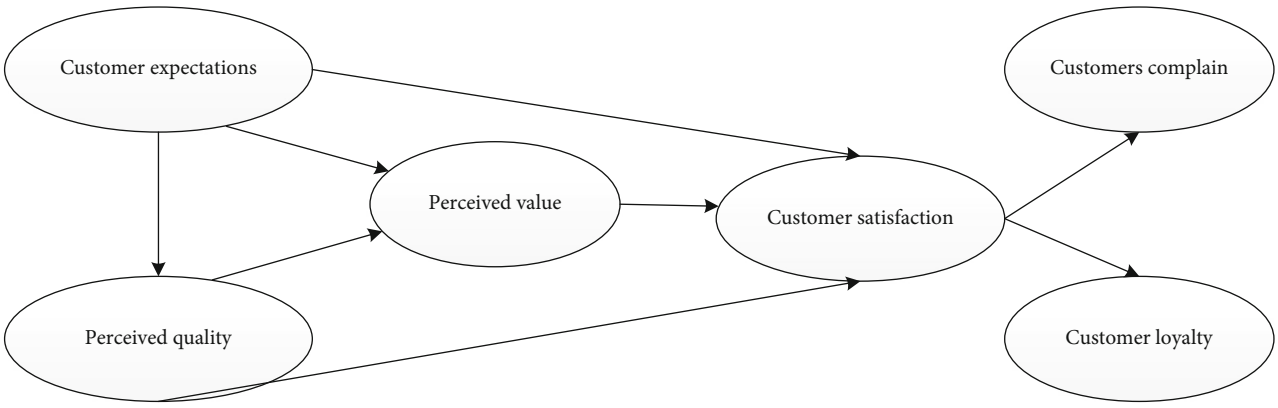

Figure 1: Customer Satisfaction Index model.

Table 1: Tourist satisfaction index system.

Latent variable	Measure variable	Latent variable	Measure variable
City tourism image	Image level Public service	Perceived value	Reasonable price Quality matches
Tourist expectations	Construction and management Pretour evaluation Expected quality	Tourist satisfaction	Overall satisfaction Compared to ideal Posttour evaluation
Perceived quality	Transportation Food Stay Entertainment Attractions Tourism features	Tourists complain Tourist loyalty	Whether there is a complaint Is there a complaint Complaint handling Revisit Recommend friends and relatives Continue to select attractions

Table 2: Subdivision evaluation index of tourist satisfaction index system.

Measure variable	Evaluation index [17]	Measured variables [18]	Evaluation index [19]
Construction and management	Urban planning and architecture Roads and landscaping Current historical and cultural atmosphere Public facilities (roads, sanitation, rest) Environmental quality (air, water quality, noise) Rural construction (including rural tourism) Safety and emergency rescue system Citizen image and behavior	Public service	Traffic signs Taxi Bus Self-driving facilities Station, wharf
Public service	Water supply Mobile phone, internet coverage Bank card convenience Public toilet	Tourism features	Characteristic culture (including performing arts, festivals) Featured buildings, pedestrian streets Characteristic ancient towns, ancient villages, and ethnic villages Specialty restaurants or local specialties Special tourism products, handicrafts, etc. Featured recreation and sports Tourism resources Featured recreational tourism service items

Table 3: Descriptive statistics of sample data.

Measurement standard	Sample size	Minimum	Maximum value	Numerical value	Standard error	Skewness
Tourism image	300	3	10	7.56	0.093	-0.420
Overall service level	300	3	10	7.74	0.094	-0.325
Overall expectations of tourism quality	300	4	10	6.37	0.125	-0.103
Expectation of service quality in tourism process	300	4	10	6.19	0.132	-0.126
Overall quality	300	2	10	6.39	0.104	0.134
Hardware facilities	300	2	10	6.34	0.138	0.110
Software facilities	300	2	10	6.42	0.145	-0.043
Reasonable price	300	4	10	7.28	0.098	-0.678
Overall cost performance	300	3	10	6.79	0.107	-0.457
Satisfaction level	300	3	10	7.54	0.098	-0.836
Satisfaction compared to needs	300	3	10	7.26	0.104	-0.657
Satisfaction compared to ideal	300	3	10	7.33	0.097	-0.802
Possibility to travel again	300	3	10	7.53	0.117	-0.892
Possibility to recommend others to travel	300	3	10	7.18	0.123	-0.595

Among them, $(1/n)\sum_i^n \widehat{\eta}_{4i}$ is the arithmetic mean of customer satisfaction latent variable $\widehat{\eta}_{4i}$, min $(\widehat{\eta}_{4i})$ is the lowest score of customer satisfaction latent variable $\widehat{\eta}_{4i}$, and max $(\widehat{\eta}_{4i})$ is the highest score of customer satisfaction latent variable $\widehat{\eta}_{4i}$.

3.2. Analysis of Tourist Satisfaction Index. In order to evaluate the tourist satisfaction index, the article uses normalization to process the original data, and the processing formula is [23]

$$Y_j = \frac{X_j - X_{\min}}{X_{\max} - X_{\min}}. \tag{8}$$

The multilinear weighting algorithm calculates the tourist satisfaction index [24]:

$$\begin{aligned} F_j &= \lambda_j \times Y_j, \\ F_t &= \sum_{j=1}^{n} F_j. \end{aligned} \tag{9}$$

Calculate the proportion of indicators:

$$\begin{aligned} P_{ij} &= \frac{Y_{ij}}{\sum_{i=1}^{m} Y_{ij}}, \quad m = 1, 2, 3, \cdots, \\ E_j &= -k \sum_{i=1}^{m} p_{ij} \ln\left(P_{ij}\right). \end{aligned} \tag{10}$$

The coefficient of difference is as follows:

$$G_j = 1 - E_j. \tag{11}$$

Determine indicator weights:

$$\theta_j = \frac{G_j}{\sum_{j=1}^{n} G_j}, \quad n = 1, 2, 3, \cdots. \tag{12}$$

The tourist satisfaction value [25] is as follows:

$$\lambda_j = \frac{W_j \theta_j}{\sum_{j=1}^{m} W_j \theta_j}. \tag{13}$$

4. Simulation Experiments

4.1. Data Collection. The experiment conducted an empirical analysis on the satisfaction of tourists with different attributes and the satisfaction of the influencing factors. The attributes of tourists are compared according to gender and age. The data source is from the tourist satisfaction data provided by a provincial tourism bureau in the second quarter of 2010. For the degree survey data, the experiment was conducted in the form of a questionnaire survey. 300 questionnaires were distributed to the public, and 270 valid questionnaires were issued. The survey locations covered 2 5A-level scenic spots and some 4A-level scenic spots in the province. According to the results of the questionnaire survey, it can be found that there are more female tourists than males, accounting for 58%. From the perspective of age, the number of tourists in the 25-54 age group is the largest, accounting for 60% of the respondents. In terms of education level, the number of tourists with a bachelor's degree is the largest, accounting for 43.21% of the total number. Descriptive statistical analysis was carried out on the sample data, and the specific data are shown in Table 3.

According to the statistical data in Table 4 and Figure 2, it can be seen that there is no significant difference in the satisfaction of tourists of different genders. In terms of influencing factor indicators, individual factors did not pass

Table 4: Differences in tourist satisfaction by gender.

Measurement standard	Satisfaction	Influencing factors	Satisfaction	Male satisfaction	Female satisfaction	*P* value
Scenic spot	7.14	Landscape	7.25	7.27	7.24	0.168
		Appreciate the value	7.22	7.15	7.25	0.135
		Environment	7.10	7.20	7.10	0.129
		Toll	7.02	7.00	6.89	0.131
Entertainment	7.06	Full facilities	7.01	7.02	6.97	0.161
		Rich in activities	7.05	7.04	7.07	0.035
		Special	7.12	7.10	7.14	0.153
Stay	6.82	Health	6.80	6.73	6.82	0.137
		Comfortable	6.93	6.87	6.96	0.133
		Price	6.70	6.85	6.68	1.112
Shopping	6.70	Product category	6.66	6.49	6.75	0.001
		Commodity price	6.60	6.56	6.73	0.126
		Shopping	6.81	6.90	6.79	0.094
Travel	6.54	Convenient	6.53	6.52	6.54	0.206
		Full facilities	6.55	6.57	6.53	0.150
Food	6.52	Taste	6.40	6.71	6.13	0.004
		Environment	6.50	6.66	6.38	0.015
		Feature	6.69	6.74	6.56	0.068

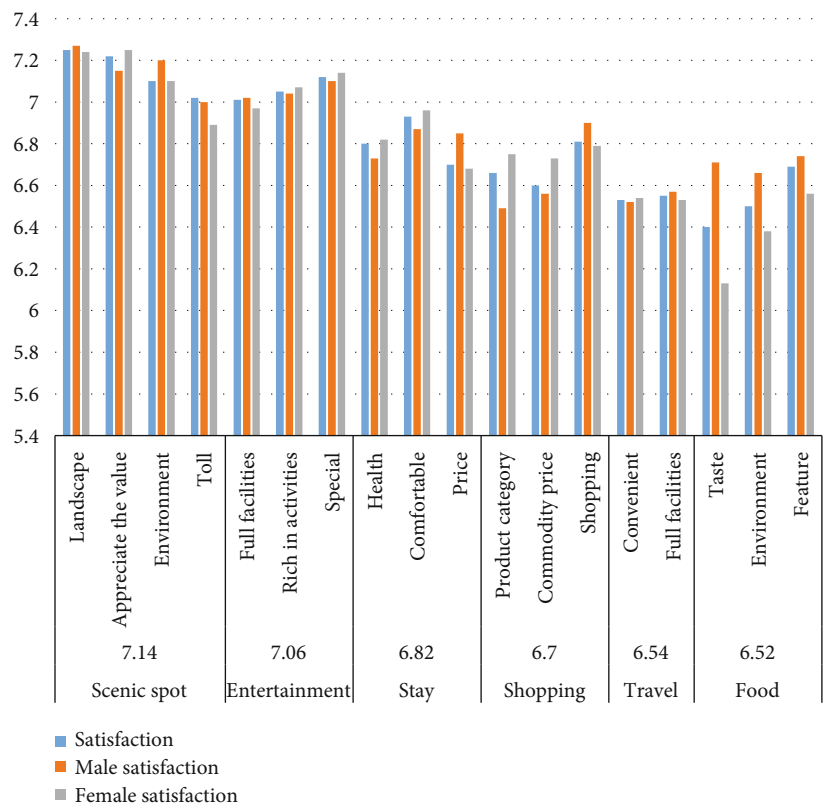

Figure 2: Tourist satisfaction statistics by gender.

the *T* test and the variety of commodities, the taste of catering, the environment of catering, and the abundance of entertainment activities. There are clear differences in sex. In terms of the variety of commodities and the richness of entertainment activities, especially in terms of commodity types, women's satisfaction is significantly higher than that of men, and in terms of food and beverage indicators, in terms of the taste and environment of food and beverages, men are significantly more satisfied than women (high degree).

Table 5: Differences in tourist satisfaction by age group.

Measurement standard	Satisfaction	Influencing factors	Satisfaction	15-24	25-54	Over 55	*P* value
Scenic spot	7.14	Landscape	7.25	7.40	7.21	7.30	0.057
		Appreciate the value	7.22	7.20	7.23	7.21	0.145
		Environment	7.10	7.16	7.11	7.07	0.125
		Toll	7.02	7.24	6.92	7.16	0.131
Entertainment	7.06	Full facilities	7.01	6.88	7.03	7.01	0.234
		Rich in activities	7.05	7.02	7.07	7.10	0.143
		Special	7.12	7.07	7.13	7.15	0.156
Stay	6.82	Health	6.80	6.91	6.76	6.75	0.065
		Comfortable	6.93	7.06	6.91	6.96	0.124
		Price	6.70	6.79	6.65	6.62	0.059
Shopping	6.70	Product category	6.66	6.81	6.58	6.59	0.012
		Commodity price	6.60	6.51	6.67	6.49	0.023
		Shopping	6.81	6.89	6.79	6.80	0.164
Travel	6.54	Convenient	6.53	6.52	6.69	6.48	0.000
		Full facilities	6.55	6.67	6.54	6.72	0.068
Food	6.52	Taste	6.40	6.62	6.35	6.48	0.004
		Environment	6.50	6.61	6.48	6.69	0.072
		Feature	6.69	6.71	6.67	6.64	0.054

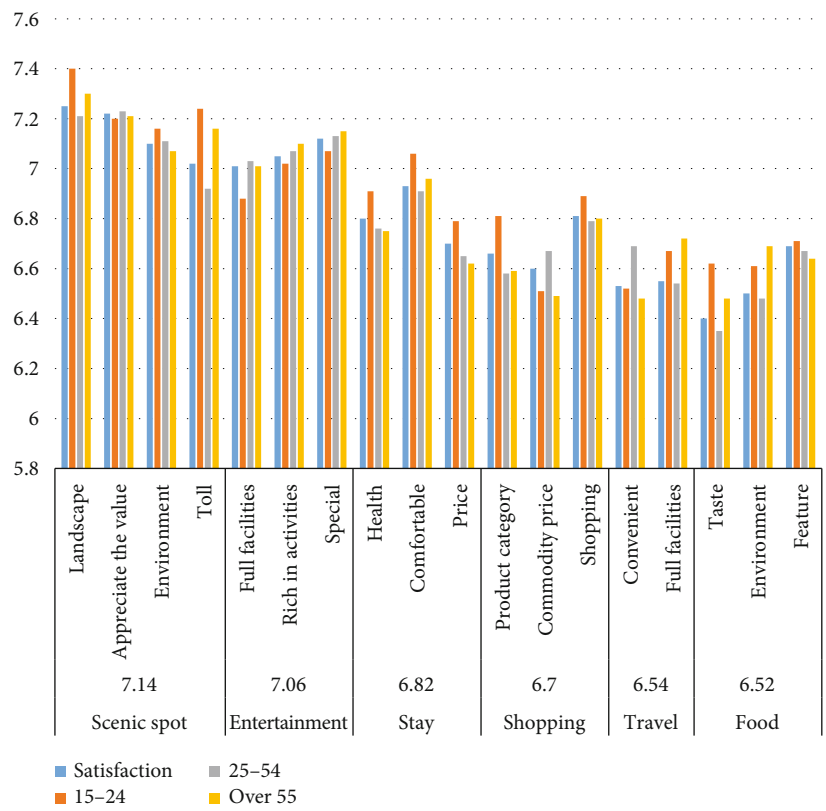

Figure 3: Statistical chart of tourist satisfaction by age group.

According to the statistical results in Table 5 and Figure 3, from the perspective of age, the 25-54 age group has the largest number of tourists, accounting for 59% of the surveyed, 14-24 years old accounted for 27%, and over 55 years old accounted for 14%. It can be seen that the tourists in the scenic spot are mainly young and middle-aged. The difference in satisfaction of tourists of different ages is not obvious, but in terms of the influencing factor indicators,

Table 6: Contribution rate of observed variables to principal components.

Evaluation variable	Principal component 1	Principal component 2	Total
Natural environment expectations	0.855	0.06	0.915
Social service expectations	0.761	0.001	0.763
Landscape features	0.582	0.351	0.933
Scenic traffic	0.623	0.293	0.916
Sanitation	0.906	0.003	0.910
Scenic capacity	0.901	0.028	0.929
Viewing facilities	0.832	0.095	0.927
Scenic spot commodity prices	0.718	0.199	0.917
Scenic spot ticket evaluation	0.683	0.274	0.957
Ideal scenic spot evaluation	0.687	0.281	0.967
General impression	0.765	0.097	0.862
Complaint	0.711	0.212	0.923
Revisit	0.676	0.275	0.951

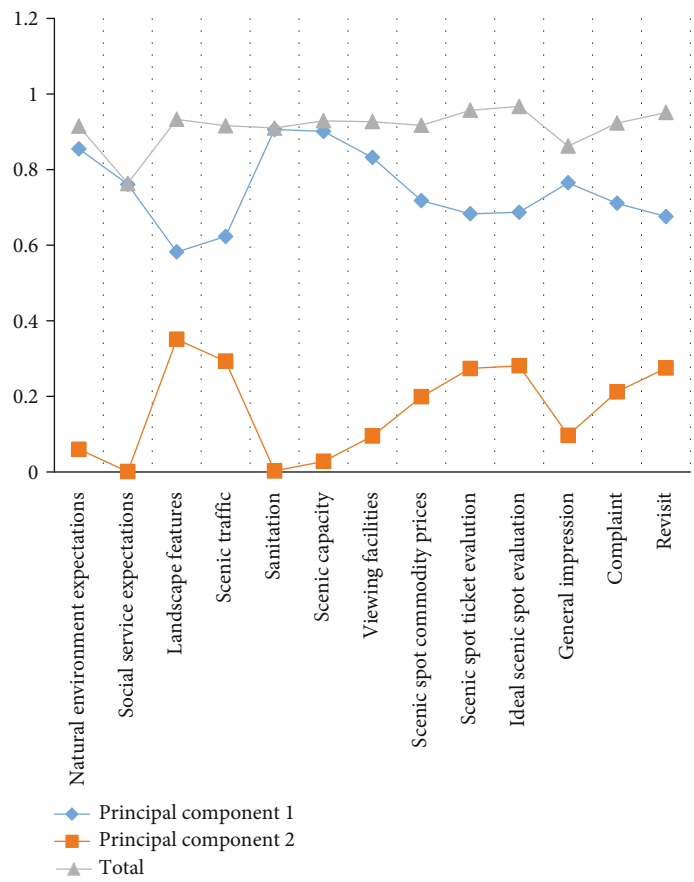

Figure 4: Statistical diagram of the contribution rate of observed variables to principal components.

there are also individual factors that have not passed the significance test. In terms of commodity types and catering tastes, especially in terms of commodity types, the satisfaction of the 15-24-year-old age group is significantly higher than that of other age groups; and in the commodity price index, the 15-24-year-old age group is significantly more satisfied. The satisfaction of the age group over 55 is significantly lower than that of the age group of 25-54. In terms of travel convenience, the satisfaction of the age group of 25-54 is relatively high.

4.2. Data Analysis. According to the contribution rate that affects the satisfaction of tourists, 13 evaluation indicators are selected for investigation and research on tourists' expectations of the scenic spot, perception of the scenic spot infrastructure, and scenic spot characteristics. Since there is

Table 7: Satisfaction of observed variables and weighted scores of structural variables.

Evaluation variable	Tourist satisfaction	Tourist perceived quality	Satisfaction
Natural environment expectations	74.25	0.150	0.121
Social service expectations	67.50	0.075	0.060
Landscape features	73.75	0.071	0.057
Scenic traffic	59.75	0.058	0.046
Sanitation	69.75	0.119	0.096
Scenic capacity	66.50	0.176	0.141
Viewing facilities	59.00	0.102	0.082
Scenic spot commodity prices	67.75	0.075	0.061
Scenic spot ticket evaluation	81.00	0.063	0.051
Ideal scenic spot evaluation	82.00	0.067	0.054
General impression	77.25	0.059	0.048
Complaint	68.00	0.075	0.060
Revisit	46.50	0.028	0.023

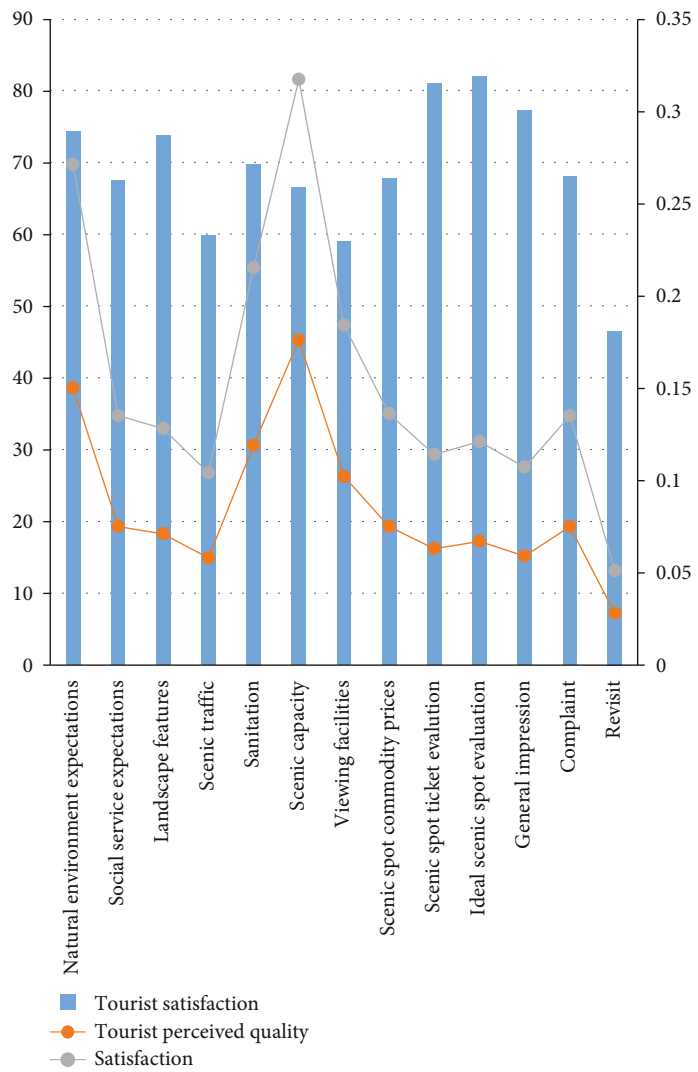

Figure 5: Statistical chart of observed variable satisfaction and weighted scores of structural variables.

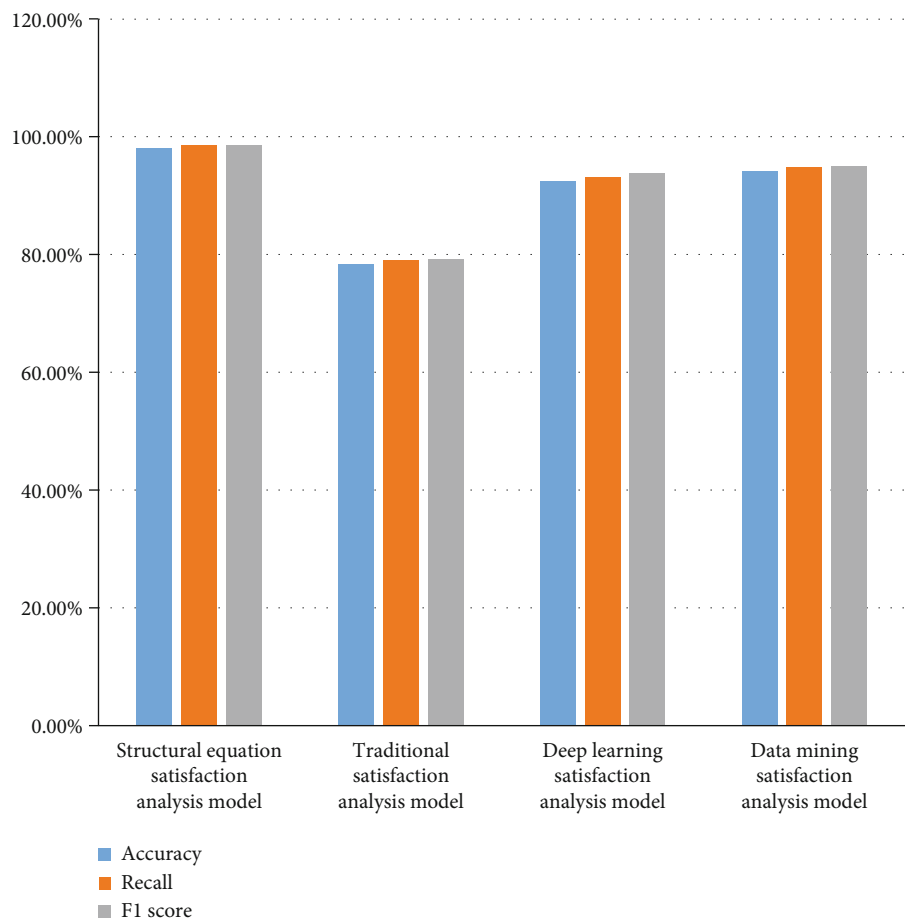

Figure 6: Statistical chart of test data in the experimental set.

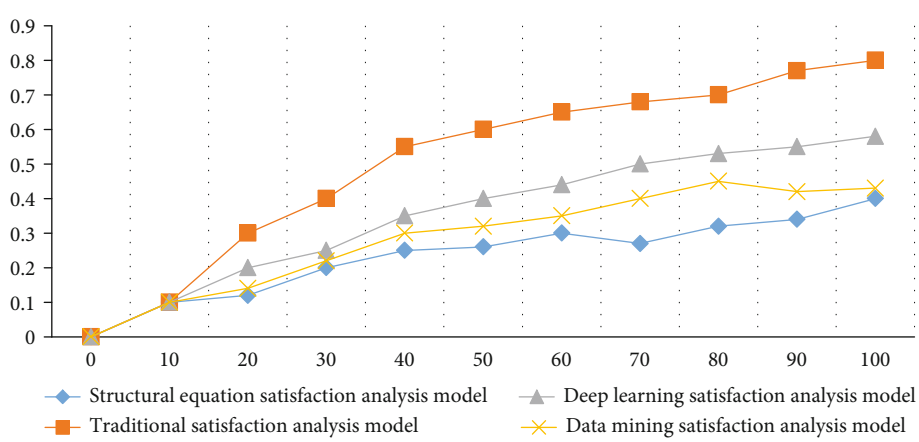

Figure 7: Statistical chart of tourist satisfaction evaluation error.

Table 8: Test data of each model on the experimental set.

Model	Accuracy	Recall	F1 score
Structural equation satisfaction analysis model	98.12%	98.56%	98.69%
Traditional satisfaction analysis model	78.32%	79.10%	79.23%
Deep learning satisfaction analysis model	92.45%	93.14%	93.79%
Data mining satisfaction analysis model	94.21%	94.89%	95.10%

Table 9: Errors in tourist satisfaction evaluation.

	Structural equation satisfaction analysis model	Traditional satisfaction analysis model	Deep learning satisfaction analysis model	Data mining satisfaction analysis model
0	0	0	0	0
10	0.1	0.1	0.1	0.1
20	0.12	0.3	0.2	0.14
30	0.2	0.4	0.25	0.22
40	0.25	0.55	0.35	0.3
50	0.26	0.6	0.4	0.32
60	0.3	0.65	0.44	0.35
70	0.27	0.68	0.5	0.4
80	0.32	0.7	0.53	0.45
90	0.34	0.77	0.55	0.42
100	0.4	0.8	0.58	0.43

information overlap and correlation between the evaluation indicators, the principal component analysis method is used to analyze and study them. The research results are shown in Table 6.

According to the experimental results in Table 6 and Figure 4, we can conclude that the contribution rate of principal component 1 is 74.621, the contribution rate of principal component is 16.688, the cumulative contribution rate is 91.309, and the amount of information loss is only 9.691, which meets the requirements of principal component analysis for the amount of information loss. It shows that the selection of two principal components can basically reflect the evaluation of tourists' satisfaction. The evaluation indicators with the largest contribution rate to the principal component 1 are the capacity of the scenic spot (0.90 1), the hygiene of the scenic spot (0.906), the viewing facilities of the scenic spot (0.832), the expectation of the natural environment of the scenic spot (0.855), the overall evaluation of the scenic spot (0.765), the society of the scenic spot, and service expectation (0.761); the largest contribution rate to principal component 2 is the scenic landscape feature (0.351), the scenic traffic (0.293), the scenic ideal evaluation (0.281), the revisiting (0.275), the scenic spot ticket evaluation (0.27 4), the Scenic area complaints (0.212), and scenic spot commodity prices (0.199). Among them, the observation indicators with a larger contribution rate to principal component 1 are mainly tourists' expectations and actual perceived quality of tourist attractions, and the observation indicators with a larger contribution rate to principal component 2 are mainly tourists' evaluation of tourist attractions. The structural variables can be simplified as tourists' perceived quality and tourists' satisfaction. The observed variables that characterize the perceived quality of tourists are the scenic capacity of the scenic spot, the hygiene of the scenic spot, the viewing facilities of the scenic spot, the expectation of the natural environment of the scenic spot, the expectation of the social service of the scenic spot, and the scenic spot. For the overall impression, the observational variable indicators that characterize the structural variables of tourist satisfaction are scenic landscape features, scenic traffic, scenic ideal evaluation, revisiting, scenic ticket evaluation, complaints about scenic spots, and scenic spot commodity prices. According to the analysis of the evaluation indicators affecting tourist satisfaction, the revision of the tourist satisfaction evaluation model is shown in Table 7.

According to the experimental data in Table 7 and Figure 5, we can conclude that among the structural variables, the perceived quality of tourists has a strong positive correlation with the satisfaction of tourists, and the path coefficient is 0.805. In the relationship between structural variables and observed variables, in terms of the perceived quality of tourists, each observed variable has a strong impact on it. Taking the expected load coefficient on the natural environment as the standard 1, the load coefficient of the viewing facilities (1.091) has a greater impact on it. The impact of natural environment expectations is stronger, and the relative natural environment expectations such as scenic environmental capacity (0.897), scenic traffic (0.869), scenic overall impressions, and landscape characteristics (0.821) are relatively weak. In terms of tourist satisfaction, revisiting (1.303), scenic spot ticket price (1.153), and scenic spot ideal evaluation (1.177) all have more influence on it than the scenic spot commodity price (1.000).

4.3. Model Comparison. In order to verify the performance of the tourist satisfaction analysis model based on the structural equation model, the experiment compares the proposed model with the other three models to test the superiority of the model performance. In the experiment, after running 4 different models on the experimental set, observe the experimental results of the 4 models. Among them, the experimental set is a set of samples set aside separately during the model training process, which can be used to adjust the hyperparameters of the model and to perform a preliminary evaluation of the ability of the model. The experiment also recorded the satisfaction evaluation error comparison curves of the four models. The steps to record the satisfaction evaluation error comparison curves are to first use the tourist satisfaction evaluation model of data mining technology to randomly generate the evaluation data format and then to randomly generate the tourist satisfaction. The evaluation is processed, the tourist satisfaction

evaluation coefficient and the comprehensive evaluation vector are calculated, and the complexity of the tourist satisfaction evaluation data is used as an independent variable to analyze and count the evaluation error value. The specific experimental data are as follows in Figures 6 and 7.

According to the experimental data in Tables 8 and 9, the test result of the satisfaction analysis model based on structural equation proposed in this article is the highest among the four models, with an accuracy rate of 98.12%, a recall rate of 98.56%, and an F1 value. The test result of the traditional satisfaction analysis model is the lowest among the four models. The experimental results also show that the performance of the structural equation satisfaction analysis model is the best. According to the evaluation error tables of the four models, we can conclude that when the complexity of the tourist satisfaction evaluation data is less than 30%, the evaluation errors of the four tourist satisfaction evaluation models are all less than 0.3 points, but with the complexity of the data, the degree is getting higher and higher, and the evaluation errors of the other three models of tourist satisfaction evaluation models are getting larger and larger. When the complexity of the tourist satisfaction evaluation data reaches 100%, the evaluation error reaches a maximum of 0.8 points and the model proposed in the article. The error is basically controlled within 0.4, so it can be concluded that the satisfaction evaluation model based on structural equation can reduce the error of tourist satisfaction.

5. Conclusion

Under the background of the fast pace of life, traveling abroad has gradually become one of the ways for people to relax and enjoy life. In the process of traveling, tourists also evaluate the work level of tourists, the quality of classic tourism resources, and tourism perception experience. It is an important reference indicator for the competitiveness and development level of tourist destinations. This paper takes the analysis of tourist satisfaction index as the research object and uses structural equation model to analyze the relationship between the influencing factors of tourist satisfaction and the degree of influence, which can accurately and efficiently analyze the value of tourist satisfaction index. There are also some shortcomings in the analysis process of the article. For example, the results of the questionnaire survey have regional limitations. The article only conducts a questionnaire survey on tourists' satisfaction within a certain province. The conclusion of the empirical analysis has obvious characteristics of hell. In the research work, it is possible to have an in-depth understanding of the personal factors, tourism motivation, and consumption behavior of tourists.

Data Availability

The experimental data used to support the findings of this study are available from the corresponding author upon request.

Conflicts of Interest

The authors declared that they have no conflicts of interest regarding this work.

References

[1] M. J. Song and J. Y. Lee, "A study on tourist satisfaction of the Daegu City Tour using a structural equation model," *Journal of the Korean Data & Information Science Sociaty*, vol. 22, no. 6, pp. 11–16, 2011.

[2] N. M. Salleh, T. Sarmidi, and R. Othman, *Tourist satisfaction and loyalty: a structural equation model (SEM) analysis*, vol. 10, no. 3, pp. 24–36, 2011.

[3] J. A. Mazanec, "Exploring tourist satisfaction with nonlinear structural equation modeling and inferred causation analysis," *Journal of Travel & Tourism Marketing*, vol. 21, no. 4, pp. 73–90, 2007.

[4] W. Qian, H. B. Sun, and F. O. Science, "Research on satisfaction of tourist based on structural equation model——a case study in Kunming," *Journal of Qufu Normal University (Natural Science)*, vol. 13, no. 3, pp. 52–63, 2015.

[5] Z. T. Deng, "Research on tourist satisfaction of rural tourism destination based on structural equation model——a case study from Liangzi Lake tourist area in Hubei," *Tourism Forum*, vol. 20, no. 3, pp. 11–17, 2012.

[6] L. Zeng and R. Li, "Tourist satisfaction, willingness to revisit and recommend, and mountain Kangyang tourism spots sustainability: a structural equation modelling approach," *Sustainability*, vol. 13, no. 19, pp. 10620–10636, 2021.

[7] X. Wang, J. Zhang, C. Gu, and F. Zhen, "Examining antecedents and consequences of tourist satisfaction: a structural modeling approach," *Tsinghua Science and technology*, vol. 14, no. 3, pp. 397–406, 2009.

[8] W. Jankingthong, "Structural equation model of factors affecting Thai tourist loyalty towardsMarine National Parks in Southern Thailand," *Chulalongkorn University Printing House*, vol. 3, no. 7, pp. 56–76, 2013.

[9] A. Sampaio, *Tourist Madeira wine perception: a structural equation modeling approach*, vol. 10, no. 3, pp. 56–59, 2003.

[10] P. Ramseook-Munhurrun, V. N. Seebaluck, and P. Naidoo, "Examining the structural relationships of destination image, perceived value, tourist satisfaction and loyalty: case of Mauritius," *Procedia - Social and Behavioral Sciences*, vol. 175, no. 6, pp. 252–259, 2015.

[11] M. A. Abou-Shouk, N. Zoair, and M. N. El-Barbary, "Sense of place relationship with tourist satisfaction and intentional revisit: evidence from Egypt," *International Journal of Tourism Research*, vol. 20, no. 2, pp. 172–181, 2018.

[12] T. Zhou and S. Tang, "A structural equation model of urban forest recreationists' satisfaction," *Mechanics of Materials*, vol. 675, pp. 1288–1294, 2014.

[13] P. Valle, J. A. Silva, and J. Mendes, "Tourist satisfaction and destination loyalty intention: a structural and categorical analysis," *International Journal of Business Science & Applied Management*, vol. 1, no. 1, pp. 45–53, 2006.

[14] S. Feng, "Tourist satisfaction factor analysis of the Bama healthy travel——based on the structural equation model perspective," *Journal of Hechi University*, vol. 20, no. 6, pp. 78–86, 2017.

[15] Y. Q. Wu, Z. G. Chen, and H. N. Chen, "Research on tourist satisfaction of Shanxi Qianling Mausoleum based on structural equation model from the perspective of cultural experience and perceived value," *Resource Development & Market*, vol. 12, no. 3, pp. 45–56, 2016.

[16] Z. H. Li, "On the improvement of tourist service satisfaction in tourist attractions," *Marketing Planning*, vol. 18, no. 4, pp. 39–41, 2003.

[17] S. Xiangyou, "Analysis of factors affecting service quality of travel agencies and tourists' satisfaction," *Journal of Tourism*, vol. 14, no. 5, pp. 25–30, 1999.

[18] X. Yanjun and W. Kai, "Expectation and feeling: an interactive model of tourism experience quality," *Tourism Science*, vol. 2, pp. 1–4, 2000.

[19] W. Xia and H. Mei, "Tourist satisfaction in tourist destinations: model and empirical research," *Journal of Beijing International Studies University: Tourism Edition*, vol. 137, no. 7, pp. 1–6, 2006.

[20] W. Qun, D. Zurong, and Z. Jinhe, "The index evaluation model of tourist satisfaction in tourism environment - taking Huangshan scenic spot as an example," *Geographical Research*, vol. 25, no. 1, pp. 171–183, 2006.

[21] T. Qinxue and Y. Rui, "Evaluation of tourist satisfaction in Dongda hot spring resort in Xi'an," *Anhui Agricultural Science*, vol. 37, no. 27, pp. 13421–13423, 2009.

[22] D. K. Tse and P. C. Wilton, "Models of consumer satisfaction formation: an extension," *Journal ofMarketing Research*, vol. 25, no. 2, pp. 204–212, 1988.

[23] A. Pizam, "Tourism's impacts: the social costs to the destination community as perceived by its residents," *Joumal of Travel Research*, vol. 16, no. 4, pp. 8–12, 1978.

[24] J. B. Beard and M. G. Ragheb, "Measuring leisure satisfaction," *Joumal of Leisure Research*, vol. 12, no. 1, pp. 20–33, 1980.

[25] R. B. Woodruff, "Customer value: the next source for competitive advantage," *Journal of the Academy of Marketing Science*, vol. 25, no. 2, pp. 139–153, 1997.

Hindawi
Journal of Sensors
Volume 2022, Article ID 4384870, 8 pages
https://doi.org/10.1155/2022/4384870

Research Article

Water Resource Accounting Modeling and Analysis Adapting to the Development of Market Economy under the Sustainable Development Strategy of Big Data

Shen Chen,[1] **Jing Zhu**,[2] **and Shuai Chen**[3]

[1]*Department of Audit, School of Accounting, Fujian Jiangxia University, Fuzhou, Fujian, China 350108*
[2]*College of Public Affairs, Fujian Jiangxia University, Fuzhou, Fujian, China 350108*
[3]*Business School, University of International Business and Economics, Beijing, China 100029*

Correspondence should be addressed to Shen Chen; 2006005@fjjxu.edu.cn

Received 24 February 2022; Revised 9 May 2022; Accepted 12 May 2022; Published 3 June 2022

Academic Editor: Yuan Li

As the world's average population continues to increase, residents' demand for water resources continues to increase. Traditional water resource management models and accounting methods have been unable to adapt to the development of the era of big data. We urgently need to establish a new accounting model to realize the sustainable use of water resources under the sustainable development strategy. Based on the above situation, starting from the development of water resource management and market economy, this paper models and analyzes the water resource accounting of sustainable development strategies in the big data environment. First of all, according to the needs of fine accounting of water resources, we start with the microcontrol principle of accounting. We take the basic principles of the accounting identity and responsibility right generation system as the basic method of water resource accounting. This paper proposes an accounting system framework for water resource accounting accounts and related statements. In the sustainable development strategy, the impact of human wading activities on water resources and ecological environment is discussed. Finally, the application of water basin accounting is analyzed in detail. The results show that under the sustainable development strategy, the water resource accounting model integrated into the market economy development can improve the utilization rate of modern water resources and further improve and realize the concept of sustainable development.

1. Introduction

As an important resource in our daily life, water resource is an indispensable material element for social development. Creating sustainable water resource management in the big data environment is the main way to improve water resource utilization [1]. The era of big data and digitization is developing rapidly, and the rapidly consumed water resources are the key content we need to pay attention to. Water resources are not only facing the current situation of shortage but also facing the problem of pollution in social development [2]. The traditional water resource accounting management is no longer applicable to the current big data background, in order to better save and utilize water resources. We need to carry out accounting and modern management of water resources suitable for the development of market economy under the strategy of sustainable development [3]. At present, people do not pay attention to this kind of content in the optimization of water resource management. The traditional management accounting method has been relatively backward. In order to meet the current development background and improve the utilization rate of water resources, different departments should plan their own responsibilities. We improve the confusion in the accounting management system. With the deepening of urbanization, China's market economy has developed, and the water resource market has become a relatively perfect system [4]. However, the large gap between urban and rural areas and the unbalanced economic development still perplex the market price of water resources in China. The market price system of water

resources has not been improved and established [5]. The price of rural water resources is not equal to that of cities, and even far lower than that of cities. We cannot effectively restrict the use of water resources by rural hukou. This situation has greatly hindered the management of water resource utilization in China [6].

In order to solve the above problems, we not only need to pay attention to ideology but also need to integrate science and technology into water resource allocation and management. In China's economically underdeveloped areas, the amount of investment in water resource accounting and management is small, so it is difficult to achieve an efficient and intelligent management mode. We need to take sustainable development strategy as the core content of improving water resources accounting [7]. In order to ensure the sustainable recycling of water resources, the key research direction is to ensure the sustainable development of water resources. The key factor for effective sustainable recycling and distribution is to promote social development and maintain the natural environment in combination with the development level of market economy [8]. The earth's water resources are limited energy, and the uneven distribution in some regions is easy to cause market chaos. We need effective regulation through the government to realize rational distribution and optimization. We narrow the gap between urban and rural areas and avoid obvious regional differences. We model and analyze water resource accounting from the demand of fine management of water resources and the concept of sustainable development. We apply accounting principles to water resource management and distribution.

This paper is mainly divided into three parts. The first part first analyzes the background and management status of water resources accounting in the sustainable development strategy, briefly describes the main problems faced by water resources accounting, and puts forward the research content of this paper. In the second part, under the sustainable development strategy of big data, integrating the development level of market economy, the water resources are finely divided, and the accounting control mode is studied. This paper puts forward the construction of accounting system architecture such as water resource vouchers and accounting statements. The characteristics of water resources are highlighted, and the current situation of water content and precipitation in water resource basins in China is analyzed. Finally, the water resource accounting is reflected in the form of identity, and the accurate data of water resource output value and accounting statements are studied. The specific application of water resource basin accounting. The third part analyzes the research results of water resource accounting modeling under the big data sustainable development strategy and briefly describes the specific significance of this research content.

2. Related Work

For the rational allocation and management of water resources, the realization of sustainable recycling begins with the accounting audit of water resources. We take social economy, natural resources, and social harmony as the basis of a virtuous circle [9]. To realize the sustainable development of water resources, we need to integrate the water resources of each region of the basin and make common distribution and utilization from the concept of science and technology. We observe the change of water resource basin and explore the accounting content of water resources from the overall regional structure. How to establish an accurate accounting mechanism is our main problem. Relevant departments need to strictly control the total amount of water resources in various regions and add the water resource quota and basic units to the accounting in providing accurate data [10]. The government also needs to regulate the conditions of water intake and use and strictly control the water intake and consumption of water resources. We help residents form standardized water use behavior and do a good job in social registration and coordination. The establishment of the accounting mechanism should first start from the level and development of market economy. The economic level of each region is different, and the share of water resources is also different. The price of water resources in economically underdeveloped areas is far from that in developed areas [11]. We need to fully grasp the change law of water consumption and water intake coefficient from the actual situation of local water resource distribution and market economy.

The spatial distribution of water resources in China is very unbalanced, and the areas that can recycle water resources are distributed in the South [12]. With the acceleration of industrial process and urban development, the use and waste of water resources are very serious. Since China proposed to take energy consumption, environmental protection, and ecological benefits as the comprehensive evaluation system of economic development in 2015, regional governments have begun to attach great importance to natural resource protection from the concept of sustainable cycle [13]. The accounting of natural resources is becoming more and more strict and standardized, and the accounting of water resources is the main concern of government agencies. At present, our research on water resource accounting is in the primary stage, and the scientific accounting method is not perfect. We need to realize research and application on the basis of accounting theory. As early as the 1970s, the contradiction between the demand for water resources in different countries and regions began to become the main social problem, and the accounting of water resources also came from people's cognition of the value of natural resources [14]. This contradiction has brought a new impact on water resource management. The United Nations and other accounting systems accounted for the total social value in 2008 and calculated the value in the balance sheet by measurement. Among them, the value of water resources as nonfinancial and nonproductive is presented in the balance sheet. This also means that natural resources are debt free. They did not consider the concept of environmental protection. At this stage, many western countries tried to add water resource accounting. The environmental protection department of the United States first investigated the output value and treatment cost of water resources and provided help for their country's water resource allocation

in the research data [15]. The UK allocates the expected income from the ownership of water resources meeting the conditions, treats the resources in the income part as assets, and brings them into the scope of environmental accounting table. Japan and other countries have also successively incorporated water resources into the natural resource accounting table and established corresponding physical quantity supply and demand balance accounts. According to the development status of water resource accounting in various countries, China also puts forward the accounting model to model and analyze water resources. This paper studies the modeling of water resource accounting to meet the development of market economy under the strategy of sustainable development.

3. Methodology

3.1. Research on Accounting Principle and Modeling of Water Resources Based on Big Data Sustainable Development Strategy. Clarifying the relationship between water resources and water resources assets is an important prerequisite for the preparation of water resource balance sheet, and clarifying water resources assets and their measurement methods is the theoretical basis for the preparation of water resources balance sheet. If you want to prepare a reasonable and accurate water resource balance sheet, you must clarify the relationship between water resource assets and water resources. To implement the key projects of regional reclaimed water recycling and establish a sustainable mode of regional reclaimed water recycling, the government needs to strengthen the supply of investment and financing policies and systems, innovate the project implementation mode and market-oriented investment and financing mode, and guide social capital investment.

Water resource is the basic material of natural resources and plays a major role in social and economic development. All life and environment cannot operate without the support of water resources. In order to realize the social development model of sustainable concept, we need to realize sustainable development in the division and protection of water resource management. With the increasingly serious problem of water resource pollution and shortage, in order to better manage and utilize water resources, we need to combine the concept of sustainable development with the development form of market economy and integrate it into the process of water resource management and governance. With the continuous emergence of research results on the relationship between man and nature and nature and water resources, researchers have paid great attention to the utilization and distribution of water resources. In order to alleviate the increasingly severe shortage and unequal distribution of water resources, a new direction for the sustainable development of water resources is pointed out. It is necessary to establish an authoritative accounting mechanism in the relationship between man, nature, and water resources. The accounting data is applied to the division of modern water resources.

The core content of accounting is to show the main fund activities and realize the microcontrol of fund activities by setting relevant items, bookkeeping methods, filling in forms, reviewing vouchers, registering records, filling in reports, etc. Firstly, the voucher is used as the basis for authenticity guarantee, and the three steps of accounting are used as technical support. Finally, it is presented in the form of accounting statements to evaluate and manage the quality of the data results. The basic principle of accounting is shown in Figure 1.

As can be seen from Figure 1, this microcontrol mode is related to fine division management, and many steps and contents can be overlapped. The flow and distribution of resources can be reflected from the details, calculation process, and specific implementation to the final effect. From the direction of fine management of water resource division, the main body and regional resources of water resources are accounted by using accounting identity and bookkeeping as calculation principles. We build project tables and ledgers including resource vouchers. This modeling method not only meets the table requirements and audit purposes but also highlights the characteristics of water resource accounting. The basic framework of water resource accounting is shown in Figure 2.

It can be seen from Figure 2 that in water resource accounting, accounting subjects can reflect the transaction process of things and are the main means of supervision. The primary steps and specific vouchers can be set to account for entities that meet the calculation principles. The accounting content shall be comprehensive and universal, and the accounting content shall be combined with specific indicators. The basic principles of water resource accounting mainly include several elements: assets, liabilities, and equity. Such as surface water content, bottom water content, other water content, utilization rate and water consumption are needed. In the framework of sustainable circulating water flow relationship, we can know the regional relationship of water resource sources from the perspective of accounting. It also includes water sources that can be used directly without processing. The processing process also includes water intake content, available water content, and consumed water content. In the process of relationship inference, we assume that the main body will use all water intake, and the calculation formula is as follows:

$$Wg_t = Kf + Sh_1 = GS + Sh_2 + Sh_1, \tag{1}$$

where Wg_t represents the water intake content, Kf represents the available water volume, and Sh_1 represents the water consumption. We judge the sustainable circulating water consumption according to the obtained water content as follows:

$$\begin{aligned} \mathrm{loop}_{Wg} &= SH + Sh_1 + Sh_2, \\ Wg_t &= \mathrm{loop}_{Wg} + PWg_t + \sum SH_t, \end{aligned} \tag{2}$$

where the variable loop_{Wg} represents the water content that can be recycled sustainably. When the regional inventory volume is changed, our accounting equation will change as follows:

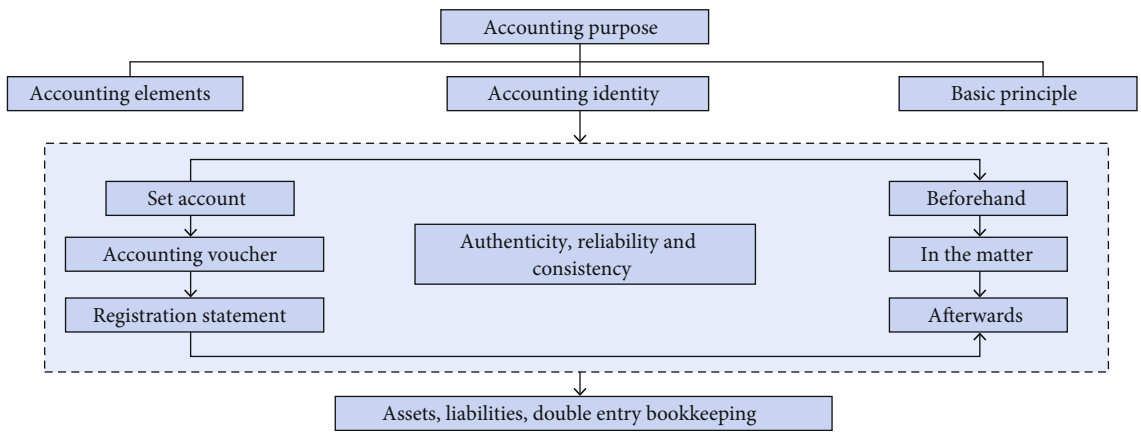

Figure 1: Basic principle diagram of accounting.

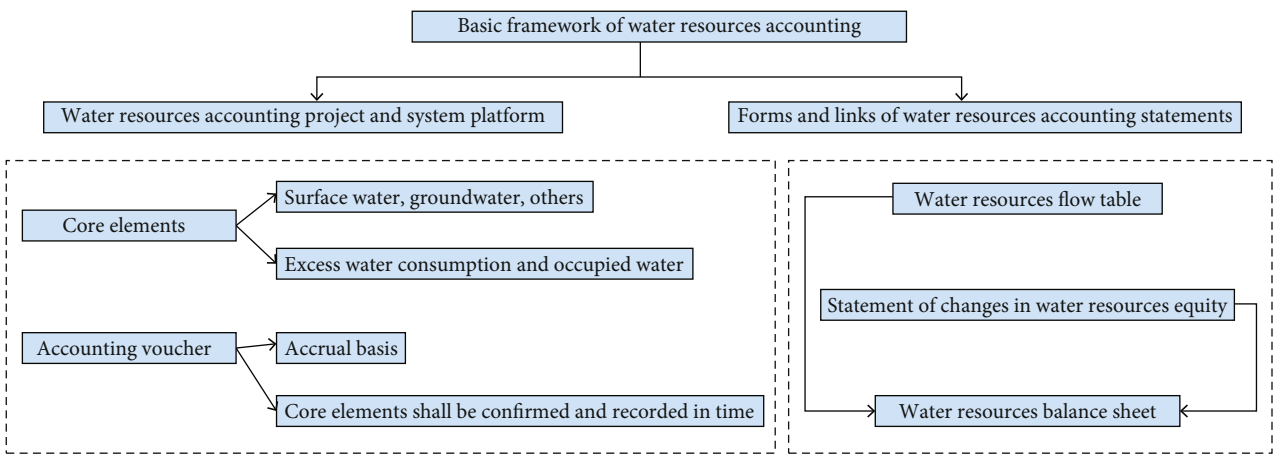

Figure 2: Basic framework of water resource accounting.

$$Wg_t - \text{Time}_{Wg} = \text{loop}_{Wg} + PWg_t + \sum SH_t. \quad (3)$$

The above formula represents the difference between the water consumption and the inventory at this stage. In accounting, we need to calculate the cost of water intake, power supply cost, and processing cost. The calculation equation is as follows:

$$\begin{aligned} \varepsilon_{tr} &= \frac{(Y_1 + Y_2) - (Y_3 + Y_1)}{2(Y_3 - Y_1)}, \\ TVW_s &= B_s \times \varepsilon_{w,s} + F_{w,s}, \\ f_{w,s} &= f^w = \frac{F_w}{Q_w} = F \times \frac{\varepsilon_w}{Q_w}, \end{aligned} \quad (4)$$

where ε_{tr} represents the water intake cost and Y_1 represents the variable of water intake times. $f_{w,s}$ represents the consumption of processing cost. From the perspective of macroaccounting, water resource accounting is a way to realize economic and social, environmental protection and resource utilization. It can maintain the harmonious survival between man and nature and adapt to the changes of natural resources. The microcontrol can reflect the information of water resource allocation, water intake process, water use, and so on.

3.2. Research on Application of Water Resource Basin Accounting Based on Big Data Sustainable Development Strategy. Several major water systems in Haihe River Basin are rich in water resources, among which Beihai River, Daqing River, and other tributaries originate from Inner Mongolia and the Loess Plateau, respectively. The annual precipitation in Hebei Plain is less, and the main flood season begins in June every year. July and August account for more than half of the annual precipitation. We analyze the precipitation trend of water resources in the basin over the years, as shown in Figure 3.

It can be seen from Figure 3 that the precipitation in each region has increased and decreased significantly. In addition to precipitation, water resource reserves also come from surface water and groundwater. Groundwater is an important source of water resource reserves, which can help industry, agriculture, and domestic water. To a certain extent, it provides guarantee for a sustainable development strategy. In practical application, we use the unit hierarchy

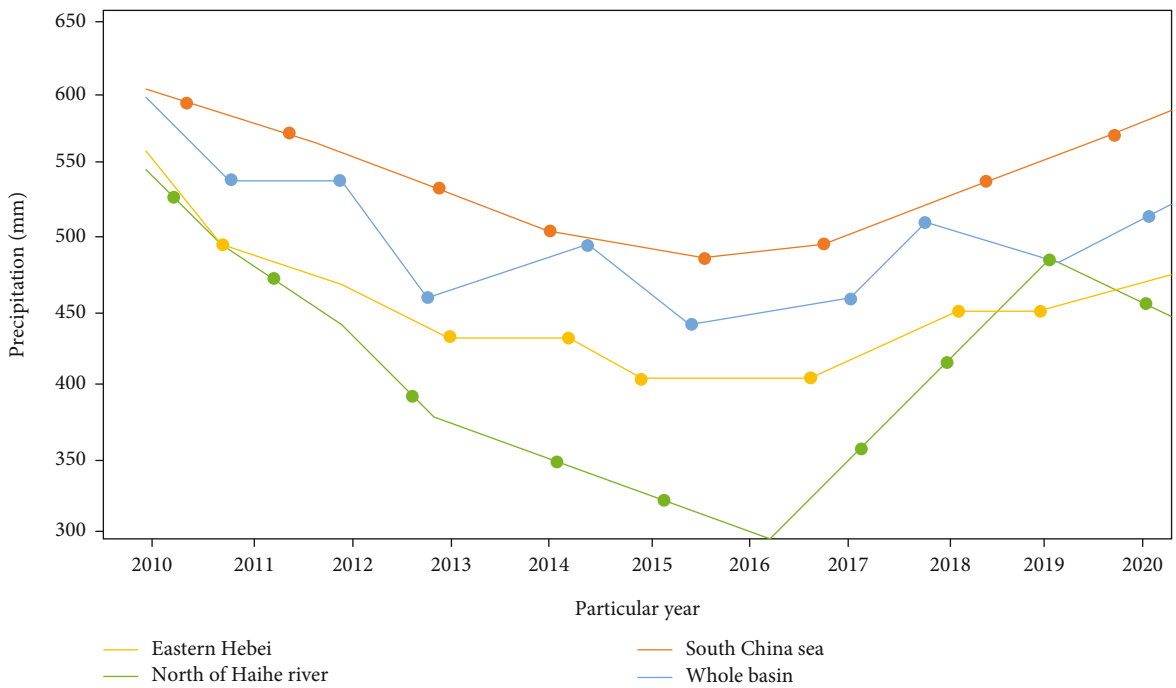

Figure 3: Trend of water resource precipitation over the years.

method to calculate the physical quantity of water resources. Mainly for the usable part of surface water resources, the accounting method is used for statistics:

$$V = \sum_{n=1}^{i} W_n. \tag{5}$$

In the formula, V is the physical quantity of water resources output value and W is the physical quantity per unit. The price change of water resources is the result of the balance between supply price and demand price. The shortage of water resources is a developing problem of dynamic balance between supply and demand. To achieve the strategic goal of sustainable utilization of water resources, we must meet the conditions of the water resource system, including the movement law of water quality and quantity in natural circulation. We study and solve various types of problems related to the balance of supply and demand and take effective measures to achieve the purpose of permanent and sustainable dynamic balance of supply and demand of water resources. This final equilibrium system can be used to objectively evaluate the price trend of water resources. In the practical application of water resource accounting, the average flow and ecological demand of each watershed area are calculated, and the formula is

$$W_r = \frac{1}{n}\left(\sum_{i=1}^{n} W_i \times K\right). \tag{6}$$

In the formula, W_r is the environmental water demand of the basin and n is the quantity in the statistical year. We calculate the annual environmental demand according to the average water volume in the minimum month:

$$W_r = 12 \times \mathrm{Min}\left(W_{ij}\right). \tag{7}$$

In the formula, W_r is the minimum demand of the basin and $\mathrm{Min}(W_{ij})$ is the minimum water consumption of each month. In accounting, it is also necessary to analyze the availability of other water resources and recycle the treated recyclable water. The main calculation formula that can be included is as follows:

$$W_Q = W_L + W_H + W_X + W_k. \tag{8}$$

The formula represents the amount of other water resources that can be utilized and the amount of reclaimed water, Haihe River water, salt water, and fresh water. According to the calculation of the formula, the data of water resource statements of various provinces and cities can be statistically determined. In view of the shortage of water resources, water intake management is not only the best way to plan the allocation and dispatching of water resources but also one of the important means to realize recyclable and sustainable utilization. Water intake permit is the main embodiment of water resource power. One of the important responsibilities entrusted by the state to various departments and management institutions is the water intake certificate. During the accounting period, we should calculate the current water right for the undistributed and transmitted water resources. When the physical quantity and unit value

of water resources are determined, the value output can be expressed by the following formula:

$$V_{\text{ass}} = A \times v. \tag{9}$$

In the formula, V_{ass} represents the value of water resources and A represents the physical quantity of assets. In practical application, the accounting of the physical quantity of water resources is mainly analyzed from the water consumption and quality degradation in each region. The characterization of water resource liabilities in different watersheds needs to be judged from the formal organization and finally accounted in a quantitative way. In the concept of water resource consumption, the water resource system of the whole region is taken as the object, and the total consumption is the difference between water use and available water. It is objective to calculate the quantity of surface water, shallow groundwater, and deep groundwater, respectively. The calculation formula is as follows:

$$\begin{aligned} D &= D_{\text{s}} + D_{\text{sg}} + D_{\text{dg}}, \\ D_{\text{s}} &= (C_{\text{in}} + C_{\text{lus}} + C_{\text{out}}) - W_{\text{sv}}. \end{aligned} \tag{10}$$

D_{s} in the formula represents the surface water consumption. This data should be analyzed from whether the surface water consumption exceeds the available. The transferred water resources are not included in the accounting scope, so the total physical liabilities of water resources are

$$D_{\text{sg}} = E_{\text{sg}} - R_{\text{g}} = L_p + D. \tag{11}$$

According to the accounting method of water resources, we calculate the output value, physical quantity, and value of water resources in the basin with the region as the unit. Finally, a water resource balance sheet is formed.

4. Result Analysis and Discussion

4.1. Analysis on Research Results of Water Resource Accounting Principle and Modeling Based on Big Data Sustainable Development Strategy. From the perspective of sustainable development of big data, we should first start from the accounting model adapted to the development of market economy, focusing on physical measurement and supplemented by value. When establishing the balance sheet of water resources, it is necessary to take the change item, time, and unit as the measurement range. The cost value and fair value in historical data are used for calculation. This paper mainly uses the balance sheet in the accounting process. Taking the natural energy of water resources as the main object, report statistics are carried out from the quantity of resources and environmental impact. The method based on the accrual basis takes the entity as the calculation content and follows the water asset calculation identity. The income and expenditure of different water right entities form a creditor's right relationship. In the accounting identity, we calculate the difference between the physical quantity of the net output value of water resources and the physical quantity of liabilities and finally obtain the physical quantity value of the net output value of water resources in each region, as shown in Figure 4.

As can be seen from Figure 4, we take Eastern Hebei, northern Haihe, and southern Haihe river basins as examples. We explore the changes of net aquatic products in the three regions with the growth of years. Finally, the change of physical quantity is filled in according to the setting principle of the balance sheet, and the results of water resource output value and purified water physical quantity are obtained. The core content of water resource accounting is to express the use of water resources activities of water-related subjects with water output and value as the main scale. The entity of water resource accounting can conduct post accounting for activities generated or completed. The main method is also used to supervise the accounting entity. Starting from the diversity and unity of subjects, we optimize the traditional single way. We adopt systematic methods and systems, establish water resources accounting identities, and determine the main factors affecting accounting. We set up calculation items and liability distribution table. Finally, the water resource accounting process is evaluated to form a complete and smooth accounting model.

4.2. Analysis of Research Results on Application of Water Resource Basin Accounting Based on Big Data Sustainable Development Strategy. Sustainable development strategy in the big data environment is the core content of our social development. Water resources in natural resources are characterized by their own randomness, fluidity, and uncertainty. Uneven distribution in some regions is easy to cause market chaos. We need effective supervision by the government to achieve reasonable layout and optimization. We narrow the gap between urban and rural areas and avoid obvious regional differences. Starting from the requirements of fine management of water resources and the concept of sustainable development, this paper models and analyzes water resource accounting. In the accounting statements of water resources, it is necessary to consider the impact of recycling characteristics and changes in assets and liabilities on regional price fluctuations. A set of reporting principles specific to changes in water resources should be formulated to highlight the characteristics of water resource assets. According to different accounting entities, the accounting results are also different. Each individual water right, as the accounting subject, such as water plants, reservoirs, and other wading areas, provides them with correct water use strategies. In wading activities, we should carry out macrocontrol of the total amount of water resources in different forms from the regional differences. We evaluate the main nature of wading activities and wading quality. We comprehensively analyze the water resource accounting cases of different subjects and study the demand for fine division of water resources in combination with the concept accounting system and relevant data. We strictly formulate the water resource management system, water right system, flow management system, value evaluation system, etc. and connect the relevant systems with water resource accounting statistics and apply the content of water resource accounting to the actual management in a quantitative and qualitative way.

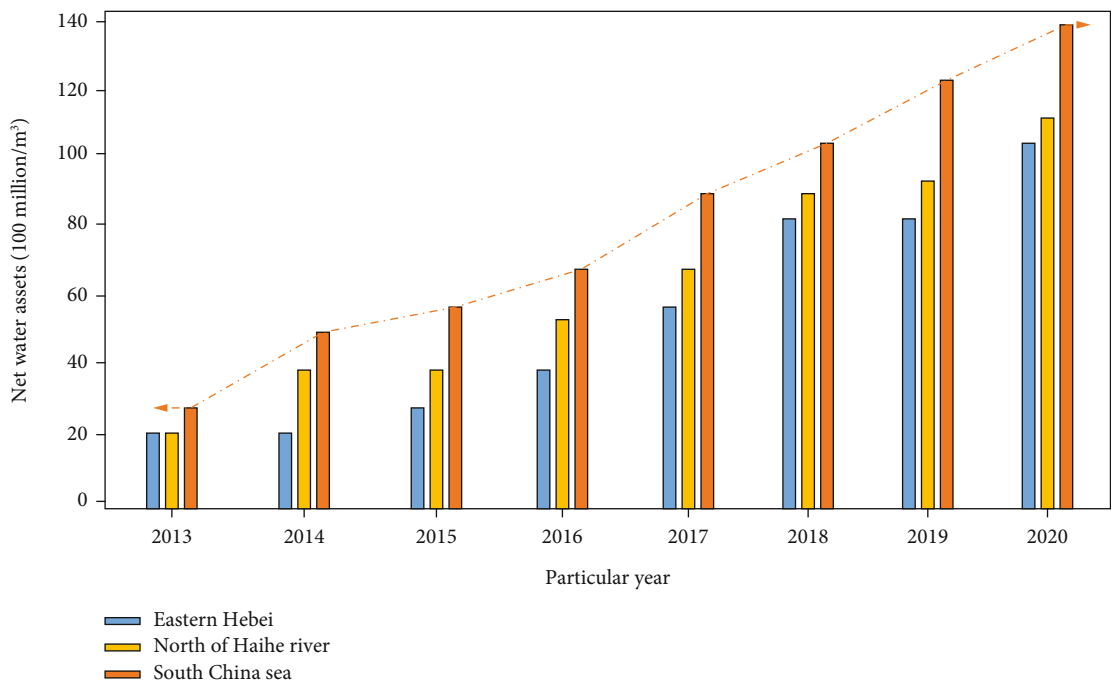

Figure 4: Net output value of water resources in each region.

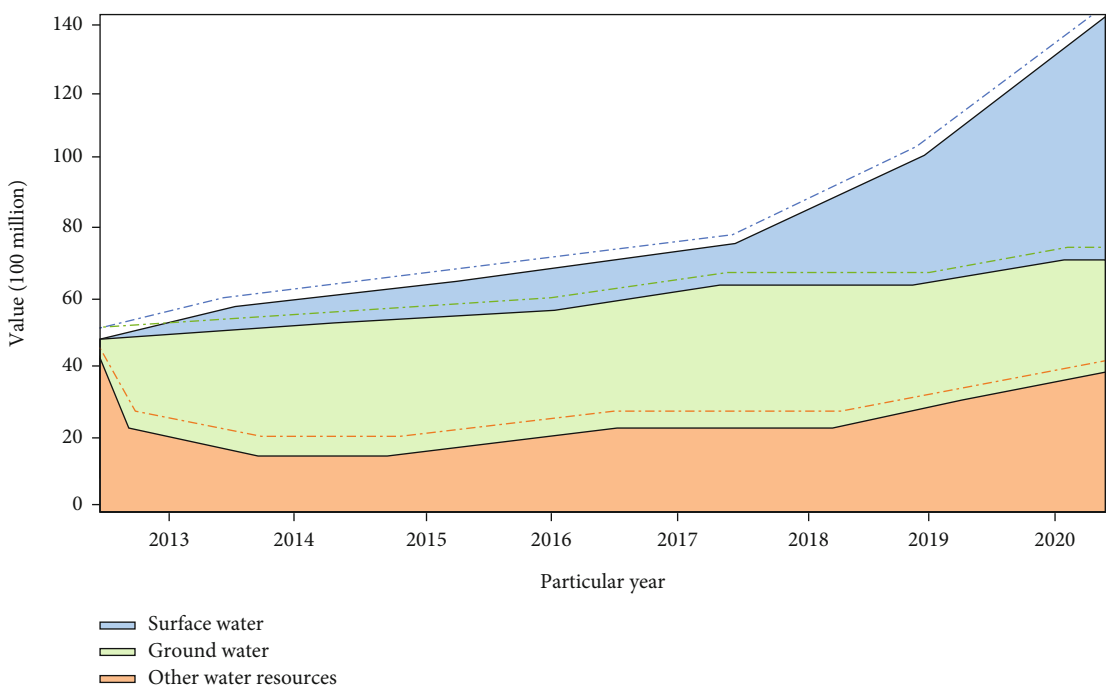

Figure 5: Analysis of available value of water resources.

According to the established the water resource accounting method and liability accounting method. Taking the water resource basin as a regional case, we take each region as the basic unit for value accounting and analysis. Finally, the available value of water resource sources is evaluated according to the accounting results. In the accounting price model, we analyze the price of natural water resources from the available quantity. We calculate the available value of surface water, underground water, and other water resources, as shown in Figure 5.

It can be seen from Figure 5 that in the total value, the available value of surface water is the highest and that of other water resources is the lowest. According to the above research results, under the theme of sustainable development strategy, we should start from the changes of market economy in different regions and uniformly allocate the divided quantity of

water resources in combination with the availability. The process of accounting includes control decision-making and demand management. This bookkeeping method and vouchers are used as the basis, and the liability statement is used as the output embodiment. We ensure the accuracy and authenticity of accounting. The research reflects the integrity and continuity of accounting. As the main branch of environmental analysis, water resource accounting provides effective help for resource scientific planning. It is of great significance to the conservation and utilization of water resources. If conditions permit, we can also take data research from the water resource accounting information of listed companies to explore the relationship between accounting and industrial behavior and income. Finally, combined with the concept of sustainable cycle, a new accounting model is formed.

5. Conclusion

This paper applies the content of accounting to the analysis of the availability of water resources in the basin and discusses the impact of different water sources on the availability. The results show that the accounting model is helpful to optimize and improve the water resources management system and provide an effective basis for the development, utilization, protection, and conservation of water resources. According to the research results of this paper, under the theme of sustainable development strategy, we should carry out unified distribution of water resources from the changes of market economy in different regions and combined with the availability of water resources. The accounting process includes control decision-making and demand management. Based on this bookkeeping method and vouchers, the balance sheet is the output embodiment. We ensure the accuracy and authenticity of accounting. This study reflects the integrity and continuity of accounting. As the main branch of environmental analysis, water resource accounting provides effective help for resource scientific planning. This is of great significance to the protection and utilization of water resources. However, this paper does not study the data in the water resource accounting information of listed companies to explore the relationship between accounting and industry behavior and income. This needs further analysis and development in future research.

Data Availability

The experimental data used to support the findings of this study are available from the corresponding author upon request.

Conflicts of Interest

The author declared that they have no conflicts of interest regarding this work.

Acknowledgments

The project was supported by the Fujian Provincial Social Science Fund, Fujian Research Center of the Theoretical System of Socialism with Chinese Characteristics in China, the project name: Research on Enterprises' Social Responsibility Oriented Internal Control and Sustainable Development Strategy (Grant No. FJ2019ZTB044).

References

[1] H. Zheng and S. Malin, "Preparation of water resources balance sheet in Hubei Province," *Statistics and Decision Making*, vol. 37, no. 19, pp. 43–47, 2021.

[2] K. Yu and Shuangyu, "Research on the construction of water resources accounting system for hydropower projects in China," *Friends of Accounting*, vol. 8, no. 13, pp. 56–62, 2021.

[3] E. Levner, D. A. L. . Pablo, and J. Ganoulis, "Risk management of transboundary water resources using the green supply chain approach," *International Journal of Risk Assessment and Management*, vol. 10, no. 4, pp. 357–372, 2008.

[4] P. Hirsch, "Water governance reform and catchment management in the Mekong region," *The Journal of Environment & Development*, vol. 15, no. 2, pp. 184–201, 2006.

[5] L. Wang and H. Jing, "Some thoughts on strengthening the supervision of water conservancy funds under the centralized accounting mode," *Haihe Water Conservancy*, vol. 4, no. 3, pp. 66–68, 2020.

[6] Z. Zhifang, C. Qiyue, W. Yu, and X. Xiao, "Research on water resources balance sheet accounting system – from the perspective of outgoing audit of natural resources assets," *Journal of Xi'an University of Finance and economics*, vol. 32, no. 2, pp. 67–72, 2019.

[7] J. Ling, G. Hong, L. Wang, Q. Changhai, and P. Zhou, "Application principles and key issues of accounting theory in fine management of water resources," *Water Conservancy Economy*, vol. 37, no. 2, pp. 8–12, 2019.

[8] L. Xinying, Y. Wang, and Z. Bin, "Exploration on accounting of water rights transaction – water saving management mode based on contract," *Finance and accounting study*, vol. 12, no. 5, pp. 1–3, 2019.

[9] X. Wang, "Discussion on the necessity of water resources accounting in water rights transaction," *Accounting study*, vol. 5, no. 21, pp. 98-99, 2018.

[10] J. Yujia and G. Xu, "Further research on enterprise water accounting and management," *Journal of Hebei University of Geosciences*, vol. 41, no. 4, pp. 64–69, 2018.

[11] T. Guiliang, W. Ding, and S. Xiaojie, "Water resources balance sheet: elements, framework and pilot compilation," *People's Yellow River*, vol. 40, no. 11, pp. 65–68, 2018.

[12] L. Yan, "Theoretical thinking and method discussion on water resources accounting," *The Accountant*, vol. 8, no. 14, pp. 11-12, 2017.

[13] Z. Pu, J. Ling, and G. Hong, "Research on physical water resources accounting framework of water equity entity," *Accounting Research*, vol. 11, no. 5, pp. 24–31, 2017.

[14] S. Guo, Z. Chengmin, S. Xinmei, and T. Yue, "Research on the implementation of environmental accounting in Huaihe ecological economic belt," *The Accountant*, vol. 6, no. 13, pp. 70-71, 2016.

[15] D. Guan and K. Hubacek, "A new and integrated hydro-economic accounting and analytical framework for water resources: a case study for North China," *Journal of Environmental Management*, vol. 88, no. 4, pp. 1300–1313, 2008.

Hindawi
Journal of Sensors
Volume 2022, Article ID 3690312, 17 pages
https://doi.org/10.1155/2022/3690312

Research Article

Convolutional Autoencoder-Based Deep Learning Approach for Aerosol Emission Detection Using LiDAR Dataset

Mazhar Hameed,[1] Fengbao Yang,[1] Sibghat Ullah Bazai,[2] Muhammad Imran Ghafoor,[3] Ali Alshehri,[4] Ilyas Khan,[5] Shafi Ullah,[2] Mehmood Baryalai,[6] Fawwad Hassan Jaskani,[7] and Mulugeta Andualem[8]

[1]*School of Information and Communication Engineering, North University of China, Taiyuan, China*
[2]*Department of Computer Engineering, Balochistan University of Information Technology, Engineering, and Management Sciences, Quetta, Pakistan*
[3]*Department of Electrical Engineering, Superior University, Pakistan*
[4]*Department of Computer Science Applied College University of Tabuk Saudi Arabia, Saudi Arabia*
[5]*Department of Mathematics, College of Science Al-Zulfi, Majmaah University, Al-Majmaah 11952, Saudi Arabia*
[6]*Department of Information Technology, Balochistan University of Information Technology, Engineering, and Management Sciences, Quetta, Pakistan*
[7]*Department of Computer Systems Engineering, The Islamia University of Bahawalpur, Pakistan*
[8]*Department of Mathematics, Bonga University, Bonga, Ethiopia*

Correspondence should be addressed to Mazhar Hameed; mazhar_hameed@hotmail.com and Mulugeta Andualem; mulugetaandualem4@gmail.com

Received 3 December 2021; Revised 3 April 2022; Accepted 29 April 2022; Published 1 June 2022

Academic Editor: Zhenxing Zhang

Quantifying atmospheric aerosols and their linkages to climatic repercussions is necessary to understand the dynamics of climate forcing and enhance our knowledge of climate change. Because of this reactivity to precipitation, temperature, topography, and human activity, the atmospheric boundary layer (ABL) is one of the most dynamic atmospheric regions: ABL aerosols have a big impact on the evolution of climate change's radiative forcing, human health, food security, and, eventually, the local and global economy. Continuous monitoring and instrumental and computational approaches are required for the detection and analysis of ABL pattern behavior. This paper provides a deep learning-based outer layer aerosol detection system based on Light Detection and Ranging (LiDAR) data fusion. The suggested method applies sequential models to turn low-level data into compressed features using object-based analysis, feature-level fusion, and autoencoder-based dimensionality reduction. Convolutional neural networks (CNNs) were used to convert compressed data into high-level properties that could be used to categorize air particles in the outer layer. This research describes deep learning approaches that allowed for detecting 40% more atmospheric features at a horizontal resolution of 5 km during daytime operations when applied to LiDAR data. Compared to existing deep learning algorithms for edges and complicated near-surface sceneries during the day, a convolutional autoencoder (CAE) trained using LiDAR dataset standard data products showed the potential for improved aerosol discrimination with 98% accuracy.

1. Introduction

In the Earth's climate system, air quality and hydrological cycle with an extent that is mainly dependent upon the atmospheric properties height, thickness, and type and air characteristics such as clouds and aerosols play a vital role [1]. Clouds of liquid water on the surface of Earth tend to reflect inbound sunlight, cooling the surface of Earth. However, ice clouds in the upper troposphere absorb and reradiate heat emitted from the surface, warming up the surface of

the Earth. Aerosol particles include windblown desert dust, wildfire smoke, sulfurous particles from volcanic eruptions, and fossil fuel particulate matter [2]. Aerosols cool or warm the surface, depending on their size, composition, and location in the atmosphere [3].

A CNN is a supervised machine learning method used for the recognition of picture features. Commercial uses of CNNs include a wide variety of object detection and semanticized issue segmentation [3]. CNNs have also been used to predict tropical cyclone intensity precisely using satellite imagery and hailstorm detection in radar images with higher accuracy than previous techniques. After instantiation of CNN's layer architecture, the model is trained with truth data sets, which develops expertise to predict proper characteristics in the image [4]. While the training of a CNN can take a long time, the forecasts are rapid compared to older algorithms or a manual approach. A collection of CNNs has been built to forecast the positions of clouds and aerosols in CATS LiDAR data to increase the speed at which LiDAR data may be distributed and establish feasibility to give real-life time layer type products [5].

Natural and artificial aerosol emissions can significantly threaten urban and regional air quality, such as biomass burning. As a result, it is crucial to understand the optical, microphysical, and geometrical characteristics of local or targeted aerosol emissions in the boundary layer. The LiDAR sensor, which uses a laser as its source, may offer highly temporal and spatially vertically resolved profiles of aerosols [6]. As a result, LiDAR remote sensing observations will aid in the research and characterization of aerosol emissions from source to destination and improve air quality. This section welcomes submissions on the most recent results and advancements in LiDAR distant detection of optical, microphysical, and mathematical spray properties from airborne-mounted LiDARs, territorial ground-based LiDAR organizations, global satellite missions, across all instrument platforms (Raman, high-spectral resolution, DIAL, and others), fleeting and spatial scales, and from airborne-moon missions. LiDAR control through a remote and the identification of anthropogenic aerosols that have an impact on air quality from industrial, biomass burning, and agricultural sources, as well as campaigns targeted at giving a full assessment of climate and health consequences, are especially encouraged [7]. Man-made aerosol emissions in cities are linked to their impacts on micrometeorology and the radiative budget, i.e., their function in heating/cooling the atmospheric column and promoting/suppressing convection, and are given specific emphasis [8]. We have used convolutional autoencoder models (CAE) [7] to detect aerosols from fusion LiDAR dataset [8]. CAE's ability to extract the aerosol type is influenced by the optical inputs' physical substance and uncertainty, as well as the CAE structure and training technique, notably the size of the data set employed for this purpose. An aerosol model detailing the optical characteristics of distinct particles was created to provide a consistent depiction of the aerosol types. This model can provide a representative and statistically meaningful synthetic database in order to recreate known aerosol features. This synthetic data collection is important since few observational data sets are statistically relevant, well-characterized, and representative of the whole range of aerosol species. Normalization is a common practice in data preparation for machine learning. You must normalize your data to a standard scale without distorting the range of numbers or surrendering any information if you want it to be consistent [9]. The aerosol model was constructed in order to train the CAE by simulating a large number of LiDAR observations (i.e., a synthetic data set) [10]. The most likely aerosol type inside the detected layers is the output data from generative adversarial neural networks (GANs) [10].

Deep learning techniques consist of deep layers where feature extraction and classification are not separately performed. Deep learning is a subclass of machine learning that processes data and makes patterns for use in decision-making. The deep learning technique teaches the machine to perform intelligent tasks. Deep learning contains numerous techniques such as a CNN, CAE, and GAN model [11]. The CNN works automatically for detecting features and classifying the raw dataset. Deep learning is a more advanced technique for recognizing hidden features more accurately and efficiently [12].

The detection of aerosols with manual detection is a challenging task due to the various properties of the environment. Hence, an automated and accurate system is required for aerosol emission detection [13]. The research is aimed at designing an intelligent aerosol emission detection system using fusion LiDAR data and applying deep and machine learning techniques to predict the emissions' area [14].

The aerosol emissions recognition has been considered as an essential application for numerous security branches and health systems. Several researchers have applied handcrafted techniques to identify such anomalies in the scene [15]. Using handcrafted features from linear binary configuration from three orthogonal planes, Gaussian mixture model, Markov random field, etc. for irregularity recognition is not acceptable as they solely rely on human assumption. Hence, the training data is not explained correctly to learn discriminative features characteristic of aerosols [16]. The acquired data from remote sensing and satellites are the key characteristics and contributions of this research. We used the convolutional autoencoder (CAE) neural network to process the data, which takes photos and extracts the hidden patterns of the input images before reconstructing the features from the hidden pattern. We then established a sequential model in the autoencoder model, which allows us to simply build sequential layers of the network from input to output. Then, we have applied GAN, which helps to solve such tasks as pattern recognition from descriptions, getting high resolution of images from low-resolution ones and predicting which is the aerosol emission area or not [1].

All of this research [17] have revealed a diverse group of people. A wide range of aerosols is challenging to categorize due to many flaws (e.g., many aerosol types have identical optical characters). Other challenge in the categorization of aerosols is the difficulty in linking their optical qualities to their physical properties source [18]. In actuality, atmospheric aerosols are made up of a variety of substances. There are a lot of sources, and data on pure aerosol kinds

Table 1: Comparative analysis of previous studies conducted on LiDAR.

Ref	Technique	Source of data	Outcome	Accuracy
Xiu et al. [1]	Semantic segmentation	LiDAR dataset	The entire waveform of LiDAR	89%
Zhang et al. [2]	Computer vision techniques	Land SAT8 data	Retrieval of Forest aboveground biomass	90.3%
Melotti and Premebida [5]	Multimodal deep learning	Self-created dataset	Object recognition combining camera	93%
Zhang et al. [7]	Multisource data fusion	LiDAR dataset	Data fusion	88%
Wahid et al. [6]	Object exploration vision techniques	Self-created dataset	Distributed soft actor critics	86.45%

are scarce. Systematic measurements and intense measurement campaigns employing various aerosol measurement methods have been carried out to address these difficulties.

Many Earth systems, such as temperature, air quality, and hydrology, are affected by the atmospheric properties of clouds and aerosols, and their effects are highly influenced by their height, thickness, and kind. At ground level, liquid water clouds tend to reflect incoming sunlight, which helps chill the surface [18]. Additionally, clouds in the upper troposphere that comprise ice are capable of absorbing heat from the surface and reemitting it, therefore contributing to the rise in surface temperature [19]. Dust, smoke, sulfur, and particles of fossil fuel burning are all examples of aerosol particles. The ability of aerosols to cool or heat the surface depends on their size, composition, and position in the atmosphere [20]. Many types of aerosols, including dark-colored ones, such as black carbon from fossil fuel combustion, are known to absorb radiation. Table 1 shows the previous studies' comparative analysis.

For this reason, the current study presents and contributes as follows:

(i) The use of LiDAR and orthophotofusion combined with a deep learning (DL) strategy to detect aerosols

(ii) DL has progressed past multilevel perceptron and now includes the following

This particular study employs an autoencoder framework and a convolutional neural network (CNN) to accomplish feature dimensionality reduction and object classification of aerosols and no aerosols in LiDAR and orthoimage data after segmentation.

2. Materials and Methods

An aerosol model was used to investigate the optical characteristics of pure aerosols produced by a single source (e.g., dust produced by the deserts and marine particles produced by the oceans). Continental, continental polluted, dust, marine, smoke, and volcanic are the six forms of pure aerosols addressed in this article. The aerosol model combines the global aerosol dataset with iterative computations of each aerosol type's intensive optical properties, as well as a numerical technique for T-matrix. The OPAC software application was used to determine the chemical makeup of each pure aerosol type (aerosol and cloud optical properties). To replicate the vast spectrum of particles in the atmosphere, the chemical composition of each aerosol type was modified within specified boundaries. For sound wavelengths of 350, 550, and 1000 nm, the aerosol model was utilized to create a synthetic database. These wavelengths were selected from OPAC's 61 wavelengths (0.25–40 m) for which GADS possesses microphysical aerosol parameters. After that, the wavelengths are rescaled in angstroms to match the traditional LiDAR wavelengths (i.e., 355, 532, and 1064 nm). This was deemed to be an acceptable assumption for all aerosol types, given the minimal difference between the LiDAR and model wavelengths. The aerosol model can be expanded to cover more wavelengths if necessary.

Every type of pure aerosol is made up of an internal combination of fundamental components in variable mix ratios that do not interact physically or chemically. Water-soluble, insoluble, soot, mineral, sulfate, and sea salt are all collected by OPAC (accumulation, coarse). The microphysical properties of each component are stored in the GADS database. Smoke and continentally contaminated kinds, however, cannot attain values above 1.2 for angstrom (550 to 350 nm) with the present GADS soot refractive index values.

Figure 1 depicts the workflow of the suggested technique combining a convolutional autoencoder, a sequential algorithm, and a GAN. The following are the details of the block diagram.

2.1. Data Acquisition of UAV LiDAR Datasets. The input photos are from the remote sensing LiDAR data of the aerosol emission dataset, $128 \times 128 \times 3$ input form. The convolutional autoencoder uses this image as an input (CAE). To recover the hidden patterns, CAE separates the input image into convolutional and pooling layers. It will then be supplied into the deconvolutional and unspooling layers, which will reconstruct the features of the hidden pattern. We used a sequential approach, which made it simple to build subsequent network layers in the order of input to output. Then, we employed a GAN to tackle problems like picture generation from descriptions or features, converting low-resolution image frames to high-resolution image frames, detecting which emission activity is active or not, and recovering image frames containing a given pattern.

One of the most well-known datasets in the field of aerosol detection is the LiDAR fusion dataset. It contains data from an aerial view, LiDAR, and other sensors attached to

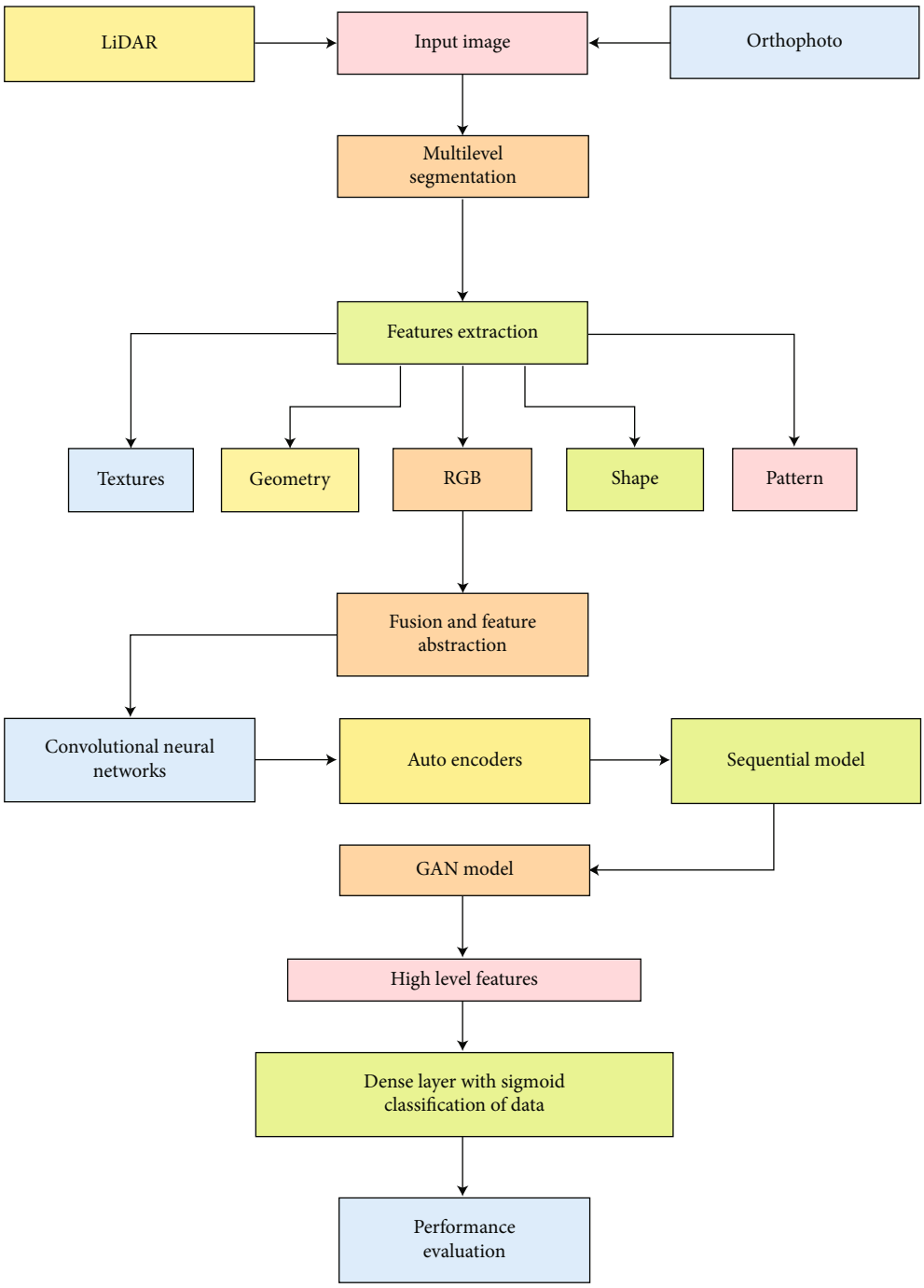

Figure 1: Proposed methodology.

the top of a drone that flies through various environments and scenarios.

This collection contains LiDAR frames that have been converted to 2D depth images. These 2D depth images show the same scene as the corresponding LiDAR frame but are more user-friendly.

The 360 LiDAR frames, like those in the dataset, are arranged in a cylinder around the sensor. The 2D depth images in this dataset might be represented as if the cylinder of the LiDAR frame had been split in half and straightened into a 2D plane. The distance of the reflecting item from the LiDAR sensor is represented by the pixels in these 2D depth photographs. The number of laser beams utilized to scan the surroundings is represented by the vertical resolution of the 2D depth image (64 in our case). These 2D depth images could be utilized for segmentation, detection, recognition, and other tasks, drawing on a large body of computer vision literature on 2D images. We have compared our model with a hybrid model of GAN and autoencoder to compare the performances.

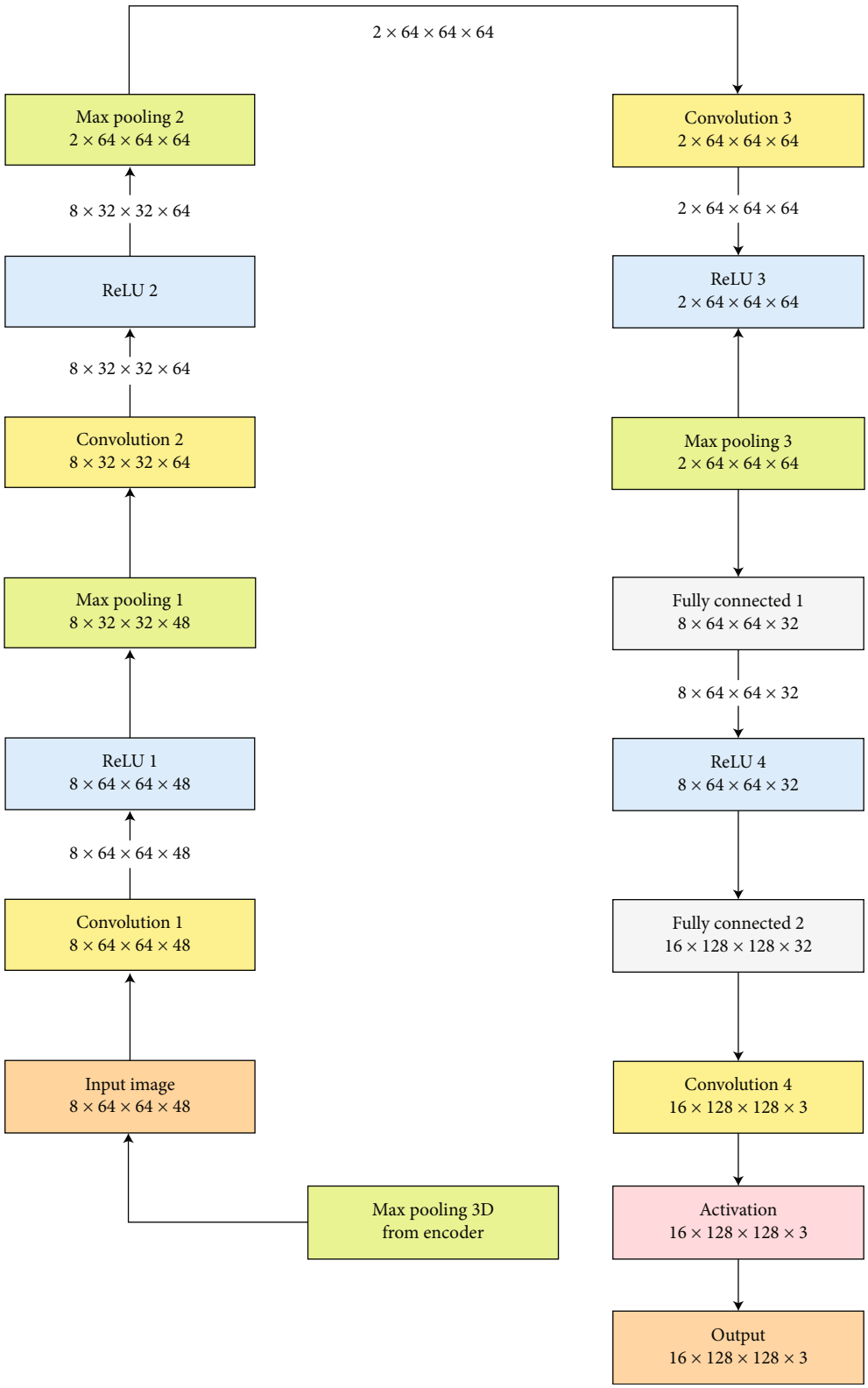

Figure 2: Generative adversarial network (GAN).

2.2. Model Training. The proposed technique defined the rule when emissions occurred. We trained the model, which contains spatial feature descriptors. The image description explains the visual feature of each frame. Each frame has its characteristics such as shape, color, andtexture. This description provides a feature vector. The convolutional autoencoder model is adequately trained with blocks of pixels that contain only standard segments. The frames'

input and output volume mistakes are reduced. The model is trained correctly on the regular images, and then the model shows the low reconstruction error. Each testing input image produces a reconstruction error. The reconstruction error depends upon custom loss. We set the threshold on the value. If the value crossed a threshold limit, it shows an aerosol emission and represents a regular event below the threshold limit. Thus, the system will be able to recognize the rare events that occur in the images.

2.3. Model Parameters. The training model is used for reducing the reconstruction error of the input volume. The proposed Model used an Adam optimizer, and the learning rate automatically depends upon the updated history of the model's weight. The minimum patch size is 64. Every training image size is trained for a maximum of 50 epochs, or until the aerosol layers are lost and the 10 consecutive epochs are reduced. The spatial autoencoder activation goal is chosen to be the hyperbolic curve. Despite its regularization capacity, we did not use the rectified linear unit (ReLU) to guarantee the regularity of the encoding and decoding functions because triggered values from ReLU have no upper bound.

2.4. Convolutional Autoencoder Model. An autoencoder is an encoder-decoder system that reconstructs the input as the output. We achieved autoencoder by two subsystems: the encoder converts the input image frame into a feature vector for internal representation [6]. The decoder, on the other hand, translates the internal representation back to the original reconstructed image. Autoencoder provides a reconstruction error [19]. The minimum reconstruction error means a slight difference between the input and the reconstructed image frames [20].

2.5. Sequential Model. The sequential model was used, which makes it simple to stack sequential network layers from input to output. Figure 2 shows generative adversarial network (GAN).

2.6. Generative Adversarial Network Model. GAN is a generative modelling method based on the CNN method. In machine learning, generative modeling is an unsupervised learning problem [21]. It comprises pitting two neural networks against each other to automatically find and learn regularities or patterns in incoming data. Adversarial competition consists of two parts: generator: replicate authentic data in order to create fictitious data and discriminator: detecting the generator by distinguishing between accurate and fictitious data [12].

As a result, we used GAN to perform tasks such as image generation from descriptions or features, obtaining high resolution image frames from low resolution ones, predicting which emission activity is active and which is not and retrieving image frames containing a given pattern. Figure 3 shows classification using the generative adversarial model.

2.7. Model Description. As shown in Figure 1, the UAV fused LiDAR dataset utilized in this investigation was collected above the Universiti Sains Malaysia campus on February 3, 2018, at midday. A Canon PowerShot SX230 HS (5 mm) camera was used to collect data from a UAV flying at a height of 353 meters (5 mm). The photographs were created using three channels (RGB) with a ground resolution of around 9.95 cm/pixel, a resolution of 4000 3000-pixels, and an 8-bit radiometric resolution. An orthomosaic snapshot of the collected image series was produced with an average root mean square errors (RMSE) of 0.192894 m. (1.08795 pix). The DSM was also created with Agisoft PhotoScan Professional. The chosen subset spans a total area of 1.68 km^2. The DSM's resolution was 79.6 cm/pixel, while Agisoft's point clouds had a point density of about 1.58 points/m^2. Figure 1 depicts the operational flow of the suggested technique using a convolutional autoencoder, a sequential algorithm, and a generative adversarial network (GAN). The following are the details of the block diagram:

The input photos come from the UAV aerosol real-world aerosol collection and have a 128x128x3 input shape. The convolutional aAutoencoder uses this image as an input (CAE). CAE extracts latent patterns from input pictures using convolutional and pooling layers (128x128x3). It will then be fed into the deconvolutional and max-pooling layers, which will recreate the hidden pattern's characteristics. We used the sequential model, which allows us to stack sequential network layers from input to output effortlessly. Then, we used GAN to help with tasks like picture generation from descriptions or features, obtaining high resolution image frames from low-resolution ones, predicting whether aberrant activity is there or not, and retrieving image frames containing a given pattern.

Feature descriptors output feature descriptors/feature vectors from an input image frame. Feature descriptors are a set of integers that encode useful information. To validate the results, the UAV data was divided into two categories: testing (20%) and training (80%). Convolutional autoencoder and GAN model are two deep learning algorithms. The purpose of each model is to generate reconstructed images in a hybrid way by using an output layer from previous models. The sequential model has been used in CAE for sequencing the stack layers.

2.8. Raw Image Data Processing. The UAV aerosol dataset is used for testing and evaluation of the offered method. The aerosol dataset contains 13 different real-world anomalies. The real-world anomalies are abused, arrest, assault, and explosion, etc. We know that images are combinations of frames; so, we have converted the images into frames for preprocessing and feature extraction. The converted image frames in the form of JPEG and applied image resizing are as follows: the image resizing is essential because the dimension of each image's frame is not the same. The resized images are fed into the temporal volumes.

2.9. Model Training. The proposed technique defined the rule when abnormal events occurred. The maximum regular frames are different as compared to the abnormally frames. We trained the model, which contains spatial feature descriptors. The image description explains the visual feature

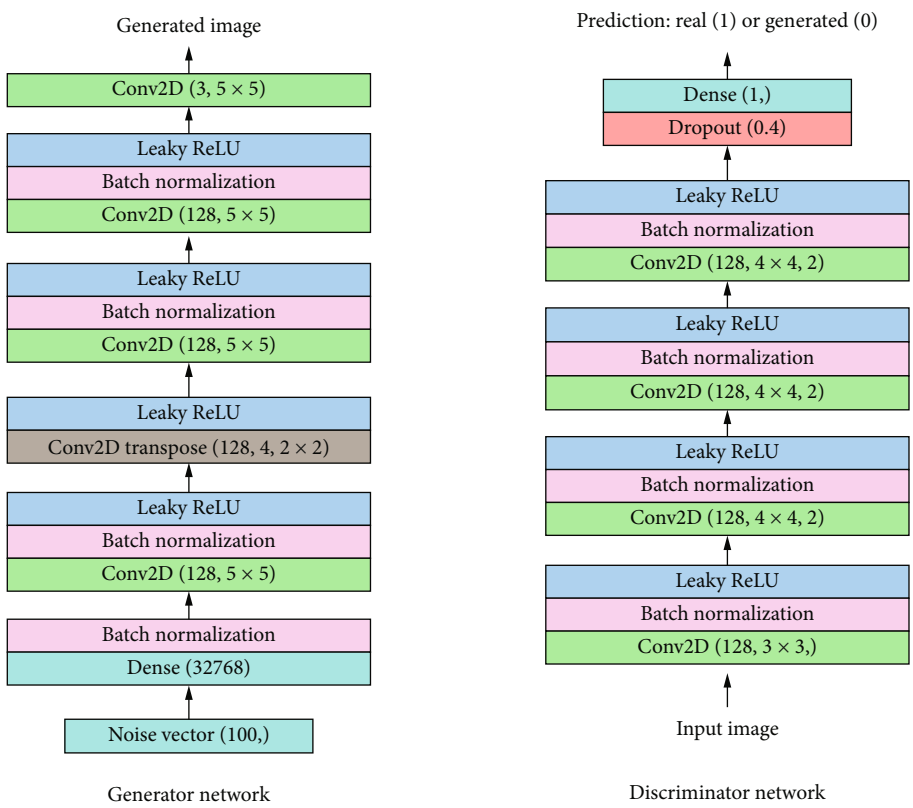

Figure 3: Classification using the generative adversarial model.

of each image's frame. Each frame has its characteristics such as shape, color, texture, and motion. This description provides a feature vector. The convolutional autoencoder model is adequately trained with images blocks contains only regular segments. The error between the input and output volume of the frames is reduced. The model is trained correctly on the standard image's frames, and then the model shows the low reconstruction error. Each testing input images volume produces a reconstruction error. The reconstruction error depends upon custom loss. We set the threshold on the value. If the value crossed a threshold limit, it shows an abnormal event, and below the threshold limit, it represents a typical event. Thus, the system will be able to recognize the rare events that occur in the images. In the following Table 2, we have shown the features that are extracted in the model.

One can find a wide variety of information about surface elements like topography, texture, and shape by studying them on images and LiDAR surveys. Using a lot of different characteristics might lead to overfitting, and that it is especially true when the training set is quite small. The other downsides of using several characteristics are that they increase the level of noise, the volume of redundant information, and the time it takes to compute. To deal with the problem of high-dimensional feature space, an autoencoder-based technique is proposed that reduces feature space dimensionality and improves low-level features by translating them into fewer features (i.e., reduced low-level features). The redesigned features will most likely be more informative than the initial raw features, assisting the full detection model creation process. CNN models were built to identify key architectural attributes, which were then processed using a series of convolution and pooling procedures to convert low-level characteristics into high-level ones. This section discusses the process after using autoencoders and CNN models to abstract low-level properties.

2.10. Model Parameters. The training model is used for reducing the reconstruction error of the input volume. The proposed model used an Adam optimizer; the learning rate automatically depends upon the updated history of the model's weight. The minimum patch size is 64. Depending on the aerosol layers, each training image size is trained for a maximum of 50 epochs. Following the loss of authentication data, the 10 consecutive epochs are no longer reduced. The spatial autoencoder activation goal is chosen to be the hyperbolic curve. Despite its regularization capacity, we did not use the rectified linear unit (ReLU) to guarantee the regularity of the encoding and decoding functions because triggered values from ReLU have no upper bound. An autoencoder is an encoder-decoder system that reconstructs the input as the output. We achieved autoencoder by two subsystems: the encoder converts the input image frame into a feature vector for internal representation.

The decoder, on the other hand, uses the internal representation to translate it back to the reconstructed images. Autoencoder provides a reconstruction error. The minimum reconstruction error means a slight difference between the input images frame and the reconstructed image frame.

Table 2: Features extraction from dataset.

Data	Feature	GLCM	Description
Orthophoto	Spectral	Angular Contrast Correlation	$\sum_{i,j=0}^{N-1} P2ij$ $\sum_{i,j=0}^{N-1} Pij(i-j)$ $\sum_{i,j=0}^{N-1} Pij((i-u)-(j-u))$
Orthophoto	Texture	Entropy Homogeneity Mean	$\sum_{i,j=0}^{N-1} P \ln(ij)$ $\sum_{i,j=0}^{N-1} P \frac{\mathrm{j}}{1+(Pij)}$ $\mathrm{q}i \sum_{i,j=0}^{N-1} f(i)Pij(\mathrm{i}) = \mathrm{q}j \sum_{i,j=0}^{N-1} f(j)Pij(\mathrm{j})$
LiDAR	Shape	Area Compactness Density	Area of segments Compactness of polygon Density of holes
LiDAR	LiDAR	DEM DSM nDSM	Digital elevation model Digital surface model Object high (DEM-DSM)

2.11. Sequential Model. The sequential model was employed in Figure 4, which allows us to easily stack sequential network layers from input to output.

2.12. Generative Adversarial Network (GAN). GAN is a generative modeling method based on the CNN method. In machine learning, generative modeling is an unsupervised learning problem. It comprises pitting two neural networks against each other to find and learn regularities or patterns in incoming data. As a result, we used a generative adversarial network (GAN) to solve tasks like image generation from descriptions or features, obtaining high resolution image frames from low-resolution ones, predicting whether abnormal activity is abnormal or not, and retrieving image frames that contain a given pattern.

3. Results and Discussion

The neural complexity addresses the lesser limits of neural resources (neuronal counts) a network needs to do a specific task within a certain tolerance. Lower limits on the information required for the intended input-output function are measured by the complexity of the information (i.e., number of examples). This study suggests a superresolution convolutional neural network (CNN) with a minimal level of complexity (SR). The computational complexity of the suggested strategy is 71.37 percent lower in CPU, TPU, and GPU than the very-deep SR (VDSR) technique, with a peak signal-to-noise ratio loss of 0.49 dB.

Autoencoder, a generative model, was used in the proposed model. Image samples are used to train the autoencoder, and testing images are used to predict the aerosol. An encoder and a decoder make up the autoencoder. For the reconstructed pictures, the trained model's loss function is calculated. At the feature extraction stage, as shown in Figure 5, A total of 21 features, including spectral, form, textural, and LiDAR-based attributes, were retrieved to recognize aerosol layers objects in LiDAR and orthophoto data. Spectral features were used to evaluate the mean pixel values in the orthophoto bands. Shape attributes are the geometric information of meaningful things that is determined from the pixels that make up these objects. To make sure that these features are used effectively, the map must be segmented accurately. Haralick texture characteristics were also used to construct texture features based on the grey-level co-occurrence matrix (GLCM) or the grey-level difference vector. Alternatively, the topography and height of objects were described using LiDAR-based characteristics. The identification and description of aerosol layers are critical elements in the reconstruction of aerosol layers objects. The preceding alluded to a method for distinguishing aerosol layers items among various objects [20]. The last, on the other hand, is concerned with defining the mathematical limit of aerosol layer objects so that their computation and concentration information can be displayed as attributes connected with the objects in a geographic information framework (GIS). From one perspective, orthophoto has a critical spatial objective limit and exhibits solid reflectance around the limits of aerosol layers. In any event, the uncanny similarity of distinct ground objects complicates orthophoto extraction of aerosol layers. However, because of the relatively tiny footprint size of the laser bar and unfavorable backscattering from lighted targets, collecting aerosol layers edges with tallness discontinuities is difficult in LiDAR [20]. The use of orthophoto and LiDAR together can increase the precision of aerosol layer detection and description measurements in this way.

Information combination is the process of using or combining data from multiple sources to frame a new dataset

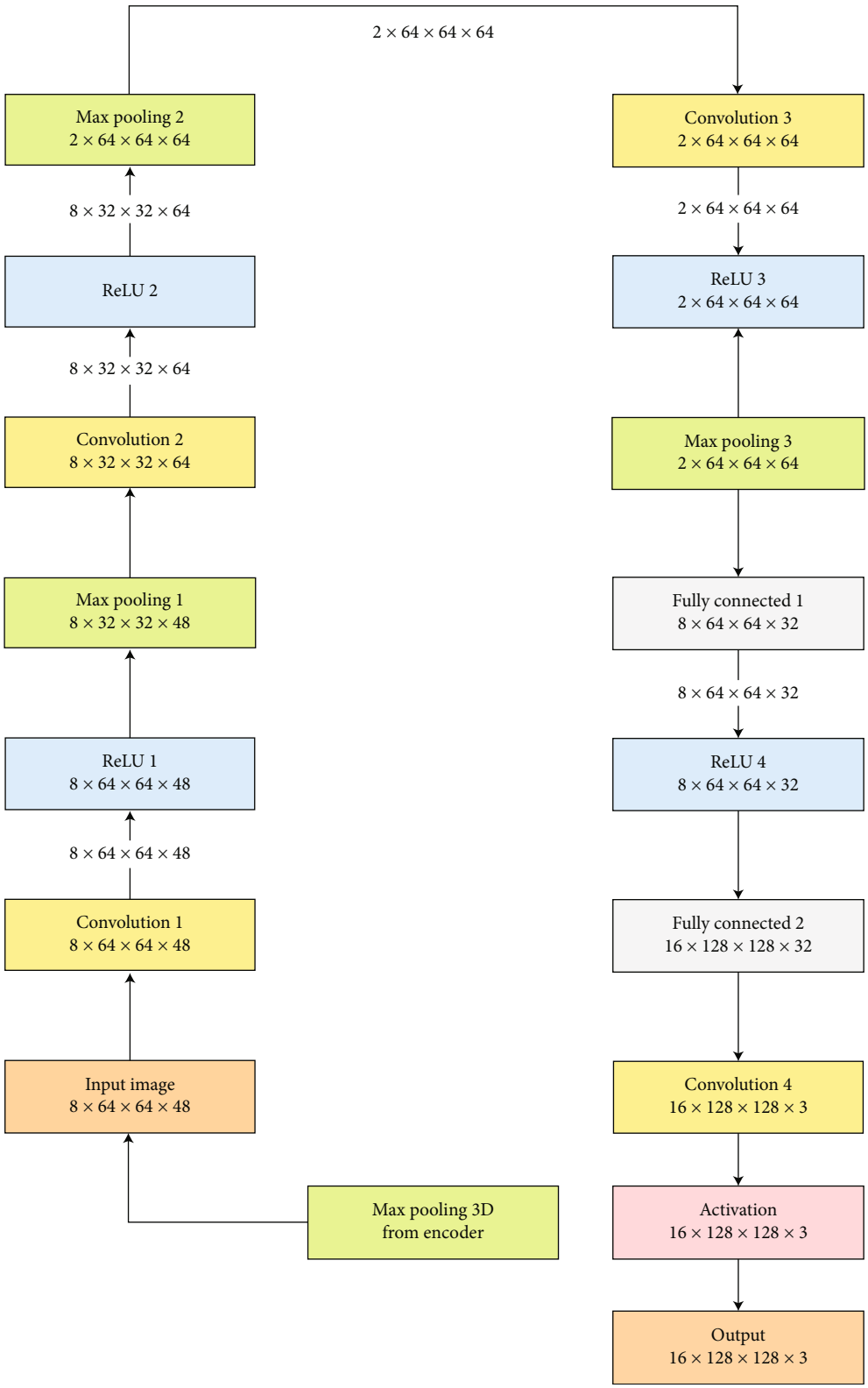

Figure 4: Sequential model.

and achieve a certain aim. [21]. Pixel, highlight, and choice combinations are the three layers of combination that can combine information from numerous sources. Because aerosol layer identification and description using object-based inquiry are more basic and proficient, the current research receives the component level. Low-level highlights for aerosol layer detection are framed using orthophoto highlights (e.g., phantom and textural highlights) and LiDAR

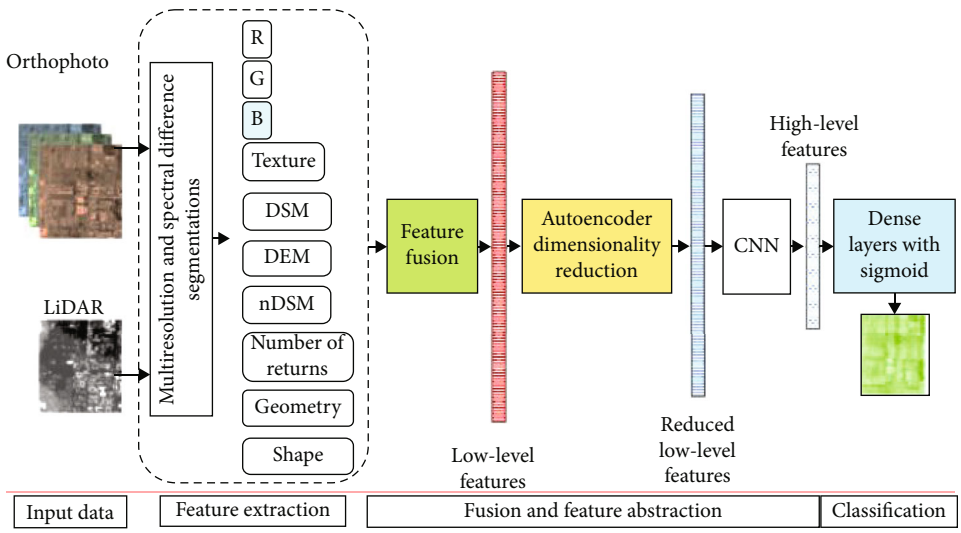

Figure 5: Experimental approach.

highlights (e.g., DSM, DEM, nDSM, and spatial highlights) (Table 1).

Many of the features associated with ghastly, textural, geological, and shape collections can be separated from orthophoto and LiDAR data. Overfitting can occur when several highlights are used, especially when the training tests are minimal. Commotion, extra information, and more computer time are some of the drawbacks of employing a large number of highlights. The current study uses an autoencoder-based technology to minimize space dimensionality and improve low-level highlights by reducing them into fewer highlights (i.e., diminished low-level highlights). The new highlights should be more informative than the old ones, and they should improve the overall system work process for recognizing aerosol layers. A CNN model is also evolved by executing several convolution and pooling actions to choose the right highlights for identifying aerosol layers and to turn lowered low-level highlights into significant level highlights. The autoencoder and CNN models are used to decrease (or abstract) low-level highlights in the next sections.

The model has been properly trained when the reconstruction error is modest. The model was not sufficiently trained if the inaccuracy was significant. Testing photos are used to evaluate the model after it has been trained. All of the layers in the autoencoder with the dense layer are fully connected. The information is passed through the bottleneck layer between the encoder and the decoder. We only use one frame at a time in a simple autoencoder. Figure depicts the autoencoder visual layer structure and properties. Each convolution layer has a 3×3 filter size with 128, 192, and 256 filters. The convolution's filtering processes are combined in the max-pooling layer, which is 3×3. The image volume is normalized using the normalization layers. The activation function is performed using RLU layers. The number of aerosol frames is detected on the softmax layer using the loss function. For training, the loss function is utilized. The sigmoid response value varies between 0.5 and 0.7. Figure 6 shows the structure of the max pooling layer.

Figure 6 shows an autoencoder that uses layers to translate the input image frame into a feature vector for internal representation (batch normalization, ReLU activation function, and Conv3D). The internal representation is used by the decoder. In the third column, it reverts to the original reconstructed picture frames, and in the second column, it expresses the shape in vector form.

3.1. Model Sequential. The sequential model is made by applying a 3D convolutional neural network, varying the number of filters in convolutional layers. It will make it suitable for a basic stack of layers where each layer has accurately one input tensor and one output tensor. It will create its weights the first time it is called on an input image since the shape of the weights depends on the shape of the image frames. Before completing training, a model configures the learning process, which is done via the compile function. It receives three arguments optimizer, loss function, and a list of metrics.

An optimizer should be the string identifier or call to an optimizer function. In the sequential model, the main aim is to minimize the loss function. It is a string identifier to call a loss function, e.g., a loss means squared error.

The output of the fully connected layer CNN is a softmax, and the sigmoid function is used for combining the result of each layer in the sequential model that is shown in Figure 7. For classification, a median filter of size three is applied to the output conclusion to smooth out variations in the classification of anomalies.

Figure 7 above shows the creation of a sequential model by applying a 3D convolutional network, changing the number of filters in convolutional layers. It will make a suitable plan for input to output weights of the shape depend upon the image frame.

3.2. Generative Adversarial Network (GAN). The GAN model has been used for the reconstruction of the image with HD resolution. Here, we use the model.

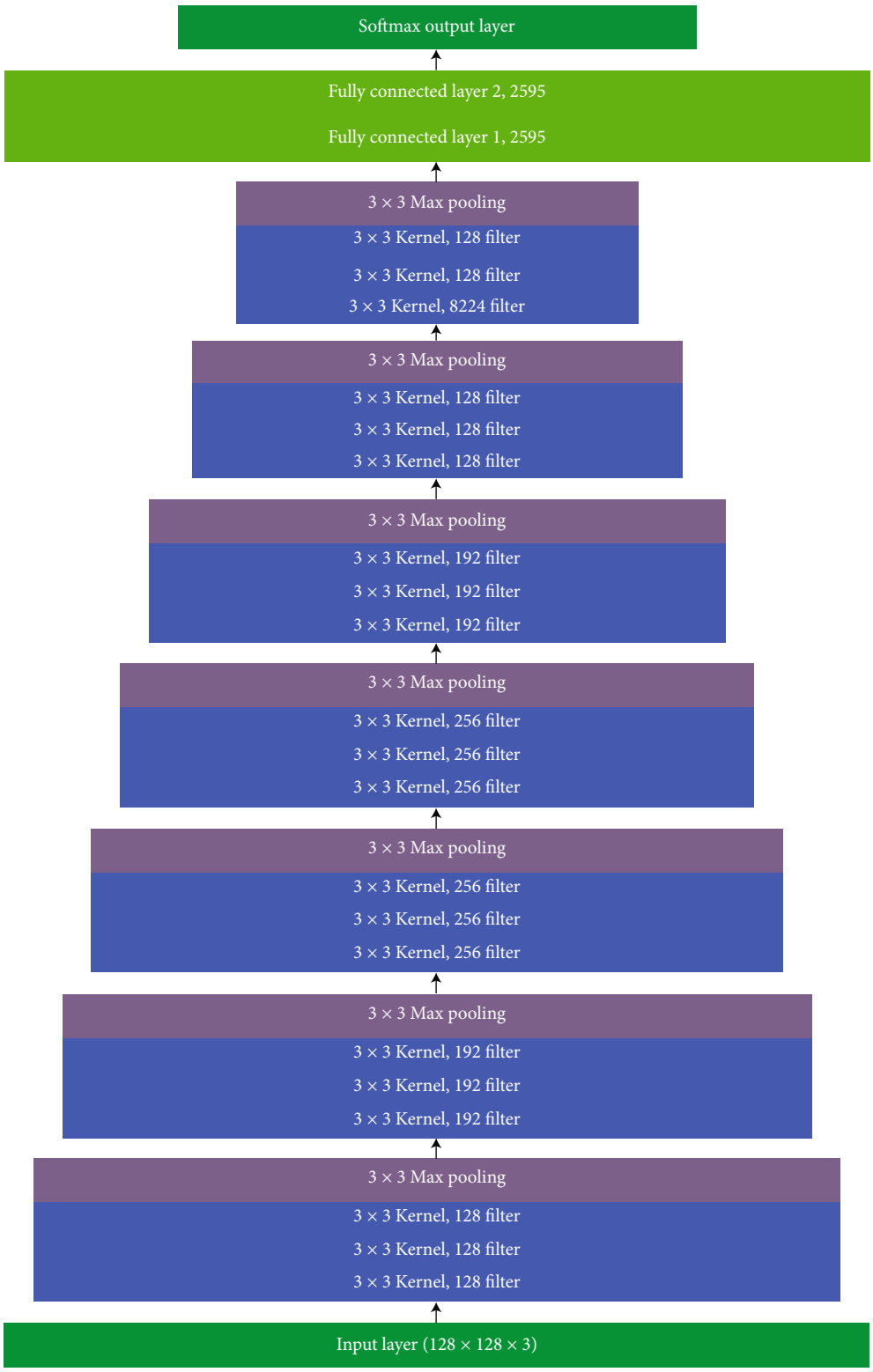

Figure 6: The structure of the max pooling layer.

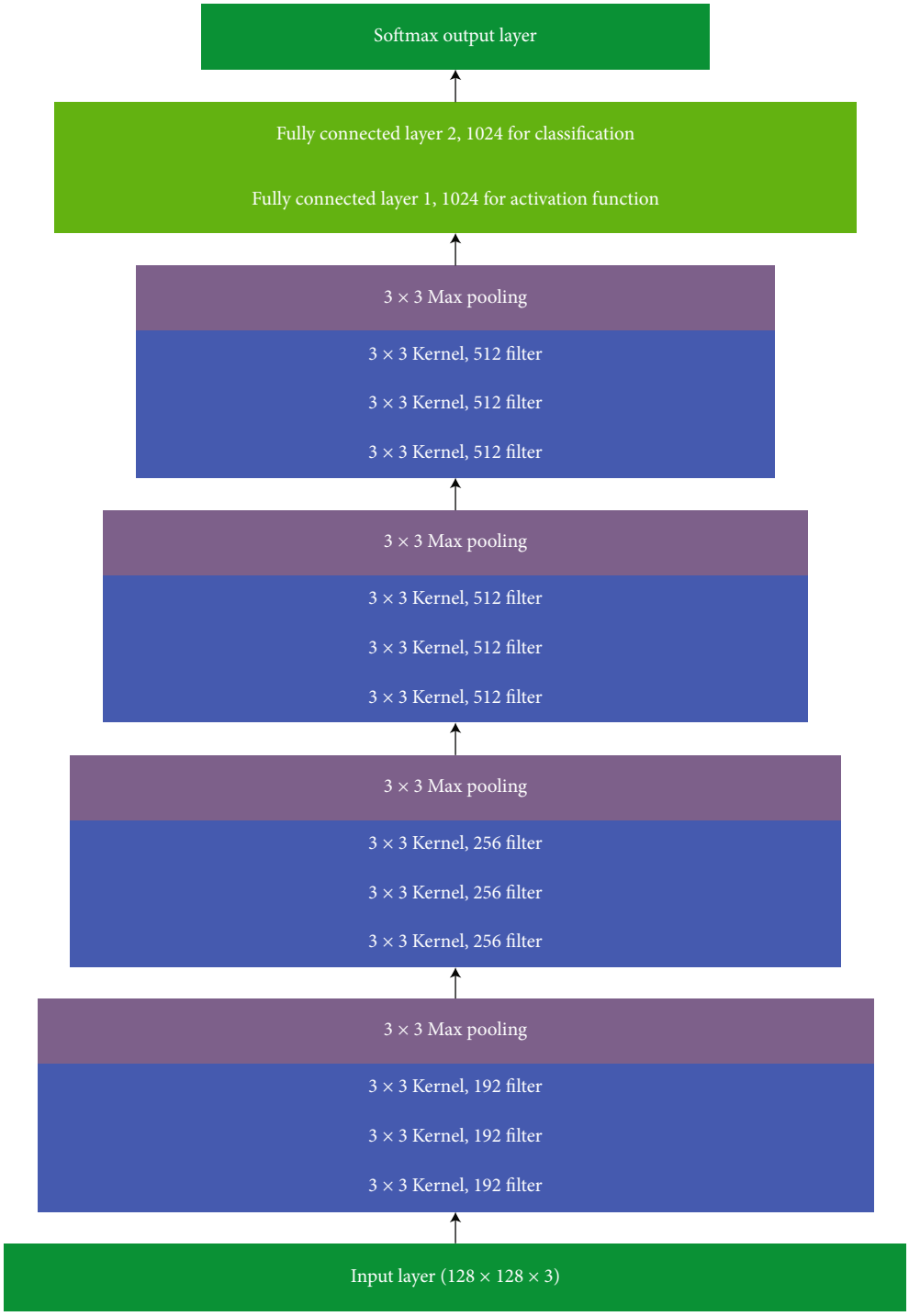

Figure 7: The internal structure of the sequential model.

Following are the parameters on which basis we have to evaluate our work. To validate the suggested technique, performance measures such as accuracy, sensitivity, specificity, and AUC are determined. The following are the performance parameters of the suggested technique:

$$\text{Specificity} = \frac{\text{TN}}{(\text{TN} + \text{FP})},$$

$$\text{Accuracy} = \frac{(\text{TP} + \text{TN})}{(\text{TP} + \text{TN} + \text{FP} + \text{FN})},$$

$$\text{Sensitivity} = \frac{\text{TP}}{(\text{TP} + \text{FN})}$$

$$\text{AUC} = \frac{\text{Sensitivity} + \text{Specificity}}{2},$$

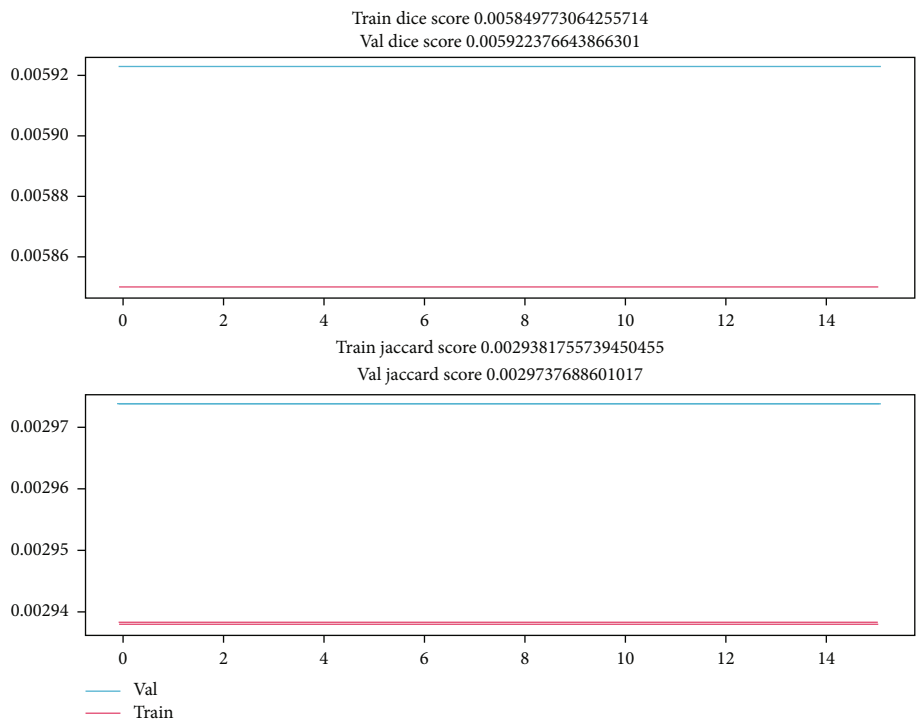

Figure 8: Training of data.

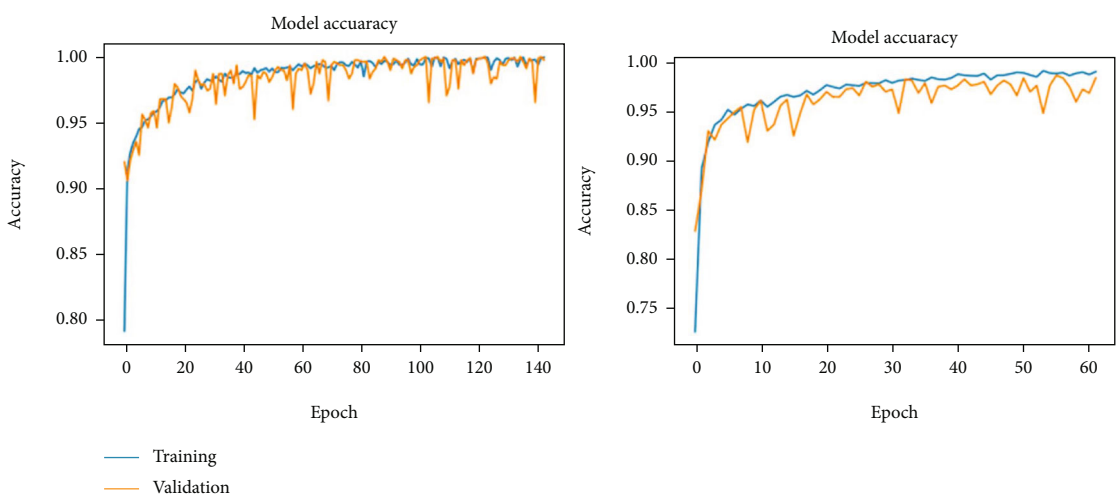

Figure 9: Model accuracy and loss.

$$\text{Recall} = \frac{\text{TP}}{\text{TP} + \text{FN}},$$

$$\text{Precision} = \frac{\text{TP}}{\text{TP} + \text{FP}},$$

$$\text{F1}_{\text{Score}} = \frac{2 * (\text{Recall} * \text{Precision})}{(\text{Recall} + \text{Precision})}. \quad (1)$$

(i) False-negative (FN): the feature detected result is 0, and predictive powers are present

(ii) True-negative (TN): the feature detected result is 0, and predictive power is absent

(iii) False-positive (FP): the feature detected result is 1, and predictive power is absent

(iv) True-positive (TP): the feature detected result is 1, and predictive power is present

3.3. Training. In the first step, we have trained our model on 70% data the training loss 0.00186344. Figure 8 shows training of data.

3.4. Testing. The testing of data on the GAN model has been carried out at 30% of set. Model accuracy to detect aerosols

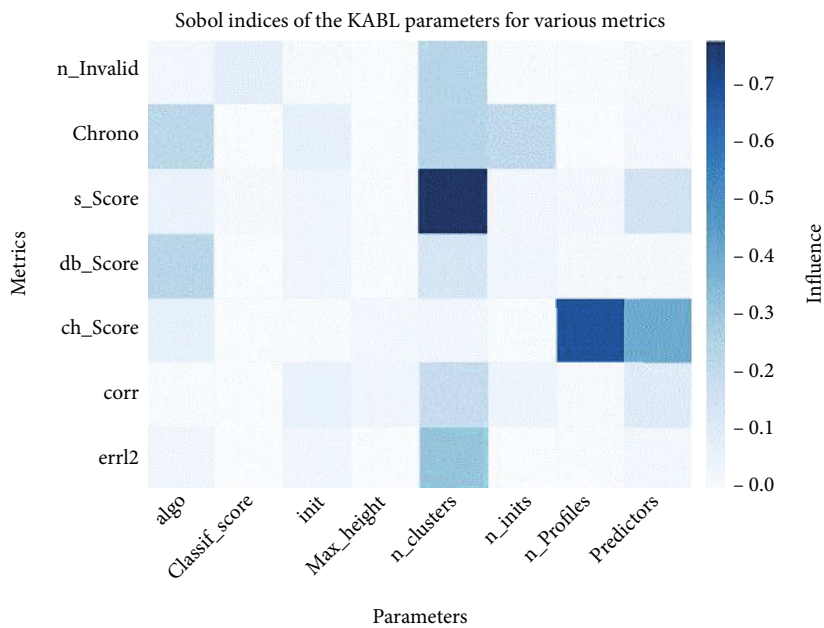

Figure 10: Confusion matrix for classification.

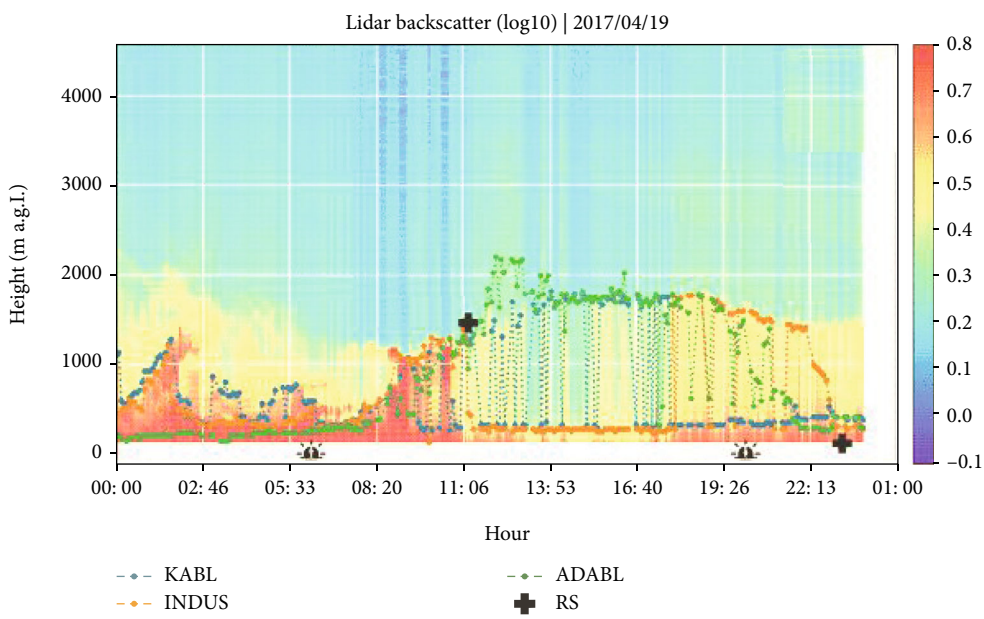

Figure 11: Aerosol detection using the GAN model.

is almost 98% at 140 epochs while at 60 epochs, it is 97%. Figure 9 shows model accuracy and loss.

Figure 10 above shows the training and validation accuracy and loss of the CAE model in classifying the images of aerosols from the datasets. The model has shown 98% accuracy of training and 98.7% accuracy of validation during experiments. Figure 11 shows aerosol detection using the GAN model.

Figure 12 shows aerosol outlier detection using at different time spans. While comparing with the GAN model on the right side at 60 epochs, CAE has shown the accuracy of 98% on training and 99% on testing with the inclusion of the GAN model. Accuracy curves for training and validation have no dropout when combining DSM and RGB (left) and loss of information when using RGB alone (right), both without dropout. Thus, the parameters were examined and hypertuned to maximize detection accuracy. According to the findings of the sensitivity analysis of these parameters, the best 10-fold crossvalidation accuracy for aerosol detection was achieved for the area in which the tests were done. The study concluded that 128 filters delivered an accuracy of 98.76% percent. The poorest results (15.5% accuracy) were seen when using 64 filters. Adam also delivers an accuracy of 81.41%, which is much superior to other optimization

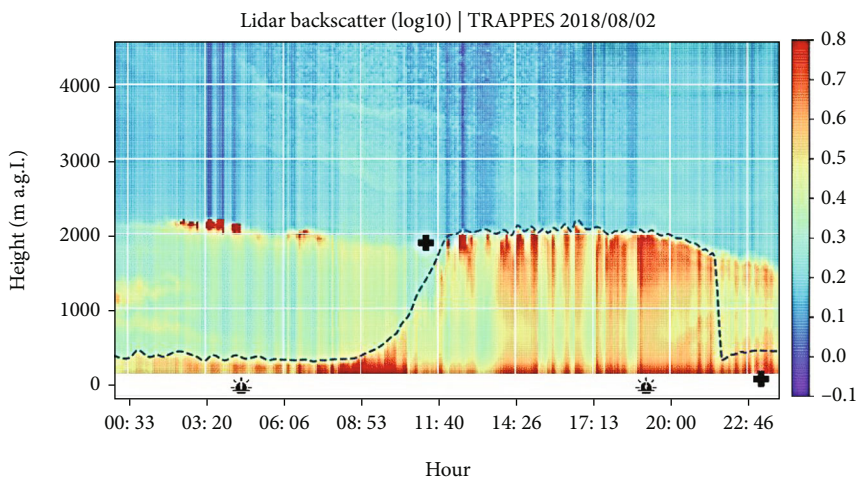

(a)

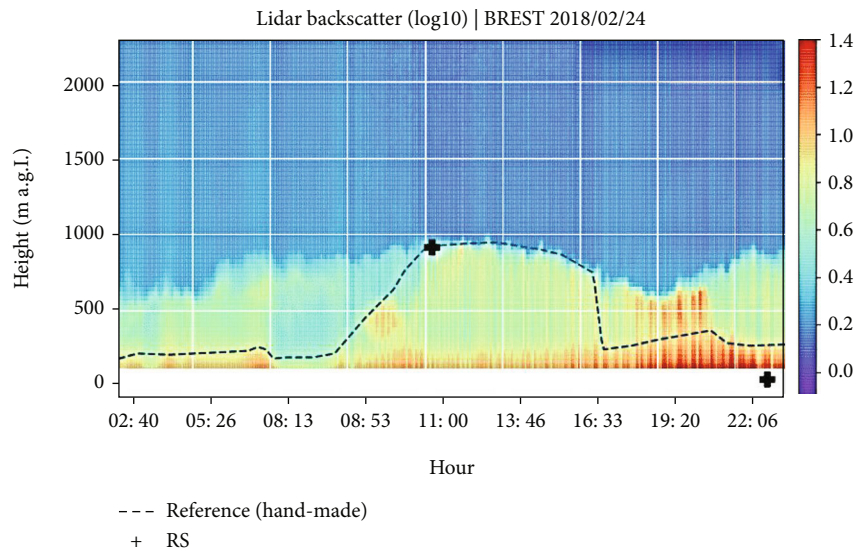

(b)

Figure 12: Aerosol outlier detection using at different time spans.

Table 3: Comparisons of current study with previous studies.

References	Techniques	Accuracy	Outcome
[2]	CNN	89%	Object recognition
[1]	Mark CNN	88%	Waveform recognition
[5]	Mod CNN	88.5%	Biomass land recognition
Our proposed	CAE with GAN	98%	Outlier aerosol recognition
	ADAM	81.41%	
	AdaGrad	23.57%	
	AdaDelta	38.95%	
	SGD	78.41%	
	RMSProp	69.55%	

techniques. Conversely, the dense layer has ignored concealed units with no consequence.

In testing, the most accurate (98.76%) results were produced using 10 or 100 units. The results for the 50- and 3-unit units were slightly less accurate (81.61 percent). The application of a smaller number of units in the fully linked layer is beneficial to the computational performance of the model; hence, it is considered best to utilize 10.

We have also compared our technique with state-of-the-art algorithms, as shown below in Table 3.

4. Conclusions

The researchers employed autoencoders and CNN models to detect aerosols in a LiDAR–orthophoto dataset, resulting in a DL method. The architecture is designed to generate objects using multiresolution and spectral difference segmentations. The identification of 9 distinct features, including spectral, textural, LiDAR, and orthofusion, was completed for the detection of aerosols. Next, they were compressed into 10 features at the feature level, using the autoencoder model. To categorize the items, they employed the high-level features generated from the modified compressed features. Building detection using this design has many advantages, including automated feature selection and removal of redundant characteristics. Convolutional neural networks (CNNs) were utilized to convert compressed information into high-level characteristics that could categorize the outer layer of atmospheric particles. This research describes deep learning approaches that, when applied to Lidar data, allowed for detecting 40% more atmospheric features at a horizontal resolution of 15 km during daytime operations. In comparison to existing deep learning algorithms for edges and complicated near-surface sceneries during the day, a convolutional autoencoder (CAE) trained using LiDAR Dataset standard data products showed the potential for improved aerosol discrimination. However, the dataset including height information (the fused orthomosaic photo and DSM) performed better in most discriminative classifications. This study demonstrated CAE's capacity to accurately categorize lower-resolution UAV-fused LiDAR images in comparison to very-high-resolution aerial shots and also indicated that dataset fusion is promising. The model has shown 98% accuracy of training and 98.7% accuracy of validation during experiments. While comparing with the GAN model on the right side at 60 epochs, CAE has shown the accuracy of 98% on training and 99% on testing with the inclusion of the GAN model. The sensitivity of CNNs with various fusion methods to the training dataset, regularization functions, and optimizers will be the subject of future research.

Data Availability

Dear Sir/Madam, as you are concerned with the availability of my code and practical work, it is confidential to my lab and cannot be shared to anyone until it gets published. And secondly, I will publish my code and lab work according to the instructions of my supervisor: Lab name: supervisor name: Regards Mazhar Hameed.

Conflicts of Interest

On behalf of all authors, the authors declare that there is no conflict of interest.

Acknowledgments

I would like to acknowledge my indebtedness and render my warmest thanks. Thanks are due to my supervisor, Professor Yang Fengbao, who made this work possible. His friendly guidance and expert advice have been invaluable throughout all stages of the work. I would also wish to express my gratitude to Miss Gao Min for her extended discussions and valuable suggestions which have contributed greatly to the improvement of the paper. This work was supported by the National Natural Science Foundation of China (Grant Nos. 61672472 and 61972363), Science Foundation of North University of China, Postgraduate Science and Technology Projects of North University of China (Grant No. 20181530), and Postgraduate Education Innovation Project of Shanxi Province.

References

[1] T. Shinohara, H. Xiu, and M. Matsuoka, "FWNet : semantic segmentation for full-waveform LiDAR data using deep learning," *Sensors*, vol. 20, no. 12, article 3568, 2020.

[2] L. Zhang, Z. Shao, J. Liu, and Q. Cheng, "Deep learning based retrieval of forest aboveground bomass from combined LiDAR and Landsat 8 data," *Remote Sensing*, vol. 11, no. 12, p. 1459, 2019.

[3] J. Rock, M. Toth, P. Meissner, and F. Pernkopf, "CNNs for interference mitigation and denoising in automotive radar using real-world data," in *Machine Learning for Autonomous Driving Workshop at the 33rd Conference on Neural Information Processing Systems (NeurIPS 2019)*, pp. 1–9, Inffeldgasse 16c Graz Austria, 2019.

[4] L. Duan, D. Zhang, F. Xu, and G. Cui, "A novel video encryption method based on faster R-CNN," in *2018 International Conference on Computer Science, Electronics and Communication Engineering (CSECE 2018)*, vol. 80, pp. 100–104, Inffeldgasse 16c Graz Austria, 2018.

[5] G. Melotti and C. Premebida, "Multimodal deep-learning for object recognition combining Camera and LIDAR data," in *2020 IEEE International Conference on Autonomous Robot Systems and Competitions (ICARSC)*, Ponta Delgada, Portugal, 2020.

[6] A. Wahid, A. Stone, K. Chen, B. Ichter, and A. Toshev, "Learning object-conditioned exploration using distributed soft actor critic," 2020, https://arxiv.org/abs/2007.14545.

[7] J. Zhang, "Multi-source remote sensing data fusion: status and trends," *International Journal of Image and Data Fusion*, vol. 1, no. 1, pp. 5–24, 2010.

[8] B. Major, D. Fontijne, A. Ansari et al., "Vehicle detection with automotive radar using deep learning on range-azimuth-doppler tensors," in *Proceedings -2019 International Conference on Computer Vision Workshop*, vol. 2019, pp. 924–932, Seoul, Korea, 2019.

[9] M. Hameed, F. Yang, M. I. Ghafoor et al., "IOTA-based Mobile crowd sensing: detection of fake sensing using logit-boosted machine learning algorithms," *Wireless Communications and Mobile Computing*, vol. 2022, Article ID 6274114, 15 pages, 2022.

[10] C. Sun, J. M. U. Vianney, and D. Cao, "Affordance learning in direct perception for autonomous driving," 2019, https://arxiv.org/abs/1903.08746.

[11] A. Atghaei, S. Ziaeinejad, and M. Rahmati, "Abnormal event detection in urban surveillance videos using GAN and transfer learning," pp. 1–7, 2020, https://arxiv.org/abs/2011.09619.

[12] P. Sedigh, R. Sadeghian, and M. T. Masouleh, "Generating synthetic medical images by using GAN to improve CNN performance in skin cancer classification," in *ICRoM 2019 - 7th international conference on robotics and mechatronics*, pp. 497–502, Tehran, Iran, 2019.

[13] M. Gan and R. Jiang, "ROUND: walking on an object-user heterogeneous network for personalized recommendations," *Expert Systems with Applications*, vol. 42, no. 22, pp. 8791–8804, 2015.

[14] V. Costa, J. Correia, N. Lourenço, and P. Machado, "COE-GAN: evaluating the coevolution efect in generative adversarial networks," in *Proceedings of the genetic and evolutionary computation conference*, pp. 374–382, Prague, Czech Republic, 2019.

[15] M. Aqeel, K. B. Khan, M. A. Azam, M. H. Ghouri, and F. Hassan, *Detection of Abnormal Events in Videos Using Convolutional Autoencoder and Generative Adversarial Network model*, IEEE, 2020.

[16] K. Kaiyrbekov and M. Sezgin, "Deep stroke-based sketched symbol reconstruction and segmentation," *IEEE Computer Graphics and Applications*, vol. 40, no. 1, pp. 112–126, 2020.

[17] S. Li, J. Kawale, and Y. Fu, "Deep collaborative filtering via marginalized denoising auto-encoder," in *Proceedings of the 24th ACM international on conference on information and knowledge management*, Melbourne, Australia, 2015.

[18] P. Kharazmi, J. Zheng, H. Lui, Z. Jane Wang, and T. K. Lee, "A computer-aided decision support system for detection and localization of cutaneous vasculature in dermoscopy images via deep feature learning," *Journal of Medical Systems*, vol. 42, no. 2, p. 33, 2018.

[19] S. Hamdi, S. Bouindour, K. Loukil, H. Snoussi, and M. Abid, "Two-streams fully convolutional networks for abnormal event detection in videos," in *Proceedings of the 12th International Conference on Agents and Artificial Intelligence (ICAART 2020) - Volume 2*, pp. 514–521, Inffeldgasse 16c Graz Austria, 2020.

[20] M. Sewak, S. K. Sahay, and H. Rathore, "Comparison of deep learning and the classical machine learning algorithm for the malware detection," in *Proceedings -2018 IEEE/ACIS 19th International Conference on Software Engineering, Artificial Intelligence, Networking and Parallel/Distributed Computing*, pp. 293–296, Busan, Korea (South), 2018.

[21] Y. Li, Q. Pan, S. Wang, T. Yang, and E. Cambria, "A gnerative model for category text generation," *Information Sciences*, vol. 450, pp. 301–315, 2018.

Hindawi
Journal of Sensors
Volume 2022, Article ID 2580575, 10 pages
https://doi.org/10.1155/2022/2580575

Research Article

Real-Time Simulation Method of Flame Animation Based on the Deep Stripping Algorithm and Texture Mapping

Jingjing Fei

Zhejiang Fashion Institute of Technology, Ningbo 315211, China

Correspondence should be addressed to Jingjing Fei; 2010707021@zjff.edu.cn

Received 17 March 2022; Revised 13 April 2022; Accepted 5 May 2022; Published 1 June 2022

Academic Editor: Yuan Li

With the gradual integration of computers into people's work and life, it is no longer an unattainable goal to use the power of science and technology to simulate various states of matter. In the future, virtual simulation modeling technology will become more and more high-end with the improvement of the needs of the times. However, nowadays, there are many problems in generating real-time image animation. For traditional simulation methods, huge computation and realistic rendering have become technical bottlenecks. This topic takes the generation of flame animation as an example to illustrate. On the basis of the depth stripping algorithm and texture mapping method, not only particle system modeling is introduced, but also a new N-S equation is improved for research. The research results show the following. (1) The model constructed by this method has superior performance and has been greatly improved; after iteration, the error value is as low as 0.03 and the accuracy value is as high as 98%. (2) After 500 simulations, there are 399 kinds of static and 698 kinds of dynamic flames, respectively; it takes 24.01 s and 98.21 s to generate 500 incomplete animations. (3) Compared with the particle system and deep learning model for flame animation recognition and detection, the highest false alarm rate of this model is 4.6%, and the lowest is 0.9%, and the experimental effect is stable; the highest recognition of flame animation can reach 99.2%, and the lowest is 98.5%. (4) Generally speaking, experts and ordinary people have a high evaluation on the effect of this model; except for the first group, the scores are all over 80%, and the highest score can reach 85.936%. Finally, the experimental results are good, which proves the effectiveness and feasibility of this method, which has certain research contribution value. However, for the follow-up work, the algorithm and model have room for further improvement.

1. Introduction

3D animation makes use of 3D space technology and related software modeling and realizes realistic dynamic and static pictures. It can even generate applications of various scenes in real time, which is the blueprint for the future of mankind. However, it is very difficult to simulate irregular natural products such as wind, water, smoke, and fire in life scenes. They cannot be defined and constructed by general mathematical models and physical attributes. Therefore, how to generate the real texture of flowing objects has always been a very challenging subject. For some skilled professionals, the process of realizing a flame is just a basic animation exercise. But the simpler the animation, the more difficult it is to control and realize the details. A flame contains a lot of knowledge in the field of computer graphics, and every dynamic and static performance is followed by unpredictable and ever-changing states. The purpose of this paper is to build the model faster and better in real time, simplify the calculation process, and reduce the redundant calculation. In addition, the paper also strengthens the color matching of flame, increases the detail texture, and ensures the realistic effect. After many investigations and consulting, there are many real simulation data about flame at home and abroad, and the research degree and cognitive degree are different.

This paper refers to the previous research literature and methods and combines new ideas of multiple modes to create innovations, which have certain theoretical and practical significance. The following literature can give some theoretical support and data support to this paper. The specific contents are as follows. The improved double depth stripping algorithm combined with Beer's law can be used to calculate

the attenuated light intensity [1]. Use the network of depth feature fusion and reconstruction to distinguish the microfiber existence characteristics of the convolution neural network [2]. Aiming at the high detection rate, low false detection rate, and real-time requirements of the video flame detection algorithm, experiments are carried out based on target tracking and multifeature fusion [3]. Based on the trust model and dynamic and static features, a probability model of multifeature fusion is established [4]. A particle system is used to control the properties of firework particles at the moment of explosion, and texture mapping is used to draw firework particles [5]. The Gyarmathy model and Perlin noise are introduced for geometric modeling, and complex flames are drawn in virtual scenes, and the real-time and fidelity aspects are studied [6]. Deep stripping and GPU are combined to draw a real-time approximate soft shadow [7]. Based on Level-Set surface deformation, the modified MacCormack and smoke density evolution curve are introduced, and a flame blue core surface evolution model is proposed [8]. The algorithm is completely implemented in GPU, fast modeling and rendering, and the final result is obtained by alpha mixing [9]. Use C4D and AE software particle special effects to make animation in three-dimensional space [10]. For local texture mapping, the region is established by picking points, and the interactive topological structure of data is studied [11]. The computer is used to simulate fluid motion, and mathematical and physical models are constructed based on N-S equations to simulate real-time flame [12]. For the Z-buffer algorithm and ray tracing algorithm, a visibility detection scheme without setting deviation is formulated [13]. TLM modeling in GPU texture mapping operation is based on UML-SystemC [14]. Texture mapping of the 3D model used the ASM algorithm, RBF interpolation function, feature point constraint, and deformation [15].

2. Theoretical Basis

2.1. Flame Animation. A flame [16] is a physical and chemical phenomenon in nature. At the same time, it is an extremely complex and unpredictable state, with hot gasification parts. In essence, a flame is an exothermic reaction, which relies on the high-speed movement of surrounding air molecules in the reaction range to emit light. In the field of vision, it is a fluid phenomenon with random motion changes, so it is difficult to describe it concretely by geometry. At the same time, due to its ever-changing state in time and space, it is difficult to truly simulate the dynamic feeling of flame combustion. Making an excellent flame animation through simulation experiments is a piece of deep knowledge. Therefore, the best way to accurately describe the interaction of various molecules in a mass of gas is to model. The classical modeling materials are sorted out in order to deepen understanding, as shown in Table 1.

In this paper, we mainly pursue the "realism" of flame, which belongs to the visual research purpose. Therefore, we can abandon some normative requirements in physics. The complicated motion of heated gas is abstracted and simplified as a dynamic motion field. By changing the original monotonous motion law in the sports field, the generation of flame will be more flexible and real. Among them, we define the sports field as an n-dimensional vector in the real number field. It has 1 to n function attributes with time t. The vortex field is defined as Y_{vortex}, a five-dimensional vector over a real number field. The specific formula is as follows:

$$Y_{\text{motionfield}} = \{\text{property1}, \text{property2}, \text{property3}, \cdots, \text{property}n\} \quad (n \in N),$$
$$Y_{\text{vortex}} = \{\text{Angle}, \text{Angle Delta}, \text{Pos}, \text{Velocity}, \text{Acc}\}. \tag{1}$$

The rotation angle characteristic value is as follows:

$$\text{Angle}_{j+1} = \text{Angle}_j + \text{AngleDelta} \times \Delta t. \tag{2}$$

Position and speed are as follows:

$$\begin{aligned} \text{Pos}_{j+1} &= \text{Pos}_j + \text{Velocity}_j \times \Delta t, \\ \text{Velocity}_{j+1} &= \text{Velocity}_j + \text{Acc} \times \Delta t. \end{aligned} \tag{3}$$

2.2. Deep Stripping Algorithm. Depth peeling's [21] full name is the deep stripping algorithm. This is a technology that can solve the problem of unordered rendering of opaque objects and realize sorting depth values. Using the shadow mapping proposed by Lance Williams, the depth test is simulated. Through multiple rendering methods, the color of the target will be stripped out layer by layer according to the flow. Then, according to the target requirements, the rendering results are obtained by mixing colors in a certain order.

The specific algorithm flow is as follows. (1) Firstly, render transparent objects, using the depth buffer test function to get color values. Then, copy the depth value into the depth texture. (2) Secondly, turn on the comparison function and filter the colors that can pass the test. This step mainly selects colors with large depth values. Then, the color value and the corresponding depth value of the next layer are obtained. (3) Repeat the second step continuously, separating layer after layer of color until all colors are stripped out. (4) Arrange the hierarchical colors in the order from back to front. Then, gradually render the depth and complexity of transparent objects to get the results.

Generally, API functions in the ARB extension function in OpenGL are used to realize the effect of this algorithm. OpenGL [22] is a software interface on graphics hardware and a state machine, which can write three-dimensional graphics applications. Its operation sequence is similar, and a series of processing stages are called rendering pipelines. In addition, based on the low-level mechanism of the window system, some function libraries can simplify programming.

2.3. Texture Mapping. Texture mapping [23], the Chinese whole process, is a kind of OpenGL hardware, which can save a variety of textures. It has the functions of reducing calculation amount and improving calculation speed. A texture image is attached to the surface of a three-dimensional object to improve the surface color richness. This mapping process can enhance the realism of objects. Sometimes, users can help adjust the surface shape, reflection, shadow, and

Table 1: Research status of establishing the model.

Research proponent	Method or model	General situation of research
Perlin	Empirical model [17]	It can preliminarily simulate natural textures such as marble, clouds, and flames.
Inakage	Digital synthesis algorithm	It can realistically simulate the fuzzy boundary of flame and the smoke effect around the flame.
Imakage	Texture mapping method [18]	A simple model of two-dimensional flame [19] can be constructed.
Philippe Beaudoin	Different equations [20]	Create a three-dimensional flame frame. Simulate the shape of combustion flame, including ambient temperature, oxygen content, and airflow speed.

other information through this method. It can be used with the deep stripping algorithm, illumination calculation, image mixing, and other technologies so as to design a more perfect and beautiful effect. The related function steps are as follows.

2.3.1. Two-Dimensional Mapping. According to the target, different intermediate mapping media are used to generate different textures. Then, paste the texture on a simple three-dimensional object. If S represents a mapping, there are

$$S : (u, v) \longrightarrow \left(x', y', z'\right). \tag{4}$$

2.3.2. Three-Dimensional Mapping. After the first step, the texture on the three-dimensional object that has been mapped once is mapped to the final target object surface. If O stands for mapping, there are

$$O : \left(x', y', z'\right) \longrightarrow (x, y, z). \tag{5}$$

In addition, there are some pieces of knowledge or operations related to texture mapping, which are supplemented here.

Perspective correct interpolation is as follows:

$$\begin{bmatrix} u \\ v \\ 1 \\ x_r \\ y_r \\ z_r \\ w_r \end{bmatrix} \xrightarrow{\text{homogenize}} \begin{bmatrix} \dfrac{u}{w_r} \\ \dfrac{v}{w_r} \\ \dfrac{1}{w_r} \\ \dfrac{x_r}{w_r} = x_s \\ \dfrac{y_r}{w_r} = y_s \\ \dfrac{z_r}{w_r} = z_s \\ 1 \end{bmatrix}. \tag{6}$$

The pixel footprint [24] is as follows:

$$\psi = \phi \circ \pi^{-1}. \tag{7}$$

The higher-order Taylor expansion is as follows:

$$\psi(x) = \psi(x_0) + J(x - x_0). \tag{8}$$

The three-dimensional stripe texture is as follows:

$$\begin{gathered} \text{RGB stripe}(\text{point } p, \text{real } w), \\ t = \frac{(1 + \sin(\pi p x / w))}{2}, \\ \text{return } (1 - t)c_0 + tc_1. \end{gathered} \tag{9}$$

2.4. Mathematical Physics Method. In this paper, the N-S (Navier-Stokes) equation is introduced [25]. This method is approved at home and abroad and can completely describe fluid phenomena. Its kinetic energy conservation equation is as follows:

$$\frac{\partial u}{\partial t} = (u\nabla)u - \frac{1}{\rho} + \nu\nabla^2 u + F. \tag{10}$$

The mass conservation equation is as follows:

$$\nabla u = 0, \tag{11}$$

where u represents the velocity field; ρ represents the density of the fluid; F refers to the external force; t denotes time; ν can explain the kinematic viscosity coefficient; $(u\nabla)u$ means the advection term.

The whole process steps are as follows:

$$u_0(x) \xrightarrow{\text{advact}} u_1(x) \xrightarrow{\text{diffuse}} u_2(x) \xrightarrow{\text{force}} u_3(x) \xrightarrow{\text{project}} u_4(x), \tag{12}$$

$$u_1(x) = u_0(x - \delta t u_0(x)), \tag{13}$$

$$u_2(x) = u_1(x) - \delta t \nu \nabla^2 u_1(x), \tag{14}$$

$$u_3(x) = u_2(x) + \delta t F(x), \tag{15}$$

$$\nabla^2 p(x) = \nabla u_3(x), \tag{16}$$

$$u_4(x) = u_3(x) - \nabla p(x). \tag{17}$$

Formulas (13)–(17) are the flow steps after formula (12) is decomposed. Formula (13) is the calculation of the advection term, which is operated by the semi-Lagrange formula. Formula (14) is related to the diffusion term and can be obtained by the implicit method. Formula (15) is the answer to add the external force term. Formulas (16) and (17)

represent the velocity with a divergence of 0, which is mainly obtained by the projection of the H-H theorem.

3. Research on Simulating Real-Time Flame Animation

3.1. Introducing Particle System. The simulation method of the particle system is simple and easy to realize. However, it cannot accurately describe the process of flame combustion. But it takes a large number of tiny particles as its basic elements, which can effectively represent those irregular fuzzy substances. In this experiment, each particle can have many properties, which are consistent with the various properties of the flame itself. And the particle system contains two forms: dynamic and static, and each particle experiences a different life cycle. It coincides with some concepts abstracted by us—the motion of the dynamic sports field. As for some weaknesses of the particle system, we integrate the method of the dynamic motion field to make up for the design of the flame animation model. The initialization improvement of the particle system is described as follows.

Determine the initial position of new particles with the following:

$$\begin{aligned} \mathrm{Pos}X &= \frac{1}{\sqrt{2\pi R}} \exp\left\{-\frac{(x_i - x_0)^2}{2R^2}\right\}, \\ \mathrm{Pos}Z &= \frac{1}{\sqrt{2\pi R}} \exp\left\{-\frac{(z_i - z_0)^2}{2R^2}\right\}. \end{aligned} \tag{18}$$

The location of new flame particles is as follows:

$$\begin{aligned} \mathrm{Pos}X &= \sum_{i=0}^{n} R\mathrm{and}() \times \mathrm{adjustnum}, \\ \mathrm{Pos}Z &= \sum_{i=0}^{n} R\mathrm{and}() \times \mathrm{adjustnum}. \end{aligned} \tag{19}$$

3.2. Improvement of the Model Method

3.2.1. Double-Layer Depth Stripping Algorithm. In this experiment, although the traditional depth stripping algorithm can ensure the correct color results, the rendering of N times leads to the inefficiency of this method, which reduces the final animation effect. Therefore, we need to improve the original algorithm. On the basis of the original, considering the hardware requirements and financial constraints, this paper gives priority to the proposed double-layer deep stripping algorithm. The new algorithm can increase the running speed by nearly two times. This method uses new technology, is easy to implement, and can save the maximum or minimum depth value. At the same time, the new algorithm can store multiple color values. Thus, the target of the first layer and the last two layers can be stripped out by rendering again. It ensures the correctness of the original algorithm, improves the performance of the algorithm to the maximum extent under the consideration of the existing resource constraints, and can complete the complete real-time rendering task in complex scenes.

3.2.2. Modified N-S Equation. After the introduction of the particle system, the mathematical and physical methods in this paper need to be modified. That is to say, the advection term of the N-S equation is modified to meet the needs of experiments. This is because the introduction of the particle system affects the key to flame formation in the system. If it is not changed and corrected in time, it will directly destroy the formation of flame animation. When simulating flame, the external shape of the flame is constructed by the generation and disappearance of particles. At this time, the advection item needs to add parameters:

$$u_1(x) = \alpha u_0(x - \delta u_0(x)). \tag{20}$$

It should be noted that the value range of α is $[0, 1]$. In this way, the shape of the whole part is controlled by the particle system. For the detailed natural state of the fluid, it is debugged by the improved N-S equation.

3.3. Analog Implementation. We use a flow chart to illustrate the formation and implementation of the whole flame animation, as shown in Figure 1.

This paper uses a variety of methods to simulate animation effects. Firstly, the concept of the dynamic motion field is put forward, and some shortcomings are compensated by combining the particle system. For GPU objects, OpenGL tools are used to accelerate the implementation of Navier-Stokes equations. It is worth noting that the N-S equation here has been improved on the advection term based on the characteristics of the particle system. At this time, the motion of particles can be completely controlled. Use the double-layer depth stripping algorithm to render real color, and then add the texture mapping method to enhance the realism of animation and improve the calculation speed.

4. Experimental Analysis

4.1. Experimental Environment. In this section, we show some of the main experimental equipment, as shown in Table 2.

4.2. Flame Effect Display. Based on the particle polygon patch, the running speed of the system can be accelerated without too many particles. We designed five kinds of flame particle textures. It is also necessary to map textures to enhance the realism of details in order to achieve the most ideal flame dynamic effect, as shown in Figure 2.

There are many modes in the formal simulation of flame effects, and we intercept some simulation states to show them. We can see that there are clearly visible flames and fireworks, as well as simulations of the surrounding tiny particles or smoke patterns, and the details are clearer than those in the traditional particle system animation. It can also simulate the random form of fire being blown when it is blown by the wind, as shown in Figure 3.

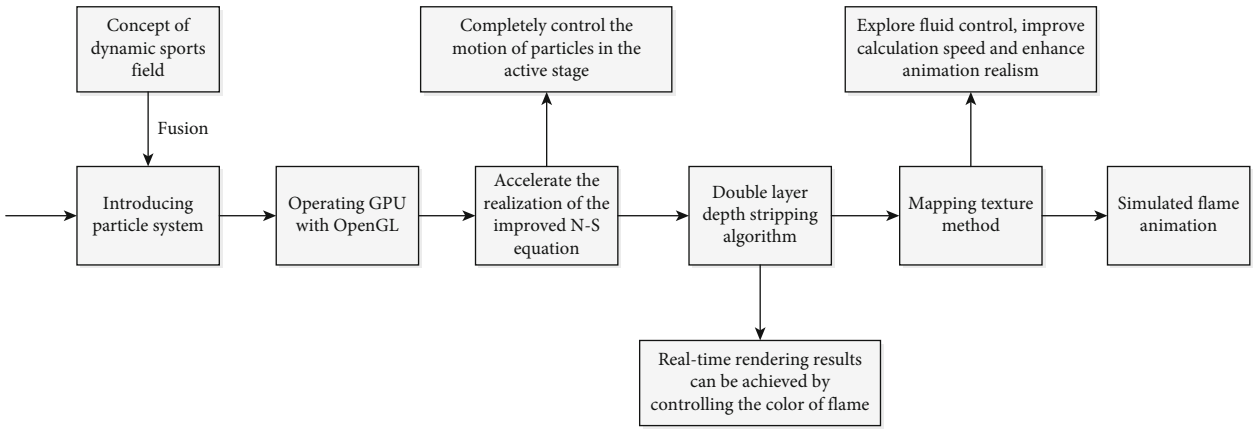

Figure 1: The flow of simulating flame.

Table 2: Hardware and software environment settings of the experiment.

Environment name	Configuration content of the environment
Processor	Intel i5-7200U
Memory	6 GB
Experimental operating system	Windows 10
CPU	3.0 GHz
GPU	NVIDIA GeForce 7900
Development tools	Microsoft Visual Studio.NET 2005 OpenGL2.0

Figure 2: Texture effect display.

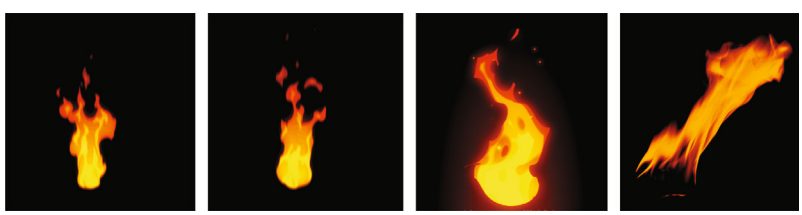

Figure 3: Simulated flame animation effect.

4.3. Performance Test. In order to verify whether the final performance of the model is superior to the traditional algorithm model after the application of this method, we test the error and accuracy of the model. Note that the model needs to be pretested to check the error. If the loss function is too large and does not reach the expected target value, the model generation is unstable, and further modification of the model is needed. As for the accuracy test, the accuracy of the algorithm is mainly judged when the model error is stable and the formal test is carried out. Both the pretest stage and the formal test stage are iterated 60,000 times, and the test results every 5000 times are recorded and evaluated after quantification, as shown in Figures 4 and 5.

In the pretest stage, we set the error target value to be less than 0.05. If the test results do not meet this requirement, then this experiment is invalid, and the model and algorithm need to be modified again. From the figure, we can find that after 5000 iterations, both methods can converge rapidly to varying degrees. At this time, the traditional method can only converge from 0.85 to 0.134, and the fluctuation value

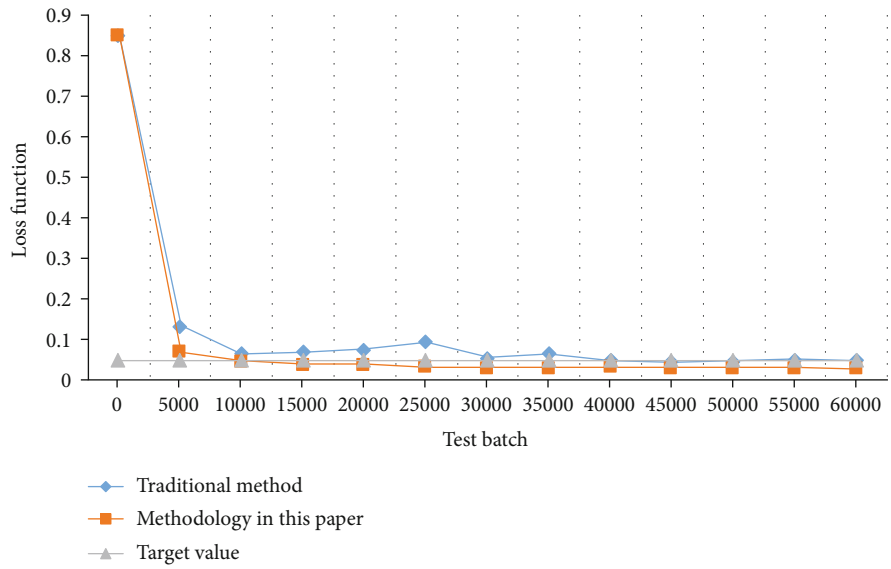

Figure 4: Pretest error analysis.

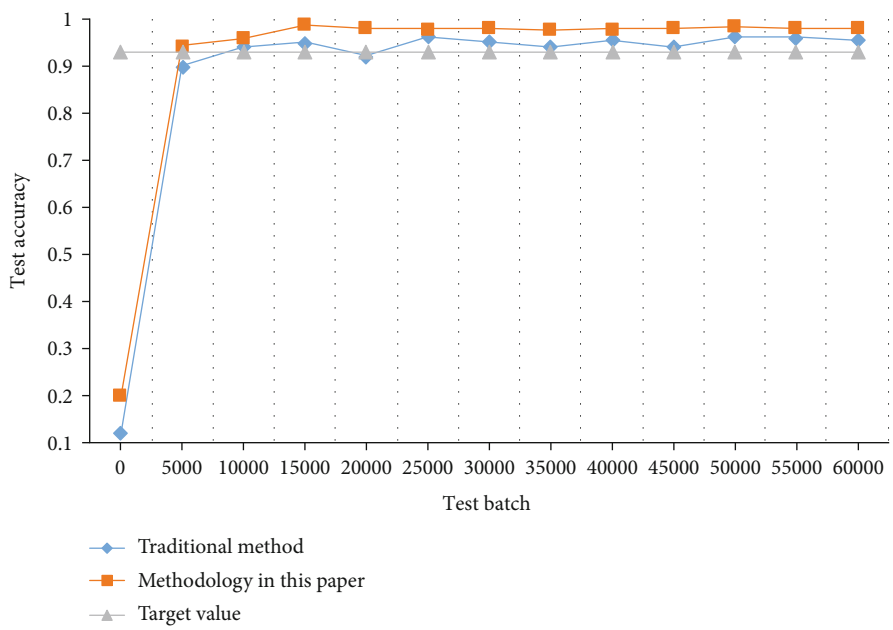

Figure 5: Test accuracy analysis.

of subsequent iterations is large, and it is not stable to the target value of about 0.05 until 40,000 iterations. The method in this paper can quickly converge to a smaller size and directly reduce it to 0.07. Then, after 30,000 iterations, the error value can be stabilized at about 0.03. Not only the target value is reached, but also the final error value is smaller, and the effect is obvious.

In the formal test phase, we set the final accuracy target value as 0.93. That is to say, the accuracy of the model should reach more than 93% before it is qualified. For the traditional method, after 10,000 iterations, the model accuracy is above 0.93, but in 20,000 tests, the test accuracy is only 0.92. The values of subsequent iterations are also unstable, and the overall curve is in a state of twists and turns, and the average accuracy can reach 95%. For this method, we can find that after 5000 iterations, the accuracy value rapidly increased to 0.943, and the subsequent test curve gradually increased and then quickly tended to be flat. Finally, after 15,000 iterations, the ultra-high-precision value of 0.98 can be basically maintained, exceeding the target value.

4.4. Flame Modal Test. The flame animation generated by us will generate different modes due to various factors. After 500 tests, count the clear flame patterns that can be captured by ultraclear lens under static and dynamic conditions. In addition, the generation time of incomplete animation (unified as the state when the flame integrity is one-fifth) and complete animation should be counted. We can find that

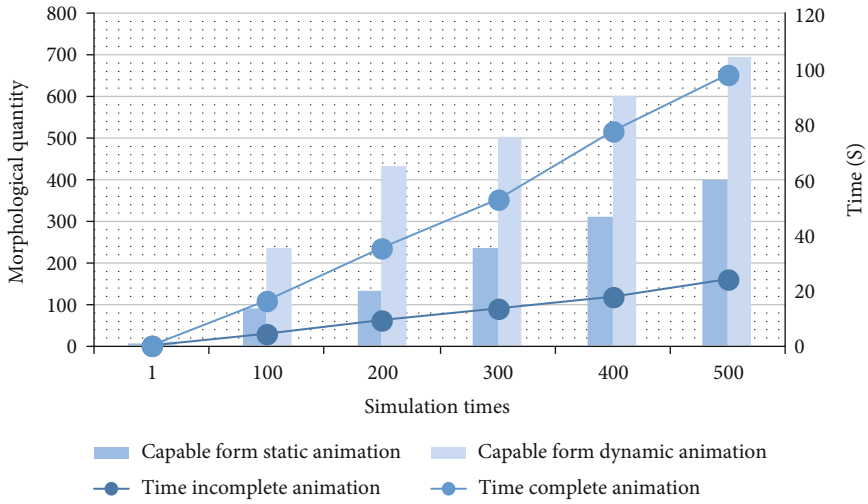

Figure 6: Capture of flame shape.

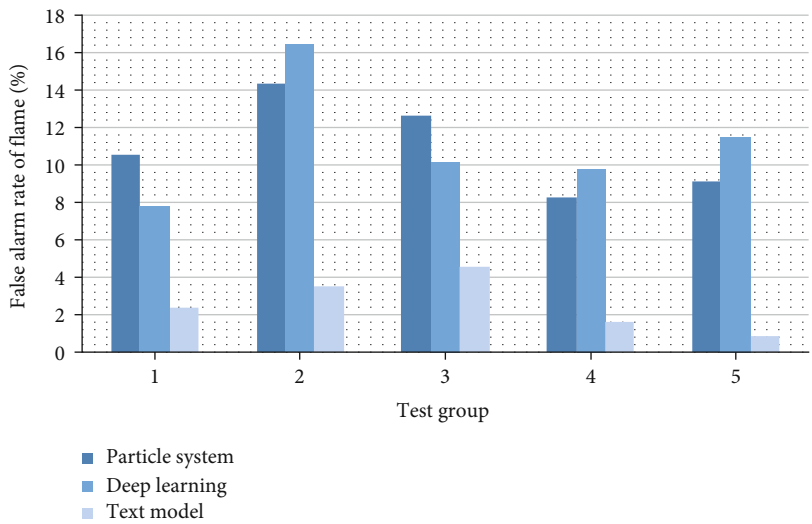

Figure 7: Nonflame identification detection.

with the increase in test times, the flame can capture more forms. The static state can capture up to 399 forms; the dynamic state can capture up to 698 different forms. In the initial state, the first test shows that the generation time of incomplete animation is only 0.05 s, and that of complete animation is 0.18 s, so the animation generation speed is very fast. After 500 simulations, it takes 24.01 s for incomplete animation and 98.21 s for complete animation. This result takes less time than originally expected, indicating that there is a faster generation speed during the test than the initial test, as shown in Figure 6.

4.5. Detection Recognition Rate Effect. After the production of flame animation, we need to use professional tools and software to identify and detect flame animation. A total of 5 test groups were set up, and each group carried out 20 recognition tests on different flame animations, with a total of 100 recognition tests. In order to better highlight the recognition effect of this method, we add the model recognition effect comparison between the unimproved particle system method and the deep learning method, as shown in Figures 7 and 8.

Before the formal test, we pretest the nonflame animation to test the false-positive rate of the three methods. Also, set up 5 sets of tests. From Figure 7, it can be found that the particle system method has the highest false alarm rate in test group 1 and test group 3. Among test groups 2, 4, and 5, the false alarm rate of the deep learning method is the highest, and the highest false alarm degree can reach 16.5%. However, the false-positive rate of this model is the lowest among the five test groups, the highest false-positive rate is only 4.6%, and the lowest is 0.9%. The effect is stable, and the interference degree is the least.

From the formal test in Figure 8, we can find that the recognition rate of flame in the animated video in this model is the highest among the five groups of data, with the highest recognition rate reaching 99.2% and the lowest recognition rate reaching 98.5%. The highest recognition rate of the

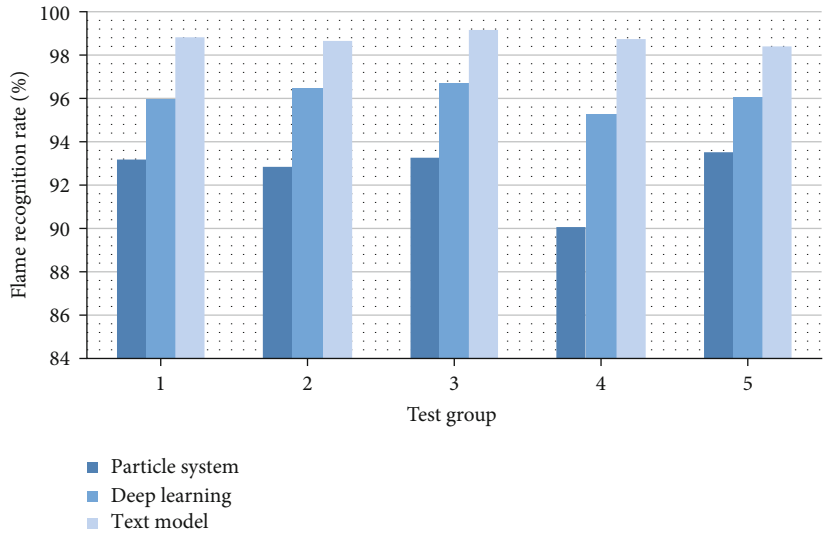

Figure 8: Flame animation recognition and detection.

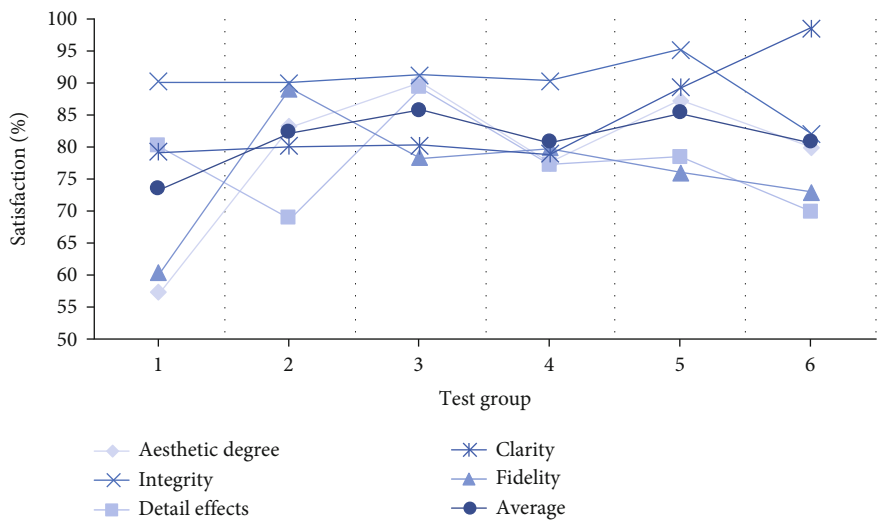

Figure 9: Satisfaction degree of effect.

particle system is 93.6%. The highest recognition rate of the deep learning model is 96.8%, which is slightly higher than that of the particle system. This proves that the flame animation produced in this experimental test is excellent and the effect is excellent.

4.6. Satisfaction Test. Making animation needs to have a certain degree of appreciation and beauty. Therefore, the flame animation completed in our experiment is evaluated from five aspects: beauty, integrity, fidelity, clarity, and detail. Five experts and 25 volunteers were invited to score six groups of flame animations based on this model. Statistical animation effect satisfaction is shown in Figure 9.

We can find that the animation integrity of the other five groups is higher than 90%, except for the integrity of the sixth group, which is 82.2%. The group with the highest aesthetic and detailed effects is the third group, which is 90.23% and 89.34%, respectively. At the same time, the third group is also the group with the highest average evaluation, reaching 85.936%. The second group has the best realistic effect, which can reach 89.23%. Group 6 is the group with the highest clarity, but the overall score is not high. The worst animation effect is the first group, with an overall score of only 73.526%.

5. Conclusion

This paper is located in a three-dimensional space angle to generate computer graphics, using CG technology to simulate virtual reality. This is an applied subject with wide application and rapid development. It intersects with many research fields and has a bright future. In this article, we take flame animation as a demonstration research example, organically combined with a variety of technical methods. In this paper, the animation model and algorithm are analyzed and tested, and the various forms of fireworks are finally captured. In addition, the dynamic and static flame

animation simulation pictures are intercepted to verify the application value of the experiment. The specific research results show that based on the deep stripping algorithm and the function of texture mapping, the flame data is visualized, and the professional simulation satisfaction evaluation is carried out. Use professional tools and software to identify and detect flame animation so as to confirm the discrimination degree of flame. It overcomes the limitation of computer performance and calculates and optimizes the error and accuracy. Improve the mathematical and physical equations to reduce the resistance that affects the real-time performance because of the complexity of calculation. The final experimental effect is close to that in nature, and the details are close to reality. Whether in the fields of games, advertisements, or special effects, it is very meaningful to study the construction of irregular real-time animation.

Although this paper simulates flame animation from a new angle and obtains ideal realistic flame effects of various forms, however, more attention should be paid to the optimization of future work. For example, OpenGL rendering efficiency is not excellent enough, and there is room for improvement in the limitation of specific hardware requirements. The generation speed of animation needs to be finely controlled. Also, the delay performance of animation may lead to poor audience perception, which needs further optimization. Improve the interface and the research on the calling effect when the parameters meet all conditions and the lack of consideration of some scenes, such as the simulation when the flame is blocked by obstructions and the firepower is weak. Texture mapping may be distorted. The above description of the shortcomings of this paper will be the focus of future work.

Data Availability

The experimental data used to support the findings of this study are available from the corresponding author upon request.

Conflicts of Interest

The authors declared that they have no conflicts of interest regarding this work.

References

[1] C. Rui, "Real-time transmission rendering of translucent objects based on deep peeling," *Modern Computer*, vol. 9, p. 5, 2021.

[2] L. Lulu, C. Shuyue, and W. Liping, "Microfiber recognition algorithm based on deep feature fusion and reconstruction," *Modern Electronic Technology*, vol. 45, no. 1, p. 6, 2022.

[3] Z. Xuemin, C. Xiaodong, and L. Yumin, "Flame detection algorithm based on target tracking and multi-feature fusion," *Television Technology*, vol. 37, no. 15, pp. 205–210, 2013.

[4] Z. Jinhua, Z. Jian, and D. Haifeng, "A flame recognition algorithm based on video multi-feature fusion," *Journal of Xi'an Jiaotong University*, vol. 40, no. 7, p. 4, 2006.

[5] H. Ang and W. Jiwen, "Fireworks animation simulation with controllable trajectory based on particle system," *Computer Technology and Development*, vol. 22, no. 7, p. 3, 2022.

[6] W. Biyun, K. Yanghong, and L. Hui, "3D dynamic flame simulation based on particle system," *Journal of Wuhan Institute of Technology*, vol. 40, no. 1, p. 6, 2018.

[7] L. Sun Mingyan, L. X. Weiwei, and W. Enhua, "Approximate soft shadow algorithm combining deep stripping with GPU," *Chinese Journal of Image and Graphics*, vol. 15, no. 9, pp. 1391–1397, 2010.

[8] H. Yi, W. Zhaoqi, and Z. Dengming, "Research on flame animation generation method based on Level-Set," *Computer Research and Development*, vol. 47, no. 11, pp. 1849–1856, 2010.

[9] Y. Wang Peng and C. H. Mengting, "A new method for rapid simulation of flame animation," *Computer Age*, vol. 9, no. 2, pp. 23-24, 2012.

[10] Z. Tingting and W. Wenbin, "Shengshi Birthday-C4D and AE are matched to realize particle special effects animation in three-dimensional space," *Film and Television Production*, vol. 11, no. 1, pp. 51–61, 2021.

[11] W. Mengwei and M. Xiuli, "Interactive texture mapping based on intermediary," *Electronic Measurement Technology*, vol. 43, no. 12, p. 6, 2020.

[12] W. Jun and W. Jiwen, "Real-time flame simulation based on N-S equation and texture mapping," *Computer and Modernization*, vol. 6, no. 12, p. 4, 2013.

[13] H. Xiangxiang, Z. Quansheng, and J. Wanshou, "Rapid visibility detection without setting deviation in multi-view texture mapping," *Journal of Surveying and Mapping*, vol. 49, no. 1, p. 16, 2020.

[14] W. Meirong, T. Ze, and W. Xiaocheng, "Research on texture mapping modeling method based on UML-SystemC," *Aviation Computing Technology*, vol. 50, no. 6, p. 5, 2020.

[15] L. Heng, L. Zhong, and Y. Ce, "Texture mapping of 3D face model based on feature constraint and deformation," *Industrial Control Computer*, vol. 1, no. 2, p. 5, 2022.

[16] W. Jidong and P. Mingyong, "Orientation optimization algorithm of 3D printing model based on deep stripping," *Journal of Computer Aided Design and Graphics*, vol. 30, no. 9, p. 7, 2018.

[17] D. Dingsheng, "A real-time flame simulation algorithm based on GPU," *Journal of Jilin Normal University: Natural Science Edition*, vol. 40, no. 2, p. 5, 2019.

[18] G. Bic, Z. Guohua, and N. Junyong, "Early fire detection algorithm based on irregular patterns of flames and hierarchical Bayesian networks," *Journal of Fire Safety*, vol. 45, no. 4, pp. 262–270, 2010.

[19] Z. Wenhui, S. Kwok, and L. Zian, "Improved direct 3D flame simulation algorithm based on particle system," *Journal of Guilin University of Electronic Technology*, vol. 34, no. 1, p. 5, 2022.

[20] Z. Juan, "Texture mapping flame simulation technology under the background of particle system," *Electronic Technology & Software Engineering*, vol. 16, pp. 69-70, 2022.

[21] P. Chuanlai, "Research on laser marking technology of curved surface parts based on two-step texture mapping," *Journal of Datong University: Natural Science Edition*, vol. 37, no. 4, p. 3, 2021.

[22] C. Jiaqing, Z. Bing, and S. Yinglei, "Flame recognition based on RGB statistical color model," *Journal of Jiangsu University of*

Science and Technology: Natural Science Edition, vol. 31, no. 2, p. 7, 2017.

[23] W. Huaibing, X. Xin, and C. Yaojie, "Three-dimensional simulation of ship traveling waves based on particle system," *Computer Technology and Development*, vol. 31, no. 8, p. 5, 2021.

[24] L. Ying, L. Qian, L. Daxiang, and Y. Wenzong, "Texture mapping algorithm of cultural relics based on PTM model," *Computer Engineering and Application*, vol. 56, no. 12, p. 6, 2020.

[25] Y. Luqing, "Image metonymy and metaphor of emotional representation in animated films–taking the image of Little Nezha in Ne Zha as an example," *Journal of Wuyi University*, vol. 40, no. 2, p. 6, 2021.

Hindawi
Journal of Sensors
Volume 2022, Article ID 8613485, 8 pages
https://doi.org/10.1155/2022/8613485

Research Article

Innovation and Discrete Dynamic Modeling of College Music Teaching Model Based on Multiple Intelligences Theory

Chen Yi

Music College of Xinjiang Normal University, Urumqi, 830002, China

Correspondence should be addressed to Chen Yi; 107621998010020@xjnu.edu.cn

Received 27 February 2022; Accepted 25 April 2022; Published 24 May 2022

Academic Editor: Yuan Li

The development of music teaching mode in colleges and universities needs to take music as the main body and carrier to spread and inherit the music theory system. With the continuous innovation and development of science and technology, the teaching mode and teaching system have also ushered in new changes. How to let students understand the process of music teaching and better appreciate the charm of music is the main problem faced by educators. Faced with the above situation, starting from the theory of multiple intelligences, this paper studies the innovation and discrete dynamic modeling of music teaching mode in colleges and universities. Firstly, this paper discusses the application effect of this method in music teaching based on the theory of multiple intelligences. This paper investigates the actual development of multiple intelligences theory in college music teaching. Combined with the characteristics of multiple intelligences theory, modeling and analysis of students' interest changes in the intelligent music education model represented by the space vector model are carried out. Finally, this paper studies the discrete dynamic modeling of students' learning effect after the optimization and innovation of music teaching mode in colleges and universities under the theory of multiple intelligences. The results show that in the innovation of music teaching mode, personalized learning services should be provided based on students' interests. The theory of multiple intelligences can help teachers to effectively analyze the diversity characteristics and changes of students in teaching activities, and it is of great help to improve students' musical performance.

1. Introduction

The music teaching classroom and teaching mode in most colleges and universities in China still stay in the traditional teaching methods. The characteristics and forms of traditional teaching have always limited the innovation and optimization of music teaching mode in Colleges and universities [1]. With the rapid development of science and technology in the big data environment, we need to pay more attention to the music teaching mode based on the students' learning status and effect and from the perspective of all-round development. Add diversified educational methods and resources to the music teaching classroom to improve students' interest in music. Pay attention to students' classroom experience and the cultivation of music knowledge quality [2]. In the process of learning subject knowledge, students can also experience the changes of music style and the charm of music itself. Effectively improve their own music cells and have a new understanding of music creation ability [3]. In music teaching, teachers need to help students form their own learning methods and thinking processes and build music knowledge and music literacy into a clear context. In the teaching mode of diversification theory, teachers should start from innovative thinking, help students comprehensively use music knowledge and take music culture as the core content of learning. The purpose is to develop students' autonomous learning and innovative learning [4].

At present, there are still many problems in the music teaching mode in colleges and universities. Affected by the traditional teaching mode, most of the classroom environment is still very backward [5]. Teaching is self-centered and takes teaching materials as the main body of knowledge structure. Students do not participate in classroom activities many times. In the innovation of teaching mode, teachers do not start from the actual situation and still take the theoretical knowledge as the teaching basis. Many teaching

researchers believe that teachers should optimize and improve the teaching mode from the students' classroom situation in the process of music teaching. Find a teaching method suitable for each student's physical and mental development, and let students form their own learning atmosphere through multiple learning in the classroom. In view of the above, American psychology professors believe that human beings should have intelligent elements to intuitively show their ability from individual elements in basic language expression and mathematical logic [6]. The teaching of multiple intelligences theory has become the main popular teaching mode, which includes eight intelligences. You can choose the appropriate mode from each intelligent teaching mode. The theory of multiple intelligences also helps to change the music teaching mode to a diversified form. In the theory of multiple intelligences, each student has his own advantages and disadvantages. These different characteristics form a new combination, allowing students to get different cognitive feelings in the learning environment. Thus, the differences between people are formed. Integrating the theory of multiple intelligences into the music teaching model of senior high school can better reflect the purpose of innovation and optimization [7].

This paper is mainly divided into three parts. The first part mainly analyzes the background and development status of music teaching mode in colleges and universities under the theory of multiple intelligences. The second part first explores the application of multiple intelligences theory in music teaching in colleges and universities. Starting from the changes of students' interest behavior and personalized needs, this paper establishes an intelligent learning environment in the innovative teaching mode of multiple intelligences theory. The students' interest model is constructed, and the spatial vector method is used to quantitatively analyze the students' personality needs. Create the student interest model from the three-dimensional space model. Finally, the discrete dynamic modeling of students' learning effect in the innovative mode of music teaching in colleges and universities under the theory of multiple intelligences is studied. The third part analyzes the research results of music teaching mode innovation and discrete dynamic modeling in colleges and universities under the theory of multiple intelligences.

2. Related Work

Music is an art form, which has a very obvious impact on human behavior and thinking. At present, the limitations brought by traditional ideas in college music teaching mode are more obvious. Starting from the modern scientific and technological society, the music teaching model should be newly optimized and improved [8]. From the development of the Internet, students' thinking and learning habits have been affected by many factors. The traditional music teaching model is no longer suitable for the students in the current Internet era. Intelligent electronic devices have become a tool that every student will use. Because of its particularity, music has extremely diversified ways of expression. In the network platform, short video and multimedia software can spread the charm and particularity of music [9]. Students can obtain music learning resources from the Internet, which brings challenges to the traditional music teaching model. Therefore, the teaching mode of multiple intelligences theory has become the main theoretical basis for changing the traditional teaching mode [10]. In the theory of multiple intelligences, each student's learning level and learning ability are different. With the cognition of society and the contact and exploration of the world, students' learning potential will be gradually displayed and expanded. This theory is also followed in college music teaching mode. Teachers should optimize teaching methods and bring intelligent teaching into them on the basis of multiple intelligences theory.

In English Teaching in the United States, students' learning differences and ability levels are divided according to the theoretical basis of multiple intelligences [11]. Carry out targeted strategy teaching for students with different learning abilities and levels. Improve the traditional teaching mode, start from teaching textbooks, and use computer technology to create interactive scenes. This virtual interactive place can help students play roles and experience deeply. Experience the charm of knowledge in learning, and achieve the purpose of improving logical thinking.

Many higher vocational schools in Japan have shifted the focus of English courses from theoretical knowledge to professionalism and practicality [12]. They believe that practical teaching can reflect students' different learning characteristics and give full play to students' subjective initiative. Using the teaching thinking of multiple intelligences theory to improve and innovate the English teaching mode, this new teaching method can bring a lot of inspiration and help to educators. It has a positive impact on students' English achievement and learning atmosphere [13].

Italy is a country full of art. These include many well-known art schools. In the art classroom of these universities, more attention is paid to the theoretical teaching method of multiple intelligences [14]. Starting from the personality of each student, this paper puts forward learning tasks according to the learning needs of different students. The students with the same learning level will be unified in formal teaching, and the students' initiative and creativity will be fully reflected in the teaching mode. This teaching model based on the theory of multiple intelligences can enhance students' love for art courses and achieve certain results in art training [15]. Based on the development and application of multiple intelligences theory in various countries, this paper also integrates this theory into the music teaching mode in colleges and universities. Some positive achievements have been made in the innovation of music teaching mode in colleges and universities.

3. Methodology

3.1. Research on Student Interest Model of College Music Teaching Innovation Model Based on Multiple Intelligences Theory. The theory of multiple intelligences plays an important role and nature in various fields of education. In the music teaching mode, it can effectively combine language

intelligence with theoretical knowledge. Language is a common tool for teachers to impart knowledge and students to each other. In the teaching process, teachers use language expression to express the subject knowledge, which is intuitively presented in front of students and can attract students' attention in class. So as to achieve the purpose of improving teaching quality and classroom learning atmosphere. In the music teaching mode, it can also use effective expression to attract students' attention and interest and transfer from the traditional theoretical knowledge to the dynamic learning process. Psychologists have proved that the process of learning is interactive. The intelligent teaching theory proposed in this paper emphasizes teaching by using students' learning interests. By stimulating students' independence and personalized needs, students can achieve the purpose of active learning. This has an important impact on students' life and study. With the advent of the Internet era, many big data technologies, cloud computing technology, and artificial intelligence have achieved effective results in various fields. Facing the process of modern society, the field of education has also ushered in new reforms and changes. The theory of multiple intelligences also emphasizes the diversification and digitization of learning knowledge. Information resources can help students form diverse interests and learning needs. Explore what you need in the ocean of knowledge, and form your own learning style. In the reform and innovation of music teaching mode in colleges and universities, we need to explore the personalized needs of students. Use big data background to provide information source for students' personalized data.

Personalized learning is also the main direction of teaching model innovation. The development of computer intelligence can effectively identify the characteristics and personality of learners. It is the main way to promote students' personality learning. Therefore, based on the above situation, some researchers propose to apply Bayesian network structure to create a student model in discrete dynamic modeling system. Analyze the characteristics of students' cognition, emotion, and interest in the intelligent learning environment. Take interest learning in music teaching as the main research object, and formulate personalized learning methods and plans. Interest mining is also one of the main problems in the field of learning resources. It combines students' hobbies and preferences with learning environment and motivation to analyze the changing trend of students' interests, so as to change teaching modes and strategies, in order to better meet the needs of students and improve students' academic performance and effect. We study the innovative model of music teaching in colleges and universities from interest modeling. By analyzing the changes of students' behavior data, we can judge the bias of interest feature set. At present, most of the learning modes are online teaching, and the online platform of music teaching can also be well developed and applied. The main research ideas and research directions of this paper are shown in Figure 1.

At the beginning of the study, the role of multiple intelligences theory in the teaching environment was explored by means of literature investigation and reading. Understand the needs of intelligent learning environment and student interest model construction. This paper analyzes the factors affecting students' learning interest and behavior changes. The innovative mode of music teaching in colleges and universities proposed in this paper is intelligent classroom. This kind of intelligent classroom can reflect the "wisdom" characteristics in the theory of multiple intelligences. The intelligent classroom infrastructure is shown in Figure 2.

As can be seen from Figure 2, the whole intelligent classroom system mainly includes several basic system structures. A variety of branches are formed from technology and facilities, network perception, and visualization to jointly establish the model. This intelligent teaching mode can reflect the interactivity of music teaching. It is obviously different from traditional teaching methods in learning form and environment. In addition to building an intelligent teaching model, we also start from students' interests and use change vectors to express students' interest characteristics. In this paper, multiple variable structures are used to represent the change structure of interest among different students. Each vector corresponds to the student's subject of interest. The representative formula is as follows:

$$\text{Student} = \{a_1, a_2, a_3 \cdots a_4\} = \{(b_1, w_1), (b_2, w_2) \cdots (b_i, w_i)\}, \tag{1}$$

where a_1 represents each student's subject of interest. We use the space vector model to represent the interest structure. Combined with the students' behavior characteristics under the theory of multiple intelligences, variables are used to represent the dimension of interest. The formula is as follows:

$$\begin{aligned} &S = \{v_1, v_2, v_3 \cdots v_i\} = \{(l_1, w_1), (l_2, w_2) \cdots (l_i, w_i)\}, \\ &S = \{v_1, v_2, v_3 \cdots v_i\} 1 \le i \le n. \end{aligned} \tag{2}$$

S represents students' interest in the subject and v_i represents the dimension of each vector. Starting from the multiple dimensions of interest behavior, we add attention, participation, and modality changes to the vector model. The expression of the model is as follows:

$$S_t = \{G_t, B_t, E_t\} = \{(G_t, W_1), (B_t, W_2), (E_t, W_3)\}. \tag{3}$$

S_t represents students' learning interest at a certain time in the teaching process, and G_t represents the classroom attention coefficient. B_t represents students' participation in the classroom. We also need to classify students' learning level in calculation. The specific steps are realized by means of mean clustering. Firstly, the specified objects are randomly selected to complete the minimum classification optimization:

$$\min \sum_{j=1}^{k} \sum_{c(i)=j} \left\| \times (i) - \widehat{\mu} \right\|^2. \tag{4}$$

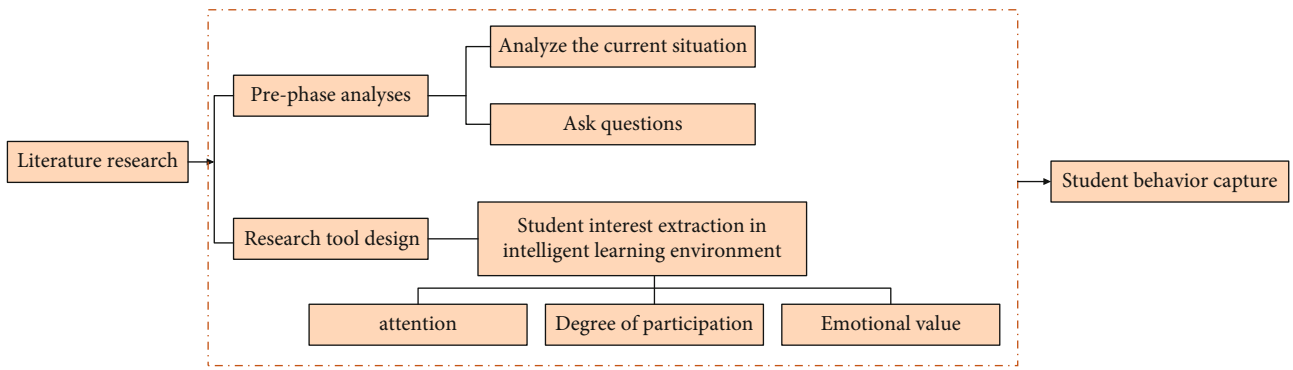

Figure 1: Research ideas and directions.

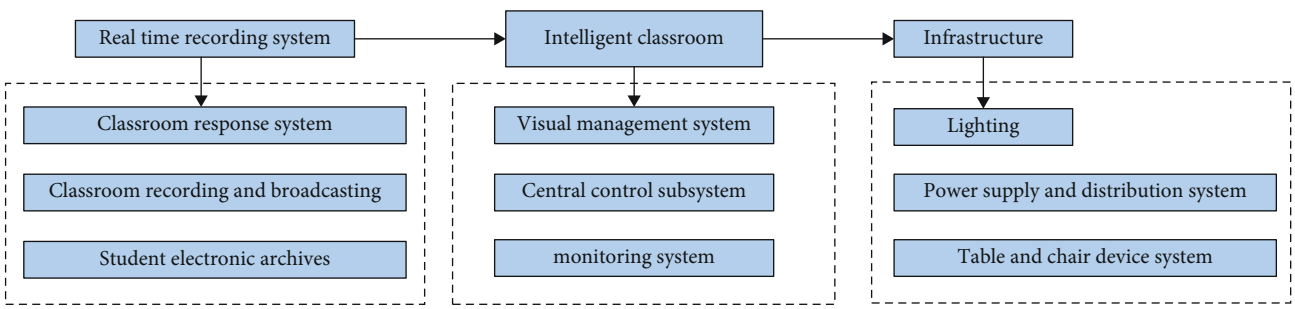

Figure 2: Intelligent classroom infrastructure diagram.

The second part adopts the minimum classification coding to simplify the homology:

$$c(i) = \arg\min \left\| \times (i) - \widehat{\mu}_j \right\|^2. \tag{5}$$

According to the three dimensions of space vector as variables, the interest behavior information is taken as the collection unit of classification. The center point is randomly selected as the interest level coefficient of students. In the division of attention level, students' behavior changes should be judged from the unit node. Calculate the weight value of student behavior change in unit time:

$$G = \sum_{i=1}^{n} s_i * w_i. \tag{6}$$

It specifies a unified unit time vector to capture the same behavior online and analyze the times of a certain kind of behavior. We found that in the music teaching mode, students' behavior can be divided into effective concentration, and the weight coefficient of attention concentration is as follows:

$$w_i = \frac{N}{N_A}. \tag{7}$$

Finally, we also need to analyze the degree of students' participation in the teaching model. The calculation formula is as follows:

$$\begin{aligned} \Pi &= \sum_{i=1}^{n} x_i w_i, \\ B &= \sum_{i=1}^{n} \sum_{j=1}^{m} x_{ij} w_{ij} * w_i. \end{aligned} \tag{8}$$

In the formula, the degree of students' participation is explored from two aspects. One is the occurrence times of attention behavior in unit time, and the other is the score of random inspection in class. B represents the coefficient of students' participation, and n represents the number of times each behavior occurs.

3.2. Research on Discrete Dynamic Modeling of Students' Learning Effect after the Innovation of Music Teaching Mode in Colleges and Universities. The traditional teaching mode is difficult to collect students' learning behavior and effect. Therefore, teachers can not adjust teaching strategies and optimize teaching methods in time, which leads to the unsatisfactory effect of students in music classroom learning. We put forward an intelligent and intelligent teaching model based on the theory of multiple intelligences. In this innovative and optimized teaching method, students' ability to accept knowledge and learning effect are analyzed through students' interest changes and behavior data. With the theory of multiple intelligences becoming the mainstream trend of teaching optimization in the field of education, we should also make rational use of it in the innovation of music teaching mode. Analyze students' interests and abilities in the teaching process.

Studying the factors affecting students' learning effect is an urgent problem to be solved to improve teaching quality. In the analysis and modeling of students' learning effect, the attention and participation in the natural environment are the main factors affecting the learning effect. One is the influence of students' own factors on learning effect. In the process of teaching and learning, the key to students' learning effect lies in their own. The second is the attention to the environment, and the external factors play a role through the internal factors. Therefore, the purpose of studying and discussing the influence of students' own factors on their learning effect is to give full play to students' subjectivity in learning. In the analysis and modeling of students' learning effect, attention and participation in the natural environment are the main factors affecting the learning effect. Firstly, we compare the samples of students randomly selected before and after the innovation of music teaching mode and judge their acceptance of the teaching mode of multiple intelligences theory from the aspect of learning interest, as shown in Figure 3.

It can be seen from Figure 3 that the interest of the sample of students before the optimization of the music teaching mode increased significantly and steadily. There was not much fluctuation. In the use of intelligent improved teaching mode, most students' learning interest has increased as a whole, so the whole sample data shows a leapfrog upward trend. In optimizing the classroom, we use student behavior data for effect analysis. Firstly, judge whether students accept new knowledge and whether they can solve and master the learning content independently from the expression characteristics. The facial features are encoded, and the students' expression features are obtained for marking. Identify the relationship between expression changes in different forms and learning effect. The weight coefficient in a certain unit time is calculated by a quantitative analysis method:

$$E = \sum_{i=1}^{n} l_i * w_i. \tag{9}$$

The calculation formula of weight can express the relationship between students' learning effect and expression characteristics in each unit time. Judge the total number from the occurrence frequency:

$$W_i = \frac{n}{N_E}. \tag{10}$$

Because of the intelligent teaching mode, the collected students' interests are in different environments and atmospheres. We need to normalize the data of attention and learning effect:

$$S_i = (G_i, B_i, E_i). \tag{11}$$

The dimension data representing the effect model are the same and can be processed in one. The standard deviation of variables between each dimension is as follows:

$$Z_i = \frac{x_i - \mu_i}{\sigma_i}. \tag{12}$$

The music teaching mode under the influence of multiple intelligences theory and the unaffected teaching mode were set up in the control group and the experimental group, respectively. The difference coefficient between the two groups is calculated by meta-analysis:

$$g_i = \frac{\bar{Y}E_i - \bar{Y}C_i}{S_i^c}, \quad i = 1, \cdots, k. \tag{13}$$

Among them, $\bar{Y}E_i$ in the formula is the experimental group, that is, the effect after the optimization of the innovation mode. $\bar{Y}C_i$ is the control group, that is, the learning effect of traditional music teaching mode. From the result data, it can be seen that the learning effect of the teaching model optimized by the theory of multiple intelligences can be significantly improved.

4. Result Analysis and Discussion

4.1. Analysis of Students' Interest Model Based on the Innovative Model of Music Teaching in Colleges and Universities under the Theory of Multiple Intelligences. At present, the music teaching mode in colleges and universities lacks obvious professionalism and rationality in curriculum arrangement and the use of teaching materials. Many colleges and universities do not pay attention to music teaching and do not have more patience and achievements in cultivating students' music literacy. With the advent of the digital age, students' learning environment is easily affected by many aspects. Colleges and universities should pay more attention to teaching quality and teaching methods in the process of music teaching to realize the teaching of multiple intelligences theory. Diversified educational ideas have become the main research object in major educational fields in the world. Teachers need to guide students to experience knowledge in music classroom. Starting with the expansion of students' own professional skills, we continue to integrate music thinking into the educational model. Give full play to the cultural connotation and charm of music, so that students' learning habits can be guaranteed. Under the guidance of multiple intelligences theory, this paper analyzes the changes of students' interests from the aspects of intelligent teaching. Create a new music teaching mode. In the calculation of students' interest model, the quantitative analysis method is used to add students' attention level and classroom participation into the calculation model.

The research selected the survey results of daily class of music teaching of students in a university. This paper compares the random samples of students before and after the reform of music teaching mode and judges their acceptance of the teaching mode of multiple intelligences theory from the perspective of learning interest. Firstly, the learning behavior and posture of students in the intelligent innovative teaching mode are obtained, and the behavior model is obtained by using the dynamic capture system. This paper adopts the market xsens MVN dynamic capture system. It

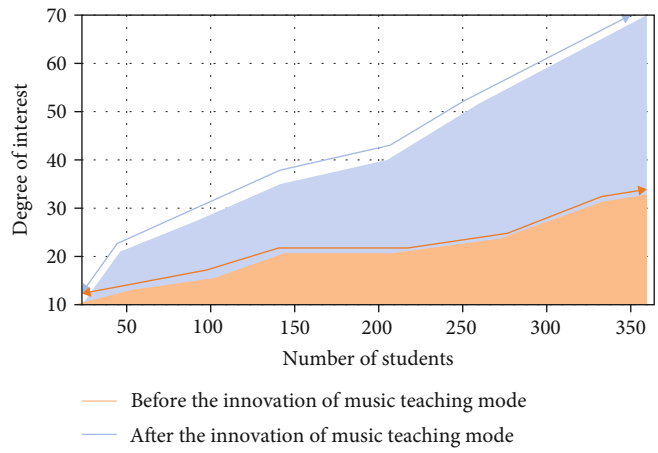

Figure 3: Changes of students' interest before and after the innovation of music teaching mode.

is a convenient, economical, and practical inertial motion capture system. Its unique feature is that it is not limited by ambient light and space distance. Pure motion capture data can be recorded without postprocessing. It is very suitable for all kinds of real-time performance applications. Taking every 4 seconds as the time node, the action target is extracted to form a video image. In the measurement of classroom participation, interactive behavior is the main object. Analyze the number of interactions between students and teachers, students, and students. We set up the control group and the experimental group for the innovative model of music teaching based on the theory of multiple intelligences. Explore the changes of the two in the degree of classroom participation, as shown in Figure 4.

It can be seen from Figure 4 that the experimental group formed by the innovative mode of music teaching can clearly see that the degree of students' participation shows an upward trend in the change of time interval. And in the calculation of attention, students can maintain a high degree of concentration in the learning process. The attention level also reflects the teaching effect after the innovation of music teaching mode. According to the change of attention coefficient and participation degree, teachers can accurately judge the change trend and personalized needs of students' interests, which has been significantly improved in teaching interaction.

4.2. Analysis of Research Results of Discrete Dynamic Modeling of Students' Learning Effect after the Innovation of Music Teaching Mode in Colleges and Universities. In the traditional classroom effect evaluation, many colleges and universities use the listening mode and evaluation form mode. It is necessary to constantly summarize the lectures to judge the effect of a course and students' learning. Although this method can improve teachers' professional level, it has uncertainty and instability. This evaluation method is easy to cause limitations of subjective results. Based on the theory of multiple intelligences, we innovate the music teaching model in Colleges and universities. In order to explore the learning effect and achievement change of students in the new model, dynamic discrete modeling is used for analysis.

Classroom attention, participation, and emotional attitude are still the main elements to evaluate students' learning effect. Attention is the behavior change and psychological activity of students, which can judge the degree of students' attention in the external environment. From a macropoint of view, the degree of classroom participation represents the change of students' interest coefficient and practical activities in the learning process. From the perspective of input, effective analysis of participation coefficient can judge the time and energy invested by students in the change of learning effect. Judge whether the learning effect of students exceeds the standard range in a certain period of time according to the changes of time and energy. Some researchers have shown that learning interest is positively correlated with time investment and learning effect. We analyze the change of students' learning effect under the music innovation mode in terms of time investment, as shown in Figure 5.

As can be seen from Figure 5, with the change of the number of students, the group learning effect and time investment participating in the innovative mode teaching show a positive correlation change. Therefore, the use of discrete dynamic modeling technology can effectively evaluate the learning process and learning effect, ensure the calculation accuracy, and quickly form scientific suggestions for teaching strategies. We integrate big data technology with education, analyze students' behavior changes and interest characteristics, and finally form a learning effect evaluation model suitable for the teaching mode of multiple intelligences theory.

Based on the above, intelligent teaching mode plays a vital role in music education, mainly as follows: first, it can promote and optimize the level of teachers. Intelligent teaching can directly optimize the level of music teachers. With the help of artificial intelligence, music teachers can carry out self-learning more efficiently and conveniently, so as to continuously optimize the level of teachers. Second, it can promote the improvement of teachers' teaching quality and efficiency. Relying on the big data analysis of intelligent teaching, teachers can quickly understand students' learning level and learning background. Teachers can quickly enter the role of teaching workers and carry out effective teaching

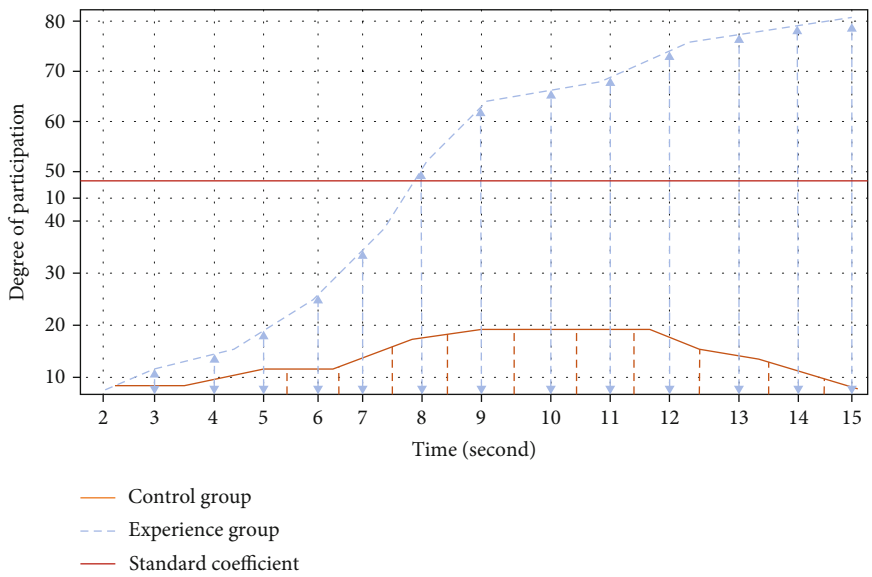

Figure 4: Comparison of participation between control group and experimental group.

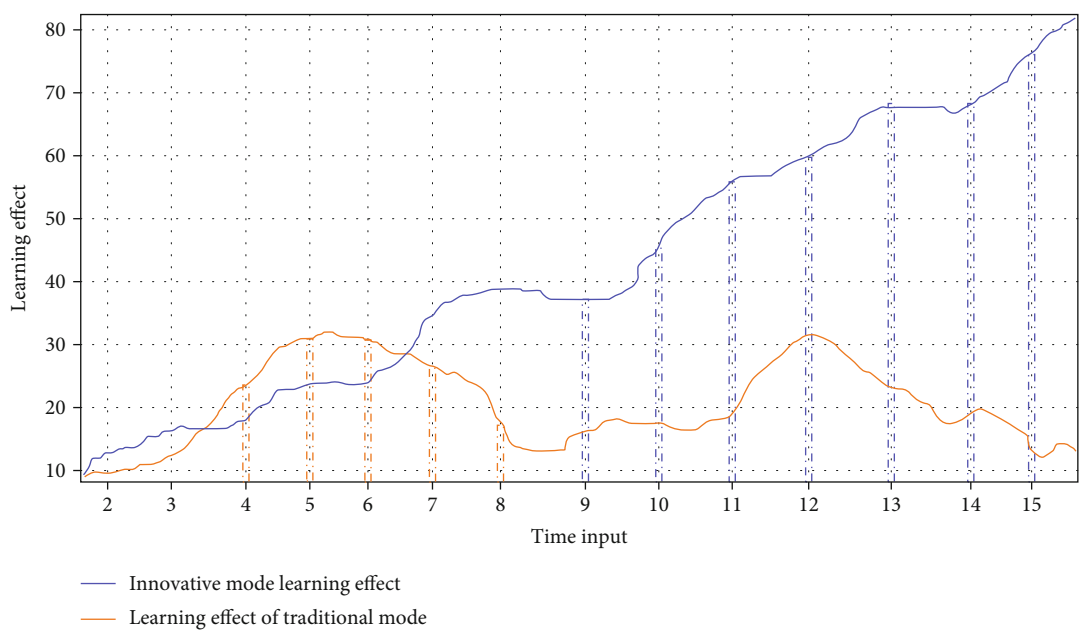

Figure 5: Changes of students' learning effect before and after music innovation mode.

work for students. Meet the educational needs of every student, and effectively improve teachers' teaching quality and efficiency. Third, it can improve students' learning efficiency. By introducing artificial intelligence, students' subjective initiative in learning music can be mobilized. Help students realize the shortcomings in their own learning, urge students to learn, and then effectively improve students' learning efficiency.

5. Conclusion

With the changes of the times, the traditional teaching model is no longer suitable for today's students and educational environment. Under the influence of the Internet, students' interests change very complex, and their personalized needs are also different. More and more online teaching modes and intelligent teaching modes gradually replace traditional teaching. In the process of education, multiple intelligences theory emphasizes that teachers should properly guide and intervene to form students' independent learning habits. Based on the above situation, we analyze and study the innovation of music teaching mode in colleges and universities on the basis of multiple intelligences theory. Firstly, the related contents of multiple intelligences theory are briefly described, and the traditional music teaching mode

is changed from the basic theory. With the support of the Internet and big data, the intelligent teaching environment is adopted for innovation and improvement. In the intelligent teaching mode, the changes of students' interests and personalized needs are analyzed and modeled, and the main factors affecting the teaching effect are judged from the students' interest model. Finally, the discrete dynamic modeling technology is used to detect the learning effect of students in the innovation mode in the big data environment. According to the learning effect of students, judge whether the innovation of music teaching mode in colleges and universities under the theory of multiple intelligences is applicable and significant. The results show that the theory of multiple intelligences has a positive impact on the innovation of music teaching model in Colleges and universities. It can help teachers form a student-centered education model with students' interest changes and personality needs as the main body. It has an important impact on students' diversified development and the improvement of their potential. The research has some innovation. However, this paper does not help students establish the relationship between knowledge well in the research process. For difficult knowledge, it lacks effective supporting means to help students understand and explore difficult knowledge. Therefore, in the future research, it is also necessary to conduct in-depth research on the establishment of learning relationship ties.

Data Availability

The experimental data used to support the findings of this study are available from the corresponding author upon request.

Conflicts of Interest

The author declared that there are no conflicts of interest regarding this work.

References

[1] W. Jiaxin and L. Shuai, "Research on the reform of social work teaching mode in Colleges and Universities under the theory of multiple intelligences – Taking Tibet University for nationalities as an example," *Shanxi Youth*, vol. 34, no. 19, pp. 39-40, 2021.

[2] S. Xiaoping, "Analysis of multiple intelligences theory in the field of comprehensive exploration of primary school art," *Teacher Expo*, vol. 24, pp. 89-90, 2021.

[3] M. Zaiwen, "Optimization of physics classroom teaching mode in Senior High School under the theory of multiple intelligences – Taking "Newton's first law" as an example," *New Curriculum*, vol. 23, pp. 94-95, 2021.

[4] S. Haiyan, "Research on group cooperative teaching model of primary school English based on multiple intelligences theory," *New Curriculum Teaching*, vol. 8, pp. 80-81, 2021.

[5] X. Zhuohua and H. Jing, "On the training mode and teaching design reform of financial news talents from the perspective of multiple intelligences theory," *Higher Education Forum*, vol. 3, pp. 40–44, 2021.

[6] C. Xiuqing, "Construction and application of effective English reading teaching model in junior middle school from the perspective of multiple intelligences theory," *Campus English*, vol. 29, pp. 123-124, 2020.

[7] W. Lingling, Y. Guoliu, and W. Yan, "Application of multiple intelligences theory in clinical practice teaching of obstetrics and gynecology," *China Continuing Medical Education*, vol. 13, no. 3, pp. 50–54, 2021.

[8] L. Ning and D. Jin, "Research on public English teaching model for postgraduates based on multiple intelligences theory," *Journal of Hebei Energy Vocational and Technical College*, vol. 20, no. 2, pp. 81–83, 2020.

[9] W. Wei, "Research on college English teaching model of multiple intelligences," *Educational Modernization*, vol. 7, no. 42, pp. 11–14, 2020.

[10] Q. Xiaojin, "Application of multiple intelligences theory in biology teaching in junior middle school," *Enlightenment and Wisdom (middle)*, vol. 3, no. 5, p. 67, 2020.

[11] S. Hongrui, "Research on the application of multiple intelligences theory in college English reading class," *Science and Technology Vision*, vol. 9, no. 14, pp. 58–60, 2020.

[12] D. Yiwei and Z. Rui, "Research on diversified teaching model of nursing English under the guidance of multiple intelligences theory," *Intelligence*, vol. 7, no. 5, p. 107, 2020.

[13] C. Jie, "Research on business English reading teaching in higher vocational colleges guided by multiple intelligences theory," *Cultural and Educational Materials*, vol. 5, no. 2, pp. 230-231, 2020.

[14] H. Qingbin, "Analysis on the construction of college English teaching under the theory of multiple intelligences," *Shanxi Youth*, vol. 15, no. 24, p. 297, 2019.

[15] X. Jianjun, "Exploration and practice of "data structure" course based on diversified teaching mode," *Microcomputer Application*, vol. 35, no. 12, pp. 54–57, 2019.

Hindawi
Journal of Sensors
Volume 2022, Article ID 6869150, 11 pages
https://doi.org/10.1155/2022/6869150

Research Article

Optimization and Design of General Machinery Production Line Management Process Based on Intelligent Computing Model

Zhenzu Li,[1] Yuli Yu,[1] Junjie Zeng,[1] Liyu Xiang,[2] Jiahao Liu,[3] and Haibin Zeng[4]

[1]*School of Business Administration, Zhuhai College of Science and Technology, Zhuhai, Guangdong 519040, China*
[2]*School of Urban Culture, South China Normal University, Foshan, Guangdong 528225, China*
[3]*School of Economical law, Southwest University of Political Science & law, Chongqing 401120, China*
[4]*Department of Law, Guangdong Police College, Guangzhou, Guangdong 510230, China*

Correspondence should be addressed to Yuli Yu; yuyuli@zcst.edu.cn

Received 11 March 2022; Revised 17 April 2022; Accepted 5 May 2022; Published 24 May 2022

Academic Editor: Yuan Li

Machinery is the most important basic tool for modern times, and it is also an indispensable sharp weapon for creating big country projects. The production line management of general machinery is particularly important. Traditional production line management causes a lot of labor waste, time waste, and low production efficiency, so the efficiency of production line management also determines the quality and output of general machinery. Therefore, it has become an industry consensus to realize intelligent management in the manufacturing process of general machinery. General machinery is not only a complex industrial structure but also has a series of preconditions that are not conducive to production, such as the diversity of parts and the low precision of preparation in the early stage. Therefore, to realize automation in the field of construction machinery manufacturing, it usually faces more challenges. Whether it is traditional production process or automatic production process, the realization of intelligent production line is the primary problem, because both production efficiency and product quality are determined by the efficient production line management efficiency and exquisite process. The workload of production line management is heavy, which is time-consuming, labor-consuming, and expensive. Adhere to the goal of quality first, and how to improve the efficiency of the production line has become the biggest problem at present. Based on the above problems, this paper adopts intelligent computing model to improve the efficiency of production line management and optimize the process. A series of tedious processes from product adoption to final shipment of production lines need intelligent technology to simplify the process, which can effectively improve the production efficiency of general machinery, reduce production costs, and improve the production quality of machinery. Supply chain management theory is used to manage suppliers' production behavior, so as to reduce costs and improve quality and service, thus improving the competitiveness of batch production lines and enterprises. Advanced manufacturing technology is used to realize automation and flexible production of batch production lines, thus improving the rapid response ability of production lines to market demand.

1. Introduction

In the production process of general machinery, before the intelligent technology of mechanical engineering is applied to the production process of mechanical engineering, most mechanical production is completed by assembly line operation, which has high labor cost and cannot guarantee the product quality. Towards intelligence, the symbols on 5G system are detected through deep echo state network [1]. This paper expounds five principles of using intelligent application in medical imaging [2] and expounds that the whole enterprise should develop intelligently, which is proved that the methodology of scientific cognition is the foundation of intelligent management of enterprise overall development. This paper introduces the strategic target complex of intelligent management for the overall development of industrial enterprises. It introduces the influence of risk on the intelligent management process of the overall development of railway tank machinery manufacturing industrial enterprises [3]. The problem of constructing

knowledge base of scheduling decision support system based on empirical data obtained from system diagram calculation experiment is solved, and the proposed method and the actual efficiency of the developed model are determined by research [4]. This paper summarizes the current research status of intelligent body and especially pays attention to the detection and expression of emotions in virtual environment [5]. This paper expounds the intelligent application of fecal immunochemical detection in population screening [6]. This paper introduces the transition from agriculture to digitalization, intelligence, and robot technology [7]. It provides a new idea for the automatic production line of automobile control arm [8]. Considering man-machine cooperation and task allocation, the performance of the production line is evaluated and optimized [9]. This paper introduces the development technology and realization method of intelligent production line based on C language of single chip microcomputer [10]. The literature expounds that using facility location redescription and single commodity flow constraint to eliminate subsequences, effective formulas that can provide high-quality solutions for large-scale instances can be obtained from classical models by making binary production variables explicit [11]. Literature research puts forward a reference practice system for practical training of key progress of SM and systematically constructs a mobile robot-based production line (MRPL) to improve participants' interest in theoretical study and professional skills [12]. A numerical example based on the information collected from the engine crankshaft leasing batch production line shows that the R and OM policy can effectively maximize the leasing profit, reduce the complexity of joint decision-making, and extend the OM theory [13]. The literature analyzes the shortage of the production line, puts forward the optimization method, and simulates the results by using genetic algorithm [14]. The solution proposed in the literature considers the energy availability and energy price of renewable energy and uses genetic algorithm with multiple constraints to optimize the production line scheduling [15]. The intelligent manufacturing process is studied, and the automatic production line based on multiple industrial robots is introduced [16]. By implementing three different line balancing technologies to improve the production line efficiency of the edging unit, a simulation verification platform for data interaction with the control system is proposed, which can verify the control system at low cost [17]. The purpose of this study is to analyze the market demand of jelly beverages in the eastern region in the next five years, select the best place to increase the factory capacity, and conduct a feasibility study on building additional production lines [18]. The literature introduces the replacement of rigid production line with flexible box [19]: production line balance analysis using genetic algorithm [20]. The literature introduces the design and application research of automatic production line of mechanical parts [21] and the application of position weight ranking method in spring production line balance [22]. The optimization and design method of general mechanical production line management flow [23, 24] based on intelligent computing model proposed in this paper can improve the traditional production mode and improve the working efficiency of the production line, and the intelligent method can realize the optimal method and the global optimal scheme in the global design. From the production line of enterprises, the production efficiency of enterprises can be improved, the production cost of enterprises can be reduced, and the production efficiency can be improved.

2. Production System Structure

The production system of machinery industry is the goal of enterprise's own production, management, and long-term development. It is an organic whole that combines various production parts and engages in certain production activities according to the development goal and demand. The production factors input by the production system include people, machines, materials, methods, environment, and energy. The manufacturing process is the process of producing the products that meet the requirements according to the production flow. The essence is the organic combination of the logistics process, the information flow process, and the capital flow process. The management process is the effective management of personnel, equipment, inventory, and other elements. The output of production system is mainly products and services. The general machinery production system takes the enterprise's own development and the market demand as the ultimate goal, increases the product value, satisfies the customer's expectation product, and realizes the enterprise profit. The structural diagram of general machinery production system is shown in Figure 1.

2.1. Content and Optimization. The study of the project of the productive evaluation of production system: firstly, the productive evaluation system of production system is established from three dimensions: task demand response ability, production resource management ability, and job fatigue degree. Secondly, taking the company's engine assembly line as the research object, based on system simulation technology, different levels of simulation models are constructed from macro to micro, and the productivity of the assembly line is comprehensively evaluated, and the evaluation results are verified by the system dynamics model. Finally, according to the evaluation results, the assembly line is optimized, as shown in Figure 2.

2.2. Improvement Ideas of Machining Production Line. Optimized processing efficiency: The traditional production line consumes a long time in the processing of parts and components, and the manufacturing efficiency is low. The commonly used optimization scheme is double production line setting or double station setting. Under the background of public welfare development of machining production line and continuous optimization of production equipment, the operation efficiency and production quality of production work can be improved to a certain extent by improving production equipment, optimizing production links, and applying advanced technologies, such as applying electronic control hydraulic drive devices.

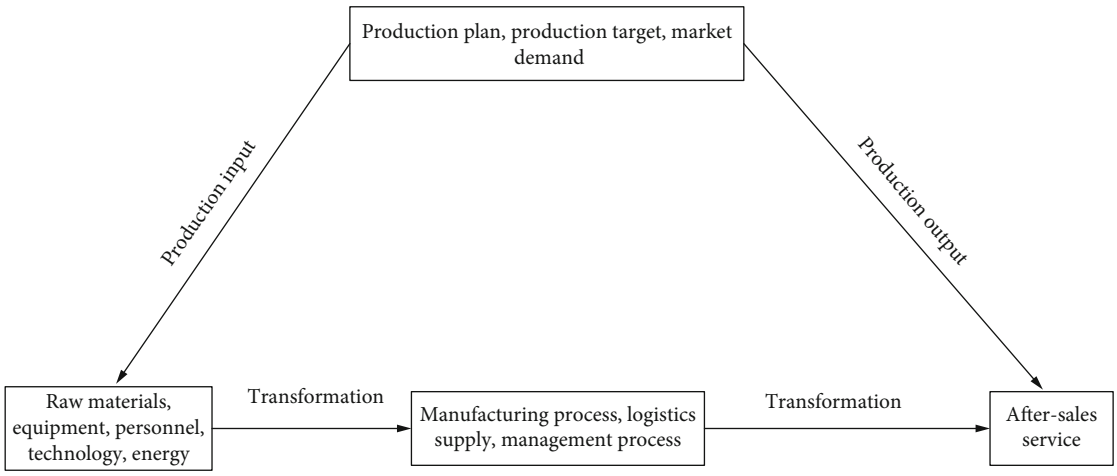

Figure 1: Production system structure.

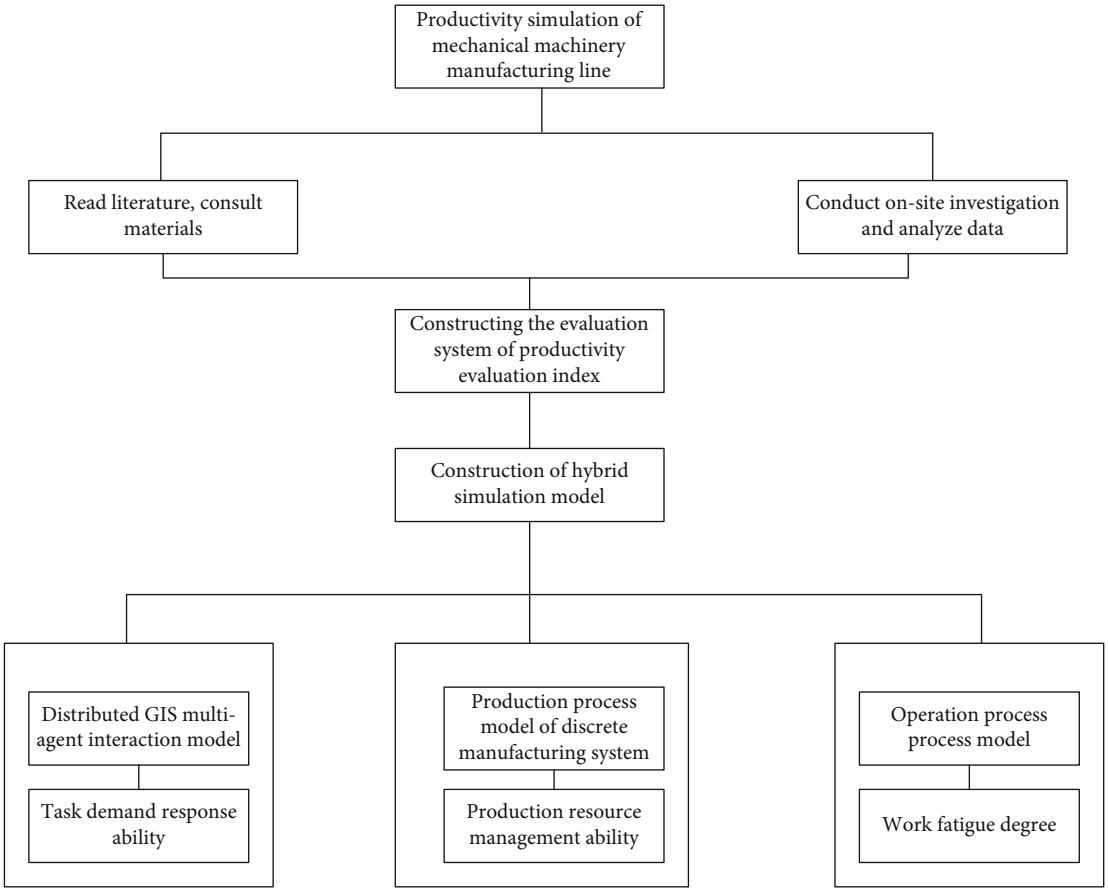

Figure 2: Production line optimization.

Change the operation mode of flexible manufacturing system: the control system of traditional machining production line is mainly relay circuit type. Under the background of the development and popularization of NC machine tools, the production structure of previous production machine tools has changed to some extent, and at the same time, the structure of parts has also changed, such as the change of design standards and production standards. Compared with previous production systems, flexible manufacturing system can coordinate with numerical control technology, enhance the connection between multiple links in the production process, and make it meet the basic requirements of expected manufacturing in terms of production quality and process control. The application of flexible manufacturing system can adjust the form of production and processing according to different production tasks, so that the

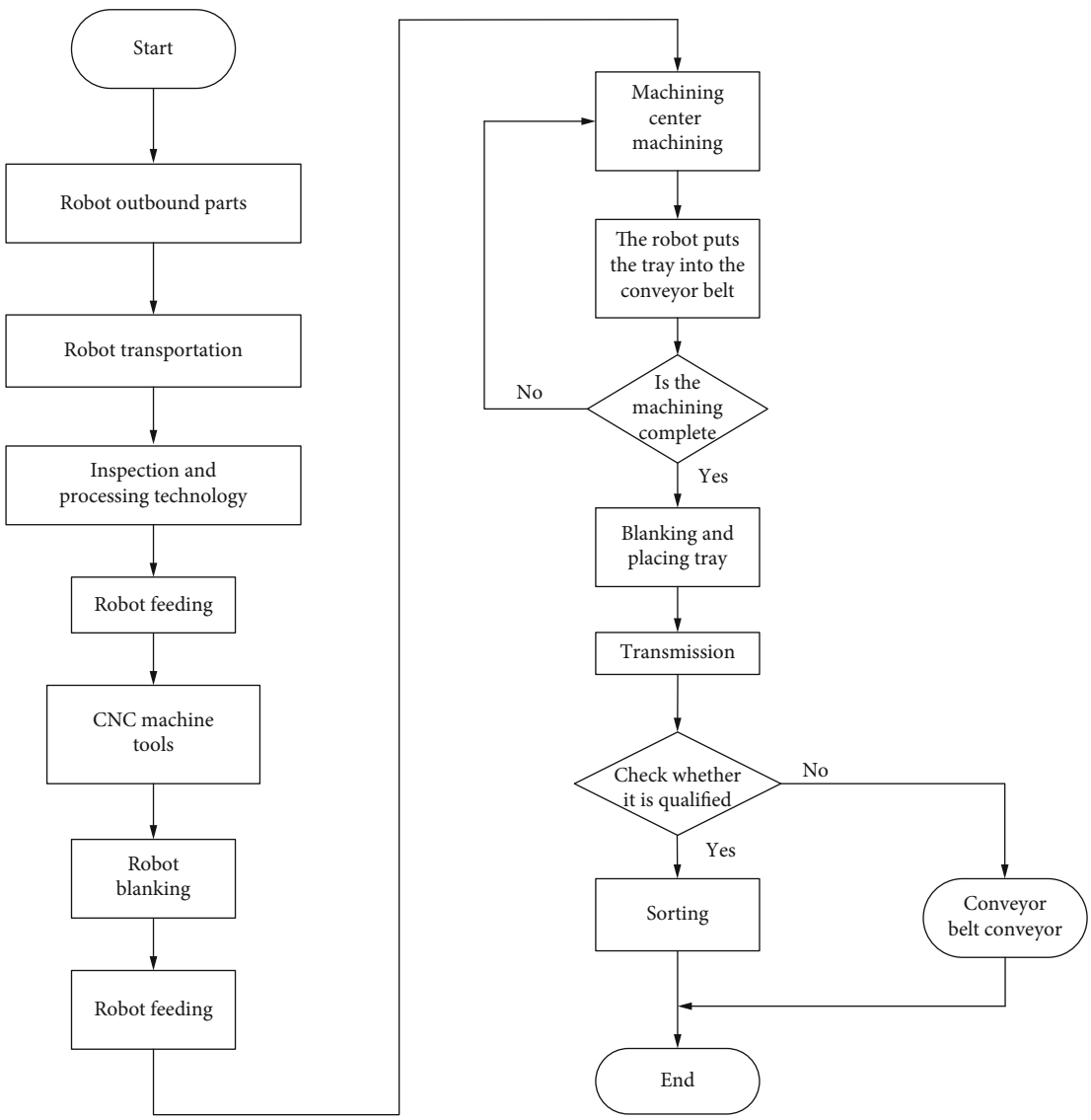

Figure 3: Process flow chart.

Table 1: Comparison of solution values.

Algorithm	Optimal solution	Average solution	Standard solution
Whale algorithm [25]	0.01231	0.01197	0.035
Improved whale algorithm [26]	0.03804	0.03195	0.031
Genetic algorithm [27]	0.02371	0.02762	0.027
Particle swarm optimization [28]	0.03196	0.02474	0.028

The best results after increasing the number of iteration steps of the above four algorithms are compared with, for example, Figure 4.

production efficiency of enterprises can be guaranteed to a certain extent and then meet the requirements of users for production components.

2.3. Improve Machining Quality and Precision. With the development and maturity of machining industry system, the intensity of market competition continues to rise. In order to stand out in the competition, relevant machining enterprises need to firmly grasp the customer dynamics and make the finished products meet the customer's needs through the production and application of new production lines according to their processing and production needs, so as to adapt to the development of market environment through the optimization of production management and production process. With the development of small machinery manufacturing, the fine requirements between its components are becoming more and stricter. In this regard, the first step for general machining enterprises to compete with other enterprises is to improve the precision of parts and to carry out fine machining through high-tech technologies and tools in the manufacturing process, so as to improve the cutting quality of parts and make them reach the desired height in terms of size and observation. Secondly, in the

Table 2: Data comparison table.

Model	1	2	3	4	5	6	7
Whale algorithm	0.291	0.263	0.242	0.263	0.253	0.272	0.211
Improved whale algorithm	0.411	0.392	0.383	0.381	0.393	0.374	0.374
Genetic algorithm	0.312	0.246	0.253	0.274	0.282	0.227	0.245
Particle swarm optimization	0.336	0.224	0.258	0.281	0.254	0.239	0.239

A bar chart of the statistics of the data in the above table is shown in Figure 5.

Table 3: Data comparison table.

Model	1	2	3	4	5	6	7
Whale algorithm	0.292	0.251	0.249	0.254	0.272	0.272	0.283
Improved whale algorithm	0.403	0.373	0.377	0.384	0.391	0.393	0.391
Genetic algorithm	0.323	0.255	0.253	0.242	0.245	0.253	0.255
Particle swarm optimization	0.330	0.232	0.251	0.273	0.277	0.237	0.321

A bar chart of the statistic of the data in the above table is shown in Figure 6.

Table 4: Data comparison table.

Model	1	2	3	4	5	6	7
Whale algorithm	0.282	0.243	0.245	0.255	0.266	0.269	0.287
Improved whale algorithm	0.411	0.363	0.367	0.366	0.371	0.377	0.388
Genetic algorithm	0.223	0.244	0.252	0.244	0.240	0.247	0.253
Particle swarm optimization	0.330	0.233	0.250	0.268	0.273	0.277	0.278

A bar chart of the statistic of the data in the above table is shown in Figure 7.

Table 5: Data comparison table.

Model	1	2	3	4	5	6	7
Whale algorithm	28.4%	23.1%	24.8%	25.2%	26.3%	26.7%	27.8%
Improved whale algorithm	40.02%	36.1%	36.7%	36.8%	37.2%	37.5%	38.3%
Genetic algorithm	23.3%	24.2%	25.1%	25.4%	25.6%	27.2%	27.3%
Particle swarm optimization	33.1%	33.3%	32.4%	33.4%	37.1%	31.5%	28.2%

A bar chart of the statistics of the data in the above table is in Figure 8.

Table 6: Comparison of experimental data of each algorithm.

Algorithm	Construction period	Cost	Quality	Safety	Environmental protection
Whale algorithm	0.4	0.6	0.4	0.4	0.2
Improved whale algorithm	0.3	0.2	0.8	0.8	0.65
Genetic algorithm	0.3	0.4	0.6	0.6	0.3
Particle swarm optimization	0.4	0.5	0.6	0.5	0.2

A bar chart of the statistic of the data in the above table is shown in Figure 9.

process of measurement, it is necessary to control the thermal effect of cutting parts, and the parts are easy to deform in the cutting process because of the high knife edge temperature. According to the characteristics of thermodynamic effect, machining enterprises can implement axial and radial dual control through production precision monitoring, automatic observation equipment, and hollow tool cone, so as to improve the machining quality and fineness of parts.

3. Production Line Optimization Algorithm

Every element in the general machinery production line must be assigned to the corresponding process. The mathematical expression is

$$\sum_{k=1}^{k} X_{ik} = 1\,;\,(i = 1, 2, 3, \cdots, m). \tag{1}$$

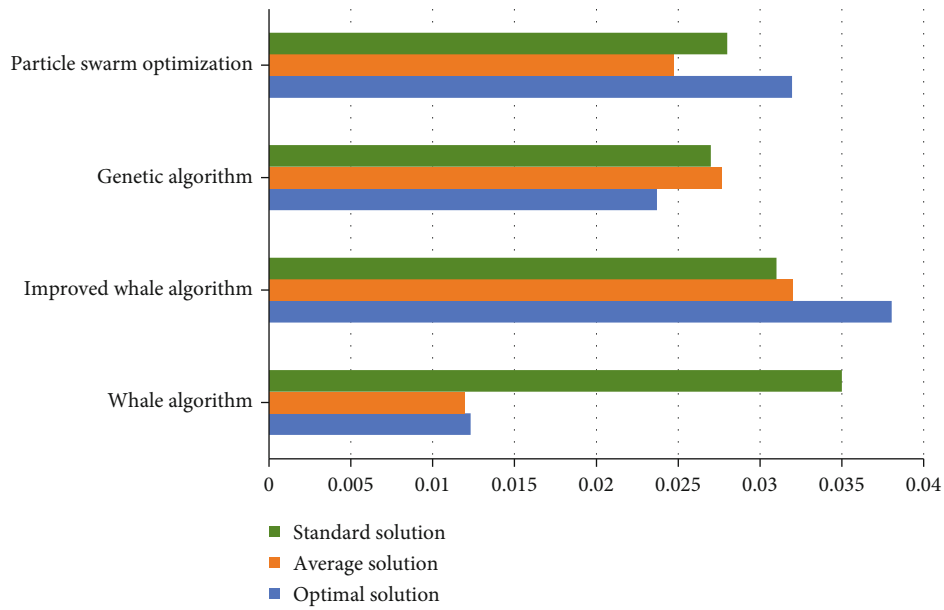

Figure 4: Comparison diagram of optimal values of algorithms.

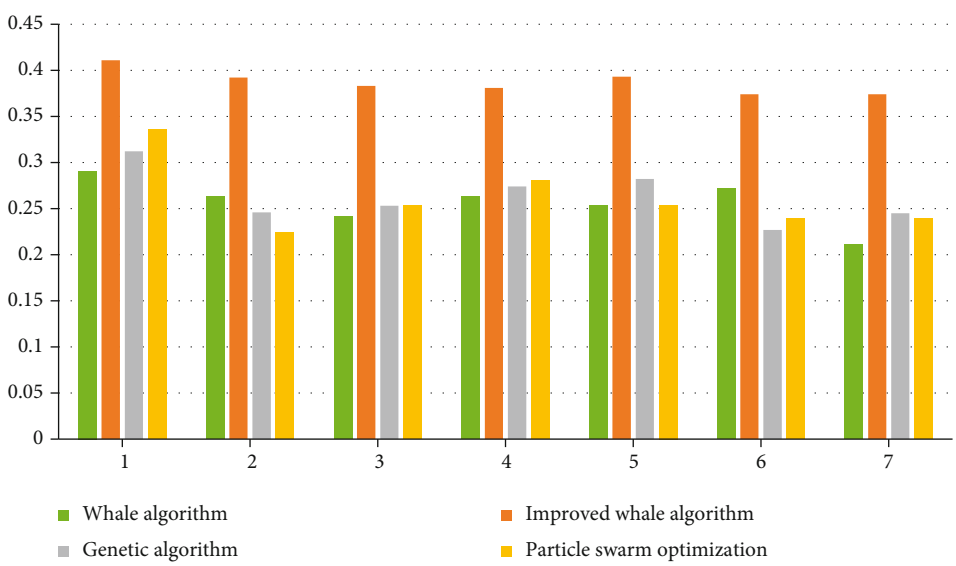

Figure 5: Comparison of algorithm accuracy.

Its expansion is

$$\begin{cases} X_{11+}X_{12} + X_{13}+\cdots+X_{1k} = 1, \\ X_{21+}X_{22} + X_{23}+\cdots+X_{2k} = 1, \\ \ldots \\ X_{m1+}X_{m2} + X_{m3}+\cdots+X_{mk} = 1. \end{cases} \tag{2}$$

In a general machinery production line, the operation where element i is j, when j is assigned to operation k, then element i must be manufactured before element j. The mathematical expression is

$$\sum_{k=1}^{K} k\left(X_{jk} - X_{ik}\right) \geq 0\,;\,(i, j) \in Pread. \tag{3}$$

Its expansion is

$$\left(X_{j1} - X_{i1}\right) + 2\left(X_{j2} - X_{i2}\right) + 3\left(X_{j3} - X_{i3}\right) + k\left(X_{jk} - X_{ik}\right) \geq 0. \tag{4}$$

The total manufacturing time of each process must be less than the production beat (CT). Production beat is an

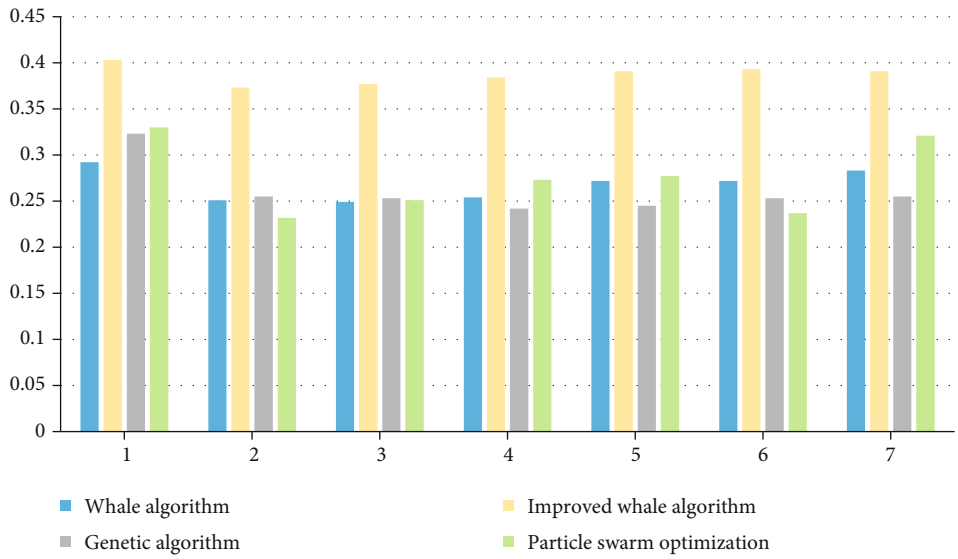

Figure 6: Comparison chart of algorithm recall rate.

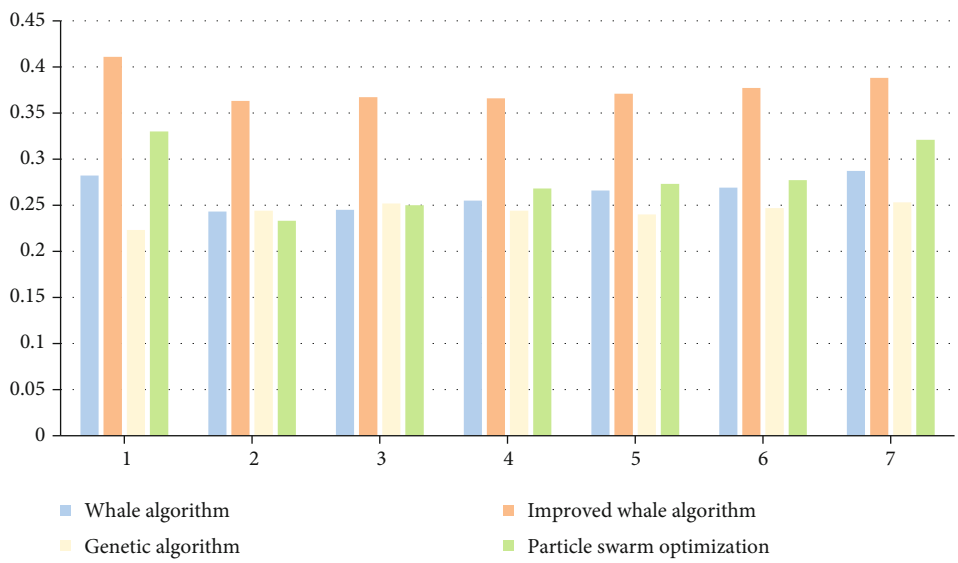

Figure 7: Comparison diagram of algorithm F value.

index used to measure the efficiency of production line. CT $= T_a/T_d$, and its mathematical expression is

$$\sum_{i=1}^{m} X_{ik} t_i \leq \mathrm{CT}\,;\,(k = 1, 2, 3.., K). \tag{5}$$

Its expansion is

$$\begin{cases} X_{11}t_1 + X_{21}t_2 + X_{31}t_3 + \cdots + X_{m1}t_m \leq \mathrm{CT}, \\ X_{12}t_1 + X_{22}t_2 + X_{32}t_3 + \cdots + X_{m2}t_m \leq \mathrm{CT}, \\ \cdots \\ X_{1K}t_1 + X_{2K}t_2 + X_{3K}t_3 + \cdots + X_{mK}t_m \leq \mathrm{CT}. \end{cases} \tag{6}$$

If a workstation in the production line has a job element assigned to it, the indication value of the workstation is 1, and its mathematical expression is

$$\sum_{k=1}^{K} X_{ik} \leq mA_k, \tag{7}$$

$$\begin{cases} X_{11+}X_{12} + X_{13} + \cdots + X_{1k} \leq mA_k, \\ X_{21+}X_{22} + X_{23} + \cdots + X_{2k} \leq mA_k, \\ \cdots \\ X_{m1+}X_{m2} + X_{m3} + \cdots + X_{mk} \leq mA_k. \end{cases} \tag{8}$$

3.1. Improved Unbalanced Programming Model of

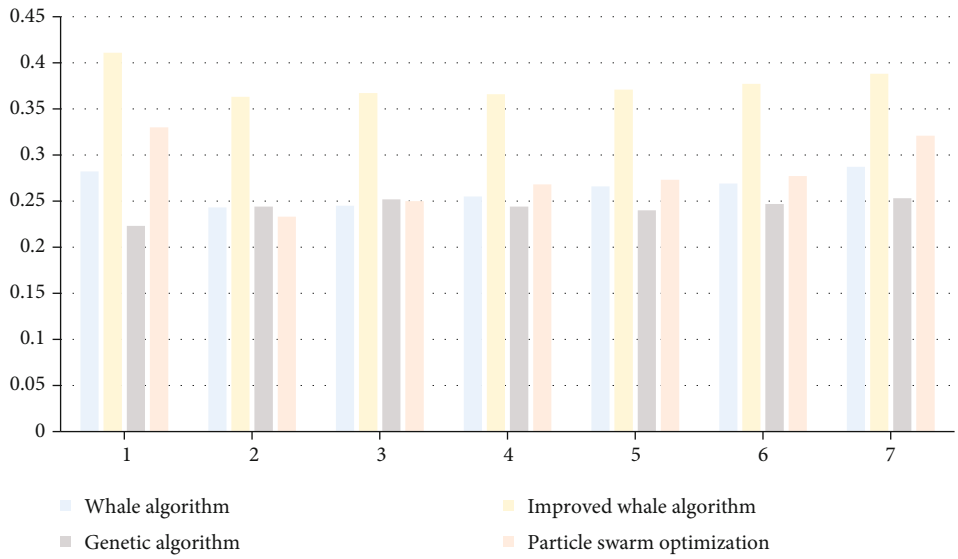

Figure 8: Comparison diagram of algorithm convergence.

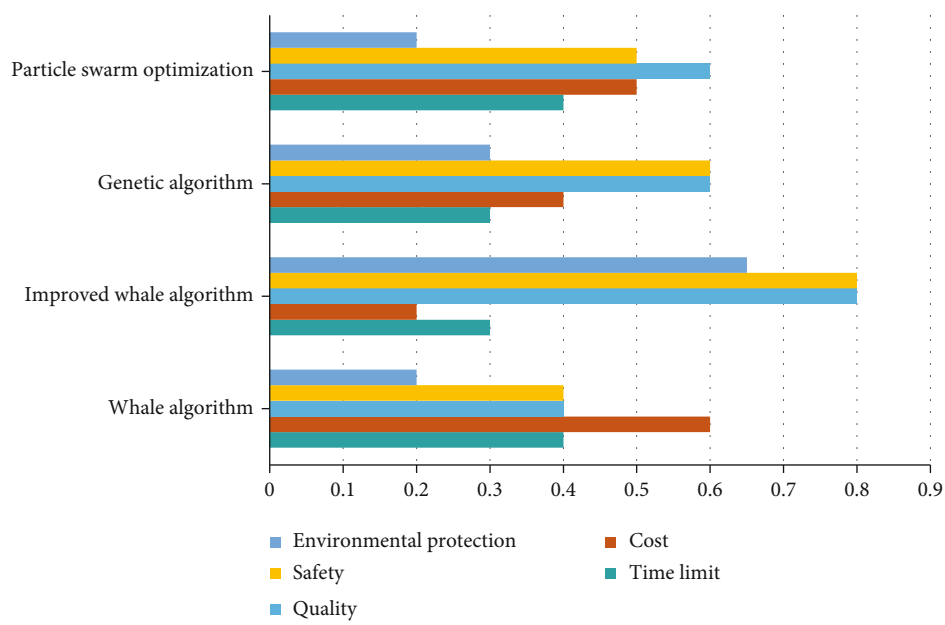

Figure 9: Comparison chart of various elements.

Production Line. Objective function:

$$\min = \sum_{k=1}^{K} A_k. \tag{9}$$

Constraint condition:

$$\sum_{k=1}^{K} X_{ik} = 1\,;\,(i = 1, 2, 3, 4, .., m), \tag{10}$$

$$\sum_{k=1}^{K} k\left(X_{jk} - X_{ik}\right) \geq 0\,;\,(i, j) \in Pread, \tag{11}$$

$$\sum_{i=1}^{m} X_{ik} t_i \leq CT\,;\,(k = 1, 2, 3, .., k), \tag{12}$$

$$\sum_{k=1}^{k} X_{ik} \leq mA_k\,;\,(k = 1, 2, 3, .., k), \tag{13}$$

where the value of the first row in the A_k matrix and X_{ik} represents the values of the i rows and k columns of the matrix X. Formula (9) is the target value requirement, and formulas (10)-(13) are for the constraints in Formula (9). Under the condition of satisfying Formula (10) to Formula (13), find the minimum value of Formula (9). The minimum value in Equation (9) is the target value for implementing the objective function.

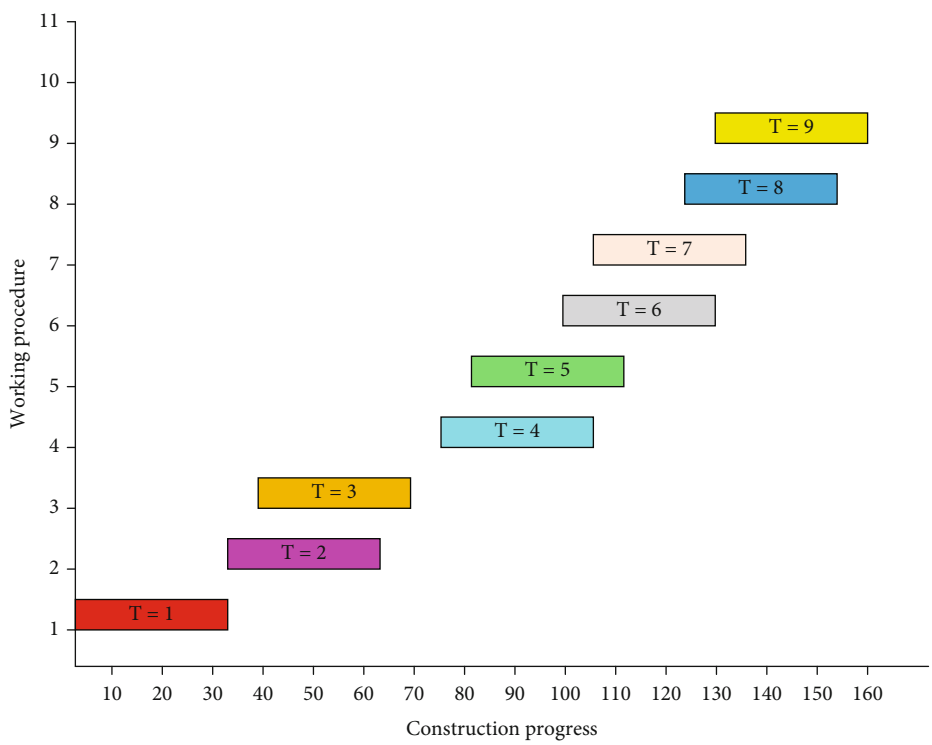

Figure 10: Process management diagram.

3.2. Evaluation Index of Production Line. The production line balance rate of its general machinery:

$$W = \frac{\sum_{i=1}^{N} T_i}{N * T}. \tag{14}$$

Equipment utilization, expressed in JPH:

$$\text{JPH} = \frac{\text{Output}}{\text{time}}. \tag{15}$$

Enterprise production capacity:

$$P = \frac{T}{\text{CT}}, \tag{16}$$

where T_i represents the value of each production line, and $N * T$ represents the total value. JPH represents the ratio of utilization, output, and time. P denotes production capacity, and T denotes production.

3.3. Whale Algorithm

3.3.1. Basic Whale Optimization Algorithm. Whales kill prey and approach the prey position and update their position by different mechanisms. There are three mechanisms for updating the position of whales in whale optimization algorithm:

The first:

$$X_i^{t+1} = X_p^t - A * D, D = \left| C * X_p^t - X_i^t \right|. \tag{17}$$

The second:

$$X_i^{t+1} = D * e^{bl} * \cos(2\pi l) + X_p^t, \tag{18}$$

$$X_i^{t+1} = \begin{cases} X_p^t - A * D, pr < 0.5, \\ D * e^{bl} * \cos(2\pi l) + X_p^t, pr \geq 0.5, \\ D = \left| X_p^t - X_i^t \right|. \end{cases} \tag{19}$$

The third:

$$X_i^{t+1} = X_R^t - A * D, D = \left| C * X_R^T - X_i^T \right|, \tag{20}$$

where X_p^t represents the global optimal position, then $X_i^t = (X_{i,1}, X_{i,2}, .., X_{i,d})$ represents the whale's position in the D-dimensional search space.

3.3.2. Improved Whale Algorithm. Elite reverse solution definition:

$$\overline{X_{i,j}^e} = K * \left(d_{a_j} + d_{b_j} \right) - X_{i,j}^e. \tag{21}$$

Reset method:

$$\overline{X_{i,j}^e} = \text{rand} \left(d_{a_j}, d_{b_j} \right). \tag{22}$$

The purpose of the improved whale algorithm is to achieve the problem of local trapped optimum and to

improve the convergence effect of the algorithm by adding the whole algorithm in the global query time.

3.3.3. Golden Sinusoidal Mechanism. The sinusoidal mechanism is equal to a new metaheuristic optimization algorithm proposed in 2017. Its inspiration comes from the scanning in the unit circle of sine function, which is similar to the spatial search of the solution of the problem to be optimized, and the search space is reduced by the golden section ratio to approach the optimal solution of the algorithm. Compared with traditional metaheuristic optimization algorithm, Gold-SA algorithm has the characteristics of simple principle, few parameters, and strong optimization ability.

The position update formula of the ith individual is as follows:

$$X_i^{t+1} = X_i^t * |\sin(R_1)| + R_2 * \sin(R_1) * \left|x_1 * P_i^t - x_2 * X_i^t\right|. \tag{23}$$

The golden section number is a definition:

$$x_1 = -\pi + (1 - \tau) * 2\pi, \tag{24}$$

$$x_2 = -\pi + \tau * 2\pi. \tag{25}$$

Divide a line segment into two parts so that the ratio of one part to the total length is equal to the ratio of the other part to this part. Its ratio is an irrational number, and the approximation of its first three digits is 0.618. Because the shape designed according to this proportion is very beautiful, it is called the golden section, also known as the ratio between China and foreign countries. The function of this value is not only reflected in the art fields, such as painting, sculpture, music, and architecture, but also plays an important role in management and engineering design.

4. Experiment Analysis

The automatic production line used in general machining is mainly to realize the intelligentization of machinery in the processing and production process. On this basis, digital technology is added. The production process flow of each stage is shown in Figure 3.

4.1. Simulation Experiment. Intelligent algorithms are used to optimize the production process of general machinery. The results of the two algorithms are compared with the data of the optimal solution, the average solution, and the standard solution, as shown in Table 1.

4.2. Model Comparison. Traditional production lines consume a long time in the processing of parts, and the production and manufacturing efficiency is low. In order to improve the traditional mode of the general mechanical production line and improve the management efficiency and work efficiency, an intelligent and efficient production and operation model is adopted, and the accuracy, recall rate, F value, and convergence of the seven processes of the production line are compared in an intelligent way, as shown in the following table.

The accuracy of general machinery in different production processes is compared, such as Table 2.

The recall rate of general machinery in different production processes is compared, such as Table 3.

General machinery performs F value pairs in different production processes, such as Table 4.

Convergence of general machinery in different production processes is shown in Table 5.

It can be seen from the chart of model comparison that the accuracy, recall, F value, and convergence of the improved whale algorithm are always higher than the other three algorithm models in different processes of the production line.

4.3. Contrast Experiment. In order to further explore whether the improved whale algorithm is effective for general machinery production line management optimization, the influence degree of enterprise stakeholders is different, so the influence degree of different goals on enterprises is also different. Compare the statistical data of experimental results with four algorithms as shown in Table 6.

In order to show the decision schemes given by these four optimization schemes more intuitively, the Gantt chart corresponding to the improved whale algorithm is given, as shown in Figure 10.

5. Conclusion

Aiming at the optimization of production line management of general machinery, this paper optimizes each process by improving whale algorithm method, which takes the factors of production schedule, such as construction period, safety, cost, and quality as evaluation indexes. In this paper, some achievements have been made in the research of general machinery production line optimization, and the conclusions are as follows:

(1) Through the comparison diagram of simulation experiment, it can be seen that although it is not the optimal solution, the optimal value of the improved whale algorithm is more stable than that of the other three algorithms

(2) Through model comparison, the comprehensive indexes of all production processes of the four algorithms are compared, and the improved whale algorithm is about 10% higher than the other three algorithms

(3) The effectiveness of the algorithm is further tested in the comparative experiment. By comparing the factors such as construction period, cost, quality, safety, and environmental protection of the production line, and using Gantt chart, it is fully proved that the improved whale algorithm is more effective and fast in job sequencing

Data Availability

The experimental data used to support the findings of this study are available from the corresponding author upon request.

Conflicts of Interest

The authors declared that they have no conflicts of interest regarding this work.

Acknowledgments

The study was supported by the "National Innovation and Entrepreneurship Training Program for College Students, China (Grant no. 202113684001S)."

References

[1] K. Bai, Y. Yi, Z. Zhou, S. Jere, and L. Liu, "Moving toward intelligence: detecting symbols on 5G systems through deep Echo state network," *IEEE Journal on Emerging and Selected Topics in Circuits and Systems*, vol. 10, no. 2, pp. 253–263, 2020.

[2] E. Colak, R. Moreland, and M. Ghassemi, "Five principles for the intelligent use of AI in medical imaging," *Intensive Care Medicine*, vol. 47, no. 2, pp. 154–156, 2021.

[3] "The impact of risks on the process of intellectualization of Management of the Holistic Development of industrial Enterprises of the Railway Tansport Machine-Building," *Inform*, vol. 5, no. 508, pp. 451–457, 2020.

[4] V. Morkun and I. Kotov, "Intellectualization of emergency control of power systems on the basis of incorporated ontologies of knowledge-bases," *Acta Mechanica et Automatica*, vol. 13, no. 2, pp. 86–94, 2019.

[5] M. Brzozowski, M. O'Brien, S. V. Ley, and A. Polyzos, "Flow Chemistry: Intelligent Processing of Gas–Liquid Transformations Using a Tube-in-Tube Reactor," *Accounts of Chemical Research*, vol. 48, no. 2, pp. 349–362, 2015.

[6] S. P. Halloran, "Intelligent use of the fecal immunochemical test in population-based Screening," *Annals of Internal Medicine*, vol. 169, no. 7, pp. 496-497, 2018.

[7] E. A. Skvortsov, E. G. Skvortsova, I. S. Sandu, and G. A. Iovlev, "Transition of agriculture to digital, intellectual and robotics technologies," *Economy of Region*, vol. 14, no. 3, pp. 1014–1028, 2018.

[8] X. Liu and W. U. Junchen, "The structure design of the end picker for the automobile control arm stamping production line," *Journal of Physics: Conference Series*, vol. 1965, no. 1, p. 012025, 2021.

[9] F. Wei, "Production line optimization based on man-machine collaborative improvement," *Journal of Physics: Conference Series*, vol. 1948, no. 1, p. 012177, 2021.

[10] W. Qinghua, "Research on simulation platform of intelligent production lines," *Journal of Physics: Conference Series*, vol. 1948, no. 1, p. 012153, 2021.

[11] A. de Oliveira, S. Willy, O. S. Maristela, and R. Socorro, "Optimization models for a lot sizing and scheduling problem on parallel production lines that share scarce resources," *RAIRO-Operations Research*, vol. 55, no. 3, pp. 1949–1970, 2021.

[12] S. Wang, L. Jiang, J. Meng, Y. Xie, and H. Ding, "Training for smart manufacturing using a mobile robot-based production line," *Frontiers of Mechanical Engineering*, vol. 16, no. 2, pp. 249–270, 2021.

[13] X. Tangbin, "Integrated remanufacturing and opportunistic maintenance decision-making for leased batch production lines," *Journal of Manufacturing Science and Engineering*, vol. 143, no. 8, 2021.

[14] L. Silin and C. Songqing, "Simulation and optimization of a factory automation production line based on plant simulation," *Journal of Physics: Conference Series*, vol. 1820, no. 1, p. 012172, 2021.

[15] M. Bruno, "Production line optimization to minimize energy cost and participate in demand response events," *Energies*, vol. 14, no. 2, pp. 462–462, 2021.

[16] L. Ye and W. Kai, "Multi-robot automatic production line," *IOP Conference Series: Earth and Environmental Science*, vol. 632, no. 4, p. 042063, 2021.

[17] X. Jiang, Q. Song, W. Fu, Y. Xu, and H. Ding, "Design of Simulation Verification Platform for ship sub assembly digital production line control system," *Journal of Physics: Conference Series*, vol. 1650, no. 3, p. 032167, 2020.

[18] S. F. S. Puspita, R. Syarief, and D. S. Hendrawan, "Feasibility study of construction additional production lines on jelly drink plant at PT XYZ," *International Journal of Engineering and Management Research*, vol. 10, no. 4, pp. 51–55, 2020.

[19] K. Roth, "Flexible boxes replace rigid production lines," *IST International Surface Technology*, vol. 13, no. 3, pp. 8–11, 2020.

[20] "Analysis of production line balancing using genetic algorithms," *Materials Science and Engineering*, vol. 801, no. 1, p. 012106, 2020.

[21] W. Bin, "Research on design and application of automatic production line for mechanical components," *Materials Science and Engineering*, vol. 831, no. 1, p. 012009, 2020.

[22] I. Siregar, "Application of ranked positional weights method in springbed production line balancing," *Materials Science and Engineering*, vol. 801, no. 1, p. 012098, 2020.

[23] M. R. Bahubalendruni and B. B. Biswal, "A review on assembly sequence generation and its automation," *Proceedings of the Institution of Mechanical Engineers, Part C: Journal of Mechanical Engineering Science*, vol. 230, no. 5, pp. 824–838, 2016.

[24] X. Lin and Y. Lu, "Research on Mathematical Model of Cost Budget in the Early Stage of Assembly Construction Project Based on Improved Neural Network Algorithm," *Mathematical Problems in Engineering*, vol. 2020, 7 pages, 2020.

[25] H. Hu, Y. Bai, and T. Xu, "A whale optimization algorithm with inertia weight," *WSEAS Transactions on Computers*, vol. 15, pp. 319–326, 2016.

[26] A. Reddy and K. Narayana, "Optimal total harmonic distortion minimization in multilevel inverter using improved whale optimization algorithm," *International Journal of Emerging Electric Power Systems*, vol. 21, no. 3, 2020.

[27] G. M. Morris, D. S. Goodsell, R. S. Halliday et al., "Automated docking using a Lamarckian genetic algorithm and an empirical binding free energy function," *Journal of Computational Chemistry*, vol. 19, no. 14, pp. 1639–1662, 1998.

[28] J. Robinson and Y. Rahmat-Samii, "Particle swarm optimization in electromagnetics," *IEEE Transactions on Antennas and Propagation*, vol. 52, no. 2, pp. 397–407, 2004.

Hindawi
Journal of Sensors
Volume 2022, Article ID 7014070, 17 pages
https://doi.org/10.1155/2022/7014070

Research Article

Research on UI Design and Optimization of Digital Media Based on Artificial Intelligence

Meng Xia[1] **and Yucui Zhou**[2]

[1]*Guangdong Polytechnic of Science and Technology, Guangdong Zhuhai 519090, China*
[2]*Tianjin University of Technology, Tianjin 300384, China*

Correspondence should be addressed to Yucui Zhou; zyc2003@email.tjut.edu.cn

Received 11 March 2022; Accepted 27 April 2022; Published 24 May 2022

Academic Editor: Yuan Li

At present, artificial intelligence technology has developed rapidly and has been gradually applied to various fields of society. With the popularization and development of computers, under the influence of artificial intelligence technology, digital media art and artificial intelligence technology merge with each other, which makes modern culture bloom with greater charm. Based on the era of artificial intelligence, this paper discusses the development core of the integration of artificial intelligence technology and digital media art, analyzes the current development status of digital media art and technology, and finally puts forward the innovative development direction and future trend. At present, China's artificial intelligence technology has gradually entered a prosperous stage in the continuous development and has become one of the high and new technologies in the new era, bringing many changes to people's work and life. With the development of society, modern people are pursuing the two-way needs of material and spirit, and art, as a special field, has attracted much attention. By involving artificial intelligence in the art field, it has become a new challenge to be faced at present, which will promote art and technology to present different forms of expression. Of course, the artistic content of digital media art will be richer, and the attention will be higher. Under the background of artificial intelligence era, the integration of artificial intelligence and digital media is the core industry at present, which promotes the development of China's economy in a better direction.

1. Introduction

This work explains artificial intelligence through the definition of intelligent agent and its role in production system, reactive agent, real-time conditional planner, neural network, and rich decision system. This book emphasizes the importance of the task environment as a decisive factor in the proper design of agents [1]. Integer programming benefits from many innovations in models and methods, and some promising directions for expounding these innovations in the future can be seen from a framework linking artificial intelligence and operational research perspectives. We looked at four key areas. Each shows useful features with the development on the horizon [2]. Logic is now widely regarded as one of the basic disciplines of computing and has applications in almost every aspect of the discipline, from software engineering and hardware to programming languages and artificial intelligence. After extensive discussion between the author of the manual and the second reader, the catalogue of these two volumes was finally determined [3]. This paper introduces constrained programming, which is a powerful example of combinatorial search problem, and it absorbs a wide range of technologies from artificial intelligence, computer science, database, programming language, and operational research [4]. This work explains artificial intelligence through the definition of intelligent agent and its role in production system, reactive agent, real-time conditional planner, neural network, and rich decision system. This book emphasizes the importance of the task environment as a decisive factor in the proper design of agents [5]. This article introduces the evolution of this book from a lecture for students with little knowledge of calculus, and readers do not need any prerequisites related to knowledge of programming languages. In university settings,

this book can be used as an introductory course in computer science, information systems, or engineering departments [6]. Pattern recognition techniques can usually improve efficiency by limiting the application of machine methods to appropriate problems. Pattern recognition, together with learning, can be used to generalize based on accumulated experience and further reduce searches [7]. Since 2010, Ant Conference has officially devoted itself to the whole field of swarm intelligence, without any specific research direction. The full-text document was presented orally at the plenary meeting, and an expanded version of the best papers presented at the meeting will be published in a special issue of the journal [8]. In the uncertain subjective and objective world, randomness is the most fundamental. This paper discusses the relationship between randomness and fuzziness, and the result is the automation of representation, processing, and thinking of uncertain information and knowledge [9]. International e-commerce conference aims to bring together researchers interested in current applications. The technology involves not only lower-level technical problems, but the revised best papers are published in CCIS series [10]. This paper discusses the implementation of artificial intelligence (AI) technology on the World Wide Web. These implementations include a pilot agent with natural language processing and rule-based artificial intelligence, which is a new complex [11]. In artificial intelligence, the process of searching for problem solutions can be realized without domain knowledge or with domain knowledge [12]. This paper examines the organizational dynamics when communication becomes a prominent part of the organizational structure. That is, to understand this change in large-scale action networks, it is necessary to distinguish at least two possible logics: the familiar collective action logic related to high-level organizational resources and the formation of collective identity [13]. A system for controlling access to digitized data is provided. A transmitter program capable of communicating with a security rights management server is provided to a non-secure client. Prior to use, an authentication process is performed between the transmitting pad and the server to authenticate the browser, which expires if authentication does not occur within a predetermined time period [14]. A system for allowing the use of media content in an interactive digital media program is described in which object mapping data and programs are downloaded to a user terminal and used in conjunction with the presentation of media content [15]. The new digital media has greatly changed the communication environment, especially for young people. These communication platforms provide new tools for young people to participate in promoting sexual health and reducing risks. Many comparative studies of follow-up and measurement of behavioral results show the effectiveness of new digital media in changing adolescent sexual behavior [16]. The purpose of this study is to understand the cognitive process of designers when sketching in digital and traditional media. The results show that traditional media has advantages over digital media and these results also provide enlightenment for computer aided architectural design [17]. The Internet has changed the way people get news, do business, communicate with each other, socialize, and interact with government officials. A number of researchers, almost all working in the countries they analyzed, contributed to the project by studying Internet-related laws and practices, testing the accessibility of selected websites and interviewing a wide range of sources [18]. Digital media strategy is an important part of contemporary political activities, which makes citizenship thinner in that people can easily become political speakers without substantive participation [19]. Interactive tables can enhance teamwork and collaborative work in many fields. One application of this new technology is collaborative search of digital content. The results show that these two strategies are equally effective and the possible benefits of team-centered disadvantages exceed expectations [20]. Digital media watermarking discusses the new aspects of digital watermarking in the world. Not only in terms of technology, but also in terms of business and law, this book discusses digital watermarking as it relates to many areas of digital media [21]. An apparatus, program product, and method utilize a set of rules associated with particular individuals to restrict or otherwise control the use of character substitution or similar techniques for similarity data of those individuals in media presentation. Thus, during generation of the media presentation, a personalized version of the media presentation may be generated [22]. This paper presents a method for managing digital objects. You can search and display objects by dragging and dropping tags onto them, and then according to the degree to which the tag search criteria match. In addition, visual cues can indicate whether the displayed objects meet their own search criteria [23]. The invention relates to an armrest-type personal digital media system that allows individuals to use portable, mobile digital devices combined with an armrest system, allows users to enjoy their own digital entertainment options, and also provides users with multiple functions such as seat armrests including memory interface modules [24].

2. The Performance Characteristics of Digital Media

2.1. Interactivity. Interactivity is an important feature of digital media technology. People can choose and receive information according to their own thinking habits and subjective consciousness and can form mutual communication and feedback between people and machines. When people can choose and control information according to their own subjective wishes and when people interact with machines, they will get more vivid information displayed by rich multimedia and then change the original boring visit into a two-way interactive way of information acquisition, so people will feel more entertaining.

2.2. Virtuality. Digital media technology has created a fictional world for people, and "0" and "1" have become the "materials" of this world and constructed the "realistic scene" of this world. Upgrading technology can change ideas and make the world better understood. Virtuality enriches the true meaning of "reality." Reality is no longer just daily

life, but more into the virtual reality of the world to experience the virtual unreality and reality of the feeling.

2.3. Spectacularity. Digital media can restore the impossible or imaginary scenes in the real world and then make people feel the shocking audiovisual experience that they have never experienced before. The success of this phenomenon shows the superb ability of digital media.

2.4. Fusion. Artistic creations based on digital technology and information technology break down the barriers between art categories caused by production and dissemination tools, put different types of artistic creation on one platform, and use unified digital technology tools and language so that different artistic categories can be freely integrated, eliminating the estrangement and occlusion between artistic categories, and finally presenting a more colorful artistic experience.

3. Artificial Intelligence Industry Upgrading Mechanism

3.1. Technical Factor Model of Economic Growth. The theoretical research in this section is based on Romer's R&D model. In the AK model, the production function is expressed as

$$F_i = F\left(k_i, \sum_{i=1}^{n} K_i, \bar{x}_i\right). \tag{1}$$

F_i Represents the output level of manufacturers, k_i represents the professional knowledge during production, $\bar{x}_i$ represents the vector of production factors, and $\sum_{i=1}^{n} K_i$ represents the cumulative level of social knowledge.

Although AK model reveals that technological progress is the result of the efforts of economic activity subjects, but it cannot explain the motivation of the main body of economic activities to carry out technological innovation. Combined with the framework of imperfect competition, Romer revises the original model and constructs R&D model, which internalizes technological progress and thinks that technological progress determines the increase of intermediate product types, while the input of intermediate product types directly affects economic growth, so innovation leads to productivity growth.

The production function Y of the product is expressed as

$$Y = H_y^{\theta} L^{\mu} \sum_{i=1}^{\infty} x_i^{1-\theta-\mu}. \tag{2}$$

When there is technological progress, the infinite diminishing effect disappears. Given the values of human capital H_y and labor force L, the total demand function of durable goods based on this can be obtained as shown as

$$\max \int_0^{\infty} \left[H_y^{\theta} L^{\mu} \sum_{i=1}^{\infty} x_i^{1-\theta-\mu} - p(i)x(i) \right] di. \tag{3}$$

The first-order condition for maximization is

$$p(i) = (1-\theta-\mu) H_y^{\theta} L^{\mu} x_i^{-\theta-\mu}. \tag{4}$$

In the formula, the profit maximization formula is

$$\pi = \max p(x)x - r\varphi x, \tag{5}$$

where $\bar{x}$ is the maximum value of $\bar{p}$ on the demand curve.

The producer enters the intermediate product sector and buys a new design with a value P_A equal to the discounted value of the net income that can be obtained as shown as

$$\int_t^{\infty} e^{-\int_t^{\tau} r(s)ds} \pi(\tau) d\tau = P_A(t). \tag{6}$$

If P_A is a constant, Formula (7) can be obtained:

$$\pi(t) - r(t) \int_t^{\infty} e^{-\int_t^{\tau} r(s)ds} \pi(\tau) d\tau = 0. \tag{7}$$

Formula (8) can be obtained by substituting P_A:

$$\pi(t) = r(t) P_A. \tag{8}$$

According to Ramsey model, Formula (9) can be deduced:

$$\int_0^{\infty} u(C(t)) e^{-pt} dt, \tag{9}$$

where $u(C(t))$ is shown:

$$u(C(t)) = \frac{c^{1-\sigma} - 1}{1-\sigma}, \sigma \in [1, \infty). \tag{10}$$

The profit that the seller can obtain from continuous investment is $\pi = (\lambda + \mu)\bar{p}\bar{x}$, and if the profit that can be obtained is equal to the newly designed price P_A, Formula (11) can be deduced:

$$P_A = \frac{\pi}{r} = \frac{1}{r}(1-\theta-\mu) H_y^{\theta} L^{\mu} x_i^{-\theta-\mu}. \tag{11}$$

The total income of human capital from the research department is $P_A \delta A$, as shown as

$$H_y = \frac{1}{\delta} \frac{\lambda}{(\lambda+\mu)(1-\theta-\mu)} \gamma. \tag{12}$$

When the values of H_y and $\bar{x}$ are fixed, L and A have the same growth rate; If the value of $\bar{x}$ is fixed, then K and A have

the same growth rate. If the growth rates of A, Y and K are Z, then the relationship between Z and interest rate R is shown:

$$z = \delta H_A = \delta H - \frac{\lambda}{(\lambda + \mu)(1 - \theta - \mu)} \gamma. \tag{13}$$

Therefore, economic growth rate is directly proportional to human capital, inversely proportional to technology, and has nothing to do with population size, while technological progress is the driving force of economic growth. In addition, Romer also stressed that government behavior can support technological innovation, and the positive externalities of technology and knowledge elements will lead to increasing returns to scale, thus promoting economic growth. Under the maximum utility, the government needs to increase investment in scientific research and education to ensure sufficient knowledge output.

3.2. Model of Intelligent Technology Expanding Product Category. Taking artificial intelligence technology as an expansion of the categories of raw products and consumer goods, the production function Y of Formula (2) can be rewritten as shown as

$$Y = H_y L^{\mu} \sum_{j=1}^{N} x_{ij}^{1-\mu}. \tag{14}$$

x_{ij} is the consumption of type j transition products, and the decomposability of transition products shows that their number is not equal to the current number of items, that is to say, new products are not the products directly copied and used by the original technology, nor do they supplement the original technology, so the discovery of new products will not cause the obsolescence of existing products.

N denotes the number of transition products used directly, and the increase in N denotes the utility brought about by technological development. In order to study this utility, the transition products are expressed as established units, and assuming that the quantities used are consistent, then Formula (14) can be further rewritten as

$$Y = H_y L^{\mu} N x_i^{1-\mu} = H_y L^{\mu} (N x_i)^{1-\mu} N^{\mu}. \tag{15}$$

If H_y, L, and Nx_i are given, Formula (15) shows that the value of Y increases with the increase of N. This reflects the connotation of technological progress. In this paper, it is indicated that the income increased by artificial intelligence technology by allocating a given number of intermediate products Nx_i to a more number of transitional products N. For a given L, if the increase of Nx_i is realized by increasing x_i, there will be a diminishing return, and if the increase of Nx_i is realized by using existing x_i and increasing N, there will be no diminishing return. Therefore, using artificial intelligence technology to increase the number of transition products will not cause a decline in profits.

3.3. Model of Intelligent Technology to Improve Product Quality. The improvement of product quality is accompanied by the replacement of old products. Referring to the research of Aghion and Howitt (1992, 1998), it is assumed that the final product is unique, the transitional product category is N, and the production function of the enterprise is expressed as

$$Y = H_y L^{\mu} \sum_{j=1}^{N} \bar{x}_{ij}^{1-\mu}, \tag{16}$$

where $\bar{x}_{ij}$ represents the quality change of the intermediate product of Class J. If the initial quality of the intermediate product is 1 and the quality after m changes is Q^m, then the input of the J department after quality adjustment is

$$\bar{x}_{ij} = Q^{mj} x_{ij}. \tag{17}$$

Assuming that quality levels within departments can be completely substituted, the total input of departments can be regarded as the weighted sum of the quality of each level, and the net present value of the total profit of J department undergoing quality adjustment at time point t_{mj} can be expressed as

$$V(m_j) = \int_{t_{mj}}^{t_{mj+1}} \pi(m_j) e^{-\int_{t_{mj}}^{w} r(v) dv} dw. \tag{18}$$

t_{mj} indicates the time of the m_j quality adjustment, t_{mj+1} indicates the time of the competitor's next adjustment, and the time for the product to maintain its advantage after the m_j quality adjustment is $t_{mj+1} - t_{mj}$. With the competitor developing new adjustment means, the old product loses its leading position.

The product category expansion model reflects the basic innovation research, and will not replace the old products, while the product quality improvement model reflects the progress of production technology, which may replace and eliminate the old products. Both of them show the contribution of the improvement of technical level in economic growth.

4. Experiment and Result Analysis

4.1. Experiment 1. In this paper, Python 3.6 is used as the main programming language, and neural network is constructed based on Pytorch 1.6. NVIDIAGeForceGTX-1080Ti is used as the main graphics card. The specific environment configuration is shown in Table 1.

4.1.1. Details of the Experiment

(1) Data Preparation. The interface image is preprocessed. In order to adapt to the horizontal screen interface, the interface image is rotated at 90 degrees and 270 degrees in this paper, and the offline rotation is carried out instead of random online rotation, which is equivalent to expanding the number of interface images in the training set to three times the original, that is, nearly 171 K pairs of training data. In this paper, different sizes of images are scaled for different

Table 1: Experimental software and hardware environment.

Type of experimental environment	Experimental environment
CPU	Intel(R) Core(TM) i5-9400F@2.20GHz
Memory	16 GB
Graphics card	NVIDIA GeForce GTX-1080Ti
Operating system	Ubuntu 18.04
Neural network framework	Pytorch 1.6
Parallel computing framework	cuda 10.1, cudnn 7.6

backbone networks (the downsampling magnification of images in backbone networks is different, so adaptive adjustment is needed). Based on the consideration of video memory and time, when simple convolution neural network is used as backbone network, the interface images are scaled to $201 * 301$ (consistent with UI2code, which is convenient for comparative experiments). When VGG16 and ResNet 34 are used as backbone networks, the image is scaled to $480 * 850$. Because of the image rotation operation, the width and height of the above scaling size are selected according to the original interface image, and the larger one of the widths of the interface image is scaled to 301 or 850, and the smaller one is scaled to 201 or 480.

(2) Model Implementation. The overall training flow of neural network translator based on Transformer proposed in this chapter is as follows: Firstly, screenshots of application screen interface are sent to convolution neural network in batches for image feature extraction. Then, it is stretched and embedded with position coding and then sent to the encoder (the input of each layer needs to be encoded with spatial position). The encoder encodes the image features into a context vector C. Then, the interface tree text corresponding to the interface screenshot is sent to the decoder for mask operation so that the decoder can observe the specific text in time steps, and then the context vector C generated by the encoder and the text after mask calculation are calculated together to calculate the probability distribution of output prediction, and finally, the control text search is carried out to finally generate the interface tree.

In this paper, the task of generating interface tree is regarded as the task of image description (generating depth-first traversal sequence of interface tree from high-fidelity interface image). Because text sequence generation is essentially a multiclassification task, cross entropy loss function is adopted in model training, and Adam optimizer is used to update weights. Parameters are set $\beta 1 = 0.9$, $\beta 2 = 0.98$, learning rate is set to 1, hot start is added, warmup $= 10000$ is set, and learning rate is dynamically adjusted. In this paper, the model dimension of Transformer is set to 512, and the number of multihead self-attention of the model is set to heads = 8. Based on the consideration of video memory and time, the batch size of training data is set to 10, and the layers of encoder and decoder are set to 3. In order to prevent over-fitting, dropout = 0. 1 is added in the training process, and the training rounds are set to 30.

For the consideration of model performance and translation time, the greedy search strategy is used to generate the interface tree. In order to further improve the effect of generating the interface tree, the model with the best performance under the greedy search strategy is used to generate the interface tree by cluster search.

4.1.2. Evaluation Indicators. In this paper, the generation effect of interface tree is mainly evaluated by the following three evaluation indicators.

(1) Perfect Matching Rate. Perfect matching rate is a relatively strict evaluation index, that is, when the generated GUI interface tree is exactly the same as the real label in the data set, it is regarded as a successful matching of the interface tree; otherwise, it is a failure. In this paper, the perfect matching rate is used to strictly distinguish the performance of models, That is, the model with higher perfect matching rate of the generated interface tree performs better. However, there is only one case where the generated interface tree matches the real interface tree successfully. However, there may be many cases of matching failure, that is, the effect of one wrong node and 100 wrong nodes is the same, that is to say, the perfect matching rate can only judge how many interface trees have been inferred successfully, but cannot judge how close the generated interface tree is to the real interface tree in case of error.

(2) BLEU Score. BLEU is commonly used in machine translation to evaluate the similarity between the generated text and the target text as shown as follows:

$$BLEU = BP * \exp\left(\sum_{n=1}^{N} w_n \log p_n\right). \tag{19}$$

BP is the length penalty factor, which is set to 1 when the generated text length is greater than the target text length; otherwise, it is $e^{1-r/c}$; R represents the target text length; C represents the length of the generated text; p_n represents the accuracy of n-gram; w_n denotes the weighting of n-gram precision, and the sum is 1.

The range of BLEU score is [0, 1], which is often expressed as percentage score. The higher the score, the higher the similarity between the generated text and the target text. If it matches completely, the BLEU is 1, which is 100%. In this paper, the highest n-gram is 4.

(3) Edit Distance. Besides using BLEU, this paper also uses edit distance to measure the similarity between the generated interface tree and the real interface tree. This article uses two editing distances: One is the Levinstein editorial distance, mainly used to judge the editing distance of string text, because the interface tree can be regarded as a text string of depth-first traversal sequence, Levinstein edit distance is used to measure its similarity, and the other is tree edit

distance, which is mainly used to judge the edit distance between two trees. This paper uses it to judge the structural similarity between the generated interface tree and the real interface tree.

The Levinstein edit distance algorithm measures the similarity of two strings by calculating the minimum number of edits a string needs to make to become another string. The fewer edits required, the smaller the edit distance between two strings, that is, the more similar they are.

The difference of tree editing distance is that preprocessing operation is needed, that is, calculating the key node set of two trees. The so-called key node refers to the highest-level node with the same leftmost leaf node. In the calculation of tree edit distance, the following order traversal sequence of the tree is mainly used to calculate the edit distance similar to Levinstein, and the dynamic programming algorithm is used to gradually move up from the lower level of the tree, and the forest edit distance may evolve in the calculation process.

4.2. Experimental Results and Analysis. In this paper, 5 K screenshots of application interfaces are randomly selected in the data set for testing, and greedy search and cluster search are used to generate interface trees, respectively. First, greedy search is used to judge the advantages and disadvantages of the model, and on this basis, the best results are selected for cluster search to further explore the performance of the model. Except for cluster search, greedy search is used as the generation method of experimental results. Because only UI2code is similar to this paper in the existing research, which can directly generate the interface tree represented by Android real controls, but pix2code and ReDraw cannot do it, so the experimental results of this paper are mainly compared with UI2code.

In order to further explore the performance of the model, this chapter chooses several different convolutional neural networks as the backbone network to extract image features and adjusts the number of layers of the model encoder and decoder. In this paper, three kinds of convolution neural networks are mainly used: simple network, VGG16, and ResNet34. The loss curves of model training are shown in Figure 1, Figure 2 and Figure 3, and the experimental results of greedy search are shown in Table 2.

As can be seen from Figures 1, 2, and 3, the model of ResNet34 as the backbone network converges faster, and the loss curve is smoother. The ours model in Table 2 represents the Transformer-based neural network translator model proposed in this chapter, and the suffix simple represents different backbone networks adopted by the model. According to the experimental results displayed, the following conclusions can be drawn:

(1) The Transformer-based neural network translator proposed in this section is obviously affected by the ability of image feature extraction, when a relatively simple convolution neural network is adopted. Because the extracted image features are not rich enough, the overall performance of the model cannot be brought into full play. When using convolution neural network with stronger image feature extraction ability, such as ResNet34, the ability of the model can be brought into full play, and the perfect matching rate between the generated interface tree and the real interface tree can be obviously improved. Specifically, the simple convolution neural network with only six convolution layers and four pooling layers has limited extraction ability. The perfect matching rate of the generated interface tree is relatively low. The perfect matching rate of the generated interface tree is only 67.56%, and the BLEU is 92.59%. The average Levinstein edit distance (LD) of the randomly selected 5K test images is 3.49, and the average tree edit distance (TD) is 2.61. However, with the deepening of the convolutional neural network and the introduction of the residual network, the effect of the model is significantly improved. When VGG16 is used as the backbone network, the perfect matching rate between the generated interface tree and the real interface tree can reach 68.96%, BLEU can also reach 93.18%, LD is further reduced to 3.16, and TD is as low as 2.34; when ResNet34 is used as the backbone network, the effect of the model can be further improved, the perfect matching rate of the interface tree can reach 70.44%, the BLEU can reach 93.21%, and the LD and TD can be further reduced to 3.09 and 2.31. Affected by the backbone network, the perfect matching rate between the interface tree generated by the model in this chapter and the real interface tree increased from 67.56% of simple to 70.44% of ResNet34, an increase of nearly 3 percentage points. At the same time, BLEU also increased from 92.59% to 93.21%, an increase of nearly 0.6 percentage points, and LD and TD also decreased obviously

(2) When the simple convolutional neural network is used in the backbone network, the number of layers of the encoder and decoder has a great influence on the model effect. If the model uses the same six-layer structure as the original transformer , then the perfect matching rate of the generated interface tree is low, only 64.88%; when the number of model layers is reduced to, the perfect match rate is 67.56% at 3 layers. The semantic complexity of interface tree generation is lower than that of machine translation task. Other indicators have been significantly improved. According to this discovery, all subsequent experiments will use three-layer encoder and decoder structure

(3) The Transformer-based neural network translator proposed in this section can generate an interface tree directly from high-fidelity UI images. In 5 K test images, 3522 images (70.44%) can directly generate a completely correct interface tree, and generally speaking, the generated interface tree is similar to the real interface structure (BLEU reaches 93.21%, LD and TD are only 3.09 and 2.31, respectively)

In order to prove the superiority of the neural network translator proposed in this paper more obviously, it is

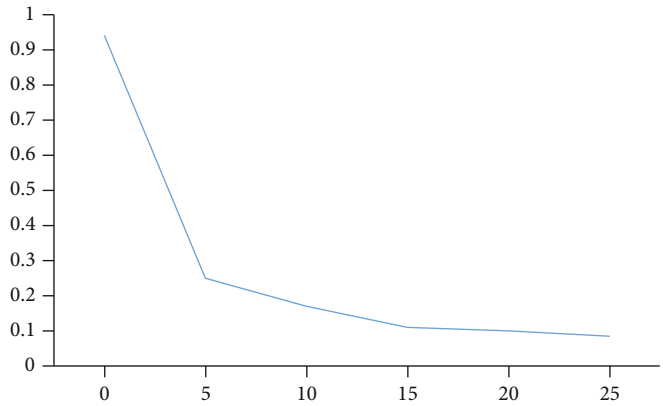

Figure 1: Loss change curve of simple model.

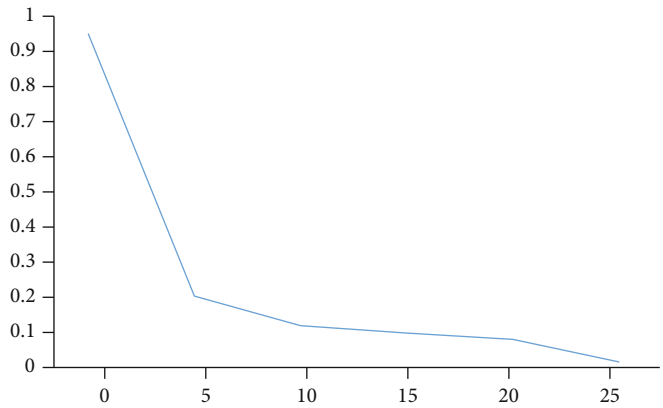

Figure 2: Loss variation curve of VGG16 model.

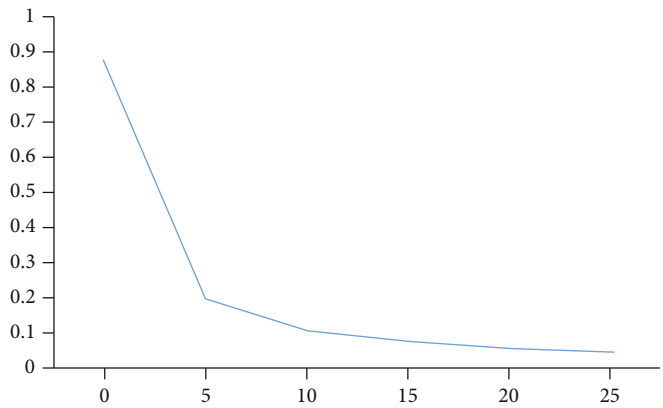

Figure 3: Loss change curve of ResNet34 model.

compared with the UI2code model with a better effect at present, and the experimental results of greedy search are shown in Table 3.

As shown in Table 3 (the postJustOnce model suffix indicates that spatial position coding is added only to the first layer of the encoder, and all layers of the encoder are added unless otherwise specified), when the model proposed in this section uses the same simple convolution neural network as UI2code, compared with it, the perfect matching rate can be improved by 7.1%, 8.67% on BLEU, and 3.31 and 2.96 on LD and TD, respectively. This is mainly due to Transformer's solution to the problem of feature information length dependence and strong feature coding and decoding ability, which proves Transformer's good

Table 2: Comparison of greedy search results in backbone networks.

Type of experimental environment	Experimental environment
CPU	Intel(R) Core(TM) i5-9400F@2.20GHz
Memory	16 GB
Graphics card	NVIDIA GeForce GTX-1080Ti
Operating system	Ubuntu 18.04
Neural network framework	Pytorch 1.6
Parallel computing framework	cuda 10.1, cudnn 7.6

Table 3: Comparison of greedy search results of each index of the model.

Scheme model	Perfect matching rate	BLEU	LD	TD
UI2code	60.46%	83.92%	6.8	5.57
ours-simple	67.56%	92.59%	3.49	2.61
ours-ResNet34	70.44%	93.21%	3.09	2.31
ours-ResNet34-posJustOnce	69.50%	93.19%	3.12	2.33

performance in interface tree generation. Furthermore, when ResNet34 is used in convolution neural network, 3522 (70.44%) GUI interface trees generated in this model can completely match the real application interface structure, while only 3023 (60.46%) of UI2code completely match the real interface tree, which is 9.98% higher than that in this paper. At the same time, on BLEU, the BLEU score of the neural network model proposed in this paper is 93.21%, and the BLEU score of UI2code is only 83.92%; compared with this article, it is improved by 9.29%. In terms of editing distance, the model proposed in this paper only needs 3.09 string editing operations or 2.34 tree editing operations to get the real interface tree on average, while UI2code needs 6.8 string editing operations or 5.57 tree editing operations on average. Compared with UI2code, the interface tree generated by this research method is closer to the real interface tree. In particular, this chapter explores different spatial position coding methods. When spatial position coding is only used in the first layer of the encoder, the perfect matching rate is 69.50%, while when spatial position coding is added in each layer of the encoder, the perfect matching rate is improved to 70.44%. Therefore, the latter position coding method is adopted in the subsequent experiments of this paper.

In order to further explore the interface tree generation ability of the model, this chapter will use the cluster search strategy to generate the interface tree for the model with the best performance under the greedy search strategy. The specific interface tree generation effect is shown in Table 4 and Figures 4, 5, 6, and 7.

In Figure 4, Figure 5, Figures 6, and 7, broken lines with different colors represent different models. The models proposed in this chapter are represented by blue, UI2code is represented by orange, the x-axis represents Beamwidth, that is, the number of results maintained at the same time during cluster search, and the y-axis displays numerical values, which are divided into perfect match rate, BLEU, Levinstein editing distance, and tree editing distance. As shown in Figures 4 and 5, with the increase of Beamwidth, the perfect matching rate and BLEU of the model will be improved, especially when Beamwidth = 2. At the same time, the model proposed in this paper is better than UI2code in all values of Beamwidth. As shown in Figures 6 and 7, as Beamwidth becomes larger, the edit distance between the generated interface tree and the real interface tree (whether it is Levinstein edit distance or tree edit distance) is reduced, which indicates that the proximity between the generated interface tree and the real interface tree is gradually increasing. The edit distance between the generated interface tree and the real interface tree is much lower than that of UI2code. From the specific values in Table 4, it can be seen that the method in this section can achieve the best generation effect when Beamwidth = 5, with a perfect match rate of 71.16%, BLEU of 93.36%, LD of 2.90, and TD of 2.14. Compared with UI2code under the same search conditions, the perfect match rate is improved by 8.3%, BLEU is improved by 5.05%, LD is reduced by 1.82, and TD is reduced by 1.32.

It should be pointed out in particular that in the process of tree editing distance calculation, this paper finds that in the generation of interface tree, there are some generated text sequences that cannot form a tree ("{" and "}" in the text sequence cannot be closed perfectly). For this reason, this paper counts the occurrence times of "{" and "}" in the generated text sequence. When the occurrence times of "{" are less than the occurrence times of "}", "}" is removed from the end of the text until all "{" and "}" match each other; when "{" occurs more often than "}", add "}" at the end of the text until all "{"and "}" match each other. According to the above operation, the interface tree can be filled simply and quickly. In 5 K test images, the number of incomplete interface trees generated by each model is shown in Figure 8. As can be seen, although the model in this chapter has completely surpassed UI2code in evaluation indicators such as perfect matching rate, it can be seen from the perfect matching rate and TD (tree editing distance) that the interface tree generated by the model in this chapter is more similar to the real interface structure, but in the same way, there are still nearly 100 interface images that cannot generate a complete interface tree; even if different backbone networks are replaced, this problem has not been significantly improved, which proves that the problem mainly lies in the codec stage of Transformer. After in-depth analysis of the model, it is considered that it is mainly caused by the self-attention mechanism of Transformer and the next section will analyze this problem.

This chapter describes the software and hardware environment of the experiment and the training parameters; after that, the experimental results are analyzed and compared with the existing research. It is found that the perfect matching rate and BLEU score of GUI interface generated by the Transformer-based neural network translator are much higher than those of the existing research, and the

Table 4: Comparison of cluster search results of each index of the model.

Scheme model	Beam width	Perfect matching rate	BLEU	LD	TD
UI2code	1	60.46%	83.92%	6.8	5.57
UI2code	2	61.76%	88.19%	5.07	3.81
UI2code	3	62.12%	88.25%	4.88	3.61
UI2code	4	62.52%	88.27%	4.74	3.5
UI2code	5	62.86%	88.31%	4.72	3.46
ours-ResNet34	1	70.44%	93.21%	3.09	2.31
ours-ResNet34	2	71.12%	93.34%	2.91	2.16
ours-ResNet34	3	71.14%	93.36%	2.9	2.16
ours-ResNet34	4	71.16%	93.36%	2.9	2.16
ours-ResNet34	5	71.16%	93.36%	2.9	2.14

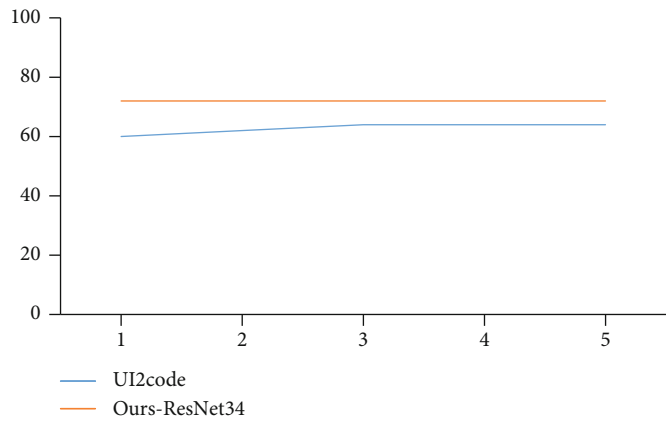

Figure 4: Comparison of cluster search results of each index of perfect matching rate.

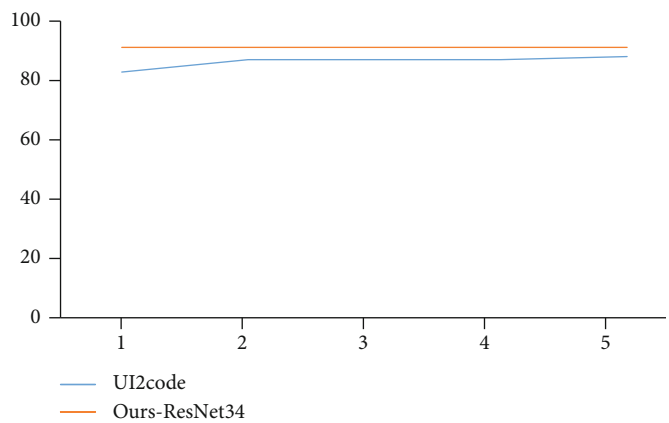

Figure 5: Comparison of cluster search effect of each index of BLEU score.

Levinstein editing distance and tree editing distance are obviously lower than those of the existing research, which proves the effectiveness of the method in this chapter.

4.3. Experiment 2. The experimental environment in this chapter is consistent with that in the previous section. Python 3.6 is used as the main programming language, and neural network is constructed based on Pytorch1.6. The graphics card mainly adopts NVIDIAGeForceGTX-1080Ti, and the specific environment configuration is shown in Table 1.

4.3.1. Details of the Experiment

(1) Data Preparation. The data used in this chapter is consistent with the previous section. There are 57 K pairs of data (interface image and interface tree label) in the training set,

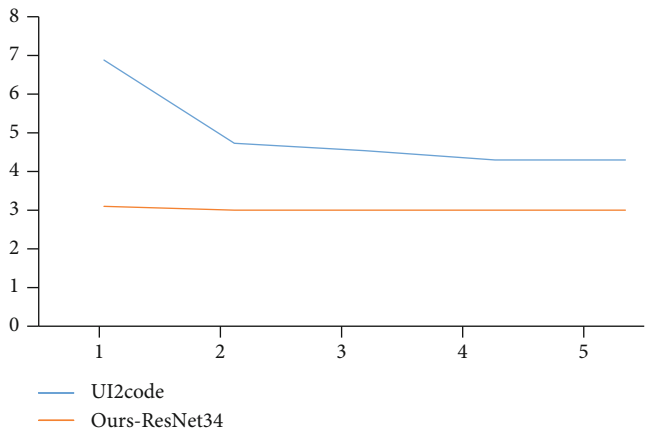

Figure 6: Comparison of cluster search results of various indicators of Levinstein editing distance.

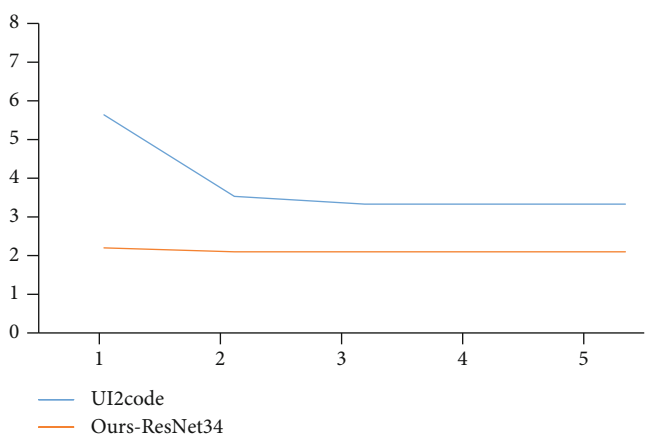

Figure 7: Comparison of cluster search effect of each index of tree editing distance.

3 K pairs in the verification set, and 5 K pairs in the test set. The training set is expanded to 171 k pairs of data after two different rotation enhancements. There are also two scaling scales for image data in this chapter: 201 ∗ 301 for simple network and 480 ∗ 850 for VGG16 and ResNet is 34.

(2) Model Implementation. The overall training process is as follows: Firstly, screenshots of application screen interface are sent to convolution neural network in batches for image feature extraction, Then, it is stretched and encoded with spatial position information and sent to the encoder (each layer of the encoder needs to be encoded with spatial position information). In each layer of the encoder (except the highest layer), in addition to the original self-attention calculation module, there is also a priori memory module, using it to extract prior information. At the same time, the prior information is propagated to all subsequent encoder layers to participate in the attention calculation of this layer. The encoder encodes the image features into a context vector C. Then, the interface tree text corresponding to the interface screenshot is sent to the decoder for masking operation so that the decoder can observe the specific text in time steps, and the context vector C and the text after masking calculation are calculated together to output the probability distribution predicted by the decoder, and finally, the control text search is carried out to finally generate the interface tree.

4.3.2. Model Training. Because the model is mainly changed in the encoder stage, however, the backbone network and decoder of image feature extraction have not been changed, so when the model is trained concretely, it is still as shown in 4.1. 1b, using cross entropy loss function, using Adam optimizer to update the weight, keeping the parameters set $\beta 1 = 0.9$ and $\beta 2 = 0.98$, setting the learning rate to 1, and still adding hot start, setting warmup = 10000, and dynamically adjusting the learning rate. In this section, the model dimension of Transformer is set to 512, and the number of multi-head self-attention of the model is set to heads = 8. Based on the consideration of video memory and time, the batch size of training data is set to 10, and the respective layers of encoder and decoder are layers = 3. In order to prevent over-fitting, dropout [71] = 0.1 is added in the training process, and the training rounds are set to 30.

4.3.3. Experimental Results and Analysis. In this section, the perfect matching rate, BLEU and editing distance are still used to evaluate the generation effect of interface tree. The 5 K screenshots of application interfaces used in the test are also consistent with the previous section. At the same time, greedy search and cluster search are used to generate interface trees, respectively. First, greedy search is used to judge the advantages and disadvantages of the model. On this basis, the best results are selected for cluster search to further explore the performance of the model. Except for cluster search, greedy search is used as the generation method of experimental results. The experimental results in this section are mainly compared with the improved model and UI2code proposed in this paper.

(1) Overall Performance Analysis. In order to fully explore the performance of prior memory self-attention proposed in this chapter, several different convolution neural networks are selected as backbone networks for image feature extraction. In this paper, three convolution neural networks are mainly used: simple convolution neural network, VGG16, and ResNet34. The loss curves of improved model training are shown in Figure 9, Figure 10, and Figure 11, and the experimental results of greedy search are shown in Table 5.

As can be seen from Figure 9, Figure 10, and Figure 11, when ResNet34 is used as the backbone network of the improved model, the convergence speed of the model is faster than that of the other two backbone networks, and the loss curve is smoother. The ours-PM model in Table 5 represents the improved Transformer neural network translator based on prior memory and self-attention proposed in this chapter, and the suffix simple represents different selected backbone networks. From the experimental results shown, the following conclusions can be drawn:

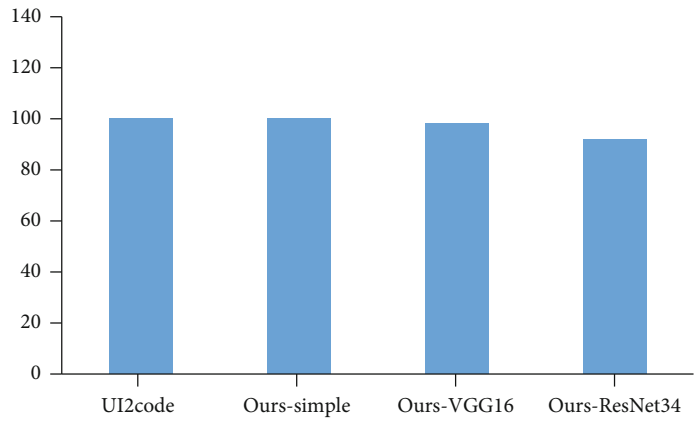

Figure 8: Number of incomplete interface trees generated by each model.

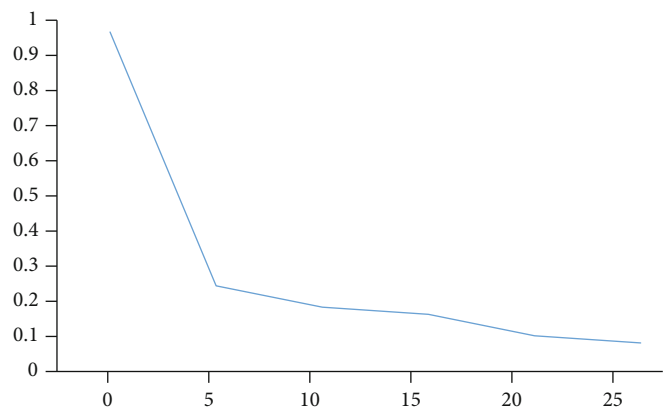

Figure 9: Loss change graph of improved simple.

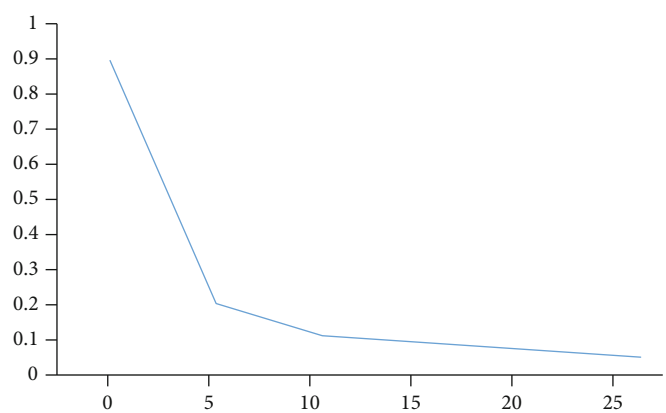

Figure 10: Loss change curve of improved VGG16.

(1) The improved Transformer neural network translator based on prior memory self-attention proposed in this chapter can show better effect when the image feature extraction ability is strong. When using simple convolution neural network for image feature extraction, it will seriously affect the model to extract prior information, resulting in the generation effect of interface tree is not significantly improved. When using convolution neural network with stronger image feature extraction ability, the ability of the improved model can be better reflected. Specifically, when using the simple convolution neural network constructed in this paper, the perfect matching rate of the generated interface tree can only reach

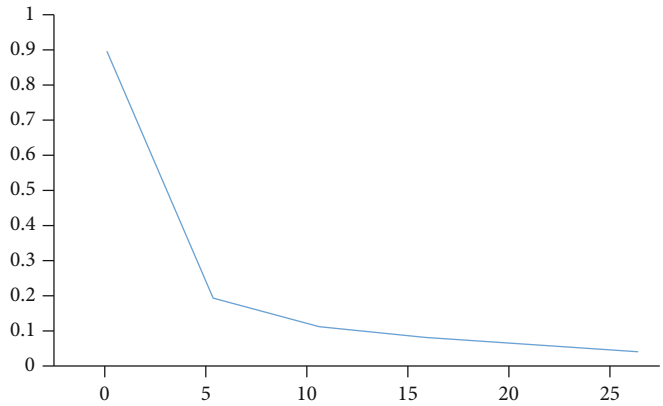

Figure 11: Loss change graph of improved ResNet 34.

Table 5: Comparison of greedy search results of backbone network of improved model.

Scheme model	m	Perfect matching rate	BLEU	LD	TD
ours-PM-simple	10	66.33%	92.13%	3.62	2.72
ours-PM-simple	20	67.76%	92.67%	3.47	2.56
ours-PM-VGG16	20	70.28%	93.42%	3.01	2.32
ours-PM-ResNet34	20	71.32%	93.66%	2.91	2.11

67.76%, which can only increase by 0.2% compared with that before improvement; BLEU can only reach 92.67%, which is only 0.08% higher than that before improvement. LD (Levinstein editing distance) and TD (tree editing distance) are 3.47 and 2.56, respectively, which are 0.02 and 0.05 lower than that before improvement. When the backbone network is replaced by VGG16 with stronger feature extraction ability, the perfect matching rate between the interface tree generated by the model and the real interface tree can reach 70.28%, which is 2.52% higher than simple; BLEU reaches 93.42%, which is 0.75% higher; and LD and TD are 3.01 and 2.32, respectively, which are 0.46 and 0.24 lower than simple, respectively. When ResNet34 is used as the backbone network of image feature extraction, the performance of the model can be further improved; the perfect matching rate can reach 71.32%, which is 1.04% higher than VGG16; the BLEU reaches 93.66%, which is 0.24% higher; and the LD and TD are 2.91 and 2.11, respectively, which are 0.1 and 0.21 lower than VGG16

(2) The setting of m can greatly affect the interface tree generation effect of the improved model, when simple convolution neural network is also used as the backbone network. At the same time, set m to 10. The perfect matching rate can only reach 66.33%. When M is expanded to 20, the perfect matching rate can reach 67.76%, and other indicators are improved to varying degrees. This may be due to different sizes of M, which can obtain different prior knowledge. When $M = 10$, the prior knowledge is too little to model well, and when $M = 20$, the modeling ability of the model can be improved. Therefore, the follow-up experiments in this paper adopt $M = 20$

(3) The improved Transformer neural network translator based on prior memory self-attention proposed in this chapter can more accurately generate interface trees directly from high-fidelity UI images. In 5 K test images, 3566 (71.32%) interface images can directly generate a completely matched interface tree. Generally speaking, compared with the improved network, the generated interface tree can further improve the ability of generating interface tree, and the generated interface tree is closer to the real interface structure (BLEU reaches 93.66%, and LD and TD further decrease to 2.91 and 2.11, respectively)

In order to directly prove the advancement of the improved Transformer neural network translator based on prior memory and self-attention proposed in this chapter, we compare it with the improved Transformer neural network translator and compare it with the best UI2code model and the existing improved Transformer model in the existing research. The experimental results of greedy search are shown in Table 6.

As shown in Table 6, in all 5 K test UI images, when the improved Transformer neural network translator based on prior memory self-attention proposed in this chapter adopts the same simple convolution neural network as UI2code, compared with it, the perfect matching rate can be improved

Table 6: Comparison of greedy search results of each index of the model.

Scheme model	Perfect matching rate	BLEU	LD	TD
UI2code	60.46%	83.92%	6.8	5.57
ours-simple	67.56%	92.59%	3.49	2.61
ours-PM-simple	67.76%	92.67%	3.47	2.56
ours-ResNet34	70.44%	93.21%	3.09	2.31
ours-PM-ResNet34	71.32%	93.66%	2.91	2.11
M^2-ResNet34	70.46%	93.63%	2.93	2.16

by 7.3%. It can be improved by 8.75% on BLEU and reduced by 3.33 and 3.01 on LD and TD, respectively. On the one hand, it benefits from Transformer's powerful feature information long dependence modeling ability; on the other hand, the prior knowledge of prior memory self-attention modeling proposed in this chapter also contributes to some extent (compared with the traditional Transformer before improvement, the above four indicators have been improved to some extent). In addition, when ResNet34 is used in convolution neural network, the ability of prior memory and self-attention can be brought into full play, and 3566 (71.32%) generated interface trees can completely match the real interface trees, which is 10.86% higher than UI2code and 0.88% higher than before improvement. Compared with UI2code, BLEU has increased by 9.74% and 0.45% compared with before improvement. Compared with UI2code, LD is reduced by 3.89 and 0.18 compared with that before improvement. Compared with UI2code, TD is 3.46 lower and 0.2 lower than before improvement. Compared with UI2code and the improved model, the improved Transformer neural network translator based on prior memory and self-attention proposed in this chapter can learn the transformation knowledge from high-fidelity UI image to interface tree more fully, and the generated interface tree is closer to the real interface tree. In particular, this paper compares the improved model with the Transformer improved model M2Transformer, which performs best on MSCOCO data set at present. M2Transformer model uses self-learning mk and mv matrices to model prior knowledge. Different from this model, the learning of prior knowledge is calculated according to self-attention mechanism, and the prior knowledge of the lower layer of encoder is transmitted to all subsequent higher layers. Each layer of M2Transformer decoder does not take the output of the last layer of encoder as a context vector matrix, but takes the output of all layers of encoder as a context vector input, establishes mesh connection with each layer of decoder, and calculates their respective weight parameters. When ResNet34 is used as the backbone network, the perfect matching rate of the interface tree generated by M2Transformer can reach 70.46%. Compared with the improved network proposed in this paper, it has certain advantages, but the perfect matching rate of the improved model based on prior memory self-attention can reach 71.32%, and other indicators have been improved to varying degrees, which further proves the superiority of the improved model proposed in this paper.

At the same time, in order to further explore the interface tree generation ability of the model, the model with the best performance under the greedy search strategy will use the cluster search strategy to generate the interface tree. The specific generation effect is shown in Table 7 and Figures 12, 13, 14, and 15.

In Figures 12, 13, 14, and 15, orange represents UI2code model, blue represents Transformer-based neural network translator proposed in this paper, and red represents improved Transformer neural network translator based on prior memory self-attention proposed in this paper. The x-axis represents Beamwidth, and the y-axis displays values, which are divided into perfect match rate, BLEU, Levinstein edit distance, and tree edit distance. As shown in Figures 12 and 13, with the increase of Beamwidth, the perfect matching rate and BLEU of the improved model have a certain improvement, which is more obvious when Beamwidth = 2. As shown in Figures 14 and 15, with the increasing Beamwidth, the editing distance of the improved model has decreased to a certain extent, which indicates that the generated interface tree is more and more close to the real interface tree. Generally speaking, when Beamwidth takes different values, the improved model proposed in this chapter is better than the model before improvement and is far better than UI2code.

At the same time, it can be seen from Table 7 that the improved model proposed in this chapter can achieve the best interface tree generation effect when Beamwidth = 5, with perfect matching rate reaching 72.22%, BLEU 93.80%, LD 2.75, and TD 2.0. Compared with the improved model, under the same search conditions, the perfect matching rate increased by 1.06%, BLEU increased by 0.44%, LD decreased by 0.15, and TD decreased by 0.14. Compared with UI2code, under the same search conditions, the perfect match rate increases by 9.36%, BLEU increases by 5.49%, LD decreases by 1.97, and TD decreases by 1.46.

At the same time, it should be noted that in view of the problem of generating incomplete interface trees in the model before improvement, the prior memory self-attention proposed in this chapter effectively alleviates this situation. In 5 k test images, the number of incomplete interface trees generated by the model is shown in Figure 16, which is reduced by nearly 50% compared with UI2code and the model before improvement.

According to the above experimental results, the interface tree generation effect of improved Transformer neural network translator based on prior memory self-attention

Table 7: Comparison of cluster search results of each index of the model.

Scheme model	Beam width	Perfect matching rate	BLEU	LD	TD
UI2code	1	60.46%	83.92%	6.8	5.57
UI2code	2	61.76%	88.19%	5.07	3.81
UI2code	3	62.12%	88.25%	4.88	3.61
UI2code	4	62.52%	88.27%	4.74	3.5
UI2code	5	62.86%	88.31%	4.72	3.46
ours-ResNet34	1	70.44%	93.21%	3.09	2.31
ours-ResNet34	2	71.12%	93.34%	2.91	2.16
ours-ResNet34	3	71.14%	93.36%	2.9	2.16
ours-ResNet34	4	71.16%	93.36%	2.9	2.16
ours-ResNet34	5	71.16%	93.36%	2.9	2.14
ours-PM-ResNet34	1	71.32%	93.66%	2.91	2.11
ours-PM-ResNet34	2	71.90%	93.70%	2.79	2.01
ours-PM-ResNet34	3	72.10%	93.80%	2.76	2
ours-PM-ResNet34	4	72.22%	93.80%	2.76	2
ours-PM-ResNet34	5	72.22%	93.80%	2.75	2

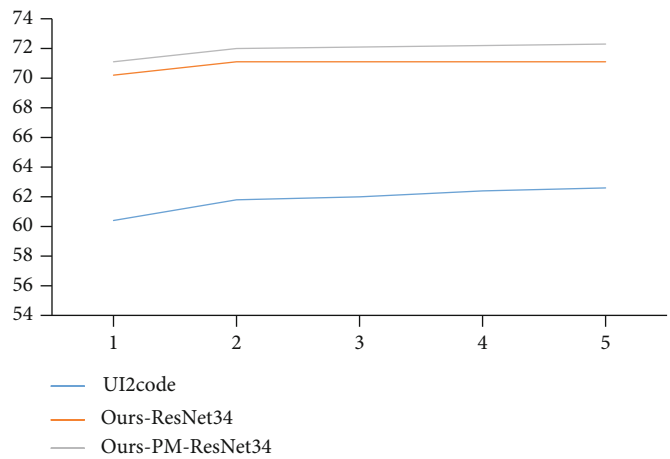

Figure 12: Comparison of cluster search results of each index in perfect matching rate model.

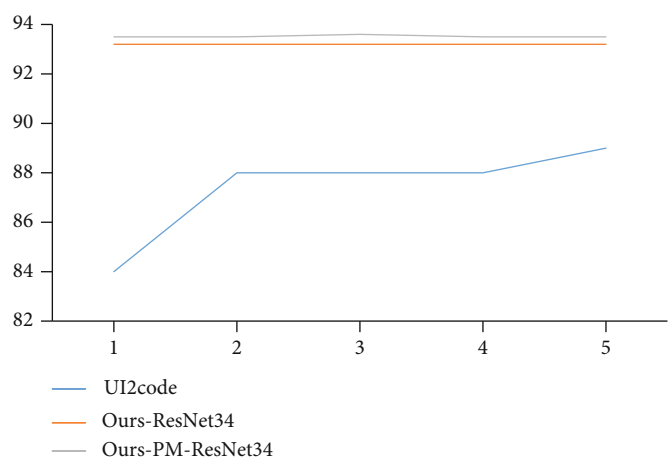

Figure 13: Comparison of cluster search results of each index in BLEU score model.

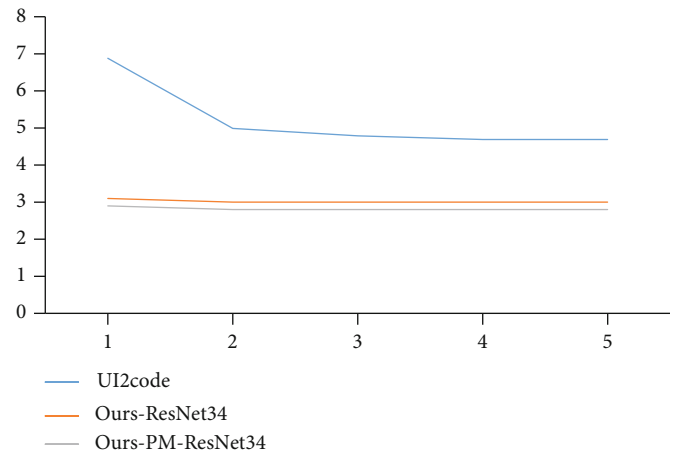

Figure 14: Comparison of cluster search results of each index in Levinstein editing distance model.

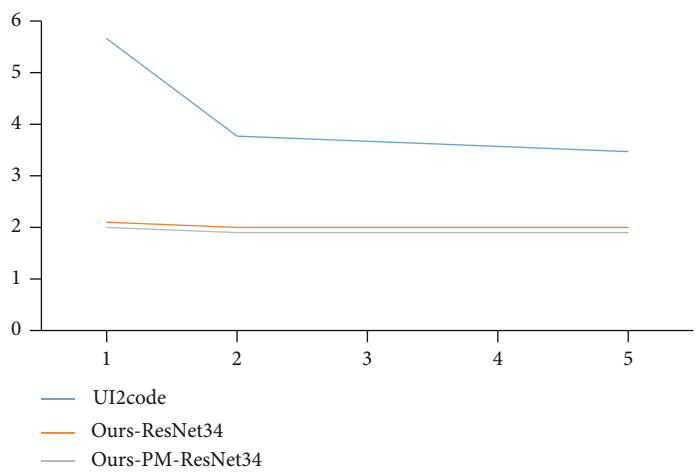

Figure 15: Comparison of cluster search results of each index in tree editing distance model.

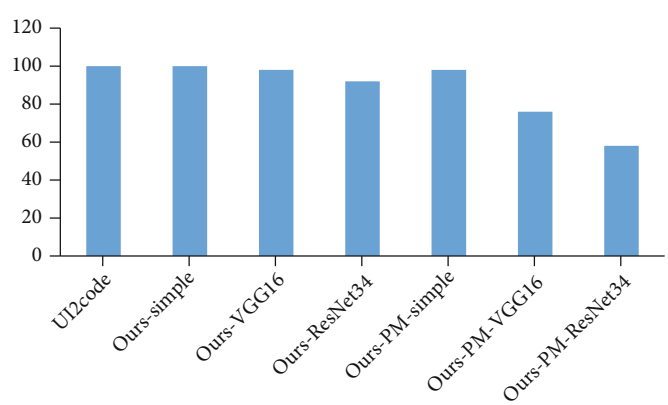

Figure 16: Number of incomplete interface trees generated by each model.

has better performance in perfect matching rate, BLEU, LD, TD and complete interface tree generation. The generated interface tree is more consistent with the real interface hierarchy, which proves that the prior memory self-attention proposed in this chapter can enhance the understanding ability of the model to the interface image features and can effectively improve the generation effect of the interface tree.

5. Conclusion

In this paper, convolutional neural network and Transformer encoder and decoder are used to generate interface tree from high-fidelity UI design image. The results show that compared with the existing research, the model proposed in this paper has significantly improved the perfect matching rate and BLEU and the average Levinstein editing distance and tree editing distance between the interface tree generated in this paper and the real interface tree are smaller. This shows that the interface tree generated by this method is more similar to the real application interface structure. But further analysis of the generated interface tree shows that at present, there are incomplete interface trees in the interface trees generated by the model (nearly 100 incomplete interface trees out of 5000), which shows that the learning ability of the model for the hierarchical structure relationship of interface trees needs to be improved. Further analysis of the proposed model shows that this is mainly caused by the characteristics of Transformer self-attention. To solve this problem, on the basis of Transformer's original self-attention mechanism, this paper puts forward the self-attention mechanism of transcendental memory. A priori knowledge is modeled by adding a memory module of continuous storage to each layer of Transformer's encoder. At the same time, the prior information of this layer is obtained by using it for attention calculation. It is transmitted to all the subsequent high level and participates in the attention calculation of the high level, which avoids that all the information in each layer of the encoder comes from a single input information source, which can enhance the understanding ability of the model to the image features and make the model better learn the hierarchical structure relationship of the interface.

Data Availability

The experimental data used to support the findings of this study are available from the corresponding author upon request.

Conflicts of Interest

The authors declared that they have no conflicts of interest regarding this work.

Acknowledgments

This work was supported by the Project of Key Scientific Research Platform of Colleges and Universities of Guangdong Province of China (Grant No. 2020CJPT006); the Project of Higher Vocational Education Computer Specialty Teaching Steering Committee of Guangdong Province of China (Grant No. JSJJZW); the special project in key fields of "artificial intelligence" in Colleges and Universities of Guangdong Provincial Department of Education—research on speaker role intelligent analysis technology of multi-person conversation speech in complex noise scene (2019KZDZX1045 and 2021015); and the Teaching Reform Research Project (Grant No. JG201954).

References

[1] N. J. Nilsson, "Artificial intelligence: a modern approach," *Applied Mechanics & Materials*, vol. 263, no. 5, pp. 2829–2833, 2003.

[2] F. Glover, "Future paths for integer programming and links to artificial intelligence," *Computers & Operations Research*, vol. 13, no. 5, pp. 533–549, 1986.

[3] A. Robinson, J. K. Eaton, and L. Eaton, "Handbook of logic in artificial intelligence and logic programming," *Oxford University Press*, vol. 2, no. 4, pp. 391–429, 1993.

[4] F. Rossi, P. V. Beek, and T. Walsh, "Handbook of constraint programming : foundations of artificial intelligence," *Elsevier Science Inc*, vol. 26, no. 19, pp. 643–691, 2006.

[5] S. Russell and P. Norvig, "Artificial intelligence: a modern approach, 3rd edition," *Applied Mechanics & Materials*, vol. 263, no. 5, pp. 2829–2833, 1995.

[6] M. Negnevitsky, "Artificial intelligence: a guide to intelligent systems," *Information & Computing Sciences*, vol. 48, no. 48, pp. 284–300, 2005.

[7] M. Minsky, "Steps toward artificial intelligence," *Proceedings of the IRE*, vol. 49, no. 1, pp. 8–30, 1961.

[8] F. Wang, "Proceedings of the national conference on artificial intelligence," *Springer Verlag*, vol. 36, no. 5, pp. 823–834, 2011.

[9] D. Li, "Artificial intelligence with uncertainty," *International Conference on Computer & Information Technology*, vol. 15, 2008.

[10] M. Dorigo, M. Birattari, and G. D. Caro, "Proceedings of the national conference on artificial intelligence," *World Scientific and Engineering Academy and Society (WSEAS)*, vol. 4, no. 3, 2007.

[11] D. M. Gabbay, C. J. Hogger, and J. A. Robinson, "Handbook of logic in artificial intelligence and logic programming. Vol. 5: logic programming," *Oxford Univ Pr*, vol. 31, no. 27, pp. 863–904, 1994.

[12] N. J. Nilsson, "Artificial intelligence: a new synthesis," *Morgan Kaufmann Publishers Inc*, vol. 9, no. 4, pp. 274–315, 1998.

[13] M. R. Genesereth and N. J. Nilsson, "Logical foundation of artificial intelligence," *Brain broad research in artificial intelligence & neuroscience*, vol. 11, no. 5, pp. 372–435, 1987.

[14] W. L. Bennett and A. Segerberg, "The logic of connective action: digital media and the personalization of contentious politics," *Perspectives on Politics*, vol. 31, no. 34, pp. 3728–3848, 2012.

[15] M. W. Rabne, J. A. Barker, and T. Alrashid, "Rights management system for digital media," *US*, vol. 8, no. 13, pp. 384–396, 1999.

[16] D. A. Wistendahl and L. K. Chong, "System for mapping hot spots in media content for interactive digital media program," *US*, vol. 8, no. 1, pp. 542–620, 1998.

[17] K. Guse, D. Levine, S. Martins et al., "Interventions using new digital media to improve adolescent sexual health: a systematic review," *Journal of Adolescent Health Official Publication of the Society for Adolescent Medicine*, vol. 51, no. 6, pp. 535–543, 2012.

[18] Z. Bilda and H. Demirkan, "An insight on designers' sketching activities in traditional versus digital media," *Design Studies*, vol. 24, no. 1, pp. 27–50, 2003.

[19] P. Howard, M. Hussain, P. N. Howard, and M. M. Hussain, "Democracy fourth wave digital media and the Arab Spring," *Systematic Botany*, vol. 31, no. 4, pp. 805–821, 2013.

[20] B. Herr-Stephenson, P. G. Lange, C. J. Pascoe, D. John, and T. Catherine, "MacArthur Foundation series on digital media and learning," *MIT Press*, vol. 7, no. 13, pp. 638–692, 2007.

[21] F. House, "Freedom on the net: a global assessment of internet and digital media," *Freedom House*, vol. 12, no. 9, pp. 261–319, 2013.

[22] C. Clar, M. Dyakova, K. Curtis et al., "Just telling and selling: current limitations in the use of digital media in public health: a scoping review," *Public Health*, vol. 128, no. 12, pp. 1066–1075, 2014.

[23] P. N. Howard, "Deep democracy, thin citizenship: the impact of digital media in political campaign strategy," *The Annals of the American Academy of Political and Social Science*, vol. 597, no. 1, pp. 153–170, 2005.

[24] M. R. Morris, A. Paepcke, and T. Winograd, "NNNNSearch: comparing techniques for co-present collaborative search of digital media," *IEEE international workshop on horizontal interactive human-computer systems*, vol. 5, no. 2, pp. 97–128, 2006.

Hindawi
Journal of Sensors
Volume 2022, Article ID 1781553, 14 pages
https://doi.org/10.1155/2022/1781553

Research Article

Effects of Variable Proportions of Concrete Fragments on Urban Soil Moisture Transport: An Experimental and Simulation Study

Changkun Yang,[1] Gengmin Jiang,[1,2] Siyu Wang,[1] Xinyu Han,[1] Jun Xu,[1] and Dongsheng Zhao[1]

[1]*College of Civil Engineering and Architecture, Nanyang Normal University, Nanyang 473061, China*
[2]*International Joint Laboratory of Watershed Ecological Security for Water Source Region of Middle Route Project of South-North Water Diversion in Henan Province, Nanyang 473061, China*

Correspondence should be addressed to Gengmin Jiang; 20131112@nynu.edu.cn

Received 18 March 2022; Accepted 28 April 2022; Published 20 May 2022

Academic Editor: Yuan Li

In order to investigate the effects of typical anthropogenic concrete fragments on moisture infiltration and evaporation in urban soils, the effects of typical anthropogenic concrete fragments on wetting peak transport distance, cumulative infiltration, cumulative evaporation, evaporation rate, and soil profile moisture at four levels (0, 5%, 10%, and 20%) were investigated by indoor soil column experiments. The results showed that the presence of concrete fragments promoted the wetting peak transport distance and cumulative infiltration, and the promotion effect increased gradually with the increase of the ratio, but there was a threshold value, and the promotion effect was least when the ratio was 20%. When the evaporation period was 35 d, concrete fragment treatment can increase the cumulative evaporation and promote the evaporation of urban soil moisture; the promotion effect increases with the increase of the proportion, but there is a threshold value; when the proportion is 20%, the promotion effect is the smallest. The evaporation rate was consistent with the different stages of evaporation process during evaporation. The concrete fragment treatment reduced the time required for moisture to reach the same depth during infiltration; the moisture coefficient of variation of the concrete fragment treatment during evaporation showed a trend of decreasing, then increasing, and then decreasing, which increased the uncertainty of moisture in the evaporation process. The model simulation results show that the models such as the power function, Kostiakov model, and Rose model fit well, and the coefficient of determination R^2 is greater than 0.99, among which the Kostiakov model fits best. The research results can provide a theoretical scientific basis for building an efficient ecological city.

1. Introduction

Urban soils are urban or suburban soils with a thickness greater than 50 cm due to mixing, landfilling, or contamination of soils under anthropogenic nonagricultural action [1]. In the process of urbanization, influenced and disturbed by human activities, urban soil is artificially excavated, carried, and mixed; a large amount of construction waste and domestic waste and other artificially invaded bodies are mixed in irregularly, directly damaging the urban soil structure and leading to a high degree of spatial heterogeneity in urban soil [2–4]. Once mechanically crushed and artificially trampled, it causes soil compaction, increases soil bulk, reduces soil pore ratio, and deteriorates aeration, which in turn affects moisture infiltration [5, 6]. At present, there are more studies on soil moisture infiltration experiments at home and abroad, and many scholars have studied the infiltration process of soil containing gravel by taking soil-stone mixed media as the research object, and a large number of research results have been obtained. For example, Zhou and Shao [7] found that within a certain infiltration calendar, the cumulative infiltration volume and the transport of wetting peaks showed a decreasing trend with the increase of gravel content and the increase of diameter. Wu et al. [8] found that the stable infiltration rate significantly decreased with increasing gravel content under the

same particle size gravel; compared to the Philip model, the Kostiakov model could better fit the variation of infiltration rate with time. Zhang et al. [9] found by horizontal infiltration experiments that the infiltration rate and infiltration coefficient k values showed a trend of increasing and then decreasing with the increase of gravel and reached the maximum value when the gravel content was 10%. Valentin and Casenave [10] found that the infiltration rate of gravel-containing soils increased with the size of the gravel, but a threshold value existed. Abrahams and Parsons [11] concluded that there is a positive correlation between infiltration and gravel content for plots not disturbed with mechanical tools and a negative correlation between infiltration and gravel content for disturbed plots. Grant and Struchtemeyer [12] pointed out by indoor runoff tests that removing gravel from the soil reduces the pore space in the soil, and infiltration performance is reduced. Previous work has focused more on the effect of natural debris such as gravel and rocks mixed into soil on moisture infiltration, focusing more on soils in agricultural fields, woodlands, and district hills; little research has been done on the effect of typical anthropogenic intrusions such as concrete fragments mixed into urban soils on moisture infiltration processes.

Soil evaporation occupies the predominant proportion for total water loss from soil and causes a serious waste of water resources. As an important part of the moisture cycle in urban ecosystems, urban soil evaporation occupies an important position in maintaining the moisture balance and energy balance of urban soils [13]. Studying the effects of typical anthropogenic intrusions such as concrete fragments on urban soil moisture evaporation can help improve the utilization of water resources and has important and far-reaching significance for the protection of ecological environment. At the present stage, many scholars have taken gravel and biochar as the research objects to study the effects of the above substances on soil moisture evaporation in depth. Coppola et al. [14] found that the presence of gravels reduces soil evaporation, mainly because they reduce the moisture retention capacity and promote the infiltration of deep moisture. Liu et al. [15] found that gravel in soil has a facilitating effect on soil moisture evaporation, but this facilitating effect is limited, and the effect of gravel on soil evaporation decreases with the extension of evaporation ephemeris and the increase of cumulative evaporation. van Wesemael et al. [16] showed that under certain rainfall conditions, soil moisture will be at a high level, and gravel in soil will form large pores with soil pore space, which changes the coherence of moisture flow in the soil and facilitates the evaporation of soil moisture. Pan et al. [17] found that embedded rock fragments increase evaporation of soil moisture, which is essentially due to the fact that the thermal conductivity of rock fragments is greater than that of soil, leading to an increase in soil temperature. Ibrahim et al. [18] applied conocarpus biochar in sandy loam soil and found that the cumulative evapotranspiration of biochar treated soil (32.2-35.5 mm) was lower than that of untreated soil (40.9 mm). Wang et al. [19] found that the addition of biochar could increase the soil moisture content, which increased from 38.0% to 41.2% with the addition of biochar from 10 g/kg to 150 g/kg under the treatment with particle size of 1-2 mm. The above studies show that admixtures such as gravel and biochar present in the soil can affect the soil moisture evaporation process by changing the pore structure of the soil, while studies on the effect of typical anthropogenic intrusions such as concrete fragments on the urban soil moisture evaporation process have always been extremely rare.

The current research on soil moisture transport mechanism is mostly focused on gravel, biochar, and other research objects, and the direction of research is also focused on agricultural land, forest land, district hills, and other types of soils. The research on the moisture transport process of urban soils by typical anthropogenic intruders such as concrete fragments is relatively rare, and the infiltration experiment process is more often considered unilaterally, lacking a comprehensive study of both infiltration and evaporation [20]. Therefore, it is important to strengthen the study on the effect of concrete fragments with different ratios on urban soil moisture transport process and its simulation. In this paper, we conducted an indoor soil column experiment to simulate the effect of concrete fragments with different ratios on urban soil moisture transport, combined with the results of field survey to simulate the real urban soil environment and explore the mechanism of the effect of concrete fragments and other anthropogenic intruders on urban soil moisture infiltration and evaporation characteristics, in order to provide a scientific basis for the construction of ecological cities.

2. Materials and Methods

2.1. Experimental Design. This experiment was conducted from September to December 2021. The experiment soil was collected from Wolong District, Nanyang City, Henan Province, China, and the soil was analyzed for soil particle size using a laser particle size analyzer (Mastersize 2000, Malvern, UK), and the results are shown in Table 1. The soil was sampled at a depth of 0-50 cm, and the soil samples were removed from large-size impurities such as man-made intruders and dead leaves of the root system, then naturally dried, milled, and sieved through a 2 mm sieve. The average initial mass moisture content of the sampled soil was 3.2%, and the main physical properties of the concrete fragments are shown in Table 2. The concrete fragments used in the experiment were collected from construction sites, crushed with a geological hammer, and screened for 3 ~ 4 cm particle size. Before the experiment, it was found through research that the concrete fragments in urban soil were concentrated in the soil depth of 20-30 cm, and a small amount existed in the soil layer of 15-20 cm and 20-25 cm. Therefore, this study combined with the actual soil conditions, the typical anthropogenic invasive body-concrete fragments as the research object, set four ratios (0, 5%, 10%, 20%), see Table 3 for details.

2.2. Experimental Device. The soil moisture infiltration and evaporation experimental device are shown in Figure 1. The infiltration experimental device consists of three parts:

Table 1: Particle size composition of the experimental soil.

Diameter	<0.002	0.002 ~ <0.05	0.05~ 2
Soil texture	Viscous particles	Powder particles	Sand grain
Mass fraction/%	7.60	53.38	39.02

soil column, marsupial, and movable base. The soil column is made of 5 mm thick Plexiglas material with an inner diameter of 20 cm and a height of 70 cm. Scale strips are attached parallel to the four directions of the soil column to observe the position of the wetting peak in centimeters with an accuracy of millimeters. Holes were made at 20, 30, 40, 50, and 60 cm of the soil column to insert soil moisture temperature sensors. The bottom of the soil column is equipped with a valve of 8 mm diameter, which aims to provide a smooth airflow environment for the infiltration experiment and avoid cyclone phenomenon during the experiment. The marsupial has an inner diameter of 20 cm and a height of 100 cm and is equipped with a valve at the bottom end, which is connected to the soil column through a plastic hose to provide a constant water head for the experiment. The moving base of the soil column is made of stainless steel with a height of 15 cm, which is easy to move and carry the column. The evaporation experimental device is mainly composed of soil column, evaporation dish, and electronic scale. The evaporation dish has an inner diameter of 20 cm and a height of 30 cm. Electronic scale range is 50 kg, and precision is 1 g.

2.3. Experimental Process

2.3.1. Infiltration Experiment Process. Before filling the soil, Vaseline was evenly applied to the inner wall of the soil column in order to weaken the influence of dominant flow at the wall. The bottom of the soil column was filled with gravel of 10 cm height as a counter-infiltration layer, and gauze (1 layer) and filter paper (1 layer) were laid flat on the gravel counter-infiltration layer in turn to avoid fine soil particles from entering the counter-infiltration layer. When filling the soil column, the depth of soil filling is 50 cm, and the thickness of soil filling is 5 cm each time, and the soil capacity is 1.4 g/cm^3, and the mass of soil filling is 2198 g per 5 cm. Only pure soil is filled at 2 cm above and below the location of soil moisture temperature sensors. The concrete fragments are mixed with soil evenly and filled according to the ratio set in the experiment. To avoid abrupt changes in structural and hydrodynamic characteristics between soil layers, interlayer brushing was required.

The infiltration experiment was carried out by the one-dimensional vertical head infiltration method. In order to reduce the atmospheric evaporation from the surface soil, the windows and other ventilation openings in the laboratory were closed and shaded during the experiment. After the start of infiltration, the soil column wetting peak transport was observed according to the principle of dense before and after infiltration, and the stopwatch was timed to observe every 1 min from 0 to 10 min, 4 min at each interval from 10 to 30 min, 6 min at each interval from 30 to 60 min, 10 min at each interval from 60 to 120 min, and 15 min at each interval from 120 to 180 min. At the same time, the readings of the marsupial were recorded, and the wetting peak and the accumulated infiltration amount were taken as the average of the readings in four directions. During the infiltration process, the sensor was set to automatically record the soil volume moisture content every 30 s, and the recording time was 240 min. When the observed wetting peak transported to 45 cm, the water supply was stopped, and the waterproof plastic film was used to seal the soil column, and the infiltration was finished.

2.3.2. Evaporation Experiment Process. The evaporation experiment soil column is the soil column after the end of the infiltration experiment. After the end of the infiltration experiment, the soil column was left to stand for 24 hours to start the evaporation experiment. At the beginning of the evaporation experiment, the soil column was moved to a suitable position, and the experiment was carried out by natural evaporation for 35 d. While the experiment was carried out, the evaporation amount of water surface was measured by using an evaporation dish with an inner diameter of 20 cm. Evaporation of soil column was measured by weighing method. Three times of data were recorded and averaged. During the experiment, the average temperature and humidity of the experiment were recorded, and the laboratory was not ventilated during the evaporation experiment. Mass of soil column was weighed by electronic scale for every 24 hours, and soil moisture evaporation was calculated and converted into evaporation amount. During evaporation, the soil moisture temperature sensor recorded the soil volumetric moisture content every 4 hours until the end of the evaporation experiment. The average daily evaporation of moisture from the water surface was 0.7966 mm/d, and the changes of temperature and humidity during the experiment are shown in Figure 2. Soil moisture evaporation (W) and evaporation rate (i) were calculated according to the following:

$$W = \frac{k(\Delta M/\rho)}{A}, \tag{1}$$

$$i = \frac{W}{\Delta t}. \tag{2}$$

In the above expression, W is the soil moisture evaporation, mm; ΔM is the mass difference of the soil column for a given time interval, g; ρ is the moisture density, 1 g/cm^3; A is the cross-sectional area of the soil column, cm^2; k is the unit conversion factor, $k = 10$ mm/cm; i is the soil moisture evaporation rate, mm/d; and Δt is the time interval, d.

2.4. Model Fitting. The trend of the wetted peak transport distance over time was described by fitting the wetted peak transport distance data through a power function relationship [21].

$$F_z = ab^t, \tag{3}$$

where F_z is the wetting peak transport distance, cm; t is the time, min; a is numerically equal to the first timing of the

Table 2: Main physical properties of concrete fragments.

Type	Saturated moisture absorption rate/%	Porosity/%	Average density/g·cm^3	Shape
Concrete fragments	6.46	13.58	2.23	Irregular block

Table 3: Proportion of concrete fragment treatments.

Soil depth/cm		Treatment			
		T0	T1	T2	T3
0 ~ 15		0%	0%	0%	0%
15~ 35	15~ 20	0%	5% × 40%	10% × 40%	20% × 40%
	20~ 25		5%	10%	20%
	25~ 30		5%	10%	20%
	30~ 35		5% × 40%	10% × 40%	20% × 40%
35~ 50		0%	0%	0%	0%

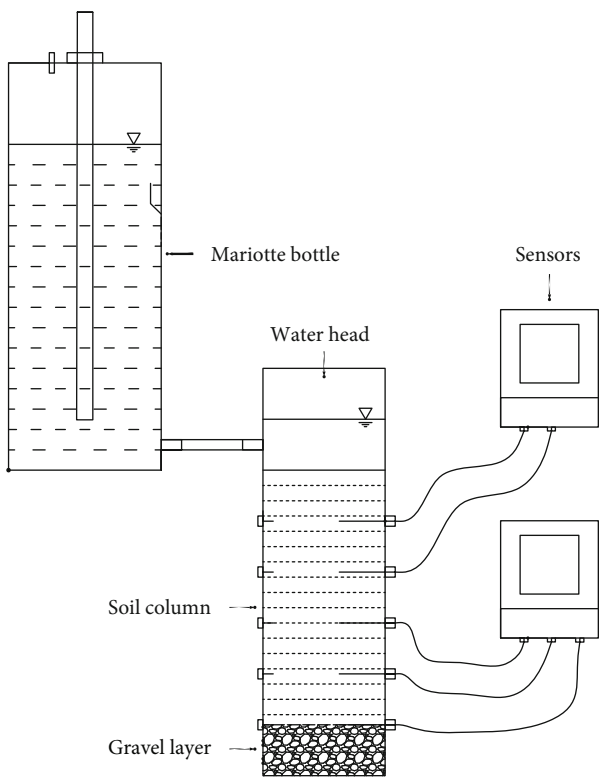

Figure 1: Schematic diagram of the experimental device.

wetting peak transport distance; and b characterizes the degree of decay of the wetting peak transport speed.

The Kostiakov model [22] was used to fit the infiltration experiment data to describe the trend of cumulative infiltration with time.

$$I = kt^{\beta}, \tag{4}$$

where I is the cumulative infiltration of soil moisture, mm; t is the infiltration time of soil moisture, min; and k and β are experimental simulation parameters with no actual physical significance.

The Rose model [23] was applied to fit the evaporation experiment data to describe the trend of cumulative evaporation with time.

$$E = ct_e^{1/2} + dt_e, \tag{5}$$

where E is the cumulative evaporation of soil moisture, mm; t_e is the number of days of soil moisture evaporation, d; c is the moisture diffusion parameter; and d is the stable evaporation parameter.

2.5. Evaluation Indicators. Indicators such as relative root mean square error (RRMSE) and Nash coefficient (NS) were used to evaluate the model fitting effect.

$$\text{RRMSE} = \frac{\sqrt{1/n \bullet \sum_{i=1}^{n} (S_i - M_e)^2}}{\overline{M_e}}, \tag{6}$$

$$\text{NS} = 1 - \frac{\sum_{i=1}^{n} (S_i - M_e)^2}{\sum_{i=1}^{n} \left(M_e - \bar{M}\right)^2}, \tag{7}$$

where n is the number of measured and simulated values, S_i is the simulated value, M_e is the measured value, and $\bar{M}$ is the average value of M_e.

A smaller RRMSE value indicates a better fit of the model, and a closer NS value to 1 indicates a more efficient simulation of the model.

2.6. Data Processing and Analysis. The experimental data in this paper were all averaged from three replicates, plotted, and function-fitted with the Origin 2021 software; the device schematic was drawn with the AutoCAD 2019 software, and Excel was used for data processing and analysis.

3. Results and Analysis

3.1. Effect of Different Proportions of Concrete Fragments on the Infiltration Characteristics of Urban Soil

3.1.1. Effect of Different Proportions of Concrete Fragments on the Transport of Wetting Peaks. Figure 3 shows the variation of the wetting peak transport distance with the infiltration time for different ratios of concrete fragments. With the extension of infiltration time, the wetting peak transport distance of different ratios of concrete fragments increased continuously, and the wetting peak curve gradually transitioned from relatively steep at the beginning of infiltration to flat. At the early stage of infiltration, the wetting peaks of different ratios of concrete fragments were basically the same, and the wetting peaks of each treatment basically overlapped. With the process of infiltration, the time required for the wetting peaks of each treatment to move to the same depth was from small to large: T2 < T1 < T3 < T0, and this

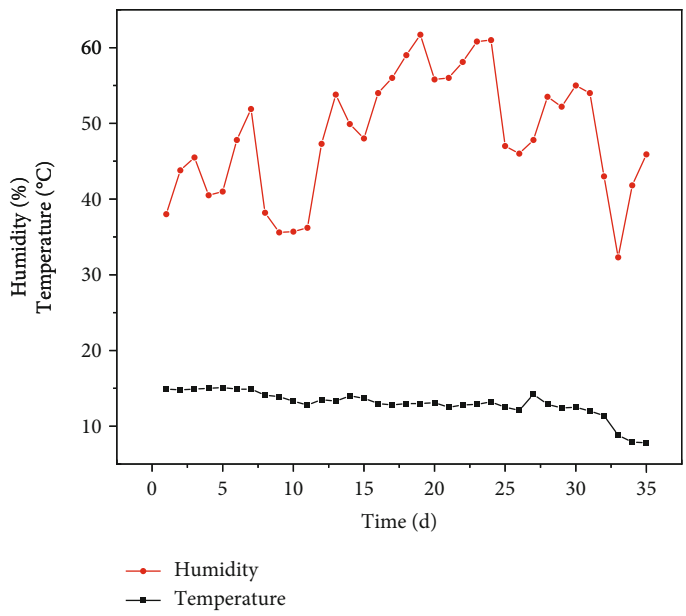

Figure 2: Temperature and humidity changes during evaporation.

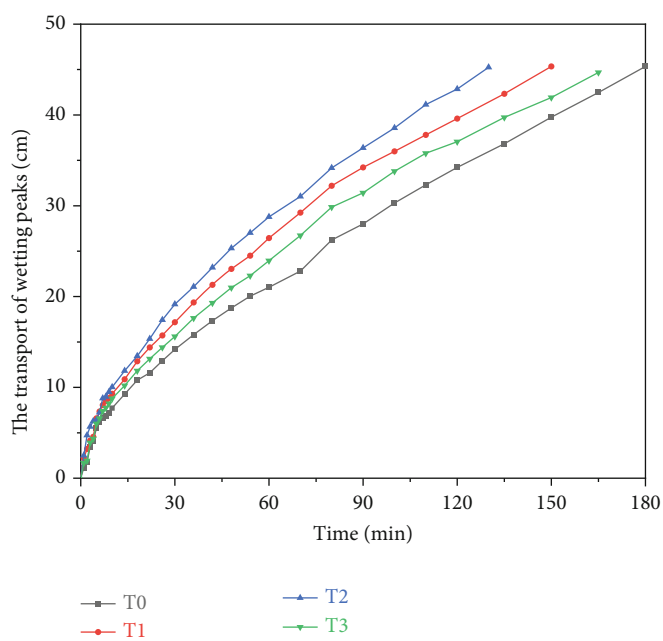

Figure 3: Variation of wetting peak transport distance with infiltration time.

difference gradually increased until the end of infiltration. From the results of each treatment, the different ratios of concrete fragments treatment had a significant effect on the wetting peak transport of urban soil. The time required to transport the wetting peak to the same depth of $h = 45$ cm was 180 min (T0), 150 min (T1), 130 min (T2), and 165 min (T3) for each treatment, and the time required to reach the same depth was 16.67% (T1), 27.78% (T2), and 8.33% (T3) lower for the concrete fragment treatment than the control treatment (T0), respectively.

The data indicate that the different proportion of concrete fragment treatment has a facilitating effect on the wetting peak transport of urban soil. The promotion effect gradually increased with the increase of the proportion, but there was a threshold value; when the proportion was 20%, its promotion effect on urban soil wetting peak transport

was less than that of the proportion 5% treatment, that is, T2 > T1 > T3.

The relationship between the wetting peak transport distance F_Z (cm) and the infiltration time t (min) for different ratios of concrete fragment treatment conforms to the power function relationship $F_Z = at^b$, and the fitting results are shown in Table 4.

As can be seen from Table 4, the fitted coefficient of determination R^2 for each concrete fragment's treatment condition is greater than 0.99 and T2 > T1 > T3 > T0, indicating that the power function equation $Fz = at^b$ can better describe the variation law of wetting peak transport distance with infiltration time for different ratios of concrete fragment treatment. With the increase of the proportion, the variation law of parameter a is T2 > T1 > T3 > T0, and parameter b shows the variation law of T2 < T1 < T3 < T0, which indicates that the decay degree of the wetting peak transport curve of different proportion of concrete fragment treatment gradually increases, and the decay law changes to T2 > T1 > T3 > T0. The variation law of RRMSE from small to large is T2 < T1 < T3 < T0, which indicates that the systematic error of the power function model simulation gradually increases and the fitting effect of the model decreases. NS shows a change of T2 > T1 > T3 > T0 and gradually approaches to 1, which indicates that the fitting efficiency of the model simulation increases.

3.1.2. Effect of Different Proportions of Concrete Fragments on the Cumulative Infiltration Volume. Figure 4 reflects the cumulative infiltration process of soil under different ratios of concrete fragments. It can be seen from Figure 4 that the cumulative infiltration rate of urban soil treated with different ratios of concrete fragments increases with time, and the curve of cumulative infiltration rate gradually slows down from steep at the beginning of infiltration, and different ratios of concrete fragments have obvious effects on the cumulative infiltration rate. At 120 min, the cumulative infiltration rate of different ratios of concrete fragments was basically stable at 120 min, and the cumulative infiltration volume at that time was chosen to measure the infiltration capacity of the soil before stable infiltration. The cumulative infiltration volume of the treatment increased by 19.66% (T1), 29.06% (T2), and 13.68% (T3) compared to the control treatment (T0). Further analysis of Figure 3 shows that the cumulative infiltration volume of different ratios of concrete fragment treatment in the same infiltration calendar time from the beginning to the end of infiltration was T2 > T1 > T3 > T0.

The data indicate that the infiltration capacity of urban soils was enhanced to some extent by different proportions of concrete fragment treatment. With the increase of the proportion, the enhancement of the infiltration capacity of each treatment gradually increased, but like the promotion of the wetting peak transport distance, there is a threshold value; when the proportion is 20%, its enhancement of the infiltration capacity of urban soil is the smallest, that is, T2 > T1 > T3.

The cumulative infiltration volume I (mm) and infiltration time t (min) between the concrete fragment treatment with different ratios fit the Kostiakov infiltration model, and the fitting results are shown in Table 5.

Table 4: Fitting results of wetting peak transport distance and infiltration time.

Treatment	a	b	R^2	RRMSE	NS
T0	1.6286	0.6362	0.9976	0.0343	0.9977
T1	2.3497	0.5913	0.9991	0.0199	0.9991
T2	2.5995	0.5862	0.9992	0.0175	0.9993
T3	2.0658	0.6030	0.9986	0.0253	0.9986

As can be seen from Table 5, the coefficient of determination R^2 fitted under each concrete fragment's treatment condition is greater than 0.99. The results indicate that the Kostiakov model has a better simulation of the cumulative infiltration amount in the process of soil moisture infiltration. With the increase of the ratio, the parameter k showed the variation law of T2 > T1 > T3 > T0, and the variation law of the parameter β was T2 < T1 < T3 < T0, which was basically consistent with the variation law of the parameters a and b of the fitting results of the wetting peak transport distance and infiltration time. The RRMSE gradually increases with the increase of the ration, which shows that T2 < T1 < T3 < T0, where the T2 treatment. The simulation error of the Kostiakov model for T2 treatment is the smallest, and the simulation effect was the best. The NS value of each treatment decreases with the increase of the proportion and gradually moves away from 1, which is T2 > T1 > T3 > T0, among which the Kostiakov model simulation of T0 treatment has the lowest fitting efficiency.

3.2. Effect of Different Proportions of Concrete Fragments on Evaporation Characteristics of Urban Soils

3.2.1. Effect of Different Proportions of Concrete Fragments on the Cumulative Evaporation Volume. Figure 5 shows the cumulative evaporation curves under different ratios of concrete fragment treatment during the evaporation experiment. From Figure 5, it can be seen that the cumulative evaporation gradually increased with the increase in the proportion of concrete debris during the experiment. At the end of the evaporation experiment, the cumulative evaporation increased by 4.65% (T1), 6.20% (T2), and 1.72% (T3) for the concrete fragment treatment compared with the control treatment (T0). At the early stage of the experiment (0-10 d), the cumulative evaporation of each treatment was relatively close to each other with no obvious pattern. Among them, the accumulated evapotranspiration was the largest in T1 treatment and the smallest in T3 treatment. In the middle of the experiment (11~ 24 d), evaporation entered the transition period, and the differences between T0 and T3 and T1 and T2 treatments decreased, and the corresponding curves gradually approached, and the differences between these two groups gradually increased with evaporation calendar time until the end of the experiment. At the later stage of the experiment (25~ 35 d), with the evaporation process, the cumulative evaporation curves of different proportions of concrete fragment treatments gradually showed certain

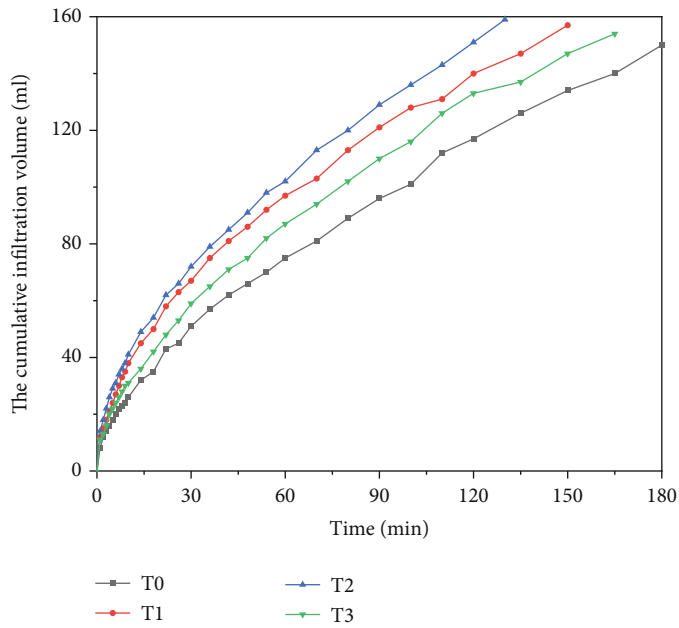

Figure 4: Variation of cumulative infiltration volume with infiltration time.

Table 5: Fitting results of cumulative infiltration volume and infiltration time.

Treatment	k	β	R^2	RRMSE	NS
T0	6.4002	0.6052	0.9988	0.0230	0.9989
T1	10.9456	0.5317	0.9993	0.0161	0.9993
T2	11.9468	0.5285	0.9995	0.0137	0.9995
T3	8.3511	0.5725	0.9991	0.0194	0.9991

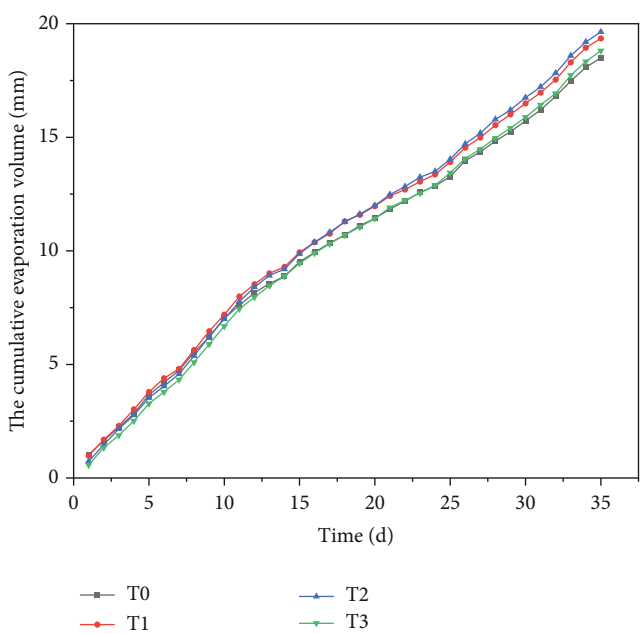

Figure 5: Variation of cumulative evaporation with evaporation calendar time.

differences, from large to small as T2 > T1 > T3 > T0, and the differences between the treatments gradually increased. In summary, the presence of concrete debris can increase the cumulative evaporation of urban soil when the evaporation period is longer, and to a certain extent, it can promote the evaporation of urban soil, but this promotion effect is limited by the ratio, and the cumulative evaporation of higher ratio treatment (T3) is smaller.

The accumulated evaporation volume E (mm) and evaporation time te (d) for different ratios of concrete fragment treatment conditions can be fitted between the Rose evaporation model, and the fitting results are shown in Table 6.

As can be seen from Table 6, the fitted coefficient of determination R^2 for each concrete fragment's treatment condition is greater than 0.99, indicating that the Rose model has a good simulation of the evaporation process of urban soil under different ratios of concrete fragment treatment conditions. The parameters c and d did not show a significant pattern with increasing proportion. The RRMSE of each treatment gradually increased with the increase of proportioning and was at a high level; among them, the RRMSE value corresponding to the T0 treatment was the smallest, and the error was the smallest. The NS value decreased with the increase of proportioning and showed that T2 > T1 > T 3 > T0; among them, the NS value corresponding to the T2 treatment was the largest; that is, the Rose model simulation of the T2 treatment had the highest fitting efficiency.

3.2.2. Effect of Different Proportions of Concrete Fragments on Evaporation Rate. Figure 6 shows the changes of evaporation rate of urban soil moisture during evaporation experiment for different ratios of concrete fragment treatment. From Figure 6, it can be seen that the soil moisture evaporation rate transitioned from the fluctuating change in the early stage to the deceleration rate stage and finally tended

Table 6: Fitting results of cumulative evaporation and evaporation time.

Treatment	c	d	R^2	RRMSE	NS
T0	0.9696	0.3548	0.9956	0.0314	0.9957
T1	0.9837	0.3769	0.9953	0.0328	0.9954
T2	0.7930	0.4201	0.9954	0.0334	0.9955
T3	0.7226	0.4069	0.9945	0.0368	0.9947

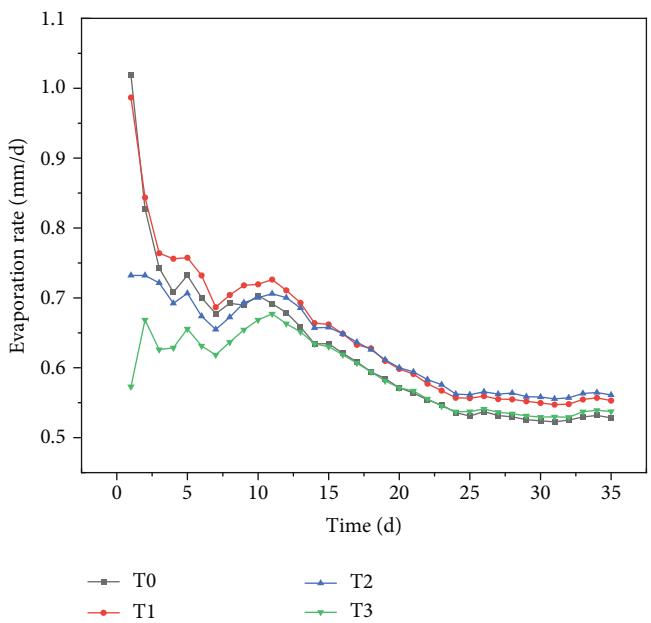

Figure 6: Variation of evaporation rate with evaporation calendar time.

to a stable state; this is more consistent with the three stages of change law of constant evaporation, evaporation decay, and evaporation stagnation of the soil evaporation process. At the early stage of the experiment (0 ~ 10 d), the temperature and humidity environment around the soil column dominated, and after the end of infiltration, the higher level of soil volumetric moisture content provided sufficient moisture and diffused to the air, and the evaporation rate was in a fluctuating undulating state with large evaporation rate. In the middle of the experiment (11 ~ 24 d), as the moisture in the soil is continuously consumed by evaporation, the volumetric moisture content of the soil gradually decreases, and it is necessary to obtain the moisture required for evaporation from the deeper soil, and the influence of the concrete fragments in the soil begins to present, at which time the evaporation rate gradually decreases with the evaporation calendar, and evaporation enters the decay process. Later in the experiment (25 ~ 35 d), as evaporation proceeds, the surface of the soil becomes very dry, and the moisture available in the soil for evaporation becomes less and less, and the evaporation process transitions from the decay stage to the stagnation stage, when the actual evaporation is small, and the evaporation rate is in a stable state with low evaporation rate. The evaporation rate change process in the late stage of the experiment indicates to a certain extent that the evaporation rate promotion effect of concrete fragments on urban soil is limited. The average evaporation rates for different ratios of concrete crushed block treatments at the later stage of the experiment were 0.5288 mm/d (T0), 0.5534 mm/d (T1), 0.5611 mm/d (T2), and 0.5348 mm/d (T3), respectively, with lower evaporation rates, indicating that the effect of concrete crushed block on evaporation from urban soils is less when the evaporation epoch is longer or the cumulative evaporation is larger.

3.3. Effect of Different Ratios of Crushed Concrete on Moisture in Urban Soil Profiles. The infiltration and evaporation characteristics of urban soil moisture changed significantly under different ratios of concrete fragment treatment conditions, and the urban soil moisture distribution under each treatment also showed significant differences as a result. Figures 7–11 reflect the variation curves of volumetric moisture content of soil at different depths with infiltration time during the infiltration experiment. Figure 12 reflects the variation process of the coefficient of variation corresponding to different depths of soil with soil depth during the evaporation experiment.

From Figures 7–11, it can be seen that with the increase of infiltration time, the volumetric moisture content of each layer in each treatment column showed a sudden increase followed by a steady trend from top to bottom. The moment of the sudden increase is basically the same as the moment of the wetting peak. Further analysis showed that the time required for the volumetric moisture content to reach the same depth of the soil to show a sudden increase followed by a steady change was different for the treatments with different proportions of concrete fragments, which were T2 < T1 < T3 < T0, and the difference increased with the increase of infiltration time. In other words, the infiltration time of moisture reaching the same depth of soil was different among treatments, from fast to slow, as T2, T1, T3, and T0, and the difference between treatments gradually became larger as infiltration proceeded. The above phenomenon, to a certain extent, reflects that the moisture infiltration of urban soil is promoted by different ratios of concrete fragment treatment, which is basically consistent with the effect of different ratios of concrete fragment treatment on the transport of wetting peak and cumulative infiltration of urban soil as described above.

Table 7 shows the coefficients of variation of soil moisture at different depths during evaporation. From the table, it can be seen that the mean volumetric moisture content of urban soils with different ratios of concrete fragment treatment did not vary significantly with soil depth during the evaporation experiment. The maximum mean moisture content of all treatments was at the soil depth of 40-50 cm, with the maximum mean moisture content in treatment T3 and the minimum in treatment T1. The coefficient of variation reflects the degree of dispersion of volumetric moisture content, with CV ≤ 10% being weak variation, 10 % < CV < 100% being moderate variation, and CV ≥ 100% being strong variation [24]. The coefficient of variation

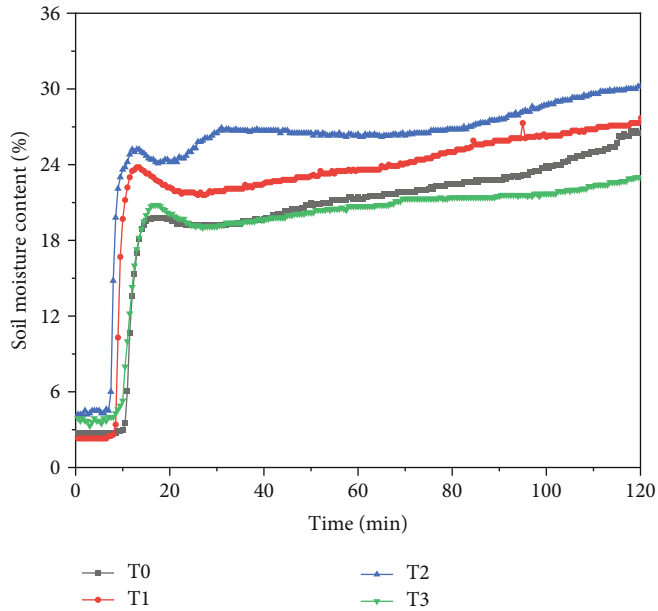

Figure 7: Variation of volumetric moisture content of 0 ~ 10 cm soil layer with infiltration time.

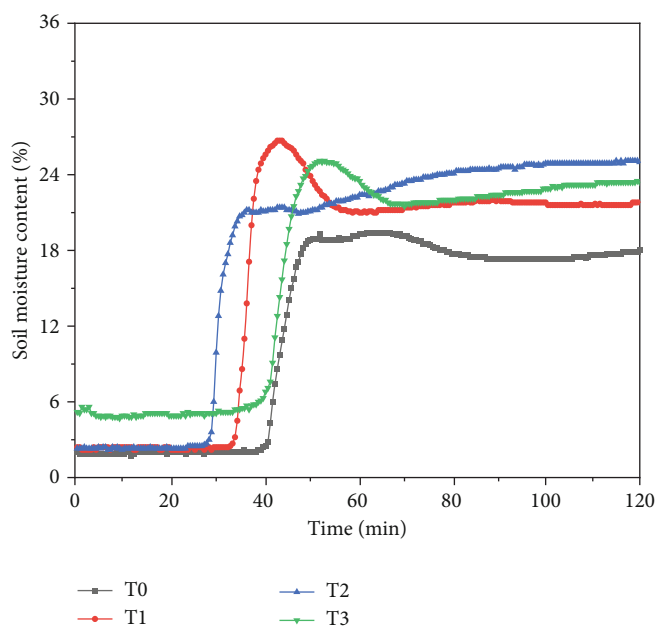

Figure 8: Variation of volumetric moisture content of 10-20 cm soil layer with infiltration time.

(CV) of the moisture content at each soil depth for the different ratios of concrete fragment treatments was less than 10%, which is weak variation. The variation of the coefficient of variation with soil depth was different for each treatment; the coefficient of variation of the control treatment increased with increasing soil depth, while the coefficient of variation of the concrete fragment treatment showed a decrease, then an increase, and then a decrease with increasing soil depth, and the variation process is shown in Table 7. The variation of the coefficient of variation with soil depth for the T1, T2, and T3 treatments indicates to some extent that the presence of concrete fragments changed the variability of the vertical distribution of urban soil moisture. The variability of the vertical distribution of soil moisture in T1, T2, and T3 treatments with soil depth indicates to some extent that the presence of concrete fragments changes the variability of the vertical distribution of soil moisture in the city.

4. Discussion

The presence of rock fragments changes the physical properties of the soil such as porosity, bulkiness, and curvature, thus having a profound effect on the infiltration of soil moisture [25]. In this study, it was found that both the wetting

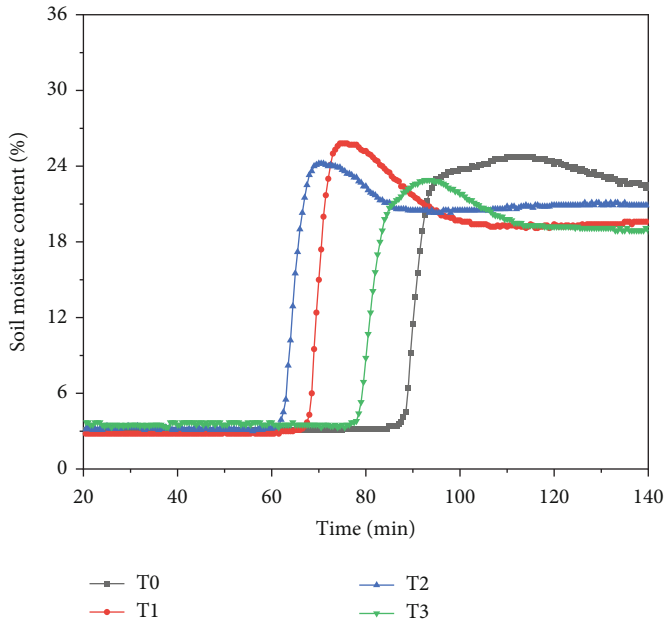

Figure 9: Variation of volumetric moisture content of 20-30 cm soil layer with infiltration time.

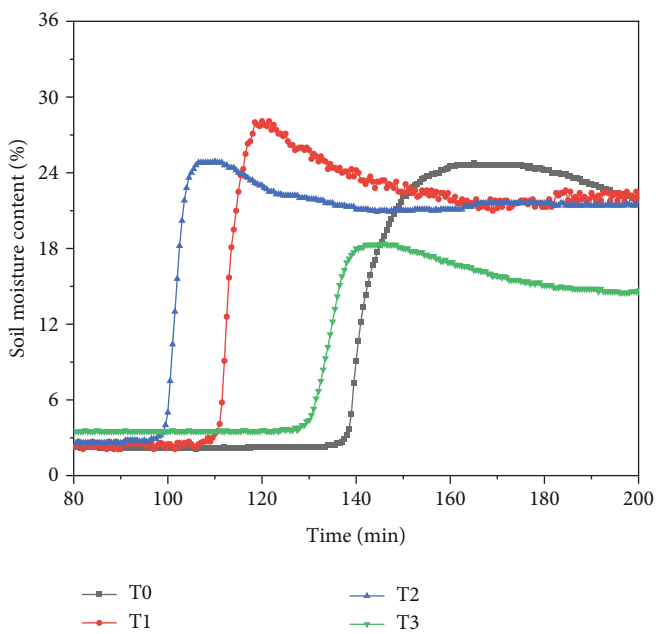

Figure 10: Variation of volumetric moisture content of 30-40 cm soil layer with infiltration time.

peak curve and the cumulative infiltration curve of urban soil moisture infiltration process showed a trend of steep and then flat change. The main reason is that at the beginning of infiltration, the soil surface layer quickly enters into saturation, and the lower soil layer, which is at a lower initial moisture content, produces a large suction gradient with the saturated soil layer, which in turn accelerates moisture conduction and results in a larger infiltration rate, and as infiltration proceeds, the suction gradient gradually decreases, the infiltration rate decreases, and the infiltration curve transitions from steep at the beginning to smooth [9, 26]. Like gravel fragments, the presence of concrete fragments changes the physical properties of urban soils and affects urban soil moisture channels, which in turn has an impact on urban soil moisture infiltration processes. In this study, the presence of concrete fragments promoted urban soil moisture infiltration, and with the increase of the ratio, its contribution to the wetting peak transport distance and cumulative infiltration increased gradually, but there was a threshold value, and when the ratio was 20%, its contribution was lower than that of the 5% treatment, and the contribution effect was minimal. The main reason for this may be

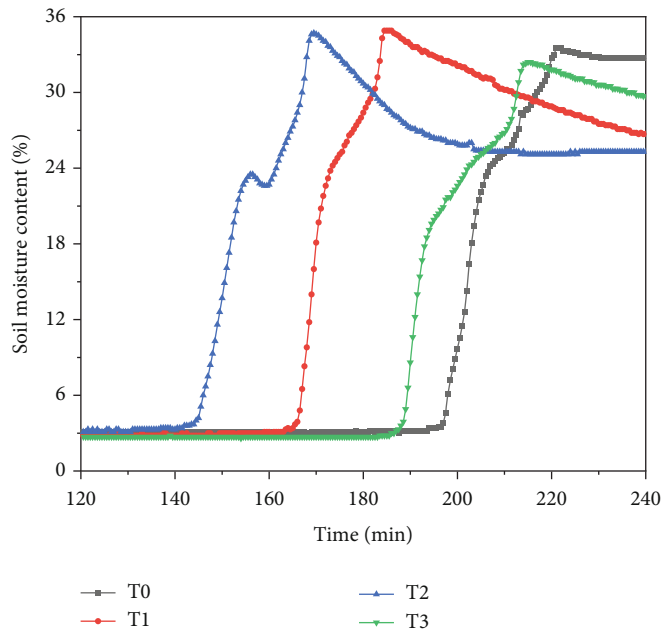

Figure 11: Variation of volumetric moisture content of 40-50 cm soil layer with infiltration time.

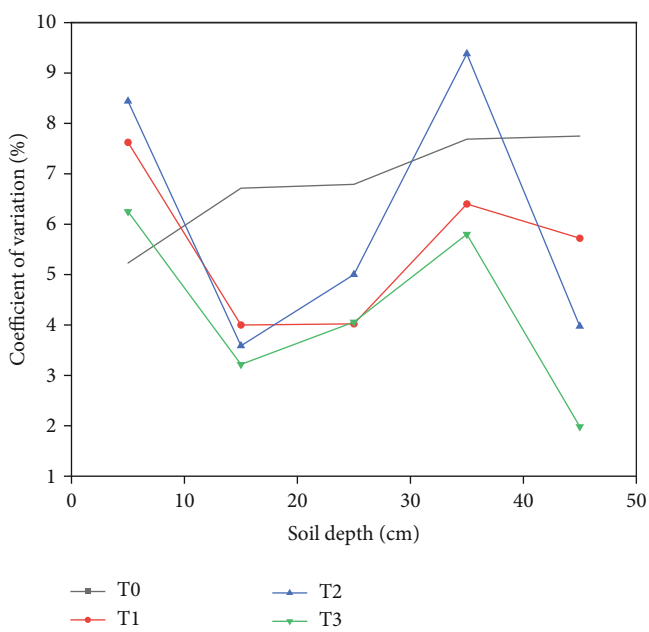

Figure 12: Variation of coefficient of moisture variation with soil depth.

that with the increase of concrete fragments in urban soils, the number of macropores in the soil increases, and the effective pore space decreases instead, and the soil moisture channels become more complex. A sufficient number of macropores will produce a dominant flow phenomenon and promote moisture infiltration; at the same time, the decrease of effective pores and the increase of moisture curvature due to complex moisture channels will have a hindering effect on moisture infiltration. When the former effect is greater than the latter, it will promote moisture infiltration, and vice versa, it will hinder moisture infiltration [27]. The results of this experiment show that the promoting effect of dominant flow dominates; it is worth mentioning that this promoting effect does not increase all the time with the increase of concrete fragment ratio, and there exists a threshold value; when the level of concrete fragment ratio is higher, the promoting effect is weakened, and this is the reason why the promoting effect of the ratio 20% concrete fragment treatment on the wetting peak transport and cumulative infiltration is the least.

In this study, it was found that the cumulative evaporation increased with the increase of concrete fragment ratio during the evaporation experiment, and the evaporation rate of urban soil was in accordance with the law of soil evaporation phase change. The reasons for this include, in addition to the change in soil texture by the concrete fragments, the effects arising from the difference in moisture content at different periods during the evaporation experiment. At the early stage of the experiment, due to the high moisture content of the surface soil, the pores are filled with free moisture, and the surface of the soil column can be approximated as the free moisture surface or evaporation surface, and the accumulated evaporation is basically the same during this period; at this time, the evaporation rate is only limited by the meteorological conditions and influenced by the temperature and humidity of the experiment, and the evaporation rate is in a fluctuating state. As evaporation continues, the moisture in the soil is gradually consumed, and after the moisture content decreases to a certain critical value, the soil changes from saturated to unsaturated state, and the suction force of the soil is rapidly increased by the small change in moisture content, resulting in a rapid decrease in the vapor pressure on the surface of the soil, a decrease in the moisture difference of the evaporation surface, a weakening of the ability to drive the upward migration of moisture, and a

Table 7: Coefficients of variation of soil moisture at different depths during evaporation.

Treatment	Soil depth/cm	Mean/%	Standard deviation/%	Maximum value/%	Minimal value/%	Coefficient of variation/%
	0 ~ 10	14.87	0.78	17.60	13.10	5.23%
	10~ 20	14.96	1.00	17.60	13.30	6.71%
T0	20~ 30	19.23	1.31	21.40	16.60	6.79%
	30~ 40	17.35	1.33	20.90	15.20	7.69%
	40~ 50	26.83	2.08	30.00	22.40	7.75%
	0 ~ 10	11.06	0.84	13.40	9.50	7.62%
	10~ 20	15.65	0.63	16.80	14.20	4.00%
T1	20~ 30	18.04	0.73	19.70	16.20	4.02%
	30~ 40	20.98	1.34	24.00	17.90	6.40%
	40~ 50	25.74	1.47	27.40	21.70	5.72%
	0 ~ 10	16.70	1.41	19.80	13.80	8.44%
	10~ 20	15.82	0.57	17.50	14.30	3.59%
T2	20~ 30	17.78	0.89	19.40	15.70	5.00%
	30~ 40	19.09	1.79	23.10	16.50	9.38%
	40~ 50	26.84	1.07	28.50	24.70	3.98%
	0 ~ 10	10.13	0.63	11.80	9.00	6.25%
	10~ 20	17.29	0.56	18.30	15.60	3.22%
T3	20~ 30	17.30	0.70	19.10	15.40	4.06%
	30~ 40	15.75	0.91	18.70	13.40	5.80%
	40~ 50	28.09	0.56	29.00	26.20	1.98%

gradual transition of the evaporation rate to the decay stage [28]; the presence of the concrete fragments present in the urban soil starts to become the main factor, and the accumulated evaporation rate at this time also varies somewhat depending on the concrete fragment ratio. In this study, it was also found that the presence of concrete fragments increased the cumulative evaporation and promoted evaporation from urban soils when the evaporation period was long enough, but the effect of this promotion was limited by the ratio, and the evaporation rate was also at a low state. The reason for this is that at the later stage of the experiment, the surface of the soil becomes very dry, the soil can supply less and less moisture for evaporation, the evaporation of moisture gradually changes from liquid water-based to moisture vapor diffusion-based, evaporation enters a stagnant stage, the evaporation rate is basically in a stable state at a lower level, and the accumulated evaporation maintains the difference in the middle of the experiment under the influence of the concrete crushed block ratio until the end of the evaporation experiment [28]. In addition, concrete fragments have a porous structure and have certain pores themselves, and during the experiment, concrete fragments with pores served as a medium to connect the soil above and below the concrete fragments, which shortened the moisture channel to some extent. This is also one of the reasons to promote the evaporation of moisture from urban soil.

In this study, it was found that different ratios of concrete fragment treatment changed the profile moisture of urban soil during infiltration and evaporation. During infiltration, as the proportion of concrete fragments increased, it took less time for moisture to infiltrate to the same depth, increasing the rate of moisture infiltration, mainly due to the promotion of dominant flow, but when the proportion reached 20%, the promotion of dominant flow was significantly weakened. During evaporation, the coefficient of variation of moisture in the control treatment tended to increase with the increase in the ratio of concrete fragments, while the coefficients of variation in the other treatments showed a decrease, then an increase, and then a decrease, indicating that concrete fragments changed the vertical spatial variability of urban soil moisture during evaporation. This is because the presence of concrete fragments changed the original textural homogeneity of the urban soil, resulting in the deformation of the natural structure of the urban soil, the reduction of the volume of pores located between the agglomerates of soil particles, and the alteration of soil permeability, which increased the uncertainty of moisture movement in the urban soil containing concrete fragments treated with concrete fragments, and in this study, the moisture movement of the urban soil treated with concrete fragments was faster than that of the control treatment. In this study, the moisture movement of the urban soil treated with concrete chips was faster than that of the control treatment, and the moisture content of the soil layer where the concrete chips were located decreased instead, and the coefficient of variation decreased, then increased, and then decreased. In contrast, the urban soil in the control treatment was homogeneous in texture, and its moisture content increased with the depth of the urban soil, and its coefficient of variation showed an increasing trend.

As with natural gravel, moisture transport in urban soils containing concrete fragments is an extremely complex process. In this study, the effect of four ratios of concrete

fragments on moisture transport in urban soils was initially investigated based on indoor soil column simulations. The moisture transport process of various anthropogenic intruders remaining in the urban soil is also affected by other factors such as plants and meteorology and is a complex multi-interface process. Therefore, it is necessary to conduct further experiments on anthropogenic intruders to investigate the moisture movement characteristics of urban soil under different types, ratios, and particle sizes of anthropogenic intruders and to elucidate the influence of anthropogenic intruders on urban soil moisture transport in depth.

5. Conclusions

The presence of concrete fragments all contributed to urban soil moisture infiltration. The promotion effect of concrete fragment treatment on wetting peak transport and cumulative infiltration was increased with increasing ratio, but there was a threshold value, and the promotion effect was minimized at 20% ratio.

The presence of concrete fragments can promote evaporation of urban soil moisture. When the evaporation period is long enough, the concrete fragment treatment can increase the accumulated evaporation and promote the evaporation of urban soil moisture to some extent; the promotion effect increases with the increase of the ratio, but there is a threshold value; when the ratio is 20%, the promotion effect is the smallest. The evaporation rate of urban soil during evaporation was in accordance with the soil moisture evaporation pattern at different stages.

The presence of concrete fragments affects the urban soil profile moisture and reduces the time required for moisture to reach the same depth during urban soil infiltration. During evaporation, the coefficient of variation of moisture in the concrete fragment's treatment showed a variation pattern of decreasing, then increasing, and then decreasing, increasing the uncertainty of moisture transport in urban soils.

Data Availability

The data presented in this study are available on request from the corresponding author.

Conflicts of Interest

The authors declare no conflict of interest.

Acknowledgments

This research was financially supported by the Key Research and Development Project of Henan Province (Project No. 182102310838), the Doctoral Research of Nanyang Normal University (Project No. ZX2014083), the laboratory-based open project of Nanyang Normal University (Project No. SYKF2021073), and the industry-university cooperation collaborative education project of the Department of higher education of the Ministry of Education (Project No. 202101354024).

References

[1] J. G. Bockheim, "Nature and properties of highly disturbed urban soils. Philadelphia, Pennsylvania," *Div. S-5, Soil Science Society of America, Chicago, Illinois*, 1974.

[2] H. Meuser, *Contaminated Urban Soils*, Springer Science & Business Media, Berlin, Germany, 2010.

[3] P. J. Craul, "A description of urban soils and their desired characteristics," *Journal of Arboriculture*, vol. 11, no. 11, pp. 330–339, 1985.

[4] J. Zhang and Q. Xu, "Formation characteristics of urban soils and their protection," *The Soil*, vol. 4, pp. 189–193, 1997.

[5] T. Xie, Y. Hou, W. P. Chen, M. E. Wang, S. T. Lv, and X. Z. Li, "Impact of urbanization on the soil ecological environment," *Acta Ecologica Sinica*, vol. 39, no. 4, pp. 1154–1164, 2019.

[6] A. Lehmann and K. Stahr, "Nature and significance of anthropogenic urban soils," *Journal of Soils Sediments*, vol. 7, no. 4, pp. 247–260, 2007.

[7] B. Zhou and M. Shao, "Effect of content and size of rock detritus on infiltration," *Acta Pedologica Sinica*, vol. 44, no. 5, pp. 801–807, 2007.

[8] X. Wu, Z. Meng, X. Dang, and J. Wang, "Effects of rock fragments on the water infiltration and hydraulic conductivity in the soils of the desert steppes of Inner Mongolia, China," *China. Soil and Water Research*, vol. 16, no. 3, pp. 151–163, 2021.

[9] W. Zhang, C. Wei, Y. Li, G. Wang, and D. Xie, "Effects of rock fragments on infiltration and evaporation in hilly purple soils of Sichuan Basin, China," *China. Environmental Earth Sciences*, vol. 62, no. 8, pp. 1655–1665, 2011.

[10] C. Valentin and A. Casenave, "Infiltration into sealed soils as influenced by gravel cover," *Soil Science Society of America Journal*, vol. 56, no. 6, pp. 1667–1673, 1992.

[11] A. D. Abrahams and A. J. Parsons, "Relation between infiltration and stone cover on a semiarid hillslope, southern Arizona," *Journal of Hydrology*, vol. 122, no. 1-4, pp. 49–59, 1991.

[12] W. J. Grant and R. A. Struchtemeyer, "Influence of the coarse fraction in two Maine potato soils on infiltration, runoff and erosion," *Soil Science Society of America Journal*, vol. 23, no. 5, pp. 391–394, 1959.

[13] F. Wu, J. Zhan, and İ. Güneralp, "Present and future of urban water balance in the rapidly urbanizing Heihe River Basin, Northwest China," *Northwest China. Ecological Modelling*, vol. 318, pp. 254–264, 2015.

[14] A. Coppola, G. Dragonetti, A. Comegna et al., "Measuring and modeling water content in stony soils," *Soil and Tillage Research*, vol. 128, pp. 9–22, 2013.

[15] D. Liu, L. Fei, K. Hao, N. Zhou, and Z. Feng, "Study on water evaporation characteristics of red soil and stony medium," *Ground Water*, vol. 43, no. 3, pp. 119–121, 2021.

[16] B. van Wesemael, J. Poesen, C. S. Kosmas, N. G. Danalatos, and J. Nachtergaele, "Evaporation from cultivated soils containing rock fragments," *Journal of Hydrology*, vol. 182, no. 1-4, pp. 65–82, 1996.

[17] Y. Pan, S. Lyu, S. Li et al., "Simulating the role of gravel in freeze–thaw process on the Qinghai–Tibet Plateau," *Theoretical and Applied Climatology*, vol. 127, no. 3-4, pp. 1011–1022, 2017.

[18] A. Ibrahim, A. R. A. Usman, M. I. Al-Wabel, M. Nadeem, Y. S. Ok, and A. Al-Omran, "Effects of conocarpus biochar on hydraulic properties of calcareous sandy soil: influence of

particle size and application depth," *Archives of Agronomy and Soil Science*, vol. 63, no. 2, pp. 185–197, 2017.

[19] T. Wang, C. E. Stewart, C. Sun, Y. Wang, and J. Zheng, "Effects of biochar addition on evaporation in the five typical Loess Plateau soils," *Catena*, vol. 162, pp. 29–39, 2018.

[20] Z. Fang, J. Du, S. Zhang et al., "Influence of anthropogenic intrusions on the soil infiltration characteristics in urban green land," *Journal of Soil and Water Conservation*, vol. 34, no. 4, pp. 124–130, 2020.

[21] W. Niu, X. Zou, J. Liu, M. Zhang, W. Lü, and J. Gu, "Effects of residual plastic film mixed in soil on water infiltration, evaporation and its uncertainty analysis," *Transactions of the Chinese Society of Agricultural Engineering*, vol. 32, no. 14, pp. 110–119, 2016.

[22] A. N. Kostiakov, "On the dynamics of the coefficient of water percolation in soils and the necessity of studying it from the dynamic point of view for the purposes of amelioration," *Trans. Sixth Comm. Int. Soc. Soil Sci.*, vol. 1, pp. 7–21, 1932.

[23] C. W. Rose, G. F. Byrne, and J. E. Begg, "Accurate hydraulic lysimeter with remote weight recording," *Division of Land Research technical paper*, 1966.

[24] C. A. Cambardella, T. B. Moorman, J. M. Novak et al., "Field-scale variability of soil properties in central Iowa soils," *Soil Science Society of America Journal*, vol. 58, no. 5, pp. 1501–1511, 1994.

[25] X. Lai, Q. Zhu, M. J. Castellano, and K. Liao, "Soil rock fragments: unquantified players in terrestrial carbon and nitrogen cycles," *Geoderma*, vol. 406, article 115530, 2022.

[26] Z. Li, Y. Liu, and Q. Yang, "Review on effects mechanism of soil water infiltration," *Journal of Irrigation and Drainage*, vol. 30, no. 5, pp. 124–130, 2011.

[27] B. Q. Ouyang, C. S. Tang, D. Y. Wang, S. K. Xu, and B. Shi, "Advances on soil moisture evaporation," *Rock and Soil Mechanics*, vol. 37, no. 3, pp. 625–636, 2016.

[28] A. Ilek, J. Kucza, and W. Witek, "Using undisturbed soil samples to study how rock fragments and soil macropores affect the hydraulic conductivity of forest stony soils: some methodological aspects," *Journal of Hydrology*, vol. 570, pp. 132–140, 2019.

Hindawi
Journal of Sensors
Volume 2022, Article ID 7426303, 13 pages
https://doi.org/10.1155/2022/7426303

Research Article

Oral Business English Recognition Method Based on RankNet Model and Endpoint Detection Algorithm

Xia Xu[1] and Kunxue Xiao[2]

[1]*School of Foreign Languages, Xinyang University, Xinyang, Henan 464000, China*
[2]*School of Foreign Languages and Literatures, Chongqing University of Education, Chongqing 400065, China*

Correspondence should be addressed to Kunxue Xiao; xiaokx@cque.edu.cn

Received 20 March 2022; Revised 31 March 2022; Accepted 4 April 2022; Published 11 May 2022

Academic Editor: Yuan Li

The prosodic feature of "stressed syllables" plays an important role in business English learning. For the majority of nonnative language learners learning English, the pronunciation of native language can easily affect the expression of spoken English. For those who cooperate and communicate in business, if they want to have more idiomatic and accurate spoken English, they need to control the necessary condition of stress first. This puts forward new requirements for the existing speech recognition technology: more accurate recognition of stressed syllables, reading complex and different emotional colors, and helping to correct oral expression. The experimental results show that (1) the higher the Fisher Ratio of the feature, the easier it is to distinguish the stressed syllables; adjusting the weight of features can effectively improve the recognition accuracy. (2) The recognition rate will decrease with the increase of noise. (3) InwMS method can distinguish features better than min-max method, but the recognition rate of stressed syllables is very low. Linear recognition based on single feature is not recommended. (4) The error rates of the two methods are 20.6% and 19.32%. If any feature of the fusion feature is removed, the error recognition rate of the model will increase by at least 3%. (5) For sentence stress recognition based on fusion features, the recognition error rate on RankNet model is as high as 42.51%. The final result of system operation is good, simple, and convenient.

1. Introduction

With the rapid development of economic globalization, neither the country nor the individual can stay out of it, and the whole world is closely linked. If people want to seek better cooperation, mutual communication and help are essential and important factors. Combined with the rapid development of computer technology in recent decades, using intelligent systems, software, and other methods to assist in learning business English has been widely popular in people's study, work, and life. Due to the wide circulation of English, it occupies an important position in economic and trade exchanges. How to learn oral English well and use it in business cooperation is a hot topic that occupies the study list for a long time. In this paper, researchers through the study of a lot of relevant literature summed up the previous experiments to get some empirical conclusions and make use of the discovery to create new value.

Compare the syllables and morphemes of simple words and compound words [1]. It is found that lexical parameters and audibility have influence on word speech recognition in monosyllabic speech test [2]. The quality of final vowels of words plays an important role in English major stress [3]. Acoustic cues of word stress promote offline and online language processing to a certain extent [4], because speakers are sensitive to auditory feedback in stressed and unstressed syllables [5]. The effects of stress are analyzed for syllable position, pitch, duration, and amplitude [6]. Using four deep neural network architectures, the problems of phonetic symbols, lexical stress assignment, and syllability can be solved [7]. In order to improve the recognition ability of accented syllables in spoken English, a word stress recognition model is established based on natural language processing and endpoint detection algorithm [8]. According to syllable stress, transfer learning and CNN neural network are used to recognize English phonetic emotion [9]. When the speech cluster is in

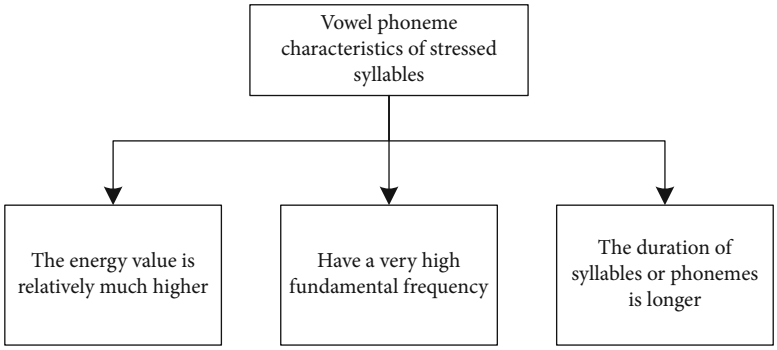

Figure 1: Factor characteristics of stress.

the middle of the word, the stress has a great influence, and the recognition is more accurate [10]. If you realize stress placement and emphasize syllables when learning English, it is helpful to learn English words [11]. The hybrid algorithm based on HMM and clustering is used to recognize English speech, which improves the recognition speed by 20.1% [12]. After experiments under different parameters, the CNN algorithm optimized by LPC has higher accuracy of English speech recognition [13]. CTC word model for acoustic detection of speech recognition needs to train more data and has better performance [14]. Applying speech recognition to college English listening teaching can effectively improve students' listening [15].

The above documents are explained from different methods and angles. It not only shows the importance and related characteristics of learning oral stress, but also provides us with excellent ideas and good experimental methods for our research. Although there are many speech research results that are good, but so far the speech system targeted is not strong, and speech recognition technology is not perfect and mature. In addition to the inability to accurately identify the position of learners' stressed pronunciation, learners cannot get a reasonable assessment report of stressed pronunciation, which cannot effectively achieve the purpose of oral business English learning. There is not yet a successful business English learning system for recognizing stressed syllables in spoken English. Most systems are faced with the problems of incomplete recognition function and imperfect performance. Therefore, this paper uses natural language processing and endpoint detection algorithm to integrate the technology of the system, so as to have a better application in speech recognition of stressed syllables.

2. Theoretical Basis

2.1. Oral Business English. Business English [16], as the name implies, mainly involves business interaction. Under the trend of internationalization, the purpose of this type of language is to help learners adapt to work and life in the workplace. In addition to simple and basic English language learning, learners not only need to improve their English expression level, but also need to understand business terminology, western business management concepts, and conventions; Foreigners' thinking mode and psychological state are different from our own country, which involves the conceptual requirements at the cultural level. If you want to do business with foreigners well, you need to know the ways and means to cooperate with them and respect their business requirements and standards.

Therefore, the functionality of "spoken language" is very important, which has three main components: words, grammar, and sentences. Oral fluency and pronunciation accuracy are very important in real interpersonal communication. As it happens, English is a language of stress and rhythm. It is self-evident that stress plays an important role in learning words and sentences, which helps to lay a solid foundation for rhythm and intonation, and it includes important grammatical and semantic characteristics. Some literature also well illustrates that the core of mastering business English and oral English learning is the stressed syllables of words and sentences. It is shown Figure 1:

2.2. Natural Language Processing. Natural language processing [17] (NLP) is an interdisciplinary subject of intelligence science and English. For machines, digital information is its expression. Through the bridge of NLP, we can create a way for human beings to communicate with machines, so that human beings can understand what machines are communicating and expressing. However, NLP also has five major difficulties: (1) language has no simple and intuitive rules. Its laws are complicated, and it is difficult for ordinary people to understand and observe. (2) Openness of English can be interconnected with other languages. (3) Language is an open collection. Users can discover and create new expressions by themselves. (4) Language is often associated with concrete practice, and it depends on the knowledge of various disciplines. (5) If you want to use a language well and smoothly, you need to base yourself on the environment and context of the language, as shown in Table 1:

2.3. Endpoint Detection Algorithm. Speech signal processing is very important. Endpoint detection algorithm technology is used to distinguish speech and nonspeech signals, so as to accurately determine the starting point and ending point of speech. In reality, the real environment of speech recognition is easily affected by noise, so the endpoint detection algorithm should reduce the interference of mute and noise. If the detection of speech signal endpoint is not accurate, it is easy to cause recognition errors, which directly determines the success or failure of the whole speech recognition work in some aspects. The performance of speech recognition can be

Table 1: Four applications of NLP.

Typical applications of NLP	
Emotional analysis [18]	The network is full of complex and redundant text information. These messages have different effects for different people or machines. However, if you make use of these texts. It can be found that the emotions they express are nothing more than positive or negative feedback
Machine translation	Language and language need to be translated before undifferentiated communication can be realized. Nowadays, the application of machine translation is mature, such as Google translation and Baidu translation
Chat robot [19]	It represents the future intelligent application, which promotes the application of chat robots to produce more new values. Using this kind of robot, smart home, intelligent entertainment, and other aspects glow with new vitality
Speech recognition [20]	The application of speech recognition has entered thousands of households and is widely used in medical treatment, communication, home appliances, games, and other industries. Whether it is the voice-to-text function in QQ or WeChat, voice navigation for cars etc., its use is not a complex laboratory high-tech, but a national-level application

improved effectively if the collection amount of speech data is effectively processed and the processing time is saved.

(1) Short-term average energy [21]

$$E_n = \sum_{m \longrightarrow -\infty}^{\infty} [x(m) \cdot \omega(n-m)]^2. \tag{1}$$

For $h(n) = \omega^2(n)$, there are

$$E_n = \sum_{m \longrightarrow -\infty}^{\infty} x^2(m) \cdot h(n-m). \tag{2}$$

Short-term average amplitude:

$$M_n = \sum_{m \longrightarrow -\infty}^{\infty} |x(m)| \cdot \omega(n-m), \tag{3}$$

where $\omega(n)$ is Hamming window and $h(n)$ can realize framing processing. When the value obtained by $E(n)$ is large, it can be applied to the voiced segment, and when the value obtained by $E(n)$ is small, it can be applied to the unvoiced segment, distinguishing the starting point and the ending point of the speech signal. E_n and M_n reflect the strength of the speech signal.

(2) Short-term average zero-crossing rate

$$Z_n = \sum_{m \longrightarrow -\infty}^{\infty} |\operatorname{sgn}[x(n)] - \operatorname{sgn}[x(n-1)]| \cdot \omega(n-m),$$
$$\operatorname{sgn}[x(n)] = \begin{cases} 1, x(n) \geq 0, \\ -1, x(n) < 0. \end{cases} \tag{4}$$

General take:

$$\omega(n) = \begin{cases} \dfrac{1}{2N}, & 0 \leq n \leq N-1, \\ 0, & else. \end{cases} \tag{5}$$

Threshold zero crossing rate [22]:

$$Z_n = \frac{1}{2} \sum_{m \longrightarrow -\infty}^{\infty} \{|\operatorname{sgn}[x(n) - T] - \operatorname{sgn}[x(n-1) - T]| + |\operatorname{sgn}[x(n) + T] - \operatorname{sgn}[x(n-1) + T]|\} \cdot \omega(n-m). \tag{6}$$

2.4. Speech Feature Extraction

(1) Energy characteristics

$$Q_n = T[x(m)w(n-m)]. \tag{7}$$

(2) Duration characteristics. Longer syllables can be judged as stressed syllables

(3) Fundamental frequency characteristics [23]

Discrete signal sequence:

$$R(k) = \sum_{m \longrightarrow -\infty}^{\infty} x(m) \cdot x(m+k). \tag{8}$$

Random signal sequence:

$$R(k) = \lim_{N \longrightarrow -\infty} \frac{1}{2N+1} \sum_{m \longrightarrow -N}^{\infty} x(m) \cdot x(m+k). \tag{9}$$

Autocorrelation function:

$$x(k) = x(n + N_P),$$
$$R(k) = R(k + N_P). \tag{10}$$

(4) LPC [24]

$$R(i) = \sum_{n=-\infty}^{+\infty} S_w(n+i)S_w(n),$$
$$H(z) = S(z)/U(z) = G/\left(1 - \sum_{k=1}^{P} \alpha_k z^{-k}\right), \tag{11}$$
$$S(z) = \sum_{k=1}^{p} \alpha_k S(n-k) + Gu(n).$$

(5) Mel cepstrum coefficients

Output of triangular filter:

$$Y_i = \sum_{k=F_{i-1}}^{F_i} \frac{k - F_{i-1}}{F_i - F_{i-1}} X_k + \sum_{k=F_{i+1}}^{F_{i+1}} \frac{F_{i-1} - k}{F_{i+1} - F_i} X_k, i + 1, 2, \cdots, 24. \tag{12}$$

DCT Transform [25]:

$$C_k = \sum_{j=1}^{24_i} \log(Y_j) \cos\left[k\left(j - \frac{1}{2}\right)\frac{\pi}{24}\right], k = 1, 2, \cdots, p. \tag{13}$$

First-order difference cepstrum calculation:

$$\Delta c_1(m) = \sum_{k=-2}^{2} k c_{l-k}(m), 1 \le m \le p. \tag{14}$$

Mel frequency conversion relation:

$$Mel = \ln\left(1 + \frac{f}{700}\right) \cdot \frac{1000}{\ln(1 + 1000/700)}. \tag{15}$$

(6) Fractal dimension feature extraction

Box counting dimension:

$$D_B(s) = \lim_{\varepsilon \longrightarrow 0} \frac{\ln(N(\varepsilon))}{\ln(1/\varepsilon)}. \tag{16}$$

Minkowski dimension:

$$D_M = \lim_{\varepsilon \longrightarrow 0}\left(2 - \frac{\ln(A_G(\varepsilon))}{\ln(\varepsilon)}\right),$$
$$A_G(\varepsilon) = area\left(\bigcup_{t \in F} G_\varepsilon(t, f(t))\right). \tag{17}$$

2.5. Algorithm Evaluation Index

(1) Recognition of stressed syllables of words

$$R_{\text{right}} = N_{\text{right}}/\left(N_{\text{right}} + N_{\text{error}}\right),$$
$$R_{\text{error}} = N_{\text{error}}/\left(N_{\text{right}} + N_{\text{error}}\right), \tag{18}$$
$$R_{\text{miss}} = N_{\text{miss}}/\left(N_{\text{right}} + N_{\text{error}} + N_{\text{miss}}\right).$$

(2) Recognition of sentence stress

$$R_i = \frac{N_i}{N}. \tag{19}$$

Among them, R_{right}, R_{error}, R_{miss}, R_i represents the correct recognition rate, wrong recognition rate, omission rate, and rereading recognition accuracy of evaluation indicators, respectively.

3. Recognition of Stressed Syllables Based on RankNet

3.1. Speech Recognition Process

3.1.1. NLP Corpus Preprocessing. The original speech data of NLP needs to be preprocessed. Mark the grammatical categories of words in sentences. Finally, the proper nouns in the text are identified and divided into blocks. First of all, the English is preprocessed to achieve the desired effect, and then after data cleaning. The text is segmented by using the word segmentation tool. Then the main part of the word is extracted, which is a process of getting the root after removing the prefix of the word. Word form is to use dictionaries to restore complex words to the most basic forms. Then, the grammatical categories of words in sentences are marked. Finally, the proper nouns in the text are identified and divided into blocks, as shown in Figure 2:

3.1.2. Stress Recognition Process. Compared with the traditional stressed syllable recognition process, it is relatively simple, and its functions are not perfect. In this paper, English words and sentences should be stressed and recognized. Therefore, we specially set up a two-layer stress recognition process, as shown in Figures 3 and 4:

The first layer mainly tests words. After feature extraction, phonemes are aligned according to time, and phoneme corpus is labeled to form training sample data. The second layer is sentence stress recognition. When the first layer

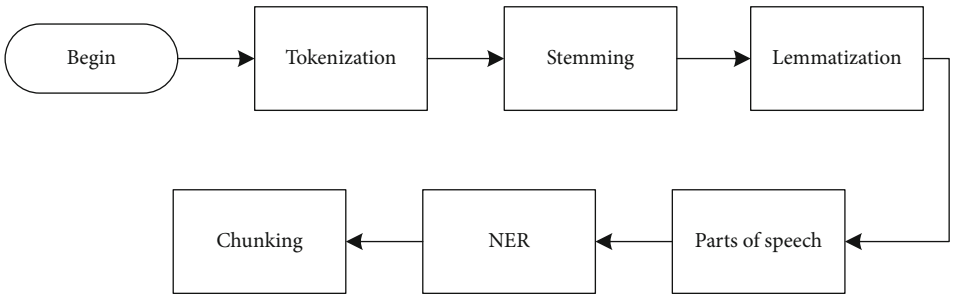

Figure 2: Steps of English corpus preprocessing.

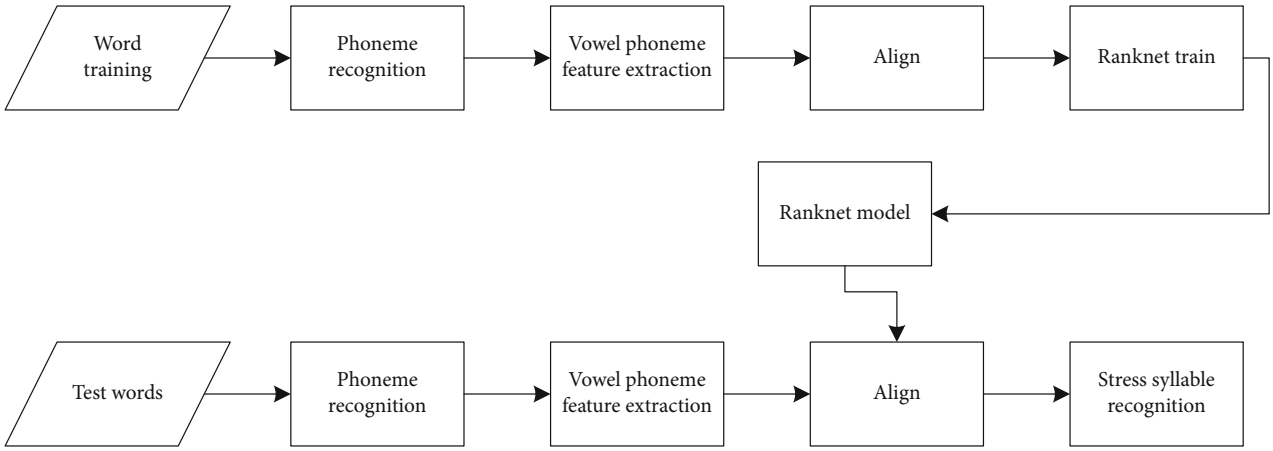

Figure 3: Layer 1 process: word stress recognition.

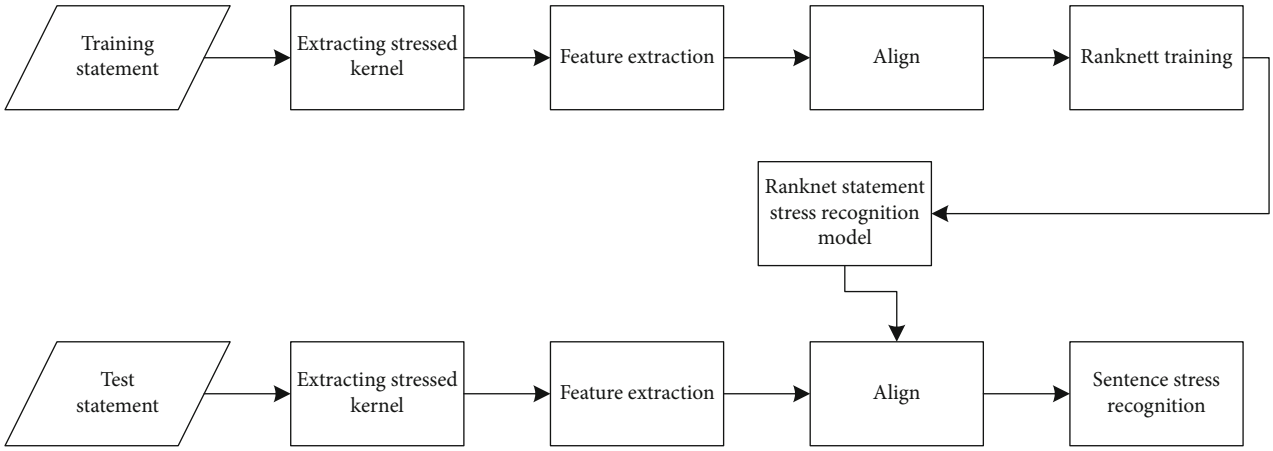

Figure 4: Layer 2 process: statement stress recognition.

recognizes the word with each stressed syllable, the stressed syllable kernel of the word is taken out to participate in the recognition of sentence stress.

3.2. RankNet Model. RankNet is based on artificial neural network. It mainly solves the ranking from the perspective of probability. This self-learning technique forms a pair of data functions. Its basic processing unit is neuron. It consists of an output y_i and a large number of input objects x_i:

$$Y_j(t) = f\left(\sum_{i=1}^{n} w_{ji}x_i - \theta_j\right). \tag{20}$$

RankNet's network model is shown in Figure 5:

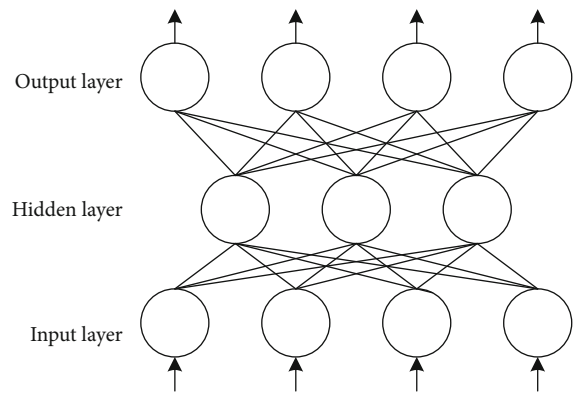

Figure 5: RankNet network architecture.

Table 2: RankNet.

RankNet	BP neural network
The input layer of RankNet is mainly composed of pairs of feature vectors	The input layer of typical BP neural network is very different, that is, feature vectors one by one
The loss function is mainly the output cross entropy of paired inputs. In back propagation, the output cross entropy loss function of a pair of input eigenvectors is used. According to the gradient of the connection weights of each layer, the connection weights between the input layer and the hidden layer and between the hidden layer and the output layer are adjusted	For BP neural network, its typical loss function is minimum mean square error. The interlayer connection weight is updated according to the error value between the actual output and the expected output

RankNet uses gradient descent algorithm and uses iterative operation to add hidden nodes to increase the adjustable parameters, thus obtaining the approximate exact solution, as shown in Table 2:

3.3. Speech Endpoint Detection. Speech endpoint detection is mainly used in silence, transition, sound and end stages. At different stages, their state transitions are different, where EH, EL, represent the high and low thresholds value of the short-term energy; RH, RL represent the high and low thresholds of the autocorrelation function value. As shown in Figure 6:

One threshold is relatively low and sensitive to signal changes; one threshold is higher. The dual-threshold endpoint detection algorithm is mainly based on short-term energy and zero-crossing rate fusion algorithm. Two different thresholds can be determined for speech endpoint detection by these two algorithms. One threshold is relatively low and sensitive to signal changes; one threshold is relatively high; when the double threshold is exceeded for a period of time, the two are properly matched, which means that the starting endpoint of the speech signal can be judged.

$$\begin{aligned} ZT &= \min\,(\mathrm{IF}, zc + 2fzc), \\ ETL &= \min\,(I_1, I_2), \\ ETU &= 5ETL, \\ I_1 &= 0.03(EMAX - EMIN) + \mathrm{EMIN}, \\ I_2 &= 4EMIN. \end{aligned} \tag{21}$$

Among them, IF is generally 25, which represents the empirical value; zc and fzc represent the mean and standard deviation of the zero-crossing rate, respectively. The short-term average energy or average amplitude of each frame is recorded as E; the maximum value and the minimum value are recorded as $EMAX$ and $EMIN$, respectively.

DTW algorithm can save computing time, as shown in Figure 7:

3.4. Stress Recognition System. In this chapter, we mainly explain the overall framework of stressed syllables in the system. The final system structure diagram includes three sections. The first section is the feature extraction module, which mainly provides preliminary judgment and evaluation results. This module is the data basis of stressed syllables. The second section is a single feature analysis module, in which stressed syllables are judged by linear discriminant function; fractal dimension curve marks position. Finally, the location information is sent to the final section of the speech evaluation. This section can specifically train and analyze the evaluation results of statistics, as shown in Figure 8:

4. Simulation Experiment Analysis

After a series of preliminary design, the specific process and implementation of each module has been described. Our accented syllable recognition system for oral business English is also basically completed.

4.1. Feature Selection and Evaluation. The selection of speech features needs a certain judgment basis. We can optimize the

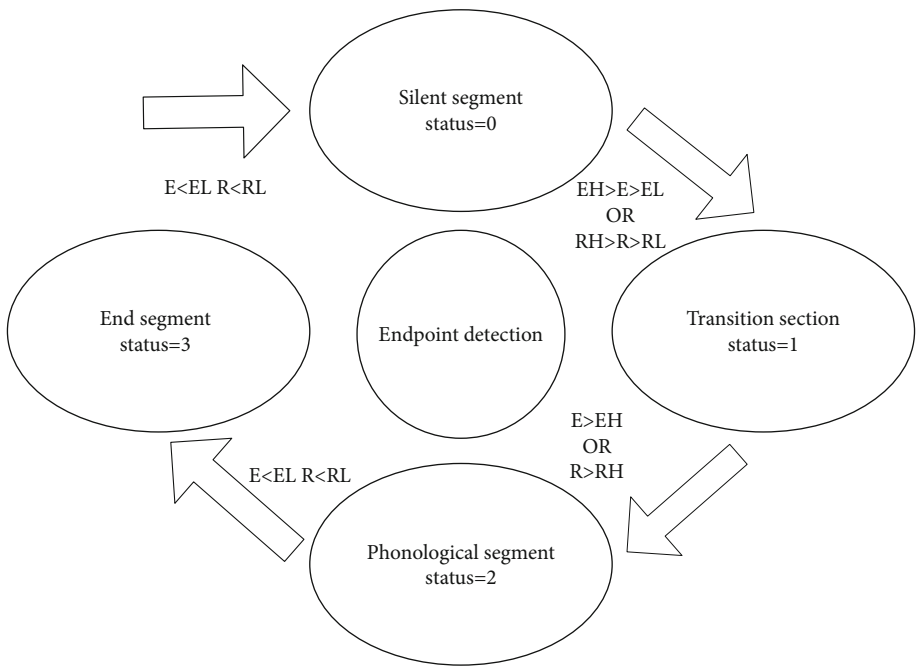

Figure 6: Endpoint detection state transition.

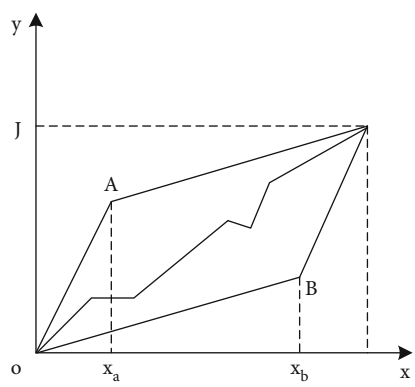

Figure 7: Efficient DTW algorithm.

distinction between the two categories and judge the influence of features on the recognition of stressed syllables. The higher the Fisher Ratio numerical results, the stronger the ability to distinguish stressed syllables:

$$\gamma_{\text{Fisher}} = \sigma_{\text{between}} + \sigma_{\text{within}}. \tag{22}$$

Divergent summation of such feature data:

$$\sigma_{\text{between}} = \sum_{i=1}^{c} \left(m_k^{(i)} - m_k \right)^2. \tag{23}$$

Divergent sum of such characteristic data for each class of samples:

$$\sigma_{\text{within}} = \sum_{i=1}^{c} \left[\frac{1}{n_i} \sum_{c \in \omega_i} \left(c_k^{(i)} - m_k^{(i)} \right)^2 \right]. \tag{24}$$

We tested eight-dimensional feature vectors and measured the recognition ability of stressed syllables of each feature, judge by Fisher Ratio values in training set and test set.

(1) After testing, we can find that Eavg in the third dimension and FDchr in the eighth dimension have higher Fisher Ratio, both of which are above 0.8. Secondly, the second dimension and the fourth dimension have higher values, and the Fisher Ratio values of Emax and Echr characteristics are both above 0.7. The remaining characteristic values are very low. For individual words, the ability to distinguish stressed syllables from unstressed syllables is poor, as shown in Figure 9:

(2) After the stress recognition process of the first layer, the sentence stress recognition of the second layer is carried out, and these eight feature types are still tested. We can see that this time, the highest Fisher Ratio value in the test set is the first dimension, with a value as high as 0.4 duration. The highest value in the training set is the eighth dimension, and Fisher Ratio value is as high as 0.16. Different test sets and training sets have different influences on stressed syllables. This means that the recognition ability of stressed syllables in these two dimensions is very strong. However, the recognition ability and effect of other dimensions are weak, as shown in Figure 10:

4.2. Endpoint Detection Comparison. On MATLAB platform, based on efficient DTW speech recognition system, the experimental environment is tested under three conditions: no noise, 5 dB, and 10 dB. In the experiment, 20

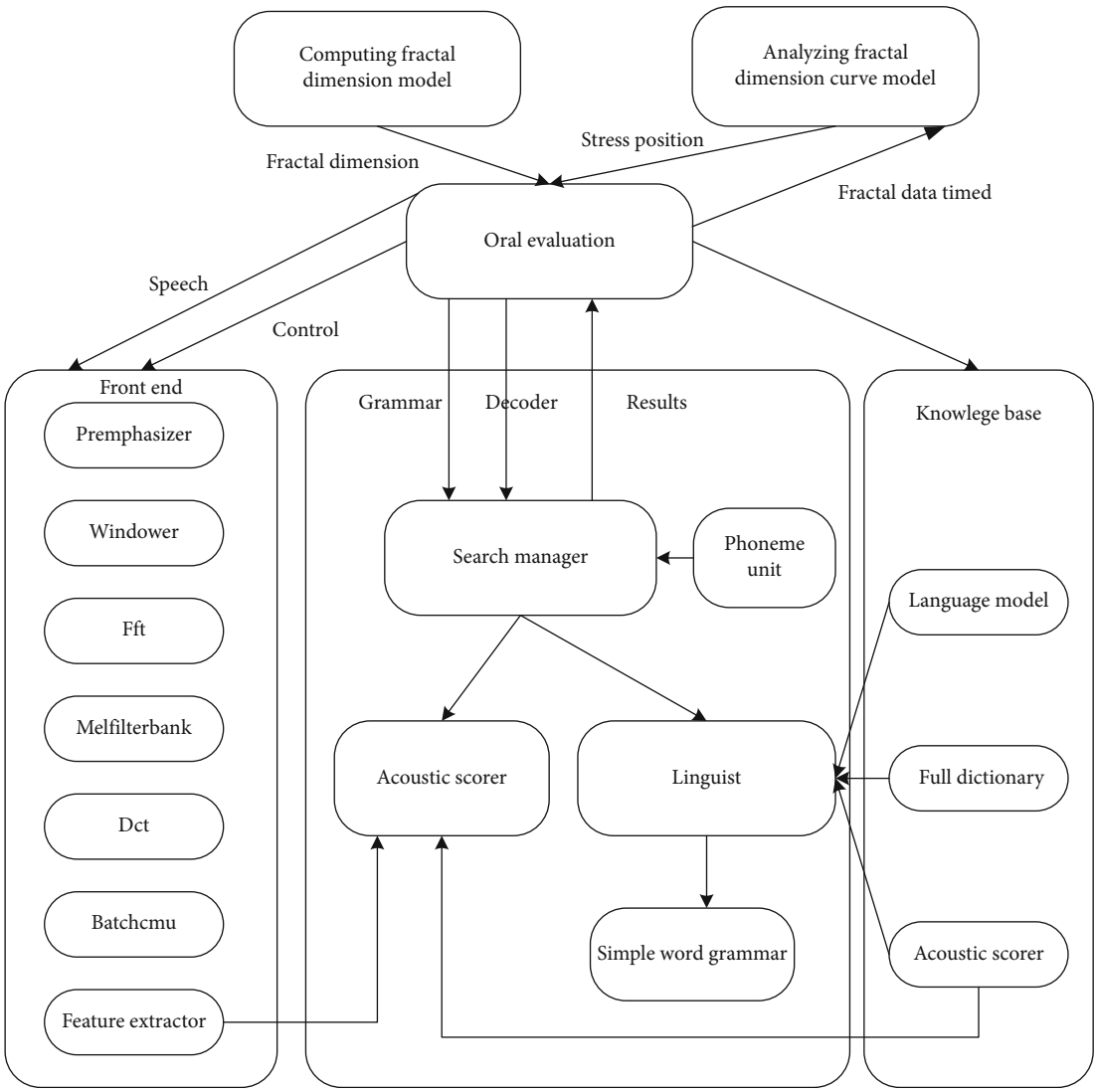

Figure 8: Improved system architecture framework based on Sphinx-4.

volunteers were invited to record the detected voice data. Among them, men and women are 50%, and each person has 10 phonetic materials. The recognition performance of dual-threshold speech endpoint detection algorithm is tested. In order to better illustrate the advantages of the detection algorithm selected in this paper, we will also use the traditional endpoint detection algorithm for data comparison. The recognition rate calculation formula is as follows:

$$\text{Recognition rate} = \frac{\text{Total number of sounds-number of misjudged sounds}}{\text{Total speech number}}. \tag{25}$$

After simulation experiment, the recognition rate of the two algorithms decreases with the increase of noise. In the same environment, the recognition rate of polysyllabic syllables is generally slightly lower than that of monosyllabic syllables. In the case of no noise, the recognition rates of the algorithms are not much different. However, with the increase of noise environment, the syllable recognition rate of this algorithm is obviously improved, and the effect is obviously superior to the traditional algorithm, as shown in Figure 11:

4.3. Stress Syllable Recognition

4.3.1. Recognition of Stressed Syllables Based on Linear Discrimination. We tested eight different phonetic features to study which features are the most effective for recognizing stressed syllables. Among them, the evaluation standard of experimental results is the recognition rate of word stress, as shown in Figure 12:

The average horizontal line is set at 70%. It can be found from the figure that the minimum and maximum normalization methods are all higher than the horizontal values, and the results are relatively balanced, so it is impossible to compare the vowel phonemes of a word. While MS normalization method is obviously superior, each feature presents a good degree of discrimination, but their recognition rate of

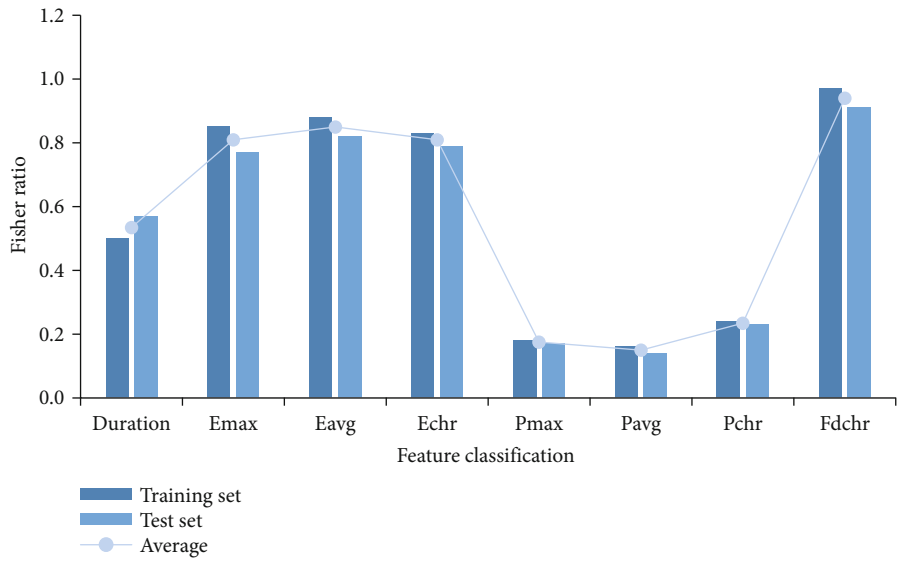

Figure 9: Word stress recognition per dimensional feature.

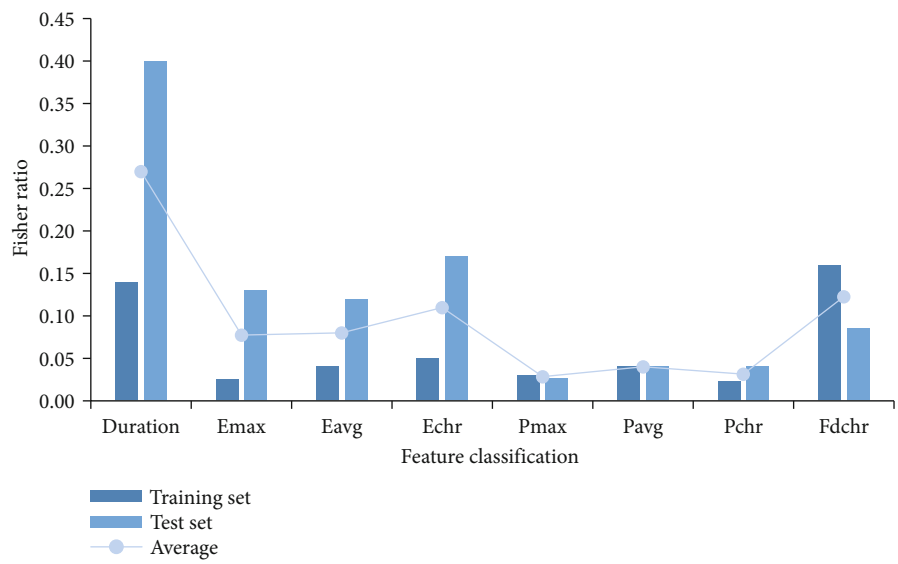

Figure 10: Sentence stress recognition per dimensional feature.

stressed syllables is very low, which cannot reflect the situation of stressed syllables well.

4.3.2. Recognition of Stressed Syllables Based on RankNet. In view of the poor results of the former method, we choose the RankNet model established in this paper, which integrates various features instead of adopting a single feature recognition method, so as to compare vowel phonemes of words and improve the recognition rate of stressed syllables, as shown in Figure 13:

The recognition rate of stressed syllables with fused features has been well improved. The error rates of the two methods are 20.6% and 19.32%, respectively. The robustness of the model is good.

Using InwMS normalization method, if any feature is removed, the error recognition rate of the model will increase by at least 3%. When dealing with duration, Eavg and FDchr, the error rate is the highest, which exceeds 24%. It can be seen that the recognition distinction of a single feature recognition is not necessarily the same in feature fusion, and their position is not necessarily important. Features are complementary, as shown in Figure 14:

4.3.3. Sentence Stress Recognition Based on RankNet. Under INwMS normalization method, the error recognition rates of accented syllables of A, B, and C are compared. A stands for R_{error}; B stands for RF_{error}; C stands for RF^2_{error}. On the test set, the reread recognition error rate of RankNet is 42.51%, as shown in Figure 15:

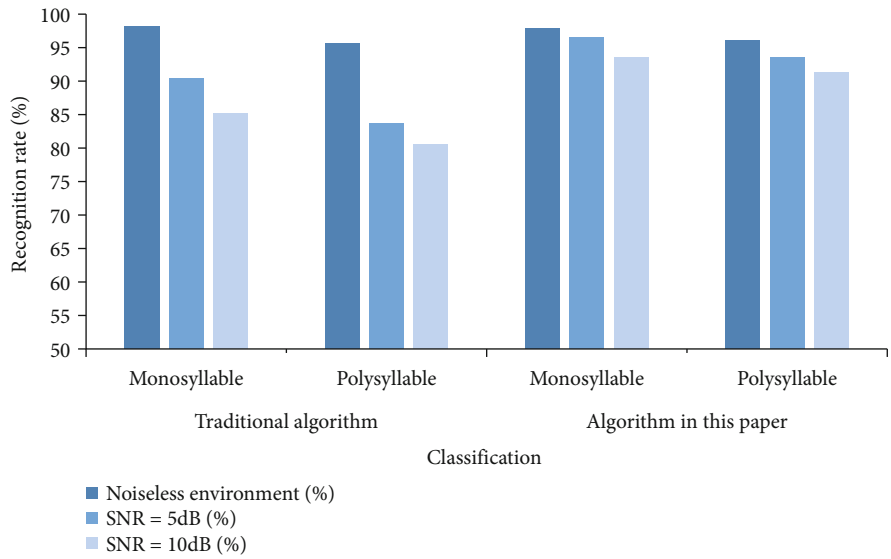

Figure 11: Recognition rate of two endpoint detection algorithms.

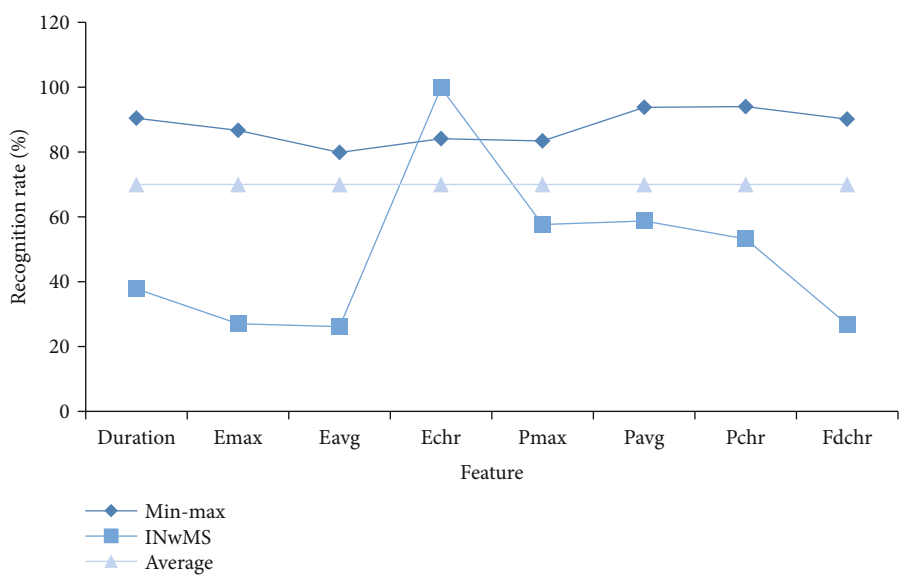

Figure 12: Recognition result of linear discrimination.

5. Conclusion

With the rapid increase of business cooperation, there are more and more people who need spoken English. However, the uneven language teaching is extremely lacking, and there is a big blank market for the system software used for oral English assistance. The research results of this paper show that

(1) in feature selection, the higher the Fisher Ratio is, the better it can distinguish stressed syllables

(2) the double-threshold speech endpoint detection algorithm is obviously superior to the traditional algorithm. Among them, the recognition rate decreases with the increase of environmental noise; the recognition rate of polysyllables is slightly lower than that of monosyllables

(3) min-max method cannot compare the vowel phonemes of words; although InwMS method can distinguish features better, the recognition rate of stressed syllables is low. Therefore, the recognition result of linear judgment of a single feature is of little significance

(4) testing the fusion features improves the recognition rate of stressed syllables. The error rates of the two normalization methods are 20.6% and 19.32%, respectively

(5) if any feature is removed, the error recognition rate of the model tested for fusion features will increase

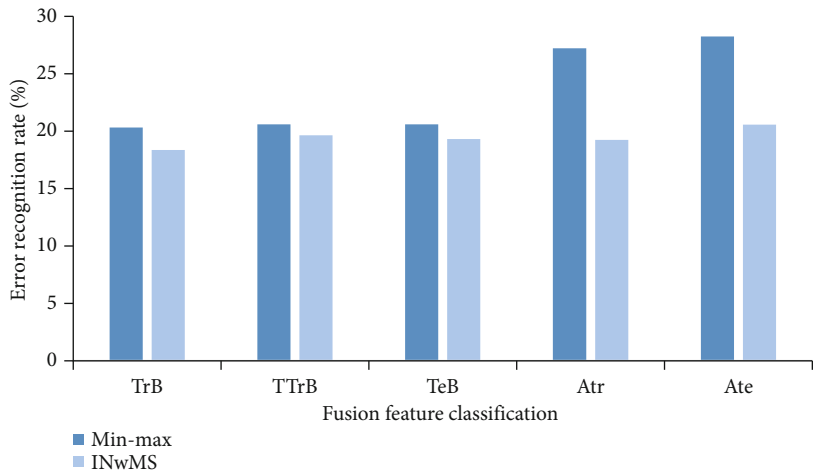

Figure 13: Recognition of stressed syllables by fusing features.

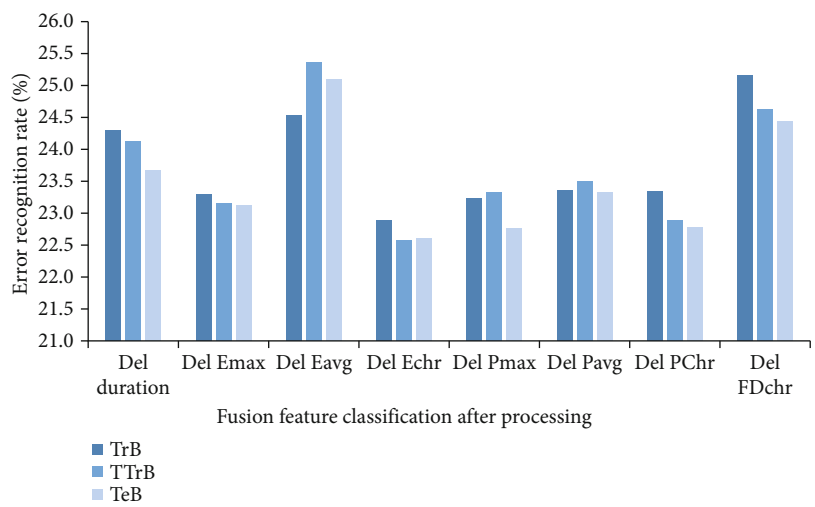

Figure 14: Fusion feature-recognition result of removing a feature.

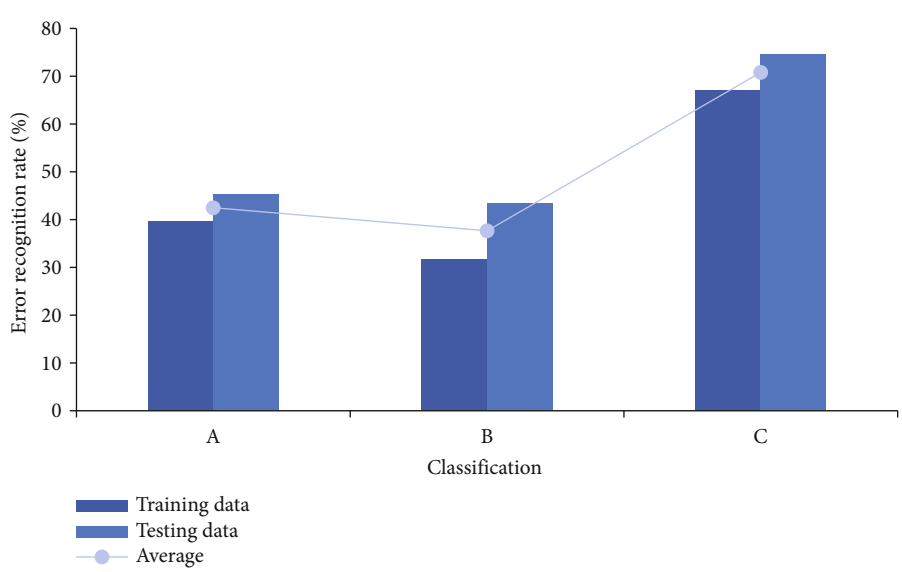

Figure 15: Sentence stress recognition result of fused features.

by at least 3%. After individual features are removed, the error rate of feature recognition rises linearly

(6) under INwMS normalization method, for sentence stress recognition based on feature fusion, the rereading recognition error rate of RankNet on the test set is as high as 42.51%

The established RankNet algorithm model has stable recognition effect and good reliability. The final experimental training is a good practice of combining experiment with theory, which has more obvious advantages than other traditional methods. The method in this paper still has some shortcomings. For example, the phonetic corpus is small in scale; there will still be missed judgments and misjudgments in noise environment. In the future work, we try some ways to further improve the recognition performance, for example, develop distributed systems to reduce maintenance costs; increase the size of the corpus to make the phonetic representation more extensive; further expand and refine the grammar, rhythm, and rhythm of stressed syllables; improve the speech endpoint detection algorithm to overcome the influence of noise. With the continuous research of speech-related topics, its development will be constantly innovated with the development of the times, and more new ideas will be put into practice to strive for breakthrough progress.

Data Availability

The experimental data used to support the findings of this study are available from the corresponding author upon request.

Conflicts of Interest

The authors declare that they have no conflicts of interest regarding this work.

References

[1] S. Lee, Y. Lee, and Y. Kwon, "The effect of syllable and morpheme on visual word recognition: comparison between simple words and compound words," *Journal of Language Sciences*, vol. 27, no. 4, pp. 75–96, 2020.

[2] A. Winkler, R. Carroll, and I. Holube, "Impact of lexical parameters and audibility on the recognition of the Freiburg monosyllabic speech test," *Ear and Hearing*, vol. 41, no. 1, pp. 136–142, 2020.

[3] C. Moore-Cantwell, "Weight and final vowels in the English stress system," *Phonology*, vol. 37, no. 4, pp. 657–695, 2020.

[4] C. Kaland, "Offline and online processing of acoustic cues to word stress in Papuan Malay," *The Journal of the Acoustical Society of America*, vol. 147, no. 2, pp. 731–747, 2020.

[5] S. Bakst and C. A. Niziolek, "Effects of syllable stress in adaptation to altered auditory feedback in vowels," *The Journal of the Acoustical Society of America*, vol. 149, no. 1, pp. 708–719, 2021.

[6] V. Y. Yu, "Effects of syllable position, fundamental frequency, duration and amplitude on word stress in Mandarin Chinese," *Journal of Psycholinguistic Research*, vol. 50, no. 32, pp. 293–312, 2020.

[7] B. Lrincz, "Concurrent phonetic transcription, lexical stress assignment and syllabification with deep neural networks," *Procedia Computer Science*, vol. 176, pp. 108–117, 2020.

[8] Q. Zhang, "Recognition of English spoken stressed syllables based on natural language processing and endpoint detection algorithm," *Journal of Intelligent and Fuzzy Systems*, vol. 39, no. 4, pp. 5713–5724, 2020.

[9] X. Chen, "Simulation of English speech emotion recognition based on transfer learning and CNN neural network," *Journal of Intelligent and Fuzzy Systems*, vol. 40, no. 2, pp. 2349–2360, 2021.

[10] L. Cilibrasi and V. St Ojanovik, "The interplay of stress saliency and word beginning saliency: an experimental study," *Linguistica Pragensia*, vol. 30, no. 2, pp. 113–126, 2020.

[11] M. S. Ahmed, "The impact of students' realization of stress placement on identifying the class of the English word and its meaning," *International Journal of Psychosocial Rehabilitation*, vol. 24, no. 10, pp. 3707–3719, 2020.

[12] X. Zhu, "Hybrid algorithm of English speech recognition based on hidden Markov model and clustering," *Computer Measurement and Control*, vol. 28, no. 5, p. 5, 2020.

[13] C. Xiaohong and T. Hua, "Research on English speech recognition based on deep machine learning," *Journal of Guiyang University: Natural Science Edition*, vol. 16, no. 3, p. 5, 2021.

[14] L. Xia and T. Gaofeng, "Research on English acoustic detection system based on speech recognition," *Automation Technology and Application*, vol. 38, no. 12, p. 3, 2019.

[15] W. Qionghua, "An empirical study on the application of speech recognition in college English listening teaching," *Research on Communication Power*, vol. 4, no. 24, p. 2, 2020.

[16] A. L. Agostinho and L. M. Hyman, "Word prosody in Lung'Ie: one system or two?," *Probus*, vol. 33, no. 1, pp. 57–93, 2021.

[17] A. Mai, "Phonetic effects of onset complexity on the English syllable," *Laboratory Phonology*, vol. 11, no. 1, p. 4, 2020.

[18] A. K. Emmendorfer, J. M. Correia, B. M. Jansma, S. A. Kotz, and M. Bonte, "ERP mismatch response to phonological and temporal regularities in speech," *Scientific Reports*, vol. 10, no. 1, p. 12, 2020.

[19] A. Kukhto, "The acoustics of word stress in Gaeilge Chorca Dhuibhne," *The Journal of the Acoustical Society of America*, vol. 148, no. 4, pp. 2726–2726, 2020.

[20] E. Banzina, L. C. Dilley, and L. E. Hewitt, "The role of secondary-stressed and unstressed–unreduced syllables in word recognition: acoustic and perceptual studies with Russian learners of English," *Journal of Psycholinguistic Research*, vol. 45, no. 4, pp. 813–831, 2016.

[21] L. Lei, "Design and research of embedded English speech recognition control system for intelligent seeder," *Agricultural Mechanization Research*, vol. 40, no. 12, p. 5, 2018.

[22] L. Lin, "Research on the application of automatic speech recognition technology in English phoneme teaching for non-English majors," *Journal of Kaifeng Institute of Education*, vol. 38, no. 4, p. 2, 2018.

[23] H. Yunxiao, S. Qing, F. Yuxiang, and G. Qing, "Speech endpoint detection algorithm based on MFCC distance in complex noise," *Computer Engineering*, vol. 46, no. 3, p. 6, 2020.

[24] D. Honghu, Q. Mao, and Z. Xiaobing, "Improved endpoint detection algorithm based on LMS adaptation," *Journal of Changzhou Institute of Technology*, vol. 34, no. 1, p. 10, 2021.

[25] J. Yu and Z. Xiaoqun, "Research on endpoint detection algorithm applied to speech annotation in noisy environment," *Journal of Nanjing University of Posts and Telecommunications: Natural Science Edition*, vol. 41, no. 1, p. 9, 2021.

Hindawi
Journal of Sensors
Volume 2022, Article ID 1314736, 13 pages
https://doi.org/10.1155/2022/1314736

Research Article

Multidimensional Analysis and Evaluation of College English Teaching Quality Based on an Artificial Intelligence Model

Man Li

School of Foreign Languages, Xi'an Aeronautical Institute, Shaanxi 710077, China

Correspondence should be addressed to Man Li; mandy@xaau.edu.cn

Received 11 March 2022; Revised 31 March 2022; Accepted 8 April 2022; Published 9 May 2022

Academic Editor: Yuan Li

In view of the lack of teaching resources and the impossibility of real-time sharing and application of teaching resources in English teaching, this paper proposes a multidimensional analysis and application of English teaching quality based on an artificial intelligence model. This paper analyzes the basic framework and application of the Internet of Things technology and puts forward the corresponding hierarchical classification and teaching quality monitoring mode. Secondly, the monitoring framework of the Internet of Things to achieve the quality of English teaching and then the basic theory of the Internet of Things is analyzed. Finally, the experiment shows that the average score of English has been greatly improved by comparing the traditional teaching mode and the new classroom quality monitoring mode under the Internet of Things technology. The main dimensions of teaching quality, such as teachers' quality, teaching attitude, teaching content, and teaching methods, are analyzed in depth, and the coefficient of most sample data is more than 0.7, which has a good application effect. Whether running on the test set or the mixed test set, the accuracy of the new classroom quality monitoring model proposed in this paper is the highest among the three models. The correct rate on the test set can reach 99.71%, the correct rate on the mixed test set can reach 98.01%, and the correct rate can reach 98.67%, which shows the superiority of the performance of the new classroom quality monitoring model.

1. Introduction

As the most widely used language in the world, English has not only become an international language, but also its international status is getting higher and higher. How to master English well and lay a solid foundation for themselves in the increasingly internationalized society in the future is the concern of many Chinese college students. Under such circumstances, more and more attention has been paid to English teaching in higher education. Different from English teaching in other countries, college English teaching in China has its unique characteristics in different aspects, such as social and political background, educational policy, and teaching mode. Now that we are in an era of Internet, everything around us is undergoing earth-shaking changes, including our lives and studies. My country's higher education is also facing a huge reform, and traditional learning methods can no longer meet the requirements of today's students. The literature [1] analyzes the influencing factors of college English classroom teaching quality evaluation. English teaching under the intelligent monitoring teaching mode pays more attention to students' self-consciousness, discovering, and solving problems in the scene, which greatly improves students' interest in learning English and promotes the all-round development of students' English learning. The literature [2] revolves around the development of autonomous learning as one of the learning strategies related to planning, goal-oriented design, monitoring, and metacognitive capabilities. The literature [3] explains that the guarantee of English teaching quality should follow the principles of scientificity, comprehensiveness, process, and development. With the development of

science and technology, many colleges and universities have introduced computer teaching technology, and computer English teaching technology is also in the process of continuous promotion. It is necessary to establish a complete teaching quality evaluation system, which can not only improve the quality of English teaching but also can also find and solve problems in time. The literature [4] emphasized the importance of monitoring system to English teaching. The article combines the characteristics of the English classroom and designs a variety of color conversions to help students strengthen their memory. According to the effective results, the color conversion teaching method can help students master more than 90% of the classroom knowledge, which not only ensures the fun of the classroom and attracts the students' interest in learning but also improves teaching efficiency. The literature [5] shows that in the information age, all fields need to be developed in an all-round way. The traditional teaching model can no longer meet the needs of current students, and the education field is facing a major reform. The literature [6] examines four factors that have a major impact on the success of college English as a second language teaching. The focus of the article is how to maintain high-quality English teaching. It lists several important factors that affect English teaching, including teacher qualifications, teaching models, and teaching methods. The literature [7] shows that college English teachers need to use selected branches from the field of educational psychology in their teaching so that students can achieve better results. How to let students experience high-quality English teaching courses depends on the teacher's teaching methods. Teachers should answer students' questions patiently through detailed explanations and guide each student to give correct English learning methods. The literature [8] proposes integrating educational ecology theory into college English teaching reform, optimizing courses and teaching models, and creating an ecological environment. The progress of China's diplomacy has made English the focus of many students' learning, and language monitoring theory is an important part of improving the efficiency of English teaching. The literature [9] introduced the theory of language monitoring and analyzed its application in college English teaching. The literature [10] introduced a blended English teaching model, which is a model of autonomous learning. The literature [11] proposes a detailed teaching quality monitoring and evaluation plan based on the characteristics of the course. Many non-English majors in universities do not pay enough attention to English learning, although the education department has explained that the listening and speaking ability of non-English majors is a very important part. The reason is that many colleges and universities lack a teaching quality monitoring system, and the purpose of the article is to achieve the goal of cultivating students' listening and speaking ability. The literature [12] analyzes the problems in the autonomous learning of college English and then points out the basic idea of how to implement monitoring. The literature [13] establishes a higher vocational English education and teaching operation mechanism and perfects the quality monitoring system of flipped classroom teaching. The literature [14] analyzed the current situation of college English pronunciation courses and analyzed the current problems. The literature [15] proposes a hybrid learning model that combines traditional classroom teaching mode and network teaching mode. The advantages of network education include the maximum utilization of resources, the autonomy of learning behavior, the modification of teaching form, and the automation of teaching management. The application of network technology in distance education is characterized by anyone, at any time, at any place, starting from any chapter and learning any course. The convenient and flexible "Five Any" of network education directly embodies the characteristics of active learning in learning mode and fully meets the needs of modern education and lifelong education. Interactive learning forms, teachers and students, and students and students, through the network for all-round communication, close the psychological distance between teachers and students, and increase the opportunities and scope of communication between teachers and students. Through the statistical analysis of the types, number, and frequency of students' questions by computer, teachers can understand the doubts, difficulties, and main problems that students encounter in their study and guide students more pertinently.

2. Learning English Teaching Quality Monitoring and Intelligent Analysis

2.1. The Status Quo of College English Teaching. In the process of English teaching in many colleges and universities, there are still many problems and shortcomings, and English teaching is not paid enough attention [16]. Many colleges and universities lack advanced teaching equipment and teaching resources. English is different from other subjects we learn. English is not our mother tongue, and there are differences in culture and thinking. English grammar is the most difficult problem to solve. There are many English learners. The number of teachers is limited, and it is inevitable to use Internet technology to solve the problem of lack of resources. Construct a quality monitoring system for college English teaching, as shown in Table 1.

2.2. Form a Complete and Scientific Teaching Quality Monitoring System. A complete and scientific teaching quality monitoring system consists of the following aspects: First, it must have a clear teaching goal. In the process of quality monitoring, you must recognize that the direction of the object you are monitoring is correct and toward the goal. Second, formulate quality standards for teaching links. The process of teaching implementation is not accomplished overnight. It is composed of different links. During the implementation of the teaching link, quality standards must be established. It is necessary to ensure that the objects you monitor can meet the standards in every teaching link, only each of the previous ones. Only when the small link reaches the standard and a good foundation is laid, can you get a full harvest in the final big link. In this way, only with a complete and scientific teaching quality monitoring system, can the teaching process be improved towards the established goal

Table 1: College English teaching quality monitoring system.

Component	Content
Class preparation	Establish the learning goals of this course, including language goals and cultural background goals
	Choose relevant background knowledge to help students build a new knowledge framework
	Explore flexible teaching methods and equipment (such as multimedia)
	Design a variety of interactive teaching activities
	Investigate and understand the background and learning status of students in this class
	Invite some students to prepare together
Teaching process	Adopt various forms of classroom introduction
	State the learning goals of each lesson
	Provide opportunities to use different learning strategies
	Provide students with comprehensive use of listening, speaking, reading, writing, and translation activities
	Summarize teaching activities (including language goals and cultural goals)
	Evaluate teaching effects through different activities
Reflection after class	Is it valid to import?
	Is the learning objective clear?
	Whether the preclass assessment of students is accurate
	Whether the class activity link is successful
	Does the teacher give feedback on the student's learning situation in a timely manner
	Is there any connection between classroom teaching and career goals?

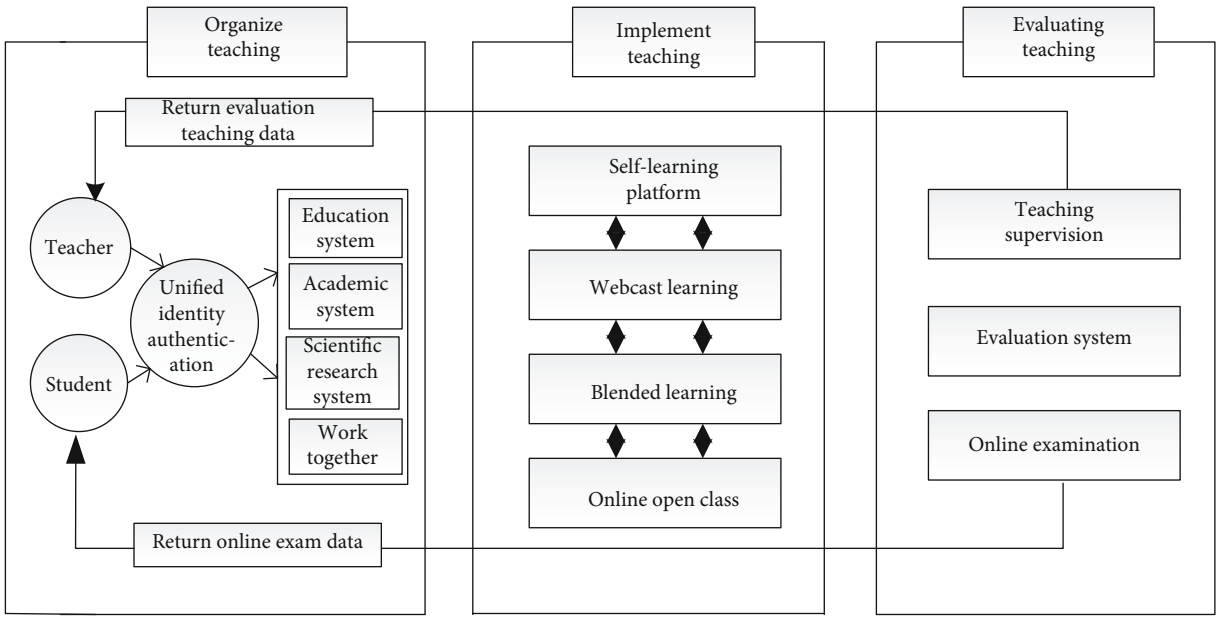

Figure 1: Teaching quality monitoring model.

and its shortcomings can be improved, and high-efficiency and high-quality teaching can be formed. The monitoring mode of college English teaching quality is shown in Figure 1.

2.3. The Role of Teaching Quality Monitoring System in Improving Teaching Quality. The teaching quality monitoring system has a guiding role. It can guide teachers in the direction of improvement, make teachers understand their shortcomings, and correct shortcomings to improve their teaching level [17]. He can guide students in the direction of learning, so that each student can master their own learning methods and formulate different learning goals for each student's different learning foundations, so that students can study with high quality and high efficiency. Second, the teaching quality monitoring system has a monitoring function. Third, the monitoring of teaching quality has a stimulating effect. It can inspire teachers to tap their own potential, find their own advantages, and develop them [18]. Fourth, the teaching quality monitoring system has a decision-making support role. After summarizing the collected information, it is convenient for school leaders to

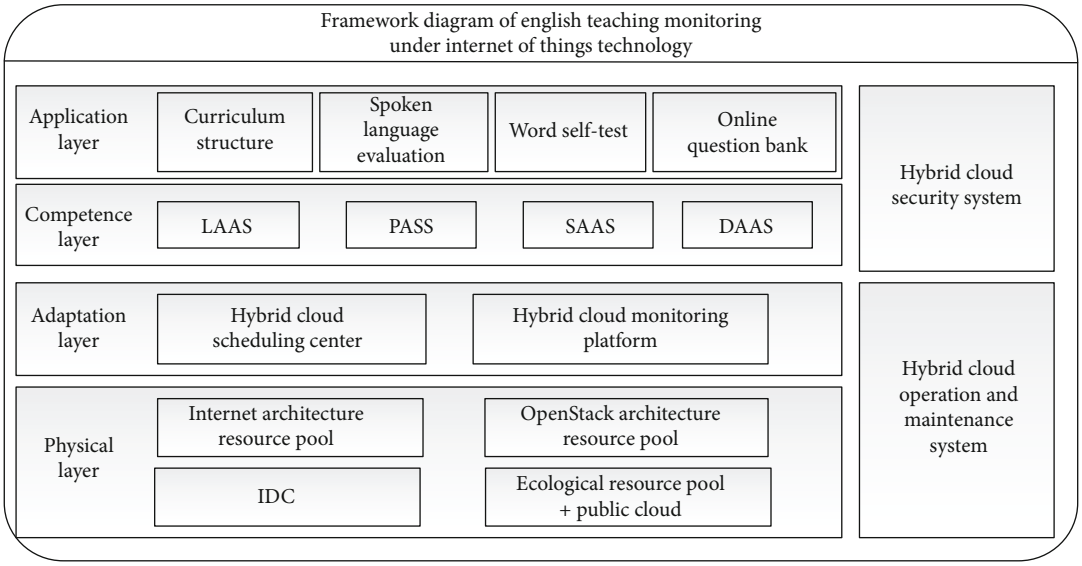

Figure 2: Framework diagram of English teaching monitoring.

Table 2: Achievement statistics of traditional teaching mode.

Group	N	Mean	Standard deviation	Standard error of the mean
Test group	100	66.2000	1.71270	.54160
Control group	100	66.8000	1.96921	.62272
Standard group	100	68.0000	2.15214	.78142

check. The framework diagram of using the Internet of Things technology to realize the monitoring of English teaching is shown in Figure 2.

3. English Teaching Quality Monitoring Based on Internet of Things Technology

3.1. Analysis of Classroom Teaching Behavior. S stands for student and T stands for teacher. It mainly studies classroom observation methods of teacher and student behavior in English classrooms [19]. The number of S behaviors is recorded as N_s, and the number of T behaviors is recorded as N_t, and the formula [20] is obtained.

$$N = N_s + N_t \tag{1}$$

The teacher behavior share R_t is

$$R_t = \frac{N_t}{N} = \frac{(N - N_s)}{N} = 1 - \frac{N_s}{N}. \tag{2}$$

The calculation formula for behavioral conversion rate Ch is

$$\mathrm{Ch} = \frac{g - 1}{N}. \tag{3}$$

The behavior conversion rate indicates the interactivity in teaching, and the greater the value, the more frequent the switching between student and teacher behaviors.

The mathematical formula is

$$S(m, n) = (f * g)(m, n) = \sum_{i=-\infty}^{\infty} \sum_{j=-\infty}^{\infty} f(i, j) g(m - i, n - i). \tag{4}$$

The convolution in the neural network is

$$S(m, n) = (I * K)(m, n) = \sum_{i} \sum_{j} I(m + i, n + i) K(i, j). \tag{5}$$

The following is the logical function:

$$s(x) = \frac{1}{1 + e^{-x}}. \tag{6}$$

The following is the hyperbolic tangent function:

$$\tanh(x) = \frac{e^{x} - e^{-x}}{e^{-x} + e^{-x}}. \tag{7}$$

The following is the linear rectification function:

$$\mathrm{ReLU}(x) = \begin{cases} 0, & x < 0, \\ x, & x \geq 0. \end{cases} \tag{8}$$

The function of the normalized index layer is to complete the calculation of the normalized index function in most linear classifiers [21]; the following is the specific algorithm input vector:

$$X = (x_1, x_2, \cdots, x_n). \tag{9}$$

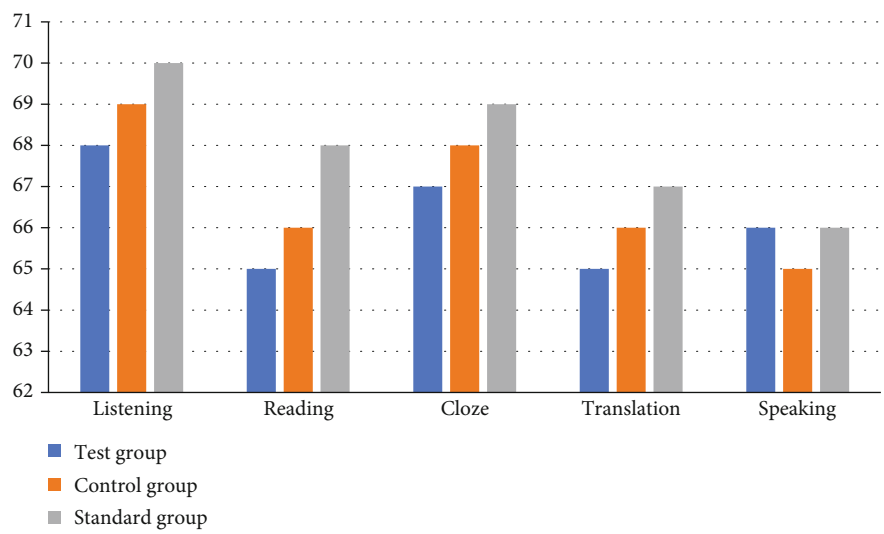

Figure 3: Result statistics of traditional teaching mode.

Table 3: New classroom quality monitoring model.

Group	N	Mean	Standard deviation	Standard error of the mean
Test group	100	85.5000	2.71270	.65405
Control group	100	86.2000	2.96921	.62272
Standard group	100	88.0000	3.15214	.78142

Calculate n scalar values:

$$y_k = \frac{e^{x_k}}{e^{x_1} + \cdots + e^{x_n}}, \tag{10}$$

spliced into

$$Y = (y_1, y_2, \cdots, y_n). \tag{11}$$

The following is the detection rate:

$$\mathrm{DR} = \frac{m_1}{M_1}. \tag{12}$$

The following is the false detection rate:

$$\mathrm{FAR} = \frac{m_2}{M_2}. \tag{13}$$

The following is the missed detection rate:

$$\mathrm{FRR} = \frac{m_3}{M_3}. \tag{14}$$

3.2. English Grammatical Analysis Model. The most commonly used evaluation algorithm for grammatical error correction is MaxMatch(M^2), and the calculation of correction rate P is publicized as

$$P = \frac{\sum_{i=1}^{n} |g_i \cap e_i|}{\sum_{i=1}^{n} |e_i|}. \tag{15}$$

The following is the correction rate R:

$$R = \frac{\sum_{i=1}^{n} |g_i \cap e_i|}{\sum_{i=1}^{n} |g_i|}. \tag{16}$$

The key evaluation index in MaxMatch is $F_{0.5}$, and the formula is defined as follows:

$$F_{0.5} = \frac{(1 + 0.5^2) * R * P}{R + 0.5^2 * P}. \tag{17}$$

Soft attention mechanism, weight a_{ij}, is determined by the $i-1$ hidden state s_{i-1} and each hidden state variable in the input [22, 23]; the calculation formula is

$$a_{ij} = \frac{\exp(e_{ij})}{\sum_{k=1}^{T_x} \exp(e_{ik})}, \tag{18}$$

$$e_{ij} = a(s_{i-1}, h_j), \tag{19}$$

where h_j is the output of the hidden layer of the encoder layer at time j and S_{i-1} is the output of the hidden layer of the decoder layer at time $i-1$.

The following is the input calculation of neuron:

$$\mu = \frac{1}{H} \sum_{i=1}^{H} x_i, \tag{20}$$

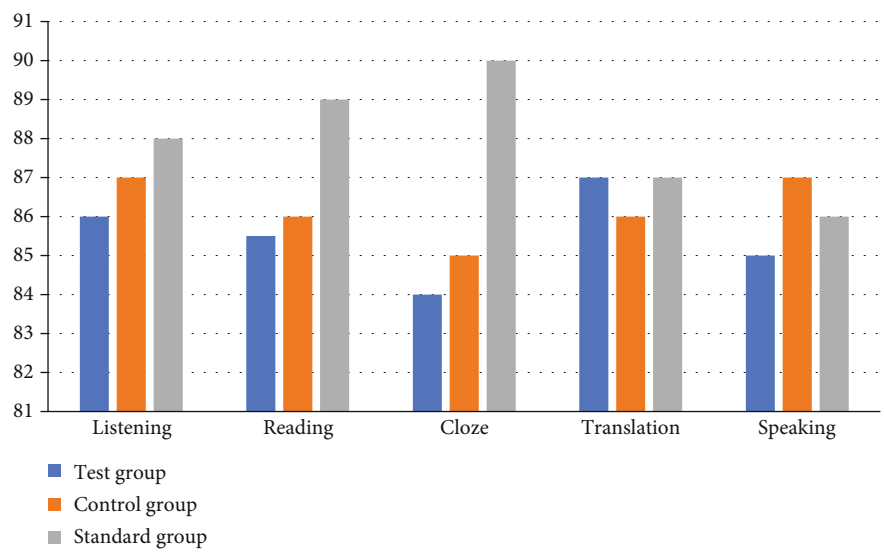

Figure 4: Score statistics of the new classroom quality monitoring model.

Table 4: Reliability coefficient.

Reliability factor	Representation
0.60-0.65	Better not
0.65-0.70	Minimum acceptable value
0.70-0.80	Pretty good
0.80-0.95	Very good

Table 5: Teacher quality sample data.

Sample number	Clear educational goals	Solid English professional knowledge	The level of teaching explanation
1	0.90	0.87	0.86
2	0.80	0.54	0.51
3	0.76	0.44	0.48
4	0.87	0.55	0.82
5	0.79	0.60	0.31
6	0.91	0.95	0.79
7	0.96	0.92	0.98
8	0.71	0.91	0.98
9	0.99	0.73	0.33
10	0.72	0.60	0.50

where μ is the average value of input neurons.

$$\sigma = \sqrt{\frac{1}{H}\sum_{i=1}^{H}(x_i - \mu)^2}. \tag{21}$$

The following is the antifiltering algorithm:

$$p(\omega_i|\omega_1,\cdots,\omega_{i-1}) = p(\omega_i|\omega_{i-n-1},\cdots,\omega_{i-1}). \tag{22}$$

When $n = 2$, bigram is

$$p(\omega_i|\omega_1,\cdots,\omega_m) = \prod_{i=1}^{m} p(\omega_i|\omega_{i-1}). \tag{23}$$

When $n = 3$, bigram is

$$p(\omega_i|\omega_1,\cdots,\omega_m) = \prod_{i=1}^{m} p(\omega_{i-2}\omega_{i-1}). \tag{24}$$

Estimate the value of $p(\omega_i|\omega_{i-2}\omega_{i-1})$; the formula is

$$p(\omega_i|\omega_{i-2}\omega_{i-1}) = \frac{c(\omega_{i-2}\omega_{i-1}\omega_i)}{c(\omega_{i-2}\omega_{i-1})}. \tag{25}$$

According to the N-gram grammar model introduced above, we can get

$$P(S) = P(\omega_1, \omega_2,\cdots,\omega_m). \tag{26}$$

Confusion is as follows:

$$\mathrm{PP}(S) = P(\omega_1, \omega_2,\cdots,\omega_m)^{-1/m} = \sqrt[m]{\frac{1}{P(\omega_1, \omega_2,\cdots,\omega_m)}}. \tag{27}$$

According to the chain method, it can be written as

$$\mathrm{PP}(S) = \sqrt{\prod_{i=1}^{m} p(\omega_i|\omega_{i-n-1},\cdots,\omega_{i-1})}. \tag{28}$$

3.3. Construction of Teaching Quality Evaluation Model. The original teaching quality evaluation data is standardized

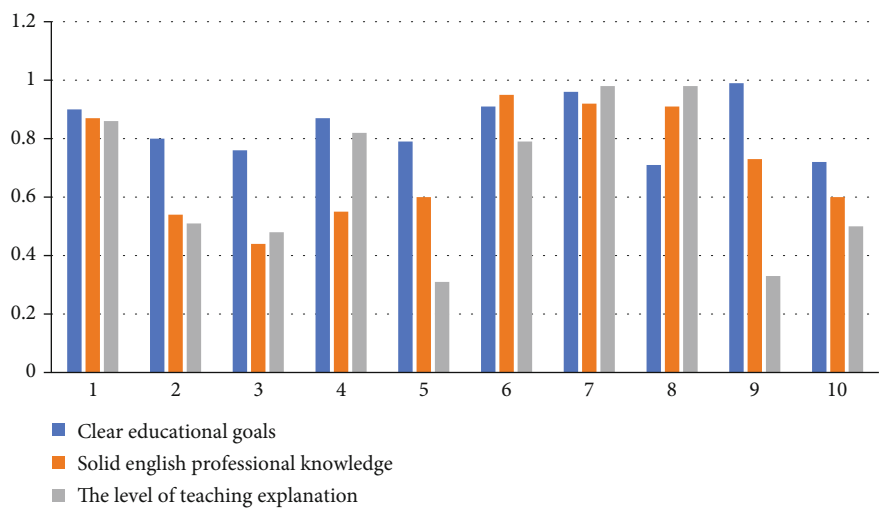

Figure 5: Teacher quality sample results.

Table 6: Sample data of teaching attitude.

Sample number	Counseling and answering questions patiently and positively	Teach seriously	Rigorous attitude
1	0.87	0.92	0.90
2	0.43	0.59	0.89
3	0.46	0.44	0.75
4	0.95	0.63	0.68
5	0.82	0.64	0.75
6	0.81	0.85	0.93
7	0.91	0.86	0.87
8	0.91	0.95	0.91
9	0.74	0.71	0.61
10	0.45	0.51	0.68

[24], and the calculation is publicized as

$$x'_{ij} = \frac{(x_{ij} - \bar{x})}{S_j}, \tag{29}$$

where x_{ij} is the score of the i-th sample in the j-th index, x'_{ij} is the standardized value, and $\bar{x}$ and S_j are the mean and standard deviation of the j-th index, respectively.

The following is the normalized value:

$$Z_{ij} = x'_{ij} + A. \tag{30}$$

Quantify teaching quality evaluation indicators:

$$p_{ij} = \frac{Z_{ij}}{\sum_{i=1}^{m} Z_{ij}} \quad (i = 1, 2, \cdots, m; j = 1, 2, \cdots, n), \tag{31}$$

where w_j is the weight of the j-th index and p_{ij} is the proportion of the i-th sample in the j-th index.

Calculate the index entropy value E_j:

$$E_j = -k \sum_{i=1}^{m} p_{ij} \ln \left(p_{ij}\right), \tag{32}$$

in

$$k = \frac{1}{\ln (n)}, E_j \geq 0. \tag{33}$$

Calculate the coefficient of difference G_j:

$$G_j = 1 - E_j. \tag{34}$$

Calculate the weight of the indicator w_j:

$$w_j = \frac{G_j}{\sum_{j=1}^{n} G_j}. \tag{35}$$

Calculate the teaching quality of the sample F_i:

$$F_i = \sum_{j=1}^{n} w_j p_{ij}. \tag{36}$$

4. Simulation Experiment

4.1. Comparative Experiment. In order to test the quality of English teaching in colleges and universities, the experiment selected 300 non-English major students from a certain university. The students came from different majors such as management, computer, auditing, and accounting. Divide these students into the experimental group, control group, and standard group, with 100 people in each group. We chose 3 teachers with the same teaching age to teach the students in 3 groups, and the teaching time is one academic year. The experiment compares the student performance of the traditional teaching model with the student performance

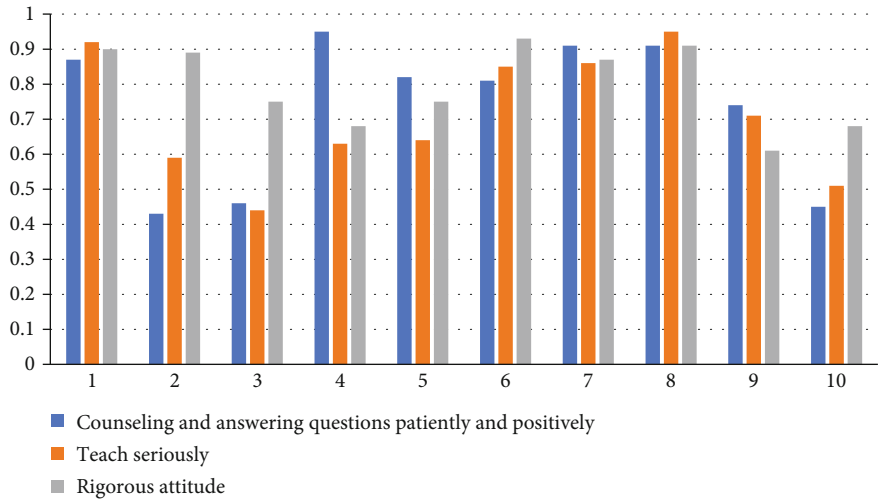

Figure 6: Sample results of teaching attitudes.

Table 7: Sample data of teaching content.

Sample number	Conceptual theory is accurate	Full of content	Focus on practice	Depth of expertise
1	0.94	0.94	0.89	0.71
2	0.56	0.64	0.81	0.59
3	0.92	0.79	0.35	0.71
4	0.68	0.81	0.86	0.92
5	0.75	0.72	0.71	0.83
6	0.70	0.63	0.74	0.47
7	0.82	0.87	0.99	0.90
8	0.91	0.92	0.48	0.95
9	0.88	0.42	0.61	0.55
10	0.70	0.62	0.56	0.65

of the new classroom quality monitoring model and observes the superiority of the new classroom quality monitoring model in English education [25]. In order to ensure the objectivity of the experimental data, the three sets of data were tested separately. The main test content included 5 parts: listening, reading, cloze, translation, and speaking. The specific experimental data are as follows:

From the data in Table 2 and Figure 3, we can conclude that under the traditional teaching mode, the average scores of the experimental group, control group, and standard group are 66.2, 66.8, and 68, respectively, and there is no big difference in the scores of the three groups. Among them, the standard group has the highest score among the three groups. The listening modules of the three groups are the highest among all the test modules. The standard group has a listening score of up to 70 points, and the control group has a listening score of 69 points. The listening score of the experimental group is 68 points. The other test modules are relatively lower, the overall performance presents a lower level, and the students' learning of English is poor.

Based on the data in Table 3 and Figure 4, we can conclude that under the new classroom quality monitoring mode, the average scores of the experimental group, control group, and standard group are 85.5, 86.2, and 89, respectively. Among them, the standard group had the highest scores in listening, reading, and cloze, which were 88, 89, and 90, respectively, and the control group had the highest score in oral English, with 87 points. Compared with the traditional teaching model, the average score of the experimental group has increased by 19.3, the average score of the control group has increased by 19.4, and the average score of the standard group has increased by 20. Overall, the students' English learning level has been greatly improved. The experimental results also show that the new classroom quality monitoring model can improve the quality of teaching.

4.2. Simulation Experiment

4.2.1. Data Collection. In order to test the quality of English teaching in a certain university, the experiment combines the results of teachers' English teaching evaluation to find out the factors affecting English teaching and adopts a questionnaire survey. The undergraduates of a university were taken as an example. The questionnaires are distributed by class. The main content of the questionnaires is the teaching quality evaluation system, which mainly includes multiple-choice questions and short answer questions. The reliability of the returned questionnaires is analyzed. The division of reliability coefficients is shown in Table 4.

The stronger the reliability and consistency of the two indicators in the reliability analysis, the smaller the error and the higher the reliability; the fewer problems will arise after the questionnaire is issued.

4.2.2. Data Preprocessing. According to the collected questionnaire results, the evaluation system of English teacher classroom quality is divided into first-level indicators and

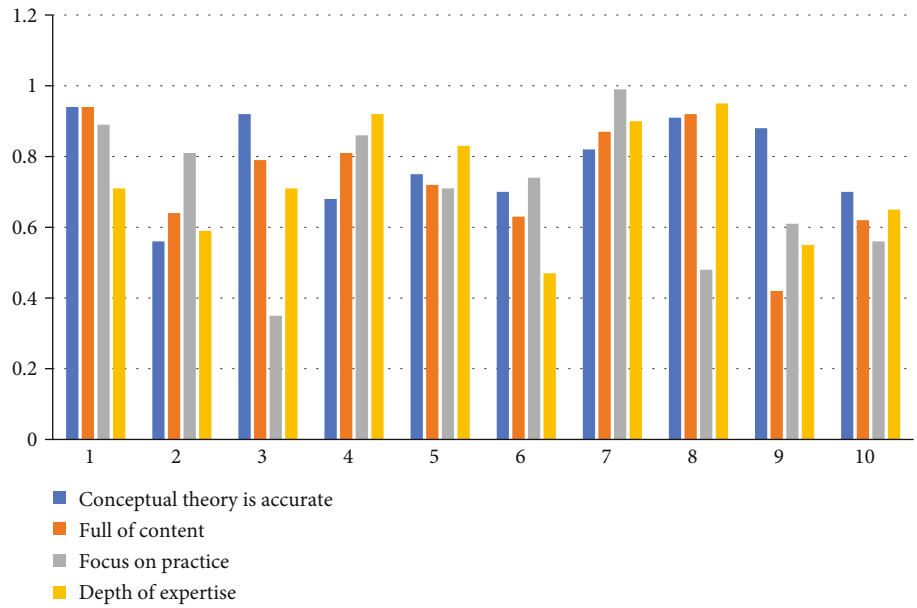

Figure 7: Sample results of teaching content.

second-level indicators. The first-level indicators can be subdivided into 5 levels, and the second-level indicators can be subdivided into 18 levels. The questionnaire is scored by students, and the results are collected to obtain experimental data. The experiment is scored from four aspects: teacher quality, teacher's teaching attitude, teaching content, and teaching method. The specific experimental results are as follows:

(1) Teacher Quality. Based on the data in Table 5 and Figure 5, we can conclude that the reliability coefficient of sample number 1 is always maintained at 0.80-0.95. The experimental data representing sample number 1 is very reliable, and the reliability coefficients with clear educational goals are maintained. Above 0.7, it shows that most teachers' educational goals are very clear. The solid reliability coefficient of English majors remains in the range of 0.70-0.90, which accounts for most of the sample. The teacher's teaching level only has a small number of reliability coefficients, a lower situation.

(2) Teaching Attitude. Based on the data in Table 6 and Figure 6, we can conclude that the reliability coefficient of No. 1 is always maintained at 0.80-0.95, which means that the experimental data of sample No. 1 is very reliable, and the reliability coefficient of sample No. 1 is serious in teaching, reaching 0.92, which not only shows the seriousness of the teacher's teaching and the credibility of the experimental data. Generally speaking, the reliability coefficients of teachers' patience and enthusiasm for answering questions, seriousness in teaching, and rigorous attitude are mostly maintained in the range of 0.70-0.90, which shows the authenticity of the experimental data.

(3) Teaching Content. Based on the data in Table 7 and Figure 7, we can conclude that the theoretical accuracy reliability coefficient of sample number 1 reaches 0.94, and the other reliability coefficients of number 1 also remain above 0.70, indicating the authenticity of the experimental data. In general, the overall reliability coefficient of the teaching content sample data is mostly maintained within the range of 0.70-0.95, and only a few parts show a low situation, which also shows that the overall status of the diversity of teaching content is good.

Table 8: Sample data of teaching methods.

Sample number	Increased interest in learning	Knowledge understanding	Problem analysis ability	Improved ability to innovate
1	0.83	0.92	0.94	0.87
2	0.56	0.54	0.51	0.85
3	0.57	0.62	0.43	0.51
4	0.93	0.82	0.91	0.87
5	0.85	0.86	0.73	0.68
6	0.79	0.63	0.87	0.89
7	0.93	0.92	0.97	0.92
8	0.83	0.96	0.97	0.98
9	0.79	0.89	0.68	0.59
10	0.62	0.65	0. 68	0.76

(4) Teaching Method. According to the data results in Tables 8, 9 and Figure 8, we can conclude that the overall reliability coefficient of the teaching method sample data presents a relatively high situation, and the reliability coefficient of the improvement of innovation ability can reach up to 0.98, indicating the authenticity and authenticity of the experimental data. In effectiveness, the reliability coefficient of sample data 1 presents a high state.

Table 9: Evaluation criteria table.

	Metrics	Formula
Accuracy	The accuracy rate measurement standard refers to the ratio of recommended English teaching resources to the number of recommended teaching resources. The larger the index value, the more accurate the recommendation result [26].	Precision = $\text{hits}_u/\text{recset}_u$
Recall rate	The recall rate standard refers to the ratio of recommended English teaching resources to the theoretical maximum number of hits. The larger the index value, the more accurate the recommendation result.	Recall = $\text{hits}_u/\text{testset}_u$
$F1$ measurement	The $F1$ measurement index can effectively balance the accuracy rate and the recall rate by favoring the smaller value. The larger the index value, the more accurate the recommendation result.	$F1 = 2 \times \text{precision} \times \text{recall}/\text{precision} + \text{recall}$

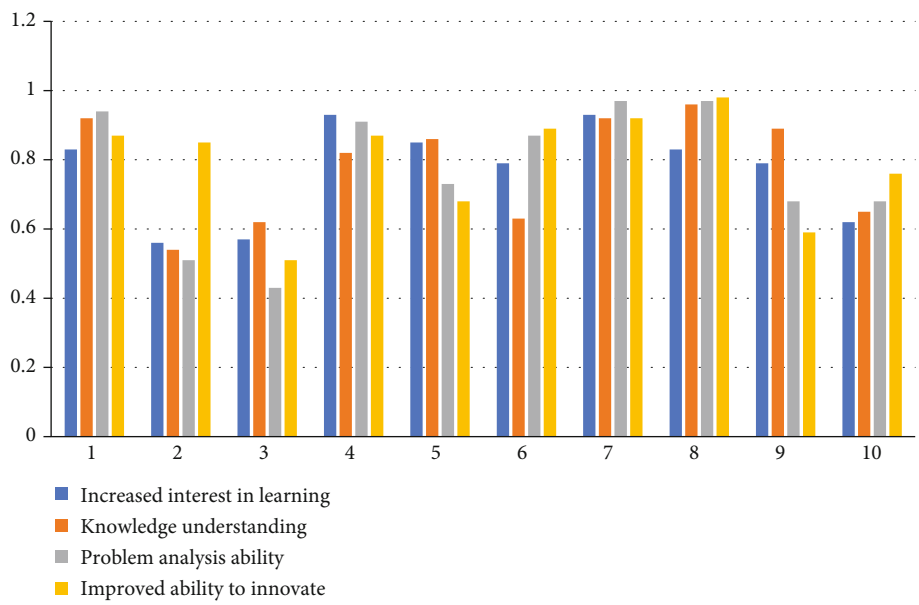

Figure 8: Teaching method sample results.

Table 10: Performance of each model on the test set.

Model	Accuracy rate	Precision rate	Recall rate	$F1$ score
New classroom quality monitoring	99.71%	98.83%	97.74%	98.82%
BP neural network teaching	51.64%	51.29%	97.83%	67.30%
Genetic Algorithm Teaching	88.21%	87.81%	88.62%	89.21%
Adaptive teaching	90.12%	92.21%	90.26%	91.32%
ASS model teaching	97.97%	98.10%	97.89%	98.00%

4.3. Model Performance Testing

4.3.1. Evaluation Criteria

4.3.2. Experimental Results and Analysis. In order to test the performance of the new classroom quality monitoring model, we run the model proposed in the article and other teaching models in different dimensions to test the superiority of the model. The experiment runs each model on the test set and the mixed test set and records the experimental data. The specific experimental data are shown in Tables 10 and 11.

The test set is used to evaluate the generalization ability of the final model, and the hybrid test set is used to adjust the hyperparameters of the model and preliminarily evaluate the ability of the model.

According to the data in Figure 9, we can conclude that the accuracy rate of the new classroom quality monitoring

Table 11: Performance of each model on the mixed test set.

Model	Accuracy rate	Precision rate	Recall rate	$F1$ score
New classroom quality monitoring	98.01%	98.67%	97.73%	98.20%
BP neural network teaching	67.70%	66.37%	70.75%	69.55%
Genetic Algorithm Teaching	90.49%	91.25%	89.63%	89.83%
Adaptive teaching	92.68%	91.49%	94.75%	90.77%
ASS model teaching	96.72%	98.54%	95.53%	97.01%

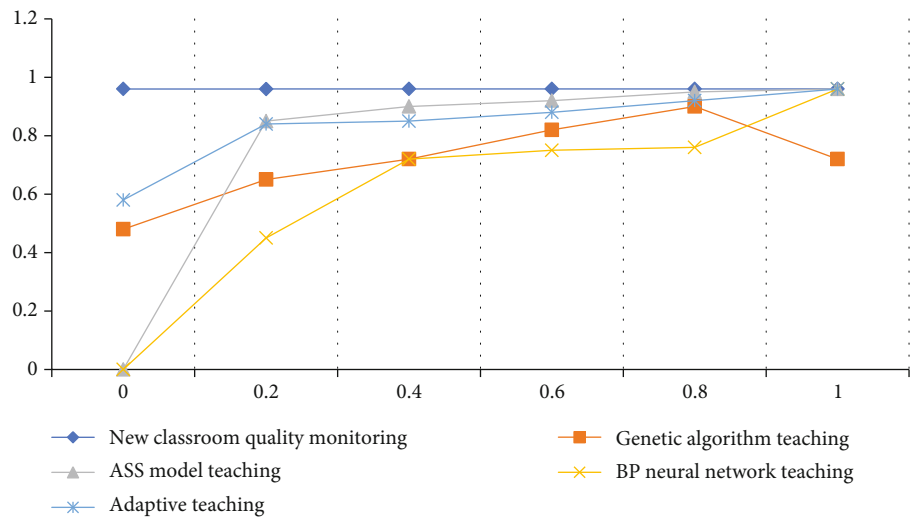

Figure 9: ROC curve on the test set.

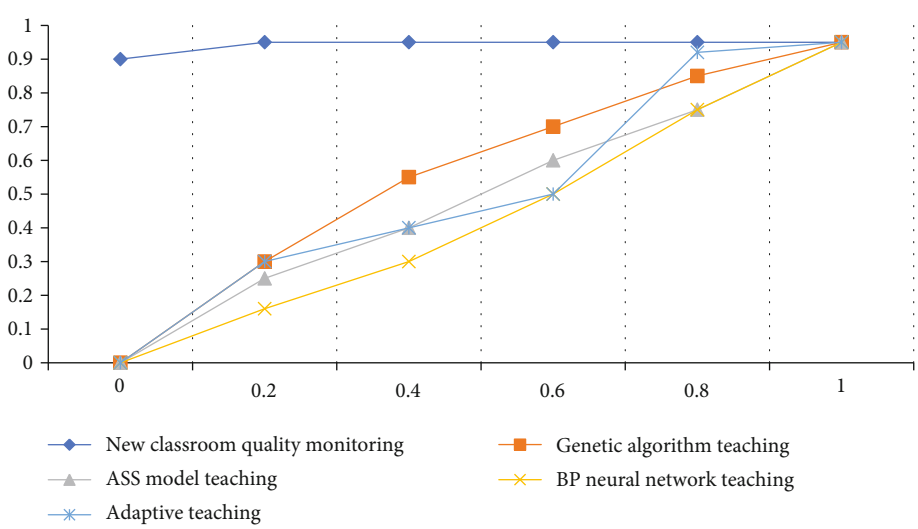

Figure 10: ROC curve on the mixed test set.

teaching model proposed in the article is the highest among several models, which can reach 99.71%, indicating that the teaching performance of the new classroom quality monitoring teaching model is the highest. Among them, the accuracy of the BP neural network teaching model is the lowest at 51.64%, indicating that the detection efficiency of the BP neural network teaching model is not good enough.

According to the data in Figure 10, we can conclude that whether it is in the test set or the mixed test set, the accuracy of the new classroom quality monitoring model proposed in

the article is the highest among the three models, and it is the highest on the mixed test set. The highest accuracy rate can reach 98.01%, and the accuracy rate can reach 98.67%, which also illustrates the superiority of the performance of the new classroom quality monitoring model. ROC curve combines sensitivity and specificity as a graphical method, which can accurately reflect the relationship between specificity and sensitivity of analytical methods, and is a comprehensive representative of the accuracy of the test. ROC curve does not fix the classification threshold and allows the existence of intermediate state, which is helpful for users to combine professional knowledge, weigh the impact of missed diagnosis and misdiagnosis, and select a better cut-off point as a diagnostic reference value. To provide an intuitive comparison between different tests under a common scale, the more convex the ROC curve is, the closer it is to the upper left corner, indicating that its diagnostic value is greater, which is conducive to the comparison between different indicators.

5. Conclusion

At present, there are more and more English learners, and the English grammar module is also an important part of the English learning process. However, due to the particularity of English teaching, there are still some shortcomings in English teaching in many universities in our country. With multifaceted support, there is still a lot of room for improvement in English teaching. Therefore, we should combine the current problems and make in-depth summaries to create a more intelligent and accurate English teaching model to make English teaching easier and more efficient.

The characteristics of college English teaching in China in the transitional period are that the professional boundaries are not clear enough, the basic teaching is not paid attention to, the teaching mode is diversified, and the teaching effect is improved. After the transformation, college English teaching is more in line with the needs of society and the times than before. College English teaching in the transitional period can improve college students' English learning ability by improving college students' interest in English courses, changing college English teachers' teaching ideas, improving college English teachers' professional quality, improving college English teaching equipment and facilities, and paying attention to the application training of college English teaching. In the transitional period, college English teachers must be student-centered in their teaching work.

Data Availability

The experimental data used to support the findings of this study are available from the corresponding author upon request.

Conflicts of Interest

The authors declared that they have no conflicts of interest regarding this work.

References

[1] L. Panpan, "Study on monitoring index system of college English classroom teaching quality based on BOPPPS model [C]," in *2019 9th International Conference on Education and Social Science (ICESS 2019)*, Shenyang, Liaoning, China, 2019.

[2] F. J. Wei, "On the autonomous learning ability in college English teaching [J]," *Journal of Hebei Normal University (Educational Science Edition)*, vol. 20, no. 2, pp. 11–17, 2011.

[3] L. Xiong and Z. Ling, "On building computer-based college English teaching quality assurance system," in *2010 International Conference On Computer Design and Applications*, pp. V2-284–V2-288, Qinhuangdao, China, 2010.

[4] H. Yin, "Research on the quality of college English teaching design based on BOPPPS model [C]," in *2018 International Conference on Social Science and Education Reform (ICSSER 2018)*, Xi'an, Shaanxi, China, 2018.

[5] M. R. Agravat, "Continuing Professional Development (CPD) for ensuring quality, monitoring and evaluating quality, in Teaching English–an analysis of survey," *Global Journal of Engineering Sciences*, vol. 5, no. 12, pp. 52–55, 2008.

[6] I. M. Krsmanović, B. I. English, and V. M. Petrović, "Factors affecting quality in teaching English (as a second language)," vol. 2, no. 12, pp. 11–19, 2010.

[7] M. Ediger, "Teaching college English," *Academic Achievement*, vol. 4, no. 8, pp. 114–120, 1991.

[8] M. L. Zhang, M. A. Xing-Yu, and S. Yang, "The exploration of ecological college English teaching mode based on the target of cultivating international talents [J]," *Journal of Jilin Teachers Institute of Engineering and Technology*, vol. 12, no. 2, pp. 110–115, 2012.

[9] Y. Xiao, "College English teaching based on language monitoring [J]," *The Science Education Article Collects*, vol. 12, no. 8, pp. 21–27, 2017.

[10] W. Wei, "On construction of the teaching quality monitoring of college English——about listing and speaking course under the curriculum system of TMM [J]," *Journal of Jixi University*, vol. 14, no. 2, pp. 54–60, 2015.

[11] B. I. Chun-Yi, "The plan of teaching quality monitoring and assessment in college English viewing, listening and speaking course [J]," *Journal of Hubei Correspondence University*, vol. 12, no. 7, pp. 21–25, 2015.

[12] L. I. Bei-Bei, "Analysis of monitoring college English autonomous learning based on net environment [J]," *Journal of Yangzhou College of Education*, vol. 12, no. 1, pp. 117–121, 2015.

[13] Y. Xu, "Research on the teaching evaluation and quality monitoring system of higher vocational English flipped classroom under the network environment [J]," *Journal of Jiamusi Vocational Institute*, vol. 14, no. 7, pp. 21–32, 2016.

[14] K. H. Chen, "On constructing a diversified evaluation system in English pronunciation teaching in college [J]," *Journal of Dongguan University of Technology*, vol. 14, no. 7, pp. 11–19, 2016.

[15] H. U. Chun-Yan and Y. Sun, "A primary analysis on monitoring modes in the blended learning of college English——based on college English teaching man agement platform (level a)[J]," *Overseas English*, vol. 17, no. 4, pp. 45–49, 2012.

[16] W. Fang and Z. Lili, "Research and practice of teaching quality monitoring system in applied undergraduate colleges and universities [J]," *Chinese Business*, vol. 8, pp. 130–133, 2009.

[17] L. Xiuqing and G. Shan, "Research on the quality monitoring index system of college English classroom teaching [J]," *China Adult Education*, vol. 12, pp. 151-152, 2010.

[18] P. D. Grey, "Book review: "Making content comprehensible for English learners, the SIOP model"," *Acda Didactica Norge*, vol. 6, no. 1, p. 22, 2012.

[19] Y. Chen, "Application of SIOP teaching mode in business secretary English course [J]," *Journal of Wuxi Institute of Technology*, vol. 17, no. 3, 2018.

[20] D. Jonassen and P. Hnning, "Mental models: knowledge in the headand knowledge in the world [J]," *Educational Knowledge*, vol. 39, no. 5/6, pp. 37–41, 1999.

[21] L. Zhou, H. Li, and K. Sun, "Teaching performance evaluation by means of a hierarchical multifactorial evaluation model based on type-2 fuzzy sets," *Applied Intelligence*, vol. 46, no. 1, pp. 34–44, 2017.

[22] Y. Feng, Y. U. Gan, and H. Zhou, "Teaching quality evaluation model based on neural network and analytic hierarchy process [J]," *Computer Engineering and Applications*, vol. 49, no. 17, pp. 235–3068, 2013.

[23] X. Zhao, "TOPSIS method for interval-valued intuitionistic fuzzy multiple attribute decision making and its application to teaching quality evaluation," *Engineering and Technology*, vol. 26, no. 6, pp. 3049–3055, 2014.

[24] L. Bai and X. X. Guo, "The model of evaluating teaching quality based on BP neural network algorithm," *Applied Mechanics and Materials*, vol. 719-720, pp. 1297–1301, 2015.

[25] N. S. Jaddi, S. Abdullah, and A. R. Hamdan, "A solution representation of genetic algorithm for neural network weights and structure," *Information Processing Letters*, vol. 116, no. 1, pp. 22–25, 2016.

[26] L. Ferrer, L. Yun, and M. Mclaren, "Study of senone-based deep neural network approaches for spoken language recognition," *IEEE/ACM Transactions on Audio Speech & Language Processing*, vol. 24, no. 1, pp. 105–116, 2016.

Hindawi
Journal of Sensors
Volume 2022, Article ID 3323866, 10 pages
https://doi.org/10.1155/2022/3323866

Research Article

Research and Analysis of Evaluation and Expansion of Physical Education Teaching System Based on Internet of Things Communication

Qingyun Wang[1] and Hua Li[2]

[1]*Sports Department of Hunan Women's College, Changsha, Hunan 410004, China*
[2]*Department of Physical Education, Hohai University, Nanjing 210014, China*

Correspondence should be addressed to Hua Li; 20080068@hhu.edu.cn

Received 28 January 2022; Revised 19 March 2022; Accepted 22 March 2022; Published 9 May 2022

Academic Editor: Yuan Li

Under the influence of China's education reform, the assessment and evaluation of physical education have gradually attracted more and more people's attention. Teaching evaluation ignores the development of students' sports lifestyle. The article uses principal component analysis to establish a teaching quality evaluation model and design an extensible teaching evaluation system. The article uses box plots to reflect the characteristics of data changes, which can clearly draw differences between samples. Three variables of experimental class, reference class, and standard class are set up to conduct controlled experiments, and statistics are made from the survey results of the 2018-2019 school year physical education evaluation student evaluation. The experimental results indicate that after using the system, students' learning satisfaction and enthusiasm have been greatly increased, and students' weekly exercise time and sports items have also increased. Before and after the use of the teaching evaluation system, the students' satisfaction with the evaluation system and the degree of movement recognition were tested. The results show that the system has a positive effect on the students' evaluation satisfaction and movement recognition.

1. Introduction

As the degree of informatization of physical education continues to deepen, attention is gradually being paid to the assessment and evaluation of physical education. The article proposes an expanded physical education teacher assessment and evaluation system. Literature [1] applies the analytic hierarchy process to establish a system of the physical education curriculum evaluation system and conduct empirical analysis, constructing an evaluation index system composed of 5 one-level indicators and 13 second-level indicators. In this practical operation, we can find that the system can clearly reflect the learning situation of college students for PE course selection, and the model can also be empirically analyzed. The system has strong operability. In the literature [2], interviews, evaluations, and tests, it is believed that the index has high reliability, validity, and easy-to-use characteristics, and it provides a scientific basis for physical education teaching. Literature [3] explained the necessity of including physical education into the college entrance examination system from different aspects; the article analyzed the importance of physical education and believed that including sports into the college entrance examination is a plan proposed by the system of caring for students, and it can also improve the importance of physical education. Literature [4] established a new event physical education teaching and curriculum evaluation based on the principles and methods of sociological statistics; this paper applies the established curriculum evaluation system to offline teaching practice, evaluates this emerging event, and explores the necessity of building a classroom curriculum evaluation system. According to the research results, the evaluation method has a great promotion effect on the course teaching and has a broad prospect for development. Through investigation and statistics, a comprehensive analysis of the intelligence method, literature [5] established a

comprehensive evaluation index system according to the ability, quality, and knowledge structure of physical education teachers. In order to accurately evaluate the performance of faculty and staff, an effective evaluation system is essential. The literature [6] is investigating the status quo of the evaluation of teachers of physical education departments in American universities and colleges for providing analysis for an effective evaluation system. The research results show that the experimental results prove that not only can provide accurate information but also explore how the respondents view the important types of information used in the current teacher evaluation system. Literature [7] combined fuzzy mathematics decision-making with the MBO performance evaluation system in management theory and constructed a reasonable model of the performance. Based on the design model, the article uses analysis and evaluation methods to comprehensively evaluate performance and provides a reference for teacher evaluation. Literature [8] studied the theoretical basis of the practical ability evaluation system of physical education students in normal colleges, the determination of evaluation weights, the formulation of evaluation standards, and the evaluation of practical ability. The research has a great role in promoting the establishment of the evaluation system of college students. General physical education evaluation is organized by the school's leaders, ignoring the importance and particularity of physical education, and selecting methods similar to other courses for curriculum evaluation; literature [9] relies on students and colleagues, quantitative analysis combined with quantitative statistics. In order to objectively, comprehensively, and truly reflect the present situation and effect of physical education, a university should have a practical teaching quality evaluation system, which is the basis for guaranteeing teaching quality. It is particularly important to establish a successful teaching quality evaluation system; literature [10] uses the analytic hierarchy process to establish a physical education teacher's teaching quality indicator system, and the distribution of weights can provide a scientific basis for constructing the quality evaluation system of college physical education teachers. The article analyzes many aspects of pedagogy [11], investigates a large amount of data, and analyzes the status quo of teaching evaluation in a university in Xi'an. Literature [12] constructed a teaching evaluation index system for the sports major; the author analyzed the education ratings of professionals in the education field and constructed a teaching evaluation index system for the sports industry. Literature [13] uses fuzzy mathematics to develop physical education teaching and evaluation of curriculum application. The educational quality evaluation of colleges and universities is a huge project. The system can directly reflect the teaching quality of schools and also provides reliable information for the Ministry of Education. Literature [14] proposes that education reform has triggered an extensive process of research, restoration, systematization, and reorganization of the education system and has resulted in profound changes in the conceptual field. Literature [15] is the basis for the systematic analysis of the connotation and characteristics of school sports policy execution above. The system includes individuals and organizations, which are divided into multiple indicators to meet the school's teaching evaluation tasks. Different literatures are put forward to analyze different teaching classes. From the above literatures, different research points can be reflected to analyze the relevance of the index system structure. It also reflects the fairness and impartiality of the evaluation system and can provide practical guidance for different teaching applications.

2. Research Status

2.1. The Evaluation of the Physical Education System

2.1.1. Sports Assessment Method. At present, many school physical examination and evaluation methods are carried out by filling in offline paper questionnaires and electronic forms. The school evaluation management staff will send the paper forms to the students, and the students will fill in according to their own opinions. And then, the staff will count and summarize the collected data and then get the final result. The statistical data is relatively large, the calculation is not convenient, and the statistical results will have some artificial errors. Based on these problems, some colleges and universities have established a teaching evaluation system. Compared with traditional evaluation methods, the calculation results are accurate, and work efficiency has been greatly improved. However, the system also has some shortcomings because of the particularity of certain courses. The evaluation of such courses lacks flexibility, which will also be improved for network technology.

2.1.2. Assessment Status Analysis. Because of the inflexibility of the system, the assessment and evaluation of some courses are still in manual operation, lacking a complete set of information technology to support the evaluation work, and the teachers present an independent and decentralized way and lack a unified set of information.

2.2. The Internet of Things Establishes the Conditions for the Construction of the System

2.2.1. The Current Progress of College Informatization Construction. As we all know, in the development process of colleges and universities, informatization construction has undergone initial hardware construction, network construction, and transition to application construction and service construction. It has transitioned from independent and partial construction to overall and overall construction. Therefore, under the impetus of this process, we are engaged in the department of physical education assessment, and evaluation will naturally think about the use of current information technology to realize its needs for assessment and evaluation.

2.2.2. IT Technology Drive at the Current Stage. At present, IT technology in information technology is changing with each passing day, especially with the mobile Internet and the IoT; some application framework technologies are emerging in an endless stream [16]. NET framework, Java's SSH MVC framework, Wabacus, Jquery framework, etc., and some advanced development environments such as

Delphi XE7, MyEclipse, VS.NET, and Android provide more feasibility and convenience for technical implementation. In the construction process, the above has also been greatly improved than before. Driven by this series of advanced technologies, informatization builders can better control the construction process in accordance with actual needs.

The application of corresponding technical means is to realize the fairness and objectivity of teaching quality evaluation in this paper. In the specific function realization, the system design and optimization can be realized by using the above technology.

2.3. Significance of the Assessment System. Most assessment and evaluation systems themselves have certain similarities and commonalities. Under the conditions of meeting actual needs, these similar and common functions are encapsulated into an independent functional module, and then, the relationship between various levels is established from an overall perspective. As well as the functional logic within the hierarchy, the design helps to establish a relatively open and universal information system.

3. Method

3.1. Physical Education Evaluation Method. The index system of the cloud model can be expressed quantitatively and accurately, and the concept can also be described in a qualitative way of discourse [17]; the sample is the N groups as an example; the N groups of samples are gathered into a rectangular array and expressed by the formula:

$$E_x = \frac{E_{X1} + E_{X2} + \cdots E_{Xn}}{n}, \tag{1}$$

$$E_n = \frac{\max\left(E_{X1}, E_{X2}, \cdots E_{Xn}\right) - \min\left(E_{X1}, E_{X2}, \cdots E_{Xn}\right)}{6}. \tag{2}$$

The principal component analysis model is defined:

$$\begin{cases} F_1 = a_{11}X_1 + a_{21}X_2 + a_{p1}X_p, \\ F_2 = a_{12}X_1 + a_{22}X_2 + a_{p2}X_p, \\ \cdots \\ F_m = a_{1m}X_1 + a_{2m}X_2 + a_{pm}X_p. \end{cases} \tag{3}$$

According to the contribution rate, select the first s principal components $F_1, F_2, \cdots F_s$ to make the contribution rate exceed 90% [18]; then add the principal components to construct a comprehensive evaluation function:

$$\begin{cases} F = h_1F_1 + h_2F_2 + \cdots h_sF_s, \\ h_s = \sum_{j=1}^{s} \frac{a_{1j}\ \mathrm{var}\left(F_j\right)}{\sum_{j=1}^{s}\mathrm{var}\left(F_j\right)}. \end{cases} \tag{4}$$

Can get parameters $X_i (i = 1, 2, 3 \cdots p)$.

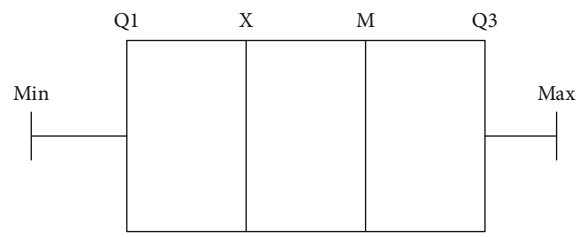

Figure 1: Box diagram.

Table 1: Student evaluation of teaching survey result table.

Class	Attitude	Ability	Content	Method	Effect
Reference class	21.45	17.09	12.85	17.11	17.11
Experimental class	21.8	17.38	13.09	17.43	17.47
Standard class	20.7	17.11	12.5	17.08	17.01

In an ideal situation, the center of gravity of P dimension in cloud theory is

$$a = \left(E_{X_1}^0, E_{X_2}^0, \cdots E_{X_n}^0\right). \tag{5}$$

The vector height of the cloud center of gravity is

$$b = \left(b_1, b_2, \cdots b_n\right). \tag{6}$$

In a perfect situation, the p-dimensional integrated cloud center of gravity vector is expressed as follows:

$$T^0 = a \times b^T = \left(T_1^0, T_2^0, \cdots T_P^0\right). \tag{7}$$

In the imperfect situation, Formula (7) can be described as follows:

$$T = \left(T_1, T_2, \cdots T_P\right). \tag{8}$$

Formula (8) is normalized into a vector [19].

$$T_i^G = \left\{ \begin{array}{l} \frac{T_i - T_i^0}{T_i^0}, , T_i < T_i^0 \\ \frac{T_i - T_i^0}{T_i}, T_i \geq T_i^0 \end{array} \right\} (i = 1, 2, \cdots p). \tag{9}$$

After processing the indicator, multiply it with the weight value of each indicator [20] to get:

$$\theta = \sum_{j=1}^{p} \left| W_j \times T_j^G \right| (0 \leq \theta \leq 1). \tag{10}$$

In this which, W_j is the J weight value.

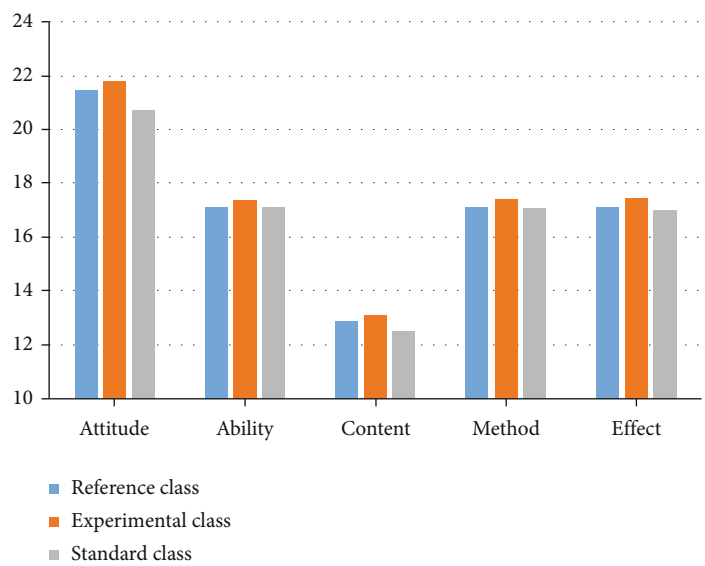

Figure 2: Survey results of teaching in physical education evaluation.

3.2. Teaching Quality Evaluation Model

3.2.1. Comparison of Professional Modules. We use box plots to reflect the characteristics of the data distribution. There are six numerical features [21], as shown in Figure 1.

We can evaluate the situation of different samples by comparing $Q_{1,i}, \bar{X}_i, M_i, Q_{3,i}$ [22]; the calculation formula is

$$R_i = \mathrm{Max}_i - \mathrm{Min}_i. \tag{11}$$

If there is a big difference between the samples, you can use the formula:

$$A_i = \frac{1}{4}Q_{1,i} + \frac{1}{2}M_i + \frac{1}{4}Q_{3,i}. \tag{12}$$

Use the concept of elasticity in economics to describe the changes in samples between different years. The general definition of elasticity can be expressed as the percentage of the rate of change of one variable (Y) $(\Delta Y/Y)$ and the rate of change of another variable $(X)(\Delta X/X)$ mathematics. The expression is

$$\varepsilon_{x,v} = \left|\frac{\Delta Y/Y}{\Delta X/X}\right| \times 100 = \left|\frac{\Delta Y}{\Delta X} \cdot \frac{X}{Y}\right| \times 100. \tag{13}$$

Divide the sample into N levels and assign different weights W_j [23], the calculation formula is

$$W_j = (N+1) - j. \tag{14}$$

Use $a_{i,j}, b_{i,j}$ to represent the number of people in the j-th level in the i sample. The calculation formula is

$$P_i = \sum_{j=1}^{n} a_{i,j} = \sum_{j=1}^{n} b_{i,j} \quad (i, j \in n), \tag{15}$$

Table 2: Students' weekly exercise status survey form.

Class	Student exercise time (hour)	Number of student exercise items (a)	Student exercise intensity (level)
Reference class	6.95	8.12	4
Experimental class	4.8	6.5	3
Standard class	5.0	7.1	2

$$D_i = \frac{\left(\sum_{i=1}^{n} a_{i.j} \cdot W_i\right)}{P_i}, \tag{16}$$

$$E_i = \frac{\left(\sum_{i=1}^{n} b_{i.j} \cdot W_i\right)}{P_i}. \tag{17}$$

Use elasticity to reflect the degree of change of each sample in different periods [24].

$$\varepsilon_i = \left|\frac{E_i - D_i}{D_i}\right| \times 100 \, (0 \le \varepsilon_i \le 100). \tag{18}$$

3.2.2. Module Comparison. The clustering treatment can better reflect the differences between groups and is a commonly used method for evaluating group characteristics [25]; the calculation formula is

$$V_h = \max\left\{\left|H_{.j1} - L_{i1.}\right|\right\}, \tag{19}$$

where $i_1 = 1, 2, \cdots, k$ and $j_1 = 1, 2, \cdots, s$.

Evaluation index A_{i1} is:

$$\Delta_{i1} = \frac{1}{4}Q_{1,V_h} + \frac{1}{2}M_{V_{j1}} + \frac{1}{4}Q_{3,V_{j1}}. \tag{20}$$

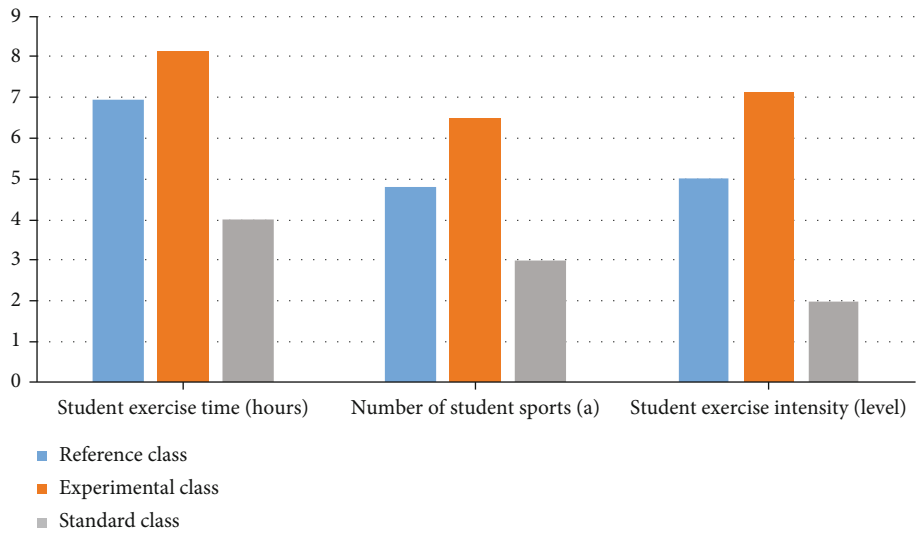

Figure 3: Diagram of students' weekly exercise status.

Table 3: Intelligent system test.

System	Number of requests	3000	3500	4000	4500	5000	5500	6000
Internet of Things system	Average response time	33	45	55	95	135	205	279
	Success rate (%)	100	100	100	100	100	100	100
Custom development model	Average response time	40	55	86	180	250	420	500
	Success rate (%)	100	99.6	99.5	99.4	99.3	98.4	99.3
Platform development model	Average response time	53	65	100	220	420	460	550
	Success rate (%)	100	98.6	98.5	98.4	98.3	98.2	98

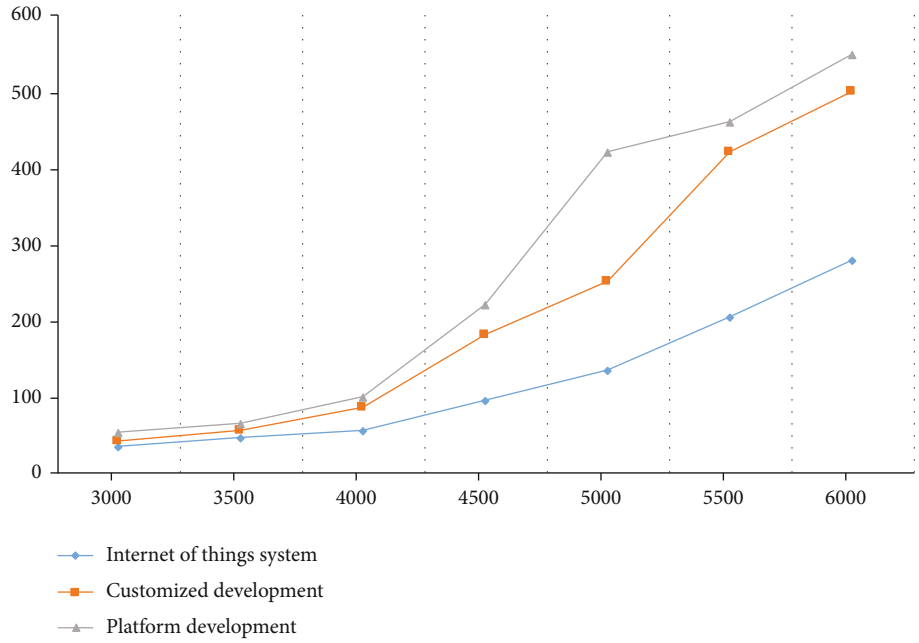

Figure 4: Average response time curve.

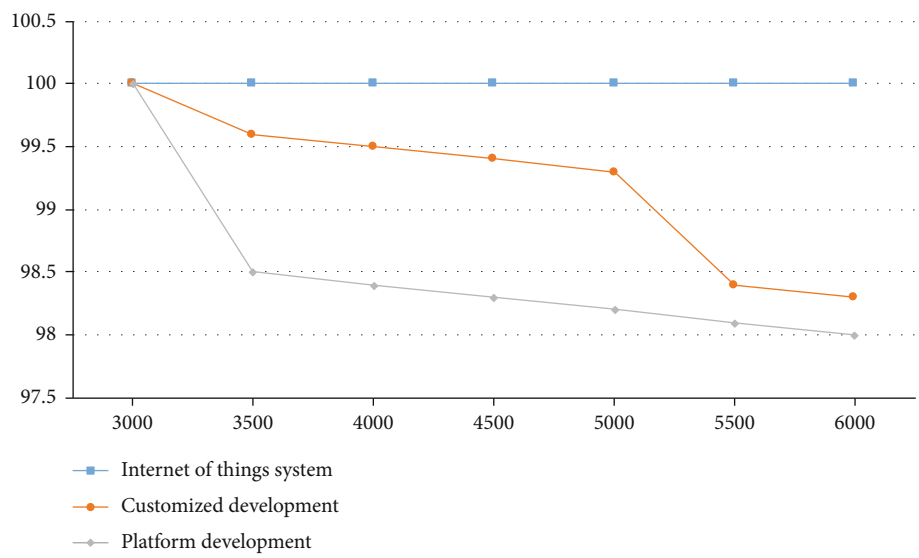

Figure 5: Success rate curve.

Table 4: Test parameters of Internet of Things system.

System	Number of requests	90	120	150	180	210	240	270
Internet of Things system	Average response time	85	290	350	450	600	800	920
	Success rate (%)	100	100	100	100	100	100	100
Custom development model	Average response time	105	300	430	550	750	1150	1500
	Success rate (%)	100	99.6	99.5	99.4	99.3	99.2	99.1
Platform development model	Average response time	160	260	500	600	900	1400	1700
	Success rate (%)	99.7	99.5	99.4	99.3	99.2	99.1	99.0

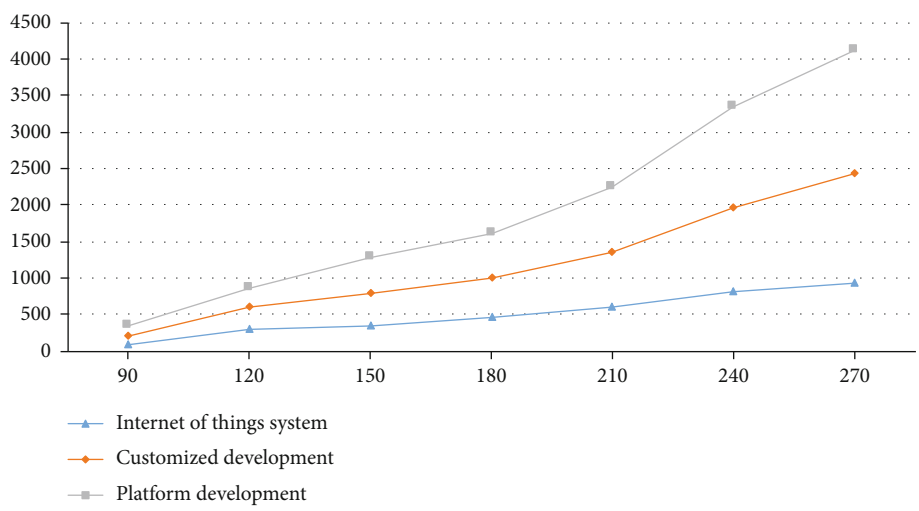

Figure 6: Average response time curve.

We can get a professional teaching quality evaluation model.

$$Y = \alpha A_i + \beta \varepsilon_i + \gamma \Delta_{i1}. \tag{21}$$

Then, there is

$$A_i = \frac{1}{4} Q_{1,i} + \frac{1}{2} M_i + \frac{1}{4} Q_{3,i}. \tag{22}$$

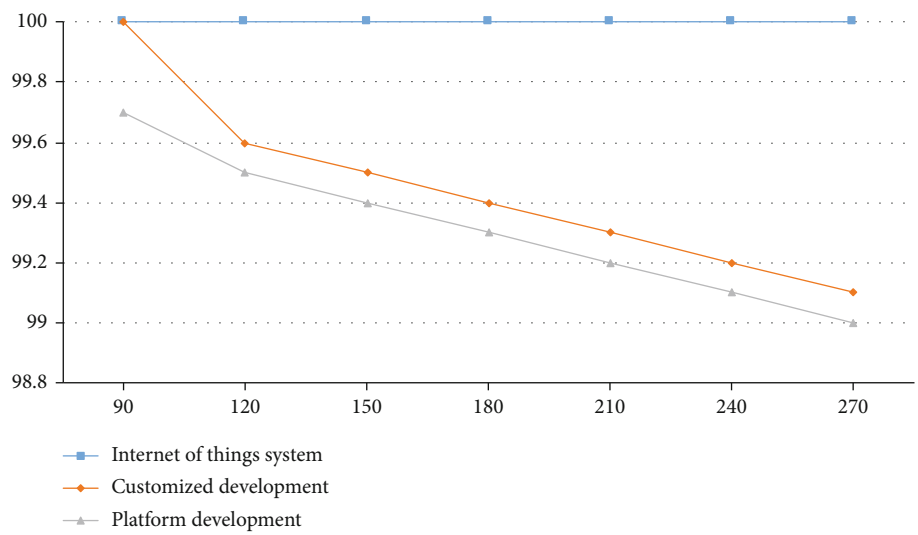

Figure 7: Success rate curve.

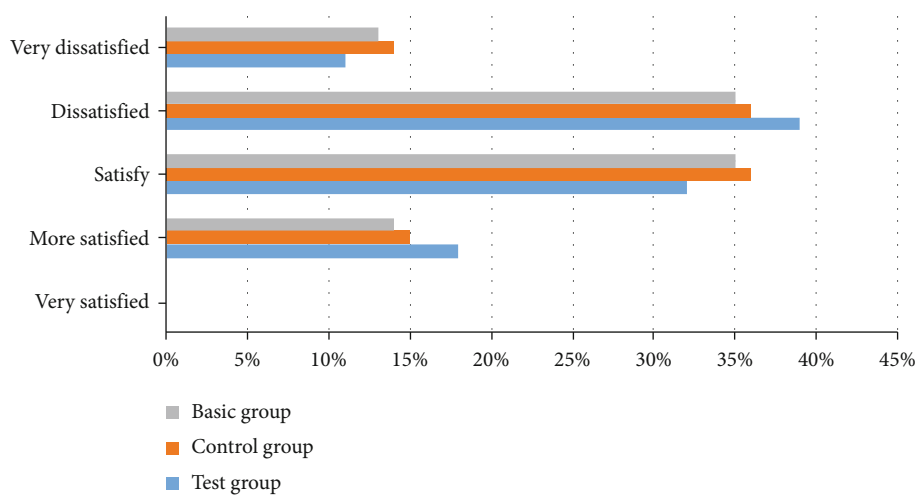

Figure 8: Student satisfaction survey before using the system.

ε_i indicates the situation of different modules:

$$\varepsilon_i = \frac{\sum_{i=1}^{n}(b_{ij} - a_{ij})(W_i/P_i)}{\sum_{i=1}^{n} a_{ij}(W_i/P_i)} \times 100 \quad (i = 1, 2, \cdots l; j = 1, 2, \cdots, n). \tag{23}$$

In this which,

$$W_i = (N + 1) - j, \tag{24}$$

$$P_i = \sum_{i=1}^{n} a_{ij} = \sum_{i=1}^{n} b_{ij}. \tag{25}$$

Δ_i can be used as the basis for evaluation:

$$\Delta_{i1} = \frac{1}{4} Q_{1V_i} + \frac{1}{2} M_{V_i} + \frac{1}{4} Q_{3V_i}. \tag{26}$$

In this which:

$$V_{i_1} = \max\left\{\left|H_{\cdot i_1} - L_{i_1 \cdot}\right|\right\}(i_1 = 1, 2, \cdots, k). \tag{27}$$

Finally got:

$$L_{i_1 \cdot} = \frac{\sum_{i_1=1}^{s} \sum_{i=1}^{p_1+p_2+\cdots p_L} a_{i_1 ij} \cdot W_i}{\sum_{i=1}^{L} SP_i}. \tag{28}$$

4. Experimental Part

4.1. Experimental Comparison Results. Using the teaching evaluation system, we conducted a school year of teaching practice. We set up three variables of experimental class, reference class, and standard class to conduct comparative experiments. We conducted statistics from the results of the 2018-2019 school year physical education evaluation student evaluation survey results. In the article, the indexes of

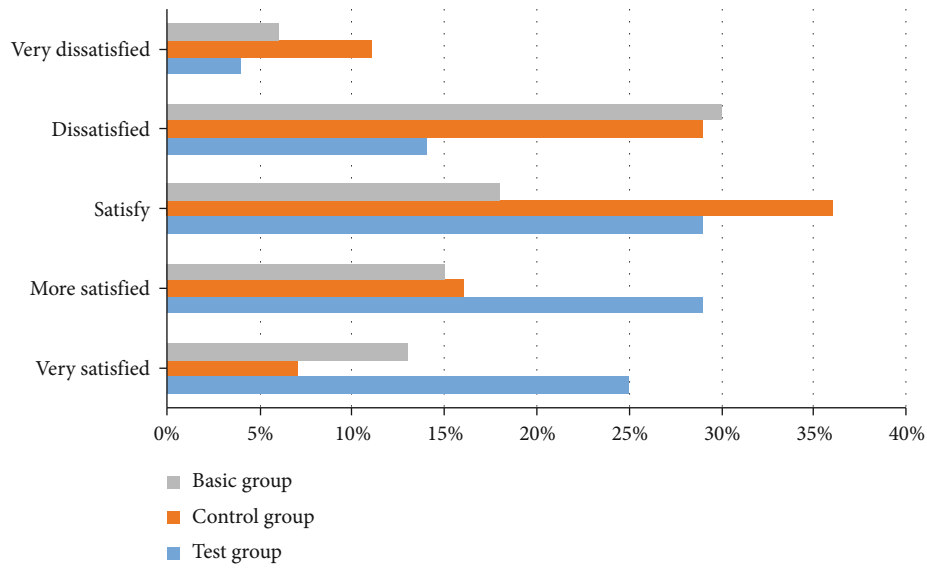

Figure 9: Student satisfaction survey after using the system.

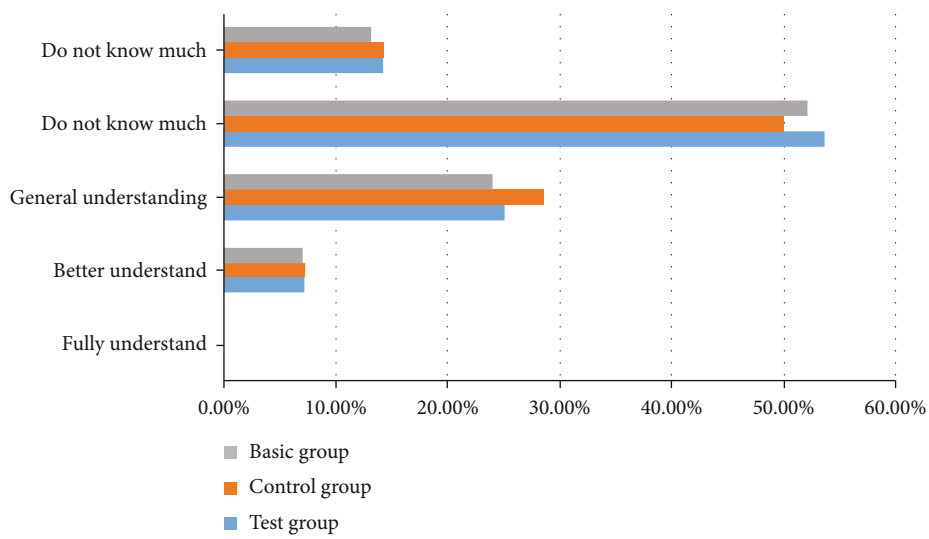

Figure 10: A survey of students' movement awareness before using the system.

teaching attitude, teaching ability, teaching content, teaching method, and teaching effect are comprehensively applied, and the students' application time, the number of items, and the intensity of exercise are compared. The paper is also divided into reference class, experimental class, and standard class for comparison. The results show that the application of these indicators plays an important role.

The specific situation is as follows. Table 1 is shown; the statistical diagram is shown in Figure 2.

From Figure 2, we can see that the students in our test are more satisfied with their teachers than the reference class and standard class. Most students give the system a higher evaluation; the system has adjusted and adjusted the previous teaching methods. Compared with the previous teaching method, students' interest in learning has shown a substantial increase; we have conducted a survey of students' weekly exercise. The specific situation is shown in Table 2, and the statistical chart is shown in Figure 3.

From Figure 3, we can see that the students' exercise time and sports items have been increased by four, which helps the students to form the consciousness of physical exercise in the subconscious.

4.2. System Test. We tested the average response time and query time of the system and their success rate and set up three modes of intelligent optimization, custom development, and platform development for comparison experiments. The specific conditions are shown in Table 3.

From Figures 4 and 5, we can get that, compared with the other two modes. The system with intelligent optimization method has obvious advantages in average response time and query efficiency. In concurrent multitasking, the

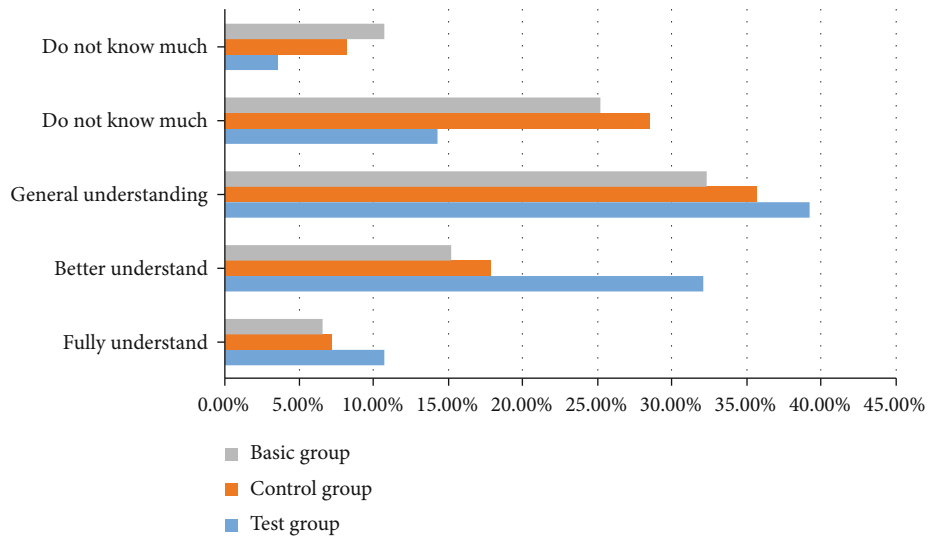

Figure 11: A survey of students' movement awareness after using the system.

average response time will increase, but the success rate will decrease.

The test parameters of multitasking capability of Internet of Things system are shown in Table 4 and Figures 6 and 7.

In the experimental part of the article, the system is tested. From the experimental results, the system with intelligent optimization scheme has lower response time and higher success rate. From the point of view of system complexity, the time complexity of intelligent optimization scheme is $n * \log(n)$, while the other two schemes are n^2 and n^3, which have higher time complexity. As far as the overall performance is concerned, the intelligent optimization system has higher performance and better complexity.

4.3. Extended Research Analysis. This experiment tested the students' satisfaction with the evaluation system and their knowledge of actions after using the teaching evaluation system. Three variables were set up: the experimental group, the control group, and the basic group. The specific experimental conditions are shown in Figures 8 and 9.

From Figures 8 and 9, we can see that the students' satisfaction with the three groups of variables has increased to a certain extent after using the system. Among them, the satisfaction of the experimental group has been greatly improved, and the dissatisfaction has been greatly improved. The experimental results show that the teaching evaluation system can improve students' summative evaluation of conventional teaching methods, and they have great satisfaction with the evaluation system.

From Figures 10 and 11, we can see that there is no significant difference in motor cognition among the students in the first three groups without using the teaching evaluation system. After using the system, there is a significant difference in motor cognition. The situation in the experimental group is more significant.

5. Conclusion

In short, the evaluation of physical education is an important link in the process of school physical education and plays an important role in constructing a complete and effective teaching process. Whether the establishment of physical teaching principles is reasonable, whether students' learning behaviors are correct, and whether the teaching effect is excellent must be confirmed by the evaluation of physical education teachers. To this end, teachers should actively study the evaluation strategy of physical education classroom teaching to give full play to the evaluation function of classroom teaching, mobilize the enthusiasm of students to participate in sports, to enhance the effectiveness and quality of school physical education, improve students' physical fitness, and lay a solid foundation for students' development. More attention should be given to classroom teaching evaluation to achieve a comprehensive evaluation of teachers and students, and on this basis, enrich teaching methods, and provide schools with better quality physical education classroom teaching.

Data Availability

The experimental data used to support the findings of this study are available from the corresponding author upon request.

Conflicts of Interest

The authors declared that they have no conflicts of interest regarding this work.

Acknowledgments

This work was supported by the Key Scientific Research Project of Hunan Provincial Department of Education in 2018 (Project No.: 18A469).

References

[1] X. Yan, D. W. Guo, and S. M. Tang, "Study of building a college physical education curriculum evaluation system," *Journal of Physical Education*, vol. 63, pp. 112–134, 2010.

[2] Y. D. Liu, F. Y. Han, and L. U. Shu-Ting, "A research on system of classroom teaching evaluation and evaluating methods in physical education institute," *Journal of Guangzhou Physical Education Institue*, vol. 11, pp. 78–100, 2000.

[3] J. L. Wang and J. X. Song, "Necessity to include physical education in the college entrance examination evaluation system," *Journal of Physical Education*, vol. 11, pp. 451–453, 2012.

[4] L. Wang and J. R. Sun, "Establishment and application of a college physical education course new event evaluation system," *Journal of Physical Education*, 2006.

[5] J. Y. Liu and Y. H. Wang, "The research of comprehensive evaluation index system on KAQ for physical education teachers in colleges," *China Sport Science and Technology*, vol. 14, pp. 46–96, 2003.

[6] C. C. Yu, *Current Faculty Evaluation at Physical Education Departments in Higher Education*, 2003.

[7] J. P. Song and D. U. Xiang-Ju, "Research on the application of fuzzy mathematics in performance evaluation system of the college physical education teachers," *Journal of Beijing Sport University*, vol. 11, pp. 78–91, 2012.

[8] X. Y. Jiang, "Study on evaluation index system of student practical teaching ability in physical education," *Journal of Gansu Lianhe University (Natural Science Edition)*, vol. 23, pp. 531–551, 2012.

[9] Y. J. Wei, "Study on evaluation system of common physical education class teaching quality in colleges," *Journal of Baoji University of Arts and Sciences (Social Science Edition)*, vol. 23, pp. 87–91, 2007.

[10] H. N. Ding, "Construction on teaching quality evaluation index system of college physical education teacher," *Bulletin of Sport Science & Technology*, vol. 12, pp. 78–101, 2003.

[11] Y. Bai, *Design and Research of Intelligent Evaluation System of Physical Education Teaching Based on Artificial Intelligence Expert Decision System*, vol. 117, Springer, Cham. Springer, Cham, 2016.

[12] X. Kuang, S. Wang, and X. Bo, "Construct the system of aerobics specialist course evaluation in physical education," *Journal of Jilin Institute of Physical Education*, vol. 2, pp. 20–31, 2008.

[13] M. A. Cai-Zhen and J. Wang, "Study on college physical education teaching quality evaluation system," *Journal of Physical Education Institute of Shanxi Normal University*, vol. 52, pp. 110–120, 2011.

[14] E. Lupu, "Evaluation-modern approach in evaluation-evaluation for physical education," *Petroleum-Gas University of Ploiesti Bulletin, Educational Sciences Series*, vol. 62, no. 2, pp. 266–273, 2010.

[15] S. Y. Wang and D. Zhou, "A scholastic physical education policy execution power evaluation index system," *Journal of Physical Education*, vol. 20, pp. 22–80, 2010.

[16] J. Guixia, "Design and implementation of mobile intelligent terminal platform for classroom teaching quality evaluation system," *Automation and Instrumentation*, vol. 6, pp. 203–207, 2014.

[17] W. Decai, "Informatization promotes the development of school-level teaching evaluation," *China Education Network*, vol. 9, pp. 69-70, 2012.

[18] L. Xiaohong, "Design and implementation of comprehensive evaluation teaching information system in colleges and universities," *Science and Technology Vision*, vol. 12, pp. 161-162, 2014.

[19] A. Watson and H. Chick, "Qualities of examples in learning and teaching," *ZDM Mathematics Education*, vol. 43, no. 2, pp. 283–294, 2011.

[20] K. Sun, "Physical education quality evaluation method based on FCE," *International Conference on Smart Grid and Electrical Automation*, pp. 518–521, 2017.

[21] S. M. Burns and L. H. Ludlow, "Understanding student evaluations of teaching quality: the contributions of class attendance," *Journal of Personnel Evaluation in Education*, vol. 18, no. 2, pp. 127–138, 2005.

[22] G. Chen and S. Li, "Network on chip for enterprise information management and integration in intelligent physical systems," *Enterprise Information Systems*, vol. 15, no. 7, pp. 935–950, 2021.

[23] E. Isidori, "Philosophy of sport education: main issues and methodology," *Physical culture and sport Studies and Research*, vol. 66, no. 1, pp. 23–25, 2015.

[24] Q. Zhou, "On teaching evaluation information system of university physical education curriculum," *Trans Tech*, vol. 2, pp. 26–30, 2013.

[25] G. Linzhou, "Theoretical thinking on the evaluation of physical education teaching in ordinary colleges and universities," *Zhejiang Sports Science.*, vol. 28, no. 4, pp. 49-50, 2006.

Hindawi
Journal of Sensors
Volume 2022, Article ID 4941243, 8 pages
https://doi.org/10.1155/2022/4941243

Research Article

The Preparation and Preservation of Soybean Protein Isolate Were Studied Based on the Internet of Things

Chunyan Niu and Xiaokun Jiang

College of Food Engineering, Jilin Agricultural Science and Technology University, Jilin Jilin 132101, China

Correspondence should be addressed to Chunyan Niu; niuchunyan@jlnku.edu.cn

Received 21 February 2022; Accepted 12 April 2022; Published 6 May 2022

Academic Editor: Yuan Li

With the gradual deepening of people's understanding of the concept of environmental protection, this situation has brought new challenges to the preservation and packaging of food. Pure green, natural, and harmless edible film has become a hot topic. Edible protein membranes include animal protein membrane, plant protein membrane, and composite protein membrane. They are mainly used in the field of food production and food safety. The traditional food film has a poor water barrier in a humid environment, which cannot effectively avoid the anaerobic respiration of fruits. At the same time, it will also cause environmental pollution. In order to solve these problems, this paper studies the preparation and preservation of soybean protein isolate based on the Internet of things. Firstly, polyphenols were fused with soybean protein isolate by ultrasonic technology to form an edible fresh-keeping film. The edible membrane of the soybean protein isolate was tested, and the optimum conditions for the formation of the edible membrane were determined by the orthogonal test. The effects of soybean protein isolate, glycerol, reducing agent, and other additives on the film-forming properties were analyzed. Finally, the changes in properties and preservation indexes after film formation were analyzed. The results showed that the film-forming temperature of polyphenol soybean protein isolate edible film was positively correlated with the film properties. The prepared food preservative film can be used for the preservation of vegetables and other foods and has a good retention effect on food nutrients.

1. Introduction

Edible food film is a substance that can cover the surface of food and is used to preserve food and prevent microbial bacteria [1]. At present, most food preservative films and edible packaging films use synthetic plastics as raw materials, such as ethylene and other chemical materials. However, synthetic plastic films are difficult to degrade in the natural environment and cannot effectively deal with residual components, which brings great harm to the environment [2]. Phthalates and other chemicals in the synthetic plastic film are easy to bring hazards and hidden dangers to human health when they are covered in food. As more and more countries pay attention to the research on green environmental protection and food preservative film, they gradually adopt the prohibition of disposable plastic appliances [3]. This form of prohibition makes the research of food preservative film and covering film particularly urgent and important. In food edible film, macromolecular natural substances such as soybean protein, starch, and plant fiber have become a hot research topic in recent years, especially the edible food preservative film based on the soybean protein isolate [4]. An edible food film can effectively preserve and protect unused or used food, blocking the oxidation, erosion, and corrosion of food caused by air and micromolecular moist steam in the air [5]. The difference between edible membrane and edible protein membrane is that the protein membrane is environmentally friendly and renewable due to the common edible membrane [6]. The edible membrane of soybean protein isolate belongs to the plant protein membrane. In addition to animal protein, soybean separation of the plant protein edible membrane is loved by researchers at home and abroad. Soybean separation takes soybean protein isolate as the main material, adding plasticizer and

auxiliary materials to press it into a film state. The price of soybean separation itself is low, it can be extracted from a variety of substances, and it is also stronger than other substances in the comparison of film-forming properties. It can block air, oxygen, oil, and other functions, but the extension property of the soybean protein isolate membrane is poor and cannot effectively block water molecules. We need to further optimize the soybean protein isolate membrane to improve the elongation, toughness, and antibacterial properties after film formation [7]. In recent years, it is found that many researchers at home and abroad often add nanoparticles to the improvement of the soybean protein isolate membrane. The membrane modification was studied by combining nanomaterials with edible protein membranes. After adding nanoparticles, the strength, toughness, and water barrier of the soybean protein isolate membrane were improved. Based on the above situation, starting from the fresh-keeping application of the soybean protein isolate film, we explore the improvement of the soybean protein isolate film by polyphenols in antioxidants. Finally, the process of film-forming and preparation and parameter changes are analyzed in real time combined with the Internet of things technology [8].

The preparation and preservation of soybean protein isolate were studied based on the Internet of things. Innovation contributions include the following: (1) Using ultrasonic technology, polyphenols were fused with soybean protein isolate to form an edible fresh-keeping film. The problem of environmental pollution caused by waste of bags is solved. (2) The optimum conditions for the formation of edible film were determined by the orthogonal test. The effects of soybean protein isolate, glycerol, reducing agent, and other additives on the film-forming properties were analyzed. (3) The changes in properties and fresh-keeping indexes after film formation were analyzed. The results showed that the film-forming temperature of the polyphenol soybean protein isolate edible film was positively correlated with the film properties. The prepared food preservative film can be used for the preservation of vegetables and other foods. Compared with the traditional food film, it solves the problem of poor water barriers in humid environments and cannot effectively avoid the anaerobic respiration of fruits.

This paper is mainly divided into three parts. The first part briefly describes the differences between the edible membrane of soybean protein isolate and the edible membrane of polyphenol soybean protein isolate and explores the current situation of edible membrane research at home and abroad. The second part first puts forward the research content of this paper from the defects of the edible membrane in the soybean protein isolate environment. The edible film was studied from the aspects of film-forming mode, nutrition, extensibility, water permeability, and oil barrier. The formation mechanism of the polyphenol soy protein isolate membrane was tested by ultrasonic. The orthogonal test was used to explore the preparation conditions of edible film. Finally, taking the polyphenol soybean protein isolate as the main research object, the fresh-keeping performance of the film and the factors affecting the performance indexes were analyzed. The third part is the analysis of the research results on the preparation method and fresh-keeping function of polyphenol soybean protein isolate edible film.

2. Related Work

Food packaging film can protect food from direct exposure to oxidizing air and can play a good role in isolating harmful substances and bacteria in the air, protecting food from corrosion and oxidation by external microorganisms to a certain extent [9]. With the concept of green environment becoming the research content of modern development, traditional synthetic plastic packaging materials cannot be degraded by the natural environment and are prone to a large number of white pollution. At present, edible biofilm has attracted more and more research and attention. The natural film formed by modified soy protein isolate can minimize the environmental harm on the basis of ensuring the food preservation period [10]. With the rapid development of modern technology, sensor technology such as the Internet of things and ultrasonic technology have become more and more developed and have been gradually applied in automobile manufacturing, biological manufacturing, material technology, and other fields [11]. We added polyphenols to the edible membrane of soybean protein isolate to optimize the film-forming property. The preparation process of film was analyzed by the Internet of things ultrasonic technology. The traditional soy protein isolate membrane has the properties of blocking oxygen, air, and oil and can be used in vegetable packaging, fruit packaging, and other foods [12]. The edible film composed of soy protein isolate can prolong the fresh-keeping period of poultry, eggs, fruits, and vegetables. The maximum limit can be extended by two weeks. As bioglycerols can change the properties of edible films, many researchers have found that soy protein isolate edible films can keep fresh and antibacterial in fruit packaging [13]. However, the traditional soy protein isolate membrane cannot effectively block water and steam. In order to optimize the traditional protein membrane, researchers at home and abroad proposed to add polyphenols in the preparation process. Polyphenols and other substances can have anticancer, antioxidation, antibacterial, and other properties and supplement the defects in soy protein isolate through stable fusion of molecular structure.

Japanese researchers mainly analyze the macromolecular structure of amino acids in the study of edible films. Edible gelatin protein film was obtained by chemical fusion degradation of animal fur and bone. This material can have high heat insulation and sealing performance and plays a good role in blocking air and grease [14] and can achieve biodegradation and compatibility. However, the disadvantage of gelatin film is the same as that of traditional soybean protein isolate film, which cannot be in direct contact with water molecules. It is easily soluble in water and has a poor barrier effect on water and steam. British researchers pay attention to the application of whey protein film in food preservation. Whey protein film can take plasticizers such as glycerol and beeswax as the basis of film-forming and fuse whey protein isolate to prepare fresh-keeping film. The film has low

oxygen permeability and can be used as food nutrition and fresh-keeping material. Compared with the soybean protein isolate membrane, it has good extensibility. It can also block fragrance substances and oils in a humid environment [15]. However, the content of amino acids in the whey protein membrane is high, and its antibacterial effect is poor. Based on the above situation, we propose to use polyphenol soy protein isolate as the research content in food preservation and edible film preparation.

3. Methodology

3.1. Preparation and Properties of Edible Membrane of Polyphenol Soybean Protein Isolate Based on Internet of Things. Polyphenol soy protein isolate is a mixed product of common protein globule structure and polyphenols. The main raw materials are soybean globulin, subunit globulin, and other substances. It contains different kinds of subunits, and each globulin is composed of acidic and basic subunits. The preparation process of soybean protein isolate without polyphenols is purified and refined from protein, which has high requirements for protein content. Common soy protein isolate can be easily obtained and refined, with emulsification and rapid film-forming. The edible film can be biodegradable and edible, and the preparation price is close to the people. However, the traditional soy protein isolate film has certain antioxidant properties and high water permeability. It cannot effectively block the invasion of water vapor and has weak ductility. With the change of the surrounding environment, the mechanical properties of the film are easy to be affected. To improve the ability of protein to resist external interference, a large number of disulfide bonds need to be added to the film. We first analyzed the molecular chain interaction in the edible protein membrane, as shown in Figure 1.

It can be seen from Figure 1 that the stability between molecules is maintained through the interaction of disulfide bond and hydrogen bond, and the polymerization degree of protein molecules presents a network structure, which can affect the performance of the final film. In this paper, natural tea polyphenols were added to the soy protein isolate membrane to improve the ductility and waterproofing of the membrane. The experimental materials and process flow are shown in Figure 2.

It can be seen from Figure 2 that the reagents required for the experiment include potassium permanganate, hydrochloric acid, sodium hydroxide, and other chemicals. There are also main raw material polyphenols and soybean protein isolate. Firstly, the edible preparation of the polyphenol protein membrane was analyzed. Firstly, polyphenols and soybean protein isolate were mixed. The mixed dissolved polyphenol soybean protein isolate was added with plasticizer and reducing agent to adjust the acidity and alkalinity of protein isolate. Finally, the film was pressed and dried to test the performance. In the film-forming preparation, polyphenols and soy protein isolate need to be added into distilled water to dissolve, mixed with glass rod, and then stirred further. This ensures that the dissolved material has highly uniform properties. In the film-forming performance test, the film integrity needs to be evaluated. During the measurement, explore the quality of the complete film and calculate the integrity efficiency of polyphenol soy protein isolate film. The calculation formula is as follows:

$$FI - \frac{M}{M+m} \times 100\%. \tag{1}$$

In the formula, FI represents the integrity efficiency of edible film and M represents the integrity quality coefficient of edible film. At the same time, the ductility strength of the film was tested, and the changes in sample parameters were analyzed from the maximum tensile strength. The evaluation is carried out with the extension test machine, and the calculation formula is as follows:

$$TS = \frac{F}{A}. \tag{2}$$

In the formula, F is the maximum tensile force formed when the sample is broken and A is the test area of the sample experimental film. The maximum elongation during the test of damaged properties is calculated as follows:

$$\begin{aligned} E &= \frac{(L - L_0)}{L_0 \times 100\%}, \\ E_0 &= \frac{L + L_0}{L \times 100\%} - E. \end{aligned} \tag{3}$$

Testing the maximum damage bearing elongation is the key content to judging the toughness and ductility of edible film. Comparing the extension range of edible film after tensile strength with the original sample, we can analyze the changes in the properties of the soybean protein isolate membrane optimized by polyphenols. Cut the edible film into the same proportion of length and width, test the light transmission performance of the film, use the vernier caliper to select the random thickness to take the average value, and the calculation formula is as follows:

$$\begin{aligned} \mathrm{OD} &= \frac{\log_{10}(A - B - C)}{A}, \\ \mathrm{OD} &= \log_{10} \frac{(L_1 + L_2 + \cdots L_N)[(A - B - C)/A]}{L_N}. \end{aligned} \tag{4}$$

In the formula, OD represents the optical density coefficient and A represents the transmittance. Next, test the water barrier performance of the edible film, cut the film into a circle, put it into the beaker to be tested, and measure the film quality under the constant weight state. The calculation formula is as follows:

$$J = \frac{C}{A}. \tag{5}$$

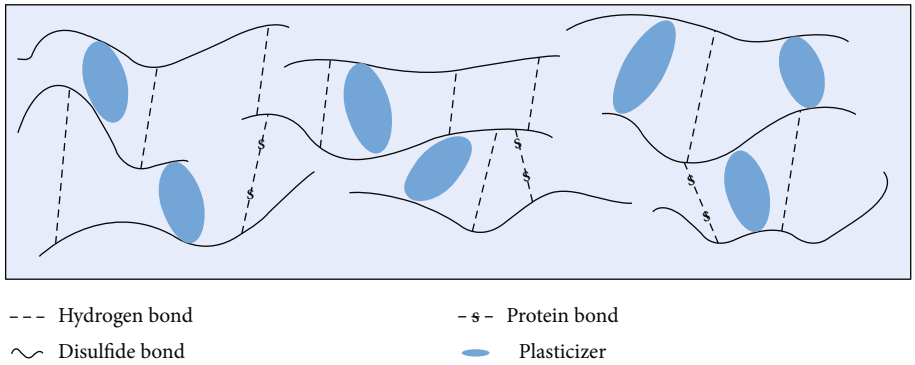

Figure 1: Molecular chain interaction in protein membrane.

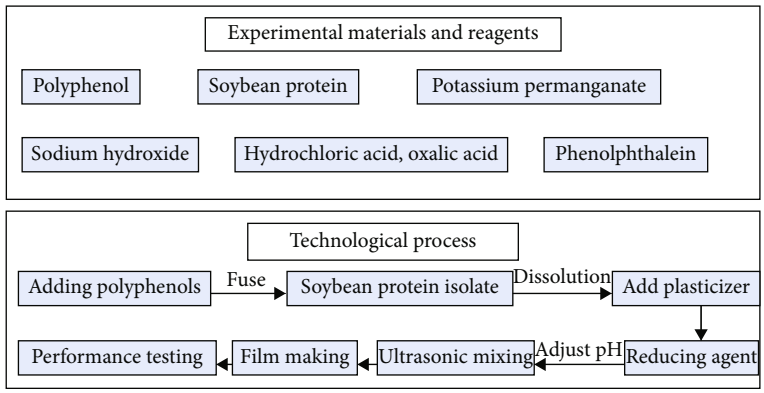

Figure 2: Experimental material and process flow chart.

J in the formula is the unit water barrier of edible film:

$$WS = \frac{M - m}{M} \times 100\%,$$
$$WVP = \frac{C \times X}{A \times \Delta P}. \quad (6)$$

In the formula, WVP is the moisture permeability coefficient of edible film, C represents the rate of passing through the film after adding water vapor, X is the film-forming thickness, and A is the effective measured area of edible film. M represents the initial mass of the measured sample. Add 5 ml of oil into the test sample test tube for the oil permeability test. Seal the opening of the fusion membrane with transparent glue, and place the oil and polyphenol soy protein isolate edible membrane in a container with humidity of 50%. The calculation formula is as follows:

$$PO = \Delta W \times \mathrm{FT} \times 100\%,$$
$$PO = \frac{PO_0(W \times \mathrm{FT})}{S \times T \times 100\%}. \quad (7)$$

In the formula, PO is the oil permeability coefficient of edible film, ΔW is the mass change after oil filtration, and FT is the film-forming thickness. Finally, the coefficient change of water vapor passing through the edible film is analyzed. Cut the film to the size of the bottle mouth of the container, seal it with double-sided adhesive tape, obtain it with hydrochloric acid solution in the interference container with different humidity, and measure the sample quality every other hour for two days. The calculation formula for water vapor penetration coefficient is as follows:

$$WPO = \frac{\Delta W \times \mathrm{FT}}{T \times S \times \Delta P}. \quad (8)$$

In the formula, ΔW represents the change of sample mass during weighing time, S represents the effective area of film-forming measurement, and ΔP represents the difference from water vapor pressure on both sides. Finally, we found that the mechanical properties of the edible membrane were affected by different contents of protein in soybean protein isolate after adding polyphenols. With the increase of protein and polyphenols, the extensibility of the soybean protein isolate membrane fluctuated up and down.

3.2. Application of Polyphenol Soy Protein Isolate Edible Film in Fresh Keeping Based on Internet of Things. In the edible film of polyphenol soy protein isolate, there are usually three modification methods, including physical, chemical, and enzyme. Chemical acetylation, phosphorylation, glycosylation, and cross-linking reactions are more effective than enzymatic methods in changing the structure and function of proteins. Physical modification is to change the structure of protein in soybean protein isolate by changing the

temperature, humidity, ultrasonic, and other physical technologies in the surrounding environment. Realize the effect on protein function. Most polyphenol soy protein isolates will be modified in high temperature difference, because heat can destroy the protein structure and expose amino acid molecules to the fusion agent. Enzyme modification can make the protein molecular structure form a variety of joint states, which has an obvious impact on the solubility and emulsification of edible films. The film prepared by traditional pectin has high water resistance and water vapor permeability and shows good tensile properties in convenient ductility. The fresh-keeping performance of soybean protein isolate edible film added with polyphenols is evaluated from the weight loss rate, and the calculation formula is as follows:

$$\mathrm{LOSE} = \frac{\Delta P - P_0}{\Delta P}. \tag{9}$$

In the formula, LOSE represents the weight loss efficiency, ΔP represents the quality coefficient of fruits and vegetables before preservation, and P_0 represents the fruit quality after preservation measures. Add the sample to the potassium permanganate extract for preparation, place it in two 50 ml containers, respectively, and determine the content of reducing sugar. Finally, test the vitamin content of the fresh-keeping film, add oxalic acid, weigh it, add it to the beaker, and filter it. The formula is as follows:

$$X = \frac{(V - V_0) \times T}{M \times V_4 \times V_3}. \tag{10}$$

In the formula, X is the vitamin content, T is the number of samples consumed, and V_4 is the total volume of samples to be tested. From the previous work, the polyphenol agent was added, and the tensile strength and light transmittance of traditional soybean protein isolate edible film and polyphenol soybean protein isolate edible film were compared by using Internet of things ultrasonic power, as shown in Figure 3.

It can be seen from Figure 3 that in the orthogonal experiment, in the edible membrane parameters of polyphenol soybean protein isolate, the light transmittance increases with the increase of tensile strength. We found from the experiment that the effect of edible film on the preservation function is the weight loss coefficient. The effect of film-forming on the weight loss rate of fruits and vegetables was obvious. The control group and experimental group were set up. Put the fruits and vegetables with different treatment methods at the same room temperature, as shown in Figure 4.

It can be seen from Figure 4 that the weight loss rate of fruits and vegetables added with edible film in the experimental group was higher, and the water evaporation effect of fruits and vegetables was higher. With the increase of experimental time, fruits and vegetables without edible film treatment had obvious weight loss.

4. Result Analysis and Discussion

4.1. Preparation and Properties of Edible Polyphenol Soy Protein Isolate Membrane Based on Internet of Things. After modification, the functions of protein such as emulsification and film-forming have been significantly improved, and the molecular structure is relatively stable. It can make up for the defect of ordinary protein film. The ultrasonic function of the Internet of things is used to destroy the interaction of protein molecules and promote the transformation of substances into liquids. The edible film of soybean protein isolate added with polyphenols showed a good optimization effect from the barrier analysis. The film thickness is related to transparency. Transparency and thickness are the key contents in every edible film product parameter. The thickness of the film depends on the quality of insoluble substances in dairy materials, especially the content of precipitates. Too much sediment added to the membrane structure will cause matrix damage. Therefore, the thickness of the composite film is generally greater than that of the ordinary protein film. The thickness of the edible film of soybean protein isolate after adding polyphenols also increases, but the transparency is still within the standard range. In the experiment, the water barrier of the film can be tested to analyze the content of water molecules in the effective area of the film at constant temperature and humidity. Water vapor transmittance is the key factor for testing water isolation performance. The lower the permeability coefficient, it means that the edible film can effectively prevent water erosion. The process of packaging food is relatively stable and can prolong the shelf life. The internal structure density of the film will also be affected by the transmittance of water vapor. Most irregular areas are easy to cause voids, so that water vapor can pass through the gaps. However, after adding polyphenols, the internal structure of the edible membrane changed and filled irregular voids greatly.

From the analysis of nutritional characteristics, the nutritional index of soybean protein isolate added with polyphenols is high, which mainly comes from the mixture of soybean protein and polyphenols. Soybean protein contains the amino acid energy needed by the human body. After appropriate proportion and blending, the digestion efficiency can also reach 90%. This nutrient is easily recycled and absorbed by the human body, and soybean protein also has the effect of promoting the development of the human brain, which often appears in health products. The traditional edible membrane of soy protein isolate cannot effectively isolate water molecules in a humid environment, and the water vapor transmittance is high. It is greatly limited in barrier grease. The soybean protein isolate membrane added with polyphenols can improve the barrier performance of oil and reduce the diffusion of water and oil, ensuring the quality stability of food in transportation. The molecular weight of polyphenols combined with proteins can form molecular groups with high density, in which the disulfide bond and hydrogen bond are relatively stable in the mixed structure, which can compress the irregular gap and make the edible membrane have a certain tightness.

4.2. Application of Polyphenol Soy Protein Isolate Edible Film in Fresh Keeping Based on Internet of Things. In the field of food preservation, edible films have been loved and concerned by major enterprises for their efficacy, safety, and

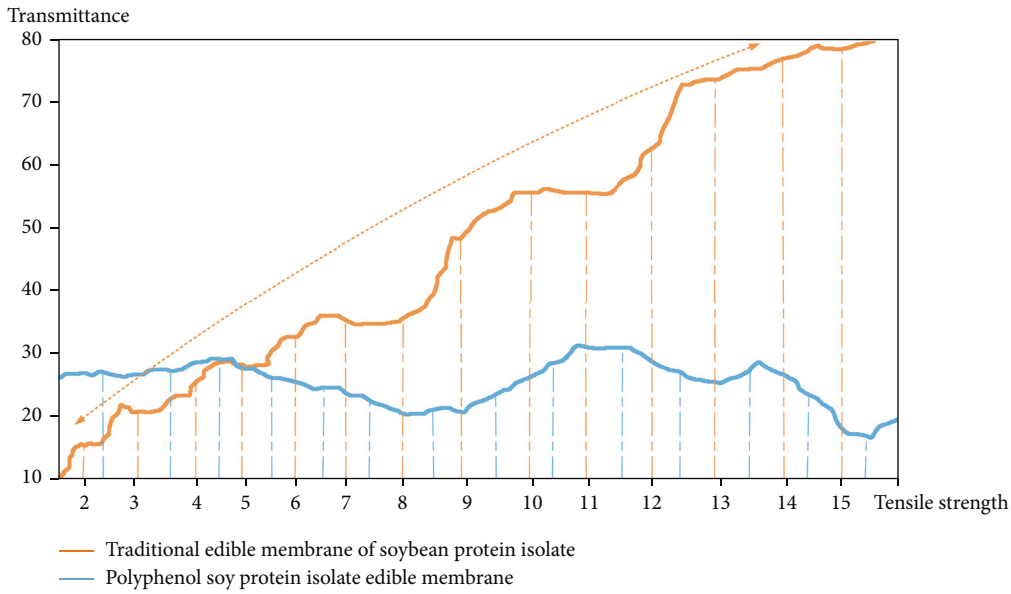

Figure 3: Comparison of tensile strength and transmittance of two edible protein films.

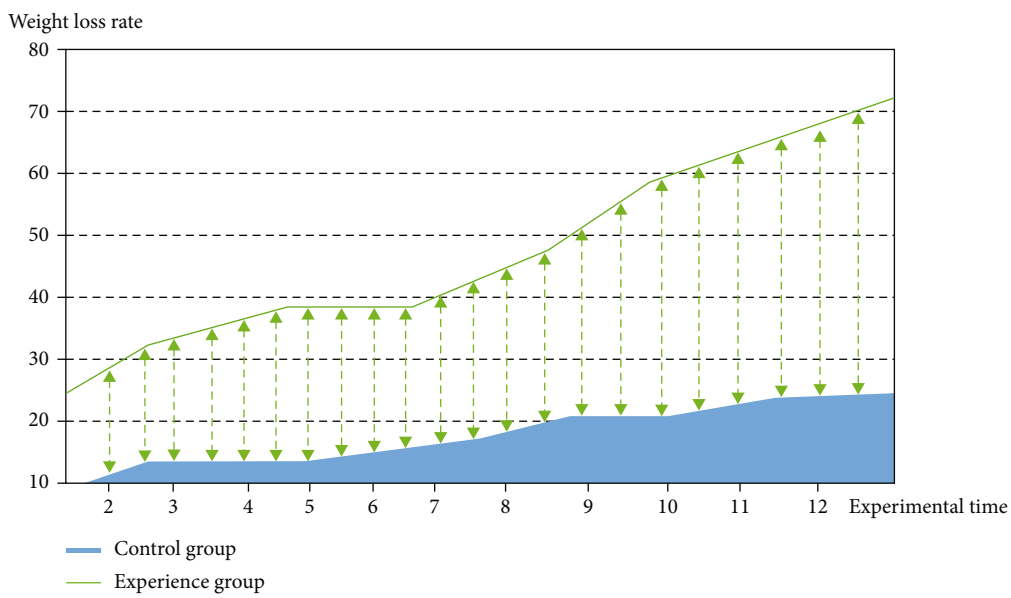

Figure 4: Comparison of weight loss rate of fruits and vegetables between experimental group and control group.

environmental protection. There are more and more studies on the fresh-keeping effect of edible film at home and abroad. Fruit and vegetable preservation and food freezing processing are the means to protect food quality and improve food shelf life. China started late in the research of edible protective film, but the research efficacy of various types of edible film has been realized by adding various plasticizers and biomolecules on the basis of soybean protein isolate film. Among them, the materials that are cheap and easy to collect mainly include soybean protein isolate and starch. Soy protein isolate has high nutritional value, is easy to be absorbed and digested by the human body, and has plasticity and film-forming property. An ordinary soybean protein isolate membrane has good performance in isolating oxygen, oil, and bacteria, but there are still some defects. The protein molecular bond rigidity of the soybean protein isolate membrane is strong, it is easy to break in practical use, and its ductility and elongation are also low. In order to improve and overcome the defects of the soybean protein isolate membrane, we added polyphenols, sugars, glycerol, and other substances on the original basis. In this paper, the fresh-keeping effect of soybean protein isolate edible film added with polyphenols was analyzed and studied. The water permeability of the polyphenol protein membrane decreased with the increase of polyphenols. It shows that the water separation performance has been improved to a certain extent. When the ratio of polyphenols reaches 3 : 1, the water barrier performance is the best. This phenomenon

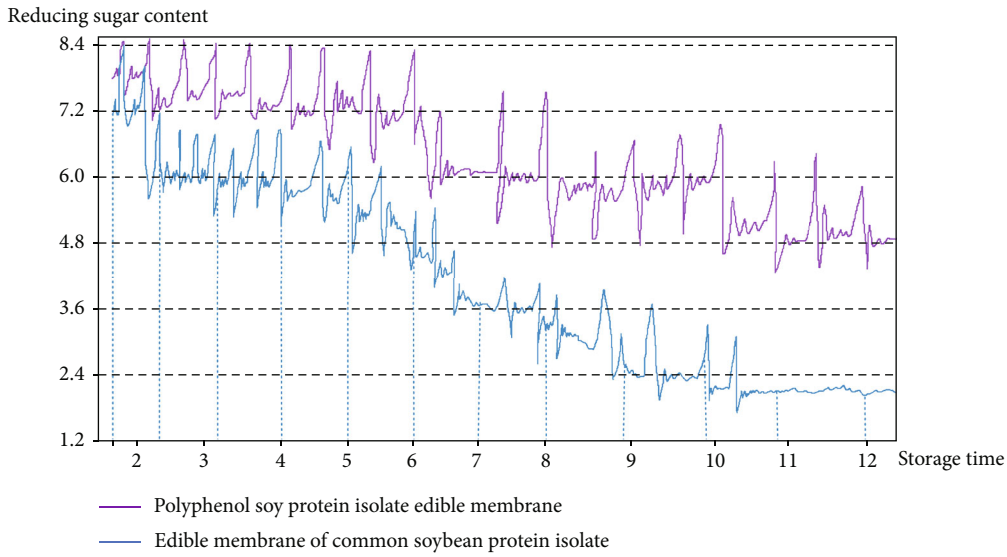

Figure 5: Comparison of influencing factors of reducing sugar in two edible protein membranes.

is positively correlated with the extensibility of the edible membrane. The tightness of the film-forming structure is the main factor related to the two properties. In the above study, we have effectively evaluated the preservation performance of film-forming treatment and continue to explore the impact of film-forming treatment on reducing sugar and acid-base based on the original sample data. The comparison of reducing sugar influencing factors between polyphenol soybean protein isolate edible membrane and ordinary soybean protein isolate edible membrane is shown in Figure 5.

It can be seen from Figure 5 that the reducing sugar in the determination results can represent the changes of nutrients during the storage of fresh food. With the increase of storage time, the sugar content of food covered with polyphenol soy protein isolate edible membrane decreased slowly. With the increase of time, the sugar content in food as a respiratory consumption substance decreases rapidly. The optimized preservative film can greatly preserve the original food. In the acid-base effect, the food acidity of edible film of polyphenol soybean protein isolate decreases slowly, which can inhibit the nutrient loss caused by the erosion of nutrients in the air. With the increase of storage time, acid-base is consumed as oxide, and the optimized edible film can better maintain the acid-base content in food. Finally, we analyze the changes of vitamin content in fruit and vegetable food. With the increase of preservation time, the vitamin content in fruit and vegetable food gradually decreases. The use of optimized edible fresh-keeping film can delay the decline rate to a certain extent, reducing the water loss and vitamin nutrient loss of food in oxygen.

5. Conclusion

Different kinds of edible films have different characteristics. The application of various edible films in the food field is distributed according to the properties of the films. As the natural green edible protein membrane can realize the functions of biodegradation, reduction, and utilization and reduce environmental pollution, many researchers began to pay attention to the properties and preparation process of these substances. The traditional edible membrane of soy protein isolate can effectively isolate oxygen and bacteria and has certain nutritional value, but there are still some defects. Based on the above situation, this paper proposes to study the preparation and fresh-keeping application of polyphenol soybean protein isolate edible film in the environment of the Internet of things. Firstly, the functional defects and modification of traditional soybean protein isolate membrane were analyzed, and the properties of the protein membrane added with various substances were compared. Polyphenols were added to soybean protein isolate for fusion to improve film-forming efficiency, water barrier, and ductility. Aiming at the problem of high water vapor transmittance of ordinary protein membranes, the orthogonal experiment was carried out by ultrasonic to explore the best proportion of edible membranes. Finally, the edible film added with polyphenols was analyzed from the fresh-keeping performance to explore the effects of weight loss rate, reducing sugar content, and vitamin content on the fresh-keeping effect. The results show that the edible membrane of polyphenol soybean protein isolate can improve the defect of poor water barrier and improve the integrity of food protection in a humid environment. It can effectively avoid anaerobic respiration of fruits and vegetables and reduce physiological activity and weight loss rate. It provides an excellent basis for food preservation and has great commercial value. Although many properties of modified protein membranes have been studied in this paper, there are still some deficiencies. The soybean protein isolate membrane has certain antioxidant performance and high water permeability. Therefore, further modifications are needed in future research.

Data Availability

The data used to support the findings of this study are available from the corresponding author upon request.

Conflicts of Interest

The authors declare no conflicts of interest.

Acknowledgments

The study was funded by the Key Discipline Project of Jilin Institute of Agricultural Science and Technology, Research on the Heavy Metal Adsorption Law of Pitaya Peel Extract (2019.10-2022.12), and Jinong Institute (2019) (No. X Y 005).

References

[1] Y. Xing, Z. Junnan, C. Lin, and W. Na, "Preparation and properties of edible soybean protein isolate membrane," *Packaging Engineering*, vol. 41, no. 23, pp. 83–89, 2020.

[2] C. Xiuyu, L. Qian, and L. Huijie, "Preparation and properties of soybean protein isolate/cellulose/starch composite edible membrane," *Journal of Jilin Institute of chemical technology*, vol. 34, no. 11, pp. 12–17, 2017.

[3] N. Chunyan, X. Liang, and L. Shuai, "Development of edible membrane of apple polyphenol soybean protein isolate," *Scientific and technological innovation*, vol. 31, pp. 86-87, 2017.

[4] L. Yimin and L. Yongping, "Effect of soy protein isolate composite membrane on oil absorption rate of fried potato chips," *Grain processing*, vol. 42, no. 4, pp. 46–48, 2017.

[5] N. Chunyan, W. Jing, W. Shanhong, and Z. Yuhao, "Preparation of edible polyphenol soy protein isolate film and its application in fresh preservation," *Food industry*, vol. 38, no. 5, pp. 78–80, 2017.

[6] N. Chunyan, W. Shanhong, P. Qingguo, L. Yihong, and G. Yu, "Preparation of edible film of corn resistant starch," *Industry and technology Forum*, vol. 16, no. 6, pp. 61-62, 2017.

[7] Z. Dong, S. Pengpeng, W. Haichao, G. Guizhen, and C. Wengen, "Preparation and properties of edible soybean protein isolate membrane," *Food and machinery*, vol. 32, no. 9, pp. 187–191, 2016.

[8] C. Shanshan, T. Hongjiang, W. Yajing, and M. Zhongsu, "Optimization of preparation process of edible film of sunflower seed shell nano cellulose/chitosan/soybean protein isolate," *Journal of agricultural engineering*, vol. 32, no. 8, pp. 306–314, 2016.

[9] M. Teng, L. Dandan, L. Haiyun, O. Jun, H. Zaibin, and Z. Hourui, "Study on preparation technology of edible composite membrane," *Soybean science*, vol. 33, no. 2, pp. 277–280, 2014.

[10] Y. Ruiyue, "Study on film-forming process of edible soybean protein isolate," *Heilongjiang grain*, vol. 2, pp. 51–54, 2014.

[11] L. Jirui and S. Qian, "Preparation and performance analysis of edible film of cinnamon essential oil. Anhui agricultural," *Science*, vol. 49, no. 20, pp. 189–191, 2021.

[12] W. Youming, X. Meng, B. JieFei, and C. Hongwei, "Optimization of potato starch film preparation process based on response surface methodology," *Journal of Xuzhou Institute of Engineering (Natural Science Edition)*, vol. 36, no. 2, pp. 22–26, 2021.

[13] C. Jingxin, M. Yang, G. Yonghong, D. Zhu, L. V. Jingyi, and M. I. Hongbo, "Research progress of sodium alginate edible film and its application in food preservation," *Journal of Bohai University (Natural Science Edition)*, vol. 42, no. 2, pp. 102–110, 2021.

[14] Z. Luyao, X. Jiao, W. Yunlu, L. Fei, H. Linlin, and L. Quanhong, "Research progress of polysaccharide based edible membrane," *Food industry*, vol. 42, no. 5, pp. 311–315, 2021.

[15] Y. Qianqian, X. Kong Qing, Z. Q. Fei, D. Haizhou, and L. Yuchen, "Preparation and properties of modified starch based edible film," *Chinese Journal of grain and oil*, vol. 36, no. 2, pp. 41–46, 2021.

Hindawi
Journal of Sensors
Volume 2022, Article ID 5075122, 11 pages
https://doi.org/10.1155/2022/5075122

Research Article

Movement Analysis and Action Optimization of Physical Education Teaching Practice Based on Multisensing Perception

Zhishuang Li[1] and Fengqing Li[2]

[1]*Sports Department of Shijiazhuang Tiedao University, 050043, China*
[2]*Hebei Institute of Communications, Shijiazhuang 051430, China*

Correspondence should be addressed to Fengqing Li; lifq@hebic.edu.cn

Received 26 January 2022; Revised 14 March 2022; Accepted 21 March 2022; Published 2 May 2022

Academic Editor: Yuan Li

Correct and effective physical education teaching can not only improve students' physical quality but also exercise students' willpower, which is an important content to promote students' all-round development. However, according to the current teaching situation in our country, in the actual teaching process, there is a situation of incongruity between teaching and sports development, which leads to the decline of the quality of physical education teaching in our country and affects the development of students' comprehensive quality. Based on these problems, starting from the relationship between teaching and sports, this paper analyzes the coordinated development between physical education teaching and training in colleges and universities and builds a physical education teaching quality monitoring system. The research results of this paper show that (1) when using traditional recognition of various motion patterns, it can recognize various behavior patterns, and the average recognition accuracy is 90.1%. The accuracy is 94.3%. Compared with the traditional recognition mode, the average recognition accuracy is increased by 4.2%, and the recognition result is better. Compared with the recognition results of the first set of experiments, for the more difficult to distinguish upstairs and downstairs, the recognition accuracy is increased by 9% and 7%, respectively, and the recognition accuracy of backward is increased by 6%. (2) Before receiving the teaching, the test results of each index of the members of the routine group and the training group were basically the same, and there was no major difference. After the T-test was performed between the conventional group and the training group, the results showed that the P values of the evaluation results of the two groups were both above 0.05. The experimental results showed that the initial conditions of the two groups could be regarded as the same before receiving the teaching. Combining the evaluation results of the two groups before the training, we can conclude that under the condition that the initial conditions are basically the same, and the training conditions and environment are basically the same, the trainees who have received the mode training method have obtained better physical fitness indicators. The improvement and the effect are greatly optimized compared with the mode training. (3) Among the 8-spoke images captured by the experiment, the multisensor motion analysis model proposed in this paper has the highest action recognition accuracy. When the first picture is taken, the recognition accuracy is 98%. The recognition accuracy rate is also increasing, and when the eighth image is taken, the action recognition accuracy rate reaches 99%. Among the three different models, the multisensor motion analysis model proposed in the article has the shortest page response time. When the number of tests is 10, the average page response time is 0.4 seconds. When the number of tests increases to 70, the average page response time reaches 1.0 seconds, and the success rate of the multisensor motion analysis model has remained at 100%. The average response time will increase with the increase of the number of tests, and the experimental results also show that the detection performance of the multisensor motion analysis model is the highest.

1. Introduction

With the continuous reform and development of education in our country, the physical quality of our students is generally poor, and the institutional health of adolescents is not only related to individuals and families but also to the strength of society and the nation. At present, the reasons for the decline of the youth system in my country are caused

by many factors, such as poor sports awareness and academic stress improvement. In the process of daily class, teachers should pay attention to the analysis of the accuracy of movements, so that students can fully understand the importance of sports. While improving students' physical quality, they can also exercise students' willpower. Literature [1] puts forward a good application for sports application and evaluation, especially from the theoretical basis of the evaluation system of physical education students' practical ability in normal colleges and universities. Literature [2] relies on students and colleagues, and quantitative analysis combined with quantitative statistics reflects the quality of physical education teaching. Reference [3] uses the analytic hierarchy process to establish a physical education teacher's teaching quality index system and assigns weights to it. Reference [4] illustrates the continuous development and application of artificial intelligence technology, which provides a new perspective for the reevaluation and setting of physical education teaching in schools and teachers. Reference [5] proposes to use inertial sensors to collect information about human motion and apply the collected information to analyze and identify human motion. Reference [6] discusses a theoretical framework for studying posture coordination strategies in standing. Reference [7] designed a human action recognition algorithm based on multifeature fusion and motion information. Reference [8] illustrates that physical exercise and positive attitudes towards physical activity must be one of the basic areas of activity in higher education institutions. Reference [9] analyzes the use of special equipment in the current special physical training and proposes the key elements that should be paid attention to and the principles that should be followed in the special physical training. Literature [10] adopts the methods of literature review and logical analysis to analyze the restrictive factors of physical education teaching environment. Reference [11] utilizes the latest powerful vision-based ego-motion estimation and uses a nonparametric Bayesian modeling approach to design an unsupervised learning model. Reference [12] is based on achievement goal theory and aims to verify the influence of the motivational climate of physical education on the motivation, interest, and intention of students to engage in physical activities or sports. Literature [13] investigated the relationship between teacher feedback and physical education performance, and the results showed that corrective, descriptive, normative, or positive feedback or feedback focused on skill outcomes may be associated with achievement. The findings in [14] showed a positive linear trend between the number of self-regulation phases that participants received training and their free-throw shooting performance and shooting adaptation. Literature [15] reviewed the literature on students' physical education attitudes and discussed issues related to attitude measurement.

2. Physical Education Practice Movement Analysis and Movement Optimization

2.1. Problems Existing in the Reform and Development of Physical Education Teaching. Many students ignore the importance of physical exercise in their daily learning. The traditional teaching methods are limited to indoor teaching. Students lack extracurricular exercises and cannot exert their subjectivity in learning. First of all, we need to change the traditional concepts of teachers and students. Many people generally think that physical education is a course for relaxation and play, but ignore the importance of physical movement teaching. Wrong sports movements may cause damage to the human bones. In order to solve these problems, teachers can play relevant video explanations before the formal teaching, so that students can have a general understanding. In the formal teaching process, some games can be added to stimulate students' enthusiasm for learning. Build a physical education teaching quality monitoring system, as shown in Table 1.

2.2. Sports Action Analysis and Action Optimization. In teaching, teachers refine the scientific and step-by-step nature of teaching by analyzing the composition of action elements. It can be known from experience that these methods can make students' learning efficiency have a positive meaning, because in the case of traditional teaching, teachers often have low requirements for students, and students' enthusiasm for learning will also be reduced. It is not very important whether to learn or not to learn the knowledge of fur. Therefore, the understanding of movements is not in place, and it will not be improved in future learning. Therefore, teachers must use our skills in the process of teaching. Refinement and strict requirements will make students' learning more meaningful. This is the basic principle that teachers should do. The construction of a physical education teaching quality monitoring system is shown in Figure 1.

3. Motion Analysis for Multisensing Perception

3.1. Motion Image Extraction Process. Use a certain algorithm to calculate the probability of each Gaussian distribution as the foreground according to each pixel on the image, and extract the pixels in the image. The mixed Gaussian model formula is as follows [20]:

$$I_t(x,y) = \sum_{i=1}^{k} \omega_{i,t} \times \eta(I_t(x,y)), \mu_{i,t}, \sum_{i,t}\Bigg), \tag{1}$$

where K is the number of models, $I_t(x,y)$ is the pixel value at time t, $k\sum_{i,t}$ is the covariance matrix, $\sum_{i,t} = \sigma^2 I$ and σ^2 are the variance, I is the three-dimensional unit matrix, $\mu_{i,t}$ is the mean, and $\omega_{i,t}$ is the weight of the ith Gaussian at time t.

Probability density formula is calculated as follows:

$$\eta(I_t(x,y)), \mu, \sum = \frac{1}{(2\pi)^{n/2}|\sum|^{1/2}} e. \tag{2}$$

Table 1: Physical education quality monitoring system.

Component	Content
Class preparation	Establish the learning objectives of physical education courses, including sports action analysis and action explanation [16].
	Select relevant background knowledge to help students build a new knowledge framework [17].
	Explore flexible and diverse teaching methods and devices (e.g., multimedia).
	Design a variety of interactive teaching activities.
	Survey to understand students' background and learning status.
	Invite some students to prepare lessons together.
Teaching process	Use various forms of classroom introduction.
	State the learning objectives of each lesson.
	Provide opportunities to use different learning strategies.
	Provide students with comprehensive use of listening, speaking, reading, writing, and translation activities [18].
	Summarize teaching activities (including language goals and cultural goals).
	Evaluate teaching effectiveness through different activities.
Reflection after class	Is it valid to import?
	Are the learning objectives clear?
	Accurate preclass assessments of students.
	The success of the classroom activities.
	Whether teachers give feedback on students' learning in a timely manner.
	Is there a link between classroom teaching and career goals [19]?

Sort the following models:

$$p_{i,t} = \frac{\omega_{i,t}}{\sigma_i}, \quad \left|I_t(x,y) - \mu_{i,t-1}\right| < 2.5\sigma_i. \tag{3}$$

Update the following algorithm:

$$\begin{cases} \omega_{i,t} = (1-\sigma)\omega_{i,t-1} + \alpha, \\ \mu_{i,t} = (1-\beta)\mu_{i,t-1} + \beta I_t(x,y), \\ \sigma_{i,t}^2 = (1-\beta)\sigma_{i,t-2}^2 + \beta\left(I_t(x,y) - \mu_{i,t}\right)^{\mathrm{T}}\left(I_t(x,y) - \mu_{i,t}\right), \\ \beta = \alpha\eta\left(I_t(x,y), \mu_{i,t}, \sum_{i,t}\right), \end{cases} \quad \omega_{i,t} = (1-\alpha)\omega_{i,t-1}. \tag{4}$$

Get the pixel difference between the ist and the $i-1$th frame images [21]:

$$D(x,y) = F_i(x,y) - F_{i-1}(x,y). \tag{5}$$

Calculate the following learning rate:

$$\alpha \begin{cases} 0.05, D(x,y) > \dfrac{S}{10}, \\ 0.10, \dfrac{S}{10} < D(x,y) \le \dfrac{S}{3}, \\ 0.15, \dfrac{S}{3} < D(x,y) \le \dfrac{S}{2}. \end{cases} \tag{6}$$

Equation (22) takes the Gaussian distribution in front of the ranking as the foreground [22].

$$B = \arg\min\left(\sum_{K=1}^{b} \omega_k > T\right). \tag{7}$$

3.2. Motion Feature Extraction. During the training process of athletes, the video obtained by the camera is used to extract the foreground image, and a square window W is constructed, and the length of the window is $n \times n$, Let the point coordinate of the center of the window be (x, y); $I(x, y)$ is the grayscale value of the image at (x, y). The calculation formula of gray value is as follows:

$$E(\Delta x, \Delta y) = \sum_{(x,y)\in W} \omega(x,y)\left[I(x+\Delta x, y+\Delta y) - I(x,y)\right]^2. \tag{8}$$

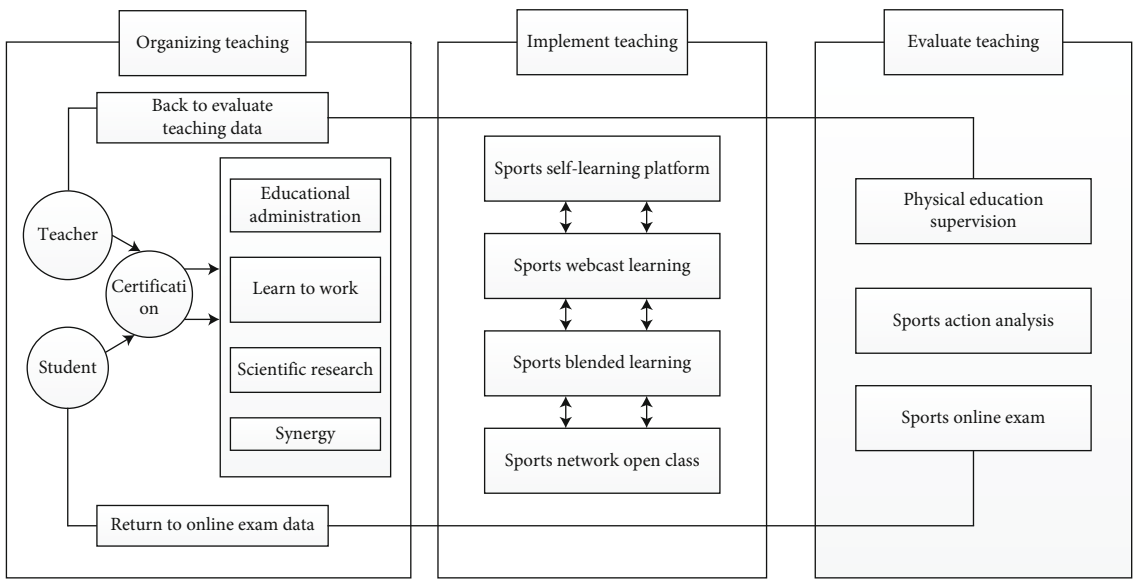

Figure 1: Physical education quality monitoring system.

Expand $I(x+\Delta x, y+\Delta y)$ in the following matrix form:

$$E(\Delta x, \Delta y) = [\Delta x, \Delta y] M \begin{bmatrix} \Delta x \\ \Delta y \end{bmatrix} \tag{9}$$

in

$$\sum_{(x,y)\in W} \omega(x,y) \begin{pmatrix} I_x^2 & I_x I_y \\ I_x I_y & I_y^2 \end{pmatrix}. \tag{10}$$

The number of movements of the measured body is identified in time t, and the fatigue assessment formula for the human body is as follows:

$$\begin{aligned} P &= \frac{0.001 \times n}{t}, \\ F &= 1 - P, \end{aligned} \tag{11}$$

where n is the number of exercises, P is the probability value of nonfatigue value, and F is the probability value of human fatigue [23].

3.3. Evaluation of Training Effect. The fuzzy scheduling function of physical training effect evaluation is as follows:

$$\begin{aligned} X_j(t+1) = p_j(t+1) \mp \beta \times \left| m\text{best}(t+1) - X_j(t) \right| \\ \times \ln \left(\frac{1}{u_j(t+1)} \right). \end{aligned} \tag{12}$$

Let $Z^{(1)}$ be the mean sequence of $X^{(1)}$:

$$Z^{(1)} = \left(Z^{(2)}(1), Z^{(1)}(3), \cdots, Z^{(1)}(n) \right), \tag{13}$$

$$Z^{(1)}(K) = \frac{1}{2} \left(x^{(1)}(k) + x^{(1)}(k-1) \right). \tag{14}$$

Then, there are

$$x^{(0)}(K) + az^{(1)}(k) = b, \tag{15}$$

where a is the development coefficient and b is the gray scale action.

Substitute the original data series $X^{(0)}$ into Equation (15) to get the following:

$$\begin{aligned} x^{(0)}(2) + az^{(1)}(2) &= b, \\ x^{(0)}(3) + az^{(1)}(3) &= b, \\ &\cdots \\ x^{(0)}(n) + az^{(1)}(n) &= b, \end{aligned} \tag{16}$$

$$A = \begin{bmatrix} a \\ b \end{bmatrix} = \left(B^{\mathrm{T}} B \right)^{-1} \cdot B^{\mathrm{T}} Y. \tag{17}$$

Substitute the resulting a, b into Equation (17) to get the following:

$$\hat{x}^{(1)}(t+1) = \left[x^{(0)}(1) - \frac{b}{a} \right] \cdot \exp(-at) + \frac{b}{a}, \quad (t = 0, 1, 2, \cdots, n-1). \tag{18}$$

Obtain the quantitative relationship of physical training effect evaluation.

$$\hat{x}^{(0)}(i) = \hat{x}^{(1)}(i) - \hat{x}^{(1)}(i-1), \quad (i = 1, 2, \cdots, n). \tag{19}$$

Table 2: The first group of motion pattern confusion matrices.

Sport mode	Running	Walk	Top	Go downstairs	Lie down	Lie flat	Lying flat
Running	190	4	2	1	2	1	0
Walk	1	180	7	5	7	0	0
Top	0	7	81	5	6	0	1
Go downstairs	0	6	7	83	4	0	0
Back	2	6	3	2	87	0	0
Lie down	5	0	0	0	3	92	0
Lie flat	5	1	0	1	0	0	93

Define $\sigma(k)$ as the residual value:

$$\sigma(k) = x^{(0)}(k) - \hat{x}^{(0)}(k). \tag{20}$$

Definition $\varepsilon(k)$ is the relative difference of residuals:

$$\varepsilon(K) = \frac{x^{(0)}(k) - \hat{x}^{(0)}(k)}{x^{(0)}(k)} \times 100\%. \tag{21}$$

Prediction function for evaluation of physical training effect [24].

$$p_{ij}^{(k)} = \frac{n_{ij}^{(k)}}{N_i}. \tag{22}$$

4. Simulation Experiments

4.1. Comparative Experiment. In order to obtain objective characteristic data of various sports modes, the experiment selected 30 testers in a sports academy, including 15 males and 15 females. 30 testers will complete 8 types of exercise modes: standing, walking, running, going upstairs, going downstairs, lying down, lying flat, and going backwards. 30 testers complete the experiment at the same time and place. During the experiment, the behavioral habits of the testers are not restricted, and the testers can complete the training actions according to their own behavioral habits. The article adopts comparative experiments. The first one adopts the traditional human motion pattern information collection method, and the second adopts the motion pattern recognition method fused with accelerators and sensors. The experimental results of the two methods are shown in Table 2 and Table 3, respectively.

According to the data in Table 2 and Table 3, Table 4 lists the recognition accuracy in two different ways. Due to the high degree of distinction between standing and other actions, the recognition accuracy is 100%. The degree of discrimination is small, and the recognition accuracy is low. The specific identification data are shown in Table 4.

According to the experimental data in Figure 2, we can conclude that when using traditional recognition of various motion patterns, it can recognize various behavior patterns, and the average recognition accuracy is 90.1%. The average recognition accuracy is 94.3%. Compared with the traditional recognition mode, the average recognition accuracy is increased by 4.2%, and the recognition result is better. Compared with the recognition results of the first set of experiments, for the more difficult to distinguish upstairs and downstairs, the recognition accuracy is increased by 9% and 7%, respectively, and the recognition accuracy of backward is increased by 6%.

4.2. Specific Data Analysis. In order to study the sports situation of students after physical education teaching, the experiment selected 40 students to test the standard degree of sports movement and divided 40 student volunteers into two groups. The experiment will compare the results of physical education assessment with and without teaching and analyze the differences between the two comparison experiments. The 40 students selected in the experiment are basically the same in height, weight, and age, and the P values are all greater than 0.06, indicating that the experiment can ensure that the conditions of the two groups can be regarded as basically the same, so the experiment can exclude the error caused by the body and other elements in the experimental results. The basic statistics of student volunteers are shown in Table 5 and Figure 3.

According to the experimental results in Table 6, we can know that before receiving the teaching, the test results of various indicators of the members of the routine group and the training group are basically the same, and there is no major difference. In the push-up test, the routine group can reach 11 times in one minute, the training group can reach 13, the triple jump routine group can reach 41, and the training group can reach 43. After throwing a 2 kg medicine ball on the spot, the routine group can reach 9.5 meters, and the training group can reach 14.5 meters. The 50-meter running routine group can reach 5.5 seconds, the training group can reach 5.1 seconds, the long jump routine group can reach 1.9 meters, the training group can reach 2.3 meters, the 60s double-shake routine group can reach 25 times, the training group can reach 50 times, the half-meter movement routine group can reach 18.2 seconds, the training group can reach 17.5 seconds, repeated 40 times across the conventional group and 44 times in the training group, and the control group can reach 1000 meters for 4.59 minutes and 4.35 minutes in the experimental group. After the T-test was performed between the conventional group and the training group, the results showed that the P values of the evaluation results of the two groups were both above 0.05. The experimental results showed that the initial

Table 3: The second group of motion pattern confusion matrices.

Sport mode	Running	Walk	Top	Go downstairs	Lie down	Lie flat	Lying flat
Running	194	3	1	1	1	0	0
Walk	1	188	5	3	3	0	0
Top	0	3	90	4	3	0	0
Go downstairs	0	4	3	91	2	0	0
Back	0	3	2	2	93	0	0
Lie down	3	2	0	0	1	94	0
Lie flat	3	1	0	0	1	0	95

Table 4: Statistics of recognition results.

Model	Standing	Walking	Running	Upstairs	Downstairs	Back	Down	Lying down
First group	100%	95%	90%	81%	83%	87%	92%	93%
Second group	100%	97%	94%	90%	91%	93%	94%	95%

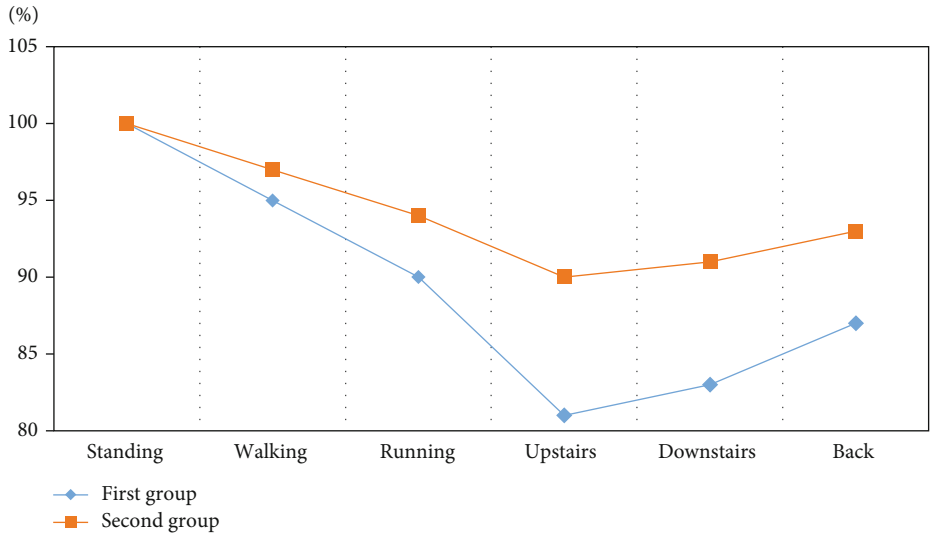

Figure 2: Statistical chart of recognition results.

Table 5: Statistics on the physical condition of volunteers.

	Regular group	Training group	P value	T value
Height (cm)	175 ± 2.00	175 ± 1.41	1.100	-0.150
Weight (kg)	70.10 ± 2.61	70.10 ± 2.17	0.978	-0.087
Age	16.6 ± 0.51	17 ± 0.00	0.701	-2.049

conditions of the two groups could be regarded as the same before receiving the teaching.

As can be seen from Table 7 and Figure 4, by analyzing the evaluation results between the conventional group and the training group, the overall situation of the members of the conventional training group was slightly improved compared with the pretraining test. The P values of the test scores of meter running, long jump, half-meter movement, and repeated crossing tests are all less than 0.05, indicating that there is a large gap between the two. Among them, the P value of the 50-meter running is less than 0.000, which has a very significant difference, while the triple jump has a significant difference. The P value of 60s and 60s double shake is greater than 0.05, and it can be seen that the difference between the conventional group and the training group after these two tests is not significant. Combining the evaluation results of the two groups before the training, we can conclude that under the condition that the initial conditions are basically the same, and the training conditions and environment are basically the same, the trainees who have

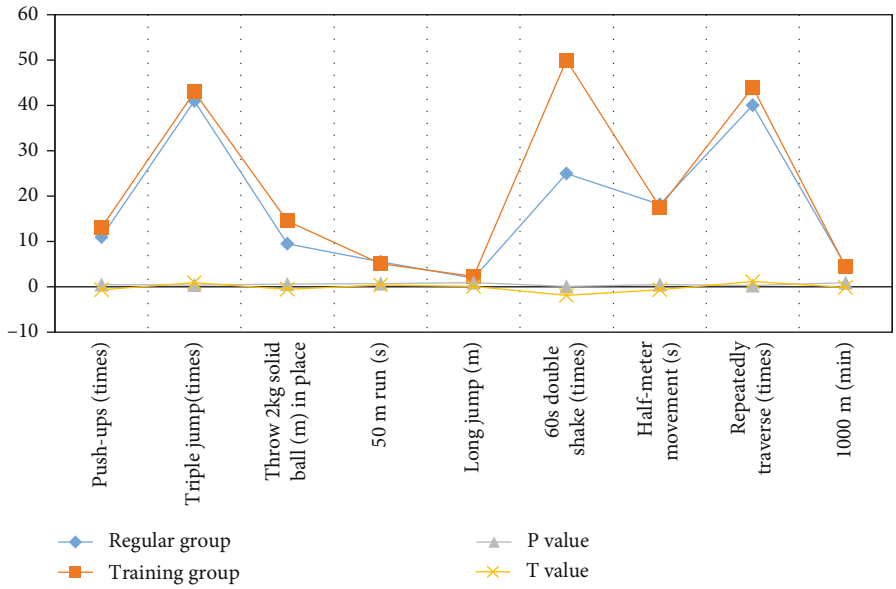

Figure 3: Statistics of physical fitness index evaluation results before teaching.

Table 6: Physical fitness index evaluation results of the routine group.

Test content	Regular group	Training group	*P* value	*T* value
Push-ups (times)	11.0	13.0	0.512	-0.673
Triple jump (times)	41.0	43.0	0.378	0.911
Throw 2 kg solid ball (m) in place	9.5	14.5	0.611	-0.521
50 m run (s)	5.5	5.1	0.685	0.414
Long jump (m)	1.9	2.3	0.920	0.102
60s double shake (times)	25.0	50.0	0.081	-1.880
Half-meter movement (s)	18.2	17.5	0.495	-0.701
Repeatedly traverse (times)	40.0	44.0	0.262	1.168
1000 m (min)	4.59	4.35	0.887	-0.144

Table 7: Physical fitness index evaluation results of the experimental group.

Test content	Regular group	Training group	*P* value	*T* value
Push-ups (times)	13.0	15.0	0.003	-3.578
Triple jump (times)	42.0	44.0	0.192	-1.372
Throw 2 kg solid ball (m) in place	12.1	15.3	0.009	-3.026
50 m run (s)	4.6	4.2	0.000	5.062
Long jump (m)	2.1	2.5	0.028	-2.456
60s double shake (times)	44.0	52.0	0.086	-1.864
Half-meter movement (s)	18.9	17.1	0.018	2.677
Repeatedly traverse (times)	42.0	46.0	0.010	-2.973
1000 m (min)	4.4	4.36	0.335	0.998

received the mode training method have obtained better physical fitness indicators. The improvement and the effect are greatly optimized compared with the mode training. It is shown in Table 8.

4.3. Model Testing. In order to verify the performance of the action analysis model based on multisensor perception proposed in the article, the experiment compares the performance of the proposed model with the support vector

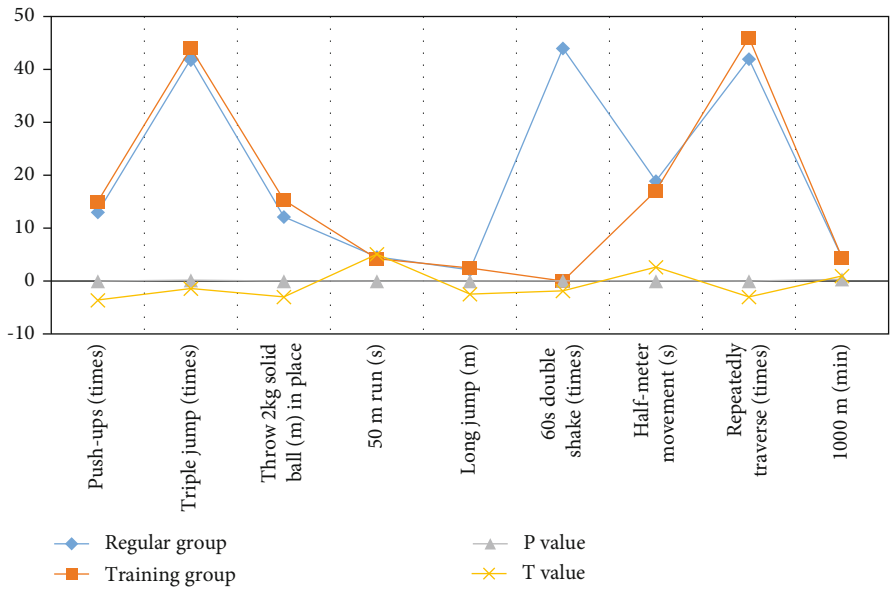

Figure 4: Statistics of physical fitness index evaluation results after teaching.

Table 8: Action model recognition accuracy.

	1	2	3	4	5	6	7	8
Multisensor motion analysis model	98%	98.1%	98.2%	98.4%	98.5%	98.6%	98.6%	99%
Support vector machine motion analysis model	97%	97.2%	97.4%	97.6%	97.7%	97.8%	97.9%	98%
Decision tree motion analysis model	96%	96.2%	96.3%	96.4%	96.4%	96.5%	96.7%	96.8%

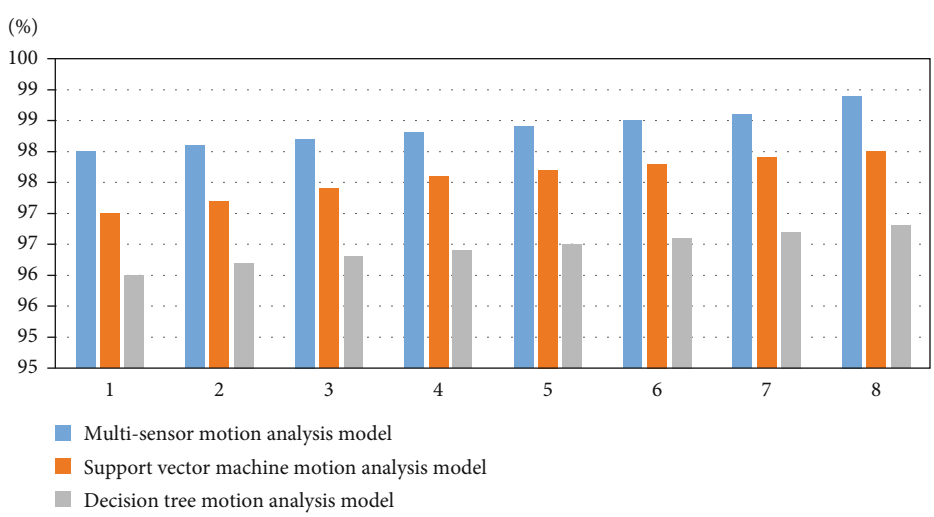

Figure 5: Action model recognition accuracy.

machine motion analysis model and the decision tree motion analysis model. Starting from two aspects, observe the detection results of 3 different models. The experimental method to test the correct rate is to shoot 8 images on the same circuit board at different distances, select the one with the closest shooting distance as the template, and test the remaining 7 sets of images with different scale multiples one by one, matching the accuracy of the model. The way to detect page response time for different models is to continuously increase the number of tests and observe the average response time of different models. The specific experimental data are as follows:

According to the experimental results in Figure 5, we can conclude that among the 8-spoke images captured in the experiment, the multisensor motion analysis model proposed in this article has the highest action recognition accuracy. When the

Table 9: Statistical results of page response time.

Model	Testing frequency	10	20	30	40	50	60	70
Multisensor motion analysis model	Average response time (MS)	0.4	0.5	0.6	0.7	0.8	0.9	1.0
	Success rate (%)	100	100	100	100	100	100	100
Support vector machine motion analysis model	Average response time (MS)	1.0	1.1	1.2	1.3	1.4	1.5	1.6
	Success rate (%)	100	99.6	99.5	99.4	99.3	98.4	99.3
Decision tree motion analysis model	Average response time (MS)	1.2	1.3	1.4	1.5	1.6	1.7	1.8
	Success rate (%)	100	98.6	98.5	98.4	98.3	98.2	98.1

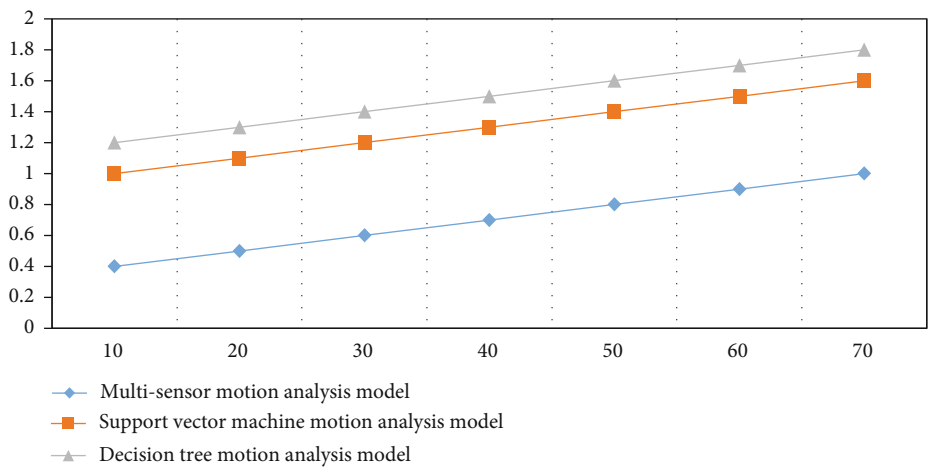

Figure 6: Statistical graph of page response time.

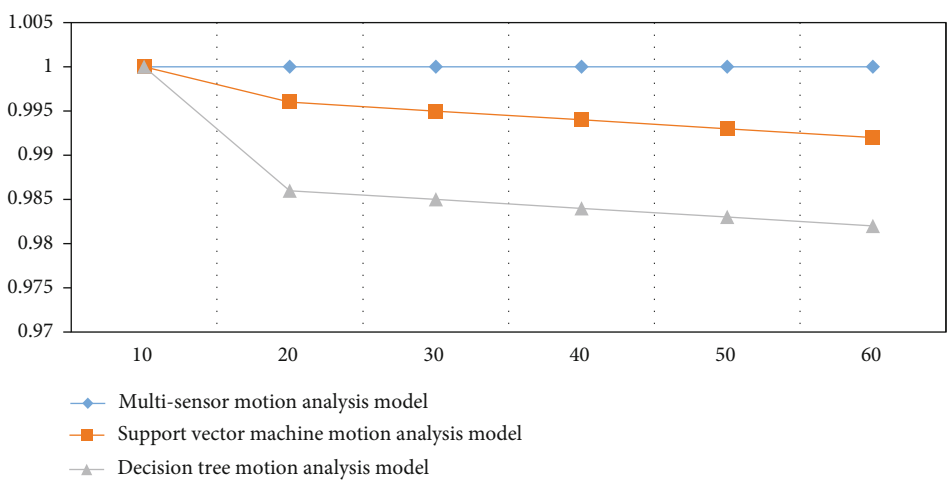

Figure 7: Success rate graph.

first picture is taken, the recognition accuracy is 98%. With the increase in the number of pictures taken, the accuracy of action recognition also increases. When the eighth picture is taken, the accuracy of action recognition reaches 99%. The recognition accuracy of the decision tree motion analysis mode is the lowest among the three models. When the eighth picture is taken, the recognition accuracy is the highest, which can reach 96.8%. The recognition accuracy of the support vector machine motion analysis model is between the two. The statistical results of page response time are shown in Table 9.

According to the data in Table 9, Figure 6, and Figure 7, we can conclude that among the three different models, the multisensor motion analysis model proposed in this article has the shortest page response time. When the number of tests is 10, the average page response time is 0.4 seconds. When the number of tests increased to 70, the average response time of the page reached 1.0 seconds, and the success rate of the multisensor motion analysis model remained at 100%. The average response time of the decision tree motion analysis model is the longest. When the number of

tests reaches 70, the average response time of the page is 1.8 seconds, and the success rate remains within 99% to 100%.Support vector machine analysis model average response time. In between, the success rate generally remains in the 98% to 100% range. The average response time will increase with the increase of the number of tests, and the experimental results also show that the detection performance of the multisensor motion analysis model is the highest.

5. Conclusion

Physical education course teaching is a highly practical course, and both teaching and learning are interdependent and inseparable [25]. Today, we are in a new century dominated by economy. The development of computer computing has spread to all corners of society, and advanced technological development has shown its advantages in various fields. Therefore, our educational methods must also be carried out to a certain extent reform. In terms of sports and sports talent training, my country has also integrated Internet thinking into physical education. It can be seen from the policy instructions that the country is paying more and more attention to the development of sports. In the future research work, in the growth process of young people, we should not pay attention to their achievements, but should pay attention to their physical health and mental health and realize the all-round development of young people. The government should give sufficient financial support to ensure diversified development of adolescent health.

Data Availability

The experimental data used to support the findings of this study are available from the corresponding author upon request.

Conflicts of Interest

The authors declared that they have no conflicts of interest regarding this work.

References

[1] X. Y. Jiang, "Study on evaluation index system of student practical teaching ability in physical education," *Journal of Gansu Lianhe University (Natural Science Edition)*, vol. 6, no. 23, pp. 531–551, 2012.

[2] Y. J. Wei, "Study on evaluation system of common physical education class teaching quality in colleges," *Journal of Baoji University of Arts and Sciences (Social Science Edition)*, vol. 20, no. 23, pp. 87–91, 2007.

[3] H. N. Ding, "Construction on teaching quality evaluation index system of college physical education teacher," *Bulletin of Sport Science & Technology*, vol. 18, no. 12, pp. 78–101, 2003.

[4] Y. Bai, *Design and Research of Intelligent Evaluation System of Physical Education Teaching Based on Artificial Intelligence Expert Decision System*, vol. 47, no. 117, 2016Springer, Cham, 2016.

[5] L. Zhang, "Research on human body movement posture based on inertial sensor," *International Journal Bioautomotion*, vol. 22, no. 2, pp. 179–186, 2018.

[6] A. D. Kuo and F. E. Zajac, "Human standing posture: multi-joint movement strategies based on biomechanical constraints," *Progress in Brain Research*, vol. 8, no. 7, pp. 297–349, 1993.

[7] W. Shen, K. Deng, X. Bai, T. Leyvand, B. Guo, and Z. Tu, "Exemplar-based human action pose correction," *IEEE Transactions on Cybernetics*, vol. 44, no. 7, pp. 1053–1066, 2014.

[8] L. K. Kozhevnikova, "Physical training as means of a healthy way of life and cultural leisure formation of student's youth," *Physical Education of Students*, vol. 10, no. 12, pp. 34–38, 2010.

[9] M. A. Yun-Feng, "Youth physical fitness training method for short track speed skaters," *China Winter Sports*, vol. 10, no. 12, pp. 21–32, 2018.

[10] Y. Yu, "Analysis on the optimization of physical education teaching environment," *Bulletin of Sport Science & Technology*, vol. 12, no. 8, pp. 32–45, 2016.

[11] K. Kitani, "Ego-action analysis for first-person sports videos," *Pervasive Computing, IEEE*, vol. 11, no. 2, pp. 92–95, 2012.

[12] A. Escartí and M. Gutiérrez, "Influence of the motivational climate in physical education on the intention to practice physical activity or sport," *European Journal of Sport Science*, vol. 1, no. 4, pp. 1–12, 2001.

[13] S. Silverman, K. J. Tyson, and J. Krampitz, "Teacher feedback and achievement in physical education: interaction with student practice," *Teaching & Teacher Education*, vol. 8, no. 4, pp. 333–344, 1992.

[14] T. J. Cleary, B. J. Zimmerman, and T. Keating, "Training physical education students to self-regulate during basketball free throw practice," *Research Quarterly for Exercise and Sport*, vol. 77, no. 2, pp. 251–262, 2006.

[15] S. Silverman and P. R. Subramaniam, "Student attitude toward physical education and physical activity: a review of measurement issues and outcomes," *Journal of Teaching in Physical Education*, vol. 19, no. 1, pp. 97–125, 1999.

[16] A. T. Özdemir and B. Barshan, "Detecting falls with wearable sensors using machine learning techniques," *Sensors*, vol. 14, no. 6, pp. 10691–10708, 2014.

[17] F. Attal, S. Mohammed, M. Dedabrishvili, F. Chamroukhi, L. Oukhellou, and Y. Amirat, "Physical human activity recognition using wearable sensors," *Sensors*, vol. 15, no. 12, pp. 31314–31338, 2015.

[18] Q. W. Xing, Z. Q. Hua, and W. J. Wei, "Pedestrian navigation method based on the kinematic mechanism of human lower limbs," *Chinese Journal of Inertial Technology*, vol. 23, no. 1, pp. 24–28, 2015.

[19] W. X. Qian, Q. H. Zeng, and J. W. Wan, "Pedestrian navigation method based on kinematic mechanism of human lower limb," *Journal of Chinese Inertial Technology*, vol. 23, no. 1, pp. 24–28, 2015.

[20] X. X. Zhang, Z. Rong, and M. F. Guo, "Yaw error self-observation algorithm for pedestrian navigation via foot-mounted inertial navigation system," *Journal of Chinese Inertial Technology*, vol. 23, no. 4, pp. 457–466, 2015.

[21] V. Lugade, E. Fortune, M. Morrow, and K. Kaufman, "Validity of using tri-axial accelerometers to measure human movement–Part I: posture and movement detection," *Medical Engineering & Physics*, vol. 36, no. 2, pp. 169–176, 2014.

[22] S. G. Trost, Y. Zheng, and W. K. Wong, "Machine learning for activity recognition: hip versus wrist data," *Physiological Measurement*, vol. 35, no. 11, pp. 2183–2189, 2014.

[23] M. Zhang and A. A. Sawchuk, "Human daily activity recognition with sparse representation using wearable sensors," *IEEE Journal of Biomedical and Health Informatics*, vol. 17, no. 3, pp. 553–560, 2013.

[24] C. Catal, S. Tufekci, E. Pirmit, and G. Kocabag, "On the use of ensemble of classifiers for accelerometer-based activity recognition," *Applied Soft Computing*, vol. 37, no. 21, pp. 1018–1022, 2015.

[25] L. Gao, A. K. Bourke, and J. Nelson, "Evaluation of accelerometer based multi-sensor versus single-sensor activity recognition systems," *Medical Engineering & Physics*, vol. 36, no. 6, pp. 779–785, 2014.

Hindawi
Journal of Sensors
Volume 2022, Article ID 3452727, 12 pages
https://doi.org/10.1155/2022/3452727

Research Article

Exploration of Water-Saving and High-Yield Irrigation Model for Tomato under Microsprinkler Irrigation with Plastic Film in a Greenhouse Based on Spatial Analysis

Mingzhi Zhang,[1,2] **Lu Wang**,[3] **Hui Wang**,[3] **Na Xiao**,[1] **and Jianfei Liu**[4]

[1]*Huanghe Science and Technology University, Zhengzhou 450000, China*
[2]*Henan Provincial Water Conservancy Research Institute, Zhengzhou 450000, China*
[3]*Shanxi Water Conservancy Development Center, Taiyuan 030002, China*
[4]*Shanxi Provincial Department of Water Resources, Taiyuan 030002, China*

Correspondence should be addressed to Na Xiao; xiaonaguofeng@126.com

Received 16 January 2022; Accepted 30 March 2022; Published 2 May 2022

Academic Editor: Liu Hongxiao

The purpose of this study was to analyse the suitability of the frequency and amount of microsprinkler irrigation under plastic film technology (MSPF) in a greenhouse. This study was aimed at determining the effects of different irrigation frequency and irrigation amount of the MSPF on the quality, yield (Y), and water use efficiency (WUE) of tomato, and the optimal irrigation period and irrigation amount of tomato with MSPF were determined by spatial analysis method. Irrigation frequency was set 3 levels, 3 d (F1), 5 d (F3), and 7 d (F3), respectively. Irrigation amount was set 3 levels, 0.7 E_{pan} (I1), 1.0 E_{pan} (I2), and 1.2 E_{pan} (I3) (E_{pan} is the diameter of 20 cm standard pan evaporation, mm), respectively. The results show that increase in the single fruit weight (SFW), transverse diameter (TD), vertical diameter (VD), total soluble solids (TSS), total soluble sugar (TSU), soluble solid content (SSC), sugar-acid ratio (SAR), soluble protein (SP), vitamin C (VC), lycopene (L), Y, and WUE of spring and autumn tomatoes was observed initially with decreasing irrigation frequency; however, decrease in all these variables was observed thereafter. Similarly, SFW, TD, VD, and SAR of spring and autumn tomatoes first added and then reduced with increasing irrigation amount, whereas TSS, SP, TSU, VC, L, and WUE exhibited an overall decreasing trend. On the basis of spatial analysis, the comprehensive score, Y, and WUE of F2I2 tomato were predicted to simultaneously reach more than 95% of the maximum, which is consistent with the earlier studies on comprehensive evaluation of yield and WUE.

1. Introduction

With improvement in the quality of life, the demand for good quality vegetables also increases [1]. Tomato (*Solanum lycopersicum L.*) is one of the main vegetables grown under protected cultivation system in Northwest China and possesses rich nutrition and health care value [2, 3]. The water requirement for the growth of facility crops mainly comes from irrigation. Although the rapid development of facility agriculture ensures the stable yield of vegetables, the irrigation of facility agriculture has also aggravates the water resource crisis in Northwest China [4, 5]. Studies have shown that changes in the irrigation frequency and irrigation amount of tomato in facility agriculture not only affected the water consumption of tomato but also changed the dry matter accumulation, fruit quality, and yield of tomato [6–8]. Therefore, under the premise of not increasing farmers' input, optimizing the existing irrigation frequency and irrigation amount of greenhouse tomato to achieve the best balance of water-saving, yield-increasing and quality improvement of tomato is important for the efficient utilization and sustainable development of facility water resources in this area.

The MSPF has a significant effect of saving water and increasing yield, and it has a good prospect in the field of facility agriculture tomato planting [5, 9, 10]. The results

Table 1: Experimental factor and design.

No.	Treatment	Irrigation frequency (d)	k_{cp}	Irrigation amount (mm)		Irrigation times	
				Spring of tomato	Autumn of tomato	Spring of tomato	Autumn of tomato
1	F1I1	3	0.7	247.12	152.73	33	47
2	F1I2	3	1.0	353.03	218.19	33	47
3	F1I3	3	1.2	423.64	261.83	33	47
4	F2I1	5	0.7	247.12	152.73	21	28
5	F2I2	5	1.0	353.03	218.19	21	28
6	F2I3	5	1.2	423.64	261.83	21	28
7	F3I1	7	0.7	247.12	152.73	15	20
8	F3I2	7	1.0	353.03	218.19	15	20
9	F3I3	7	1.2	423.64	261.83	15	20

show that irrigation frequency and irrigation amount can change soil water distribution and crop yield and quality [2, 11]. In terms of irrigation frequency, farmers often initiate irrigation after delayed drought stress on the crop physiological index. Decreased crop yield and poor quality are common due to untimely irrigation. Drip irrigation for 7–9 days has been found to improve the quality and yield of tomato [12]. In terms of irrigation amount, the actual amount of crop irrigation is much higher than the crop water requirement, resulting in a great waste of water resources, leading to a series of ecological environment and food production problems [13, 14]. Studies have shown that drip irrigation can improve the quality and yield of tomato when the irrigation amount is 0.7 E_{pan} [2].

At present, there are few studies on the effects of single factor and interaction of irrigation frequency and irrigation amount of MSPF on the fruit quality, yield, and water use efficiency (WUE) of greenhouse tomato; at the same time, there are few reports on the guidance of greenhouse tomato irrigation based on pan evaporation. Tomato fruit quality, yield, and WUE are the 3 major indices constituting the comprehensive benefit of greenhouse tomato. It is difficult to meet the peak value of the 3 major indices at the same time by selecting the most suitable combination of irrigation frequency and irrigation amount. There are few studies on how to optimize the three main indexes. Therefore, this study sought to explore the quality, yield, and WUE of greenhouse tomato in response to different irrigation frequencies and irrigation amount of MSPF based on pan evaporation-controlled MSPF amount. Regression analysis of data based on the least square method using Mathematica 12.0 was performed by taking principal component analyses (PCA) for the comprehensive scores of spring and autumn tomato quality, yield, and WUE as dependent variables and irrigation frequency and irrigation amount as independent variables. The maximum confidence interval (CI) of 95% was used to screen the optimal irrigation frequency and amount. The most suitable irrigation frequency and irrigation amount combination model of MSPF for tomato quality, yield, and WUE in arid and semiarid sandy loam areas was obtained. This paper provides valuable data support for water saving, yield increase, and quality improvement of facility vegetables in this area through greenhouse experiments and multiobjective optimization data analysis.

2. Materials and Methods

2.1. Experimental Site and Management. The experimental greenhouse is located in the Modern Agricultural Science and Technology Exhibition Center of Xi'an City, Shaanxi Province. The test center has a warm temperate semihumid continental monsoon climate, located in the arid and semiarid regions of Northwest China, with an altitude of 435 m. The field water holding capacity of the soil in the greenhouse is 25.40% (mass water content), and its type is sandy loam, and the mass fractions of sand, silt, and clay are 63.9%, 29.63%, and 6.47%, respectively. The average bulk density of the 1.0 m soil layer was 1.48 g/cm^3, the water holding capacity of field weight was 27.40%, and the depth of groundwater table on the site exceeded 30 m. The contents of organic matter, total phosphorus (P), total potassium (K), total nitrogen, available nitrogen, available P, and available K in the plough layer before sowing were 15.53 g/kg, 10.12 g/kg, 2.01 g/kg, 1.36 g/kg, 70.45 mg/kg, 112 mg/kg, and 85.23 mg/kg, respectively.

The greenhouse tomato variety in this experiment is "Jingfan 401" (Jingyan Yinong Seed Technology Co., Ltd., Beijing). The length of the ridge was 3.4 m and the width of the ridge was 1.2 m. Tomato was planted in one pipe and two rows on ridges. The plant spacing was 40 cm and the row spacing was 50 cm. A 1-meter block copolymer waterproof membrane was embedded in each treatment of the experimental plot to prevent the interaction of horizontal water transport among the plots. The field management measures, such as fertilisation, irrigation, and pesticides, were kept similar in all treatments. In this experiment, the spring and autumn tomatoes were transplanted on March 27, 2019, and August 23, 2019, irrigated on April 4, 2019, and August 30, 2019, stopped irrigation on July 15, 2019, and January 17, 2020, and reaped on July 25, 2019, and January 30, 2020. During the growth period of tomato, except for the different treatment factors, the other treatments were consistent. The microsprinkler hose selected for MSPF is Hebei Plentirain Irrigation Equipment Technology Co., Ltd. (Hebei, China). The thin-walled oblique hole in the

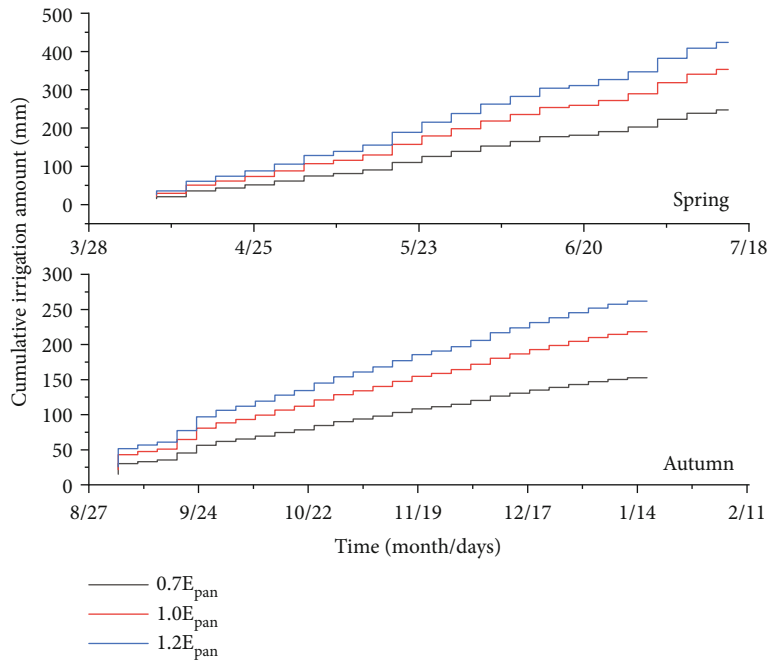

Figure 1: 5-day irrigation records.

microsprinkler hose has three microholes, and the diameter of the microhole is 0.7 mm. The diameter of the microsprinkler hose is 32 mm, and the working pressure is 0.6 bar. The white agricultural insulation film was produced by Hedong pastoral plastic product factory (Hebei, China).

2.2. Experimental Design. This paper mainly studies the effects of irrigation frequency and water amount of MSPF on the quality, yield, and water use efficiency of greenhouse tomato. Irrigation frequency and irrigation amount are set at 3 levels, in which the interval of irrigation frequency was 3 days, 5 days, and 7 days, respectively; the irrigation amount was controlled by the basis of the cumulative evaporation (E_{pan}, a 20 cm diameter standard pan) [15], which was realised by a control coefficient (k_{cp}). The k_{cp} (the crop pan coefficient) was 0.7, 1.0, and 1.2. A completely randomized trial design was used, and the treatments are shown in Table 1. Each of the treatments was repeated 3 times, a total of 27 experimental plots.

Pan evaporation amount was monitored at 8.00 am on the same day of each irrigation frequency. Formula (1) is used to calculate irrigation amount [5, 16]. The irrigation records of spring and autumn tomatoes are shown in Figure 1.

$$W = A * E_{pan} * k_{cp}. \quad (1)$$

In the formula, W represents the irrigation amount and A represents the plot area.

2.3. Determination of Tomato Quality and Calculation of Related Indices

2.3.1. Measurements. The fruit shape indices (weight of single fruit, vertical diameters, and transverse diameters), tomato flavor indices (total soluble solids, soluble solid content, and sugar/acid ratio), and tomato nutrition indices (soluble protein, vitamin C, and lycopene) of spring and autumn tomatoes were determined. Three tomato fruits were randomly selected in each plot when the tomatoes were ripe at the first stage. Individual fruits were homogenized to determine the fruit flavor and nutritional indexes. The specific measurement method is as follows:

Weight of single fruit (SFW): the SFW was gauged by electronic scale (LQ-C20002 Kunshan Youkeweite Electronic Technology Co., Ltd., Jiangsu, China)

Vertical diameters (VD): the VD was gauged by vernier calipers [5]

Transverse diameters (TD): the TD was gauged by vernier calipers [5]

Total soluble solid content (TSS): the TSS was gauged by hand-held refractometer (PR-32α Atago, Tokyo, Japan)

Total soluble sugar content (TSU): the TSU was gauged by anthrone method [17]

Soluble solid content (SSC): the SSC was gauged by anthrone method [2]

Titratable acids content (TA): the TA was gauged by acid-base titration [18]

Sugar/acid ratio (SAR): SAR = SSC/TA [5]

Soluble protein content (SP): the SP was gauged using Coomassie brilliant blue assay [2]

Vitamin C content (VC): the VC was gauged by the classical titration method [19]

Lycopene content (L): the L was gauged by ultraviolet spectrophotometer [20]

2.3.2. Quality Comprehensive Evaluation. The above 9 indices are taken as variables of comprehensive quality evaluation. Firstly, standardisation and homogenisation were performed. Secondly, the principal component load matrix

of each variable was obtained using principal component analysis (PCA) to evaluate the comprehensive concept quality of tomato, and a quantitative comprehensive score was derived for the comprehensive evaluation of tomato quality [5].

2.4. Determination of Tomato Yield and Water Use Efficiency and Calculation of Related Indices

2.4.1. Yield. When the fruits are ripe, 4 tomato plants are randomly selected in each plot, and the ripe fruits are collected every three days and weighed, and the weights are recorded separately and finally converted into hectare yield (Y, kg/hm^2).

2.4.2. Water Use Efficiency. Automatic detection of soil moisture was performed by soil moisture sensor (TRIME-PICO-IPH, IMKO, Inc., Ettlingen, Germany). Formula (2) is used to calculate water consumption (ET_a, mm) and formula (3) is used to calculate crop water use efficiency (WUE, kg/m^3) [5, 21]:

$$ET_a = I \pm 1000 \times H \times (\theta_{t1} - \theta_{t2}), \quad (2)$$

where I is the irrigation quota of spring and autumn tomatoes growth period (mm), H is the depth ($H = 0.80$ m), and θ_{t1} and θ_{t2} is 0-0.80 m average soil volumetric water contents at times t1 and t2 (cm^3/cm^3), respectively.

$$\mathrm{WUE} = \frac{Y}{ET_a}. \quad (3)$$

2.5. Data Analysis. Statistical analysis was performed by SPSS 22.0 (IBM Crop., Armonk, New York, NY, USA), and the contribution degree was obtained by the efficacy estimation in univariate analysis. The statistics was plotted by OriginPro 2019b (Origin Lab Corporation, Northampton, MA, USA). The Wolfram Mathematica 12.0 (Wolfram Research, New York, NY, USA) was used to return analysis of data.

3. Results

3.1. Effects of Different Irrigation Frequency and Irrigation Amount on Quality of Tomato

3.1.1. Shape Indices. As shown in Table 2, the SFW and VD of spring tomato and autumn tomato fruits were greatly affected by irrigation frequency (F, $P \leq 0.05$). The F increased from F1 to F3, and the SFW, TD, and VD of spring tomato and autumn tomato were first added and then reduced. The SFW, TD, and VD of spring tomato and autumn tomato fruits were greatly affected by irrigation amount (I, $P \leq 0.05$). With increase in I, the SFW, TD, and VD of spring tomato and autumn tomato were added.

3.1.2. Flavor Indices. As shown in Table 3, the TSS of spring tomato and autumn tomato were greatly affected by F. The TSS, TSU, and SAR of spring tomato and autumn tomato were greatly affected by I. The flavor index of the spring tomato and autumn tomato treated with F2I2 was not significantly different from that of F1I2. The TSS of the spring tomato and autumn tomato in F1I2 were significantly higher than that of F1I3 (approximately 22.53% and 29.80%, respectively) and F3I3 (approximately 13.95 and 17.80%, respectively). The TSU of the spring tomato and autumn tomato F1I2 were significantly higher than that of F1I3 (approximately 22.67 and 16.01%, respectively) and F3I3 (approximately 36.12% and 17.36%, respectively). The F increased from F1 to F3, the TSS, TSU, and SAR of spring tomato and autumn tomato were first added and then reduced, and the TSS, TSU, and SAR of spring tomato and autumn tomato were reduced and2 added from I1 to I3 for I.

3.1.3. Nutritional Indices. As shown in Table 4, the SP and VC of spring tomato and autumn tomato were greatly affected by F. The SP, VC, and L of spring tomato and autumn tomato were greatly affected by I. No significant difference in nutritional index between F2I2 and F1I2 treatments was observed. The SP of F2I2 treatment was significantly higher than that of F3I3 treatment. The VC of F2I2 with spring and autumn tomato was significantly higher than that of F1I3 (approximately 26.02% and 17.02%, respectively), F2I3 (approximately 17.07% and 11.88%, respectively), F3I1 (approximately 9.43% and 10.63%, respectively), F3I2 (approximately 10.41% and 6.07%, respectively), and F3I3 (approximately 26.62% and 28.19%, respectively). The L of F2I2 with spring and autumn tomato was significantly higher than that of F1I3 (approximately 17.01% and 10.77%, respectively), F2I3 (approximately 14.56% and 8.76%, respectively), and F3I3 (approximately 34.00% and 18.31%, respectively). The F was added from F1 to F3, and the SP, VC, and L of spring tomato and autumn tomato were added initially and reduced thereafter, while these parameters decreased with increased from I1 to I3.

3.1.4. Comprehensive Evaluation of Tomato Quality Based on PCA. As shown in Table 5, the first PC1 mainly represents the appearance of fruit, and its cumulative contribution rate is more than 50%; the second PC2 mainly characterizes fruit flavor and nutrition, and its cumulative contribution rate is more than 32%. It can be seen from Figure 2 that the comprehensive quality score of F2I2 treatment is within 95% confidence interval of the peak value of spring and autumn tomato quality score, indicating that the quality of spring tomato and autumn tomato with F2I2 treatment can reach the best.

3.2. Effects of Different Irrigation Frequency and Irrigation Amount on Yield and WUE of Tomato. As shown in Table 6, the yield, ET_a, and WUE of spring tomato and autumn tomato were greatly affected by F and I. The significantly higher tomato yield of F2I2 was compared with F1I1, F2I1, F3I1, and F3I2 yields (33.44% and 31.00%, 31.88% and 28.03%, 44.08% and 43.38%, and 27.49% and 16.73%, for spring and autumn tomatoes, respectively). The ET_a of F2I2 was significantly lower in F1I3, F2I3, and F3I3 (12.63% and 15.98%, 18.15% and 9.50%, and 11.87% and

Table 2: Effects of different irrigation frequency and irrigation amount on fruit shape of tomato.

Treatment	Spring of tomato fruit			Autumn of tomato fruit		
	SFW (g)	TD (mm)	VD (mm)	SFW (g)	TD (mm)	VD (mm)
F1I1	85.79 ± 39.3b	48.27 ± 9.2b	50.97 ± 9.56d	111.88 ± 18.74b	42.64 ± 4.08c	50.25 ± 6.47c
F1I2	114.03 ± 35.56ab	52.94 ± 6.48ab	59.88 ± 4.8bcd	153.36 ± 30.81a	49.68 ± 5.91ab	59.96 ± 5.35ab
F1I3	134.88 ± 67.31a	52.04 ± 11.79ab	65.68 ± 12.62abc	151.46 ± 51.12a	49.26 ± 5.12ab	60.06 ± 6.34ab
F2I1	106.16 ± 35.23ab	48.69 ± 7.1b	57.58 ± 9.94cd	113.23 ± 36.48a	45.23 ± 3.54bc	50.25 ± 4.64c
F2I2	139.42 ± 25.75a	57.86 ± 4.17a	67.39 ± 3.17ab	161.52 ± 31.06a	51.75 ± 3.36a	62.86 ± 3.54a
F2I3	146.37 ± 34.56a	59.8 ± 6.2a	71.01 ± 10.65a	153.37 ± 30.21a	51.47 ± 7.01a	58.2 ± 3.04ab
F3I1	83.23 ± 48.65b	47.72 ± 11.41b	52.92 ± 10.31d	125.43 ± 44.19ab	48.78 ± 8.02ab	56.85 ± 7.7b
F3I2	105.24 ± 28.54ab	53.97 ± 8.38ab	58.85 ± 4.94bcd	149.29 ± 17.5ab	51.09 ± 4.63ab	61.33 ± 2.01ab
F3I3	118.7 ± 40.01ab	54.46 ± 5.96ab	62.94 ± 9.57abc	157.17 ± 55.09a	49.34 ± 6.12ab	61.58 ± 4.28ab
			F-value			
F	3.317*	2.102 ns	5.228**	0.136 ns	1.738 ns	3.106*
I	7.167*	6.468**	14.079**	9.186**	7.192**	23.728**
F∗I	0.113 ns	0.463 ns	0.214 ns	0.268 ns	0.930 ns	1.798 ns

Table 3: Effects of different irrigation frequency and irrigation amount on fruit flavor of tomato.

Treatment	Spring of tomato fruit			Autumn of tomato fruit		
	TSS (%)	TSU (%)	SAR	TSS (%)	TSU (%)	SAR
F1I1	5.22 ± 0.21ab	7.6 ± 1.01abc	6.87 ± 1.35ab	4.85 ± 0.39a	7 ± 1.14ab	6.52 ± 0.9ab
F1I2	5.01 ± 0.16bc	7.42 ± 1.29abc	8.24 ± 1.94a	4.58 ± 0.47a	6.78 ± 1.54abc	6.14 ± 1.17ab
F1I3	4.54 ± 0.06d	6.32 ± 1.37cd	6.87 ± 1.35ab	4.19 ± 0.28b	6.09 ± 0.89cd	6.05 ± 1.14ab
F2I1	5.43 ± 0.26a	8.7 ± 0.88a	7.89 ± 0.96a	5.17 ± 0.55a	7.35 ± 0.87a	6.89 ± 1.24a
F2I2	5.17 ± 0.66ab	7.75 ± 1.6ab	8.2 ± 1.61a	4.94 ± 0.47a	7.06 ± 0.84ab	6.35 ± 1.18ab
F2I3	4.84 ± 0.42cd	6.97 ± 1.37bcd	6.25 ± 1.26b	4.41 ± 0.81ab	6.25 ± 0.98bc	5.55 ± 0.75b
F3I1	5.23 ± 0.15ab	7 ± 1.44bcd	7.79 ± 1.74a	4.54 ± 0.75ab	6.99 ± 1.6bc	6 ± 0.93ab
F3I2	4.9 ± 0.38bc	6.8 ± 1.54bcd	7.5 ± 1.53ab	4.09 ± 0.44a	6.71 ± 1.5abc	5.89 ± 1.56ab
F3I3	4.22 ± 0.12e	5.69 ± 1.22d	6.16 ± 0.89b	3.81 ± 0.24b	6.02 ± 1.18d	5.47 ± 0.63b
			F-value			
F	8.714**	6.609*	0.286 ns	12.215**	0.538 ns	0.597 ns
I	38.232**	8.416**	8.217*	12.800**	4.931*	3.473*
F∗I	1.191 ns	0.249 ns	1.246 ns	0.180 ns	0.015 ns	0.519 ns

13.82%, for spring and autumn tomatoes, respectively). The WUE of F2I2 was significantly higher than F1I3, F2I3, F3I2, and F3I3 (26.44% and 25.97%, 23.36% and 12.27%, 23.05% and 12.33%, and 37.89% and 24.35%, for spring and autumn tomatoes, respectively). With decrease in F, the yield and WUE initially increased and then decreased; however, ET_a exhibited an overall decreasing trend, in which the tomato yield of F2 (109.916.20 and 90368.06 kg/ha, for spring and autumn tomatoes, respectively) was higher than that of F1 and F3 by 5.27% and 3.24% and 19.31% and 11.30%, and the WUE was higher than that of F1 and F3 by 8.44% and 7.24% and 11.46% and 11.06%, for spring and autumn tomatoes, respectively. With the addition of I, the Y of spring tomato and autumn tomato was added at first and then reduced, in which I2 spring tomato and autumn tomato Y was higher than I1 by about 24.44% and 26.15% and also higher than I3 by about 1.64% and 3.06%. The WUE of spring tomato and autumn tomato was higher than that of I1 by about 8.44% and -5.21% and also higher than that of I3 by about 14.46% and 19.10%.

3.3. Optimization of Irrigation Frequency and Irrigation Amount Based on Tomato Quality, Yield, and WUE. Considering the difference in irrigation frequency and irrigation amount of spring and autumn tomato, we used Mathematica 12.0 to analyse the experimental results of two tomato crops (Table 7). The quality of tomato was superior when it was irrigated once every 5 days, and the irrigation amount was approximately 0.8-0.9 E_{pan}. Similarly, the yield reached its maximum value when it was irrigated once in 4–5 days, and the irrigation amount was approximately 1.1 E_{pan}. Furthermore, the WUE reached the maximum when it was irrigated once in 5 days, and the irrigation amount was approximately 0.7-0.8 E_{pan}. Thus, our study indicates that achieving the peak values of quality, yield, and WUE at

Table 4: Effects of different irrigation frequency and irrigation amount on fruit nutritional of tomato.

Treatment	Spring of tomato fruit			Autumn of tomato fruit		
	SP (mg/g)	VC (mg/g)	L (%)	SP (mg/g)	VC (mg/g)	L (%)
F1I1	5.4 ± 0.35ab	19.62 ± 1.55ab	59.18 ± 7.33abc	5.26 ± 0.5ab	16.93 ± 2.89ab	60.65 ± 8.86aab
F1I2	5.27 ± 0.63ab	17.94 ± 1.28bc	58.45 ± 4.53abc	4.91 ± 0.38ab	16.17 ± 2.12ab	59.03 ± 8.91ab
F1I3	5.12 ± 0.71bc	15.23 ± 1.53d	53.4 ± 6.59c	4.45 ± 0.63ab	14.83 ± 1.91bc	53.54 ± 8.69bc
F2I1	5.7 ± 0.51a	20.85 ± 4.24a	65.73 ± 7.15a	5.2 ± 0.15a	17.86 ± 1.82a	61.3 ± 5.12a
F2I2	5.39 ± 0.39ab	19.19 ± 2.44ab	62.48 ± 8.15a	5.10 ± 0.55ab	17.36 ± 0.54ab	59.31 ± 3.74ab
F2I3	5.07 ± 0.32bc	16.83 ± 2.62cd	54.54 ± 10.93bc	4.87 ± 0.34ab	15.51 ± 1.37abc	54.53 ± 6.12abc
F3I1	5.31 ± 0.52ab	17.54 ± 1.37bc	61.45 ± 5.86ab	4.83 ± 0.5ab	15.69 ± 1.7ab	58.14 ± 5ab
F3I2	4.95 ± 0.56bc	17.38 ± 1.37bc	58.29 ± 5.83abc	4.96 ± 0.51ab	16.36 ± 2.24abc	56.9 ± 6.78abc
F3I3	4.73 ± 0.19c	14.92 ± 1.1d	46.63 ± 5.04d	4.44 ± 0.2b	13.54 ± 1.66c	50.13 ± 6.86c
			F-value			
F	4.400*	7.979**	4.292*	3.440*	5.475**	1.758 ns
I	6.924**	20.392**	16.757**	10.041**	11.005**	8.314**
F∗I	0.374 ns	0.539 ns	1.014 ns	1.131 ns	0.487 ns	0.050 ns

Table 5: Principal component loading matrix.

Variables	Spring		Autumn	
	PC1 (55.00%)	PC2 (32.16%)	PC1 (50.92%)	PC2 (38.09%)
X1	-0.143	0.971	-0.348	0.905
X2	-0.203	0.921	-0.185	0.953
X3	-0.212	0.968	-0.337	0.915
X4	0.932	-0.280	0.883	-0.321
X5	0.971	-0.076	0.893	-0.276
X6	0.764	-0.124	0.912	-0.287
X7	0.920	-0.208	0.972	-0.161
X8	0.924	-0.216	0.930	-0.306
X9	0.956	-0.203	0.786	-0.474

similar irrigation frequency and amount is challenging. Further analysis indicated a 95% CI of the maximum ((comprehensive score of quality, 164.64-173.30 (spring) and 146.23-153.93 (autumn)), (yield, 113491.66-119464.90 (spring) and 93518.24-98440.25 (autumn)), (WUE, 32.02-33.70 (spring) and 36.91-38.85 (autumn)) of all 3 parameters as the acceptability interval to optimize all 3 parameters simultaneously. The shadow areas of quality comprehensive score, yield, and WUE overlap were found to increase gradually with increase in CI. The irrigation frequency and irrigation amount for the comprehensive score of quality, yield, and WUE at 95% CI of the maximum value have been shown in Figures 2 and 3, respectively. The comprehensive score, yield, and WUE of tomato were found to exhibit more than 95% of the maximum value simultaneously when treated with F2I2.

4. Discussion

4.1. Effects of Irrigation Frequency on Greenhouse Tomato Quality and Yield. Many researchers believe that tomato grows ideally at high altitude, and the growth also requires constant soil water potential and high soil oxygen diffusion rate [22–24]. In this paper, the yield and WUE of tomato increased initially and decreased subsequently with decrease in irrigation frequency (Table 6) under similar irrigation amount. This fluctuation might be attributable to the fact that the high frequency small quota irrigation keeps water in a small soil volume, leading to water retention mainly concentrated in the shallow soil (0-20 cm) in MSPF. The shallow soil has high water-filled pore space (WFPS) and poor soil air permeability, which reduces the deep migration and distribution of deep crop roots, which is not conducive to the growth of tomato [25–27]. Low frequency and high quota irrigation increase the volume difference of soil dry and wet zone and prolong its duration, leading to persistent water stress in nonhumid area. Similarly, large quota irrigation easily increases soil compactness, reduces soil porosity and ventilation, and limits the increase in yield [27]. In this study, compared with the irrigation frequency of 3 and 7 days, the 5-day soil volume moisture content of the tillage layer was higher than that of 1.72% and 3.23% and 1.54% and 3.62% (for spring and autumn tomatoes, respectively, Figure 4) at during tomato maturity, indicating that irrigation once in 5 days effectively decreases unnecessary water evaporation and deep leakage. Wang et al. [28] showed that change in tomato yield with irrigation frequency occurs predominantly due to the change in SFW, which is inconsistent with our finding indicating that the change in SFW does not affect the yield (Table 2). This might be attributed to fruit thinning during fruit expansion. Difference in ET_a in different irrigation frequencies was not found to be significant (Table 3). Furthermore, change in WUE caused by increase in irrigation frequency might be attributed to the change in yield (Table 6). Our findings are not consistent with those of a study by Jacob Fara et al. [12] that demonstrated superior yield and WUE of drip irrigation with 7-day irrigation compared with those of 5-day irrigation. The difference in our result may be attributed to the differences in physical

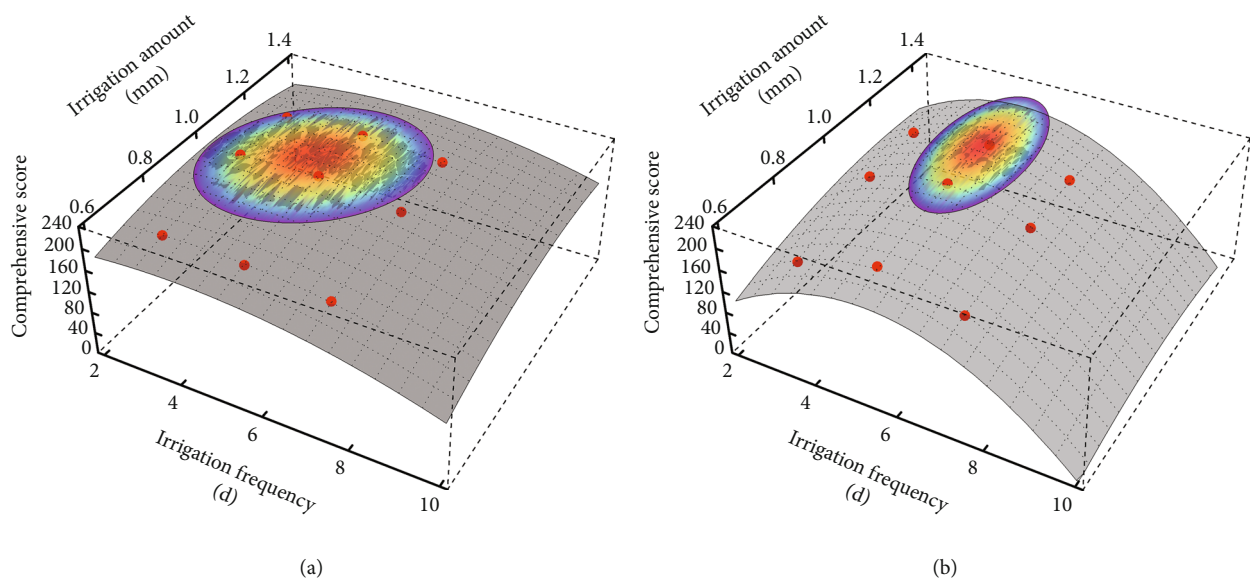

Figure 2: Comprehensive score chart of quality principal components of spring tomato (a) and autumn tomato (b). Note: the circular dotted points in the figure represent the spring (a) and autumn (b) measured and calculated value of comprehensive score of tomato quality, and the shadow regions represent 95% confidence interval of maximal comprehensive score.

Table 6: Effects of different irrigation frequency and irrigation amount on tomato yield and WUE.

Treatment	Spring			Autumn		
	Y (kg/hm^2)	ET$_a$ (mm)	WUE (kg/m^3)	Y (kg/hm^2)	ET$_a$ (mm)	WUE (kg/m^3)
F1I1	89898.31 ± 12173.48cd	318.32 ± 16.73e	28.26 ± 3.68bc	74791.67 ± 10196.15cd	206.26 ± 24e	36.59 ± 5.92ab
F1I2	114602.01 ± 19370.81a	364.43 ± 8.03cd	31.47 ± 5.42ab	95180.56 ± 17617.6ab	275.01 ± 22.62c	34.96 ± 7.84ab
F1I3	108739.06 ± 24907.83ab	428.2 ± 10.58b	25.43 ± 5.95cd	92625 ± 11596.79ab	317.75 ± 8.26a	29.16 ± 3.7c
F2I1	90964.34 ± 14880.36cd	265.59 ± 17.24f	34.13 ± 4.15a	76527.78 ± 13027.18cd	198.19 ± 9.19e	38.54 ± 5.95a
F2I2	119961.18 ± 15863.47a	374.12 ± 15.82c	32.16 ± 4.75ab	97979.17 ± 12550.56a	266.97 ± 7.57cd	36.73 ± 4.83ab
F2I3	118823.08 ± 12774.65a	457.08 ± 21.81a	26.07 ± 3.12cd	96597.22 ± 12447.91a	294.99 ± 8.01b	32.72 ± 3.85bc
F3I1	83258.23 ± 12514.06d	267.46 ± 10.83f	31.23 ± 5.25ab	68333.33 ± 12007.99d	195.36 ± 9.8e	35 ± 6.07ab
F3I2	94097.43 ± 15084.14cd	360.55 ± 8.52d	26.13 ± 4.38cd	83937.5 ± 10271.14bc	256.91 ± 2.68d	32.7 ± 4.21bc
F3I3	99024.6 ± 17708.7bc	424.49 ± 8.34b	23.32 ± 4.09d	79638.89 ± 13283.92cd	309.79 ± 9.94a	25.77 ± 4.65c
			F-value			
F	10.847**	19.247**	6.516**	10.501**	11.054**	7.299**
I	19.545**	1089.676**	18.539**	23.832**	610.180**	18.901**
F∗I	1.154 ns	29.560**	2.826*	0.403 ns	3.025*	0.360 ns

and chemical characteristics of the soil [29]. In addition, the soil before planting tomato was treated with a 60 cm deep loosening tillage by Jacob Fara et al., which could have changed the physical properties of the soil, improved its aeration and water storage capacity, and reduced the effect of moisture stress on tomato growth [30, 31].

Liu et al. [2] demonstrated a decreasing trend in the tomato yield of drip irrigation with decrease in irrigation frequency, which is inconsistent with our finding indicating that the tomato yield of MSPF initially increases and subsequently decreases. The difference could be attributed to different methods used for controlling the irrigation frequency. In the study conducted by Liu et al., cumulative evaporation was used to control the irrigation frequency for tomato yield, in which the cumulative evaporation of the highest irrigation frequency was 10 mm, the irrigation frequency during the growth period was 30 times, and the irrigation amount was 210–250 mm. In this paper, the frequency was controlled by time, the highest irrigation frequency was 3 days, the irrigation frequency was 33 times during the growth period of tomato, and the irrigation amount was 150–240 mm. Soil moisture, as the medium of nutrient transformation in soil and nutrient uptake by plant roots, has a direct relationship with fruit quality [2]. When irrigation was based on cumulative evaporation, it was noticed that the higher the irrigation frequency, the smaller is the amount of single irrigation and

Table 7: Regression equations between irrigation frequency and amount and tomato yield and water use efficiency.

	Dependent variable	Regression equation	R^2	Combination of treatment for max z		
				x/d	y	z_{max}
Spring	Comprehensive score	$z = -33.17 - 3.48x^2 - 143.44y^2 + 37.72x + 269.10y - 4.85xy$	0.99	5	0.8	173.30
	Yield (kg/hm^2)	$z = -129210.31 - 2911.56x^2 - 150334.57y^2 + 28294.42x + 338919.45y - 2327.97xy$	0.93	4	1.1	119464.90
	WUE (kg/m^3)	$z = -24.32 - 0.79x^2 - 41.25y^2 + 10.28x + 80.29y - 2.89xy$	0.89	5	0.8	33.70
Autumn	Comprehensive score	$z = 37.88 - 1.98x^2 - 110.37y^2 + 18.57x + 179.35y - 0.08xy$	0.99	5	0.9	153.93
	Yield (kg/hm^2)	$z = -127690.85 - 1987.56x^2 - 155108.02y^2 + 2052.59x + 344115.78y - 3321.00xy$	0.99	4	1.1	99181.15
	WUE (kg/m^3)	$z = -10.46 - 0.91x^2 - 43.05y^2 + 9.33x + 71.19y - 0.87xy$	0.98	5	0.8	39.43

Note: x is the irrigation frequency and y is the irrigation amount, respectively.

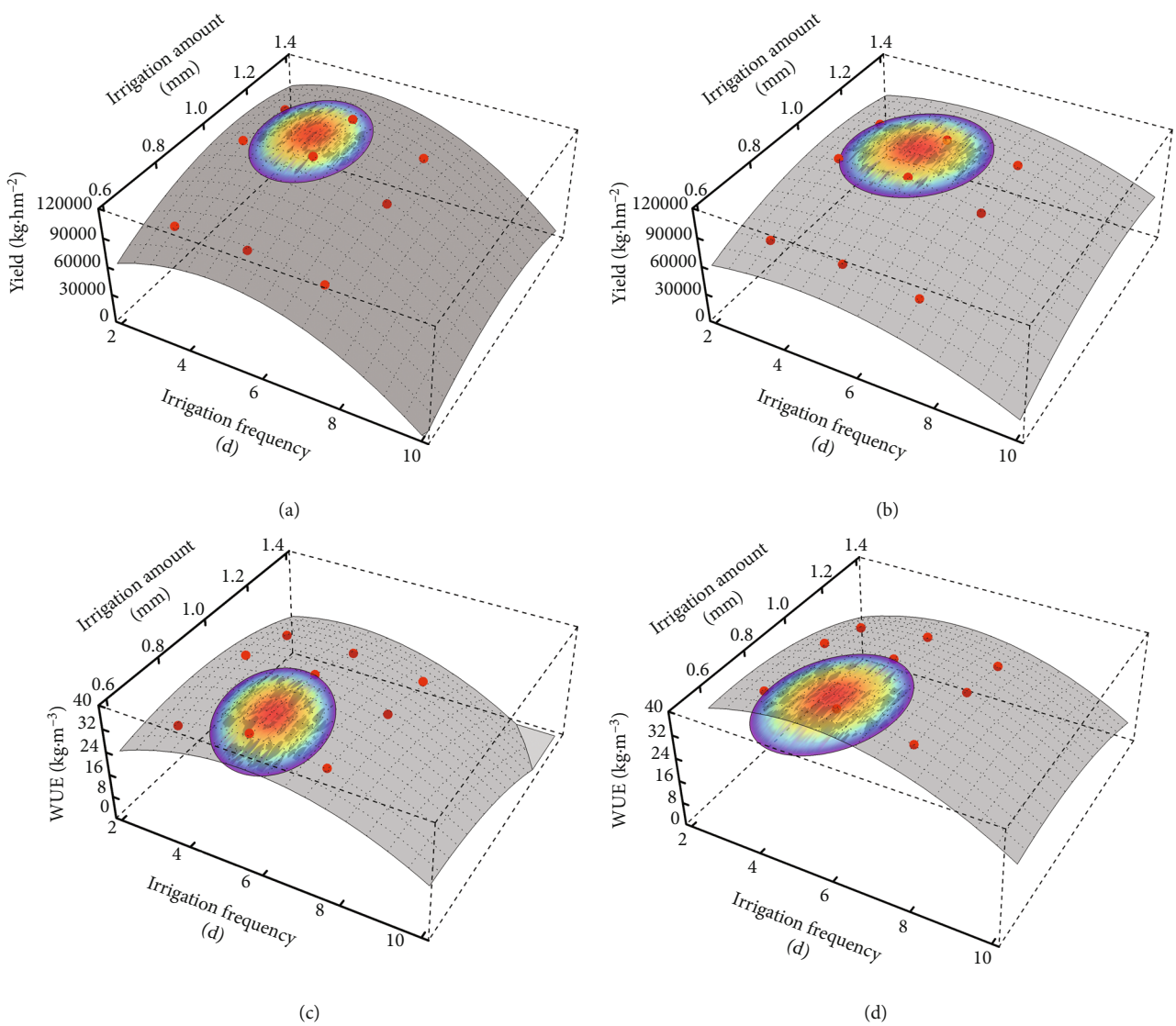

Figure 3: Relationship between yield, WUE, irrigation frequency, and irrigation amount. Note: the circular dotted points in the figure represent the spring (a and c) and autumn (b and d) measured values, and the shadow regions represent 95% confidence interval of maximal yield and WUE.

the smaller is the soil wetting body. Soil drought stress could also be easily increased. However, when the irrigation frequency was properly reduced, the amount of single irrigation could be increased and the volume and duration of soil dry and wet areas could be adjusted. Further decreasing the irrigation frequency provides a disadvantageous place for microbial and enzyme activities, resulting in obvious and long dry and wet areas that last longer, which is not conducive to the growth of tomato. Previous studies have found that an appropriate irrigation frequency could effectively alleviate soil drought and water stress, promote the production of photosynthetic products in the form of sucrose and transfer to reproductive organs, and increase the TSU of tomato [2], which might be one of the reasons for superior TSU of tomato fruit with 5-day irrigation frequency in our study. Few researchers have found that the SFW of tomato increases with increase in irrigation frequency [32]. However, we found lesser tomato SFW with the 3 days compared with that of the 5-day irrigation frequency. The highest irrigation frequency in a study by Sensoy was based on cumulative evaporation of 6 d, while it was of 3 d in this study. Additionally, the soil moisture was small, which could have easily caused the soil drought stress to limit the elevated SFW of tomato. The content of TSS in tomato was found to be higher after 5 d irrigation frequency, which might be due to the fact that the TSS of tomato pulp is composed of 65% sugars (sucrose and hexose), 13% acids (citric acid and malic acid), and 12% other secondary components, including phenols, amino acids, soluble pectin, and ascorbic acid. The percentages of soluble sugars and organic and soluble solids were 55% and 11%, respectively. The TSS of tomato increased with an increase in irrigation frequency [2, 33, 34].

4.2. Effects of Irrigation Amount on Greenhouse Tomato Quality and Yield. Previous studies have found that soil

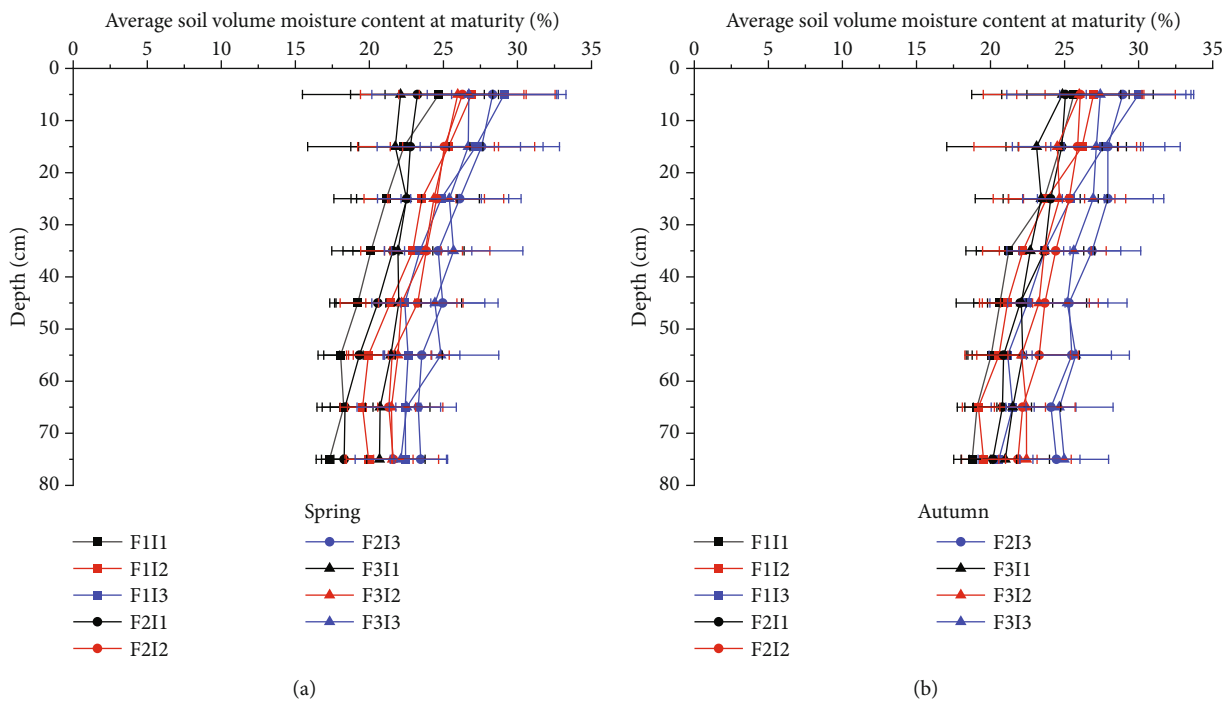

Figure 4: Soil volume moisture content of tomato.

water stress restricts crop root morphological development and reduces crop absorption and utilization of soil water and nutrients, and tomato fruit weight decreases significantly. Lower tomato fruit weight is also one of the main reasons for tomato yield reduction [35, 36]. In this study, the yield of spring and autumn tomatoes increased when the irrigation amount increased from I1 to I2, which may be due to the increase of moist body per unit irrigated area of soil tillage layer, which reduced the water stress of crop roots and increased the ability of crops to effectively absorb and utilize nitrogen. At the same time, tomato is most sensitive to soil water shortage during flowering and fruit expansion [37]. The existence of the above reasons may be one of the reasons for the reduction of tomato yield in this paper. However, when the irrigation amount increased from I2 to I3, the tomato yield did not increase but decreased slightly, which may be due to the excessive water in the soil, the increase of soil water-filled porosity, and the decrease of soil gas exchange. Limit the activities of soil microorganisms and enzymes and reduce the yield of tomato [23, 38]. In summary, the results showed that I2 treatment was a suitable irrigation amount for stable yield and yield increase of tomato in this region. In this study, it was found that the higher the irrigation amount, the higher the soil water consumption, probably because the higher irrigation amount was easy to increase the ineffective wetting body in the cultivated layer, the soil surface water content was also higher, and the soil water ineffective evapotranspiration increased; at the same time, irrigation directly increases soil water content, and soil moisture is the main factor for maintaining the best water driving force and leaf stomatal function. Plants with lower drought stress send signals to the aboveground parts, which can increase transpiration and thus increase plant water evapotranspiration [36]. Finally, the ET_a of spring tomato and autumn tomato was added by 53.80% and 53.84% (Table 6) with the increase of irrigation amount from I1 to I3. It was consistent with the conclusion that there was a positive correlation between tomato irrigation and water consumption studied by Wu et al. [39]. The yield increase of spring tomato and autumn tomato was lower than the ET_a added of spring tomato and autumn tomato by 56.08% and 48.49%, which may be one of the reasons why the crop water use efficiency of spring tomato and autumn tomato decreased by 20.07% and 16.99%. Sensoy et al. [15], Wu et al. [39], and Zhu et al. [40] studies found that the crop water use efficiency of tomato decreased when the irrigation amount under drip irrigation added from 0.5 times of evaporation to 1.0 times of evaporation, indicating that the effect of MSPF on the crop water use efficiency of tomato was the same as that of drip irrigation.

Agbna et al. [16] and Ouyang et al. [32] studies showed that the transverse diameters and vertical diameters of tomato under drip irrigation increased first with the increase of irrigation water, which was consistent with the conclusion of MSPF in this study. Previous studies have found that lower irrigation water is easy to cause soil drought stress, and the resistance of phloem sap transport to fruit in crop roots under drought stress reduces the flow from xylem to fruit and increases the solute concentration of fruit juice [5, 34, 41]. At the same time, drought stress could increase the activities of sucrose synthase and sucrose phosphate synthase and promote the conversion of sucrose to fructose and glucose [16] and further increase the sugar content of tomato fruit, which may be the reason why the TSS and TSU of tomato decreased with the increase in irrigation amount under MSPF. This conclusion is consistent with that

of Xing et al. [42], Sensoy et al. [15], and Hao et al. [17], indicating that the effect of MSPF on the flavor and nutrition index of tomato fruit is the same as that of drip irrigation. The Wang et al. [43] study showed that the contents of TSS, SP, and VC in tomato fruits under drip irrigation increased at first and then decreased with the added of irrigation amount, which was not consistent with the conclusion of this paper, which may be due to the difference of crop varieties and the different ways of controlling irrigation during tomato growth period.

5. Conclusions

In this study, the $\Phi 20$ standard pan evaporation was used as a reference to monitor tomato quality, yield, and WUE under different combinations of irrigation frequency and irrigation amount in MSPF. Our results indicate initial addition and subsequent reduction in SFW, TD, VD, TSS, SP, TSU, VC, L, SAR, yield, and WUE of tomato with decrease in irrigation frequency. Similar increased trend was observed in SFW, TD, VD, SAR, and yield of tomato with increase in irrigation amount; however, TSS, SP, TSU, VC, L, and WUE exhibited an overall decreasing trend. Superior quality and significantly higher yield of spring and autumn of tomato in F2I2 were observed compared with F1I1 (approximately 33.44% and 31.00%, respectively), F2I1 (31.88% and 28.03%, respectively), F3I1 (44.08% and 43.38%, respectively), and F3I2 (27.49% and 16.73%, respectively). The WUE of F2I2 growing during spring and autumn was also significantly higher than F1I3, F2I3, F3I2, and F3I3 (approximately 26.44% and 25.97%, 23.36% and 12.27%, 23.05 and 12.33%, and 37.89% and 24.35%). On the basis of spatial analysis, the comprehensive score, yield, and WUE of F2I2 tomato were predicted to simultaneously reach more than 95% of the maximum, which is consistent with the earlier studies on comprehensive evaluation of yield and WUE.

Data Availability

The data used to support the findings of this study are available from the corresponding author upon request.

Conflicts of Interest

The authors declared that they have no conflicts of interest to this work.

Acknowledgments

This work is supported jointly by the Key Research and Development Program of Shaanxi (2022NY-191), Ninth batch of key disciplines in Henan Province - Mechanical Design, Manufacturing and Automation (JG [2018] No. 119), Natural Science Foundation of China (No. 41807041), Science and Technology Program of Xi'an (20193052YF040NS040), Fundamental Research Funds for the Central Universities (GK202103129).

References

[1] W. J. Ntow, P. Drechsel, B. O. Botwe, and P. K. H. J. Gijzen, "The impact of agricultural runoff on the quality of two streams in vegetable farm areas in Ghana," *Journal of Environmental Quality*, vol. 37, no. 2, pp. 696–703, 2008.

[2] H. Liu, H. Li, H. Ning et al., "Optimizing irrigation frequency and amount to balance yield, fruit quality and water use efficiency of greenhouse tomato," *Agricultural Water Management*, vol. 226, no. 12, article 105787, 2019.

[3] S. Malherbeand and D. Marais, "Economics, yield and ecology: a case study from the South African tomato industry," *Outlook on AGRICULTURE*, vol. 44, no. 1, pp. 37–47, 2015.

[4] L. Mu, C. Wang, B. Xue, H. Wangand, and S. Li, "Assessing the impact of water price reform on farmers' willingness to pay for agricultural water in northwest China," *Journal of Cleaner Production*, vol. 234, pp. 1072–1081, 2019.

[5] M. Z. Zhang, W. Q. Niu, Z. G. Lu et al., "Yield and quality response of greenhouse tomato to different micropores group spacing and irrigation amount," *The Journal of Animal and Plant Sciences*, vol. 32, no. 2, 2021.

[6] O. P. Choudhary, B. S. Ghuman, and M. S. D. N. Chawla, "Yield and quality of two tomato (Solanum lycopersicum L.) cultivars as influenced by drip and furrow irrigation using waters having high residual sodium carbonate," *Irrigation Sci*, vol. 28, no. 6, pp. 513–523, 2010.

[7] G. C. Shao, M. H. Wang, N. Liu, M. Yuan, P. Kumar, and D. L. She, "Growth and comprehensive quality index of tomato under rain shelters in response to different irrigation and drainage treatments," *The Scientific World Journal*, vol. 2014, 12 pages, 2014.

[8] J. Wen, J. Li, and H. H. M. Y. A. Khan, "Impact of lateral depth and irrigation frequency on inorganic nitrogen distribution, yield, and quality of asparagus lettuce utilizing sewage effluent under drip irrigation," *Commun Soil Sci Plan*, vol. 52, no. 20, pp. 2550–2561, 2021.

[9] M. Zhang, Z. Lu, Q. Bai et al., "Effect of microsprinkler irrigation under plastic film on photosynthesis and fruit yield of greenhouse tomato," *Journal of Sensors*, vol. 2020, 14 pages, 2020.

[10] M. Z. Zhang, W. Q. Niu, Q. J. Bai et al., "Improvement of quality and yield of greenhouse tomato (Solanum lycopersicum L.) plants by micro-sprinkler irrigation under plastic film," *Appl Ecol Env Res*, vol. 18, no. 5, pp. 6905–6926, 2020.

[11] A. Sałata, S. Lombardo, G. Pandino, G. Mauromicale, H. Buczkowska, and R. Nurzyńska-Wierdak, "Biomass yield and polyphenol compounds profile in globe artichoke as affected by irrigation frequency and drying temperature," *Industrial Crops and Products*, vol. 176, article 114375, 2022.

[12] S. Jacob Fara, F. Delazari, R. Gomes, and W. L. A. D. J. H. Silvaa, "Stomata opening and productiveness response of fresh market tomato under different irrigation intervals," *Sci Hortic-Amsterdam*, vol. 255, no. 20, pp. 86–95, 2019.

[13] H. Sun, X. Zhang, X. Liu et al., "Impact of different cropping systems and irrigation schedules on evapotranspiration, grain yield and groundwater level in the North China Plain," *Agr Water Manage*, vol. 211, pp. 202–209, 2019.

[14] X. Yang, Y. Chen, S. Pacenka et al., "Effect of diversified crop rotations on groundwater levels and crop water productivity in the North China Plain," *Journal of Hydrology*, vol. 522, pp. 428–438, 2015.

[15] S. Sensoy, A. Ertek, I. Gedikand, and C. Kucukyumuk, "Irrigation frequency and amount affect yield and quality of field-

grown melon (Cucumis melo L.)," *Agr Water Manage*, vol. 88, no. 1-3, pp. 269–274, 2007.

[16] G. H. Agbna, S. Dongli, L. Zhipeng, N. A. Elshaikh, S. Guangcheng, and L. C. Timm, "Effects of deficit irrigation and biochar addition on the growth, yield, and quality of tomato," *Sci Hortic-Amsterdam*, vol. 222, pp. 90–101, 2017.

[17] L. I. U. Hao, A. W. Duan, F. S. Li, J. S. Sun, Y. C. Wang, and C. T. Sun, "Drip irrigation scheduling for tomato grown in solar greenhouse based on pan evaporation in North China Plain," *Journal of Integrative Agriculture*, vol. 12, no. 3, pp. 520–531, 2013.

[18] V. Decruyenaere, C. Clément, R. Agneessens, C. Losseauand, and D. Stilmant, "Development of near-infrared spectroscopy calibrations to quantify starch and soluble sugar content in the roots of Rumex obtusifolius," *Weed Research*, vol. 52, no. 1, pp. 1–5, 2012.

[19] W. Gould, *Tomato Production, Processing, and Technology (3rd Edition)*, CTI Publications, Baltimore, USA, 1992.

[20] D. Li, S. Wan, X. Li, Y. Kangand, and X. Han, "Effect of water-salt regulation drip irrigation with saline water on tomato quality in an arid region," *Agricultural Water Management*, vol. 261, article 107347, 2022.

[21] L. C. Cefali, E. C. L. Cazedey, T. M. Souza-Moreira, M. A. Correa, H. R. N. Salgado, and V. L. B. Isaac, "Antioxidant activity and validation of quantification method for lycopene extracted from tomato," *Journal of AOAC International*, vol. 98, no. 5, pp. 1340–1345, 2015.

[22] Y. Du, H. Cao, S. Liu, X. Guand, and Y. Cao, "Response of yield, quality, water and nitrogen use efficiency of tomato to different levels of water and nitrogen under drip irrigation in northwestern China," *Journal of integrative agriculture*, vol. 16, no. 5, pp. 1153–1161, 2017.

[23] K. Uçan, F. Kıllı, C. Gençoğlanand, and H. Merdun, "Effect of irrigation frequency and amount on water use efficiency and yield of sesame (Sesamum indicum L.) under field conditions," *Field Crops Research*, vol. 101, no. 3, pp. 249–258, 2007.

[24] E. Holzapfel and J. J. A. M. Coronata, "Number of drip laterals and irrigation frequency on yield and exportable fruit size of highbush blueberry grown in a sandy soil," *Agr Water Manage*, vol. 148, pp. 207–212, 2015.

[25] C. Jianping, C. Qiang, and C. Ping, "Effects of drip irrigation frequency o soil physical and chemical characteristics and cotton yield under subsoiling condition," *Journal of Soil and Water Conservation*, vol. 33, no. 1, pp. 263–269, 2019.

[26] F. B. K. S. Kim, "Effects of irrigation frequency on root formation and shoot growth of spray chrysanthemum cuttings in small jute plugs," *Sci Hortic-Amsterdam*, vol. 60, no. 1-2, pp. 125–138, 1994.

[27] A. N. Chachar, M. U. Mirjat, R. K. Soothar, I. A. Shaikh, M. H. Mirjat, and S. A. Dahri, "Effects of irrigation frequencies on soil salinity and crop water productivity of fodder maize," *Acta Ecologica Sinica*, vol. 40, 2020.

[28] F. Wang, Y. Kangand, and S. Liu, "Effects of drip irrigation frequency on soil wetting pattern and potato growth in North China Plain," *Agr Water Manage*, vol. 79, no. 3, pp. 248–264, 2006.

[29] W. M. Rodriguez-Ortega, V. Martinez, R. M. Rivero, J. M. Camara-Zapata, T. Mestre, and F. Garcia-Sanchez, "Use of a smart irrigation system to study the effects of irrigation management on the agronomic and physiological responses of tomato plants grown under different temperatures regimes," *Agr Water Manage*, vol. 183, pp. 158–168, 2017.

[30] X. Li, C. Zhang, and Z. H. A. J. Adeloye, "A sustainable irrigation water management framework coupling water-salt processes simulation and uncertain optimization in an arid area," *Agricultural Water Management*, vol. 231, article 105994, 2020.

[31] N. Kuang, D. Tan, H. Li, Q. Gou, Q. Li, and H. Han, "Effects of subsoiling before winter wheat on water consumption characteristics and yield of summer maize on the North China Plain," *Agricultural water management*, vol. 227, article 105786, 2020.

[32] Z. Ouyang, J. Tian, X. Yanand, and H. Shen, "Effects of different concentrations of dissolved oxygen on the growth, photosynthesis, yield and quality of greenhouse tomatoes and changes in soil microorganisms," *Agricultural Water Management*, vol. 245, article 106579, 2021.

[33] A. A. Kader, "Flavor quality of fruits and vegetables," *Journal of Science and Food Agriculture*, vol. 88, no. 11, pp. 1863–1868, 2008.

[34] J. Chen, S. Kang, T. Du et al., "Modeling relations of tomato yield and fruit quality with water deficit at different growth stages under greenhouse condition," *Agr Water Manage*, vol. 146, pp. 131–148, 2014.

[35] E. Coyago-Cruz, M. Corell, A. Moriana et al., "Effect of regulated deficit irrigation on commercial quality parameters, carotenoids, phenolics and sugars of the black cherry tomato (Solanum lycopersicum L) Sunchocola," *Journal of Food Composition and Analysis*, vol. 105, article 104220, 2022.

[36] C. Patanè, S. Tringaliand, and O. Sortino, "Effects of deficit irrigation on biomass, yield, water productivity and fruit quality of processing tomato under semi-arid Mediterranean climate conditions," *Sci Hortic-Amsterdam*, vol. 129, no. 4, pp. 590–596, 2011.

[37] Z. H. Shang, H. J. Cai, H. Chen et al., "Effect of water-fertilizer-gas coupling on soil N_2O emission and yield in greenhouse tomato," *Environmental Sciences*, vol. 41, pp. 1–18, 2020.

[38] C. Hui, H.-j. Hou, X.-y. Wang et al., "The effects of aeration and irrigation regimes on soil CO_2 and N_2O emissions in a greenhouse tomato production system," *Journal of Integrative Agriculture*, vol. 17, no. 2, pp. 449–460, 2018.

[39] Y. Wu, S. Yan, J. Fan et al., "Combined effects of irrigation level and fertilization practice on yield, economic benefit and water-nitrogen use efficiency of drip-irrigated greenhouse tomato," *Agricultural Water Management*, vol. 262, article 107401, 2022.

[40] Y. Zhu, H. Cai, L. Song, X. Wang, Z. Shang, and Y. Sun, "Aerated irrigation of different irrigation levels and subsurface dripper depths affects fruit yield, quality and water use efficiency of greenhouse tomato," *Sustainability-Basel*, vol. 12, no. 7, p. 2703, 2020.

[41] S. Guichard, N. Bertin, C. Leonardiand, and C. Gary, "Tomato fruit quality in relation to water and carbon fluxes," *Agronomie*, vol. 21, no. 4, pp. 385–392, 2001.

[42] Y. Y. Xing, F. C. Zhang, Y. Zhang, J. Li, S. C. Qiang, and L. F. Wu, "Effect of irrigation and fertilizer coupling on greenhouse tomato yield, quality, water and nitrogen utilization under fertigation," *Scientia Agricultura Sinica*, vol. 48, no. 4, pp. 713–726, 2015.

[43] J. Wang, Y. Liand, and W. Niu, "Deficit alternate drip irrigation increased root-soil-plant interaction, tomato yield, and quality," *International Journal of Environmental Research and Public Health*, vol. 17, no. 3, p. 781, 2020.

Hindawi
Journal of Sensors
Volume 2022, Article ID 7740946, 12 pages
https://doi.org/10.1155/2022/7740946

Research Article

An Examination of Impact of the Board of Directors' Capital on Enterprises' Low-Carbon Sustainable Development

Lipeng Liu,[1] Xiaoxue Liu,[2] Zihao Guo,[3] and Shuangshuang Fan[1]

[1]*School of Management, China University of Mining and Technology, Beijing 100086, China*
[2]*School of Economics, Beijing Technology and Business University, Beijing 100048, China*
[3]*Zhongtai Securities Institute for Financial Studies, Shandong University, Jinan 250000, China*

Correspondence should be addressed to Xiaoxue Liu; liuxx@th.btbu.edu.cn

Received 25 March 2022; Revised 13 April 2022; Accepted 20 April 2022; Published 28 April 2022

Academic Editor: Yuan Li

Given the increasingly serious ecological and environmental problems in China, research on enterprises' low-carbon sustainable development behavior (LCSDB) has become a heated discussion. This is also because enterprises are a primary source of carbon emissions and environmental pollution. From the perspective of the board of directors' capital (BODC), this study considers empirical evidence from 286 enterprises listed on the Shanghai and Shenzhen stock exchanges in China from 2008 to 2016 to examine the BODC's impact on enterprises' LCSDB and its mechanisms. A group test is conducted using the enterprise's property, nature of rights, and region, among other factors, to investigate the heterogeneity of the impact of board capital on enterprises' LCSDB and its regulatory role. The research indicates (1) an increase in BODC promotes enterprises' LCSDB. (2) An awareness of social responsibility (AOSR) plays an intermediary role in the relationship between BODC and corporate LCSDB. (3) Media attention enhances the BODC's role in promoting enterprises' LCSDB. (4) Government regulatory factors promote the BODC's positive impact on LCSDB. These findings significantly impact the effectiveness of decision-makers within the company, the governance mechanism to address climate change risks, and the possible connection between corporate governance reform and carbon-related policies.

1. Introduction

With the rapid development of China's economy and urbanization, ecological and environmental problems have become increasingly severe. The report of Chinese government in 2022 proposed that "the battle of pollution prevention and control should be carried out in depth throughout the country. The emission of major pollutants continued to decline, and the average concentration of fine particulate matter (PM2.5) in cities decreased by 9.1%." As a constituent cell of the social economy, enterprises are an important source of carbon emissions and environmental damage. Although the Chinese government has paid more and more attention to environmental issues in recent years, the awareness of enterprises in this regard needs to be improved [1]. Reducing high-carbon energy consumption can resolve the most important issues of today and in the future, such as climate change, the environment, and sustainable development [2]. Currently, one critical problem of close focus worldwide involves enterprises' energy consumption and the alarm toward climate change. Low-carbon technologies can be sustainable because they reduce energy consumption and environmental pollution [3]. Additionally, governments must discuss energy emission regulations and the improvement of enterprises' energy efficiency [4]. To some extent, urging enterprises to implement low-carbon sustainable development behaviors (LCSDB) is an effective way to solve current ecological and environmental problems [5]. An enterprise's LCSDB is an economic behavior that reduces external negative externalities in the environment. It also entails a process in which enterprises: integrate low-carbon concepts into different links in their operations and management through low-carbon technological innovations and institutional arrangements and reduce high-carbon energy consumption, carbon emissions, environmental pollution, and resource recycling in such aspects of the product life cycle as product

research and development, material procurement, manufacturing, marketing, logistics, and after-sales service. Enterprises' LCSDB will permeate different aspects of the business, such as its decision-making, supply chain management, production, technology, and capital utilization.

Research on corporate environmental behavior can be traced back to Pigou's (1920) suggestion that government regulations should guide enterprises' green development [6]. However, some research indicates that although government regulations promote enterprises' low-carbon operations, their influence has gradually weakened [7]. Scholars have increasingly studied the influencing factors of enterprises' LCSDB from an internal governance perspective. As the core of the corporate governance mechanism, the board of directors undertakes various tasks—such as allocating resources to align with the corporate strategy, providing creative thinking, and establishing contact with the outside world—that impact the realization of enterprises' financial and nonfinancial objectives [8]. Many scholars have interpreted the relationship between the board of directors and enterprises' sustainable development behaviors based on institutional agency theory. For example, the board of directors is important within the corporate governance structure in addressing environmental risks and ensuring the environmental supervision of raw materials [9]. The board's structure can potentially impact the formulation and implementation of corporate social and environmental responsibility policies [10]. The characteristics of the board of directors, such as its size, proportion of independent directors, and gender diversity, can positively impact enterprises' environmental and sustainable development behaviors [11].

This study explores whether the board of directors' capital (BODC) as a resource endowment positively impacts enterprises' LCSDB, which provides a more evolved perspective than the agency and resource-dependence theories [12–14]. Integrating human capital and social capital of the enterprise's board of directors provides the foundational resources for green transformation, reduces transformation risks, and promotes sustainable development. For example, directors with embedded environmental protection experience can help enterprises develop low-carbon technologies and design low-carbon management strategies; directors with a government background can help enterprises best utilize government subsidies for low-carbon operations. Therefore, this paper describes the characteristics of the BODC and examines its key and mediating role in enterprises' LCSDB, which has important theoretical and practical significance in studying the microlevel factors of enterprises' LCSDB. The BODC concept has not yet been universally defined, but roughly includes directors' own experience; ability; and social resources, or the ability to provide resources for enterprises [15]; heterogeneity of directors' age; educational background; and work experience, among others [16].

The BODC is divided into two levels: human and social capital [16]. This paper describes the BODC through five dimensions to examine its impact on enterprises' LCSDB: the educational background, environmental protection experience, gender diversity, government relationships, and director connections. Additionally, the awareness of social responsibility (AOSR) is an intermediary variable that may promote the BODC's impact on the LCSDB. Meanwhile, this study analyzes the moderating effects of environmental rules and media attention on the relationship between board capital and enterprises' LCSDB. It also tests the heterogeneity of the BODC's impact on enterprises' LCSDB by grouping given the nature of property rights and the enterprise's location. As academic literature on the influencing factors of enterprises' LCSDB scarcely involves research from the BODC perspective, this paper provides highly significant research implications.

This work also presents the following marginal contributions: (1) this study is the first to examine enterprises' LCSDB from a board capital perspective. Currently, most academic research has studied the driving factors and mechanisms of enterprises' LCSDB from the perspective of external and internal stakeholder pressures, but the research focusing on BODC is currently in its infancy. (2) In analyzing enterprises' LCSDB, this study adopts the back-propagation (BP) neural network mathematical model to construct a low-carbon behavioral index for enterprises. Neural network has the advantages of nonlinear mapping ability, self-learning, and self-adaptive ability, which can be widely used in pattern recognition and analysis [17], thus can solve problems better. As academic circles have yet to reach a unified understanding of the concept and indicators of enterprises' low-carbon behavior, this paper's results provide a high-value reference for further academic research.

The remainder of this paper is structured as follows: Section 2 reveals the theoretical analysis and hypothesis and constructs a conceptual framework between the BODC and enterprises' LCSDB. Section 3 presents the research design and methodology and describes the samples used in this study. Section 4 empirically tests the data and discusses the results. Section 5 presents the relationship between the BODC and LCSDB to facilitate sustainable development. Finally, Section 6 discusses the limitations and future research direction.

2. Theoretical Analysis and Hypothesis Development

2.1. Relationship between BODC and Enterprises' LCSDB. Studies of BODC reveal two important elements: human and social capital. The former is the result of specific human investment and ultimately accumulates the professional background, relevant experience, skills, and knowledge for enterprise decision-making [18–20]. The latter refers to individuals' or social units' ability to obtain the sum of the actual and potential resources they, or the enterprises, need in their relationship network [15]. In practical research, it is difficult to distinguish between these two concepts. To examine the BODC's mechanism of influence on LCSDB, this paper analyzes the board of directors given five aspects: the educational background, environmental protection experience, gender diversity, political connections, and director connections.

First, a close relationship exists between the board of directors' human capital and enterprises' sustainable development behavior, with a positive connection between board members' educational background and the board's responsibility for social and environmental issues [21, 22]. This is because the higher the senior executives' educational background, the more they understand and focus on sustainable development in society. Board members with embedded environmental protection work experience have accumulated rich relevant knowledge; further, companies with board members with such work experience have lower greenhouse gas emissions [23]. This may be because such board members are more inclined to make decisions conducive to the sustainable development of society. As a strategic human resource, board members are crucial to the future development of the company [24].

Previous studies have observed that gender diversity in the board of directors adds value to governance because it can bring various advantages [25]. For example, female directors are more inclined to assume social responsibilities, delay risks, and focus on social and environmental issues to improve enterprises' sustainable development behaviors [26]. Several studies have also empirically verified that female directors positively influence enterprises' sustainable development behaviors [27–29]. Second, members of the board of directors can use their political connections to help enterprises obtain government-controlled resources, such as subsidies for environmental protections; expand financing channels; and reduce financing costs. Simultaneously, directors who hold political positions have a sharp attention to industry information and better understand consumers' green preferences and competitors' LCSDB to promote their own enterprise's sustainable development and LCSDB. Moreover, when a board connection occurs—or specifically, a phenomenon in which organizations are connected through overlapping board members and executives [30]—the board connection may diffuse the LCSDB among different enterprises. Subsequently, the affiliated enterprises can reference each other's LCSDB activities, gain experience in low-carbon technology innovation, pool their resources, and accelerate green transformation. This leads to the following Hypothesis 1.

Hypothesis 1. The BODC can promote enterprises' LCSDB.

2.2. Media Attention and Environmental Regulations Mediate the Relationship between BODC and LCSDB. In the theory of institutional economics, public opinion is regarded as an informal environmental system [31], while social schools posit that public opinion is a social normative mechanism. The media is an independent social supervisory force that reveals enterprises' moral and immoral behaviors, bringing public pressure and compelling them to fulfill their social responsibilities [32]. With the enhancement of the public's awareness of environmental protections, the public will focus more on which enterprises' behaviors are harmful to the environment. The news media will typically prioritize stories that can attract public attention based on the driving force of interest [33], and thus, are more inclined to report negative information, such as enterprises' environmental pollution and high carbon emissions. Media attention provides a way for enterprises to obtain legitimacy, but also acts as a source of crisis regarding such legitimacy [34]. According to legitimacy theory, whether an enterprise's behavior is legal depends on its evaluation by the public [35]. As society closely observes environmental problems, environmental protections and the low-carbon transformation of enterprises have become important aspects of legitimacy; for example, high-carbon-emitting enterprises must improve their levels of carbon emissions to win the public's trust and establish a positive corporate image.

Additionally, environmental regulations have become an important way to effectively solve environmental problems in China's current legal society. First, the government restrains enterprises' carbon emissions behaviors by establishing carbon emissions standards, punishing highly polluting enterprises, implementing environmental assessments, and setting production technical standards. These administrative measures influence the firm to not only weigh its need to produce and emit against the costs of possible violations but also improve environmental performance [36]. Second, the government corrects enterprises' high carbon ranking by strengthening its supervision, such as through the collection of fossil fuel taxes, sewage charges, and emissions-trading plans [37]. These measures aim to increase enterprises' environmental control costs through the market mechanism to curb the demand for petrochemical energy. Enterprises will adopt clean technologies, such as desulfurization and denitrification methods, to achieve emissions reduction targets [38].

Based on this analysis, this paper proposes the following hypotheses.

Hypothesis 2. Media attention positively regulates the relationship between BODC and enterprises' LCSDB.

Hypothesis 3. Environmental regulations have a positive regulatory effect on the relationship between BODC and enterprises' LCSDB.

Figure 1 illustrates the assumptions presented in this section and the conceptual framework for the BODC's mechanism of influence on LCSDB.

3. Research Design and Empirical Analysis

3.1. Variable Definition and Construction

3.1.1. Dependent Variable: The Low-Carbon Behavioral Index. The dependent variable in this study is the enterprise's low-carbon behavioral index (LCBI), which refers to the enterprise's degree of behavior related to low energy consumption, low pollution, and low emissions, which will lead to the enterprise's economic benefits and the sustainable development of society and the environment. This paper considers prior research to posit that LCSDB is guided by the concept of sustainable development [39–45]. Specifically, this concept shapes the enterprise's low-carbon culture and

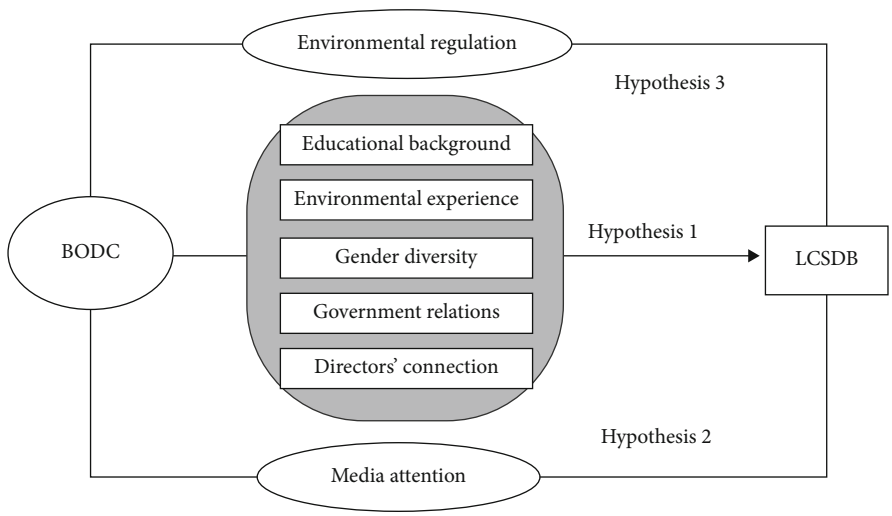

Figure 1: The mechanism of the BODC's influence on LCSDB and this paper's conceptual framework.

involves formulating low-carbon-development strategies with low-carbon technological innovations as a driving force. It includes the realization of low-carbon management in product manufacturing, logistics, marketing, and other cycles; and the selecting of low-carbon materials, low-carbon energy, and green human resource management. Carbon emissions should be reduced to achieve a mutually beneficial situation that promotes both environmental and economic benefits. Therefore, this study constructs an enterprise LCSDB evaluation system to measure the enterprise's LCBI given the six dimensions of low-carbon culture: the low-carbon strategy, innovations, investments, operations, and emissions. Table 1 shows the enterprise's LCSDB evaluation system.

Simultaneously, Liu (2021) used a BP neural network method to determine the weight of each index in the evaluation index system and address the complex relationships within this system to obtain a more objective weight [46]. The specific steps are as follows.

First, the BP neural network structure is built. The input layer is marked as vi, $(i = 1, 2, .., m)$, $I = (v1, v2, v3, \cdots vm)\ T$, the hidden layer is represented by hi, $(i = 1, 2, .., n)$, $H = (h1, h2, h3, \cdots hn)\ T$, the actual output from the output layer is expressed as $didj$, and the predicted output is expressed as Oi, $(i = 1, 2, .., n)$.

Second, the standardized treatment index is calculated; the forward and reverse indicators are standardized using the following two equations.

$$\vartheta_i = \frac{\vartheta_i{}' - \min\left(\vartheta_i{}'\right)}{\max\left(\vartheta_i{}'\right) - \min\left(\vartheta_i{}'\right)}, \tag{1}$$

$$\vartheta_{\mathrm{i}} = \frac{\vartheta_{\mathrm{i}}' - \min\left(\vartheta_{\mathrm{i}}'\right)}{\max\left(\vartheta_{\mathrm{i}}^{:}\right) - \min\left(\vartheta_{\mathrm{i}}'\right)} \mathrm{i} = 1, 2, \cdots \mathrm{m}. \tag{2}$$

Third, a forward transmission is performed; the transfer from the input layer to the metaphor layer and from the metaphor layer to the output layer is displayed in Equations (3) and (4), respectively.

$$H_j = f\left(\sum_{i=1}^{m} \alpha_{ij}\vartheta_i + v_j\right), \tag{3}$$

$$O_j = f\left(\sum_{i=1}^{k} b_i h_i + v_j\right), \tag{4}$$

where f is the activation function, and the sigmoid function is used, with v_j as the threshold.

Fourth, a directional correction is performed, with the error function given in Equation (5). The value of the error function is set to 10-5 and minimized by repeatedly correcting the weight and threshold.

$$E = \frac{1}{2}\sum_{i=1}^{n}\left(d_i - o_j\right)^2. \tag{5}$$

Fifth, we confirm the weight, which is calculated using Equation (6).

$$w_i = \frac{\sum_{k=1}^{n}\left|\alpha_{ik}\right|}{\sum_{j=1}^{m}\sum_{k=1}^{n}\left|\alpha_{jk}\right|}. \tag{6}$$

Sixth, the LCBI is obtained by calculating the weighted average.

$$\mathrm{LCBI} = \mathrm{w_i}\vartheta_{\mathrm{i}}. \tag{7}$$

3.1.2. Independent Variable: The Board's Capital. This study selected five indicators—the directors' educational background, environmental protection experience, gender diversity, political connections, and directors' connections—to construct the board capital variable (BC). If the director has a master's degree or above, the educational background

Table 1: The enterprise's LCSDB evaluation system.

General index	Secondary indicators	General index	Secondary indicators
Low-carbon culture	Management layer	Low-carbon innovations	Low-carbon technology R&D
	Employee layer		Low-carbon equipment update
Low-carbon strategy	Regulations and rules of low-carbon management	Low-carbon operations	Low-carbon production
	Low-carbon financial strategy		Low-carbon marketing
	Low-carbon human resource management (HRM) strategy		Low-carbon logistics
Low-carbon input	Low-carbon materials		Low-carbon services
	Clean energy	Low-carbon emissions	Low-carbon gas
	Green HRM		Low-carbon solid waste

is scored as one, and zero otherwise. The average score of the director's educational background was used to measure the educational background of the board of directors. If the directors have embedded environmental protection experience, this is scored as one, and zero otherwise; the average score of this experience is used to measure the board's environmental protection experience. The board's gender diversity is measured by the ratio of the number of female directors in the board of directors. If the directors have experience in central, provincial, and municipal governments, their political connections are scored as three, two, and one, respectively, while the rest are noted as zero. The average score for the directors' political connections was used to measure the board's political connections. The ratio of directors with connections to total directors was used to measure director connections. Finally, the average score of the five indicators was calculated as the BODC.

3.1.3. Moderating Variables: MC, ER, SOE, and DISTRICT. The text of news reports from the CSMAR news database was analyzed using Python software, and irrelevant reports were filtered through a keyword analysis. Subsequently, 129,658 reports related to the listed companies were obtained. A sample of text for training was taken that included news related to pollution accidents from a public environmental research center to summarize the negative environmental keywords. The news reports were also searched to weigh the sample's media attention. Finally, a surrogate variable for the MC was established that assumes a value of one if the number of negative reports is greater than the sample's median, and zero otherwise.

The ER surrogate variables were primarily measured by the administrative supervisory status of enterprises' carbon emissions in the region where the enterprise is located. This was confirmed by the number of local laws and regulations issued by the local government in the China Environmental Yearbook 2008-2016. The cumulative value of each year since 2008 was ranked according to the sample's environmental regulatory status; enterprises with scores greater than the sample's median were given a value of one, while those with values less than the sample's median were ranked as zero.

This study also constructs the SOE and DISTRICT virtual variables and scale used for the heterogeneity test. The SOE indicates whether the enterprise is state-owned, with such enterprises scored as one, and zero otherwise. If the enterprises are located in China's eastern region, then, DISTRICT is given a value of one, and zero otherwise.

3.1.4. Intermediary Variable: The Awareness of Corporate Social Responsibility. A comprehensive integration of human and social capital has resulted in the BODC increasing the awareness of corporate social responsibility, thus promoting enterprises' low-carbon sustainable development activities. In this regard, a board's consciousness of its social responsibility may mediate the explanatory and interpreted variables. To further investigate the existence of this intermediary transmission channel—or specifically, the board's capital impacting CSR awareness, and subsequently, enterprises' low-carbon sustainable development behavior—this paper measures corporate social responsibility awareness (AOSR) according to whether enterprises publish social responsibility or sustainable development reports [47]. According to Parsa et al. (2021), if an enterprise publishes social responsibility, environmental, or sustainable development reports in its first year, the index variable is set as one, and zero otherwise [48].

3.1.5. Control Variables. We chose some control variables to avoid biased results and a study largely founded on previous empirical literature, we will choose some control variables. According to Alshirah et al. (2020) and Malm et al. (2020), the control variables in this study include the board's structure (EB), return on assets (ROA), cash flows (cash), enterprise size (in size), and asset-liability ratio (LEV) [49, 50].

The variable EB indicates the number of directors on the board [51]. As boards are responsible for making a corporation's significant decisions, a larger board is more desirable because it allows the directors a greater opportunity to use their skills, experiences, knowledge, and external networks [52] to maintain the enterprise's sustainable operations and encourage social responsibility behaviors.

The variable ROA is a key indicator of profitability and is calculated as the earnings before tax divided by total assets. Although some studies disagree that a positive relationship exists between profitability and the extent of their social responsibilities [53, 54], most researchers confirm a positive relationship [55, 56].

The variable cash represents the net cash flow of business operations, calculated by subtracting the cash outflow from operating activities from the cash inflow from operating activities. The level of cash affects enterprises' investment behaviors, such as purchasing materials, hiring employees, and paying logistics expenses. Therefore, the cash situation relates to other low-carbon operational behaviors.

The variable size is calculated as the logarithm of total assets [57]. Firm size is expected to significantly impact LCSDB because larger firms must disclose more social, economic, and environmental information than smaller firms to satisfy stakeholders' needs [58]. Moreover, low-carbon investments have costly implementation costs, and thus, larger companies may have more resources and expertise to enable them to undertake LCSDB, which will also improve their image and reputation [59].

The variable LEV is measured as the total debt over assets [60]. However, previous empirical evidence has been inconclusive. Many high-leverage firms are more prone to disclose voluntary information and behavior to reduce both agency and capital costs. Table 2 presents the definition or measurement of the variables.

3.2. Samples and Data Source. According to existing literature, Chinese industries are a primary source of heavy pollution in China, and enhancing their positive environmental behaviors is key to promoting LCSDB [61–66]. Therefore, this study samples large-share companies listed on the Shanghai and Shenzhen stock exchanges from 9 heavy-pollution industries: thermal power generation, iron and steel, cement, electrolytic aluminum, coal, metallurgy, chemical, petrochemical, and papermaking industries. This study's primary research sample includes 286 listed companies selected from these industries, with data spanning 2008 to 2016; sample companies with "ST" and "∗ ST" prefixes and companies with missing financial data were then omitted. Enterprises with "ST" before the stock abbreviation will perform special treatments for the stock transactions of listed companies with abnormal financial or other conditions. Further, stock abbreviations preceded by "∗ ST" indicate risk, in that their shares may be delisted and differ from the shares of other companies. The sample data has been selected since 2008 because in reality, China's environmental pollution is more serious after 2008.

3.3. Building Models. This study examines the impacts of board capital on LCSDB by constructing the panel regression benchmark model in the following form:

$$\mathrm{LCBI}_{\mathrm{it}} = \beta_0 + \beta_1 * \mathrm{BC}_{\mathrm{it}} + \beta_2 * \mathrm{EB}_{\mathrm{it}} + \beta_3 * \mathrm{ROA}_{\mathrm{it}} + \beta_4 * \mathrm{CASH}_{\mathrm{it}} + \beta_5 * \mathrm{LnSIZE}_{\mathrm{it}} + \beta_6 * \mathrm{LEV}_{\mathrm{it}} + \varepsilon_{\mathrm{it}}. \tag{8}$$

Among them, the intercept term is β_0, β_1 to β_6 are coefficients, and $\varepsilon_{\mathrm{it}}$ is residual. If β_1 is greater than zero, the BODC can promote the LCSDB. To further investigate the mediating role of AOSR, this study constructs an extended model:

$$\mathrm{LCBI}_{\mathrm{it}} = \beta_0 + \beta_1 * \mathrm{BC}_{\mathrm{it}} + \beta_2 * \mathrm{EB}_{\mathrm{it}} + \beta_3 * \mathrm{ROA}_{\mathrm{it}} + \beta_4 * \mathrm{CASH}_{\mathrm{it}} + \beta_5 * \mathrm{LnSIZE}_{\mathrm{it}} + \beta_6 * \mathrm{LEV}_{\mathrm{it}} + \varepsilon_{\mathrm{it}}, \tag{9}$$

$$\mathrm{AOSR}_{\mathrm{it}} = \alpha_0 + \alpha_1 * \mathrm{BC}_{\mathrm{it}} + \alpha_2 * \mathrm{EB}_{\mathrm{it}} + \alpha_3 * \mathrm{ROA}_{\mathrm{it}} + \alpha_4 * \mathrm{CASH}_{\mathrm{it}} + \alpha_5 * \mathrm{LnSIZE}_{\mathrm{it}} + \alpha_6 * \mathrm{LEV}_{\mathrm{it}} + \varepsilon_{\mathrm{it}}, \tag{10}$$

$$\mathrm{LCBI}_{\mathrm{it}} = \gamma_0 + \gamma_1 * \mathrm{BC}_{\mathrm{it}} + \gamma_2 * \mathrm{AOSR}_{\mathrm{it}} + \gamma_3 * \mathrm{EB}_{\mathrm{it}} + \gamma_4 * \mathrm{ROA}_{\mathrm{it}} + \gamma_5 * \mathrm{CASH}_{\mathrm{it}} + \gamma_6 * \mathrm{LnSIZE}_{\mathrm{it}} + \gamma_7 * \mathrm{LEV}_{\mathrm{it}} + \varepsilon_{\mathrm{it}}. \tag{11}$$

In these three equations, we focus on (β_1, α_1) and (γ_1, γ_2). On the one hand, if α_1 is significant, then, the BODC will affect the corporate AOSR. On the other hand, if γ_1 and γ_2 are simultaneously significant and the absolute value of γ_3 is less than that of $\beta 1$, we can consider AOSR as mediating corporate LCSDB. If γ_2 is significant, but γ_1 is not, then, the corporate AOSR fully mediates the BODC regarding the impact of corporate LCSDB.

This study further investigates the moderating effects of MC and ER on the BODC's impact on LCSDB by constructing the following extended models:

$$\mathrm{LCBI}_{\mathrm{it}} = \beta_0 + \beta_1 \mathrm{BC}_{\mathrm{it}} + \beta_2 \mathrm{MC}_{\mathrm{it}} + \beta_3 \mathrm{MC}_{\mathrm{it}} * \mathrm{BC}_{\mathrm{it}} + \beta_4 \mathrm{EB}_{\mathrm{it}} + \beta_5 \mathrm{ROA}_{\mathrm{it}} + \beta_6 \mathrm{CASH}_{\mathrm{it}} + \beta_7 \mathrm{LnSIZE}_{\mathrm{it}} + \beta_8 \mathrm{LEV}_{\mathrm{it}} + \varepsilon_{\mathrm{it}}, \tag{12}$$

$$\mathrm{LCBI}_{\mathrm{it}} = \beta_0 + \beta_1 \mathrm{BC}_{\mathrm{it}} + \beta_2 \mathrm{ER}_{\mathrm{it}} + \beta_3 \mathrm{ER}_{\mathrm{it}} * \mathrm{BC}_{\mathrm{it}} + \beta_4 \mathrm{EB}_{\mathrm{it}} + \beta_5 \mathrm{ROA}_{\mathrm{it}} + \beta_6 \mathrm{CASH}_{\mathrm{it}} + \beta_7 \mathrm{LnSIZE}_{\mathrm{it}} + \beta_8 \mathrm{LEV}_{\mathrm{it}} + \varepsilon_{\mathrm{it}}. \tag{13}$$

In Equations (12) and (13), if β_3 is greater than zero, then, MC and ER have positive regulatory effects on the BODC's impact on LCSDB; otherwise, these have negative regulatory effects.

4. Results and Discussion

4.1. Descriptive Statistics. Table 3 presents the sample's descriptive statistics. The following can be observed: (1) the enterprises' average and median LCBI are 0.382 and 0.238, respectively, which indicates that overall, enterprises in heavy-pollution industries do not exhibit particularly remarkable low-carbon behaviors. The standard deviation of 0.493 suggests a certain difference in low-carbon behaviors among the sample enterprises. (2) The sample's maximum BC was 1.905, while the minimum BC was 0.130. This substantial range reveals that a difference exists between the samples' BODC. Further, there is a large gap

Table 2: The definition or measurement of the variables.

Variable type	Variables	Variable description or measurement method
Dependent variable	LCBI	Calculated using a BP neural network method and LCSDB evaluation system
Independent variable	BC	Average score of five indicators regarding the board of directors
Intermediary variable	AOSR	Scored as one if social responsibility, environmental, or sustainable development reports are disclosed, and zero otherwise
Control variable	EB	The number of directors on the board
	ROA	The earnings before taxes divided by total assets
	CASH	The cash outflow from operating activities subtracted from the cash inflow from operating activities
	In size	The logarithm of total assets
	LEV	Liabilities divided by total assets
Moderating variable	MC	Scored as one if the number of negative reports is greater than the sample's median, and zero otherwise
	ER	Scored as one if larger than the sample's median, and zero otherwise
	SOE	Scored as one if enterprise is state-owned, and zero otherwise
	DISTRICT	Scored as one if enterprise in located in China's eastern region, and zero otherwise

Table 3: The variables' descriptive statistics.

Variables	Mean	Median	Std. dev.	Minimum	Maximum
LCBI	0.382	0.258	0.493	0.000	2.310
BC	4.697	4.235	41.30	0.130	1.905
AOSR	0.459	1.000	0.486	0.000	1.000
EB	8.480	9.000	2.552	5.000	17.00
ROA	0.051	0.045	0.478	-0.412	0.062
CASH	0.070	0.062	0.070	-0120	0.279
In SIZE	10.20	10.12	0.587	8.982	11.55
LEV	1.924	1.316	1.502	-1.203	15.88
MC	0.556	0	0.489	0	1.000
ER	0.768	0	0.186	0	1.000

between the best- and poorest-performing samples. (3) The mean value of AOSR is 0.459; therefore, the investigated heavy-pollution enterprises do not actively disclose social responsibility or sustainable development reports. (4) The control variables' standard deviations are less than one, except for that of the enterprise's asset-liability ratio (Lev), which is greater. This indicates a relatively stable range of fluctuations.

4.2. The Relationship between BODC and LCSDB and Its Regulatory Role. Table 4 displays the test results regarding the relationship between the enterprises' BODC and LCSDB and its moderating effects. The regression results in column 1 reveal that a positive correlation exists between enterprises' BODC and LCSDB; hence, BODC promotes LCSDB, in that board members' human and social capital improve the enterprises' levels of LCSDB. The higher the BODC, the more inclined the enterprises are to implement LCSDB. Thus, Hypothesis 1 is verified.

To further investigate the regulatory effects of MC and ER on the relationship between BODC and lcsdb, columns 1 and 3 introduce the interaction terms of MC × BODC and ER × BODC, respectively. It can be noted that MC and ER have a positive moderating effect on the relationship between BODC and LCSDB; thus, Hypotheses 2 and 3 are verified.

4.3. The Mediating Role of AOSR. Table 5 illustrates the results from testing the mediating role of AOSR. The coefficient of BODC in the second column is significantly positive, indicating that BODC significantly improved AOSR among the sample enterprises. The AOSR coefficient in the third column is significantly positive, the BODC coefficient is significantly positive, and the absolute value is less than the absolute value of the BODC coefficient in the first column; therefore, AOSR plays an intermediary role between BODC and LCSDB.

4.4. Heterogeneity Test. This study further investigates the heterogeneity of the BODC's impact on enterprises' LCSDB by selecting two indicators of heterogeneity: the nature of enterprises' property rights and the enterprise's home region. Given the nature of property rights, the sample enterprises were divided into state-owned and nonstate-owned enterprises. According to their respective regions, the sample enterprises were divided into the central and western regions and eastern regions of China. After the samples were classified according to these criteria, the characteristics of heterogeneity were revealed through grouping tests. Table 6 lists the test results.

In the first column, the coefficient of BODC is significantly positive, although this coefficient in the second column was not statistically significant. In the third column, the coefficients of SOE and SOE × BODC are significant; hence, the BODC's promotional effect on enterprises' LCSDB differs due to the enterprises' different ownership. Specifically, the BODC of state-owned enterprises has a more obvious promotional effect on LCSDB. This may occur because state-owned enterprises with rich board capital are more likely to respond to the government's low-carbon

Table 4: The results from testing the relationship between BODC and LCSDB and its regulatory role.

Variables	(1)	LCBI (2)	(3)
BC	4.483∗ (1.897)	-21.354∗∗∗ (-2.329)	-12.368∗∗∗ (-2.527)
MC		125.600∗∗∗ (12.975)	
MC × BC		2.311∗∗∗ (2.862)	
ER			-2.566∗∗∗ (-1.109)
ER × BC			1.638∗∗∗ (2.354)
Control variables	Control	Control	Control
R^2	0.318	0.362	0.275
Model	Fixed-effects	Fixed-effects	Fixed-effects

Note: ∗∗∗, ∗∗, and ∗ are significant at the level of 1%, 5%, and 10%, respectively; the value of t-test is in parentheses.

environmental protection policies and more actively participate in low-carbon operations and production methods. Additionally, board members of state-owned enterprises are more likely to obtain financing for low-carbon transformations than private enterprises due to their strong political background. Simultaneously, such firms have fewer risks during the low-carbon transition because they can receive more support for policies and financial subsidies. In other situations, state-owned enterprises present more obvious low-carbon behaviors than nonstate-owned enterprises.

The coefficient of BODC in the fifth column regression was not statistically significant, while this coefficient in the fourth column regression was significantly positive. In the sixth column, the coefficient of the interaction between DISTRICT and BODC is significant, which indicates that regional heterogeneity exists in the BODC's promotional effect on enterprises' LCSDB. Specifically, this effect on enterprises in the eastern region is more obvious, possibly due to the far-reaching impact of China's reform and opening-up policy. Given the superior economic foundation and sustainable development vision in China's eastern region, such enterprises are more inclined to engage in low-carbon environmental protections under the same board capital conditions, with a stronger sense of social responsibility and organizational legitimacy.

4.5. Robustness Test. We performed several robustness tests. First, we changed the explanatory variables' measurement method. Referring to existing literature (Haynes and Hillman, 2010) [16], board capital is specifically divided into its breadth and depth, and such indicators as heterogeneity in the educational level, gender, environmental protection work experience, chain director, and political association are used as proxy indicators of the board capital's breadth. Literature measures the degree of heterogeneity using more Herfindahl-Hirschman coefficients, where Pm denotes the percentage of M members on the board of directors, and Q is the category, with its value range set as $Q \in [0, 1]$.

After standardizing the five indicators' scores, the average value is the score of the board capital's breadth, which ranges from zero to one; the higher the score, the greater the breadth. Additionally, the ratio of the number of concurrent positions of board members in the same industry to the number of concurrent positions of all chain directors is used as a measure of the board of directors' capital depth, with values ranging between one and zero. The higher the score, the higher the board's capital depth. Finally, the breadth and depth of the board's capital are added to provide a comprehensive measurement of board capital, as follows:

$$H = 1 - \widehat{\alpha}_{m\ddot{I}\mu Q} P_m^2. \tag{14}$$

Second, we controlled for the influence of endogeneity. In this study, the propensity score-matching method (PSM) was used to test Hypothesis 1; and EB, ROA, CASH, LnSIZE, and LEV were selected to carry out a repeatable one-to-one nearest-neighbor matching of the sample enterprises. The sample with the highest tendency score and the sample with the lowest score of a certain board of directors' capital sample will form a paired sample. After obtaining the pseudovalues, we determined if they met the equilibrium hypothesis. If so, the paired sample was placed into the model to regress. The experimental results demonstrate that enterprises with higher board capital achieve better LCSDB. Therefore, this study's research conclusions remain unchanged.

Finally, we control for the influence of endogeneity by regressing board capital against the lag of other control variables. We also attempted to eliminate the loss samples and add other control variables, such as the enterprise's year of establishment. After the previously noted robustness test, this study's conclusion is still valid.

5. Conclusions

This paper considered data from Chinese-listed companies in heavily polluting industries spanning 2008 to 2016 to examine how BODC affects enterprises' LCSDB and its influencing mechanism from the enterprise perspective. The results reveal that the BODC can significantly promote enterprises' LCSDB. Further, media reports and environmental regulations promote the relationship between board capital and such behavior. Simultaneously, corporations' awareness of social responsibility mediates the relationship between BODC and LCSDB. This conclusion is still valid after changing the explanatory variables, using a PSM test, combining lags, adding other control variables, and performing other robustness tests. Further research indicates that the board capital's effect on enterprises' low-carbon sustainable development behavior is influenced by the nature of property rights and the enterprise's location. Compared with private enterprises, the capital of board of directors in state-owned enterprises is more significant than that of private

Table 5: The results from testing the mediating role of enterprises' AOSR.

Variables	LCBI (1)	AOSR (2)	LCBI (3)
BC	1.256∗(1.817)	0.025∗(1.523)	1.128∗(1.648)
AOSR			22.148∗∗∗(5.287)
Control variables	Control	Control	Control
R^2	0.439	0.487	0.391
Model	Fixed-effects	Fixed-effects	Fixed-effects

Note: ∗∗∗, ∗∗, and ∗ are significant at the level of 1%, 5%, and 10%, respectively; the value of ***t***-test is in parentheses.

Table 6: Heterogeneity test results regarding the relationship between BODC and LCSDB.

	Enterprises' ownership			Enterprises' region		
	State-owned (1)	Nonstate-owned (2)	All samples (3)	Eastern District (4)	Non-Eastern District (5)	All samples (6)
BODC	5.438∗∗∗ (2.360)	1.897 (1.254)	1.620∗∗ (1.961)	2.609∗∗ (1.153)	1.102 (1.892)	4.586∗∗ (2.923)
SOE			-18.238∗ (-1.059)			
SOE × BODC			4.026∗ (1.298)			
DISTRICT						9.264 (1.256)
DISTRICT × BODC						2.358∗ (-1.985)
Control variables	Control	Control	Control	Control	Control	Control
R^2	0.529	0.285	0.311	0.286	0.331	0.203
N	1224	1350	2574	855	1719	2574
Model	Fixed-effects	Fixed-effects	Fixed-effects	Fixed-effects	Fixed-effects	Fixed-effects

Note: ∗∗∗, ∗∗, and ∗ are significant at the level of 1%, 5%, and 10%, respectively; the value of t-test is in parentheses.

enterprises in promoting enterprises' low-carbon sustainable development behavior. Compared with enterprises in the central and western regions, the board capital of enterprises in eastern China has a more significant impact on enterprises' low-carbon sustainable development behavior. The research results help enterprises actively respond to realize national sustainable development strategies from a governance structural perspective.

Given these research conclusions, this paper proposes the following: (1) enterprises should augment their boards' levels of human and social capital. The selection of board members should focus on their environmental protections, work experience, and educational background, as such characteristics will enhance and guide the transmission of low-carbon sustainable development behavioral information through the board's human capital channel. On the one hand, we should focus on the board's gender diversity, improve the ratio of female directors on the board, and enhance the board's awareness of the social environment to compel them to assume more social responsibilities. (2) The government should improve enterprises' low-carbon transformation environment through financial support and knowledge-sharing to drive sustainable low-carbon transformations. This will involve strengthening and improving relevant laws and regulations, which will protect the ownership of inventions and patent rights in pursuing low-carbon innovation. The government must also attempt to transfer low-carbon technologies, knowledge, and operations to enterprises, as such resources have become a font of wisdom and a strong support for enterprises' low-carbon transformations. In addition, the government should not only focus on controlling the total carbon emissions of heavily polluting enterprises but also pay attention to the control of energy consumption and vigorously encourage enterprises to improve relevant technologies and processes. (3) The media should increase the publicity of low-carbon sustainable development of enterprises and make the concept of "low-carbon development" a new social value orientation. The media should play a greater role in guiding low-carbon awareness and low-carbon behavior and supervising the implementation of low-carbon behavior by enterprises and residents. At the same time, the media guide and encourage residents to disseminate and share low-carbon elements through a variety of social media, including self-media social

circles. (4) In considering regional heterogeneity, the government must enhance the low-carbon development environment and policy support for low-carbon transformations in the central and western regions and help the low-carbon transformation of western enterprises through production, learning, and research. Alternatively, and in considering that financing constraints may impact the low-carbon transformation of enterprises in the central and western regions, the government can promote low-interest environmental loans to mitigate environmental enterprises' funding limitations, thus promoting enterprises in the central and western regions to enhance their low-carbon behaviors.

6. Limitations and Future Research

The main limitations of this paper are mainly reflected in three aspects. First, the number of heavily polluting industries in China is about 16, and the types of industries involved are more complex. However, the sample of this paper only selects 9 representative industries instead of analyzing the whole sample. In order to deeply reveal the relationship between corporation's BODC and LCSDB, the wider the research industry, the more reliable the results may be. Moreover, when studying the mechanism of the impact of BODC on corporation's LCSDB, this study only considers the intermediary variable of AOSR. However, in fact, when the board of directors of an enterprise is rich in capital, it may have a strong ability to bear the risk of low carbon green innovation and a good profitability, which can provide relevant protection for low-carbon behavior. Therefore, the transmission mechanism of this paper is relatively limited and lacks a richer perspective. In addition, most of the data used in this study are public historical data, and there is a lack of field interviews with the research objects to obtain first-hand data. The advantage of field interview is that it can obtain more extensive information, such as how the capital of the board of directors affects the psychology of enterprise management and then affects LCSDB.

In future research, we look forward to further mining the mechanism of the impact of BODC on LCSDB. Selecting a wider range of data acquisition channels and increasing methods such as expert evaluation, enterprises' interview, and questionnaire to verify and test the multiple data. Furthermore, it is expected to establish a comprehensive framework affecting LCSDB in the future, rather than limited to the microlevel of enterprise board of directors. At the same time, considering the influencing factors such as external environmental regulation, market competition, and consumer preference, we will study how the above factors cooperate with the BODC to jointly affect the low-carbon behavior of enterprises and how the impact degree and contribution value for each factor. So as to better provide suggestions for the realization of low-carbon development of enterprises. Additionally, with the implementation of carbon inclusion and improvement of the carbon market trading system, we will consider exploring the multiple path to realize LCSDB from more dimensions, including corporate social responsibility, environmental regulation, carbon market, and carbon inclusion in the future research.

Data Availability

The data used to support the findings of this study are available from the corresponding author upon request.

Conflicts of Interest

The authors declare no conflict of interest.

Authors' Contributions

Lipeng Liu did the writing and editing, revisions, investigation, data curation, data analysis, validation, reviewing, and proofreading. Xiaoxue Liu did the conceptualization, supervision, funding acquisition, reviewing, and editing. Zihao Guo did the writing and editing, revisions, data curation, data analysis, validation, reviewing, and proofreading. Shuangshuang Fan did the data analysis, data curation, investigation, reviewing, and proofreading.

Acknowledgments

This work was supported by the Major Project of the National Social Science Fund of China (21&ZD151).

References

[1] W. Zhang, M. Zhang, S. Wu, and F. Liu, "A complex path model for low-carbon sustainable development of enterprise based on system dynamics," *Journal of Cleaner Production*, vol. 321, article 128934, 2021.

[2] I. Dincer and C. Acar, "Smart energy systems for a sustainable future," *Applied Energy*, vol. 194, pp. 225–235, 2017.

[3] F. Li, X. Xu, Z. Li, P. Du, and J. Ye, "Can low-carbon technological innovation truly improve enterprise performance? The case of Chinese manufacturing companies," *Journal of Cleaner Production*, vol. 293, article 125949, 2021.

[4] H. Schwartz, "A review of "beyond smart cities: how cities network, learn and innovate"," *Journal of the American Planning Association*, vol. 80, no. 1, pp. 97-98, 2014.

[5] Z. He, W. Shen, Q. Li et al., "Investigating external and internal pressures on corporate environmental behavior in papermaking enterprises of China," *Journal of Cleaner Production*, vol. 172, pp. 1193–1211, 2018.

[6] A. C. Pigou, *The Economics of Welfare*, Macmillan and co., London, 4th edition, 2017.

[7] A. M. Leiter, A. Parolini, and H. Winner, "Environmental regulation and investment: evidence from European industry data," *Ecological Economics*, vol. 70, no. 4, pp. 759–770, 2011.

[8] J. Galbreath, "Do boards of directors influence corporate sustainable development? An attention-based analysis," *Business Strategy and the Environment*, vol. 27, no. 6, pp. 742–756, 2018.

[9] W. Ben-Amar, M. Chang, and P. Mcilkenny, "Board gender diversity and corporate response to sustainability initiatives: evidence from the carbon disclosure project," *Journal of Business Ethics*, vol. 142, no. 2, pp. 369–383, 2017.

[10] N. Hussain, U. Rigoni, and R. P. Orij, "Corporate governance and sustainability performance: analysis of triple bottom line performance," *Journal of Business Ethics*, vol. 149, no. 2, pp. 411–432, 2018.

[11] N. Chams and J. García-Blandón, "_Sustainable or not sustainable?_ The role of the board of directors," *Journal of Cleaner Production*, vol. 226, pp. 1067–1081, 2019.

[12] P. Berrone and L. R. Gomez-Mejia, "Environmental performance and executive compensation: an integrated agency-institutional perspective," *The Academy of Management Journal*, vol. 52, no. 1, pp. 103–126, 2009.

[13] C. A. Mallin and G. Michelon, "Board reputation attributes and corporate social performance: an empirical investigation of the US best corporate citizens," *Accounting and Business Research*, vol. 41, no. 2, pp. 119–144, 2011.

[14] N. Orazalin and M. Mahmood, "Toward sustainable development: board characteristics, country governance quality, and environmental performance," *Business Strategy and the Environment*, vol. 30, no. 8, pp. 3569–3588, 2021.

[15] A. J. Hillman and T. Dalziel, "Boards of directors and firm performance: integrating agency and resource dependence perspectives," *The Academy of Management Review*, vol. 28, no. 3, pp. 383–396, 2003.

[16] K. T. Haynes and A. Hillman, "The effect of board capital and CEO power on strategic change," *Strategic Management Journal*, vol. 31, no. 11, pp. 1145–1163, 2010.

[17] G. Zeng, "Analysis of learning ability of ideological and political course based on BP neural network and improved -means cluster algorithm," *Journal of Sensors*, vol. 2022, 11 pages, 2022.

[18] M. Kroll, B. A. Walters, and S. A. Le, "The impact of board composition and top management team ownership structure on post-IPO performance in young entrepreneurial firms," *The Academy of Management Journal*, vol. 50, no. 5, pp. 1198–1216, 2007.

[19] Y. Y. Kor and H. Leblebici, "How do interdependencies among human-capital deployment, development, and diversification strategies affect firms' financial performance?," *Strategic Management Journal*, vol. 26, no. 10, pp. 967–985, 2005.

[20] S. G. Johnson, K. Schnatterly, and A. D. Hill, "Board composition beyond independence," *Journal of Management*, vol. 39, no. 1, pp. 232–262, 2013.

[21] T. Hafsi and G. Turgut, "Boardroom diversity and its effect on social performance: conceptualization and empirical evidence," *Journal of Business Ethics*, vol. 112, no. 3, pp. 463–479, 2013.

[22] C. Post, N. Rahman, and E. Rubow, "Green governance: boards of directors' composition and environmental corporate social responsibility," *Business & Society*, vol. 50, no. 1, pp. 189–223, 2011.

[23] S. Homroy and A. Slechten, "Do board expertise and networked boards affect environmental performance?," *Journal of Business Ethics*, vol. 158, no. 1, pp. 269–292, 2019.

[24] B. Gao and X. Zhang, "Analysis of an enterprise human resource management performance evaluation model based on the DEA method," *Journal of Sensors*, vol. 2022, 11 pages, 2022.

[25] J. Galbreath, "The impact of board structure on corporate social responsibility: a temporal view," *Business Strategy and the Environment*, vol. 26, no. 3, pp. 358–370, 2017.

[26] I. Boulouta, "Hidden connections: the link between board gender diversity and corporate social performance," *Journal of Business Ethics*, vol. 113, no. 2, pp. 185–197, 2013.

[27] A. Diamantopoulos, B. B. Schlegelmilch, R. R. Sinkovics, and G. M. Bohlen, "Can socio-demographics still play a role in profiling green consumers? A review of the evidence and an empirical investigation," *Journal of Business Research*, vol. 56, no. 6, pp. 465–480, 2003.

[28] P. Braun, "Going green: women entrepreneurs and the environment," *International Journal of Gender and Entrepreneurship*, vol. 2, no. 3, pp. 245–259, 2010.

[29] H. Khlif, K. Hussainey, and I. Achek, "The effect of national culture on the association between profitability and corporate social and environmental disclosure," *Meditari Accountancy Research*, vol. 23, no. 3, pp. 296–321, 2015.

[30] N. Yoon, "Understanding theoretical orientation and consequences of board interlock: integration and future directions," *Nonprofit Management and Leadership*, vol. 31, no. 4, pp. 717–736, 2021.

[31] D. C. North, *Institutions, Institutional Change and Economic Performance*, Cambridge University Press, 2012.

[32] M. A. Islam and C. Deegan, "Media pressures and corporate disclosure of social responsibility performance information: a study of two global clothing and sports retail companies," *Accounting and Business Research*, vol. 40, no. 2, pp. 131–148, 2010.

[33] A. Dyck, N. Volchkova, and L. Zingales, "The corporate governance role of the media: evidence from Russia," *The Journal of finance*, vol. 63, no. 3, pp. 1093–1135, 2008.

[34] M. K. Bednar, "Watchdog or lapdog? A behavioral view of the media as a corporate governance mechanism," *The Academy of Management Journal*, vol. 55, no. 1, pp. 131–150, 2012.

[35] M. C. Suchman, "Managing legitimacy: strategic and institutional approaches," *The Academy of Management Review*, vol. 20, no. 3, pp. 571–610, 1995.

[36] B. Bye and M. E. Klemetsen, "The impacts of alternative policy instruments on environmental performance: a firm level study of temporary and persistent effects," *Environmental and Resource Economics*, vol. 69, no. 2, pp. 317–341, 2018.

[37] Y. Wang and N. Shen, "Environmental regulation and environmental productivity: the case of China," *Renewable and Sustainable Energy Reviews*, vol. 62, pp. 758–766, 2016.

[38] F. Scrimgeoura, L. Oxleyb, and K. Fatai, "Reducing carbon emissions? The relative effectiveness of different types of environmental tax: the case of New Zealand," *Environmental Modelling & Software*, vol. 20, no. 11, pp. 1439–1448, 2005.

[39] P. M. Clarkson, Y. Li, G. D. Richardson, and F. P. Vasvari, "Revisiting the relation between environmental performance and environmental disclosure: an empirical analysis," *Accounting, Organizations and Society*, vol. 33, no. 4-5, pp. 303–327, 2008.

[40] Y. Liu, "Exploring the relationship between external positive–negative pressures and the carbon management behaviour of industrial firms," *Corporate Social Responsibility and Environmental Management*, vol. 25, no. 4, pp. 628–641, 2018.

[41] Y. Liu, N. Wang, and J. Zhao, "Relationships between isomorphic pressures and carbon management imitation behavior of firms," *Resources, Conservation and Recycling*, vol. 138, pp. 24–31, 2018.

[42] R. Chang, J. Zuo, Z. Zhao et al., "Sustainability attitude and performance of construction enterprises: a China study," *Journal of Cleaner Production*, vol. 172, pp. 1440–1451, 2018.

[43] J. Lee, M. Bazilian, B. Sovacool et al., "Reviewing the material and metal security of low-carbon energy transitions," *Renewable & Sustainable Energy Reviews*, vol. 124, article 109789, 2020.

[44] B. K. Sovacool and S. Griffiths, "Culture and low-carbon energy transitions," *Nature Sustainability*, vol. 3, no. 9, pp. 685–693, 2020.

[45] M. R. B. Rubel, D. M. H. Kee, and N. N. Rimi, "Green human resource management and supervisor pro-environmental behavior: the role of green work climate perceptions," *Journal of Cleaner Production*, vol. 313, article 127669, 2021.

[46] C. Liu, "Evaluation model of low-carbon circular economy coupling development in Forest area based on radial basis neural network," *Complexity*, vol. 2021, Article ID 6692792, 12 pages, 2021.

[47] J. Jung, K. Herbohn, and P. Clarkson, "Carbon risk, carbon risk awareness and the cost of debt financing," *Journal of Business Ethics*, vol. 150, no. 4, pp. 1151–1171, 2018.

[48] S. Parsa, N. Dai, A. Belal, T. Li, and G. Tangs, "Corporate social responsibility reporting in China political, social and corporate influences," *Accounting and Business Research*, vol. 51, no. 1, pp. 36–64, 2021.

[49] M. H. Alshirah, A. Abdul Rahman, and I. R. Mustapa, "Board of directors' characteristics and corporate risk disclosure: the moderating role of family ownership," *EuroMed Journal of Business*, vol. 15, no. 2, pp. 219–252, 2020.

[50] J. Malm, H. P. Adhikari, M. W. Krolikowski, and N. B. Sah, "The old guard: CEO age and corporate litigation," *Journal of Behavioral and Experimental Finance*, vol. 31, article 100545, 2021.

[51] M. Jizi, "The influence of board composition on sustainable development disclosure," *Business Strategy and the Environment*, vol. 26, no. 5, pp. 640–655, 2017.

[52] M. Rhee and J. Lee, "The signals outside directors send to foreign investors: evidence from Korea," *Corporate Governance: An International Review*, vol. 16, no. 1, pp. 41–51, 2008.

[53] S. Brammer and S. Pavelin, "Factors influencing the quality of corporate environmental disclosure," *Business Strategy and the Environment*, vol. 17, no. 2, pp. 120–136, 2008.

[54] E. Stanny and K. Ely, "Corporate environmental disclosures about the effects of climate change," *Corporate Social Responsibility and Environmental Management*, vol. 15, no. 6, pp. 338–348, 2008.

[55] R. S. O. Wallace, K. Naser, and A. Mora, "The relationship between the comprehensiveness of corporate annual reports and firm characteristics in Spain," *Accounting and Business Research*, vol. 25, no. 97, pp. 41–53, 1994.

[56] B. Raffournier, "The determinants of voluntary financial disclosure by Swiss listed companies," *European Accounting Review*, vol. 4, no. 2, pp. 261–280, 1995.

[57] J. Martínez-Ferrero, I. M. Garcia-Sanchez, and B. Cuadrado-Ballesteros, "Effect of financial reporting quality on sustainability information disclosure," *Corporate Social Responsibility and Environmental Management*, vol. 22, no. 1, pp. 45–64, 2015.

[58] T. Cooke, "An assessment of voluntary disclosures in the annual reports of Japanese corporations," *The International Journal of Accounting*, vol. 26, no. 3, pp. 174–189, 1991.

[59] S. M. Da Silva Monteiro and B. Aibar-Guzmán, "Determinants of environmental disclosure in the annual reports of large companies operating in Portugal," *Corporate Social Responsibility and Environmental Management*, vol. 17, no. 4, pp. 185–204, 2010.

[60] G. Michelon and A. Parbonetti, "The effect of corporate governance on sustainability disclosure," *Journal of Management & Governance*, vol. 16, no. 3, pp. 477–509, 2012.

[61] T. H. H. Nguyen, M. H. Elmagrhi, C. G. Ntim, and Y. Wu, "Environmental performance, sustainability, governance and financial performance: evidence from heavily polluting industries in China," *Business Strategy and the Environment*, vol. 30, no. 5, pp. 2313–2331, 2021.

[62] M. Zhuang, W. Zhu, L. Huang, and W. T. Pan, *Research of influence mechanism of corporate social responsibility for smart cities on consumers' purchasing intention*, Library Hi Tech,, 2021.

[63] Z. Li, J. Wang, and S. Che, "Synergistic effect of carbon trading scheme on carbon dioxide and atmospheric pollutants," *Sustainability*, vol. 13, no. 10, p. 5403, 2021.

[64] C. Huang, X. Wu, X. Wang, T. He, F. Jiang, and J. Yu, "Exploring the relationships between achievement goals, community identification and online collaborative reflection," *Educational Technology & Society*, vol. 24, no. 3, pp. 210–223, 2021.

[65] D. Chen, H. Gao, and Y. Ma, "Human capital-driven acquisition: evidence from the inevitable disclosure doctrine," *Management Science*, vol. 67, no. 8, pp. 4643–4664, 2021.

[66] X. Liang, T. Lu, and G. Yishake, "How to promote residents' use of green space: an empirically grounded agent-based modeling approach," *Urban Forestry & Urban Greening*, vol. 67, article 127435, 2022.

Hindawi
Journal of Sensors
Volume 2022, Article ID 2908447, 10 pages
https://doi.org/10.1155/2022/2908447

Research Article

Evaluation of Low-Carbon Scientific and Technological Innovation-Economy-Environment of High Energy-Consuming Industries

Zhao Zhao,[1,2] Zheng Liu,[1] Tianqi Peng,[1] Lingling Li,[3] and Yuanjun Zhao[4,5]

[1]*School of Management, Shanghai University of Engineering Science, Shanghai 201620, China*
[2]*Odette School of Business, University of Windsor, Canada N9B 3P4*
[3]*Department of Central Laboratory, Shanghai Children's Hospital, Shanghai Jiao Tong University, Shanghai 200062, China*
[4]*School of Accounting, Nanjing Audit University, Nanjing 211815, China*
[5]*Institute of Intelligent Management Accounting and Internal Control, Nanjing Audit University, Nanjing 211815, China*

Correspondence should be addressed to Zheng Liu; 03140011@sues.edu.cn

Received 2 February 2022; Accepted 24 March 2022; Published 12 April 2022

Academic Editor: Yuan Li

The coordination of scientific and technological innovation with economy and environment is conducive to the sustainable development of high energy-consuming industries. Under the background of realizing the "carbon peak and neutrality" goal in China, this paper constructs the evaluation index system of scientific and technological innovation, economy, and environment of high energy-consuming industries. Based on the coupling coordination theory, this paper analyzes the coordinated development of scientific and technological innovation, economy, and environment of high energy-consuming industries from 2011 to 2019 and analyzes the factors restricting the coordinated development of the three systems. The results show that with the emphasis on scientific and technological innovation and ecological environment, the coordination degree of the complex system of scientific and technological innovation, economy, and environment of high energy-consuming industries is gradually increasing. R & D investment, the proportion of total industrial output value in GDP, and coal consumption per 10000 yuan of industrial output value are the main influencing factors of the coordination of the three systems.

1. Introduction

With the excessive consumption of resources, excessive emission of greenhouse gases, and other environmental problems outstanding, China proposes to achieve carbon peak in 2030 and carbon neutralization in 2050. As China's basic industry, high energy consumption industry has made great contributions to China's economic take-off and infrastructure construction. These six high energy-consuming industries, chemical raw materials and chemical product manufacturing industry, nonmetallic mineral products industry, ferrous metal smelting and rolling processing industry, nonferrous metal smelting and rolling processing industry, petroleum processing coking and nuclear fuel processing industry, and power and heat production and supply industry, contribute about one-third of the total industrial output value. At the same time, they also bring "high pollution, high energy consumption, and high material consumption." Problems such as the solidification of product structure, low energy efficiency, and weak low-carbon transformation of traditional high energy-consuming enterprises have become increasingly prominent, which objectively requires enterprises to continue to promote scientific and technological innovation and technological progress. Promoting the scientific and technological innovation of high energy-consuming industries and the coordinated development of economy and environment is conducive to solving the problems of environmental constraints, reducing carbon emissions, and realizing the goal of " carbon peak and neutrality."

In recent years, synergetic theory and order parameter principle are widely used in the evaluation of collaborative

development in the fields of industrial system, interindustry, interindustry and regional, industrial cluster system, and so on. Yan et al. quantitatively studied the coupling and coordinated development of energy, economy, and ecological environment in Australia from 2007 to 2016 by constructing a coupling and coordination model based on coupling theory [1]. Xu et al. used the extended Cobb Douglas function to study the relationship between the coordination degree of the world economic forum system of 31 provinces in China and regional economic development during 2007-2018 [2]. Han et al. established a comprehensive index system and coupling coordination index (CCI) and discussed the coordination relationship within the economic resource environment (ERE) system of Beijing Tianjin Hebei Urban Agglomeration from 2008 to 2017 [3]. Xie et al. established the evaluation index system of tea industry tourism ecological environment system, determined the weight coefficient of each index by entropy weight method, and evaluated the coupling coordination degree of Fujian Province and 9 cities by constructing the coupling coordination model from 2011 to 2019 [4].

Innovation is the main engine of growth in more and more economies. Thompson introduced a collective social capital growth model based on innovation, which theoretically expressed the view that social capital affects innovation and then economic growth [5]. Martin developed the concept of elasticity and tested its usefulness as a help to understand the response of regional economies to major recession shocks [6]. By constructing an endogenous growth model including R & D distortion parameters, Jones and Williams pointed out that the investment in science and technology R & D in decentralized economies is unreasonable relative to the social optimal level [7]. Based on the panel data of 11 coastal provinces and cities in China from 2006 to 2015, Li et al. calculated the efficiency of marine scientific and technological innovation by using stochastic frontier analysis (SFA). The results show that the scale of marine scientific research institutions, the structure of scientific researchers, the development degree of marine economy, and the structure of marine industry have a significant positive impact on the efficiency of marine scientific and technological innovation [8]. Cheng et al. selected 29 provinces and cities in China from 2009 to 2018 and used the feasible generalized least squares (FGLS) method to empirically analyze the impact of the new generation of information technology on the sustainable development of regional economy [9]. Liu et al.'s study was based on the essence of the development of green finance. This paper uses fuzzy principal component analysis to construct the evaluation index system of green finance. Taking the data of three provinces and cities in the Yangtze River Delta from 2015 to 2019 as an example, this paper uses QAP analysis to study the impact of financial technology on the regional development of green finance [10].

In addition, scholars also put forward corresponding strategies for carbon emissions in different industries. Liu et al. established a game model to solve the problem of agricultural carbon emission and compared the optimal decision-making and profit under three conditions: whether manufacturers invest in emission reduction and whether retailers invest in emission reduction under decentralized decision-making or centralized decision-making [11]. Wongsapai and Daroon investigated and verified the energy consumption and efficiency data from the database of designated factories in Thailand and analyzed and estimated the greenhouse gas emission reduction potential [12]. In order to reduce the environmental pollution caused by abandoned household medical devices, Liu et al. constructed an evolutionary game model between the government and household medical device enterprises based on the dynamic punishment and dynamic subsidy measures taken by the government. This paper studies the strategic choice of the government and domestic medical device enterprises from the perspective of system dynamics [13].

Generally speaking, scientific and technological innovation not only drives economic development but also brings some help to the improvement of ecological environment. Some progress has been made in the research on the coupling and coordination between scientific and technological innovation and economy and the composite system of scientific and technological innovation and environment, but the existing research is also insufficient [14]. The existing research seldom considers the coupling and coordination among the three systems of high energy-consuming industry, scientific and technological innovation, economy, and environment, as well as the internal mechanism of the coordinated development of the three systems, which is difficult to reflect the real development status of the three systems [15–17]. Under the new situation of realizing the goal of "carbon peak and neutrality," it is necessary to conduct in-depth quantitative analysis on the interaction between technological innovation, economy, and environment of high energy-consuming industries [18–21].

Based on this, from the perspective of sustainable development of high energy-consuming industries, this paper takes the "scientific and technological innovation-economy-environment" composite system as the research object, constructs the evaluation index system of three subsystems based on the coupling coordination theory, establishes the coordination degree model of the composite system, makes an empirical study on the statistical data of high energy-consuming industries from 2011 to 2019, and calculates the scientific and technological innovation subsystem. The coupling and coordination of economic subsystem and environmental subsystem analyze the factors affecting the coordination of the three, so as to explore a new way for the coordinated development of scientific and technological innovation, economy, and environment in high energy-consuming industries, in order to provide reference for transforming the development trend of China's high energy-consuming industries, accelerating technological innovation, promoting economic progress, and improving the environment. It has important theoretical value and practical significance for exploring the basic problems of innovation driven and coordinated development of economic development and ecological environment in high energy-consuming industries.

2. Evaluation Index System and Evaluation Model

2.1. Evaluation Index System. Scientific and technological innovation and economic and environmental development are affected by many factors. The establishment of the index system should not only effectively represent the characteristics of the subsystem but also be measurable and desirable. Therefore, in order to study the coordination relationship between scientific and technological innovation system, economic system, and environmental system of high energy-consuming industries, under the principle of scientificity and systematicness, considering the availability of data and drawing on the practices of Wu, etc., the full-time equivalent of R & D personnel is selected to account for the number of labor force. The R & D investment intensity, the ratio of effective invention patents to R & D investment, and the proportion of new product sales revenue to industrial sales revenue are three indicators to measure the development status of scientific and technological innovation in high energy-consuming industries in Shanghai. Using Zheng's practice for reference, the proportion of total industrial output value to regional GDP, the growth rate of total industrial output value, the maintenance and appreciation rate of capital, and the economic development level of high energy-consuming industries are measured by the proportion of fixed asset investment in the total industrial output value. Using the practices of Zhou and Xiong for reference, the environmental status is measured by five indicators: ammonia nitrogen emission of industrial wastewater, sulfur dioxide emission of industrial waste gas, solid waste generation, coal consumption per 10000 yuan of industrial output value, and comprehensive utilization rate of industrial solid waste. The detailed evaluation index system is shown in Table 1.

2.2. Evaluation Model

2.2.1. Data Standardization Processing. Due to the different measurement standards and statistical caliber of each index, in order to eliminate the impact of index dimension, the deviation standardization method is used to standardize the statistical data. The data standardization processing formula of scientific and technological innovation, economy, and environment subsystem is as follows:

$$\text{Positive indicator}: X_{ij} = \frac{x_{ij} - x_{\min}}{x_{\max} - x_{\min}}, \tag{1}$$

$$\text{Negative indicator}: X_{ij} = \frac{x_{\max} - x_{ij}}{x_{\max} - x_{\min}}, \tag{2}$$

where X_{ij} represents the standardized value of the j-th index of the i-th evaluation object in the evaluation index system, and $X_{ij} \in [0, 1]$; the greater the value of X_{ij}, the greater the contribution to the system; $x_{\max}$ represents the upper limit value in the evaluation index, and $x_{\min}$ represents the lower limit value in the evaluation index.

2.2.2. Determine Index Weight. In order to ensure the objectivity of the data and overcome the influence of subjective factors, the entropy method is used to determine the weight of each index, and the calculation steps are as follows.

(1) Calculate the proportion of each evaluation index

$$p_{ij} = \frac{X_{ij}}{\sum_{i=1}^{n} X_{ij}}.. \tag{3}$$

(2) Calculate the entropy of each index

$$A_j = -k \sum_{i=1}^{n} p_{ij} \ln p_{ij}.. \tag{4}$$

Among them, $k = 1/\ln n$.

(3) Determine the weight of each evaluation index

$$w_{ij} = \frac{1 - A_j}{\sum_{j=1}^{m} \left(1 - A_j\right)}, \tag{5}$$

$$\sum_{j=1}^{m} w_{ij} = 1. \tag{6}$$

2.2.3. Coupling Model. Synergetics is a widely used modern cross-sectional discipline proposed by German physicist Haken. It studies the composite system composed of a large number of subsystems interacting in a complex way. The composite system synergy model can scientifically measure the system synergy, which is favored by the majority of researchers. The determination of order parameters is conducive to grasp the development and evolution direction of low-carbon scientific and technological innovation, economy, and environment composite system of high energy-consuming industries. Based on Shi's analysis on the coupling between regional logistics capacity and regional economic development, the coupling degree model of scientific and technological innovation and environmental subsystem of high energy-consuming industry is as follows:

$$C = \left(\frac{a \times b \times c}{\left(a + b + c/3\right)^3} \right)^{1/3}. \tag{7}$$

Among them, C is the coupling degree among the three systems, and $C \in [0, 1]$. The smaller the value of C, the worse the correlation and coupling degree between the scientific and technological innovation subsystem, the economic subsystem, and the environmental subsystem, the more uncoordinated they are and develop into a disordered state. The greater the value of C, the better the correlation and coupling between scientific and technological innovation subsystem, economic subsystem, and environmental subsystem, the more coordinated they are and develop to an orderly state.

2.2.4. Coupling Coordination Model. The coupling coordination degree model can reflect the degree of orderly and coordinated development among scientific and technological innovation, economic, and environmental systems of high energy-consuming industries. The formula is as follows:

Table 1: Evaluation index system.

Subsystem	Index	Index attribute
Scientific and technological innovation subsystem	Proportion of R & D personnel full-time equivalent in labor force	+
	R & D expenditure intensity	+
	Number of valid invention patents	+
	New product sales revenue	+
Economic subsystem	Proportion of total industrial output value in regional GDP	+
	Growth rate of total industrial output value	+
	Rate of capital accumulation	+
	Proportion of fixed asset investment in total industrial output value	+
Environment subsystem	Discharge of ammonia nitrogen in industrial wastewater	-
	Sulfur dioxide emission in industrial waste gas	-
	Solid waste generation	-
	Coal consumption per 10000 yuan of industrial output value	-
	Comprehensive utilization rate of industrial solid waste	+

Table 2: Classification of coupling degree coordination.

Z value interval of coupling coordination degree	Coordination level	Coupling coordination degree
(0.0-0.1)	1	Extreme disorder
(0.1-0.2)	2	Severe imbalance
(0.2-0.3)	3	Moderate disorder
(0.3-0.4)	4	Mild disorder
(0.4-0.5)	5	Verge of disorder
(0.5-0.6)	6	Reluctantly coordinate
(0.6-0.7)	7	Primary coordination
(0.7-0.8)	8	Intermediate coordination
(0.8-0.9)	9	Good coordination
(0.9-1.0)	10	High quality coordination

(1) Comprehensive evaluation index model

$$T = \lambda_1 a + \lambda_2 b + \lambda_3 c, \tag{8}$$

where T represents the comprehensive evaluation index of scientific and technological innovation, economy, and environment system, reflecting the contribution degree of the three. λ_1, λ_2, and λ_3 are undetermined coefficients, and $\lambda_1 + \lambda_2 + \lambda_3 = 1$. Considering the current situation of scientific and technological innovation, economy, and environment development of high energy-consuming industries, assuming that the three systems have the same status, take $\lambda_1 = \lambda_2 = \lambda_3 = 1/3$.

(2) Coupling coordination model

$$Z = \sqrt{C \times T}, \tag{9}$$

where Z represents the coordination degree of scientific and technological innovation, economy, and environment system, and $Z \in [0, 1]$. The greater the value of Z, the more coordinated the scientific and technological innovation subsystem, economy subsystem, and environment subsystem. The smaller the value of Z, the more uncoordinated the scientific and technological innovation subsystem, economic subsystem, and environmental subsystem. Based on Liao's classification rules, the coordination level of coupling degree is divided as shown in Table 2 below.

3. Empirical Analysis

3.1. Data Sources. The statistical data are related to scientific and technological innovation, economy, and environment come from China Statistical Yearbook, China Environmental Statistical Yearbook, China Scientific and Technological Statistical Yearbook, and China Industrial Statistical Yearbook from 2011 to 2019. Some index data are converted by formula. The missing values of some indicators in some years are supplemented by interpolation.

3.2. Determine Index Weight. On the basis of searching the original data from 2011 to 2019, the index data of scientific and technological innovation subsystem, economic subsystem, and environmental subsystem of high energy-consuming industry are processed, and the weight of each index is determined by entropy weight method, so as to lay a foundation for further calculation of system coupling coordination degree. The weight of each index is shown in Table 3.

3.3. Analysis of Overall Development Level. On the basis of determining the weight of each index, the comprehensive development index of scientific and technological innovation, economy, and environment system is obtained. Among them, a is the comprehensive development level of scientific and technological innovation, b is the comprehensive development level of economy, and c is the comprehensive development level of environment. On the basis of calculating the

Table 3: Weight of each index.

Subsystem	Index	Weight
Scientific and technological innovation subsystem	Proportion of R & D personnel full-time equivalent in labor force	21.27%
	R & D expenditure intensity	17.37%
	Number of valid invention patents	34.21%
	New product sales revenue	27.15%
Economic subsystem	Proportion of total industrial output value in regional GDP	37.09%
	Growth rate of total industrial output value	21.80%
	Rate of capital accumulation	21.16%
	Proportion of fixed asset investment in total industrial output value	19.95%
Environment subsystem	Discharge of ammonia nitrogen in industrial wastewater	26.12%
	Sulfur dioxide emission in industrial waste gas	25.81%
	Solid waste generation	17.89%
	Coal consumption per 10000 yuan of industrial output value	16.67%
	Comprehensive utilization rate of industrial solid waste	13.50%

Table 4: Comprehensive development level and coupling coordination dispatching of each system.

Year	a	b	c	C	T	Z	Degree of coordination
2011	0.001	0.801	0.335	0.137	0.337	0.215	Moderate disorder
2012	0.133	0.632	0.381	0.694	0.336	0.483	Verge of disorder
2013	0.271	0.589	0.360	0.691	0.344	0.488	Verge of disorder
2014	0.396	0.538	0.414	0.907	0.404	0.605	Primary coordination
2015	0.501	0.412	0.338	0.483	0.316	0.391	Mild disorder
2016	0.665	0.356	0.548	0.966	0.506	0.699	Primary coordination
2017	0.765	0.415	0.538	0.970	0.565	0.740	Intermediate coordination
2018	0.873	0.493	0.670	0.980	0.744	0.854	Good coordination
2019	0.993	0.123	0.742	0.323	0.663	0.463	Verge of disorder

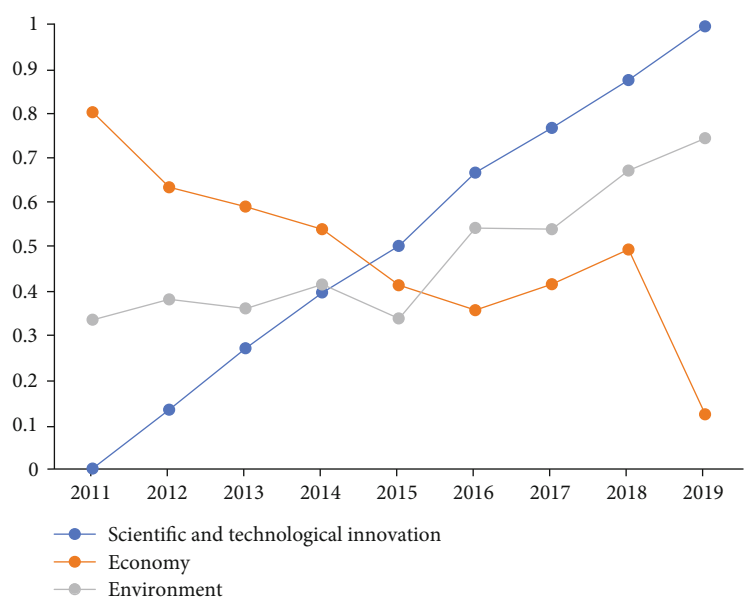

Figure 1: Comprehensive development level of scientific and technological innovation, economy, and environment of high energy-consuming industries.

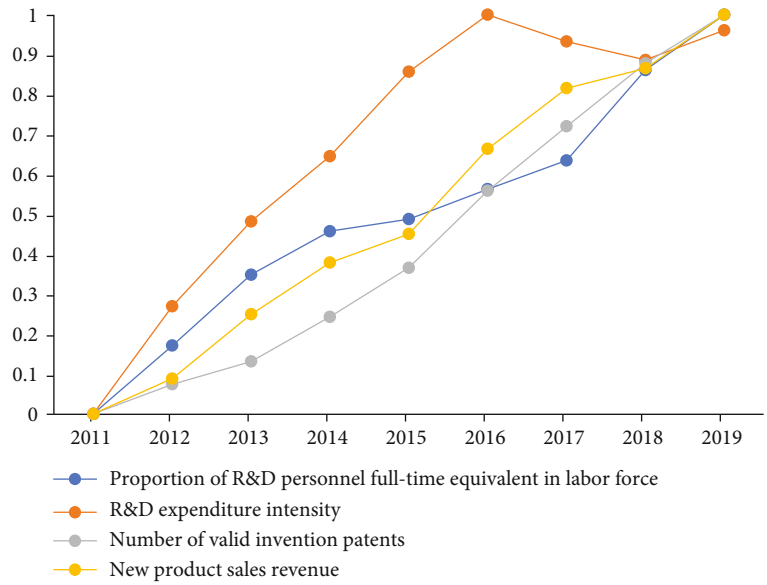

Figure 2: Order degree of scientific and technological innovation subsystem.

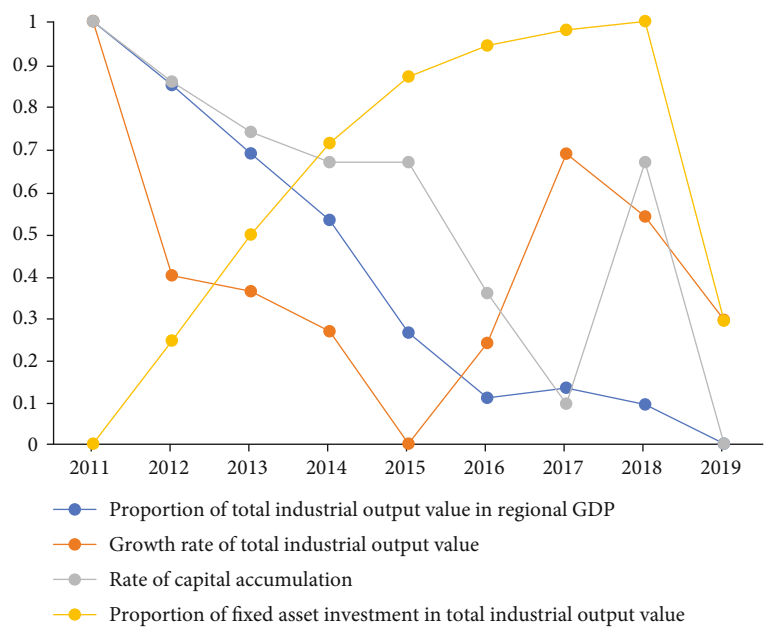

Figure 3: Order degree of economic subsystem.

comprehensive development index, the coupling coscheduling among scientific and technological innovation subsystem, economic subsystem, and environmental subsystem is calculated by bringing in formulas (7)–(9). The results are shown in Table 4 and Figure 1.

It can be seen from Table 4 above that from 2011 to 2019, the comprehensive development level of scientific and technological innovation, economy, and environment of high energy-consuming industries showed a steady upward trend year by year. The economic development lagged behind the development of scientific and technological innovation and ecological environment, which was generally characterized by lagging economic development. From 2011 to 2014, there was a large gap in the overall development level of the three systems, and the development of scientific and technological innovation and ecological environment lagged behind the economic development. The development level of the three systems was ranked as follows: economy>environment>scientific and technological innovation. Since 2015, the comprehensive development level of scientific and technological innovation has exceeded the comprehensive development level of economy and ecological environment, but the economic development level is still higher than the comprehensive development level of ecological environment. At this time, the overall development level of the three systems is as follows: scientific and technological innovation>economy>environment. From 2016 to 2019, the comprehensive development level of

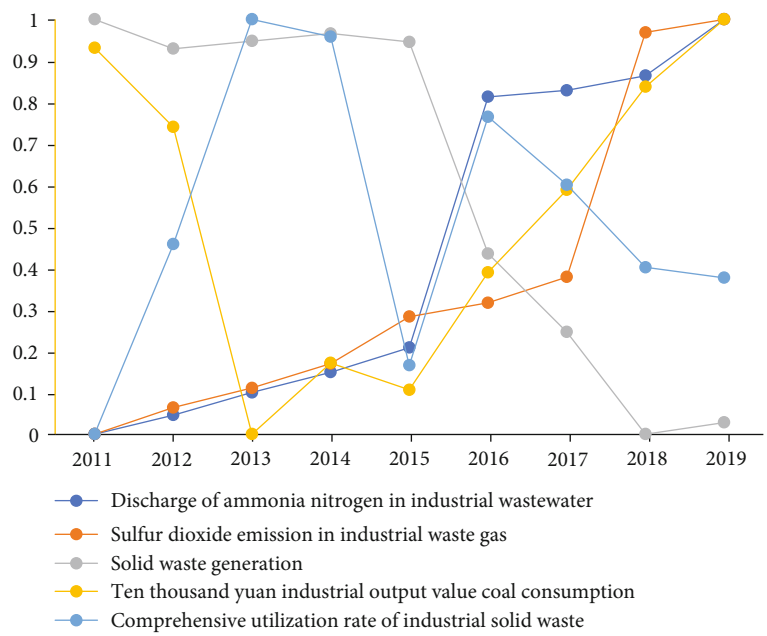

Figure 4: Order degree of environmental subsystem.

ecological environment gradually caught up with and surpassed the economic subsystem but still lagged behind the development level of scientific and technological innovation. The overall development level of the three systems is as follows: scientific and technological innovation>ecological environment>economy. On the whole, since 2010, high energy-consuming industries have attached great importance to the development of ecological environment while scientific and technological innovation and economic development. Scientific and technological innovation, as an important means to promote economic development and improve the level of ecological environment, has contributed an important amount to economic development and environmental construction.

Accordingly, the comprehensive development level of scientific and technological innovation subsystem, economic subsystem, and ecological environment system of high energy-consuming industry is gradually rising, indicating that the internal of scientific and technological innovation subsystem, economic subsystem, and ecological environment system have achieved orderly development and are in a good and orderly growth state, which jointly determines that the coupling and coordination degree of the three systems presents a rising trend.

From 2011 to 2019, the phased evolution characteristics of the coordination degree of scientific and technological innovation, economy, and ecological environment system are obvious. The coordinated development process of scientific and technological innovation, economy, and ecological environment of high energy-consuming industries is divided into three obvious stages.

In the first stage, from 2011 to 2013, the coordination of scientific and technological innovation, economy, and ecological environment system is low, and the three systems are in a state of imbalance. The coordination degree was 0.215 in 2010 and increased year by year. By 2013, the coupling coordination degree of the three systems was 0.488, which is still on the verge of imbalance. At this stage, the coordinated development level of scientific and technological innovation, economy, and ecological environment is low and the development speed is slow. This is because before 2013, the coupling and interaction between scientific and technological innovation, economy, and ecological environment of high energy-consuming industries were weak, and the interaction between them was not obvious. The extensive development mode was adopted to drive the development of the overall economy through the development of high energy-consuming industries, did not pay attention to mastering core technologies, ignored the negative impact on the ecological environment, and produced more pollutant emissions. During this period, the development of scientific and technological innovation subsystem and environment lags behind the economic subsystem, and the three subsystems with low order work together, resulting in the low level of coordinated development of the three, which is in a state of imbalance.

In the second stage, in the five years from 2014 to 2018, the coordination degree of scientific and technological innovation and economic and environmental system of high energy-consuming industries has increased significantly each year compared with the previous year, and the coordination degree has increased from 0.605 in 2014 to 0.854 in 2018. Compared with the first stage, the coordination degree has improved greatly, forming a rapid growth period, indicating the scientific and technological innovation of high energy-consuming industries. The level of coordinated economic and environmental development continued to rise rapidly. Accordingly, the coupling and interaction ability of scientific and technological innovation subsystem, economic subsystem, and environmental subsystem has gradually increased, but the speed of coupling and coordinated development has gradually slowed down in recent years. The

comprehensive development level of scientific and technological innovation has gradually surpassed the comprehensive development level of economy and ecological environment, indicating that the position of scientific and technological innovation in economic development has gradually increased and become an important force to promote economic development.

In the third stage, in 2019, the coupling degree of the three systems of high energy-consuming industry, scientific and technological innovation, economy, and environment showed a downward trend compared with the previous year and was on the verge of imbalance. The interaction and coupling ability of these three systems is weak. In 2019, due to the upgrading of Sino US trade friction, insufficient market demand, falling prices of industrial products, rising costs, and other factors, the level of economic development was low. It shows that in the future development process, we should pay attention to the economic benefits brought by science and technology and use core technology to promote the improvement of the comprehensive level of economy and ecological environment.

3.4. Analysis of Influencing Factors Restricting Coupling Coordination. Coordination is a virtuous circle situation formed in order to maximize the effectiveness of the overall system and make each subsystem or module in the system to cooperate, promote, and influence each other. In order to promote the development of the coupling and coordination level of scientific and technological innovation, economy, and environment in the direction of good coordination and finally achieve high-quality coordination, it is necessary to find out the factors restricting the coordinated development of the three in the indicators of each subsystem.

Figure 2 shows the order trend of various indicators of the scientific and technological innovation subsystem. It can be seen that the indicators of the scientific and technological innovation subsystem of China's high energy-consuming industries generally fluctuate and rise by a small margin, and the change trends of the four indicators are basically the same. It can be seen from Figure 2 that in the scientific and technological innovation subsystem, the proportion of full-time equivalent of R & D personnel in the number of labor force, the number of effective invention patents, and the sales revenue of new products are increasing year by year. Increasing the proportion of full-time equivalent of R & D personnel in the number of labor force is conducive to improving the scientific and technological innovation level of high energy-consuming industries, so as to increase the number of effective invention patents and the sales revenue of new products and improve the comprehensive development level of scientific and technological innovation subsystem. From 2011 to 2016, the proportion of R & D investment in the total industrial output value increased year by year, and the growth rate decreased year by year. It showed a downward trend from 2016 to 2018 and then showed an upward trend after 2018. The proportion of R & D investment decreased. Reducing R & D investment will inevitably reduce the development speed of scientific and technological innovation and increase capital investment. R & D and mastering low-carbon technology is the key to reducing carbon emissions and an important means to achieve the goal of "carbon peak and neutrality."

It can be seen from Figure 3 that in the economic subsystem, the proportion of total industrial output value in regional GDP decreases year by year, and other industries develop rapidly and gradually catch up with and surpass the scale of industrial development. Compared with other industries, the growth of total industrial output value is slow. Due to the influence of technology, environment, and other factors, the transformation of old and new industrial kinetic energy is slow, and the industrial structure needs to be optimized and upgraded. The quality and efficiency of development need to be improved, which restricts the improvement of the comprehensive level of the economic subsystem. Both the growth rate of industrial output value and the rate of capital preservation and appreciation have experienced a process of decline, rise, and decline. In the past two years, the growth rate of industrial output value has shown a downward trend, the contribution rate to the total output value has gradually decreased, the development of industrial industry lags, and the reduction of the rate of capital preservation and appreciation has restrained the development of industrial economy to a certain extent. From 2011 to 2018, the industrial fixed asset investment showed an upward trend, but after 2018, the fixed asset investment decreased, and the lack of funds brought obstacles to the development of high energy-consuming industries, which was not conducive to the improvement of the level of industrial economic development.

In order to ensure the sustainable coupling and coordination of the three subsystems, it is also necessary to find out the short board factors restricting environmental development. Figure 4 shows the order trend of each index of the environmental subsystem. It can be seen from Figure 4 that from 2011 to 2019, the emission of ammonia nitrogen in industrial wastewater and sulfur dioxide in industrial waste gas in the environmental subsystem showed an increasing trend year by year, and the generation of industrial solid waste decreased year by year. The high emission of ammonia nitrogen and sulfur dioxide put great pressure on the improvement of ecological environment and the reduction of pollution and carbon, which is not conducive to the realization of the "carbon peak and neutrality" goal. From 2011 to 2013, the coal consumption per 10000 yuan of industrial output value showed a downward trend and increased year by year after 2013. Coal and other fossil energy are the main sources of carbon emission in China. The increase of fossil energy consumption is easy to lead to the increase of carbon emission in China and aggravate environmental pollution.

4. Conclusion

By constructing the synergy degree model of high energy-consuming industry's scientific and technological innovation economy environment composite system, this paper makes an empirical study on the coordinated development of high energy-consuming industry's technological innovation

economy and ecological environment. The results show that from 2011 to 2019, the synergy of technological innovation economy environment system of high energy-consuming industries generally shows an upward trend, and the comprehensive development of scientific and technological innovation and ecological environment gradually catch up with and surpass the comprehensive economic development level. The improvement of the comprehensive development level of scientific and technological innovation drives the development of economy and ecological environment, which is directly related to the low order of technological innovation subsystem. It shows that in the development of high energy consumption industry, we should overcome the short board effect in the "barrel principle" and make the subsystems develop together. In addition, in order to promote the scientific and technological innovation of high energy-consuming industries and achieve high-quality coordination of the coupling and coordination level of economy and environment, it is necessary to find out the index factors restricting the coordinated development of the three in each subsystem. Less R & D investment is the factor restricting the development of scientific and technological innovation subsystem, the low proportion of total industrial output value in GDP is the factor restricting the development of economic subsystem, and the increase of coal consumption per 10000 yuan of industrial output value is the factor restricting the development of environmental subsystem.

Taking the high energy-consuming industry as a whole as the research object, this paper studies the coordinated development of low-carbon technological innovation, economy, and environment, without empirical research and comparative analysis on the evolution and difference of the composite system between the six high energy-consuming industries. In the follow-up research, it can be considered to study the collaborative relationship between high energy-consuming industries, so as to provide a certain reference for improving or improving the level of collaborative development among industries.

Data Availability

The data used to support the findings of this study are available from the corresponding author upon request.

Conflicts of Interest

All authors declare no conflicts of interest in this paper.

Acknowledgments

This study was supported by the soft science research project of Shanghai Science and Technology Committee (Grant no. 22692104000), the Key Lab of Information Network Security of Ministry of Public Security (Grant no. C20609), the Municipal Key Curriculum Construction Project of University in Shanghai (Grant no. S202003002), and the Shanghai Philosophy and Social Science Planning Project (Grant no. 2020BGL007).

References

[1] X. Yan, M. Chen, and M. Y. Chen, "Coupling and coordination development of Australian energy, economy, and ecological environment systems from 2007 to 2016," *Sustainability*, vol. 11, no. 23, p. 6568, 2019.

[2] S. Xu, W. He, L. Yuan, D. M. Degefu, Y. Yang, and H. Li, "The relationship between coordination degree of the water–energy–food system and regional economic development," *Sustainability*, vol. 13, no. 3, p. 1305, 2021.

[3] H. Han, L. Guo, J. Zhang, K. Zhang, and N. Cui, "Spatiotemporal analysis of the coordination of economic development, resource utilization, and environmental quality in the Beijing-Tianjin-Hebei urban agglomeration," *Ecological Indicators*, vol. 127, article ???, 2021.

[4] X. Xie, H. Sun, J. Gao, F. Chen, and C. Zhou, "Spatiotemporal differentiation of coupling and coordination relationship of tourism–urbanization–ecological environment system in China's major tourist cities," *Sustainability*, vol. 13, no. 11, p. 5867, 2021.

[5] M. Thompson, "Social capital, innovation and economic growth," *Journal of Behavioral and Experimental Economics*, vol. 73, pp. 46–52, 2018.

[6] R. Martin, "Regional economic resilience, hysteresis and recessionary shocks," *Journal of Economic Geography*, vol. 12, no. 1, pp. 1–32, 2012.

[7] C. I. Jones and J. C. Williams, "Too much of a good thing? The economics of investment in R&D," *Journal of Economic Growth*, vol. 5, no. 1, pp. 65–85, 2000.

[8] G. Li, Y. Zhou, F. Liu, and A. Tian, "Regional difference and convergence analysis of marine science and technology innovation efficiency in China," *Ocean & Coastal Management*, vol. 205, article 105581, 2021.

[9] L. Cheng, S. Zhang, X. Lou, Y. Yang, and W. Jia, "The penetration of new generation information technology and sustainable development of regional economy in China—moderation effect of institutional environment," *Sustainability*, vol. 13, no. 3, p. 1163, 2021.

[10] Z. Liu, J. Song, H. Wu et al., "Impact of financial technology on regional green finance," *Computer Systems Science and Engineering*, vol. 39, no. 3, pp. 391–401, 2021.

[11] Z. Liu, L. Lang, B. Hu, L. Shi, B. Huang, and Y. Zhao, "Emission reduction decision of agricultural supply chain considering carbon tax and investment cooperation," *Journal of Cleaner Production*, vol. 294, article 126305, 2021.

[12] W. Wongsapai and S. Daroon, "Estimation of greenhouse gas mitigation potential from carbon intensity and energy data analysis from Thai industrial sector," *Energy Reports*, vol. 7, pp. 930–936, 2021.

[13] Z. Liu, L. Lang, L. Li, Y. Zhao, and L. Shi, "Evolutionary game analysis on the recycling strategy of household medical device enterprises under government dynamic rewards and punishments," *Mathematical Biosciences and Engineering: MBE*, vol. 18, no. 5, pp. 6434–6451, 2021.

[14] W. Yang, X. Chen, Z. Xiong, Z. Xu, G. Liu, and X. Zhang, "A privacy-preserving aggregation scheme based on negative survey for vehicle fuel consumption data," *Information Sciences*, vol. 570, pp. 526–544, 2021.

[15] Z. Li, J. Wang, and S. Che, "Synergistic effect of carbon trading scheme on carbon dioxide and atmospheric pollutants," *Sustainability*, vol. 13, no. 10, p. 5403, 2021.

[16] H. Wang and Q. Luo, "Can a colonial legacy explain the pollution haven hypothesis? A city-level panel analysis," *Structural Change and Economic Dynamics*, vol. 60, pp. 482–495, 2022.

[17] Y. Li and Q. Li, "The application of BIM technology in budget control of port construction cost," *Journal of Coastal Research*, vol. 103, no. 1, pp. 644–648, 2020.

[18] S. Gao, "Strategy of improving the industrial and commercial administration ability of port type park," *Journal of Coastal Research*, vol. 103, no. 1, pp. 663–667, 2020.

[19] W. C. Lee, N. Hoe, K. K. Viswanathan, and A. H. Baharuddin, "An economic analysis of anthropogenic climate change on rice production in Malaysia," *Malaysian Journal of Sustainable Agriculture*, vol. 4, no. 1, pp. 01–04, 2019.

[20] H. Yu, Y. Zhao, Z. Liu et al., "Research on the financing income of supply chains based on an E-commerce platform," *Technological Forecasting and Social Change*, vol. 169, article 120820, 2021.

[21] R. Sun, J. Wang, Q. Cheng, Y. Mao, and W. Y. Ochieng, "A new IMU-aided multiple GNSS fault detection and exclusion algorithm for integrated navigation in urban environments," *GPS Solutions*, vol. 25, no. 4, pp. 1–17, 2021.

Hindawi
Journal of Sensors
Volume 2022, Article ID 1732532, 13 pages
https://doi.org/10.1155/2022/1732532

Research Article

Research on Multitarget Recognition and Detection Based on Computer Vision

XiaoYing Zhang and Yiran Chen

College of Big Data and Artificial Intelligence, Chongqing Institute of Engineering, Chongqing, 400056, China

Correspondence should be addressed to XiaoYing Zhang; 00250@cqie.edu.cn

Received 13 February 2022; Revised 10 March 2022; Accepted 15 March 2022; Published 8 April 2022

Academic Editor: Yuan Li

Information is obtained from human eyes for thinking divergence, and further associated with computer equipment, so human beings endow computers with the ability of "vision" to convey and feel information. This field has developed for many years, and many aspects can be in line with other research directions, such as artificial intelligence, which has become popular in recent years, and pattern recognition, which has been applied a lot. In order to sort out the structure and content of multitarget recognition smoothly, this paper starts from the perspective of shallow vision, uses theory and practical experiments, and chooses the core technology with the largest weight from massive computer technologies, so that the recognition algorithm can compare with the recognition algorithm. The research shows that (1) CNN shows its unique feature ability and incomparable detection accuracy from many models, and the error rate can be reduced from 28.07% to 18.40%. (2) The method of candidate region is complex, and the larger the region, the more difficult it is to calculate. The method based on regression is far beyond it in both precision and speed and is more suitable for the research of this subject. (3) When the mAP increases, the speed is forced to slow down. If the image resolution is high with the same model, the mAP will be high (SSD and YOLO models are often used). Experiments show that the recognition effect is obvious. At the end of the article, the advantages and disadvantages of this study are summarized. In the field of computer vision, people need to do more in-depth research. Follow-up can optimize multitarget recognition and detection and strive to improve the accuracy.

1. Introduction

When it comes to computer vision, we have to mention the background of deep learning. If we want new development, we need to study some old classic problems repeatedly (such as the target detection problem in this paper) and find blind spots that others cannot find from the details, resulting in qualitative changes, and "blind spots" become "breakthrough points." When you think of the word "vision," you can think of the meaning that it makes the machine detached and get the perception ability. However, this goal is difficult to achieve. Researchers have wasted a lot of effort and made a lot of useless work, and it was not until the introduction of deep learning that they got a positive meaning that cannot be omitted. Target recognition is the core, most valuable, and most basic task step. If this part of work is not done well, all subsequent steps will be greatly affected. In this paper, a variety of computer technologies are used, such as deep learning and image processing, combing and summarizing the relevant information of the better target recognition algorithm based on computer vision so far and selecting the multitarget visual recognition method (target detection algorithm based on convolution neural network) which meets the actual needs and is most suitable for this study. According to the latest cutting-edge science, we have inquired a lot of information and literature related to computer vision and cited them reasonably. The latest progress of computer vision algorithm and the improvement of computer performance in reference [1] have new functions. Reference [2] designs real-time computer vision and machine learning systems for modeling and recognizing human behavior in visual surveillance. Literature [3] investigates head posture estimation in computer vision. Reference [4] analyzes and calculates the development of horizontal

setting method and fast marching method of interface motion in computer vision. Reference [5] provides 19 enlightening basic achievements in computer vision research. In literature [6], computer vision introduces flexible decision forest models to deal with huge and diverse image and video analysis tasks. Literature [7] extracts moving targets from complex background scenes and designs the background code manual model of target motion detection algorithm. Reference [8] uses wavelet transform to detect human moving objects based on computer vision. Literature [9] investigates the ability of six different algorithms to track subpixel targets in moving background and noise. Literature [10] discusses the key algorithms of video target detection and recognition in intelligent transportation system based on computer vision technology. In reference [11], an improved algorithm combining background subtraction and mixed frame difference method is introduced on the basis of moving target detection algorithm. Literature [12] solves the problem of detecting moving objects by using tree search algorithm for object detection in image sequences. Literature [13] introduces the method of moving multitarget detection and tracking in stable scene. Literature [14] realizes target tracking and real-time obstacle detection of autonomous vehicles based on computer vision. Literature [15] develops a new m-sequence target and circular correlation processing technology based on computer vision for real-time displacement measurement.

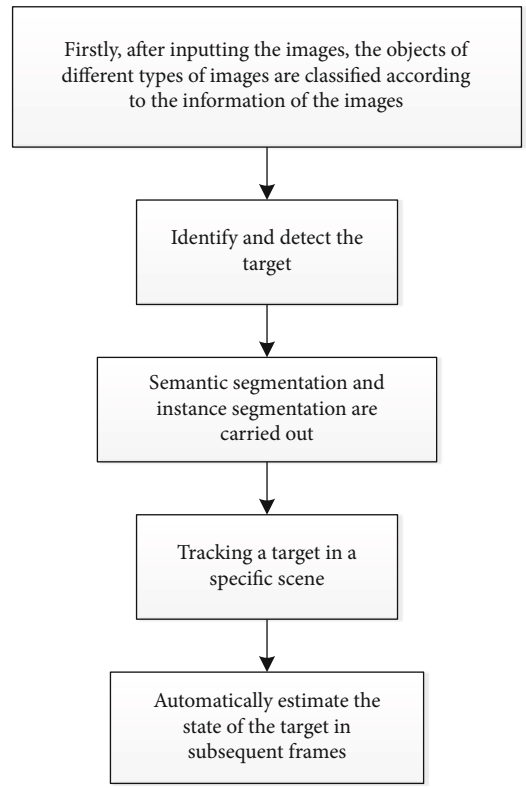

Figure 1: Typical processing flow of computer vision.

2. Theoretical Basis

2.1. Computer Vision. Computer Vision [16] is a science that studies how to make machines "see". At the beginning of last century, the function that computer vision can realize is only to analyze and recognize two-dimensional digital images. With the continuous expansion of this field, people are no longer easily satisfied with processing simple images, and people prefer that computers can recognize and even understand what they see through vision. Machine analysis extracts image features and then analyzes them. Image understanding [17] is an extension and expansion of computer vision research. The process flow is shown in Figure 1.

Main research directions of computer vision is shown in Table 1.

2.2. Deep Learning. Turing test [19], a method to test whether a machine has human intelligence, was put forward by mathematician Turing in 1950s, and it can well judge whether a machine has the same perception ability as human beings. The core idea of the Turing test is to ask computers to disguise themselves as human beings as much as possible when they take questions from people. This coincides with the desire of people in our target detection algorithm that computers disguised as human "eyes" can obtain, process, and convey information. Whether it is Turing test, deep learning, or artificial intelligence, the contents of their research topics are similar and integrated, and a lot of knowledge is interlinked. Many algorithms cannot achieve this goal, and the research and success of deep learning algorithm bring hope. Deep learning is a big science, which aroused the research wave of deep learning as early as the 1940s, but it did not achieve great success until 2012. Deep learning [20] is to learn the internal law and representation level of sample data. The feature extraction method of directly calculating the original data replaces the old method. The feature expression of unsupervised learning can be divided into three types according to different components. As shown in Table 2, there are various methods of feature expression.

2.2.1. Limit Boltzmann. DBN [21] consists of "Constrained Boltzmann Machines," as shown in Figure 2.

Let n be the visible layer node, m be the hidden layer node, v be the visible unit, and h be the hidden unit. Energy of the system:

$$E(v, h \mid \theta) = -\sum_{i=1}^{n} a_i v_i - \sum_{j=1}^{m} b_j h_j - \sum_{i=1}^{n}\sum_{j=1}^{m} v_i W_{ij} h_j. \quad (1)$$

When the model state is constant, the joint probability distribution is

$$P(v, h \mid \theta) = \frac{e^{-E(v,h|\theta)}}{Z(\theta)}, Z(\theta) = \sum_{v,h} e^{-E(v,h|\theta)}. \quad (2)$$

Table 1: Main research directions of computer vision.

Image classification	Challenges such as viewpoint change, scale change, intraclass change, image deformation, image occlusion, lighting conditions, and background clutter; nowadays, the popular image classification architecture is convolution neural network.
Object recognition and detection [18]	Subdivision detection algorithms such as face detection, vehicle detection, and character recognition are derived. Commonly used models are R-CNN and fast R-CNN.
Semantic segmentation	Every pixel of the input image is classified, and its inner meaning can be clearly described with a picture. Commonly used models are full convolution network (FCN), SegNet, and so on.
Motion and tracking	Generally speaking, large-scale convolution neural networks can be trained as classifiers and trackers. The representative tracking algorithms are full convolution network tracker (FCNT) and multidomain convolution neural network (MD net).
Visual question and answer	The purpose of this study is that users ask questions according to the input images, and the algorithm automatically answers questions according to the content of questions.
Motion recognition	In practical applications, accurate motion recognition is helpful for public opinion monitoring, advertising, and many other tasks related to video understanding.
Three-dimensional reconstruction	In the field of 3D vision, geometry-based methods are still the main methods, such as 3D reconstruction and visual SLAM.

Table 2: Feature expression method based on learning.

Category	Method name
Feature expression based on deep learning	CDBN, SBM, DeCAF, R-CNN, fast R-CNN, NIN, SPPNet, segDeepM, MatchNet, OverFe-at, SuperCNN……

The activation probability of hidden unit is

$$p\left(h_j = 1,|v,\theta\right) = \sigma\left(b_j + \sum_j v_i W_{ij}\right). \tag{3}$$

Visible cell activation probability is

$$p(v_i = 1,|h,\theta) = \sigma\left(a_i + \sum_i h_j W_{ij}\right). \tag{4}$$

The sigmoid activation function is

$$\sigma(x) = \frac{1}{1 + \exp\,(-x)}. \tag{5}$$

The output of the activation function hidden layer node is

$$v^{k+1} = \omega^k h^k + b^k, h^k = \sigma\left(v^k\right). \tag{6}$$

Softmax function:

$$p_s = \frac{\exp\,\left(v_s{}^{N+1}\right)}{\sum_j \exp\left(v_s{}^{N+1}\right)}. \tag{7}$$

When $d_s = 0$, the cross-entropy function:

$$L = -\sum_s d_s \log p_s. \tag{8}$$

2.2.2. Self-Coding Machine. As shown in Figure 3, the main structure of the self-encoding machine is as follows.

Input an N-dimensional signal x, through the input layer to the middle layer, the signal changes y, the principle of self-coding machine.

$$y = s(Wx + b). \tag{9}$$

The signal y is decoded by the decoding layer to the output layer of n neurons, and the signal becomes z.

$$z = s\left(W'y + b'\right). \tag{10}$$

Matrix transposition:

$$W' = W^T. \tag{11}$$

Typical square error:

$$L(xz) = \|x - z\|^2. \tag{12}$$

Cross entropy method:

$$L_H(x,z) = -\sum_{k=1}^{n}[x_k \log z_k + (1 - x_k) \log\,(1 - z_k)]. \tag{13}$$

2.2.3. Convolution Neural Network. Convolutional neural networks (CNN) [22] s a kind of feedforward neural networks with depth structure including convolution calculation. It is a very important deep learning algorithm. We give an example of a single-layer convolution neural network, which includes two processes: convolution and subsampling. Introducing

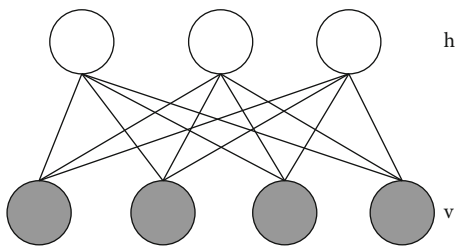

Figure 2: Constrained Boltzmann machine.

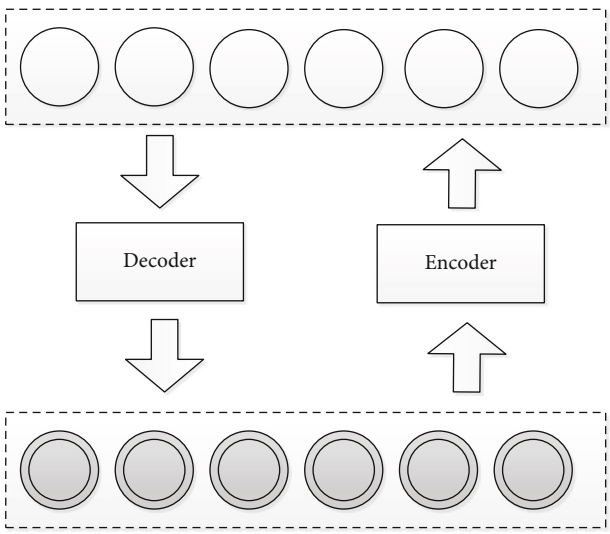

Figure 3: Self-coding machine.

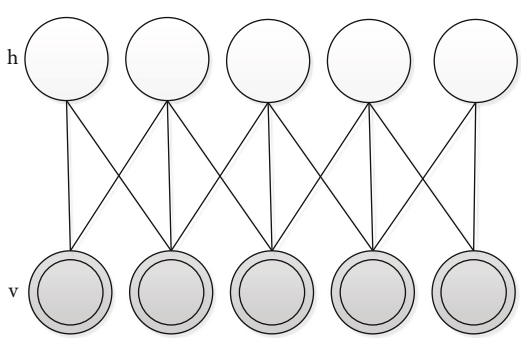

Figure 4: Single-layer convolution neural network.

different convolution kernels to extract different features and observe specific patterns of input signals; subsampling can reduce the dimension of feature map (using average pooling or maximum pooling operation), which reduces the resolution of feature map, but can keep the feature description. In the graph, every two nodes have various connections, which represent the process of convolution from the input node and then subsampling into the output node, as shown in Figure 4.

$$Z^{l+1}(i,j) = \left[Z^l \otimes \omega^{l+1}\right](i,j) + b, \tag{14}$$

$$Z^{l+1}(i,j) = \sum_{k=1}^{K_l}\sum_{x=1}^{f}\sum_{y=1}^{f}\left[Z_k^l(s_0 i + x, s_0 j + y)\omega_k^{l+1}(x,y)\right] + b, \tag{15}$$

$$L_{l+1} = \frac{L_l + 2p - f}{s_0} + 1\ (i,j) \in \{0, 1, \cdots L_{l+1}\}, \tag{16}$$

$$L_{l+1} = \frac{L_l + 2p - f}{s_0} + 1(i,j) \in \{0, 1, \cdots L_{l+1}\}, \tag{17}$$

$$L^{l+1} = L. \tag{18}$$

2.3. Target Detection Algorithm. Application fields of target detection and tracking are shown in Table 3.

If we want to detect the target, we need to use the corresponding algorithm. Because the traditional algorithm has great limitations, it must be based on image processing and hand-designed feature extraction, and it is greatly influenced by external factors such as noise and resolution, so its performance is not enough to meet people's needs. CNN's accuracy is nearly 30% higher than before [23]. The flow of traditional target detection algorithm is shown in Figure 5.

2.4. Image Processing. As shown in Figure 6, it is a flowchart about image processing.

(1) Pixel units are converted to centimeters:

$$L_{(\text{Actual})} = L_{(\text{Pixel})} * \left(\frac{100}{L_{(\text{Ruler})}}\right) cm. \tag{19}$$

(2) Image grayscale depends on RGB color scale operation [24].

Floating point algorithm:

$$\text{Gray} = R * 0.3 + G * 0.59 + B * 0.11. \tag{20}$$

Integer method:

$$\text{Gray} = \frac{(R * 30 + G * 0.59 + B * 11)}{100}. \tag{21}$$

Shift algorithm:

$$\text{Gray} = (R * 76 + G * 151 + B * 28) \gg 8. \tag{22}$$

Average method:

$$\text{Gray} = \frac{(R + G + B)}{3}. \tag{23}$$

Table 3: Application fields of target detection and tracking.

Application field	Specific application
Virtual reality	Interactive virtual world, game control, virtual studio, character animation, teleconferencing, and so on
Autonomous navigation	Vehicle navigation, robot navigation, space probe navigation, etc.
Robot vision	Industrial robots, home service robots, restaurant service robots, space probes, etc.
Advanced human-computer interaction	Sign language translation, gesture-based control, information transmission in noisy environment, etc.
Intelligent monitoring	Public safety monitoring, parking lots, supermarkets, department stores, vending machines, ATMs, access control of outsiders, traffic scenes, old and young care, etc.
Motion analysis	Content-based sports video retrieval, personalized training of golf and tennis, clinical research of patients, etc.

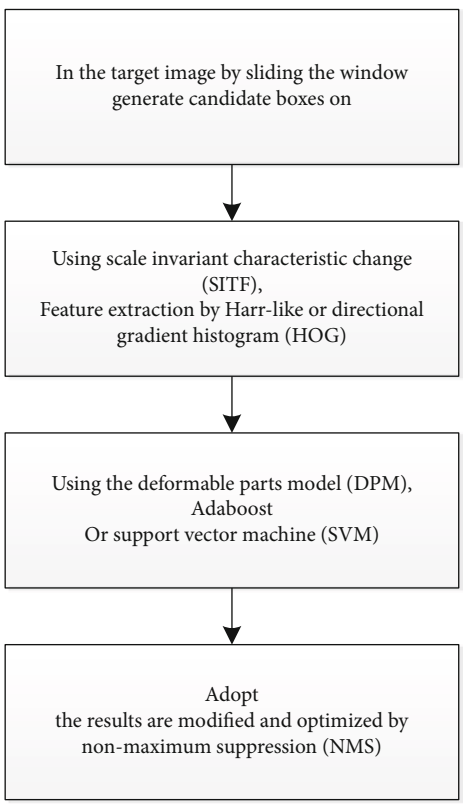

Figure 5: Traditional target detection algorithm.

Green method only:

$$\text{Gray} = G. \tag{24}$$

(3) The binarization of the image makes the image either black or white [25]. It can reduce the difficulty of subsequent image processing and further reduce the occupation of storage space

$$g(x, y) = \begin{cases} 0(\text{Gray value is less than threshold}(T)), \\ 255(\text{Gray value is greater than threshold}(T)). \end{cases} \tag{25}$$

(4) Enhancement and sharpening

$$d(x, y) = f(x, y) - g(x, y). \tag{26}$$

(5) Edge detection

$$\nabla^2 f(x, y) = \frac{\partial^2 f(x, y)}{\partial x^2} + \frac{\partial^2 f(x, y)}{\partial y^2}, \tag{27}$$

$$\nabla^2 f(x, y) = f(x+1, y) + f(x-1, y) + f(x, y+1) + f(x, y-1) - 4f(x+1, y). \tag{28}$$

3. Target Detection Algorithm Based on Convolution Neural Network

3.1. Overview of Convolution Neural Networks. All the research in this paper is mainly based on the field of computer vision, in which feature extraction and classification are indispensable parts. In the traditional image processing, the feature extraction method is usually designed by hand, which is modified on the image by human beings according to relevant theory and experience knowledge, far from being "intelligent;" moreover, this method cannot completely extract the target information, and its limitations are too great. In convolution neural network, convolution can represent feature extractor, and neural network is classifier, which meets the requirements of target recognition algorithm. Moreover, convolution neural network adopts average pooling or maximum pooling operation, which can imitate the visual and perceptual mechanism structure of living bodies and carry out supervised learning and unsupervised learning. Add three concepts to convolution neural network to reduce limitations, as shown in Table 4.

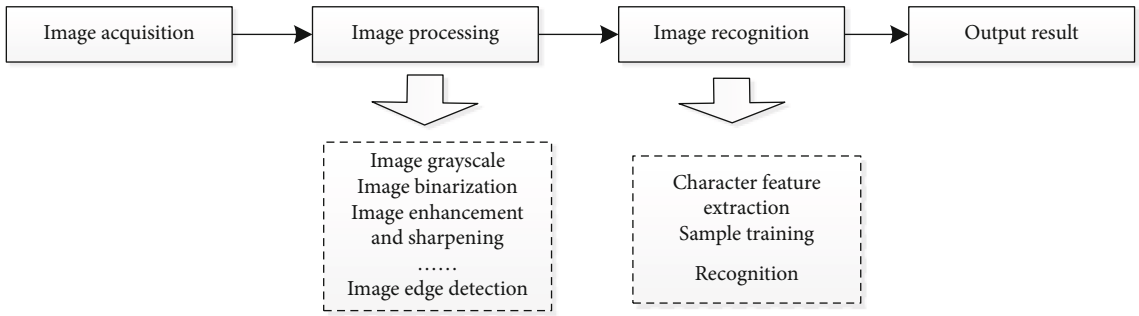

Figure 6: Image processing flow.

Table 4: Supplement of convolution neural network.

Purpose	New concept
It makes the convolution neural network more suitable for special processing of image data, and greatly reduces the limitations of traditional methods.	Local sensory angle Sparse weight Parameter sharing

Table 5: Flow comparison of two algorithms.

Object detection algorithm based on regression (one-stage algorithm)	Target detection algorithm for candidate areas (two-stage algorithm)
This kind of algorithm omits the candidate region generation stage	Select candidate regions on the input image
Feature extraction, target classification, and target regression are implemented directly in the same convolution neural network, which truly realizes end-to-end	Feature extraction and classification of candidate regions by convolution neural network

3.2. Selection of Target Detection Algorithm. As shown in Table 5 is the flow comparison of the two algorithms.

Then, as shown in Table 6, several main models under the two-stage algorithm are briefly summarized.

The one-stage algorithm can omit the candidate region generation stage. Therefore, in this study, according to the limitations of various literatures and experimental conditions, we decided to mainly select SSD model for multitarget recognition and detection based on computer vision; at the same time, we will also select YOLO model similar to SSD model to compare their performance and specific recognition work, which can better explain the situation and function of multi-target recognition and detection.

3.3. SSD Target Detection Algorithm

(1) SSD300 network architecture

SSD inherits the idea of regression from YOLO and has the running speed of YOLO and the detection accuracy of faster RCNN. SSD can complete target location and classification at one time. Among them, the shallow feature map plays a great role in target positioning, which contains position information. The deep feature map is of great significance to the classification of image objects, and it contains a lot of semantic information.

The SSD target detection algorithm adopts the feature pyramid structure detection way and utilizes each kind of feature function diagram of different size, such as Conv1, Conv2, Conv3, Conv4, Conv5, and Conv6. It can predict targets on characteristic maps of different receptive fields.

The reason why SSD model is chosen for target detection is mainly because SSD is improved on the basis of YOLO, which has more details optimized by YOLO, and SSD is widely used in many fields, so there are many data for reference, as shown in Table 7.

Feature pyramid prediction and SSD network architecture are shown in Figures 7 and 8:

Shallow feature maps are used to predict small-sized targets, while deep feature maps are used to predict large-sized targets, which improves the detection effect of small-sized targets. However, due to the lack of semantic information in the shallow feature map, SSD is still very poor in small target detection. At the same time, due to the nonuniformity of positive and negative samples, it is difficult to train.

(2) SSD training strategy

Training SSD is based on the fact that the output of ground truth information depends on the output of a fixed set of specific detectors, which can determine the end-to-end loss function and back propagation. Mapping

Table 6: Some main models of the two algorithms.

One-stage algorithm	Performance summary	Two-stage algorithm	Performance summary
YOLO series	YOLOv1 is very fast and can be monitored in real-time. The recognition effect of small targets is not good, and pictures with fixed size.	R-CNN	Ross Girshick proposed in 2014. Selective search algorithm is used instead of sliding window, which solves the problem of window redundancy and reduces the time complexity of the algorithm. Convolution neural network replaces the traditional hand-made feature extraction part, which can extract the image features more effectively and improve the external anti-interference ability.
SSD series	YOLOv2 solves the problem of difficult convergence and uses high-resolution pictures to fine-tune the network; anchor frame and convolution for prediction.	SPPNet	In 2015, Kaiming He and others proposed. The feature map is obtained by running convolution layer only once from the whole image, which greatly reduces the time consumed by feature extraction. Reduce the loss of image information and avoid repeated calculation of convolution features. The lifting speed is about 24 times to 64 times.
M2Det	YOLOv3 uses Darknet-53 as the network backbone and adopts FPN architecture.	Mask, R-CNN	In 2017, He et al. proposed Mask R-CNN, which combines faster R-CNN and FCN. The multiscale feature extraction ability of the model is strengthened, and the recognition of small target objects is more accurate. The detection speed is about 5 pieces per second.
CentripetalNet	YOLOv4 uses CSPDarknet 53 and many pervasive algorithms to achieve the best experimental results.	D2Det	Cao et al. proposed in 2020. At the same time, it solves the problems of accurate positioning and accurate classification. Dense local regression and DRP are introduced to extract accurate target feature regions from the first stage and the second stage, respectively, thus improving performance.

Table 7: SSD network classification.

Classification	Action
Standard network	This part of the network can classify images and remove the layers related to classification.
Pyramid network	This part of the network can be used to detect multi-scale feature mapping layer, so as to complete the detection of different sizes of targets.

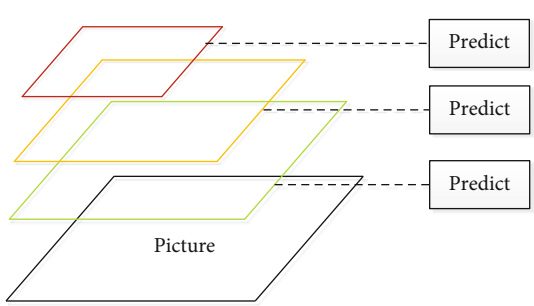

Figure 7: Feature pyramid prediction.

annotation information to default boxes is critical for some network models with default boxes. The total loss function includes position loss (loc) and confidence loss (conf).

$$L(x, c, l, g) = \frac{1}{N}\left(L_{conf}(x, c) + \alpha L_{loc}(x, l, g)\right). \tag{29}$$

Losses include classification and regression. The cross-entropy loss function of classified loss is shown in formula (30). SmoothL1 of regression loss is shown in formula (31).

$$L_{conf}(x, c) = -\sum_{i \in Pos}^{N} x_{ij}^{p} \log\left(\hat{c}_i^p\right) - \sum_{i \in Neg} \log\left(\hat{c}_i^0\right) \quad \text{where} \quad \hat{c}_i^p = \frac{\exp\left(c_i^p\right)}{\sum_p \exp\left(c_i^p\right)}, \tag{30}$$

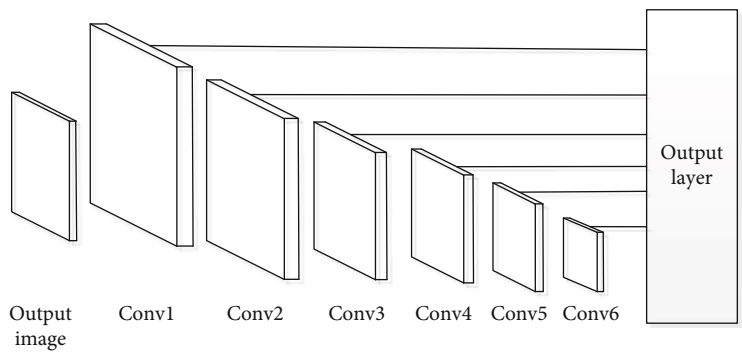

Figure 8: SSD network architecture.

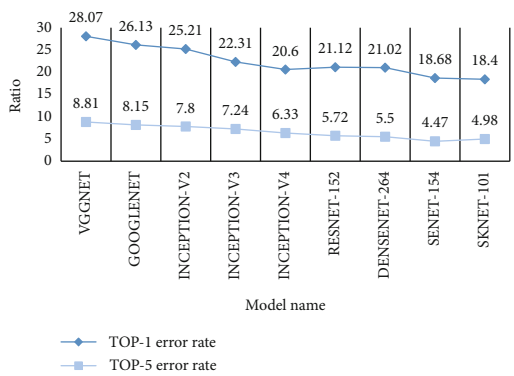

Figure 9: Performance comparison of some "CNN" models.

Table 8: Main evaluation indexes of COCO data set.

Indicators	Meaning
AP	The value of AP when IOU = 0.5: 0.05: 0.95
AP^{50}	The value of AP when IOU = 0.5
AP^{75}	The value of AP when IOU = 0.75
AP_S	AP value of small objects
AP_M	AP value of medium object
AP_L	AP value of large objects

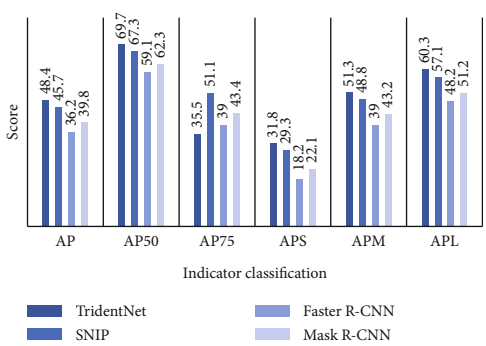

Figure 10: Target detection algorithm based on candidate regions.

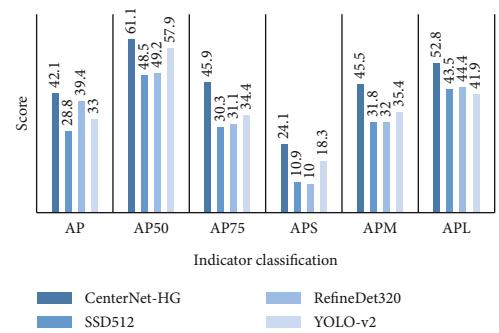

Figure 11: Object detection algorithm based on regression.

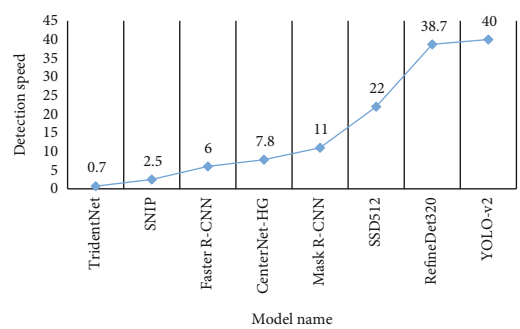

Figure 12: Comparison of detection speed of models.

$$L_{loc}(x, l, g) = \sum_{i \in Pos}^{N} \sum_{m \in \{cx, cy, w, h\}} x_{ij}^{k} \text{smooth}_{L1}\left(l_i^m - \hat{g}_j^m\right). \tag{31}$$

The receptive field in the shallow layer of SSD is smaller; for the deep layer, its receptive field is larger. The output of SSD is actually a convolution of multiple single outputs. Its training can be equivalent to splitting a complete image, and then dividing the image into countless small subimages to make a single output classification and positioning. SSD predicts the object category and position in the window; predict the background if there are no objects.

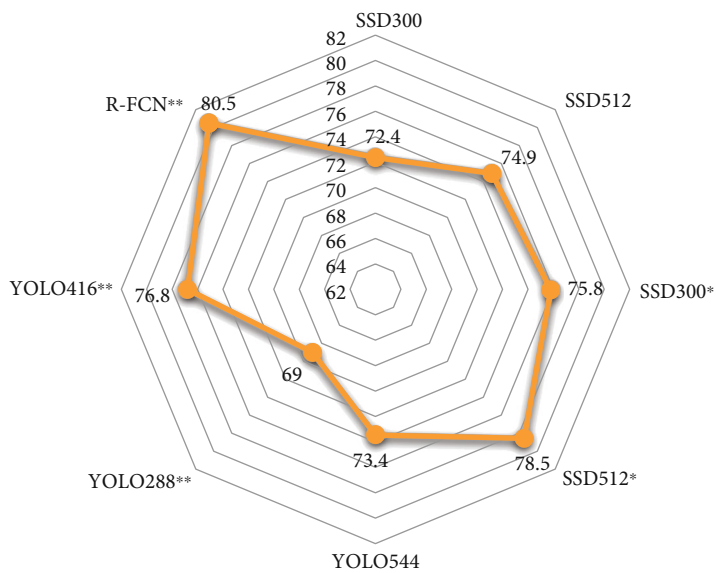

Figure 13: mAP performance metrics comparison.

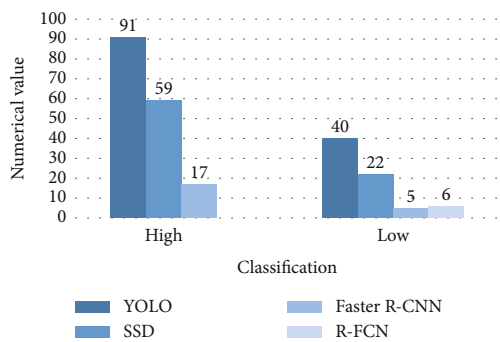

Figure 14: Maximum and minimum FPS under the same mAP.

4. Experimental Analysis

4.1. "CNN" Model Performance Comparison. We can use partial convolution neural network model to make a performance comparison, so as to highlight the strength of convolution neural network and the superiority of convolution method.

From the data shown in Figure 9, it is obvious that the error rate based on TOP-1 has dropped sharply from the original 28.07 to 18.40%; the error rate based on TOP-5 also decreased from 8.81% to 4.98%. Therefore, whether from the target demand or technical superiority, choosing a well-developed "CNN" model can help reduce the pressure and burden of target detection.

4.2. Performance Comparison on COCO Datasets. Evaluate the performance of the two algorithms, as shown in Table 8.

The details are shown in Figures 10 and 11. We can find from Figure 10 that if the algorithm chooses the candidate region method, with the refinement and improvement of the model, the accuracy of the detected results is obviously higher and higher, but the real-time situation cannot be detected all the time, which leads to the great drawback that cannot be overcome by this method. The model for the selection of the region is too complex, which virtually adds a lot of burden to the algorithm. The larger the model, the deeper the computation of the algorithm is. We can find from Figure 11 that the accuracy of regression algorithm is superior.

In order to evaluate the superiority of speed, we select some models of the two algorithms (TridentNet, SNIP, Faster R-CNN, CenterNet-HG, Mask R-CNN, SSD512, RefineDet320, and YOLO-v2) to compare the detection speed. As shown in Figure 12, the YOLO-v2 model has the fastest detection speed, and the TridentNet model has the slowest detection speed. Comparing the data of the two graphs, we can find that the speed of most regression algorithms is faster than that of candidate regions.

4.3. Comparison of SSD and YOLO. SSD and YOLO series models are the "darlings" in regression algorithms. In order to study the performance of models in multitarget recognition and detection, we choose a series of models of these two methods to compare and explain several performances.

(1) First, we select PASCAL VOC 2007 and PASCAL VOC 2012 data, and then use them to train SSD model and YOLO model. "$*$" means that the model applies small target data enhancement; "$**$" indicates that the model data results are tested by the VOC 2007 test set. One problem that needs attention is that because the test results of VOC 2007 are generally better than those of 2012, we specially selected the results of R-FCN in VOC 2007 in order to add cross-reference content. Finally, we can see from the diagram shown in Figure 13 that high-resolution images of the same model will have better mAP, but its processing speed will become slower

Figure 15: Model processing flow.

Table 9: Results analysis.

Results	Analysis
The training results based on VOC07 + 12plus (240000) are more accurate	This is because the training amount of 240,000 can make SSD have higher detection accuracy
The training results based on VOC07 + 12 (120000) have some error recognition	The training amount of 120000 is insufficient, so SSD generally uses multiple scale predictions of multiple scale feature maps and aspect ratio in images to determine the range of recognition targets, so as to separate and predict them.

Figure 16: Training result 1.

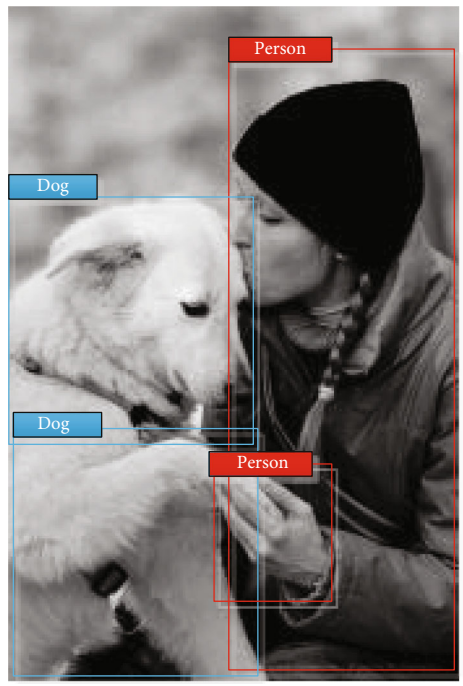

Figure 17: Training result 2.

(2) As shown in Figure 14, the highest FPS and the lowest FPS of YOLO, SSD, faster R-CNN, and R-FCN were compared under the same mAP. The input image resolution and feature extractor will affect the speed. In the figure, whether it is the highest FPS or the lowest FPS, YOLO's FPS is the highest, followed by SSD; however, the FPS data of the other two models, faster R-CNN and R-FCN, are very similar. By comparison, their FPS is very low, far less than the data of YOLO and SSD

4.4. Multitarget Recognition and Detection Based on SSD. In this section, choose clone-recursive directly on github, configure it according to the instructions and run it; GitHub provides a VOC-based model. Therefore, after careful consideration, we decided to use SSD300 model which has been trained on VOC 2007 and realized the detection of several pictures after simple prediction of trial operation results.

(3) As shown in Figure 15

The analysis of processing results is shown in Table 9: The processed picture is shown in Figures 16 and 17.

(4) We choose the model based on VOC07+12plus (240000). After the picture is processed, the situation of multi-target recognition and detection is shown in Figures 18–21

According to the test results, when there are multiple targets in an image, we can easily find that some targets in

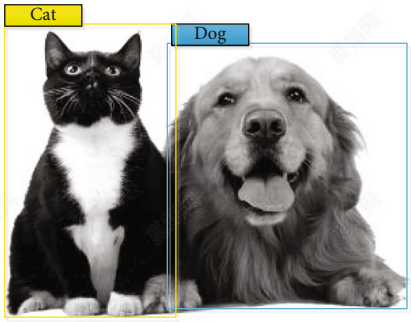

Figure 18: Test 1.

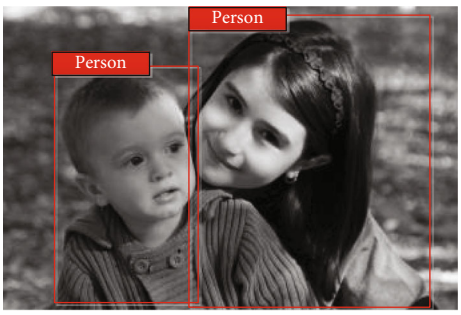

Figure 19: Test 2.

Figure 20: Test 3.

the image cannot be detected because of various problems: it may be a clear problem, and the edge of the target is blurred and difficult to distinguish. It may be that the target is too small to detect its existence. It is difficult to capture effective features due to incomplete recognition due to occlusion by

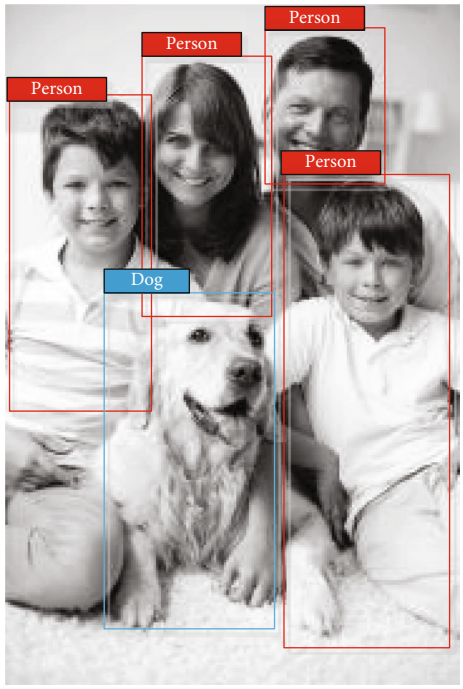

Figure 21: Test 4.

other targets. It is difficult to fully capture features during movement, and there are omissions in real-time tracking… These problems are waiting for us to actively solve.

It is difficult to detect small objects: the main reason is that the resolution of the image is very low, the feature expression ability is weak, and it is difficult to extract. The detection target is too small, resulting in low IOU, which makes the target have no corresponding anchor frame. In the training data set, large and medium-sized targets are more inclined to be detected, and small objects are difficult to be included.

The occlusion problem leads to the incomplete expression of features, which increases the difficulty of classification and location.

When detecting densely distributed targets, the position of prediction box of similar targets close to each other is difficult to determine. After NMS processing, it is easy to be regarded as a single object.

5. Conclusion

This paper combs the effects of several typical target detection algorithms, gives their performance comparison on number sets, and highlights the superiority of target detection algorithms based on convolution neural network. The research results of this paper show that

(1) CNN shows its unique feature ability and incomparable detection accuracy from many models, and the error rate can be reduced from 28.07% to 18.40%

(2) The selection of candidate region method in target algorithm is complex and difficult to control, and the larger the region, the more difficult it is to

calculate. The method based on regression is far beyond it in both precision and speed and is more suitable for the research of this subject

(3) When the mAP increases, the speed is forced to slow down. If the image resolution is high with the same model, the mAP will be high (SSD and YOLO models are often used)

(4) In image training, using VOC07 + 12plus model, the VOC detection with 240,000 training amount is most in line with the regulations, and the final effect is good

The effect of target detection is good, but based on the technology of computer vision, the existing target detection algorithm has more research space, which can be optimized and improved to improve the detection efficiency and accuracy of the algorithm, so that people can choose the most suitable algorithm when studying experiments. At present, target detection is mainly aimed at the recognition and detection in specific scenes. In complex natural life scenes, the recognition and detection of multiple targets are easily interfered by various self or environmental factors, such as small targets, blocked by other objects, too dense objects, which make it difficult to find targets, and difficult to identify and track them in real-time in moving scenes… These are a series of problems that researchers are waiting to solve.

Data Availability

The experimental data used to support the findings of this study are available from the corresponding author upon request.

Conflicts of Interest

The authors declared that they have no conflicts of interest regarding this work.

Acknowledgments

This research was supported by the Scientific and Technological Research Program of Chongqing Municipal Education Commission (Grant nos. KJZD-K202001901 and KJZD-K201901902), Chongqing Municipal Natural Science Foundation (Grant no. cstc2020jcyj-msxmX0666), and Chongqing Municipal Education Commission Humanities and Social Sciences Research Project (Grant no. 20SKGH277).

References

[1] G. Bradski and A. Kaehler, *Learning OpenCV: Computer Vision with the OpenCV Library*, O'Reilly Media, Inc, 2008.

[2] N. M. Oliver, B. Rosario, and A. P. Pentland, "A Bayesian computer vision system for modeling human interactions," *IEEE Transactions on Pattern Analysis and Machine Intelligence*, vol. 22, no. 8, pp. 831–843, 2000.

[3] E. Murphy-Chutorian and M. M. Trivedi, "Head pose estimation in computer vision: a survey," *IEEE Transactions on Pattern Analysis & Machine Intelligence*, vol. 31, no. 4, pp. 607–626, 2009.

[4] A. M. Andrew, "Level set methods and fast marching methods: evolving interfaces in computational geometry, fluid mechanics, computer vision, and materials science," *Kybernetes*, vol. 29, no. 2, pp. 239–248, 2000.

[5] P. Sinha, B. Balas, Y. Ostrovsky, and R. Russell, "Face recognition by humans: nineteen results all computer vision researchers should know about," *Proceedings of the IEEE*, vol. 94, no. 11, pp. 1948–1962, 2006.

[6] A. Criminisi and J. Shotton, *Decision Forests for Computer Vision and Medical Image Analysis*, Springer, London, 2013.

[7] K. Chen, X. Han, and T. Huang, "Target detection algorithm based on the movement of codebook model," *Science*, vol. 5, no. 2, 2012.

[8] F. Li, Fang Shuai, and X. Xinhe, "Human motion target detection based on computer vision," *Journal of Ordnance Engineering*, vol. 26, no. 6, pp. 766–770, 2005.

[9] D. Casasent, B. Kumar, and Y. L. Lin, "Subpixel target detection and tracking," *Journal of the American Veterinary Medical Association*, vol. 245, no. 9, pp. 992–992, 1987.

[10] Q. Pan and H. Zhang, "Key algorithms of video target detection and recognition in intelligent transportation systems," *International Journal of Pattern Recognition and Artificial Intelligence*, vol. 34, 2020.

[11] C. F. Zhang, Z. Y. Fang, and H. Q. Qu, "Information technology in an improved moving target detection algorithm," *Advanced Materials Research*, vol. 886, pp. 560–563, 2014.

[12] S. D. Blostein and T. S. Huang, "A tree search algorithm for target detection in image sequences," in *Proceedings CVPR'88: The Computer Society Conference on Computer Vision and Pattern Recognition*, pp. 690–695, Ann Arbor, MI, USA, 1988.

[13] G. Tao, Z. Yao, W. Ping, C. Wang, and J. Yang, "Automatic stable scene based moving multi-target detection and tracking," *Journal of Computers*, vol. 6, no. 12, pp. 2647–2655, 2011.

[14] R. Fang and C. Cai, "Computer vision based obstacle detection and target tracking for autonomous vehicles," *MATEC Web of Conferences*, vol. 336, article 07004, 2021.

[15] Y. D. Hu, Q. Xia, and R. Hou, "Computer vision-based displacement measurement with m-sequence target," *Smart Structures and Systems*, vol. 27, no. 3, pp. 537–546, 2021.

[16] C. Szegedy, W. Liu, Y. Q. Jia et al., "Going deeper with convolutions," in *Proceedings of the 2015 IEEE Conference on Computer Vision and Pattern Recognition*, pp. 1–9, Boston, MA, USA, 2015.

[17] T. Bouwmans, "Traditional and recent approaches in background modeling for foreground detection: an overview," *Computer Science Review*, vol. 11-12, pp. 31–66, 2014.

[18] A. W. M. Smeulders, D. M. Chu, R. Cucchiara, S. Calderara, A. Dehghan, and M. Shah, "Visual tracking: an experimental survey," *IEEE Transactions on Pattern Analysis and Machine Intelligence*, vol. 36, no. 7, pp. 1442–1468, 2014.

[19] W. L. Ouyang, P. Luo, X. Y. Zeng et al., "DeepID-Net: multi-stage and deformable deep convolutional neural networks for object detection," https://arxiv.org/abs/1409.3505.

[20] D. Maturana and S. Scherer, "VoxNet: a 3D convolutional neural network for real-time object recognition," in *Proceedings of the 2015 IEEE/RSJ International Conference on Intelligent Robots and Systems (IROS).*, pp. 922–928, Hamburg, Germany, 2015.

[21] S. F. He, R. W. H. Lau, W. X. Liu, Z. Huang, and Q. X. Yang, "SuperCNN: a superpixelwise convolutional neural network for salient object detection," *International Journal of Computer Vision*, vol. 115, no. 3, pp. 330–344, 2015.

[22] P. Dhankhar and N. Sahu, "A review and research of edge detection techniques for image segmentation," *International Journal of Computer Science and Mobile Computing*, vol. 2, no. 7, pp. 86–92, 2013.

[23] T. H. Rassem and B. E. Khoo, "Object class recognition using combination of color SIFT descriptors," in *Proceedings of the 2011 IEEE International Conference on Imaging Systems and Techniques (IST)*, pp. 290–295, Penang, Malaysia, 2011.

[24] S. Walk, N. Majer, K. Schindler, and B. Schiele, "New features and insights for pedestrian detection," in *Proceedings of the 2010 IEEE Conference on Computer Vision and Pattern Recognition (CVPR)*, pp. 1030–1037, San Francisco, CA, USA, 2010.

[25] S. Belongie, J. Malik, and J. Puzicha, "Shape matching and object recognition using shape contexts," *IEEE Transactions on Pattern Analysis and Machine Intelligence*, vol. 24, no. 4, pp. 509–522, 2002.

Hindawi
Journal of Sensors
Volume 2022, Article ID 9881935, 11 pages
https://doi.org/10.1155/2022/9881935

Research Article

Fluorescence Sensor Based on Polyaniline Supported Ag-ZnO Nanocomposite for Malathion Detection

Sintayehu Berhanu,[1] Fikradis Habtamu,[1] Yordanos Tadesse,[2] Fantahun Gonfa,[1] and Tesfaye Tadesse[1]

[1]*Department of Chemistry, Bonga University, Bonga, P.O. Box 334, Bonga, Ethiopia*
[2]*Department of Chemistry, Salale University, Fiche, P.O. Box 245, Fiche, Ethiopia*

Correspondence should be addressed to Sintayehu Berhanu; sintayehuberhanu38@gmail.com

Received 19 November 2021; Accepted 19 February 2022; Published 22 March 2022

Academic Editor: Zhenxing Zhang

Sensitive and selective determination of harmful organophosphate is rigorously fundamental due to its large negative influence on the environment and human health. Ultrasensitive fluorescence nanocomposite was developed for malathion detection which was based on electrostatic interaction between polyaniline and Ag-ZnO nanocomposite. The nanocomposite (Ag-ZnO/PANI) was prepared via the sol-gel technique next in situ oxidative polymerization of polyaniline. The synthesized nanocomposite was characterized by FT-IR, XRD, SEM, UV-vis, and fluorescence spectroscopic techniques. The fluorescence intensity of the nanocomposite was quenched by MA, which was proportional to the concentration of MA in the range of 0–1000 nM, with a detection limit of 13.2 nM. The proposed method was sensitive, selective, easy in design, and fast in operation. Therefore, it has been effectively used for MA detection in agricultural products with suitable recovery.

1. Introduction

Organophosphate pesticides (OPs) have been utilized worldwide because of their particular benefits such as ease of synthesis, low environmental persistence, and the moderately high death rate for insects [1, 2]. Inferable from their persistence, toxicity, and bioaccumulation, they make long-term harm to the environment and living species [3, 4]. Specifically, malathion (MA) is an organophosphate pesticide which is mainly used to enhance food production and control pests and increases harvest all over the world. However, unreasonable use of OPs results in various adverse effects on human beings, wildlife, and the environment [4–6].

Consumption of agricultural products which contain excessive amounts of malathion could combine with certain cholinesterases (such as acetylcholinesterase (AChE)) in the human body, cause serious damage to human nerve function, and even cause unsteadiness, shortness of breath, cerebral pain, loss of motion, respiratory damages, aggravated asthma, and death [3–6]. Several methods have been developed over the past few years for the determination of OPs, such as high-performance liquid chromatography [6], gas chromatography [7], enzyme-linked immune sorbent assays [8], colorimetric sensing [9], and fluorescence spectroscopy [1, 10–12].

These ordinary techniques are sensitive and accurate, but they suffer from numerous drawbacks, including substantial instruments, time-consuming processes, significant expense, long analysis time, the necessity of highly trained personnel, and the inability to be used for continuous monitoring [13]. Recently, the OP pesticide biosensors advanced to AChE inhibition. Furthermore, biocompatible nanomaterials in biosensors improve their performance by augmenting the surface area needed for AChE immobilization as well as reducing the response time [14].

Conversely, measurements based on the quenching of the photoluminescent characteristics of nanomaterials have been widely used for the detection of DNA, proteins, microorganisms, metal ions, and others. It has different advantages such as high sensitivity and selectivity, fast response time, visualization, and being inexpensive and accurate for

qualitative and quantitative detection of Ops [1, 5]. Considering the previous works, enzyme-free sensors based on metals or their oxides like CuO [15], CeO_2 [16], Fe_2O_3 [17], MnO_2 [18], and others have been utilized due to their minimal expense, excellent electrocatalytic activity, and the capacity to conduct electrochemical reactions at lower potentials [15–18].

Zinc oxide (ZnO) is perhaps the most encouraging material in sensory applications because of its high conductive electron movement and great adsorption quality [19]. However, limitations like low sensitivity, poor selectivity, and high working temperature are as yet difficulties related to these sensors [20]. To beat the drawback and to upgrade the detecting characteristics, the modification supported by different metals and organic molecules has drawn extensive interest [19–24].

There are several reports on the upgrading of the electronic, catalytic, and sensorial potential of ZnO by incorporating noble metals such as Cu, Pt, Co, Pd, and Ag [21, 25, 26]. Among these, Ag merits special consideration due to its stability, conductivity, nontoxic nature, and comparatively less expensive. The incorporation of Ag nanoparticles (NPs) with ZnO in the polymer matrix upgrades the mechanical properties and modifies the surface and conductivity of ZnO [21, 26]. Polyaniline (PANI) is also an important polymer with high conductivity and an extensional conjugated electron framework. Supporting the inorganic filler with this organic polymer is used to tune the optical, electrical, and photocatalyst properties as well as upgrade the detecting capability of ZnO [25, 27].

Subsequently, in the present study, Ag-decorated ZnO supported by PANI (Ag-ZnO/PANI) NCs was synthesized. The NC crystalline size, morphological properties, optoelectronic properties, and surface functional groups were characterized by X-ray diffraction, scanning electron microscope, UV-vis, and FT-IR techniques. The sensitivity and selectivity of the NCs to MA were studied by using a fluorescence spectrophotometer.

2. Experimental Methods

2.1. Reagents and Chemicals. Silver nitrate (169.87 g/mol), Zinc(II) acetate dehydrate (183.48 g/mol), aniline (93.13 g/mol), sulphuric acid (98 g/mol), sodium hydroxide (40 g/mol), oxalic acid (90.03 g/mol), hydrochloric acid (36.46 g/mol), ethanol (46.07 g/mol), ammonium persulfate (228.18 g/mol), and malathion (330.358 g/mol) were used. All chemicals were of analytical grade (Sigma-Aldrich) and used as received without further purification.

2.2. Synthesis of Ag-ZnO Nanoparticle. Silver-doped zinc oxide (Ag-doped ZnO) NPs were prepared by a sol-gel method [28]. 100 mmol of Zn(II) acetate dehydrate was dissolved in 200 mL of ethanol solution and stirred for 30 min. Separately, oxalic acid dehydrate (55.8 mmol) was dissolved in 80 mL of ethanol solution which was added slowly with constant stirring for 3 hr to the Zn(II) acetate solution until a white solution was formed. To this solution, 4% wt of silver nitrate was added and stirred for an additional 3 hr. The solution was dried on a water bath to form a xerogel. The xerogel was calcined at 500°C in a muffle furnace at a heating rate of 5°C/min. Then, it was kept at this temperature for 2 hr, lastly obtaining a dark brown powder of Ag-ZnO after grinding using the motor pestle.

2.3. Synthesis of Ag-ZnO/PANI Nanocomposite. The synthesis of Ag-ZnO/PANI NCs was carried out as follows: 2 g of Ag-ZnO NPs were added into 200 mL of 1 M H_2SO_4 solution. 2 mL of aniline was added dropwise to the solution and stirred for 30 min until a silvery-white color was formed. A solution of 35.1 mmol of ammonium persulfate oxidant in 100 mL of H_2SO_4 solution was added dropwise under a refrigerator and stirred for 30 min. The solution color was changed into dark green confirming the formation of the Ag-ZnO/polyaniline hybrid.

It was kept at room temperature for 24 hr, and then, the solution was filtered and washed with distilled water until the filtrate became colorless. Finally, the precipitated material was filtered and dried in a vacuum oven at 80°C for 6 hours. Thus, Ag-ZnO/PANI NC was prepared [29, 30].

2.4. Structural Characterizations. X-ray diffraction patterns were obtained using a BRUKER D8 (West Germany) and equipped with Cu Kα radiation (λ = 1.5405 Å) at room temperature in the scan range 2θ between 10 and 90°.

Accelerating voltage and the applied currents were 40 kV and 30 mA, respectively. The morphologies of the nanocomposites were done by using EVO 18 SEM. The absorbance was recorded by using the SPECTRONIC GENESYS 2PC UV-vis spectrophotometer. Fourier transform infrared (FT-IR) spectroscopy was used in the region between 4000 and 400 cm^{-1} to determine the functional groups and surface structure of the samples by a model of Shimadzu 8400S (German) using KBr plates. The fluorescence spectra were measured using Shimadzu RF 5301PC spectrofluorimeter.

2.5. Detection of MA and pH Optimization. A stock solution of 50 mg/L of MA was prepared in 100 mL of double distilled and deionized water. Sensing of OPs was performed by preparing a series of concentrations and by adjusting the pH (7) to the optimum at room temperature. The MA sensing was performed by monitoring the fluorescence behavior of the Ag-ZnO supported by the PANI NC solution.

The synthesized NC was dispersed in distilled water, and the spectra were recorded at different excitation wavelengths from 350 to 430 nm with a gap of 10 nm before the addition of OPs. Then, the fluorescence intensity of the aqueous solution of the NC was measured with a consecutive addition of 0.01 M of MA at 380 nm. To calculate the analytical parameters, the slope of the calibration curve was used based on Equation (1) [31]:

$$I_0 - \frac{I}{I_0} = m[\mathrm{MA}] + b, \tag{1}$$

where I_0 and I represent the fluorescence intensities of Ag-ZnO/PANI in the absence and presence of MA, m-slope, and b-intercept and [MA] is the concentration of MA. The

limit of detection (LOD) can be calculated using the equation of LOD =3SD/slope, where SD is the standard deviation of the calibration curve [24]. The quenching efficiency (QE) was estimated using Equation (2) [31].

$$QE = I_0 - \frac{I}{I_0}. \quad (2)$$

To optimize the experimental condition, the reaction times between the NCs and MA were investigated. Furthermore, the effect of pH was studied in the pH range of 3 to 11.

Each time, the pH was maintained by using 0.1 M HCl and 0.1 M NaOH measured by a pH meter under a constant excitation wavelength and concentration.

2.6. Detection of Real Sample. The methodology was applied for MA sensing from two different agricultural products (potatoes and tomatoes) which were purchased purposively from a local market. The samples were allowed to be dried, then grounded and spiked with MA standards of 0.05, 0.1, and 0.15 M and 0.25 μM, separately. Then, they were carefully standardized and formerly allowed to stand for 24 hr. The powders were mixed with 30 mL ethanol and 5 mL water, with ultrasonic extraction for 1 hr, and centrifuged for 30 min at 4000 rpm. The supernatant was transferred and evaporated at 50°C [32].

Finally, the fluorescence spectra of the NCs and the dry residue solution were measured in ultrapure water. The selectivity of this technique was studied by evaluation of fluorescence intensity using UV-vis spectra taken before and subsequent addition of a series of Mg^{2+}, glucose, CO_3^{2-}, Cl^-, and Cd^{2+} [30, 33].

3. Results and Discussion

3.1. Characterization of the Nanocomposite

3.1.1. FT-IR Spectra. FT-IR technique was used to determine the functional groups of PANI and Ag-ZnO. The peak at 608 cm^{-1} in Figure 1(b) is attributable to the metallic stretching of Ag-O, and the small peak centered at 609 cm^{-1} in Figure 1(a) is due to the Ag-O group revealing the existence of Ag. In addition, the bands at 492 cm^{-1} showed Zn–O bond observed. The presence of peaks due to ZnO and Ag confirms the effective interaction of their elements. All these effects indicated well incorporation as well as the presence of inorganic filler (Ag-ZnO nanoparticle) into the host matrix.

The absorption band of PANI has occurred at 1126 cm^{-1} which is due to stretching vibration of quinoid ring Figure 1(a). The peak at 3442 cm^{-1} is attributable to the free N–H vibrational stretching of the primary and secondary amine groups. Similarly, the peaks associated with the C-H and C-N stretching vibrations are located at 2932 and 1470 cm^{-1}, respectively. In addition, the peak at 1293 and 801 cm^{-1} corresponds to the C-N in-plane deformation and a = CH in-plane vibration of PANI Figure 1(b). Thus, from the FT-IR spectra, it is confirmed that the NPs existent in the macromolecular chain of PANI and aniline monomers

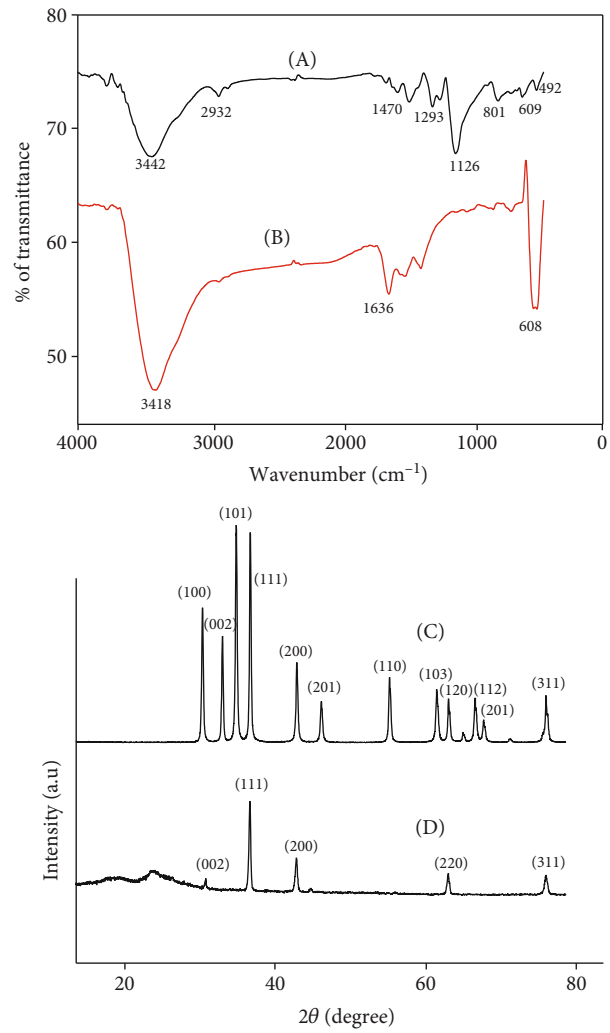

Figure 1: FT-IR spectra of Ag-ZnO/PANI (a) and Ag-ZnO (b); XRD patterns of Ag-ZnO (c) and Ag–ZnO/PANI NCs (d).

are successfully polymerized on the surface of Ag-ZnO NPs confirming that the PANI is existing in the NCs.

3.1.2. XRD Analysis. The XRD patterns of the Ag-ZnO and Ag-ZnO/PANI are shown in Figure 1. As shown in Figure 1(c), diffraction peaks located at $2\theta = 31.79$, 34.44, 36.27, 47.55, 62.87, 67.97, and 69.11° are in good agreement with (100), (002), (101), (102), (110), (103), (112), and (201) crystal plane of wurtzite structure of ZnO (JCPDS card.No.75-576).

The reflection planes at (111), (200), (120), and (311) show the characteristics of face-centered cube Ag metal in Ag-ZnO NPs (JCPDS, No. 04-0783). The average crystal grain size of Ag-ZnO NPs can be calculated according to the Scherrer equation (Equation (3)) [34], which estimated is as 35.68 nm [35, 36].

$$D_{hkl} = \frac{k\lambda}{\beta_{hkl}} \cos\theta_{hkl}, \quad (3)$$

where D_{hkl} is the particle size which is perpendicular to the

normal line of the plane ($k = 0.9$, $\lambda = 0.15405$ nm) (wavelength of X-ray), β_{hkl} is the FWHM of the diffraction line, and θ is the diffraction angle of *hkl*.

In the hybrid of Ag-ZnO/PANI, the diffraction peak of PANI was overlapped with the peak of Ag-ZnO, which results in a weak peak in the composite. The characteristic peaks corresponding to the reflection of (111), (200), (220), and (311) crystal planes were shown as 38.06, 44.23, 64.36, and 77.4°, respectively. It can be observed from Figure 1(d) that two broad amorphous peaks about $2\theta = 18°$ and 25.42° are related to the planes of the PANI molecular chain.

The average crystal size was calculated at 38.06, 44.23, and 64.36°, and the average size of the NCs estimated is about 31.52 nm. The diffraction peaks of Ag-ZnO NPS move slightly towards the direction of the 2θ decrease in the Ag-ZnO/PANI NCs, and there is variation in broadness and intensity which is due to the strong interfacial interaction among Ag-ZnO and the polymer of aniline [30, 35].

3.1.3. Morphology. Morphological features of the as-synthesized Ag-ZnO and Ag-ZnO/PANI composites are shown in Figure 2. The Ag-ZnO NPs show an irregular morphology Figure 2(a) and ensure a certain extent agglomeration, which is because the radius of Zn is smaller than that of Ag, and the two NPs have different valence states. Consequently, there are some variations between them in morphology. Ag-ZnO/PANI NCs Figure 2(b) reveal that PANI is coated on the surface of Ag-ZnO, and the image showed an aggregate of particles with no distinct morphology, but brighter spots on the surfaces possibly represented Ag metal on the nanocomposite.

3.1.4. UV-vis Spectra. UV-vis spectrum of PANI NPs is shown in Figure 3(a), and the characteristic band was observed at 415 and 310 nm with a bandgap of 2.73 eV. The absorption peak observed at this two-point is expected for aromatic nuclei with π-π $*$ electronic transitions and charge transfer from the benzenoid ring to the quinoid rings [30]. The UV-vis spectrum of Ag NPs is shown in Figure 3(b) with a strong absorption peak of about 418 nm with a bandgap of 2.8 eV, which is attributed to the surface plasmon resonance, which confirms the symmetric and narrow size of Ag NPs [37].

The UV-vis spectra of Ag-ZnO and Ag-ZnO/PANI NC are presented and compared in Figures 3(c) and 3(d). The Ag-ZnO particles represent a sharp absorption peak around 430 nm corresponding to the bandgap of 2.61 eV, and the modification of the ZnO by Ag significantly affects the bandgap [31, 38]. As expected, the Ag-ZnO particles supported by PANI could expand the wavelength response to longer. The central absorption edge for Ag-ZnO/PANI rose at 470 nm, attributable to the 2.42 eV bandgap [30].

According to Rahman et al. [38], Ag-ZnO NPs exhibit lower bandgap energies compared to ZnO. It is observed that the characteristic peaks appear in Ag-ZnO/PANI NCs with a redshift in the peak position after the addition of PANI. This substantial increase in wavelength may be due to the interaction and synergism between Ag, ZnO, and PANI within NCs. This can simplify the electron excitation with relatively low energy for enhanced detection of the malathion.

3.1.5. Photoluminescence Spectra. The photoluminescence spectra of ZnO and Ag-ZnO NPs at excitation wavelengths of 360 and 370 nm are shown in Figures 3(e) and 3(f). Broad emission bands from 380 to 490 nm and 450 to 600 nm are shown for ZnO and Ag-ZnO NPs, respectively. To study the fluorescence properties of Ag-ZnO/PANI NCs, the emission spectra can be used to describe the recombination method of photogenerated holes and electrons by the fluorescence emission intensity. The good emission intensity is related to the recombination of photogenerated charge transporters with a short lifetime. The departure of the photogenerated transporter, holes, and electrons is large because of a longer lifetime, which allows weakening of the intensity in the fluorescence spectra [37]. The maximum emission fluorescence spectrum of Ag-ZnO/PANI NCs was obtained by exciting the NCs at the excitation wavelength of 380 nm (Figure 3(g)) with a range of 510-630 nm band centered at 581 nm.

3.2. Optimization of Experiments. The stability of the sensor is fundamental; the effect of pH on fluorescence intensity in the presence of 1 μM MA solution is studied and carried out in the pH range of 3 to 11. Figure 4(a) shows that the change in pH of the solution had an observable change in the fluorescence intensity of the NCs and MA. The fluorescence had a maximum intensity at neutral pH (pH = 7). However, the fluorescence spectra of Ag-ZnO/PANI+MA are slowly declining again with further increasing or decreasing the pH from 7. This can be described depending on the protonation and deprotonation of the amine groups at the polyaniline surface and the carbonyl, sulfide, or methoxy group of MA.

It is stated that the benzenoid rings are the reason for the fluorescence emission, whereas at low pH the PANI is protonated and the quinoid rings act as a fluorescence quencher. Moreover, at low pH, the aggregation of Ag-ZnO/PANI is established by the action of intramolecular hydrogen bonds with the carbonyl, methoxy, or sulfide groups of MA on the surface of the Ag-ZnO/PANI+MA [31].

Moreover, at higher pH (8–11), the deprotonation of amino moieties of PANI has created a negative charge cloud on the surface and made anionic layers which undergo strong electrostatic interaction with different functional groups of MA. While at neutral pH there is no protonation or deprotonation of Ag-ZnO/PANI NC and MA, in addition, the maximum fluorescence is achieved. Therefore, we chose pH = 7 as the experimental condition.

Figure 4(b) illustrates the quenching efficiency of MA with increasing reaction time. Upon addition of 2 μM MA into the Ag-ZnO/PANI NC at pH 7, the fluorescence quenched quickly, and the fluorescence intensity nearly reached its lowest value after 30 sec depending on this result; the reaction time of 2 min seems to be selected for the detection of MA.

3.3. Quenching Mechanism of Sensor. The most possible mechanism for the fluorescence enhancement of Ag-ZnO/

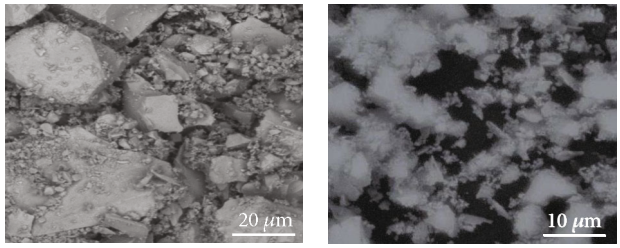

(a) (b)

Figure 2: SEM image of Ag-ZnO (a) and Ag-ZnO/PANI (b).

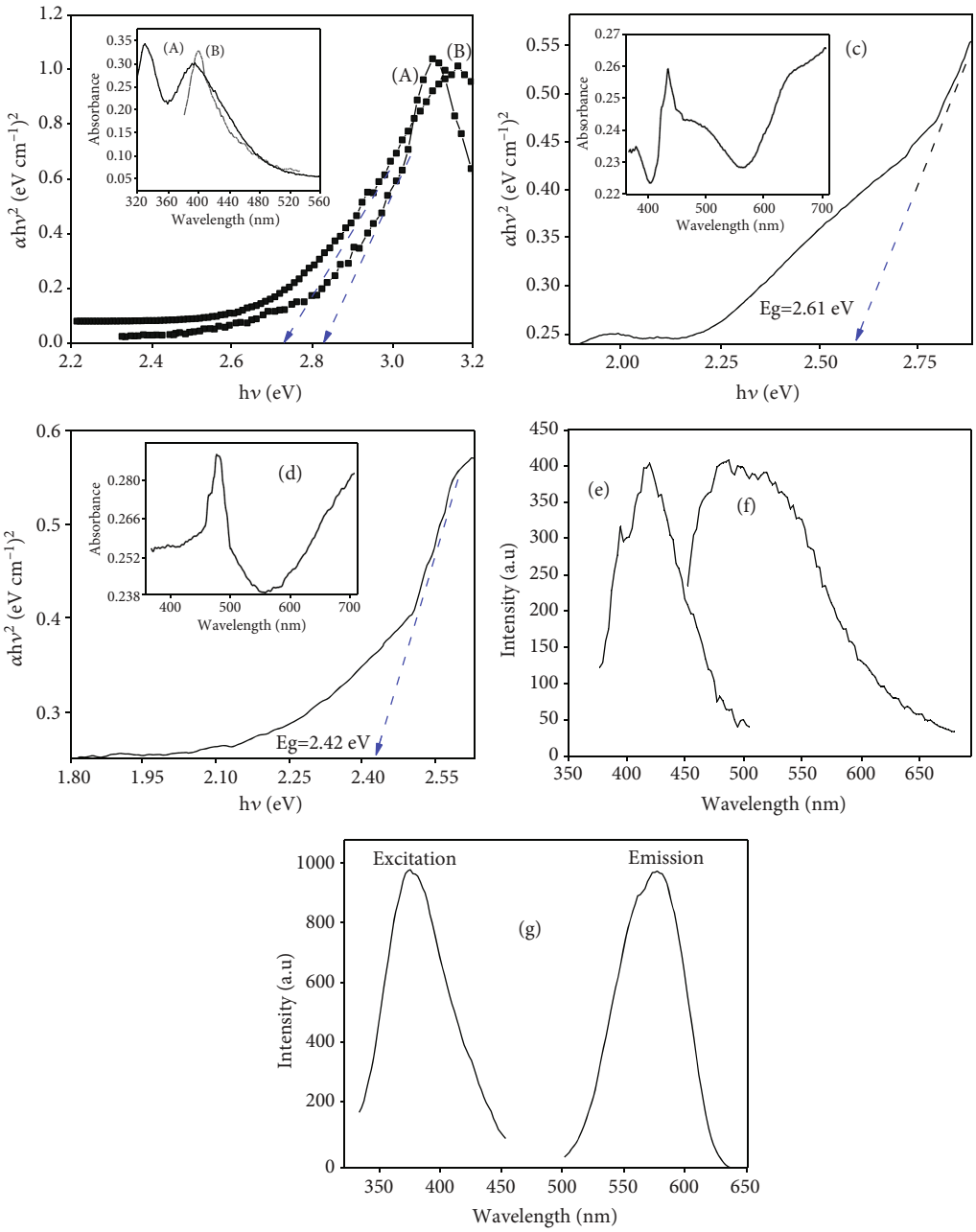

Figure 3: UV-vis absorption spectra of (a) PANI NPs, (b) ZnO NPs, (c) Ag-ZnO NPs, and (d) Ag-ZnO/PANI NCs and (e) fluorescence of ZnO NPs, (f) Ag-ZnO NPs, and (g) excitation and fluorescence emission spectrum of Ag-ZnO/PANI NCs.

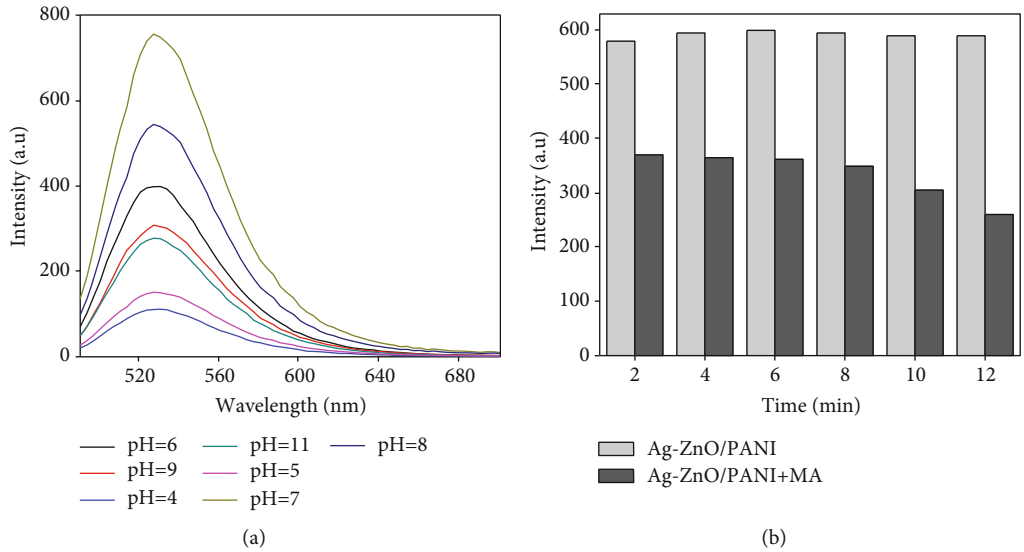

Figure 4: (a) Variation of fluorescent intensity in different pH of solutions using 1 μM of Ag-ZnO/PANI NCs and (b) the effect of reaction time on the fluorescence intensity of the Ag-ZnO/PANI + MA (2 μM) at pH 7.

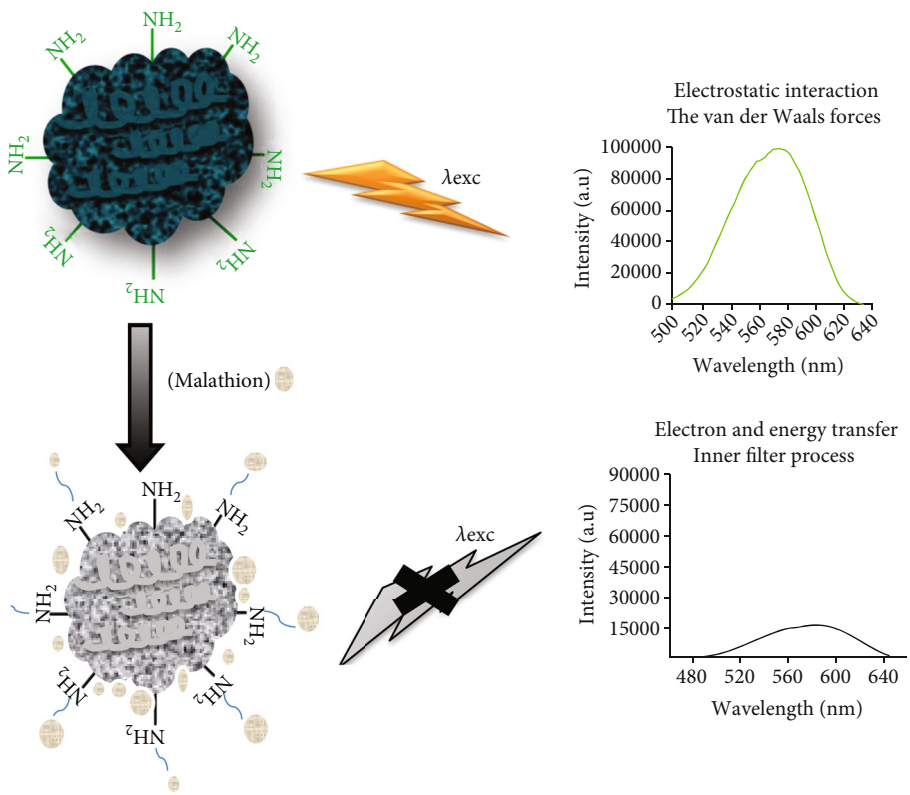

Figure 5: Schematic illustration of MA detection using Ag-ZnO/PANI NCs fluorescence sensor.

PANI NCS due to PANI adsorption onto Ag-ZnO NPs is based on the van der Waals force as well as the electrostatic force of interaction. A large number of delocalized electrons on the amine groups of PANI and the inorganic filler allow moderate electrostatic interaction. Such electrostatic effect is the main reason for the interaction between Ag-ZnO and PANI [39].

Generally, the quenching of the fluorescence spectra of Ag-ZnO/PANI NCs by MA is shown schematically in Figure 5, which possibly occur due to the inner filter process and electron and energy transfer. Inner filter effect needs an overlap

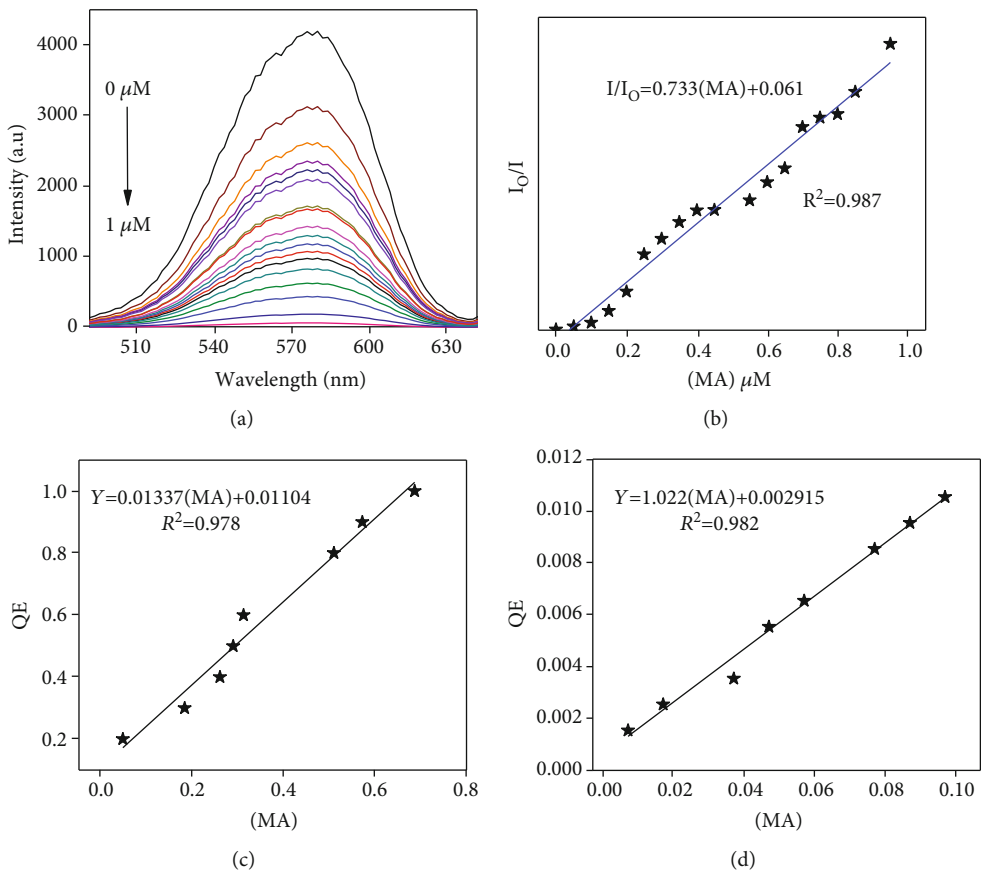

Figure 6: (a) Fluorescence quenching of Ag-ZnO/PANI NC with increasing concentrations of MA, (b) linear relationship plot representing Io/I and concentration of MA, I_o and I are the fluorescence intensities of Ag-ZnO/PANI nanocomposite in the absence and presence of MA, (c) QE versus MA concentration from 0.1 to 0.8 μM, and (d) from 0.01 to 0.1 μM at pH 7 and λex = 380 nm.

between the absorption spectrum of the MA, the excitation spectrum, and the emission band of the Ag-ZnO/PANI NC.

The absorption spectra of MA can be shielded as part of the radiation from the excitation of the Ag-ZnO/PANI NC, and the MA can absorb the emitted light by the Ag-ZnO/PANI NC. Additionally, the spectral overlap between the absorption peaks of MA and the absorption and emission spectra of Ag-ZnO/PANI NC allows the inner filter effect and subsequently reduces the intensity of the emission spectra.

Furthermore, the electron-donating amine groups of polyaniline can strongly interact with carbonyls as well as sulfide groups of MA. This effect is also told that the quenching mechanism is not associated only with the inner filter effect process but also forms the aggregate of the compound [30, 31, 37, 39, 40].

In the standard state, the fluorescence quantum yield (QY) of Ag-ZnO/PANI NCs was calculated relative to the integrated fluorescence emissions of L-tryptophan (standard solution of amino acids; QY = 0.1435) fluorescent with similar optical properties by using Equation (3) [41, 42].

$$\Phi_F = \Phi_{F(\mathrm{std})} \times \frac{F \times A_{\mathrm{std}} \times n^2}{F_{\mathrm{std}} \times A \times n_{\mathrm{std}}^2} \times \frac{F \times A_{\mathrm{std}} \times n^2}{F_{\mathrm{std}} \times A \times n_{\mathrm{std}}^2}, \quad (4)$$

where F and F_{std} are the fluorescence area of the sample and the standard amino acid, respectively; A and A_{std} are the absorbance of the NCs and standard amino and; and n and n_{std} are the refraction index of the NCs and the standard amino acid. The QY of Ag-ZnO/PANI NCs is 0.149 ≈ 15%. This value is approximately similar to the QY of the standard L-tryptophan that reported by Kirby and Steiner [43].

3.4. Sensitivity and Selectivity for MA. The sensitivity of the sensor is one of the main aspects of analysis [44]. The intensity of the NC recovers proportionally with the concentration of malathion. To check the validity of this method, we used Ag-ZnO/PANI NC to detect MA in optimum conditions. An arrangement of MA solution composed of 0-1 μM together with an appropriate amount of Ag-ZnO/PANI NCs was used to measure the fluorescence spectra.

Fluorescence intensity of the maximal emission at 571 nm was observed, which varied with the concentration of MA Figure 6(a). The blue shift (~10 nm) observed revealed the formation of an aggregate of compounds. Although, the fluorescence intensity of the NPs decreased with increasing amounts of MA and the fluorescence quenching ratio was proportional to the MA concentration of 0.01-0.95 μM.

There are two linear regions of correlation in the MA concentration range of 0.01–0.1 μM ($R^2 = 0.990$) and 0.1–

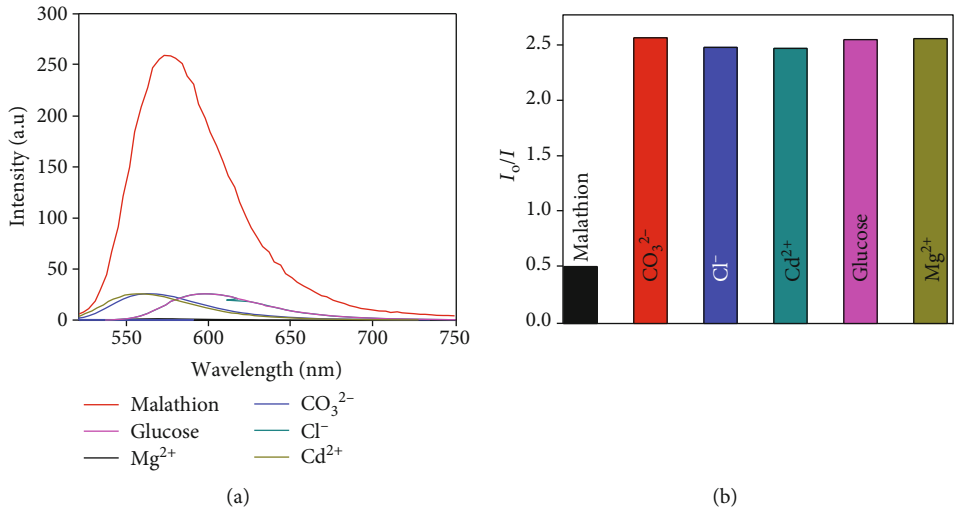

Figure 7: (a) The fluorescence intensity of Ag-ZnO/PANI NC with different interferences (Mg^{2+}, glucose, CO_3^{2-}, Cl^-, and Cd^{2+}, all interference concentrations of 0.125 μM) and MA (0.5 μM) as the Ag-ZnO/PANI NC as control and (b) UV-vis spectral variation of Ag-ZnO/PANI NC upon additions of various OPs.

Table 1: Determination of MA spiked in commercial samples.

Sample ($n = 5$)	Spiked (μM)	Found (μM/μg/L)	Recovery (%)	RSD (%)
Potato	0	0	0	0
	0.05	0.041	82	2.63
	0.1	0.093	93	2.74
	0.15	0.11	96	1.32
	0.25	0.189	93.3	2.87
Tomato	0	0	0	0
	0.05	0.043	86	2.45
	0.1	0.089	89	3.11
	0.15	0.109	72	1.41
	0.25	0.179	71.6	1.93

RSD: relative standard deviation.

0.8 μM ($R^2 = 0.987$) as shown in Figures 6(c) and 6(d), respectively. This shows that the quantitative measurement of MA using Ag-ZnO/PANI NCs sensor can be accomplished with different sensitivities (slopes of the lines) of 1.022 and 0.0133 μM according to the range of detection. The limit of detection acquired from the calibration line is 0.0081 μM (Figure 6(b)). It is found that the NC has a reasonable limit of detection for MA; therefore, the result indicates the NC was sensitive enough to monitor MA concentration.

To check the selectivity performance of the sensor towards MA detection, a similar experiment was performed with different interference such as Mg^{2+}, glucose, CO_3^{2-}, Cl^-, and Cd^{2+} Figure 7(a) using a fluorescence spectrophotometer. The shape and band maxima of the fluorescence spectra remain unchanged, and no other emission towards longer wavelengths was noticed except for the redshift (~19 nm) of glucose due to interaction with NCs. This observation suggests that the weak fluorophore–quencher interaction does not change the spectral of NCs.

The NC also showed high selectivity on UV-vis spectra Figure 7(b). Apart from MA, no other ion-induced absorption maximum shift. Furthermore, the interference investigation of these OPs indicated the NC was capable to be applied to complex environments with small interference from other ions. Hence, the fabricated sensor is quite selective and specific towards OPs on both fluorescence and UV-vis spectra.

3.5. Analysis of MA in Real Samples. The pretreated potato and tomato were added into Ag-ZnO/PANI, and the data were collected by a fluorescence spectrophotometer, and a calibration curve was used to study the spiked experiments. The results of the experiment are given in Table 1. Four samples were not detected in the absence of spiked MA, and those recovered were in the range of 91.0–99.6% and

Table 2: Comparison of performance of different MA probing methods.

Fluorescent probe	LOD (detection range)	Recovery (%)	Reference
TPCA-β-Cyclodextrin @AgNPs	0.01 μg/mL (0.1-25 μg/mL)	83-101	[10]
Eu(III)–Bathophenanthroline	0.92 mM	—	[11]
Magnetic-assisted FAM-apt	5.48 μg/mL	109.6	[12]
Apta-LFB with quantum dots nanobeads and Au nanostars	2.24 nM	—	[45]
Apt-AuNPs	4 pM (10 pM-1 μM)		[46]
Apt-SERS	500 nM-10 μM		[47]
Ag-ZnO/PANI	0.132 μM	92.0–99%	This work

LOD: limit of detection.

92.8–95.6% with acceptable results. The relative standard deviation (RSD) ranges were 1.19–5.05% and 4.01–5.06%, respectively. The sensitivity and selectivity of this method were comparable with most of the informed methods. A comparison between this work and other reported systems for MA sensing in detection limit (LOD) or linear range is summarized in Table 2.

4. Conclusion

In summary, a novel ultrasensitive fluorescence quenching probe based on Ag-ZnO/PANI NC was developed for MA detection, which has a detection limit of 0.132 μM. The fluorescence of Ag-ZnO/PANI NC is strongly quenched by MA and has several uses such as fast response time, good stability, high selectivity, and sensitivity. Additionally, the Ag-ZnO/PANI NC has been effectively used for MA detection in agricultural products with suitable results.

Data Availability

No data were used to support this study.

Conflicts of Interest

All authors declare that they have no conflict(s) of interest.

Acknowledgments

The authors are thankful for the financial support provided by the Ministry of Science and Higher Education of Ethiopia.

References

[1] R. Bala, A. Swami, I. Tabujew, K. Peneva, N. Wangoo, and R. K. Sharma, "Ultra-sensitive detection of malathion using quantum dots-polymer based fluorescence aptasensor," *Biosensors and Bioelectronics*, vol. 104, pp. 45–49, 2018.

[2] Q. Lang, L. Han, C. Hou, F. Wang, and A. Liu, "A sensitive acetylcholinesterase biosensor based on gold nanorods modified electrode for detection of organophosphate pesticide," *Talanta*, vol. 156, pp. 34–41, 2016.

[3] N. I. Valente, S. Tarelho, A. L. Castro, A. Silvestre, and H. M. Teixeira, "Analysis of organophosphorus pesticides in whole blood by GC-MS-μECD with forensic purposes," *Journal of Forensic and Legal Medicine*, vol. 33, pp. 28–34, 2015.

[4] Q. Chen, R. Sheng, P. Wang et al., "Ultra-sensitive detection of malathion residues using FRET-based upconversion fluorescence sensor in food," *Spectrochimica Acta Part A: Molecular and Biomolecular Spectroscopy*, vol. 241, article 118654, 2020.

[5] R. S. Chouhan, A. C. Vinayaka, and M. S. Thakur, "Thiol-stabilized luminescent CdTe quantum dot as biological fluorescent probe for sensitive detection of methyl parathion by a fluoroimmunochromatographic technique," *Analytical and Bioanalytical Chemistry*, vol. 397, no. 4, pp. 1467–1475, 2010.

[6] C. C. Leandro, P. Hancock, R. J. Fussell, and B. J. Keely, "Comparison of ultra-performance liquid chromatography and high-performance liquid chromatography for the determination of priority pesticides in baby foods by tandem quadrupole mass spectrometry," *Journal of Chromatography A*, vol. 1103, no. 1, pp. 94–101, 2006.

[7] X. Zhao, W. Kong, J. Wei, and M. Yang, "Gas chromatography with flame photometric detection of 31 organophosphorus pesticide residues in *Alpinia oxyphylla* dried fruits," *Food Chemistry*, vol. 162, pp. 270–276, 2014.

[8] M. Wei, J. J. S. Wang, and A. B. Chemical, "A novel acetylcholinesterase biosensor based on ionic liquids-AuNPs-porous carbon composite matrix for detection of organophosphate pesticides," *Sensors and Actuators B: Chemical*, vol. 211, pp. 290–296, 2015.

[9] T. Kohzadi, M. J. W. S. Roushani, and T. W. Supply, "Highly sensitive colorimetric determination of malathion using gold nanoparticles," *Water Science and Technology: Water Supply*, vol. 16, no. 5, pp. 1214–1220, 2016.

[10] M. Wang, K. Su, J. Cao et al., ""Off-On" non-enzymatic sensor for malathion detection based on fluorescence resonance energy transfer between β and fluorescent probe," *Talanta*, vol. 192, pp. 295–300, 2019.

[11] H. A. Azab, A. S. Orabi, and A. M. Abbas, "New probe for fluorescence detection of *azinphous ethyl*, *malathion* and *heptachlor* pesticides," *Journal of Luminescence*, vol. 160, pp. 181–187, 2015.

[12] M. Jiang, C. Chen, J. He, H. Zhang, and Z. Xu, "Fluorescence assay for three organophosphorus pesticides in agricultural products based on magnetic-assisted fluorescence labeling aptamer probe," *Food Chemistry*, vol. 307, article 125534, 2020.

[13] T. J. Dale and J. Rebek, "Fluorescent sensors for organophosphorus nerve agent mimics," *Journal of the American Chemical Society*, vol. 128, no. 14, pp. 4500-4501, 2006.

[14] Y. Hou, A. M. Soleimanpour, and A. H. Jayatissa, "Low resistive aluminum doped nanocrystalline zinc oxide for reducing gas sensor application via sol–gel process," *Sensors and Actuators B: Chemical*, vol. 177, pp. 761–769, 2013.

[15] Y. Xie, Y. Yu, L. Lu et al., "CuO nanoparticles decorated 3D graphene nanocomposite as non-enzymatic electrochemical sensing platform for malathion detection," *Journal of Electroanalytical Chemistry*, vol. 812, pp. 82–89, 2018.

[16] C. Bignon, S. Amigoni, T. Devers, and F. Guittard, "Barrier cream based on CeO_2 nanoparticles grafted polymer as an active compound against the penetration of organophosphates," *Chemico-Biological Interactions*, vol. 267, pp. 17–24, 2017.

[17] W. Wei, S. Dong, G. Huang, Q. Xie, and T. Huang, "MOF-derived Fe_2O_3 nanoparticle embedded in porous carbon as electrode materials for two enzyme-based biosensors," *Sensors and Actuators B: Chemical*, vol. 260, pp. 189–197, 2018.

[18] X. Yan, Y. Song, C. Zhu et al., "MnO_2 nanosheet-carbon dots sensing platform for sensitive detection of organophosphorus pesticides," *Analytical Chemistry*, vol. 90, no. 4, pp. 2618–2624, 2018.

[19] D. Zhang, N. Yin, and B. Xia, "Facile fabrication of ZnO nanocrystalline-modified graphene hybrid nanocomposite toward methane gas sensing application," *Journal of Materials Science: Materials in Electronics*, vol. 26, no. 8, pp. 5937–5945, 2015.

[20] H. Tian, H. Fan, H. Guo, and N. Song, "Solution-based synthesis of ZnO/carbon nanostructures by chemical coupling for high performance gas sensors," *Sensors and Actuators B: Chemical*, vol. 195, pp. 132–139, 2014.

[21] A. I. Uddin, D. T. Phan, and G. S. Chung, "Low temperature acetylene gas sensor based on Ag nanoparticles-loaded ZnO-reduced graphene oxide hybrid," *Sensors and Actuators B: Chemical*, vol. 207, pp. 362–369, 2015.

[22] V. Gilja, I. Vrban, V. Mandić, M. Žic, and Z. Hrnjak-Murgić, "Preparation of a PANI/ZnO composite for efficient photocatalytic degradation of acid blue," *Polymers*, vol. 10, no. 9, p. 940, 2018.

[23] W. K. Jo and N. C. Selvam, "Enhanced visible light-driven photocatalytic performance of ZnO–g-C_3N_4 coupled with graphene oxide as a novel ternary nanocomposite," *Journal of Hazardous Materials*, vol. 299, pp. 462–470, 2015.

[24] A. I. Uddin, U. Yaqoob, D. T. Phan, and G. S. Chung, "A novel flexible acetylene gas sensor based on PI/PTFE-supported Ag-loaded vertical ZnO nanorods array," *Sensors and Actuators B: Chemical*, vol. 222, pp. 536–543, 2016.

[25] B. Hatamluyi, Z. Eshaghi, F. M. Zahed, and M. Darroudi, "A novel electrochemical sensor based on GQDs-PANI/ZnO-NCs modified glassy carbon electrode for simultaneous determination of Irinotecan and 5-fluorouracil in biological samples," *Sensors and Actuators B: Chemical*, vol. 286, pp. 540–549, 2019.

[26] B. L. Martínez-Vargas, S. M. Durón-Torres, D. Bahena, J. L. Rodríguez-López, J. M. Peralta-Hernández, and A. Picos, "One-pot synthesis of ZnO-Ag and ZnO-Co nanohybrid materials for photocatalytic applications," *Journal of Physics and Chemistry of Solids*, vol. 135, article 109120, 2019.

[27] H. Tai, Y. Jiang, G. Xie, J. Yu, X. Chen, and Z. Ying, "Influence of polymerization temperature on NH3 response of PANI/TiO2 thin film gas sensor," *Sensors and Actuators B: Chemical*, vol. 129, no. 1, pp. 319–326, 2008.

[28] T. Chitradevi, A. J. Lenus, and N. V. Jaya, "Structure, morphology and luminescence properties of sol-gel method synthesized pure and Ag-doped ZnO nanoparticles," *Materials Research Express*, vol. 7, no. 1, article 015011, 2020.

[29] M. F. Nsib, S. Saafi, A. Rayes, N. Moussa, and A. Houas, "Enhanced photocatalytic performance of Ni-ZnO/polyaniline composite for the visible-light driven hydrogen generation," *Journal of the Energy Institute*, vol. 89, no. 4, pp. 694–703, 2016.

[30] F. Habtamu, S. Berhanu, and T. Mender, "Polyaniline supported Ag-doped ZnO nanocomposite: synthesis, characterization, and kinetics study for photocatalytic degradation of malachite green," *Journal of Chemistry*, vol. 2021, 12 pages, 2021.

[31] S. Ebrahim, A. Shokry, M. M. A. Khalil, H. Ibrahim, and M. Soliman, "Polyaniline/Ag nanoparticles/graphene oxide nanocomposite fluorescent sensor for recognition of chromium (VI) ions," *Scientific Reports*, vol. 10, no. 1, pp. 1–11, 2020.

[32] X. Hua, L. Wang, G. Li, Q. Fang, M. Wang, and F. Liu, "Multi-analyte enzyme-linked immunosorbent assay for organophosphorus pesticides and neonicotinoid insecticides using a bispecific monoclonal antibody," *Analytical Methods*, vol. 5, no. 6, pp. 1556–1563, 2013.

[33] X. Yan, H. Li, X. Wang, and X. Su, "A novel fluorescence probing strategy for the determination of parathion- methyl," *Talanta*, vol. 131, pp. 88–94, 2015.

[34] S. Mehrizi and M. H. Sohi, "Electrical resistivity and magnetic properties of electrodeposited nanocrystalline CoFe thin films," *Journal of Materials Science: Materials in Electronics*, vol. 26, no. 10, pp. 7381–7389, 2015.

[35] Y. Hou, J. Feng, Y. Wang, and L. Li, "Enhanced antibacterial activity of Ag-doped ZnO/polyaniline nanocomposites," *Journal of Materials Science: Materials in Electronics*, vol. 27, no. 7, pp. 6615–6622, 2016.

[36] K. Takahashi and T. Morizumi, "Growth of InAs whiskers in wurtzite structure," *Japanese Journal of Applied Physics*, vol. 5, no. 8, pp. 657–662, 1966.

[37] A. Shokry, M. M. A. Khalil, H. Ibrahim, M. Soliman, and S. Ebrahim, "Highly luminescent ternary nanocomposite of polyaniline, silver nanoparticles and graphene oxide quantum dots," *Scientific Reports*, vol. 9, no. 1, pp. 1–12, 2019.

[38] M. M. Rahman, A. Khan, H. M. Marwani, and A. M. Asiri, "Hydrazine sensor based on silver nanoparticle-decorated polyaniline tungstophosphate nanocomposite for use in environmental remediation," *Microchimica Acta*, vol. 183, no. 5, pp. 1787–1796, 2016.

[39] M. Mitra, A. Ghosh, A. Mondal, K. Kargupta, S. Ganguly, and D. Banerjee, "Facile synthesis of aluminium doped zinc oxide-polyaniline hybrids for photoluminescence and enhanced visible-light assisted photo-degradation of organic contaminants," *Applied Surface Science*, vol. 402, pp. 418–428, 2017.

[40] S. Poyraz, I. Cerkez, T. S. Huang et al., "One-step synthesis and characterization of polyaniline nanofiber/silver nanoparticle composite networks as antibacterial agents," *ACS Applied Materials & Interfaces*, vol. 6, no. 22, pp. 20025–20034, 2014.

[41] S. C. Ortiz, E. M. Ospino, and R. Cabanzo, "Spectroscopy characterization and quantum yield determination of quantum dots," *Journal of Physics: Conference Series*, vol. 687, no. 1, article 012097, 2016.

[42] J. El Nady, M. Ali, O. A. Kamel, S. Ebrahim, and M. Soliman, "Room temperature synthesis of aqueous ZnCuInS/ZnS quantum dots," *Journal of Dispersion Science and Technology*, vol. 41, no. 13, pp. 1956–1962, 2020.

[43] E. P. Kirby and R. F. Steiner, "Influence of solvent and temperature upon the fluorescence of indole derivatives," *The Journal of Physical Chemistry*, vol. 74, no. 26, pp. 4480–4490, 1970.

[44] M. Afshari, M. Dinari, and M. M. Momeni, "The graphitic carbon nitride/polyaniline/silver nanocomposites as a potential electrocatalyst for hydrazine detection," *Journal of Electroanalytical Chemistry*, vol. 833, pp. 9–16, 2019.

[45] N. Cheng, Y. Song, Q. Fu et al., "Aptasensor based on fluorophore-quencher nano-pair and smartphone spectrum reader for on-site quantification of multi-pesticides," *Biosensors and Bioelectronics*, vol. 117, pp. 75–83, 2018.

[46] R. Bala, R. K. Sharma, and N. Wangoo, "Development of gold nanoparticles-based aptasensor for the colorimetric detection of organophosphorus pesticide phorate," *Analytical and Bioanalytical Chemistry*, vol. 408, no. 1, pp. 333–338, 2016.

[47] Y. Nie, Y. Teng, P. Li, W. Liu, Q. Shi, and Y. Zhang, "Label-free aptamer-based sensor for specific detection of malathion residues by surface-enhanced Raman scattering," *Spectrochimica Acta Part A: Molecular and Biomolecular Spectroscopy*, vol. 191, pp. 271–276, 2018.

Hindawi
Journal of Sensors
Volume 2022, Article ID 5754751, 12 pages
https://doi.org/10.1155/2022/5754751

Review Article

Nutrient Detection Sensors in Seawater Based on ISI Web of Science Database

Lina Cao,[1] Hongyong Xiang,[2] Jingwen Xu,[3] Yufu Gao,[4] Chenlu Lin,[4] Kun Li,[5] Zhiwei Li,[4] Nana Guo,[4] P. David,[6] Chunguang He,[1] and Haijun Yang[2]

[1]*State Environmental Protection Key Laboratory of Wetland Ecology and Vegetation Restoration, School of Environment, Northeast Normal University, Changchun 130024, China*
[2]*School of Ecology and Environmental Science, Yunnan University, Kunming 650091, China*
[3]*School of Life Sciences, Northeast Normal University, Changchun 130024, China*
[4]*Key Laboratory of Vegetation Ecology, Ministry of Education, Jilin Songnen Grassland Ecosystem National Observation and Research Station, Northeast Normal University, Changchun 130024, China*
[5]*Heilongjiang Provincial Key Laboratory of Ecological Restoration and Resource Utilization for Cold Region, Heilongjiang University, Harbin 150080, China*
[6]*NKEA Instrumentation, Rue Gutenberg, Z.I. Kerandr'e, 56700 Hennebont, France*

Correspondence should be addressed to Chunguang He; 59388103@qq.com and Haijun Yang; yang@nenu.edu.cn

Received 25 December 2021; Accepted 10 February 2022; Published 7 March 2022

Academic Editor: Yuan Li

Marine ecosystem is increasingly deteriorating. In order to assess anthropogenic influence and instigate appropriate remedial actions, it is still of great significance to develop the technology of sensors applied for nutrient detection (e.g., nitrate, phosphate, and silicate) in seawater. This brief review shows an important direction for the development of nutrient detection sensors in seawater and also the limitations and challenges based on data from the ISI Web of Science database. Being different from previous review papers, in this short critical review paper (1) we unified the unit of limit of detection (LOD) for making the comparison within different researches possible; (2) only the literatures focusing on the technological development of sensors in seawater were used; and (3) not only the detection methods but also the detected analytes and publication years were discussed to supply more valuable information for the development of nutrient sensors applied in seawater. In total, 109 literatures were collected with regard to technological development. The quantity of literatures has increased most during 2011-2020. For analytes, literatures related to nitrate, phosphate, ammonium, and phosphate will continue to increase with more accurate data. For detection methods, spectrophotometry, colorimetry, fluorimetry, and electrochemistry are the most widely used sensors. LODs show thousands of orders. In general, there are lower LOD to nitrite and ammonium and fluorimetry method. Now, for analytes, nitrate (1.0983) > silicate (0.5495) > phosphate (0.4823) > ammonium (0.1324) > nitrite (0.0568). For detection methods, microfluidics (1.7617) > electrochemistry (1.2607) > colorimetry (0.4462) > spectrophotometry (0.2941) > fluorimetry (0.0558). This result indicated that the development level of detection methods is closer for nitrate, nitrite, phosphate, and silicate. For ammonium, spectrophotometry has significantly lower LOD than electrochemistry ($p < 0.05$), and fluorimetry also has significantly lower LOD than electrochemistry ($p < 0.05$). Our results imply that sensors with accurate LOD should be developed in the future. In addition, more detection methods should be considered by future sensors.

1. Introduction

Despite the fact that oceans cover more than 70% of our planet and have a profound impact on global climate, weather patterns, human health, agriculture, and commerce [1, 2], human ability to make sustained measurements of ocean processes is limited and much of the oceans remain largely unexplored [3, 4]. Meanwhile, marine ecosystem is increasingly deteriorating due to continuous development and utilization of oceans by industrial pressures and growing

population [5, 6]. These ecosystems of coastal zones, estuaries, and gulfs have been gradually destroyed with different extents, such as dumping of waste, construction of harbours, dredging, and extraction processes [7, 8]. Furthermore, frequently occurred marine natural disasters (e.g., tsunamis and red tides) bring substantial social impacts and economic losses [9, 10]. Therefore, the work of ocean environmental monitoring is urgent and monitoring the concentration changes and spatiotemporal distribution of nutrients in ocean environments is significant. In order to assess the impacts of these activities and instigate appropriate remedial actions, it is of great significance to develop the technology of sensors applied for ocean environmental monitoring, including the detection of chemical elements (e.g., nitrate, nitrite, phosphate, ammonium, and silicate), physical elements (e.g., pH, DO, and heavy metals), and biology (e.g., phytoplankton, benthonic animal, and fish).

Determining the distributions and variations of chemical elements in oceans is key to fully understanding global geochemical cycles, evaluating seawater pollution, and forecasting the occurrence of harmful algal blooms (HABs) [11, 12]. Although a wide variety of elements are essential to life in oceans, only a relatively small number of essential elements (e.g., nitrate, phosphate, and silicate) are termed as nutrients [13]. These nutrients are essential for the survival of marine organisms, such as promoting the growth of biology and microorganisms. Besides, accurate quantification of these nutrients is also necessary for forecasting the occurrence of harmful red tides and comprehending the dynamics of marine ecosystems [14]. On the contrary, inadequate nutrients will restrict the growth of phytoplankton and excessive nutrients are prone to cause eutrophication and even further lead to harmful algal blooms, extreme depletion of DO, and even death of aquatic organism [12, 15].

Traditional nutrient monitoring is difficult to determine the distributions and variations of nutrients to support ocean environmental monitoring [16]. Because they are measured by manual processing of sampling: water is collected at known locations and times, preserved and transported to laboratory for analysis by standard detection methods such as spectrophotometry, colorimetry, or fluorescence [17]. Nevertheless, these traditional methods (1) cannot satisfy the long-term in situ monitoring demands of nutrient detection in seawater and (2) are rather costly and time-consuming with expensive and bulky high-tech instruments and professional operators. Moreover, these obtained data may be not accurate enough because these seawater samples may undergo unexpected reactions during the long-time operation [14].

Currently, sensors and sensing systems are applied for nutrient monitoring to obtain primary data, to assure time-series observations on remote permanent platforms [1]. Consequently, in situ nutrient sensors, the device placed on a mobile platform such as a submersible vehicle, have a unique and important role in ocean environmental monitoring [17]. Over the years, the development of low-cost portable devices that can be employed for onsite and continuous analysis of nutrients has been attracting scientific attention [18]. Now, various nutrient sensors, including electronic sensors, chemical sensors, and biosensors, have been widely used for continuous observation in estuaries and seawater [19, 20]. And these nutrient sensors have been greatly improved during the past decades on accuracy, operability, sustainability, and other aspects [21–23]. Because of the unavoidable limitation of in situ seawater environment, the development of sensor technology has to be long duration of use, less wastewater output, low energy consumption, less reagent consumption, small volume, and strong ion selectivity. Some products with mature technology in market include Micro-Lab, EcoLAB2, and CYCL Phosphate sensors (Wetlabs, USA), SUNAV2 (Satlantic, Canada), and WIZ sensors (SYSTEA, Italy) [24, 25]. However, the main bottlenecks that restrict the development of nutrient sensors are short duration, low precision, narrow range of detection concentration, and poor reproducibility [26, 27]. To be more specific, since sample pretreatment, such as enrichment and dilution, cannot be applied in the field detection of nutrients in seawater, an ideal chemical sensor needs to have a high precision and a wide measuring range. Taking precision of sensors (LOD, limit of detection) as another example, studies have shown that the nutrient concentrations in seawater before and after algal bloom in some oligotrophic zones are order of nmol/L, and the nutrient concentrations in the same sea area vary greatly in different sea areas and at different times, and the detected concentration ranges from nmol/L to μmol/L (a difference of 5 orders of magnitude) [1, 28]. Hence, it is still necessary to utilize more appropriate methods to increase the precision of nutrient sensors in seawater, such as the limit of detection (LOD).

Previous valuable review papers have systemically reviewed either one analyte (or one group of analytes) or one category/type of sensors in seawater [1, 8, 9, 17, 29, 30]. With the increase of new literatures on nutrient sensors, how to utilize these resources to better service scientific development has been an important work. In this short critical review, after a brief introduction of necessity and need for higher precision of nutrient sensors in seawater, we collected related literatures focusing on the technological development of nutrient sensors in seawater and excluded those literatures focusing on application. We summarized the research status of nutrient sensors in seawater by quantity of literatures and then discussed the sensitivity of sensors (LOD) from two aspects of analytes and detection methods. Finally, a statistic analysis was performed to see if there existed any significant differences among five different detection methods (spectrophotometry, chromatography, colorimetry, electrochemistry, and fluorimetry) within one nutrient (nitrate, nitrite, phosphate, ammonia, and silicate). Being different from previous review papers, in this short critical review paper (1) we unified the unit of LOD to make the comparison within different researches possible; (2) only the literatures focusing on the technological development of sensors in seawater were used; and (3) not only the detection methods but also the detected analytes and publication years were discussed to supply more valuable information for the development of nutrient sensors applied in seawater. This brief review shows an important direction for the development of nutrient detection sensors in seawater and also the existing limitations and challenges.

Table 1: Summary of sensors for the nutrient detection in seawater.

Analytes	Detection methods	LOD (μM)	Ref.	Year
Phosphate	Fluorimetry	0.4000	[31]	2020
Phosphate	Colorimetry	2.4211	[32]	2020
Nitrate	Chromatography	0.2200	[33]	2020
Nitrate	Microfiber	2.7419	[34]	2020
Nitrite	Colorimetry	0.1000	[35]	2019
Nitrate	Spectrophotometry	0.0200	[36]	2019
Phosphate Ammonium	Colorimetry	1.8947 1.5000	[37]	2019
Nitrate	Spectrophotometry	0.2000	[38]	2019
Ammonium	Spectrophotometry	0.1500	[39]	2019
Ammonium	Fluorimetry	0.0021	[40]	2018
Nitrate	Spectrophotometry	0.0074	[41]	2018
Nitrate	Spectrophotometry	0.1000	[42]	2018
Phosphate	Spectrophotometry	0.1000	[43]	2018
Silicate	Electrochemistry	0.5000	[23]	2018
Nitrate	Electrochemistry	0.0009	[44]	2018
Nitrate	Electrochemistry	0.9000	[14]	2018
Ammonium	Spectrophotometry	0.2000	[45]	2018
Ammonium	Spectrophotometry	0.0800	[46]	2018
Ammonium	Fluorimetry	0.0065	[47]	2018
Nitrite	Electrochemistry	0.2000	[48]	2018
Silicate	Spectrophotometry	1.6000	[49]	2018
Ammonium	Fluorimetry	0.1600	[50]	2018
Phosphate	Spectrophotometry	0.1000	[43]	2018
Ammonium	Fluorimetry	0.0010	[51]	2017
Nitrate Nitrite Phosphate Ammonium Silicate	Spectrophotometry	0.3000 0.1000 0.1000 0.3000 0.2000	[52]	2017
Phosphate	Colorimetry	0.0300	[53]	2017
Nitrate	Electrochemistry	0.3900	[54]	2017
Nitrate	Electrochemistry	0.8000	[55]	2017
Phosphate	Colorimetry	0.0526	[56]	2017
Phosphate	Colorimetry	0.0300	[53]	2017
Phosphate	Colorimetry	0.1000	[57]	2017
Silicate	Optofluidics	0.0451	[58]	2017
Ammonium	Electrochemistry	0.6400	[59]	2017
Ammonium	Colorimetry	0.0150	[60]	2017
Nitrate	Electrochemistry	0.8000	[61]	2016
Nitrite	Fluorimetry	0.1000	[62]	2016
Ammonium	Fluorimetry	0.0074	[63]	2016
Phosphate	Spectrophotometry	0.0014	[64]	2016
Phosphate	Electrochemistry	0.1000	[65]	2016
Phosphate	Electrochemistry	4.0000	[66]	2016
Silicate	Electrochemistry	0.5000	[67]	2015
Nitrate	Microfluidics	5.0000	[68]	2015
Nitrate	Electrochemistry	3.8000	[69]	2015
Ammonium	Spectrophotometry	0.0055	[70]	2015

Table 1: Continued.

Analytes	Detection methods	LOD (μM)	Ref.	Year
Ammonium	Fluorimetry	0.0058	[71]	2015
Nitrate Nitrite	Microfluidics	0.0250 0.0200	[72]	2015
Phosphate	Fluorimetry	0.0145	[73]	2014
Ammonium	Spectrophotometry	0.0036	[74]	2014
Nitrate	Spectrophotometry	0.0300	[75]	2014
Ammonium	Fluorimetry	0.0100	[76]	2013
Phosphate	Colorimetry	0.0520	[77]	2013
Ammonium	Fluorimetry	0.0007	[78]	2013
Nitrate Phosphate Silicate Ammonium	Colorimetry Colorimetry Colorimetry Fluorimetry	0.5000 0.3000 1.0000 0.3000	[79]	2013
Phosphate	Electrochemistry	0.1900	[80]	2013
Nitrate	Spectrophotometry	0.2000	[81]	2013
Nitrate	Spectrophotometry	1.9355	[82]	2012
Silicate	Electrochemistry	0.1000	[83]	2012
Nitrate Nitrite	Microfluidics	0.0250 0.0200	[84]	2012
Ammonium	Carbon nanotube	0.0100	[85]	2012
Nitrite	Colorimetry	0.0150	[86]	2011
Nitrate	Spectrophotometry	1.7000	[87]	2011
Ammonium	Fluorimetry	0.0130	[88]	2011
Ammonium	Fluorimetry	0.0010	[89]	2011
Ammonium	Spectrophotometry	0.0035	[90]	2011
Ammonium	Fluorimetry	0.0050	[91]	2011
Phosphate	Electrochemistry	0.1200	[25]	2011
Ammonium	Colorimetry	0.0150	[92]	2011
Nitrate	Spectrophotometry	0.2000	[93]	2010
Nitrate	Spectrophotometry	0.3000	[94]	2010
Nitrate	Electrochemistry	10.0000	[95]	2010
Nitrite	Spectrophotometry	0.1000	[96]	2009
Nitrate	Electrochemistry	0.014	[97]	2009
Nitrate	Electrochemistry	0.0002	[98]	2008
Nitrate	Microfluidics	4.5000	[99]	2008
Silicate	Electrochemistry	0.3000	[100]	2008
Ammonium	Fluorimetry	0.0011	[101]	2008
Silicate	Electrochemistry	0.3000	[100]	2008
Nitrate Nitrite Phosphate	Colorimetry	0.0020 0.0020 0.0015	[102]	2008
Nitrite	Spectrophotometry	0.0001	[103]	
Nitrate	Electrochemistry	4.5000	[104]	2007
Silicate	Electrochemistry	1.0000	[105]	2007
Nitrate	Spectrophotometry	2.0000	[106]	2006
Ammonium	Spectrophotometry	0.0050	[107]	2005
Nitrate	Electrochemistry	1.0000	[108]	2005
Phosphate	Fluorimetry	0.0200	[109]	2003
	Spectrophotometry		[110]	2003

Table 1: Continued.

Analytes	Detection methods	LOD (μM)	Ref.	Year
Nitrate		0.1000		
Silicate		0.5000		
Phosphate		0.1000		
Nitrate	Spectrophotometry	0.2000	[111]	2002
Nitrate	Spectrophotometry	0.0452	[112]	2002
Nitrate	Spectrophotometry	0.0452	[112]	2002
Nitrite	Fluorimetry	0.0046	[113]	2000
Nitrate		0.0069		
Nitrate	Spectrophotometry	0.0226	[114]	1999
Nitrate	Spectrophotometry	0.1000	[115]	1998
Nitrate	Electrochemistry	0.1000	[116]	1994

2. Materials and Methods

2.1. Database Compilation. We build this database using the following topics searched in core database of Web of Science (1985-2020): "sensor" and "seawater or sea water or saline water or marine water or salt water or ocean" and "nutrient or nitrate or nitrite or phosphate or ammonia or silicate" in July 2020. Here, for supplying more valuable information for the development of nutrient sensors applied in seawater, we just collected literatures focusing on the technological development of sensors, excluded those focusing on application. In total, 42.21% of the screened literatures were published during the last five years (2016-2020). For each literature, we extracted the information: tested analytes, detection method of sensors, LOD, and publication year. All tested analytes were categorized into phosphate, nitrite, nitrate, ammonium, and silicate. As for the detection methods, we included spectrophotometry (ultraviolet spectrophotometry, visible light spectrophotometry), fluorimetry, colorimetry (visual colorimetry, photoelectric colorimetry), chromatography, microfiber, microfluidics, electrochemistry, optofluidics, and carbon nanotube. We unified all the units of LODs as μM (μmol/L).

2.2. Data Analysis. We performed one-way ANOVA to test the differences of LODs among different detection methods within one analyte. All data were checked for normality before conducting the ANOVA tests and were log-transformed to meet normality and homogeneity assumptions [19]. If significant effects are present in the ANOVA, then Tukey's test was used for post hoc analysis of significant differences among detection methods. All statistical analyses were performed by SPSS statistics software (IBM, 20.0).

3. Results and Discussions

3.1. Research Status of Nutrient Sensors in Seawater. To a certain extent, quantity of literatures could reflect scientific research status in this area. After screening from 538 literatures searched in the core database of Web of Science, we finally collected 109 literatures focusing on the technological development of nutrient sensors applied in seawater. Table 1 shows the summary of sensors for the nutrient detection in seawater. Here, we classified analytes mainly by phosphate, nitrate, ammonium, and silicate related to different detection methods with LOD and publication date.

From Table 2, we can see that the quantity of literatures has increased with the development of decades. In particular, during 2011-2020 in both analytes and detection methods, there are more literatures focusing on the technological development of sensors. Furthermore, this trend also means that more literatures may appear during the next ten years to meet the needs from all walks of life and from many different areas. Actually, nitrate determination was firstly taken by electrochemical methods in 1834 [117]. It has been attracting more attention in the world today from different perspectives. A review published in 2021 summarizes the advances in knowledge in terms of the modes of action of devices and deployment strategies, identifying the current limitations and future challenges for the electrochemical detection of nutrients in marine environments [118]. The application of electrochemical sensors including potentiometric, voltammetric, and field-effect transistor sensors for nitrate, nitrite, ammonium, and phosphate determination in aqueous environments was reviewed [16]. The recent advances in ISE sensing platforms for environmental water analysis from on board to in situ approaches were also reviewed [119].

In terms of quantity, the above obvious result may mainly attribute to (1) emerging technologies. In 2003, Thouron developed a system with three analysers to measure phosphate, nitrate, and silicate together [110]. And Zhang et al. fabricated a self-supported electrode to detect ammonia based on electrodepositing platinum-polypyrrole on Ni foam [120]. New technologies also promote the improvement of old ones. For example, scientists improved the sensitivity measurement of nitrate concentration based on new dispersion turning point (DTP) theory [34]. Meanwhile, the emergence of new technologies also brings more detection methods. For example, phosphate was detected by interfacial barrier effects of p-n junction on electrochemistry [121]. (2) Some problems previously hard to study are solved. It was well known that not extensively researches had studied voltammetric sensors for nitrate detection in seawater, because the LOD data from sensors was usually above 1 μM, higher than the nitrate concentrations in seawater, particularly the concentration of nitrate at the ocean surface (at a nanomolar level) [122]. Nine years later, Legrand et al. developed an electrode by electrodepositing silver nanoparticles on a gold disc electrode to test nitrate in synthetic seawater [54]. The sensor showed a limit of quantification of 0.39 μM and a linear range of 0.39-50 μM. The peak current intensity remained at 95% of the initial value after regular detection of 25 μM nitrate for about 26 days. And (3) more and more emerging contaminants interference is still a technical challenge. For example, the challenges of nitrate biosensors based on reductases include oxygen interference [123], low electron transfer efficiency [124, 125], and high cost and low storage temperature, which promote relevant research and generate more literatures.

Although the quantity of relevant literatures has been increasing steadily, the research status within both analytes

Table 2: Literature number of nutrient sensors.

Category	In total	Years	2011-2020	2001-2010	1994-2000
Analytes					
Nitrate	39	1994-2020	21	14	4
Nitrite	12	2000-2019	8	3	1
Phosphate	21	2003-2020	18	3	0
Ammonium	26	2005-2019	24	2	0
Silicate	11	2003-2018	7	4	0
Detection methods					
Spectrophotometry	38	1998-2019	24	12	2
Colorimetry	18	2008-2020	15	3	0
Fluorimetry	19	2000-2020	15	2	2
Electrochemistry	24	1994-2018	15	8	1
Chromatography	1	2020	1	0	0
Microfiber	1	2020	1	0	0
Microfluidics	6	2008-2020	5	1	0
Optofluidics	1	2017	1		
Carbon nanotube	1	2012	1		

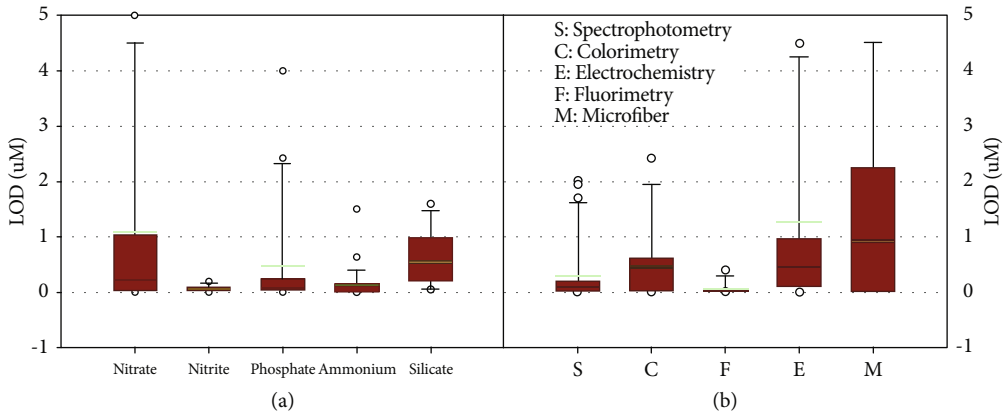

Figure 1: Average of LOD for (a) five nutrients and (b) five detection methods with more than five literatures. Green line: mean value.

and detection methods is very varied. For analytes, we can see that more research focused on nitrate, phosphate, and ammonium. This result should attribute to seriously increasing marine environmental and ecological problems, such as frequent red tide, green tide, and other ecological disasters [9, 10, 126]. Hence, for a period of time, literatures related to nitrate, phosphate, ammonium, and phosphate will continue to increase with more accurate data and new detection methods.

For the detection methods, we found a similar trend as one previous review paper that spectrophotometry, colorimetry, fluorimetry, and electrochemistry are the most commonly used sensors for the detection of nutrient detection in seawater [127]. These traditional and classic detection methods have been attracting a lot of attention for years, followed by emerging chromatography, microfiber, microfluidics, optofluidics, and carbon nanotube (Table 2). Then, other electrochemical sensors have been used for water analysis. As we know, we widely used electrochemical sensors as one of the most promising analytical tools for the rapid detection of nitrate due to its high sensitivity, quick response, ease of operation and miniaturization, low sample and power consumption, low reagent consumption, and easy combination with automation devices [18, 128]. Nevertheless, some new methods also appeared with technical advantage. For example, a new method using a microfiber mode interferometric sensor to improve the sensitivity of nitrate concentration measurement in seawater based on dispersion turning point (DTP) theory is demonstrated [34]. Through interdisciplinary research within electronics, chemistry, materials science, etc., the application of microfluidic technology shows more advantages and gradually becomes a better way to further reduce energy consumption, reduce the amounts of reagents, and promote the miniaturization of sensors [129]. Therefore, more studies should focus on the development of new detection methods for clearer understanding of the nutrient in seawaters.

3.2. Sensitivity of Nutrient Sensors in Seawater. LODs in Table 1 show thousands of orders for different analytes and

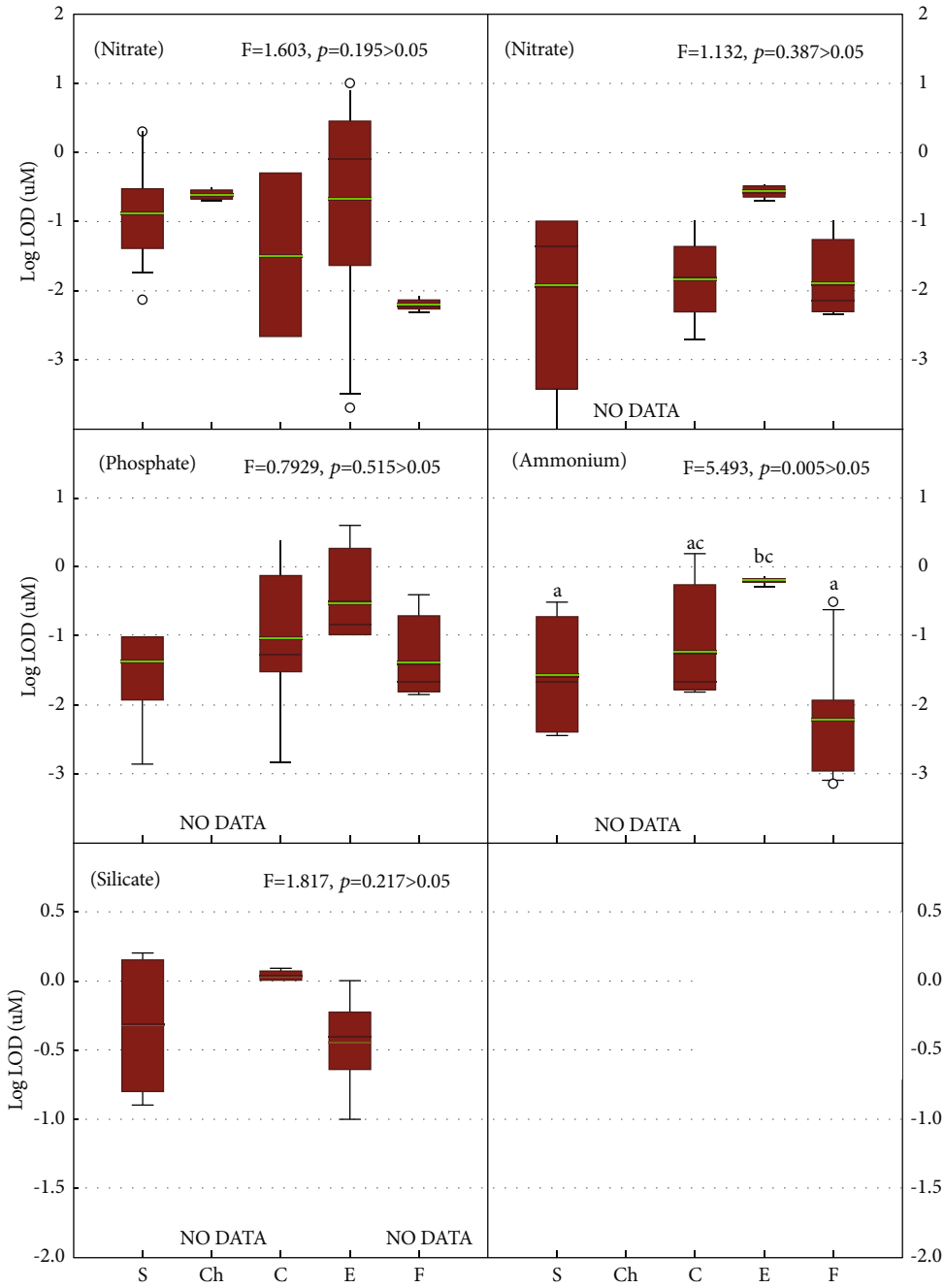

Figure 2: Analysis of one-way ANOVA for different detection methods. Green line: mean value. $p < 0.05$.

detection methods. Here, the average LOD of nutrient sensors included was μM. Among all the sensors checked, the most sensitive sensor was developed by Chen and Chumbimuni-Torres in which the indirect detection of nitrate through spectrophotometry and electrochemistry method was used [98, 103]. Above sensor could achieve an ultrasensitive LOD, as low as 0.1 nM [103]. By contrast, some other sensors are relatively "insensitive" with the LODs at the level of 2-10 μM, distributed from 2006 to 2016 [66, 68, 95, 104].

Figure 1(a) shows the average LOD of five nutrients at the level almost below1 μM with descending sequence: nitrate (1.0983) > silicate (0.5495) > phosphate (0.4823) > ammonium (0.1324) > nitrite (0.0568). Figure 1(b) only shows the average LOD of five detection methods with more than five literatures at the level almost below 1 μM (except for microfluidics at the level of 2 μM) with descending sequence: microfluidics (1.7617) > electrochemistry (1.2607) > colorimetry (0.4462) > spectrophotometry (0.2941) > fluorimetry (0.0558). For the rest four detection methods, chromatography, microfiber, optofluidics, and carbon nanotube have a LOD of 0.2200, 2.7419, 0.0451, and 0.01, respectively.

In general, both detection of nitrite and ammonium and fluorimetry method seem to have lower LODs (Figure 1).

Nevertheless, we cannot just draw a simple conclusion that these related research develop best. This result could mainly attribute to the following: (1) some new literatures based on special detection technique usually increase the mean value with their own high LODs. For example, Yang et al. used a new technique to improve the sensitivity of sodium nitrate concentration measurement in seawater based on dispersion turning point [34]. Although the sensor shows advantages of easy to construct, low cost, high precision, and high sensitivity, which provides a new optical detection method for in situ detection of marine environment or low concentration substances sensing in other liquids, its LOD is 2.7419 μM. The same situation applies to Khongpet et al. who used a compact hydrodynamic sequential injection system for consecutive online determination of phosphate and ammonium, with a LOD 1.8947 μM [37]. On a long view, these technologies are constantly developing with lower LOD. And more literatures related to these technologies will finally lower the average LOD. Before we get too excited about that, we may have to face the situation that the emergence of other new technologies (in embryonic stage) may increase the mean value with their own high LODs, again. (2) Different detection methods have their own special value. For example, a variety of approaches have been used for the determination of phosphate in seawater, including colorimetric detection, fluorescent detection, and electrochemical detection. For all are reagent-based methods, phosphate cannot be detected directly. Therefore, autonomous systems tend to employ the colorimetric method rather than fluorescent or electrochemical methods [130]. Previous study has shown that when algal blooms erupt, the nutrient concentration in seawater is on the order of 10^{-9} mol/L [131]. So it is very necessary to utilize more appropriate methods to increase the accuracy of the sensor. In addition to accuracy, the nutrient concentration in the same sea area varies significantly at different times or in different sea areas and the ranges from 10^{-9} to 10^{-6} mol/L, with a difference of 5 orders of magnitude [131]. Hence, an ideal sensor should better have wide measurement range.

3.3. Comparison of Detection Methods. Figure 2 shows the result of analysis of one-way ANOVA for different detection methods ($p < 0.05$). In general, at the present stage, we could see that not all methods (NO DATA) can be used for detection within one nutrient in seawaters such as chromatography to nitrite, phosphate, ammonium, and silicate (Figure 2). Clearly, future studies should focus on the development of chromatography sensors applied in seawater.

Furthermore, except ammonium ($p < 0.05$), there were no significant differences among different detection methods applied in any nutrient sensor. This result indicated that, for nitrate, nitrite, phosphate, and silicate, their development level of detection methods is closer to each other. For ammonium, spectrophotometry has a significantly lower LOD than electrochemistry ($p < 0.05$), and fluorimetry also has a significantly lower LOD than electrochemistry ($p < 0.05$). This result is in accordance with the consensus that electrochemical sensors have been widely used as one of the most promising analytical tools for the rapid detection of nitrate in environmental matrices due to low sample and power consumption, high sensitivity, quick response, and ease of operation and miniaturization [18, 128].

4. Conclusions

From 109 literatures, the general status of nutrient detection sensors in seawater including the research status, sensitivity, detection methods, and future challenges was reviewed, with most published during 2011-2020. For analytes, literatures related to nitrate, phosphate, ammonium, and phosphate will continue to increase with more accurate data. For detection methods, spectrophotometry, colorimetry, fluorimetry, and electrochemistry are the most widely used sensors. LODs show thousands of orders. In general, there are lower LOD to nitrite and ammonium and fluorimetry method. Now, for analytes, nitrate (1.0983) > silicate (0.5495) > phosphate (0.4823) > ammonium (0.1324) > nitrite (0.0568). For detection methods, microfluidics (1.7617) > electrochemistry (1.2607) > colorimetry (0.4462) > spectrophotometry (0.2941) > fluorimetry (0.0558). This result indicated that the development level of detection methods is closer for nitrate, nitrite, phosphate, and silicate. For ammonium, spectrophotometry has significantly lower LOD than electrochemistry ($p < 0.05$), and fluorimetry also has significantly lower LOD than electrochemistry ($p < 0.05$). Our results are expected to indicate that higher sensitivity sensors should be developed in the future. In addition, more detection methods should be considered by future sensors. We can see that although the stability, sensitivity, and detection limit of sensors have greatly improved, there are still some certain technical issues that restrict the large-scale use of this technology, including low reproducibility, low accuracy, narrow detection concentration ranges, and short continuous measurement time. Besides, good stability is important to an ideal sensor achieved by improving sensor antifouling ability, which is a hot topic partially in biocompatibility and blood compatibility [132]. So, it is a feasible solution to further explore new antifouling materials and approaches for maintaining long-term sensor durability and stability. In short, this brief review shows an important direction for the development of nutrient detection sensors in seawater and many limitations and challenges still existed. Clearly, much work still needs to be done in many areas of sensor development and for a variety of seawater environments.

Conflicts of Interest

The authors declare that there is no conflict of interest regarding the publication of this paper.

Authors' Contributions

Lina Cao and Hongyong Xiang have equal contributions.

Acknowledgments

This study was supported by the National Natural Science Foundation of China (grant numbers 32071587, 32101310,

and 41501566), Fellowship of China Postdoctoral Science Foundation (grant number 2021M692728), China Scholarship Council (grant number 202006625001), Science Foundation of Science and Technology of Education Department of Jilin (grant number JJKH20211293KJ), Natural Science Foundation of Heilongjiang (grant number YQ2021C031), University Nursing Program for Young Scholar with Creative Talents in Heilongjiang (grant number UNPYSCT-2020008), Postdoctoral Scientific Research Developmental Fund of Heilongjiang (grant number LBH-Q20166), and Program of Introducing Talents of Discipline to Universities (grant number B16011).

References

[1] C. Whitt, J. Pearlman, B. Polagye et al., "Future vision for autonomous ocean observations," *Science*, vol. 7, 2020.

[2] X. Hongyong, K. Li, L. Cao, Z. Zhang, and H. Yang, "Impacts of pollution, sex, and tide on the time allocations to behaviours of Uca arcuata in mangroves," *Science of the Total Environment*, vol. 742, article 140609, 2020.

[3] M. G. Mostofa Khan, C.-Q. Liu, W. Zhai et al., "Reviews and syntheses: ocean acidification and its potential impacts on marine ecosystems," *Biogeosciences*, vol. 13, no. 6, pp. 1767–1786, 2016.

[4] N. L. Williams, L. W. Juranek, K. S. Johnson et al., "Empirical algorithms to estimate water column pH in the Southern Ocean," *Geophysical Research Letters*, vol. 43, no. 7, pp. 3415–3422, 2016.

[5] S. D. Thomson, R. C. Quinn, A. J. Ricco, and J. E. Koehne, "Electrochemistry for life detection on ocean worlds," *Chemelectrochem*, vol. 7, no. 3, pp. 614–623, 2020.

[6] L. D. Talley, I. Rosso, I. Kamenkovich et al., "Southern Ocean biogeochemical float deployment strategy, with example from the Greenwich meridian line (GO-SHIP A12)," *Journal of Geophysical Research-Oceans*, vol. 124, no. 1, pp. 403–431, 2019.

[7] I. L. Justino Celine, A. C. Freitas, A. C. Duarte, A. P. Teresa, and R. Santos, "Sensors and biosensors for monitoring marine contaminants," *Analytical Chemistry*, vol. 6-7, pp. 21–30, 2015.

[8] M. Graham and G. Fones, "A review ofin situmethods and sensors for monitoring the marine environment," *Sensor Review*, vol. 32, no. 1, pp. 17–28, 2012.

[9] D. L. Li, X. B. Xu, Z. Li, T. Wang, and C. Wang, "Detection methods of ammonia nitrogen in water: a review," *Analytical Chemistry*, vol. 127, article 115890, 2020.

[10] T. Toste, S. Pouliquen, J. Hausman et al., "Ocean FAIR data services," *Frontiers in Marine Science*, vol. 6, 2019.

[11] A. J. Birchill, G. Clinton-Bailey, R. Hanz et al., "Realistic measurement uncertainties for marine macronutrient measurements conducted using gas segmented flow and lab-on-chip techniques," *Talanta*, vol. 200, pp. 228–235, 2019.

[12] F. Wang, J. M. Zhu, L. F. Chen, Y. F. Zuo, X. J. Hu, and Y. Yang, "Autonomous and in situ ocean environmental monitoring on optofluidic platform," *Micromachines*, vol. 11, no. 1, p. 69, 2020.

[13] M. Li, K. Xu, M. Watanabe, and Z. Chen, "Long-term variations in dissolved silicate, nitrogen, and phosphorus flux from the Yangtze River into the East China Sea and impacts on estuarine ecosystem," *Estuarine, Coastal and Shelf Science*, vol. 71, no. 1-2, pp. 3–12, 2007.

[14] C. Maria, G. Crespo, T. Cherubini et al., "In situ detection of macronutrients and chloride in seawater by submersible electrochemical sensors," *Analytical Chemistry*, vol. 90, no. 7, pp. 4702–4710, 2018.

[15] J. C. Robidart, J. D. Magasin, I. N. Shilova et al., "Effects of nutrient enrichment on surface microbial community gene expression in the oligotrophic North Pacific Subtropical Gyre," *The ISME Journal*, vol. 13, no. 2, pp. 374–387, 2019.

[16] C. Xiaoyan, G. Zhou, S. Mao, and J. Chen, "Rapid detection of nutrients with electronic sensors: a review," *Environmental Science-Nano*, vol. 5, no. 4, pp. 837–862, 2018.

[17] A. M. Nightingale, A. D. Beaton, and M. C. Mowlem, "Trends in microfluidic systems for in situ chemical analysis of natural waters," *Sensors and Actuators B-Chemical*, vol. 221, pp. 1398–1405, 2015.

[18] J. Chunbo, Y. He, and Y. Liu, "Recent advances in sensors for electrochemical analysis of nitrate in food and environmental matrices," *Analyst*, vol. 145, no. 16, pp. 5400–5413, 2020.

[19] X. Hongyong, Q. Cai, Y. Li et al., "Sensors applied for the detection of pesticides and heavy metals in freshwaters," *Journal of Sensors*, vol. 2020, 22 pages, 2020.

[20] A. G. Vincent, R. W. Pascal, A. D. Beaton et al., "Nitrate drawdown during a shelf sea spring bloom revealed using a novel microfluidic in situ chemical sensor deployed within an autonomous underwater glider," *Marine Chemistry*, vol. 205, pp. 29–36, 2018.

[21] C. Frank, D. Meier, D. Voß, and O. Zielinski, "Computation of nitrate concentrations in coastal waters using an in situ ultraviolet spectrophotometer: behavior of different computation methods in a case study a steep salinity gradient in the southern North Sea," *Methods in Oceanography*, vol. 9, pp. 34–43, 2014.

[22] J. R. Etheridge, F. Birgand, J. A. Osborne, C. L. Osburn, M. R. Burchell Ii, and J. Irving, "Using in situ ultraviolet-visual spectroscopy to measure nitrogen, carbon, phosphorus, and suspended solids concentrations at a high frequency in a brackish tidal marsh," *Limnology and Oceanography: Methods*, vol. 12, no. 1, p. 10, 2014.

[23] C. Barus, D. C. Legrand, N. Striebig et al., "First deployment and validation of in situ silicate electrochemical sensor in seawater," *Frontiers in Marine Science*, vol. 5, 2018.

[24] D. Aguilar, C. Barus, W. Giraud et al., "Silicon-based electrochemical microdevices for silicate detection in seawater," *Sensors and Actuators, B: Chemical*, vol. 211, pp. 116–124, 2015.

[25] J. Jońca, V. León Fernández, D. Thouron, A. Paulmier, M. Graco, and V. Garçon, "Phosphate determination in seawater: toward an autonomous electrochemical method," *Talanta*, vol. 87, no. 1, pp. 161–167, 2011.

[26] K. S. Johnson, J. A. Needoba, S. C. Riser, and W. J. Showers, "Chemical sensor networks for the aquatic environment," *Chemical Reviews*, vol. 107, no. 2, pp. 623–640, 2007.

[27] Z. Ye, J. Yang, N. Zhong, X. Tu, J. Jia, and J. Wang, "Tackling environmental challenges in pollution controls using artificial intelligence: a review," *Science of the Total Environment*, vol. 699, p. 134279, 2020.

[28] L. R. Adornato, E. A. Kaltenbacher, D. R. Greenhow, and R. H. Byrne, "High-resolution in situ analysis of nitrate and phosphate in the oligotrophic ocean," *Environmental Science and Technology*, vol. 41, no. 11, pp. 4045–4052, 2007.

[29] C. D. M. Campos and J. A. F. da Silva, "Applications of autonomous microfluidic systems in environmental monitoring," *Advances*, vol. 3, no. 40, pp. 18216–18227, 2013.

[30] R. D. Prien, "The future of chemical in situ sensors," *Marine Chemistry*, vol. 107, no. 3, pp. 422–432, 2007.

[31] J. M. Zhu, G. W. Han, X. J. Hu et al., "A portable and accurate phosphate sensor using a gradient Fabry–Pérot array," *Acs Sensors*, vol. 5, no. 5, pp. 1381–1388, 2020.

[32] J. M. Racicot, T. L. Mako, A. Olivelli, and M. Levine, "A paper-based device for ultrasensitive, colorimetric phosphate detection in seawater," *Sensors*, vol. 20, no. 10, p. 2766, 2020.

[33] T. L. Mako, A. M. Levenson, and M. Levine, "Ultrasensitive detection of nitrite through implementation ofN-(1-naphthyl)ethylenediamine-grafted cellulose into a paper-based device," *Acs Sensors*, vol. 5, no. 4, pp. 1207–1215, 2020.

[34] L. Yang, J. Wang, S. S. Wang, Y. P. Liao, and Y. Li, "A new method to improve the sensitivity of nitrate concentration measurement in seawater based on dispersion turning point," *Optik*, vol. 205, p. 164202, 2020.

[35] S. C. Morgan, A. D. Hendricks, M. L. Seto, and V. J. Sieben, "A magnetically tunable check valve applied to a lab-on-chip nitrite sensor," *Sensors*, vol. 19, no. 21, p. 4619, 2019.

[36] F. Tengyue, P. Li, K. Lin et al., "Simultaneous underway analysis of nitrate and nitrite in estuarine and coastal waters using an automated integrated syringe-pump-based environmental-water analyzer," *Analytica Chimica Acta*, vol. 1076, pp. 100–109, 2019.

[37] W. Khongpet, S. Pencharee, C. Puangpila, S. K. Hartwell, S. Lapanantnoppakhun, and J. Jakmunee, "A compact hydrodynamic sequential injection system for consecutive on-line determination of phosphate and ammonium," *Microchemical Journal*, vol. 147, pp. 403–410, 2019.

[38] K. S. Johnson, S. C. Riser, and M. Ravichandran, "Oxygen variability controls denitrification in the Bay of Bengal oxygen minimum zone," *Geophysical Research Letters*, vol. 46, no. 2, pp. 804–811, 2019.

[39] L. Peicong, Y. Deng, H. Shu et al., "High-frequency underway analysis of ammonium in coastal waters using an integrated syringe-pump-based environmental-water analyzer (i SEA)," *Talanta*, vol. 195, pp. 638–646, 2019.

[40] Z. Yong, J. Chen, X. Shi et al., "Development and application of a portable fluorescence detector for shipboard analysis of ammonium in estuarine and coastal waters," *Analytical Methods*, vol. 10, no. 15, pp. 1781–1787, 2018.

[41] M. Eichhorn, C. Ament, M. Jacobi et al., "Modular AUV system with integrated real-time water quality analysis," *Sensors*, vol. 18, no. 6, p. 1837, 2018.

[42] D. Meyer, R. D. Prien, L. Rautmann, M. Pallentin, J. J. Waniek, and D. E. Schulz-Bull, "In situ determination of nitrate and hydrogen sulfide in the Baltic Sea using an ultraviolet spectrophotometer," *Frontiers in Marine Science*, vol. 5, 2018.

[43] S. Sateanchok, N. Pankratova, M. Cuartero, T. Cherubini, K. Grudpan, and E. Bakker, "In-line seawater phosphate detection with ion-exchange membrane reagent delivery," *Acs Sensors*, vol. 3, no. 11, pp. 2455–2462, 2018.

[44] L. Emilie, P. Fau, M. Comtat et al., "In situ metalorganic deposition of silver nanoparticles on gold substrate and square wave voltammetry: a highly efficient combination for nanomolar detection of nitrate ions in sea water," *Chem*, vol. 6, no. 4, p. 50, 2018.

[45] M. Jian, P. Li, K. Lin et al., "Optimization of a salinity-interference-free indophenol method for the determination of ammonium in natural waters using o -phenylphenol," *Talanta*, vol. 179, pp. 608–614, 2018.

[46] L. Kunning, P. Li, W. Qiaoling, S. Feng, J. Ma, and D. Yuan, "Automated determination of ammonium in natural waters with reverse flow injection analysis based on the indophenol blue method with o -phenylphenol," *Microchemical Journal*, vol. 138, pp. 519–525, 2018.

[47] Z. Min, T. Zhang, Y. Liang, and Y. Pan, "Toward sensitive determination of ammonium in field: a novel fluorescent probe, 4,5-dimethoxyphthalaldehyde along with a hand-held portable laser diode fluorometer," *Sensors and Actuators B-Chemical*, vol. 276, pp. 356–361, 2018.

[48] Y. Zhang, J. T. Nie, H. Y. Wei et al., "Electrochemical detection of nitrite ions using Ag/Cu/MWNT nanoclusters electrodeposited on a glassy carbon electrode," *Sensors and Actuators B-Chemical*, vol. 258, pp. 1107–1116, 2018.

[49] X. Cao, S. W. Zhang, D. Z. Chu, N. Wu, H. K. Ma, and R. Ma, "Development of lab-on-chip spectrophotometric silicate sensor in situ analysis of seawater," *Spectroscopy and Spectral Analysis*, vol. 38, no. 3, pp. 895–900, 2018.

[50] C. Wang, Z. Li, Z. L. Pan, and D. L. Li, "Development and characterization of a highly sensitive fluorometric transducer for ultra low aqueous ammonia nitrogen measurements in aquaculture," *Computers and Electronics in Agriculture*, vol. 150, pp. 364–373, 2018.

[51] G. Georgia, E. Trikas, M. Petala, T. Karapantsios, G. Zachariadis, and A. Anthemidis, "An integrated sequential injection analysis system for ammonium determination in recycled hygiene and potable water samples for future use in manned space missions," *Microchemical Journal*, vol. 133, pp. 490–495, 2017.

[52] H. L. Wang, S. W. Zhang, C. L. Guo, and D. Z. Chu, "Development of an in-situ analyzer for nutrient monitoring in seawater," in *In Proceedings of the 2017 6th International Conference on Energy, Environment and Sustainable Development*, pp. 550–553, Zhuhai, China, 2017.

[53] M. M. Grand, G. S. Clinton-Bailey, A. D. Beaton et al., "A lab-on-chip phosphate analyzer for long-term in situ monitoring at fixed observatories: optimization and performance evaluation in estuarine and oligotrophic coastal waters," *Frontiers in Marine Science*, vol. 4, p. 4, 2017.

[54] L. D. Chen, C. Barus, and V. Garcon, "Square wave voltammetry measurements of low concentrations of nitrate using Au/AgNPs electrode in chloride solutions," *Electroanalysis*, vol. 29, no. 12, pp. 2882–2887, 2017.

[55] N. Pankratova, M. Cuartero, T. Cherubini, G. A. Crespo, and E. Bakker, "In-line acidification for potentiometric sensing of nitrite in natural waters," *Analytical Chemistry*, vol. 89, no. 1, pp. 571–575, 2017.

[56] D. Gillian, I. Maguire, B. Heery, C. Nwankire, J. Ducree, and F. Regan, "PhosphaSense: a fully integrated, portable lab-on-a-disc device for phosphate determination in water," *Sensors and Actuators B-Chemical*, vol. 246, pp. 1085–1091, 2017.

[57] J. M. Zhu, Y. Shi, X. Q. Zhu et al., "Optofluidic marine phosphate detection with enhanced absorption using a Fabry–Pérot resonator," *Lab on a Chip*, vol. 17, no. 23, pp. 4025–4030, 2017.

[58] X. Cao, S. W. Zhang, D. Z. Chu, N. Wu, H. K. Ma, and Y. Liu, "A design of spectrophotometric microfluidic chip sensor for analyzing silicate in seawater," in *In 3rd International*

Conference on Water Resource and Environment, Qingdao, China, 2017.

[59] L. Ding, J. W. Ding, B. J. Ding, and W. Qin, "Solid-contact potentiometric sensor for the determination of total ammonia nitrogen in seawater," *International Journal of Electrochemical Science*, vol. 12, no. 4, pp. 3296–3308, 2017.

[60] L. O. Šraj, M. I. Almeida, M. K. ID, and S. D. Kolev, "Determination of trace levels of ammonia in marine waters using a simple environmentally-friendly ammonia (SEA) analyser," *Marine Chemistry*, vol. 194, pp. 133–145, 2017.

[61] P. Nadezda, M. G. Afshar, D. Yuan, G. A. Crespo, and E. Bakker, "Local acidification of membrane surfaces for potentiometric sensing of anions in environmental samples," *Acs Sensors*, vol. 1, no. 1, pp. 48–54, 2016.

[62] C. Chen, Z. Q. Yuan, H. T. Chang, F. N. Lu, Z. H. Li, and C. Lu, "Silver nanoclusters as fluorescent nanosensors for selective and sensitive nitrite detection," *Analytical Methods*, vol. 8, no. 12, pp. 2628–2633, 2016.

[63] Z. Yong, D. Yuan, H. Lin, and T. Zhou, "Determination of ammonium in seawater by purge-and-trap and flow injection with fluorescence detection," *Analytical Letters*, vol. 49, no. 5, pp. 665–675, 2016.

[64] S. X. Li, W. J. Liang, F. Y. Zheng, H. F. Zhou, X. F. Lin, and J. B. Cai, "Lysine surface modified Fe_3O_4@SiO_2@TiO_2 microspheres-based preconcentration and photocatalysis for in situ selective determination of nanomolar dissolved organic and inorganic phosphorus in seawater," *Actuators B-Chemical*, vol. 224, pp. 48–54, 2016.

[65] C. Barus, I. Romanytsia, N. Striebig, and V. Garcon, "Toward an *in situ* phosphate sensor in seawater using square wave voltammetry," *Talanta*, vol. 160, pp. 417–424, 2016.

[66] S. Cinti, D. Talarico, G. Palleschi, D. Moscone, and F. Arduini, "Novel reagentless paper-based screen-printed electrochemical sensor to detect phosphate," *Analytica Chimica Acta*, vol. 919, pp. 78–84, 2016.

[67] D. Aguilar, C. Barus, W. Giraud et al., "Silicon-based electrochemical microdevices for silicate detection in seawater [J]," *Sensors and Actuators B-Chemical*, vol. 211, pp. 116–124, 2015.

[68] C. Deirdre, C. Fay, D. Boyle et al., "Development of a low cost microfluidic sensor for the direct determination of nitrate using chromotropic acid in natural waters," *Analytical Methods*, vol. 7, no. 13, pp. 5396–5405, 2015.

[69] C. Maria, G. A. Crespo, and E. Bakker, "Tandem electrochemical desalination-potentiometric nitrate sensing for seawater analysis," *Analytical Chemistry*, vol. 87, no. 16, pp. 8084–8089, 2015.

[70] K. Taketoshi, T. Ichikawa, K. Hidaka, and K. Furuya, "A highly sensitive and large concentration range colorimetric continuous flow analysis for ammonium concentration," *Journal of Oceanography*, vol. 71, no. 1, pp. 65–75, 2015.

[71] L. Ying, Y. Pan, Q. Guo, H. Hongzhi, W. Chancui, and Q. Zhang, "A novel analytical method for trace ammonium in freshwater and seawater using 4-methoxyphthalaldehyde as fluorescent reagent," *Journal of Analytical Methods in Chemistry*, vol. 2015, 7 pages, 2015.

[72] M. Yucel, A. D. Beaton, M. Dengler, M. C. Mowlem, F. Sohl, and S. Sommer, "Nitrate and nitrite variability at the seafloor of an oxygen minimum zone revealed by a novel microfluidic in-situ chemical sensor," *PLoS One*, vol. 10, no. 7, article e0132785, 2015.

[73] L. Krockel, H. Lehmann, T. Wieduwilt, and M. A. Schmidt, "Fluorescence detection for phosphate monitoring using reverse injection analysis," *Talanta*, vol. 125, pp. 107–113, 2014.

[74] Z. Yong, D. Yuan, Y. Huang, J. Ma, S. Feng, and K. Lin, "A modified method for on-line determination of trace ammonium in seawater with a long-path liquid waveguide capillary cell and spectrophotometric detection," *Marine Chemistry*, vol. 162, pp. 114–121, 2014.

[75] K. Wild-Allen and M. Rayner, "Continuous nutrient observations capture fine-scale estuarine variability simulated by a 3D biogeochemical model," *Marine Chemistry*, vol. 167, pp. 135–149, 2014.

[76] A. Natchanon, J.-Z. Zhang, P. B. Ortner, J. Stamates, M. Shoemaker, and M. W. Kindel, "A portable analyser for the measurement of ammonium in marine waters," *Environmental Science-Processes & Impacts*, vol. 15, no. 3, pp. 579–584, 2013.

[77] L. Francois-Eric, V. J. Sieben, E. Malcolm et al., "A high performance microfluidic analyser for phosphate measurements in marine waters using the vanadomolybdate method," *Talanta*, vol. 116, pp. 382–387, 2013.

[78] Z. Yong, D. Yuan, Y. Huang, J. Ma, and S. Feng, "A sensitive flow-batch system for on board determination of ultra-trace ammonium in seawater: method development and shipboard application," *Analytica Chimica Acta*, vol. 794, pp. 47–54, 2013.

[79] M. Gilbert, J. Needoba, C. Koch, A. Barnard, and A. Baptista, "Nutrient loading and transformations in the Columbia River estuary determined by high-resolution in situ sensors," *Estuaries and Coasts*, vol. 36, no. 4, pp. 708–727, 2013.

[80] J. Jonca, W. Giraud, C. Barus et al., "Reagentless and silicate interference free electrochemical phosphate determination in seawater," *Electrochimica Acta*, vol. 88, pp. 165–169, 2013.

[81] K. S. Johnson, L. J. Coletti, H. W. Jannasch, C. M. Sakamoto, D. D. Swift, and S. C. Riser, "Long-term nitrate measurements in the ocean using the in situ ultraviolet spectrophotometer: sensor integration into the APEX profiling float," *Journal of Atmospheric and Oceanic Technology*, vol. 30, no. 8, pp. 1854–1866, 2013.

[82] L. Bulgariu and D. Bulgariu, "Direct determination of nitrate in small volumes of natural surface waters using a simple spectrophotometric method," *Reviews in Analytical Chemistry*, vol. 31, no. 3-4, pp. 201–207, 2012.

[83] W. Giraud, L. Lesven, J. Jonca et al., "Reagentless and calibrationless silicate measurement in oceanic waters," *Talanta*, vol. 97, pp. 157–162, 2012.

[84] A. D. Beaton and L. Christopher, "Lab-on-chip measurement of nitrate and nitrite for in situ analysis of natural waters," *Environmental Science & Technology*, vol. 46, no. 17, pp. 9548–9556, 2012.

[85] C. W. Jang, Y. T. Byun, and Y. M. Jhon, "Detection of 10 nM ammonium ions in 35‰ NaCl solution by carbon nanotube based sensors," *Journal of Nanoscience and Nanotechnology*, vol. 12, no. 3, pp. 1765–1769, 2012.

[86] A. D. Beaton and J. Vincent, "An automated microfluidic colourimetric sensor applied *in situ* to determine nitrite concentration," *Sensors and Actuators B-Chemical*, vol. 156, no. 2, pp. 1009–1014, 2011.

[87] O. Zielinski, D. Voss, B. Saworski, B. Fiedler, and A. Kortzinger, "Computation of nitrate concentrations in

turbid coastal waters using an in situ ultraviolet spectrophotometer," *Journal of Sea Research*, vol. 65, no. 4, pp. 456–460, 2011.

[88] H. Burkhard, C. M. Duarte, and V. Cerda, "A miniature and field-applicable multipumping flow analyzer for ammonium monitoring in seawater with fluorescence detection," *Talanta*, vol. 85, no. 1, pp. 380–385, 2011.

[89] A. Natchanon, J.-Z. Zhang, and P. B. Ortner, "An autonomous batch analyzer for the determination of trace ammonium in natural waters using fluorometric detection," *Analytical Methods*, vol. 3, no. 7, pp. 1501–1506, 2011.

[90] C. Guohe, M. Zhang, Z. Zhang, Y. Huang, and D. Yuan, "Online solid phase extraction and spectrophotometric detection with flow technique for the determination of nanomolar level ammonium in seawater samples," *Analytical Letters*, vol. 44, no. 1-3, pp. 310–326, 2011.

[91] S. K. Bey, A. Kaed, D. P. Connelly, F.-E. Legiret, A. J. K. Harris, and M. C. Mowlem, "A high-resolution analyser for the measurement of ammonium in oligotrophic seawater," *Ocean Dynamics*, vol. 61, no. 10, pp. 1555–1565, 2011.

[92] S. R. Alves, R. B. R. Mesquita, M. T. S. O. B. Ferreira, C. F. C. P. Teixeira, A. A. Bordalo, and A. O. S. S. Rangel, "Development of a sequential injection gas diffusion system for the determination of ammonium in transitional and coastal waters," *Analytical Methods*, vol. 3, no. 9, pp. 2049–2055, 2011.

[93] R. Pidcock, M. Srokosz, J. Allen et al., "A novel integration of an ultraviolet nitrate sensor on board a towed vehicle for mapping open-ocean submesoscale nitrate variability," *Journal of Atmospheric and Oceanic Technology*, vol. 27, no. 8, pp. 1410–1416, 2010.

[94] K. S. Johnson, S. C. Riser, and D. M. Karl, "Nitrate supply from deep to near-surface waters of the North Pacific subtropical gyre," *Nature*, vol. 465, no. 7301, pp. 1062–1065, 2010.

[95] F. Katia, V. Ynam, B. Chaudret, V. Garcon, D. Thouron, and M. Comtat, "An original nitrate sensor based on silver nanoparticles electrodeposited on a gold electrode," *Electrochemistry Communications*, vol. 12, no. 10, pp. 1439–1441, 2010.

[96] W. D. Gong, M. Mowlem, M. Kraft, and H. Morgan, "A simple, low-cost double beam spectrophotometer for colorimetric detection of nitrite in seawater," *IEEE Sensors Journal*, vol. 9, no. 7, pp. 862–869, 2009.

[97] J. N. Plant, K. S. Johnson, J. A. Needoba, and L. J. Coletti, "NH4-Digiscan: an in situ and laboratory ammonium analyzer for estuarine, coastal, and shelf waters," *Limnology and Oceanography: Methods*, vol. 7, no. 2, pp. 144–156, 2009.

[98] K. Y. Chumbimuni-Torres, P. Calvo-Marzal, J. Wang, and E. Bakker, "Electrochemical sample matrix elimination for trace-level potentiometric detection with polymeric membrane ion-selective electrodes," *Analytical Chemistry*, vol. 80, no. 15, pp. 6114–6118, 2008.

[99] S. Aravamudhan and S. Bhansali, "Development of microfluidic nitrate-selective sensor based on doped- polypyrrole nanowires," *Sensors and Actuators B-Chemical*, vol. 132, no. 2, pp. 623–630, 2008.

[100] M. Lacombe, V. Garcon, D. Thouron, N. Le Bris, and M. Comtat, "Silicate electrochemical measurements in seawater: chemical and analytical aspects towards a reagentless sensor," *Talanta*, vol. 77, no. 2, pp. 744–750, 2008.

[101] A. Natchanon and J.-Z. Zhang, "Shipboard fluorometric flow analyzer for high-resolution underway measurement of ammonium in seawater," *Analytical Chemistry*, vol. 80, no. 4, pp. 1019–1026, 2008.

[102] A. Abbassi, A. Mihi, and R. Benbouta, "Monitoring of hydrogen generated by corrosion reactions of steel," *Materials and Corrosion*, vol. 59, no. 12, pp. 942–947, 2008.

[103] G. H. Chen, D. X. Yuan, Y. M. Huang, M. Zhang, and M. Bergman, "In-field determination of nanomolar nitrite in seawater using a sequential injection technique combined with solid phase enrichment and colorimetric detection," *Analytica Chimica Acta*, vol. 620, no. 1-2, pp. 82–88, 2008.

[104] S. Aravamudhan, S. Ketkar, and S. Bhansali, "Development of nitrate-selective electrochemical sensor with integrated micro-fluidics," in *In 2007 Ieee Sensors*, Atlanta, GA, USA, 2007.

[105] M. Lacombe, V. Garcon, M. Comtat et al., "Silicate determination in sea water: toward a reagentless electrochemical method," *Marine Chemistry*, vol. 106, no. 3-4, pp. 489–497, 2007.

[106] K. S. Johnson, L. J. Coletti, and F. P. Chavez, "Diel nitrate cycles observed with in situ sensors predict monthly and annual new production," *Deep Sea Research Part I: Oceanographic Research Papers*, vol. 53, no. 3, pp. 561–573, 2006.

[107] Q. P. Li, J. Z. Zhang, F. J. Millero, and D. A. Hansell, "Continuous colorimetric determination of trace ammonium in seawater with a long-path liquid waveguide capillary cell," *Marine Chemistry*, vol. 96, no. 1-2, pp. 73–85, 2005.

[108] N. Karousos, L. C. Chong, C. Ewen, C. Livingstone, and J. Davis, "Evaluation of a multifunctional indicator for the electroanalytical determination of nitrite," *Electrochimica Acta*, vol. 50, no. 9, pp. 1879–1884, 2005.

[109] Z. H. Xie, X. C. Lin, and G. N. Chen, "Novel phosphate-sensitive fluorescent composite matrix," *Chemical Research in Chinese Universities*, vol. 19, no. 2, pp. 201–205, 2003.

[110] D. Thouron, R. Vuillemin, X. Philippon et al., "An autonomous nutrient analyzer for oceanic long-term in situ biogeochemical monitoring," *Analytical Chemistry*, vol. 75, no. 11, pp. 2601–2609, 2003.

[111] K. S. Johnson and L. J. Coletti, "In situ ultraviolet spectrophotometry for high resolution and long-term monitoring of nitrate, bromide and bisulfide in the ocean," *Deep-Sea Research Part I-Oceanographic Research Papers*, vol. 49, no. 7, pp. 1291–1305, 2002.

[112] P. C. Gardolinski, A. R. David, and P. J. Worsfold, "Miniature flow injection analyser for laboratory, shipboard and in situ monitoring of nitrate in estuarine and coastal waters," *Talanta*, vol. 58, no. 6, pp. 1015–1027, 2002.

[113] R. T. Masserini and K. A. Fanning, "A sensor package for the simultaneous determination of nanomolar concentrations of nitrite, nitrate, and ammonia in seawater by fluorescence detection," *Marine Chemistry*, vol. 68, no. 4, pp. 323–333, 2000.

[114] A. R. J. David, T. Mccormack, and P. J. Worsfold, "A submersible battery-powered flow injection (FI) sensor for the determination of nitrate in estuarine and coastal waters," *Journal of Automated Methods & Management in Chemistry*, vol. 21, no. 1, pp. 1–9, 1999.

[115] A. R. J. David, T. Mccormack, A. W. Morris, and P. J. Worsfold, "A submersible flow injection-based sensor for the determination of total oxidised nitrogen in coastal waters," *Analytica Chimica Acta*, vol. 361, no. 1-2, pp. 63–72, 1998.

[116] H. W. Jannasch, K. S. Johnson, and C. M. Sakamoto, "Submersible, osmotically pumped analyzer for continuous determination of nitrate in situ," *Analytical Chemistry*, vol. 66, no. 20, pp. 3352–3361, 1994.

[117] W. L. Pearce and Faraday Reprint, "Experimental researches in electricity. vols. 1 to 3. Michael Faraday. Dover, New York, 1965. Vols. 1 and 2, 896 pp. (bound as one volume); vol. 3, 602 pp. plates. $15," *Science*, vol. 150, no. 3696, pp. 598-599, 1965.

[118] W. Hong, D. Pan, and H. Han, "Electrochemical monitoring of marine nutrients: from principle to application," *TrAC Trends in Analytical Chemistry*, vol. 138, article 116242, 2021.

[119] G. A. Crespo, "Recent advances in ion-selective membrane electrodes for in situ environmental water analysis," *Electrochimica Acta*, vol. 245, pp. 1023–1034, 2017.

[120] Z. Liang, J. Wan, J. Li et al., "Fabricating a self-supported electrode for detecting ammonia in water based on electrodepositing platinum-polypyrrole on Ni foam," *Journal of the Electrochemical Society*, vol. 167, no. 2, 2020.

[121] Y. Ding, M. G. Zhao, J. T. Yu, X. M. Zhang, Z. M. Li, and H. Li, "Using the interfacial barrier effects of p-n junction on electrochemistry for detection of phosphate," *Analyst*, vol. 145, no. 9, pp. 3217–3221, 2020.

[122] M. D. Patey, M. J. A. Rijkenberg, P. J. Statham, M. C. Stinchcombe, E. P. Achterberg, and M. Mowlem, "Determination of nitrate and phosphate in seawater at nanomolar concentrations," *Analytical Chemistry*, vol. 27, no. 2, pp. 169–182, 2008.

[123] P. Nicolas, "Interferences from oxygen reduction reactions in bioelectroanalytical measurements: the case study of nitrate and nitrite biosensors," *Analytical and Bioanalytical Chemistry*, vol. 405, no. 11, pp. 3731–3738, 2013.

[124] A. Rafiq, K. S. Bhat, M.-S. Ahn, and Y.-B. Hahn, "Fabrication of a robust and highly sensitive nitrate biosensor based on directly grown zinc oxide nanorods on a silver electrode," *New Journal of Chemistry*, vol. 41, no. 19, pp. 10992–10997, 2017.

[125] Z. Ke, H. Zhou, H. Ping, and L. Qing, "The direct electrochemistry and bioelectrocatalysis of nitrate reductase at a gold nanoparticles/aminated graphene sheets modified glassy carbon electrode," *RSC Advances*, vol. 9, no. 64, pp. 37207–37213, 2019.

[126] A. E. Santoro, N. J. Nidzieko, G. L. Van Dijken, K. R. Arrigo, and A. B. Boehm, "Contrasting spring and summer phytoplankton dynamics in the nearshore Southern California Bight," *Limnology and Oceanography*, vol. 55, no. 1, pp. 264–278, 2010.

[127] F. Monteiro-Silva, P. A. S. Jorge, and R. C. Martins, "Optical sensing of nitrogen, phosphorus and potassium: a spectrophotometrical approach toward smart nutrient deployment," *Chem*, vol. 7, no. 4, p. 51, 2019.

[128] Z. Elena and E. Bakker, "Potentiometric sensing," *Analytical Chemistry*, vol. 91, no. 1, pp. 2–26, 2019.

[129] S. A. Jaywant and K. M. Arif, "A comprehensive review of microfluidic water quality monitoring sensors," *Sensors*, vol. 19, no. 21, p. 4781, 2019.

[130] K. Wanpen, S. Pencharee, C. Puangpila, S. K. Hartwell, S. Lapanantnoppakhun, and J. Jakmunee, "Exploiting an automated microfluidic hydrodynamic sequential injection system for determination of phosphate," *Talanta*, vol. 177, pp. 77–85, 2018.

[131] K. Guebuem, Y.-W. Lee, D.-J. Joung, K.-R. Kim, and K. Kim, "Real-time monitoring of nutrient concentrations and red-tide outbreaks in the southern sea of Korea," *Geophysical Research Letters*, vol. 33, no. 13, 2006.

[132] R.-V. M. Victor, J. R. Sempionatto, B. E.-F. de Avila et al., "Delayed sensor activation based on transient coatings: biofouling protection in complex biofluids," *Journal of the American Chemical Society*, vol. 140, no. 43, pp. 14050–14053, 2018.

Hindawi
Journal of Sensors
Volume 2021, Article ID 4967954, 5 pages
https://doi.org/10.1155/2021/4967954

Research Article

An Intelligent Hydroponic Device for *Astragalus membranaceus* Bge. var. mongolicus (Bge.) Hsiao

Qiyuan Chen,[1] Zhenqing Bai,[2,3] XiuJuan Zhang,[2] and Shengli Wang[4]

[1]*Inner Mongolia Technical College of Mechanics and Electrics, Huhhot, China 010070*
[2]*Inner Mongolia Key Laboratory of Molecular Biology on Featured Plants, Inner Mongolia Academy of Science and Technology, Huhhot, China 010018*
[3]*College of Life Sciences, Yan'an University, Yan'an, China 716000*
[4]*Integrated Support Center, Inner Mongolia Huhhot Science and Technology Bureau, Huhhot, China 010070*

Correspondence should be addressed to Zhenqing Bai; shanxibzq@163.com and XiuJuan Zhang; mingyuesong@163.com

Received 5 July 2021; Accepted 17 September 2021; Published 17 November 2021

Academic Editor: Yuan Li

Astragalus membranaceus Bge. var. mongolicus (Bge.) Hsiao roots are widely used as raw materials of medicine. Due to the limited arable land, cultivating medicinal plants hydroponically is increasingly concerned. However, whether the quality of *A. membranaceus* grown hydroponically is better than that produced in a field is still unknown. In this study, we designed an intelligent hydroponic device for *A. membranaceus*, and quality of the medicinal plant cultivated by this device was compared with that cultivated in the field. Results showed that hydroponics significantly increased effective components in *A. membranaceus* when compared with field. Specifically, astragaloside IV contents in *A. membranaceus* grown hydroponically for four weeks were higher than those cultivated in the field for two years. The biomass is not significantly different between four-week hydroponics and annual cultivation. Therefore, hydroponics with our intelligent device can be used for the sustainable production of *A. membranaceus* in the future.

1. Introduction

Astragalus membranaceus (Fisch.) Bge. is a medicinal plant which is widely used in modern medicine [1–3]. It is distributed in north China and widely cultivated in Inner Mongolia [4, 5]. To date, the available agricultural land is decreasing in recent decades which limited the development of *A. membranaceus*. Facility agriculture is one of the important strategies to solve the problem of cultivated land utilization in the modern agriculture [6].

In the facility agriculture, the soilless cultivation has the advantages of saving fertilizer and water, saving labor, decreasing disease and insect, and improving high yield [6]. Among them, hydroponic nutrient mixing system can cultivate the higher-quality plant varieties [7], such as soilless cultivation of vegetables in ornamental greenhouse and the cultivation of strawberry (*Fragaria* × *ananassa* Duch.) [8, 9]. In addition, hydroponics can quickly cultivate plants, shorten plant culture period, and improve yield. Thus, making special hydroponic device for plant growth is a determinant of sustainable plant growth and industrial development [10].

Hydroponics is a good way to produce high-yield crops by taking minimal space, makes work easier for farmers in growing of plants, and also consumes less amount of water when compared to traditional method resulting in conservation of water [11]. In production, strawberry hydroponics can avoid the occurrence of some soil-borne diseases and pests [8]. Here, an intelligent hydroponic device for cultivating *A. membranaceus* was designed.

2. Materials and Methods

2.1. A. membranaceus Cultivation Conditions. Seeds of *A. membranaceus* were collected in Chifeng City, Inner Mongolia, China, and then, seeds were sown in nutrient soils (vermiculite and nutrient soil ratio was 1 : 3). The seeds were

planted with sufficient water. Then, the seedlings were cultured under 16 h light/8 h darkness and 25°C for 30 days. Watered every two days. Then, the one-month plants were cultivated in a hydroponic device. The root of these plants was harvested in one, two, and four weeks, respectively.

For Field conditions, the seeds of *A. membranaceus* were planted directly in the field, and the plants grew for one and two years in Hohhot, Baotou, and Chifeng, Inner Mongolia. The root of *A. membranaceus* in the field was harvested with four-week hydroponic plants. Collect these roots, dry them in an oven at 45°C, weigh, and count 10 roots. These roots were used in HPLC.

2.2. Structure of Designed Hydroponic Device. The intelligent hydroponic device is designed according to the needs of *A. membranaceus* growth. It has hydroponic tank, support seat, and support leg, which are bolted with each other; the surface of the support leg is bolted with a water pump. The water outlet end of the water pump is connected with a water injection pipe and a water extraction pipe. The water extraction pipe far away from the end of the water pump is connected with a three-way water valve. The water inlet ends at the top and bottom of the right side of the three-way water valve are, respectively, connected with a nutrition pipe and a water supply pipe. The water supply pipe away from the three-way water valve is connected with a special water pipe. Both sides of the top of the hydroponic tank are bolted with a support plate. The gap inside the support frame is penetrated with a moisture discharge pipe which is connected with a moisture discharge cover. The inner part of the fixing frame is bolted with a moisture exhaust fan. The pump operates 24 hours every work day, at 25°C, humidity 30%; the cultivate medium was modified Hoagland nutrient solution (Table 1).

2.3. High-Performance Liquid Chromatography (HPLC) Determination. Take 2.0 g of medicinal powder (passing through 100-mesh sieve) and accurately weigh it. Put it into a 150 ml Soxhlet extractor, add 40 ml methanol, soak it overnight (12 h), add 20 ml methanol, and heat and reflux at 85°C for 4 h. The solvent was recovered and concentrated to dryness. The residue was dissolved with 10 ml water and shaken with water-saturated n-butanol for 4 times, 40 ml each time. Wash thoroughly with ammonia test solution for 2 times, 40 ml each time. Discard ammonia solution, and evaporate with n-butanol solution. The residue was dissolved with 5 ml water and cooled down. The residue was washed off with 50 ml water and then eluted with 30 ml 40% ethanol. The eluent was continued to be eluted with 80 ml 70% ethanol. The eluate was collected and evaporated to dryness. The residue was dissolved in methanol and transferred to 5 ml volumetric flask; add methanol to volume to the scale, shake well, filter with 0.45 μm microporous membrane, and set aside.

For the chromatographic column, Agilent Zorbax sb-c18 column (250 mm × 4.6 mm) was used. The mobile phase was acetonitrile water (32 : 68); the flow rate was 1.0 ml·min^{-1}; the column temperature was 27°C; the ELSD parameters are as follows: evaporator temperature: 112°C, nebulizer temperature: 85°C, gas flow rate: 1.5 SLM, data rate: 80 Hz, led intensity: 100%, smoothing: 50 (5.0 seconds), and PMT gain: 10.0; the theoretical number of astragaloside IV was not less than 4 μl, 10 μl, 20 μl, and 10 μl of the reference solution, and the test solution was, respectively, injected into the liquid chromatograph. The determination was carried out according to the above chromatographic conditions, and the HPLC liquid chromatograms were recorded.

2.4. Data Analysis. All experiments were conducted with three biological replicates. The HPLC statistical analyses data were performed using one-way ANOVA by SPSS software (version 13.0) at the significant level of $P \leq 0.01$. All figures were generated using Origin 9.0 software.

3. Results

3.1. The Hydroponic Device Design for A. membranaceus Cultivation. In order to alleviate the problem of land use efficiency in *A. membranaceus* planting, this research designs an intelligent hydroponic device for its cultivation. In the hydroponic device, a camera is fixed at the bottom of the bracket for the interior watching of the hydroponic tank. The top of the front side of the hydroponic tank is fixedly installed with a water temperature and a water level meter for the monitor of its temperature and moisture insufficiency (Figure 1). The equipment can not only reduce the staff entry but can also discharge the moist air. It can solve the problem that the current *A. membranaceus* hydroponic device still needs the staff to enter the hydroponic greenhouse for water supplement and fertilization.

3.2. The Biomass and Astragaloside IV Contents between Hydroponic Culture and Cultivation. In order to further study whether the selected cultivation has the representativeness of astragaloside IV content in the root of *A. membranaceus* in Inner Mongolia, three different production areas cultivation were selected for comparison. The results show that the content of astragaloside IV in hydroponic root is significantly higher than that in other areas (Figure 2(a)). At the same time, in order to understand the biomass difference between hydroponics and cultivation, their biomass was statistically analyzed. The results showed that there was significant difference between hydroponic culture, annual cultivation, and biennial cultivation (Figure 2(b)). Therefore, *A. membranaceus* used in this study is universal. The nutrient solution is changed every 2 weeks in the intelligent hydroponic device which can be grown continuously for 2 months of *A. membranaceus*.

3.3. The Astragaloside IV Contents Increased in Hydroponic Device Than Cultivation. To understand the cultivation status of *A. membranaceus* in hydroponic device, we blasted the astragaloside IV between the hydroponic device and filed cultivation. Interestingly, the content in hydroponic cultivation was higher than that in the field. The astragaloside IV contents is 0.218 mg/g in two years of cultivation; its content is 0.627 mg/g in two-month seedling with four-week hydroponic cultivation (Figure 3). Meanwhile, the elapsed time of hydroponic cultivation is significantly

Table 1: Hoagland nutrient formula.

Macroelements	Final concentration (mM)	Stock solution concentration (mM)
KNO_3	5	1000
$Ca(NO_3)_2{\cdot}4H_2O$	5	1000
$MgSO_4{\cdot}7H_2O$	2	400
KH_2PO4	1	200
Microelement	Final concentration (μM)	Stock solution concentration (mM)
H_3BO_3	46.1	46.1
$MnCl_2{\cdot}4H_2O$	9.1	9.1
$ZnSO_4{\cdot}7H_2O$	0.76	0.76
$CuSO_4{\cdot}5H_2O$	0.32	0.32
$Na_2MoO_4{\cdot}2H_2O$	0.24	0.24
Fe^{2+}	Final concentration (μM)	
EDTA-Fe-Na	50	

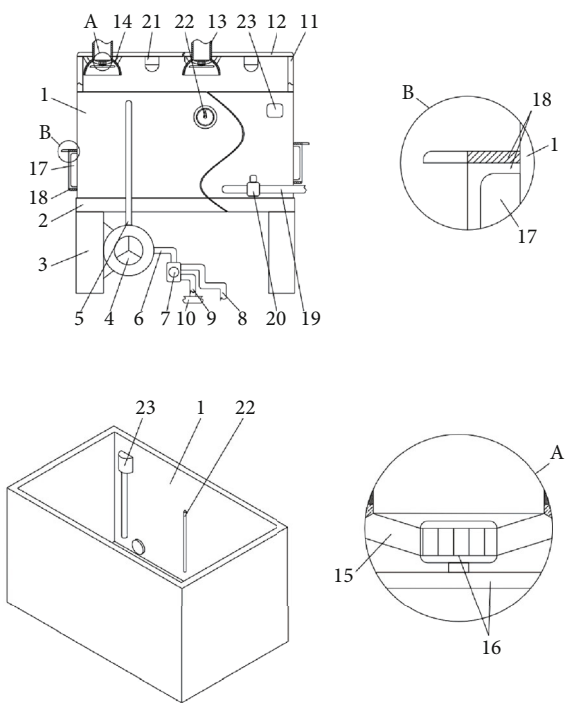

Figure 1: The hydroponic device structure of *Astragalus membranaceus* Bge. var. mongolicus (Bge.) Hsiao. An intelligent controlled Astragalus hydroponic device includes a hydroponic tank (1), a support seat (2), a support leg (3), a water pump (4), a water injection pipe (5), a water extraction pipe (6), a three-way water valve (7), a nutrition pipe (8), a water make-up pipe (9), one end of the support plate (11), a special water pipe (10), a support plate (12), the gap in the support plate (12), a moisture drainage pipe (13), a moisture drainage cover (14), a fixed pipe the inner part of the fixing frame (15), a moisture exhaust fan (16), socket (17), waterproof cover (18), drain pipe (19), drain valve (20), camera (21), water temperature gauge (22), and water level gauge (23).

shorter than that of common cultivation. From two years to two months is the significantly time efficiency improvement for *A. membranaceus*.

4. Discussion

The nutrients of plant growth come from the root absorption [12]. Field planting and indoor soil culture are common plant culture methods. At present, with the limited area of soil cultivated land in China, soilless cultivation is one of the effective ways to solve this problem [13]. The soilless cultivation technology through hydroponics, fog culture, and other ways has been widely used in vegetable and flower cultivation. The greater environmental and ecological awareness is growing the farmers who want to adopt sustainable and efficient cultivation systems [14]. Sustainable and modern cultivation systems contain cultivation devices and organic fertilization [10]. In modern agriculture, the hydroponic device is the growing process of the plant root cultivated in the nutrient-rich solutions, such as the official Real-Time Operating System (RTOS) for ARM Cortex-M microcontroller [15]. The hydroponic devices were used to produce "Biquinho" pepper with brackish water [16]. However, there are few reports on soilless cultivation of medicinal plants, such as *Coptis chinensis* Franch. [17]. *A. membranaceus* is a typical medicinal material in China. Due to the limitation of cultivated land area, developing soilless cultivation is a good way to develop plant factory production in the future [18].

In addition to the limited land use, the soil-borne disease of *A. membranaceus* is one of the main factors affecting its industrial development [19]. The soilless cultivation completely avoids this problem. But the frequent in and out of the equipment easily brings in foreign bacteria, which will affect the production of *A. membranaceus*. Moreover, the air is often humid in the hydroponic planting process, which further provides conditions for the reproduction of pathogens [6, 10]. This *A. membranaceus* hydroponic device can reduce these effects on its soilless production by external visual monitoring system. Astragaloside IV is the main active component in *A. membranaceus* that determines its quality [9, 20, 21]. In this study, the active ingredients of four-week hydroponic cultivated

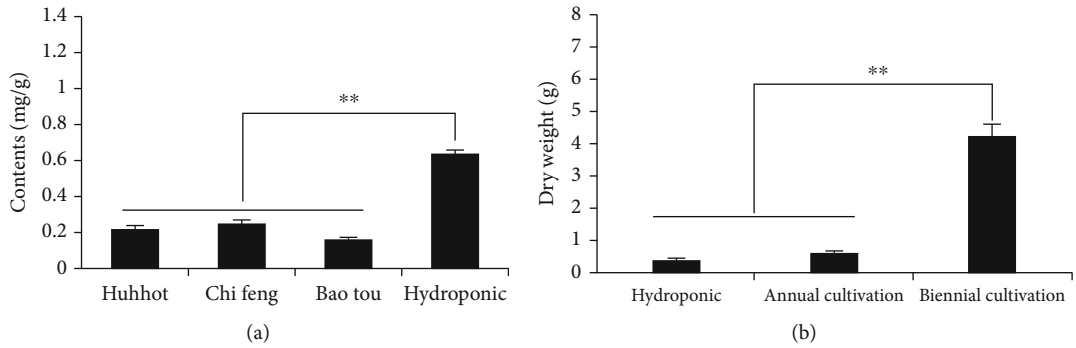

Figure 2: The astragaloside IV contents and dry weight of different cultivation areas or years in *A. membranaceus* Bge. var. mongolicus (Bge.) Hsiao: (a) the astragaloside IV contents of different cultivation areas in *A. membranaceus* Bge. var. mongolicus (Bge.) Hsiao; (b) dry weight of different years in *A. membranaceus* Bge. var. mongolicus (Bge.) Hsiao. Data are shown as the mean ± SD ($n = 3$), and the double asterisk indicates the significance ($P < 0.01$) according to one-way ANOVA tests. The double asterisk above bars represents significant differences at the level of 0.01.

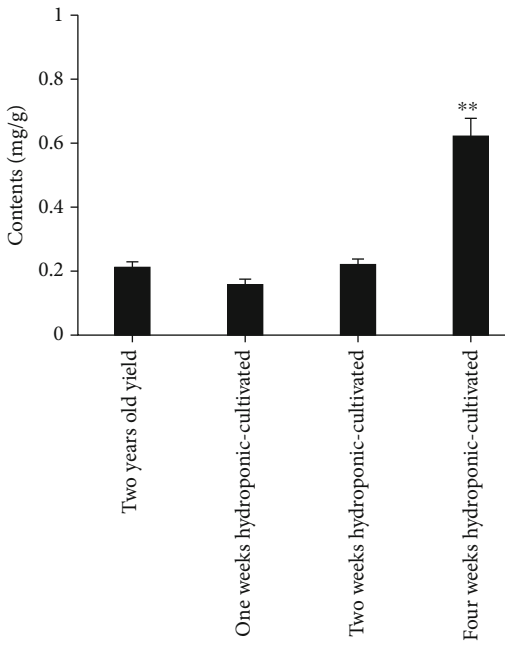

Figure 3: The contents of astragaloside IV in hydroponic device and yield plants. Data are shown as the mean ± SD ($n = 3$), and the double asterisk indicates the significance ($P < 0.01$) according to one-way ANOVA tests. The double asterisk above the bar represents significant differences at the level of 0.01.

plants can reach 2 times more than those of a two-year-old field *A. membranaceus*. Moreover, astragaloside IV contents in Hohhot cultivation used in this study are representative. There is no difference in biomass between hydroponic and annual *A. membranaceus*, which greatly shortens its culture time and unaffected by the external environment. Meanwhile, hydroponics of *A. membranaceus* can realize its sustainable culture.

In conclusion, based on the soilless cultivation of *A. membranaceus*, the intelligent hydroponic device was designed to improve its cultivation efficiency and the content of active ingredients. Meanwhile, this method avoids soil-borne diseases. Soilless culture avoids continuous cropping obstacles in conventional cultivation [22]. Therefore, this study provides theoretical support for the soilless cultivation and the development of the *A. membranaceus* industry.

Data Availability

The data used to support the findings of this study are available from the corresponding author upon request.

Conflicts of Interest

The authors have declared no conflict of interests.

Authors' Contributions

BZQ conceived the research and wrote the manuscript. CQY performed the experiments and data analysis and revised the manuscript. ZXJ gave the project support and the design guidance of the experiment.

Acknowledgments

We thank Science and Technology Projects of Inner Mongolia Autonomous Region (2020GG0286, 2020CG0075, and 2021GG0342) for financial supports.

References

[1] M. Cheng, X. L. Chi, H. Wang, and G. Yang, "Analysis of status and problems of international trade of *Astragalus membranaceus* in China," *Modern Chinese Medicine*, vol. 21, no. 4, pp. 424–428, 2019.

[2] National Pharmacopoeia Committee, *Pharmacopoeia of the People's Republic of China*, China Medical Science and Technology Press, Beijing, China, 2020.

[3] Q. Zhang, Y. J. Yu, L. Jia et al., "Establishment of regenerated plantlets system from callus of *Astragalus membranaceus* (Fisch) Bunge," *Journal of Beijing University of Agriculture*, vol. 29, no. 3, pp. 18–20, 2014.

[4] S. Y. Sun and G. L. Chen, "Effects of drought stress on reproductive growth and effective components of *Astragalus*

membranaceus var. mongholicus," *Molecular Plant Breeding*, vol. 17, no. 22, pp. 7559–7565, 2019.

[5] Y. Zhang, L. Dong, J. J. Yong, F. Y. Mao, and X. Y. Fu, "Study on the main component determination method and HPLC finger print of Radix Astragali. Lishizhen," *Medicine and Materia medica Research*, vol. 27, no. 11, pp. 2610–2613, 2016.

[6] M. Majid, J. N. Khan, Q. M. Ahmad Shah, K. Z. Masoodi, B. Afroza, and S. Parvaze, "Evaluation of hydroponic systems for the cultivation of Lettuce (*Lactuca sativa* L. , var. Longifolia) and comparison with protected soil-based cultivation," *Agricultural Water Management*, vol. 245, article 106572, 2021.

[7] R. Tandil, J. Yapson, W. Atmadja, S. Liawatimena, and R. Susanto, "Hydroponic nutrient mixing system based on STM32," *IOP Conference Series Earth and Environmental Science*, vol. 195, no. 1, article 012052, 2018.

[8] O. Grunert, E. Hernandez-Sanabria, S. Buysens et al., "In-depth observation on the microbial and fungal community structure of four contrasting tomato cultivation systems in soil based and soilless culture systems," *Frontiers in Plant Science*, vol. 11, 2020.

[9] L. L. Wang, H. L. Feng, K. Yang, H. M. Teng, and Z. H. Hu, "Research progress on biology and chemical constituents of *Astragalus membranaceus*," *Genomics and Applied Biology*, vol. 36, no. 6, pp. 2581–2585, 2017.

[10] G. E. Barrett, P. D. Alexander, J. S. Robinson, and N. C. Bragg, "Achieving environmentally sustainable growing media for soilless plant cultivation systems - a review," *Scientia Horticulturae*, vol. 212, pp. 220–234, 2016.

[11] M. S. Hariram, P. K. Kshama, M. Navaneeth, and Pratheeksha, "Fully automated hydroponics system for smart farming," *International Journal of Engineering and Manufacturing (IJEM)*, vol. 11, no. 4, pp. 33–41, 2021.

[12] K. S. Shin, D. Chakrabarty, J. Y. Ko, S. S. Han, and K. Y. Paek, "Sucrose utilization and mineral nutrient uptake during hairy root growth of red beet (*Beta vulgaris* L.) in liquid culture," *Plant Growth Regulation*, vol. 39, no. 2, pp. 187–193, 2003.

[13] S. Nwosisi and D. Nandwani, "Urban horticulture: overview of recent developments," in *Urban Horticulture. Sustainable Development and Biodiversity, vol 18*, D. Nandwani, Ed., Springer, Champions, 2018.

[14] R. Altieri, A. Esposito, G. Baruzzi, and T. Nair, "Corroboration for the successful application of humified olive mill waste compost in soilless cultivation of strawberry," *International Biodeterioration & Biodegradation*, vol. 88, no. 88, pp. 118–124, 2014.

[15] W. Atmadja, S. Liawatimena, J. Lukas, E. P. L. Nata, and I. Alexander, "Hydroponic system design with real time OS based on ARM cortex-M microcontroller," *IOP Conference Series: Earth & Environmental Science*, vol. 109, article 012017, 2017.

[16] M. Bione, T. M. Soares, A. Cova, V. Paz, and B. Neves, "Hydroponic production of 'Biquinho' pepper with brackish water," *Agricultural Water Management*, vol. 245, article 106607, 2021.

[17] W. L. Huang, Z. Q. Bai, J. Jiao et al., "Distribution and chemical forms of cadmium in Coptis chinensis Franch. determined by laser ablation ICP-MS, cell fractionation, and sequential extraction," *Ecotoxicology and Environmental Safety*, vol. 171, pp. 894–903, 2019.

[18] R. Fan, J. Luo, S. Yan et al., "Use of water hyacinth (Eichhornia crassipes) compost as a peat substitute in soilless growth media," *Compost Science & Utilization*, vol. 23, no. 4, pp. 237–247, 2015.

[19] Z. Y. Mao, H. Y. Chen, and Y. L. Li, "Effects of different cultivation modes on yield and root rot incidence rate of *Astragalus membranaceus*," *Information of Agricultural Science and Technology*, vol. 426, no. 1, pp. 52–52, 2014.

[20] Y. B. Cao, "Research progress on pharmacological activities and mechanism of astragaloside IV," *Drugs & Clinic*, vol. 32, no. 5, pp. 954–960, 2017.

[21] Z. H. Sun, J. Shao, and M. Guo, "A review on chemical components and pharmacological effects of Huangqi," *Clinical Journal of Chinese Medicine*, vol. 7, no. 25, pp. 22–25, 2015.

[22] X. Wang, Z. Wang, and W. Zhang, "Research progress on soilless culture and nutrient solution recipes of strawberry," *Tianjin Agricultural Sciences*, vol. 23, no. 6, pp. 83–86, 2017.